This work was performed for the Jet Propulsion Laboratory, California Institute of Technology, sponsored by the National Aeronautics and Space Administration under Contract NAS7-100.

N68-18634

Surveyor Spacecraft System

SURVEYOR I FLIGHT PERFORMANCE

FINAL REPORT

Volume I of III

JPL Contract 950056 / October 1966

SSD 68189R

J.D. CLOUD
Manager
System Engineering and Analysis Laboratory

K.C. BEALL
Director
Surveyor I Post Flight Evaluation

R.H. LEUSCHNER
Head
Post Flight Analysis Section

HUGHES
HUGHES AIRCRAFT COMPANY
SPACE SYSTEMS DIVISION

PRECEDING PAGE BLANK NOT FILMED.

CONTENTS

			Page
1.0	SCOPE AND PURPOSE		1-1
2.0	BRIEF SYSTEM DESCRIPTION		
	2.1	Surveyor I Mission Objectives	2-1
	2.2	Brief Spacecraft Mechanization Description	2-3
	2.3	Flight Configuration	2-15
3.0	MISSION PERFORMANCE SUMMARY		
	3.1	Introduction	3-1
	3.2	Transit Phase Description	3-1
	3.3	First Lunar Day Description	3-13
	3.4	Second Lunar Day Description	3-21
	3.5	Summary of Significant Anomalies	3-31
	3.6	Summary of Transit Deviations From EPD 180	3-31
	3.7	Mission Event Time History	3-35
4.0	SYSTEM SUMMARY AND CONCLUSIONS		
	4.1	Summary of System Performance Parameters	4-1
	4.2	Conclusions and Recommendations	4-6
5.0	PERFORMANCE ANALYSIS		
	5.1	SYSTEM	
		5.1.1 Introduction	5.1-1
		5.1.2 Mission Statistics	5.1-1
		5.1.3 Commands to Spacecraft in Flight	5.1-3
		5.1.4 Postmission Data Processing	5.1-12
	5.2	THERMAL SUBSYSTEMS	
		5.2.1 Introduction	5.2-1
		5.2.2 Summary of Thermal Events and Results	5.2-2
		5.2.3 Analysis of Thermal Control System	5.2-17
		5.2.4 Anomaly/Discrepancy Description	5.2-161
		5.2.5 Conclusions and Recommendations	5.2-162
		5.2.6 References	5.2-163
		5.2.7 Acknowledgments	5.2-164
		Appendix A	A-1
		Appendix B	B-1

PRECEDING PAGE BLANK NOT FILMED

ILLUSTRATIONS

		Page
1-1	Typical Lunar Television Pictures	xii
2-1	Surveyor Spacecraft	2-4
2-2	Atlas-Centaur 10/SC-1	2-5
2-3	Spacecraft General Arrangement	2-7
2-4	Simplified Spacecraft Functional Block Diagram	2-9
5.1-1	Postmission Data Processing Flow	5.1-13
5.2-1	Compartment A and B Radiator Thermal Environment During Lunar Day	5.2-21
5.2-2	Compartment A and B Lunar Day Thermal Dissipating Capability	5.2-23
5.2-3	Sun Angle on First Lunar Day	5.2-24
5.2-4	SC-1 A/SPP Transit Analysis	5.2-29
5.2-5	Solar Panel (EP-12) on First Lunar Day	5.2-31
5.2-6	Solar Panel Axis Motor (M-10) on First Lunar Day	5.2-33
5.2-7	Elevation Axis Motor (M-12) on First Lunar Day	5.2-35
5.2-8	Lower Mast (V-34) on First Lunar Day	5.2-37
5.2-9	Planar Array (M-8) on First Lunar Day	5.2-39
5.2-10	SC-1 Spaceframe Flight Data Compared with Predictions	5.2-41
5.2-11	Spaceframe Temperature Distribution on Test Data and SC-1 Flight Data Survey Transit Coast Phase	5.2-42
5.2-12	Spaceframe Lunar History (V-28, V-37, V-38, and V-39)	5.2-43
5.2-13	Spaceframe Lunar History (V-27, V-34, V-35, and V-36)	5.2-45
5.2-14	Crushable Block 3 Heat Shield (V-44) on First Lunar Day	5.2-51
5.2-15	Thrust Chamber Assembly Illumination Pattern Resulting From Attitude Shifts	5.2-56
5.2-16	Position of Sun Vector (-58 degree Yaw) Relative to Flight Sensor P-22	5.2-61
5.2-17	SC-1 Flight Sensor P-22 (Retro Nozzle) During Midcourse	5.2-66
5.2-18	Flight Control Electronics Boards (FC-44 and FC-45) on First Lunar Day	5.2-67
5.2-19	Canopus Temperature (FC-47) on First Lunar Day	5.2-69
5.2-20	Temperature Rise of Pitch Gyro (FC-54) and Flight Control Electronics Board 6 (FC-45) When Flight Control System Operated on Moon	5.2-72

		Page
5.2-21	Roll Gyro Temperatures (Sensor FC-46) on First Lunar Day	5.2-73
5.2-22	Pitch Gyro Temperature (Sensor FC-54) on First Lunar Day	5.2-75
5.2-23	Yaw Gyro Temperature (Sensor FC-55) on First Lunar Day	5.2-77
5.2-24	Roll Actuator (FC-71) and Vernier Engine 1 (P-7) Temperature History	5.2-81
5.2-25	Nitrogen Tank (FC-48) on First Lunar Day	5.2-83
5.2-26	RADVS Temperature on First Lunar Day	5.2-89
5.2-27	AMR Electronics Temperature (R-7)	5.2-91
5.2-28	AMR Antenna (R-27) During Midcourse	5.2-92
5.2-29	Surveyor Television Thermal Profile	5.2-95
5.2-30	Transit Heatup of Camera 3	5.2-118
5.2-31	Comparison of Predicted and Measured Temperatures — Steady-State Nonoperating	5.2-120
5.2-32	TV-9: Vidicon Collar	5.2-124
5.2-33	TV-10: ECU Chassis	5.2-125
5.2-34	TV-9: Vidicon Collar	5.2-126
5.2-35	TV-10: ECU Chassis	5.2-127
5.2-36	Lunar Surface Temperature (Based on $\epsilon_{moon} = 1.0$) Obtained from SC-1	5.2-131
5.2-37	Temperature and Shadow of Outboard Side of Compartment A During First Lunar Day and Night	5.2-135
5.2-38	Temperature and Shadow of Outboard Side of Compartment B During First Lunar Day and Night	5.2-137
5.2-39	Angle Between Sun Rays and the Normal to Outboard Side of Compartment A During First Lunar Day	5.2-139
5.2-40	Angle Between Sun Rays and the Normal to Outboard Side of Compartment B During First Lunar Day	5.2-140
5.2-41	SC-1 Flight Data for Flight Control Electronics	5.2-143
5.2-42	SC-1 Flight Data for Pitch Gyro	5.2-143
5.2-43	SC-1 Flight Data for Pitch Gyro Temperature Rise When Flight Control System was Operated	5.2-144
5.2-44	SC-1 Flight Data for Flight Control Electronics Board 6	5.2-144
5.2-45	Thermal Response of SC-1 Roll Actuator	5.2-144
5.2-46	Thermal Response of Propellant Lines on Lunar Surface	5.2-145
5.2-47	Thermal Response of Propellant Tanks on Lunar Surface	5.2-146
5.2-48	Thermal Response of Vernier Engines and Helium Tank on Lunar Surface	5.2-146
5.2-49	Thermal Response of Shock Absorber on Lunar Surface	5.2-147
5.2-50	Thermal Response of SC-1 RADVS Units on Lunar Surface	5.2-147
5.2-51	Temperature Versus Eppley Solar Intensity	5.2-151

		Page
A-1	Transmitter Traveling-Wave Tubes	A-1
A-2	Main Battery	A-3
A-3	Solar Cell Array	A-4
A-4	Boost Regulator	A-5
A-5	Auxiliary Battery	A-6
A-6	Battery Charge Regulator	A-7
A-7	Flight Control Electronics	A-8
A-8	Flight Control Electronics	A-9
A-9	IRU Roll Gyro	A-11
A-10	Canopus Sensor	A-12
A-11	Nitrogen Tank	A-14
A-12	IRU Gyros	A-15
A-13	Attitude Jet 2	A-17
A-14	Roll Actuator	A-18
A-15	Planar Array	A-19
A-16	Solar Panel Axis Motor	A-20
A-17	Elevation Axis Motor	A-21
A-18	Retro Engine Upper Case	A-22
A-19	Oxidizer Line Near Engine 2	A-23
A-20	Fuel Tank 2	A-24
A-21	Oxidizer Tank 3	A-25
A-22	Vernier Engine 1	A-26
A-23	Oxidizer Line	A-27
A-24	Vernier Engines	A-29
A-25	Retro Engine Lower Case	A-31
A-26	Fuel Tanks	A-32
A-27	Oxidizer Tanks	A-34
A-28	Helium Tank	A-36
A-29	Retro Engine Nozzle	A-37
A-30	AMR Electronics Platform	A-38
A-31	AMR ECU Heat Sink	A-39
A-32	RADVS Klystron Unit	A-40
A-33	RADVS Signal Data Converter	A-41
A-34	RADVS Velocity Sensor Antenna Preamplifier	A-42
A-35	Altimeter Radar Sensor Temperature (R-13)	A-43
A-36	AMR Edge of Antenna Dish	A-44
A-37	TV Camera Electronics	A-45
A-38	Survey TV Hood and Mirror Assembly	A-47
A-39	Compartment A Thermal Tray Top	A-48
A-40	Compartment A Lower Support	A-49
A-41	Compartment A Insulation Retainer	A-50
A-42	Compartment A External Canister	A-51
A-43	Compartment A Thermal Switch	A-52
A-44	Compartment A Thermal Tray – Top	A-54
A-45	Compartment B Lower Support	A-55
A-46	Compartment B External Canister	A-56
A-47	Compartment B Thermal Switch 4 Radiator	A-57

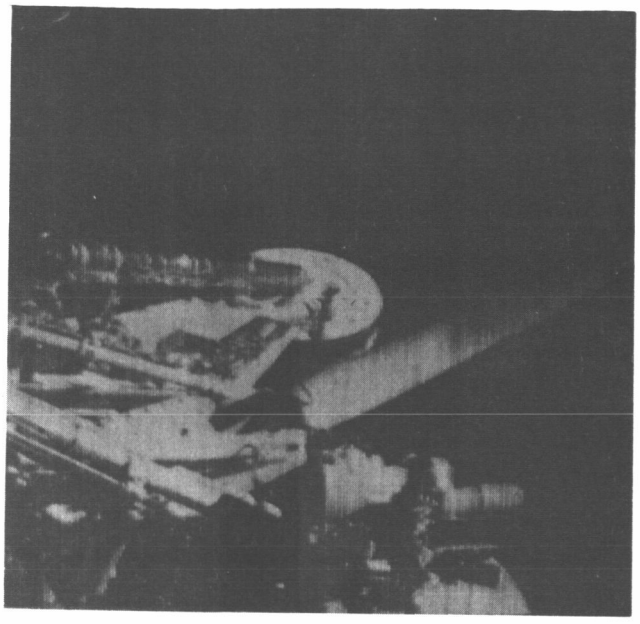
		Page
A-48	Compartment A Thermal Switch 8 Radiator	A-58
A-49	Compartment B Thermal Switch 4 Contact Ring	A-59
A-50	Upper Spaceframe	A-60
A-51	Lower Spaceframe	A-61
A-52	Thermal Tunnel	A-62
A-53	Shock Absorber 1	A-63
A-54	Leg 2 – Upper Web	A-64
A-55	Shock Absorber 2	A-65
A-56	Shock Absorber 3	A-66
A-57	A/SPP Mast	A-67
A-58	Spaceframes	A-68
A-59	Retro Attach Points	A-70
A-60	Crushable Block 3	A-73
A-61	Compartment B Thermal Switch 1 Radiator	A-75
A-62	Compartment B Thermal Switch 5 Radiator	A-76
A-63	Compartment A Thermal Switch 2 Radiator	A-77
A-64	Auxiliary Battery Outside Shell	A-78
B-1	Transmitters A and B	B-1
B-2	Main Battery and Battery Charge Regulator	B-4
B-3	Compartment A Top and Bottom Tray and Thermal Tunnel	B-7
B-4	Compartment A Interior (Near Day and Night Terminator)	B-10
B-5	Compartment A Radiators and Contact Ring	B-12
B-6	Compartment A Exterior (Near Day and Night Terminator	B-15
B-7	Compartment A and B Outer Shells	B-17
B-8	Boost Regulator and Compartment B Top and Bottom Tray	B-20
B-9	Compartment B Radiators and Contact Rings	B-25
B-10	Compartment B Exterior (Near Day and Night Terminator)	B-28
B-11	Mast, A/SPP, and Solar Cells	B-30
B-12	Auxiliary Battery/Battery Case	B-35
B-13	Flight Control Electronics and Canopus	B-38
B-14	Nitrogen and Helium Tanks	B-41
B-15	Propellant Lines	B-45
B-16	Fuel and Oxidizer Tanks	B-49
B-17	Vernier Engines and Roll Actuator	B-58
B-18	RADVS System	B-62
B-19	Upper and Lower Spaceframe	B-66
B-20	Leg 2, Gas Jet 2, and Crushable Block 3	B-72
B-21	Shock Absorbers	B-75
B-22	Retro Attach Points 1, 2, and 3	B-78
B-23	Survey Camera	B-81
B-24	TV and Flight Control	B-84

TABLES

		Page
2-1	Surveyor SC-1 Telemetry Assignments	2-13
2-2	SC-1 Flight Configuration and Telemetry Sources	2-15
3-1	SC-1 Mission Milestone – Transit Phase	3-2
3-2	SC-1 Event/Time History – Transit Phase	3-3
3-3	SC-1 Mission Milestone – Lunar Phase	3-14
3-4	Goldstone Visibility During Lunar Phase	3-15
3-5	Lunar Operations Sequences – First Lunar Day	3-16
3-6	Summary of Lunar Day Engineering Interrogations	3-22
3-7	Summary of First Lunar Day TV Sequences	3-26
3-8	Lunar Operation Sequences – Second Lunar Day	3-28
3-9	Summary of Significant Anomalies	3-32
3-10	Summary of Significant Transit Deviations From EPD 180	3-34
4-1	Summary of System Performance Parameters	4-1
4-2	Telemetry Analog Channels for Which Full 66-Hour Transit Phase Averaged Plots Are Not Useful	4-8
5. 1-1	Commands Transmitted by Prime Tracking Stations (Not Including Second Lunar Day Operations)	5. 1-1
5. 1-2	TV Pictures Made by Commands From Prime Tracking Stations (Not Including Second Lunar Day Operations)	5. 1-2
5. 1-3	Transmitter High Power Intervals	5. 1-3
5. 1-4	Thrust Power on Intervals	5. 1-3
5. 1-5	SC-1 Flight-Time Command Log	5. 1-4
5. 1-6	Predicted View Period Summary	5. 1-19
5. 1-7	Surveyor I PDP-4 Tapes	5. 1-21
5. 1-8	Designation of Nominal Coefficients Used by EDRS Program	5. 1-22
5. 1-9	Volts-to-Engineering-Units Coefficients	5. 1-23
5. 2-1	Mission A Major Events and Times	5. 2-4
5. 2-2	SC-1 Thermal Control Subsystem Flight Performance	5. 2-14
5. 2-3	SC-1 Actual High Power Operation Durations Compared With That Specified in EPD-180, Revision 5C	5. 2-18
5. 2-4	Transient Response to High Power Modes – Transit	5. 2-19
5. 2-5	Crushable Block Shield No. 3 Heat Capacity	5. 2-48
5. 2-6	SC-1 Crushable Block Shield No. 3 Radiation Properties	5. 2-48

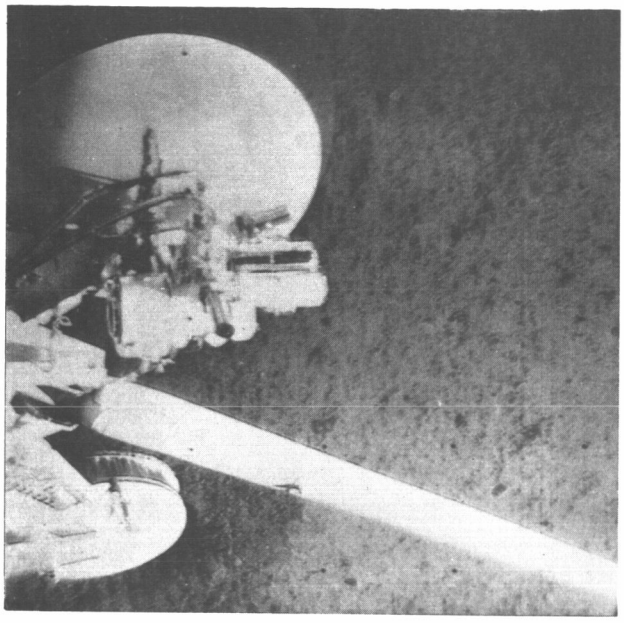
		Page
5.2-7	SC-1 Vernier Engine Exhaust Convection Heat Flux	5.2-49
5.2-8	Comparison of RADVS Flight and STV Temperature	5.2-87
5.2-9	Summary of SC-1 TV Camera Performance During First Lunar Day	5.2-115
5.2-10	Survey Camera Thermal Control Heater Operation During SC-1	5.2-116
5.2-11	Frequency of Operation of Drive Motors	5.2-129
5.2-12	Camera Power Dissipation	5.2-129
5.2-13	Proposed Lunar Surface Temperature Requirements Prior to Liftoff	5.2-148
5.2-14	Flight to STV Phase Intensity Correspondence	5.2-160

PRECEDING PAGE BLANK NOT FILMED.



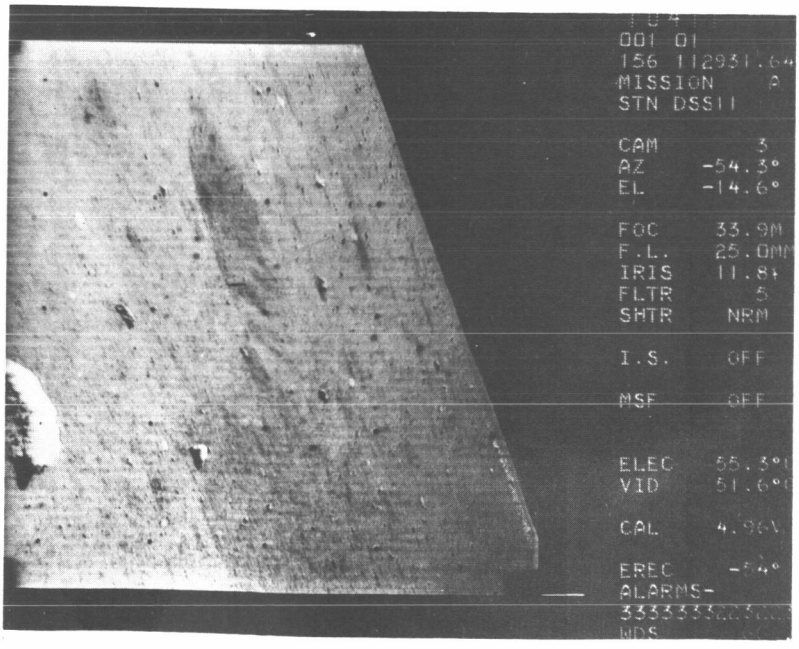
68189-568 (U)

a) Historic First Picture From the Moon



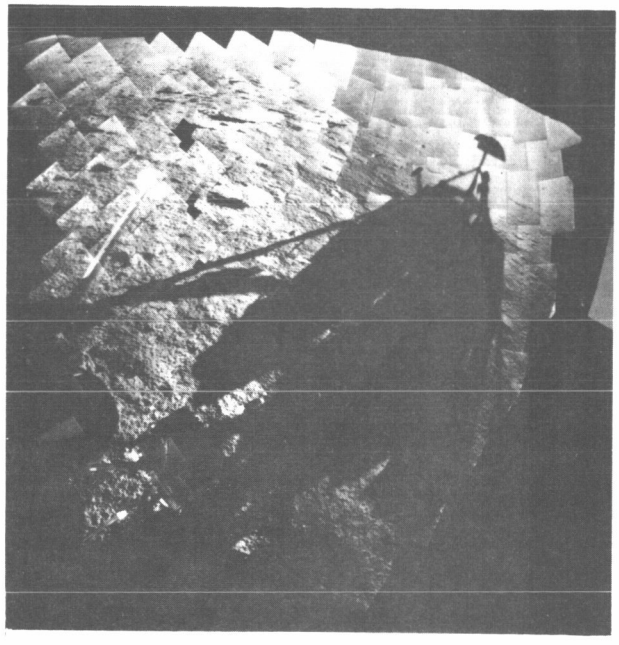
68189-569(U)

b) Subsequent 600 Line Picture of Same Footpad



68189-570(U)

c) Lunar Surface



68189-571(U)

d) Mosaic Showing Spacecraft Shadow on Lunar Surface

Figure 1-1. Typical Lunar Television Pictures

1.0 SCOPE AND PURPOSE

At 1441 GMT (0741 PDT) on Memorial Day, 30 May 1966, the first Surveyor spacecraft was launched from Cape Kennedy into a near perfect lunar trajectory by the Atlas/Centaur launch vehicle. At 0617 on 2 June GMT (2317 on 1 June PDT) after a 63-hour and 36-minute journey through space, the historical first truly soft landing of a spacecraft on the lunar surface was accomplished. This was followed by 12 days of flawless lunar operations, a 21-day quiescent period during the lunar night and subsequent morning, and a successful 7 days of operation during the second lunar day.

This report describes the actual performance of the spacecraft throughout this mission based on both real time and postmission data analysis. The period covered includes the prelaunch countdown, the transit and landing phase, and the first lunar day of operations through to the day/night terminator.

The basic purpose of this report is to document the actual performance of the Surveyor I spacecraft throughout this historic mission, compare its performance with that predicted by the spacecraft design, and recommend any changes or modifications that should be made in the spacecraft design, prediction models, or lunar operations. As this spacecraft is the first of a series of lunar landers and as it was so extremely successful, this report will tend to be overly thorough in the reporting and analysis of mission results.

2.0 BRIEF SYSTEM DESCRIPTION

The Surveyor spacecraft is designed and built by the Hughes Aircraft Company under the direction of the California Institute of Technology Jet Propulsion Laboratory for the National Aeronautics and Space Administration. It has been conceived and designed to effect a transit from earth to the moon, perform a soft lunar landing, and transmit to earth basic scientific and engineering data relative to the moon's environment and characteristics. A brief description of the Surveyor mission objectives and vehicle design is given in this section.

2.1 SURVEYOR I MISSION OBJECTIVES

The basic overall objectives of the Surveyor spacecraft system as defined in Reference 1 are as follows:

1) To develop a technology for and accomplish a series of soft landings on selected areas of the surface of the moon

2) To transport and soft land an instrumentation payload and perform experiments on the surface of the moon for the purpose of local area investigation

3) To obtain engineering data on the performance of the spacecraft system which will aid in future space exploration

4) To telemeter the scientific and engineering data back to earth for retrieval, reduction, and dissemination

5) To achieve the following capabilities as a minimum:

   a) Operation from lunar sunrise to sunset

   b) Three hours (nonoperating mode)* of predawn operations for SC-1 through SC-4 (Missions A through D) and 20 hours

*Nonoperating mode refers to the instrumentation payload only. The spacecraft bus shall be capable of providing normal engineering functions during the periods specified herein.

PRECEDING PAGE BLANK

(nonoperating mode)* of predawn operations for SC-5 through SC-7 (Missions E through G)

c) One hundred fifty hours (nonoperating mode)* of postsunset operations

A ninety-day period of operation is a desired objective.

It is planned to meet these overall objectives in a series of progressive steps, each adding a significant level of accomplishment over that of the preceding spacecraft. As such, the detailed mission objectives for the first spacecraft are defined in Reference 2 and summarized below.

2.1.1 Primary Objectives

1) Demonstrate the capability of the Surveyor spacecraft to perform successful midcourse and terminal maneuvers, and a soft landing on the moon.

2) Demonstrate the capability of the Atlas/Centaur vehicle to successfully inject the Surveyor spacecraft on a lunar-intercept trajectory.

3) Demonstrate the capability of the Surveyor communications system and the Deep Space Network to maintain communications with the spacecraft during its flight and after the soft landing.

2.1.2 Secondary Objectives

1) Obtain in-flight engineering data on all spacecraft subsystems used in cruise flight

2) Obtain in-flight engineering data on all spacecraft subsystems used during the midcourse maneuver, terminal maneuver, and main retro phase

3) Obtain in-flight engineering data on the performance of the closed-loop terminal descent guidance and control system, consisting of the velocity and altitude radars, on-board analog computer, autopilot, and vernier engines

4) Obtain engineering data on the performance of spacecraft subsystems used on the lunar surface

2.1.3 Tertiary Objectives

1) Obtain postlanding TV pictures of a spacecraft footpad and the immediately surrounding lunar-surface material

---

*Nonoperating mode refers to the instrumentation payload only. The spacecraft bus shall be capable of providing normal engineering functions during the periods specified herein.

2) Obtain postlanding TV pictures of the lunar topography

3) Obtain data on the radar reflectivity of the lunar surface

4) Obtain data on the bearing strength of the lunar surface

5) Obtain spacecraft temperature data on the lunar surface for use in the analysis of lunar surface temperatures

As will be demonstrated in the remainder of this report, all of the above primary, secondary, and tertiary objectives were met or exceeded by the Surveyor I spacecraft. In addition, the spacecraft demonstrated the capability of surviving the lunar night and successfully operating throughout the second lunar day, thereby greatly exceeding the mission objectives.

2.2 BRIEF SPACECRAFT MECHANIZATION DESCRIPTION

The Surveyor spacecraft (Figure 2-1) consists of a basic bus and an engineering payload. The spacecraft design is such that the engineering payload may be replaced by scientific payloads of equivalent power and weight requirements of subsequent flights. It is launched into a lunar orbit by the Atlas/Centaur launch vehicle (Figure 2-2).

2.2.1 Basic Bus

The basic bus (Figure 2-3) provides the capabilities of structural support, electrical power, telecommunications, attitude control, propulsion, thermal control, approach television, and engineering instrumentation. The following subsystems are a part of the basic bus:

1) Vehicle and mechanisms

2) Electrical power

3) Telecommunications

4) Flight control

5) Propulsion

6) Approach television

Figure 2-4 is a block diagram of the spacecraft system. Each of the subsystems is described briefly below.

2.2.1.1 Vehicle and Mechanisms

The vehicle and mechanisms subsystem provides support, alignment, thermal protection, electrical interconnection, mechanical actuation, and touchdown stabilization for the spacecraft. The subsystem consists of the

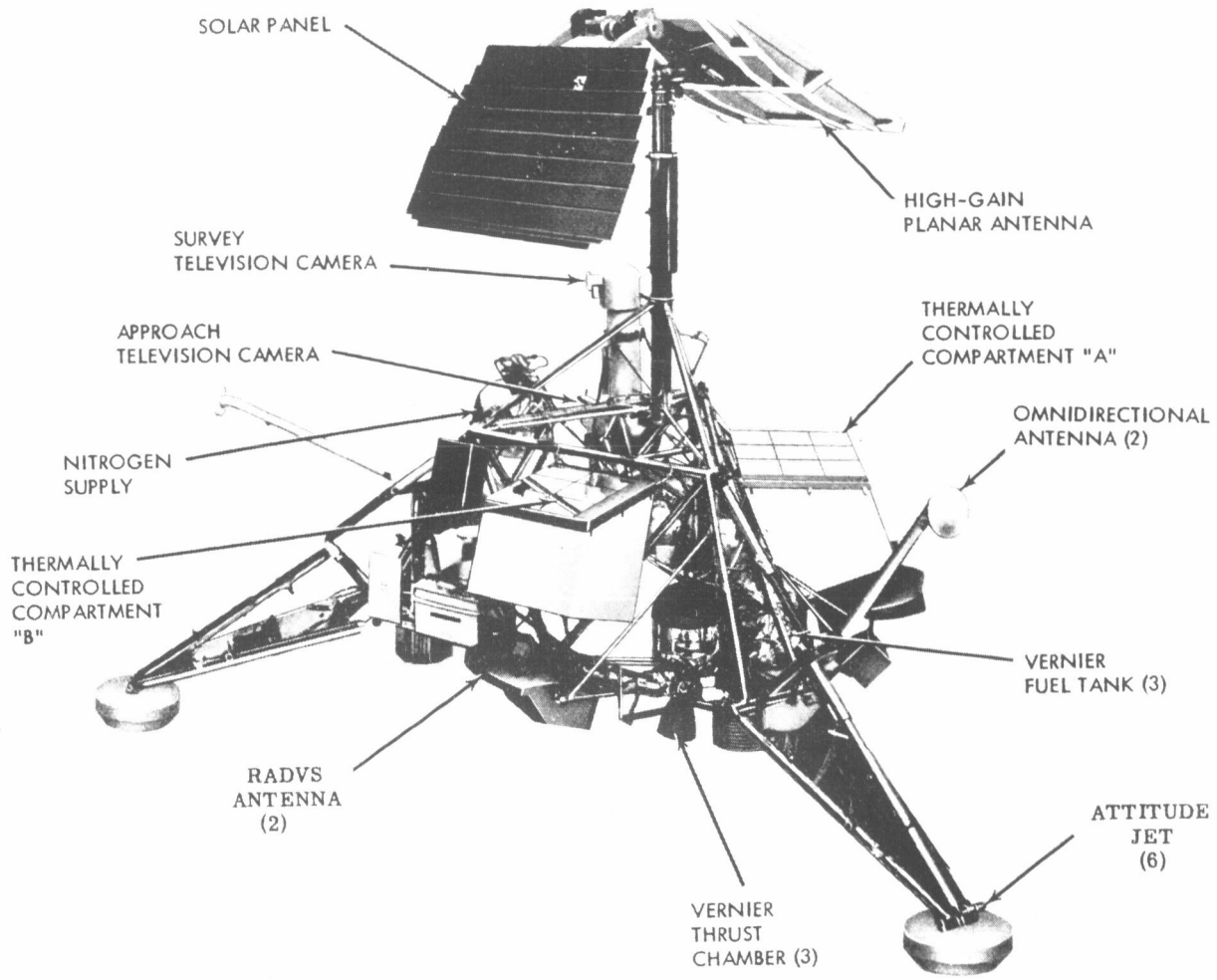
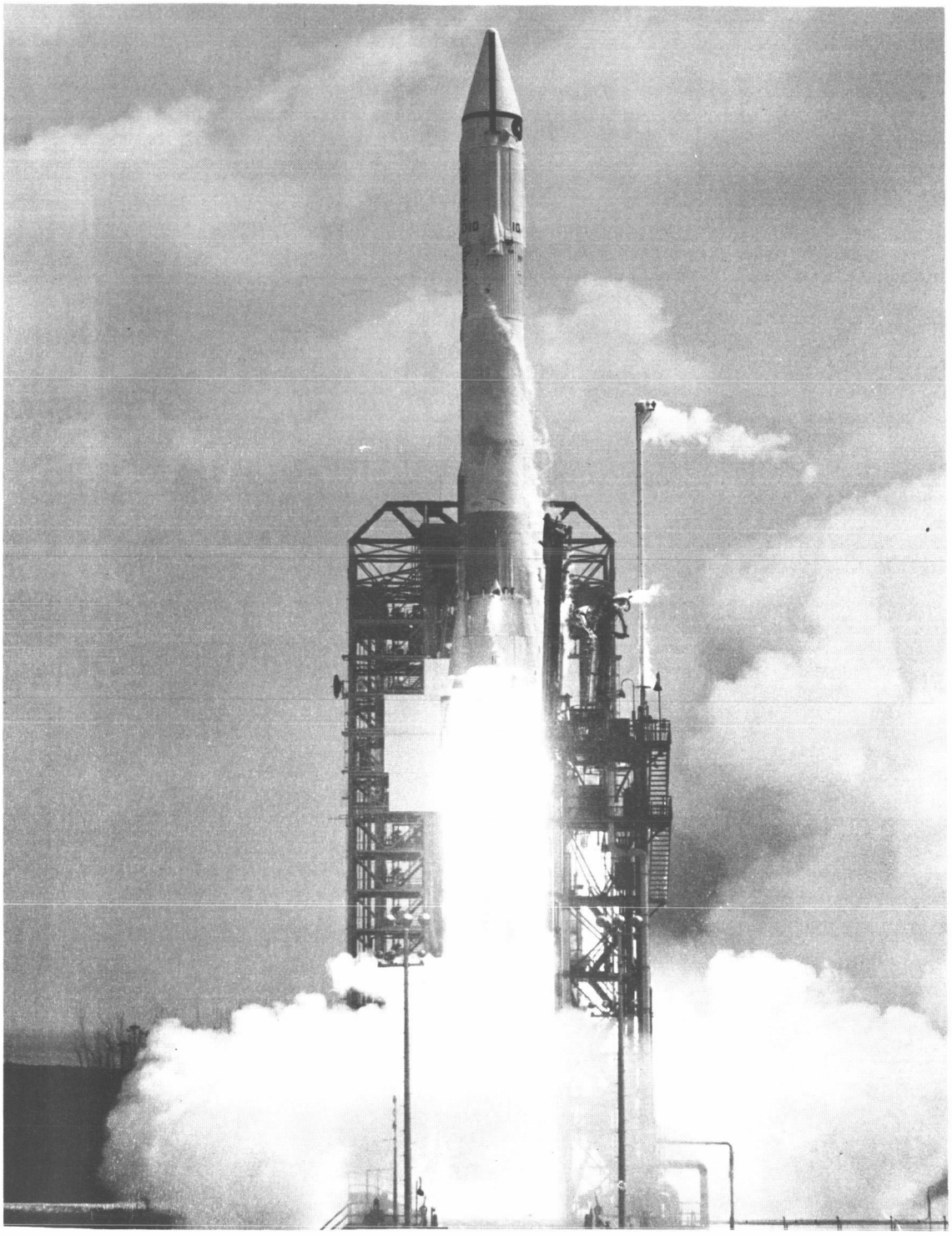


Figure 2-1. Surveyor Spacecraft



68189-565(U)

Figure 2-2. Atlas-Centaur 10/SC-1

PRECEDING PAGE BLANK NOT FILMED.

PRECEDING PAGE BLANK NO

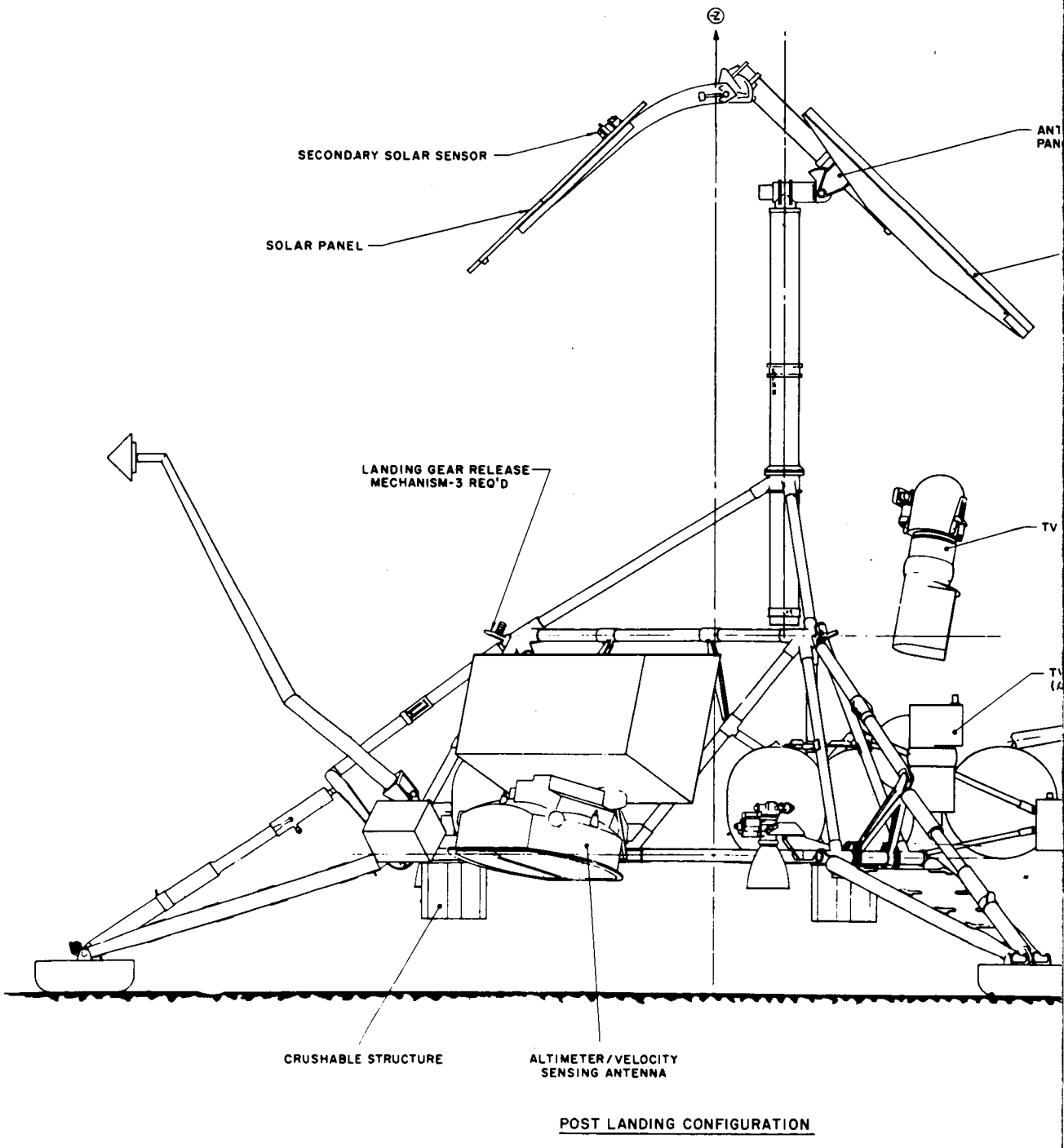


Figure 2-3. Spacecraft General Arrangement

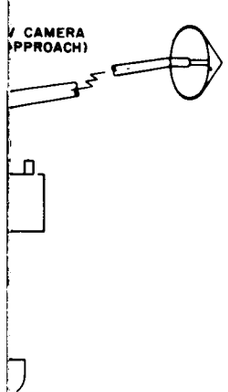
T FILMED.

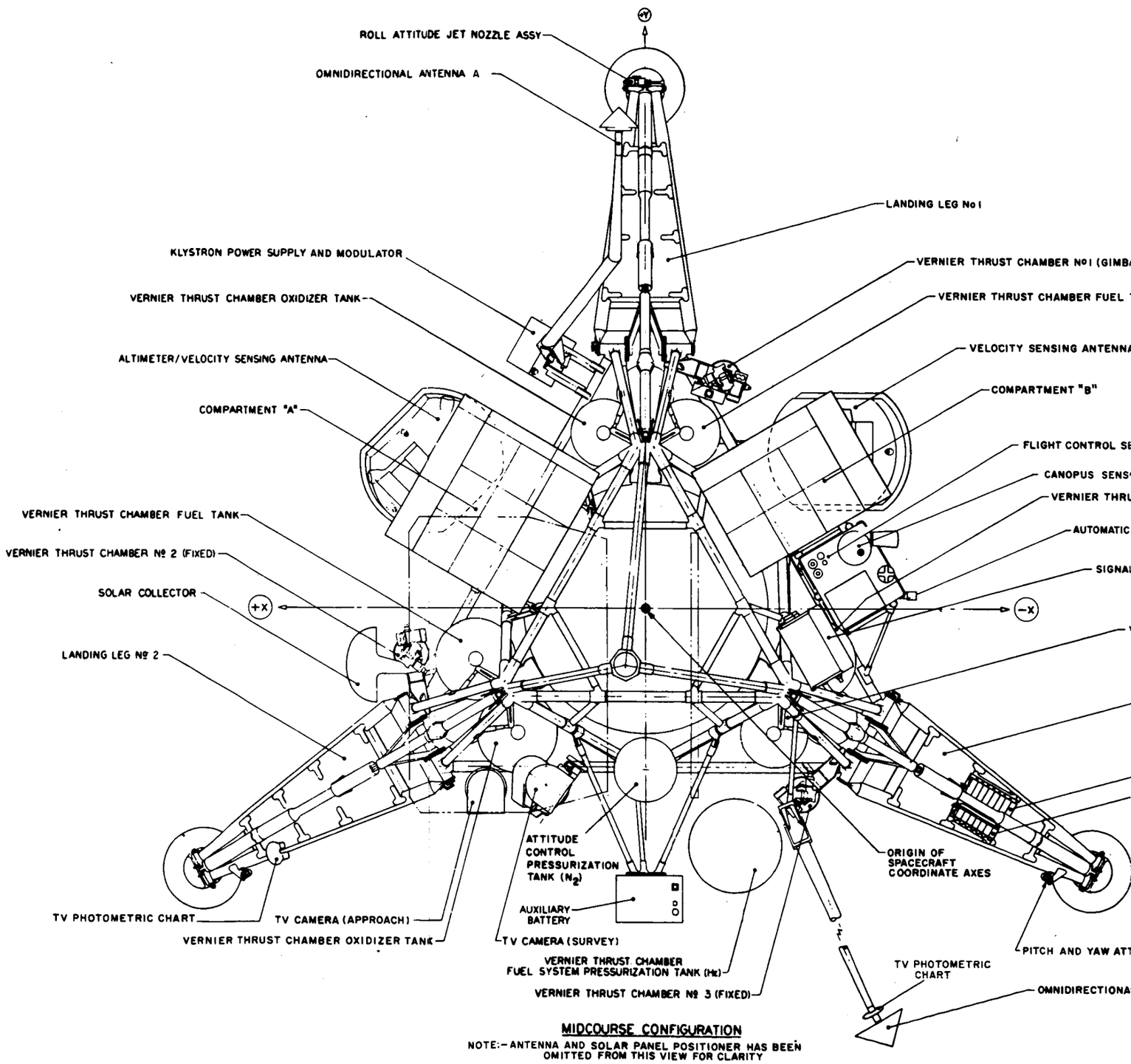
ENNA AND SOLAR
EL POSITIONER

PLANAR ARRAY ANTENNA

CAMERA (SURVEY)

V CAMERA
PPROACH)





MIDCOURSE CONFIGURATION

NOTE:- ANTENNA AND SOLAR PANEL POSITIONER HAS BEEN OMITTED FROM THIS VIEW FOR CLARITY

ALLED)

TANK

ENSOR GROUP

OR

UST CHAMBER OXIDIZER TANK

SUN ACQUISITION SENSOR

L DATA CONVERTER

VERNIER THRUST CHAMBER FUEL TANK

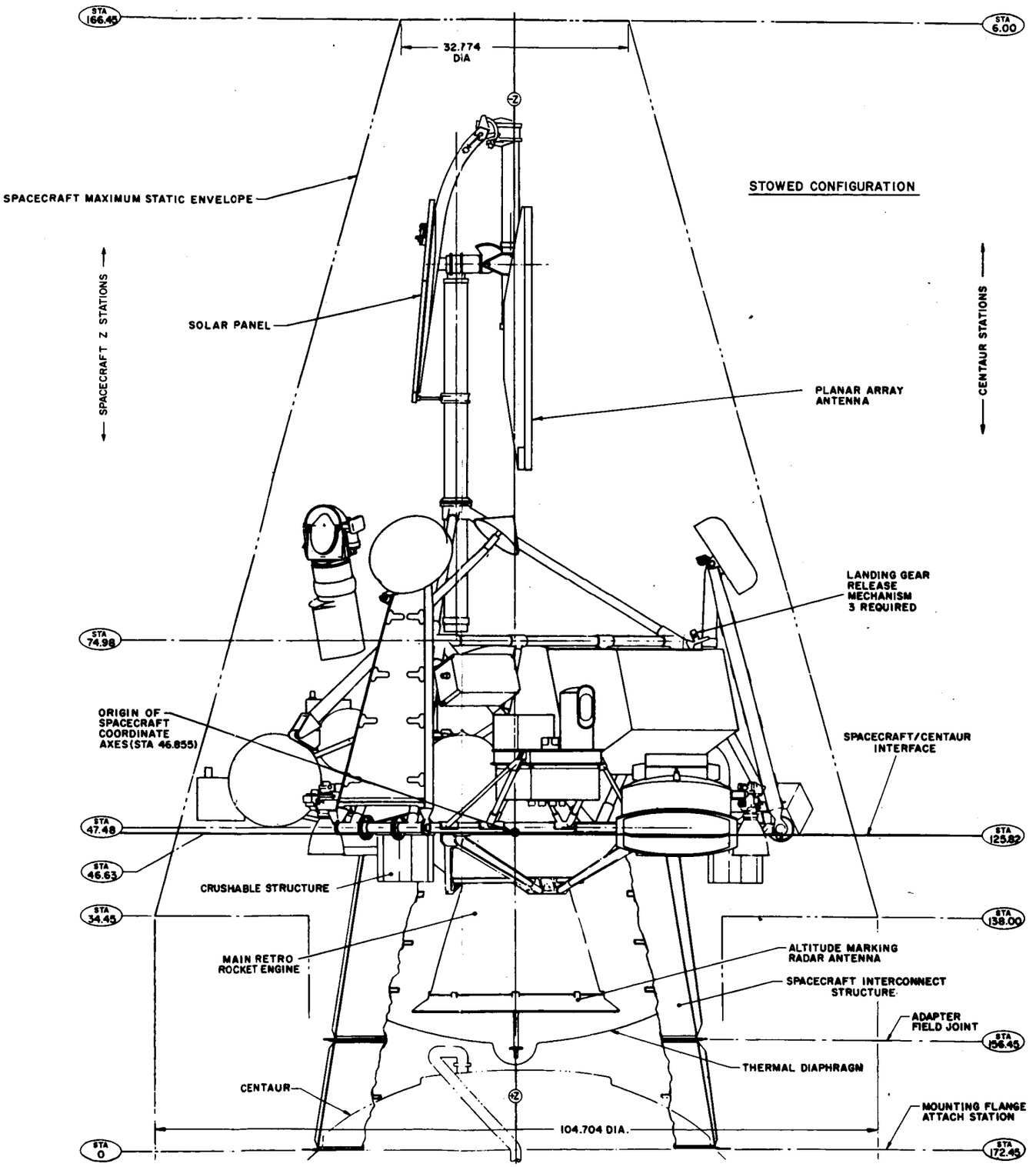
LANDING LEG No 3

ACCELEROMETER AMPLIFIER

STRAIN GAGE AMPLIFIER

ITUDE JET NOZZLE ASSY-2 REQ'D

L ANTENNA B



2-7-4

3

PRECEDING PAGESBLANK NOT FILMED.

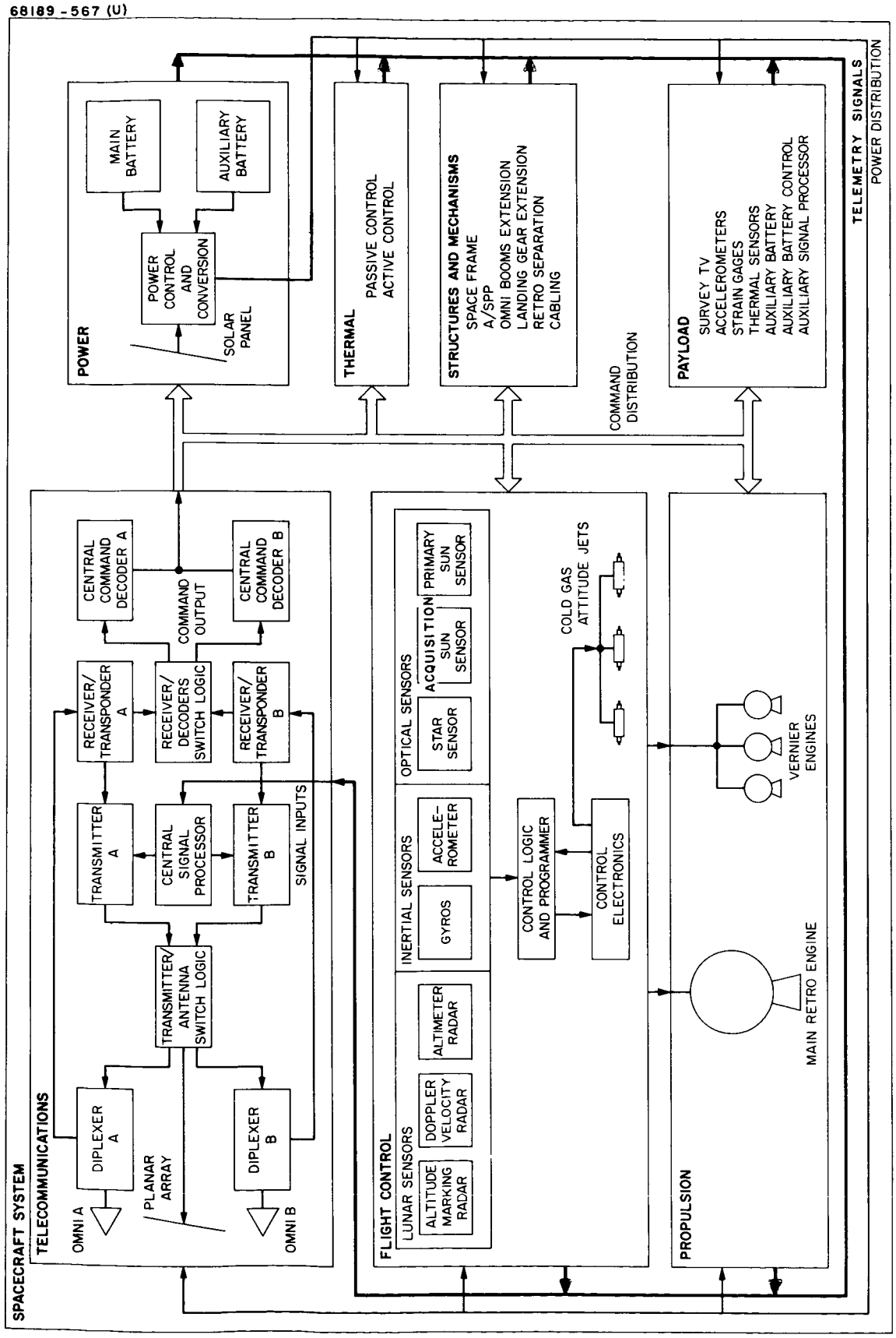


Figure 2-4. Simplified Spacecraft Functional Block Diagram

basic spaceframe, landing gear, crushable blocks, secondary sun sensor, omnidirectional antenna mechanisms, antenna/solar panel positioner, pyrotechnic devices, electrical cabling, thermal compartments, and separation sensing and arming devices.

The spaceframe is the basic structure of the spacecraft and provides a rigid mount for all components of the spacecraft and mounting surfaces and attachments for connecting to Centaur. The tripodic landing gear and crushable blocks stabilize the spacecraft and absorb impact energy during touchdown. The secondary sun sensor located on the solar panel is used as a backup for the sun acquisition sensor, and in postlunar operations assists in determining spacecraft orientation and aids in positioning the solar panel. The omnidirectional antenna mechanisms provide for omnidirectional antenna deployment. The antenna/solar panel positioner supports and positions (around four independent axes) the planar array antenna and solar panel. The pyrotechnic devices mechanically release or lock mechanisms, switches, and valves. The electrical cabling interconnect the spacecraft subsystems and components. The thermal compartments provide thermal control for temperature sensitive components. The separation sensing and arming devices ensure that certain critical squib firing circuits will remain disabled until after Centaur separation.

2.2.1.2 Electrical Power

The electrical power subsystem generates, stores, converts, and controls electrical power for distribution to the spacecraft subsystems. Most of the power required by the spacecraft is supplied by the solar panel which converts solar energy into electrical power. Excess electrical power from the solar panel is stored in the main rechargeable battery and is delivered during peak periods of demand when the solar panel output cannot meet such demands by itself. Thus, the main battery augments the solar panel during peak power periods. An auxiliary nonrechargeable battery provides a backup power source for the main battery and solar panel. The electrical power subsystem also contains an engineering mechanisms auxiliary that provides a constant current source for the operation of pyrotechnic devices.

2.2.1.3 Telecommunications

The telecommunications subsystem provides command reception, decoding, signal processing, and radio frequency transmission. The telecommunications subsystem consists of the following:

1) Radio frequency group

2) Command decoding group

3) Signal processing group

The radio frequency (data link) group which provides redundant two-way communication between the spacecraft and the DSIF consists of two transmitters, two receivers, two omnidirectional antennas, and a high gain

planar array antenna. The signal processing group processes spacecraft data for telemetry to the DSIF. The command decoding group accepts commands from the spacecraft receivers, generates sync and timing signals from each command, checks each command for correct address and command complements, and provides output signals to command the addressed spacecraft subsystems.

2.2.1.4 Flight Control

The flight control subsystem provides spacecraft velocity and attitude control during transit and terminal descent. The flight control subsystem consists of the following:

1) Flight control sensor group (FCSG)

2) Attitude jets

3) Attitude jet supply

4) Roll actuator

5) Altitude marking radar (AMR)

6) Radar altimeter/doppler velocity sensor (RADVS)

The FCSG contains inertial (gyro), optical (Canopus sensor, acquisition sun sensor, primary sun sensor) sensors, accelerometers, and flight control electronics. The sensors generate signals to the attitude jets and/or the vernier engines (including the roll actuator) for attitude control of the spacecraft for sun and Canopus acquisition, midcourse maneuver, transit, and terminal descent.

Three pairs of attitude jets provide attitude control during coast phases. The attitude jet supply contains cold nitrogen gas under pressure for the attitude jets. The roll actuator aligns vernier engine 1 for roll control during vernier engine firing periods. The AMR provides a marking signal at a nominal slant range of 60 miles from the moon to initiate the main retro engine ignition sequence. The RADVS provides range and velocity information for velocity and attitude control during terminal descent.

2.2.1.5 Propulsion

The propulsion subsystem provides thrust during the midcourse correction maneuvers and terminal descent. The propulsion subsystem consists of the main retro rocket engine and the vernier propulsion subsystem. The main retro engine is a spherical solid propellant engine that provides the bulk of the spacecraft deceleration during terminal descent.

The vernier propulsion subsystem consists of three thrust chambers, six propellant tanks, and a helium tank and valve assembly. The vernier propulsion subsystem provides thrust for the midcourse correction, for

attitude control during retro descent, and for deceleration after the main retro burnout. Thrust chamber 1 can be swiveled to provide a thrust vector about the roll axis. Thrust chambers 2 and 3 are stationary and provide thrust parallel to the roll axis for pitch and yaw control. The three thrust chambers are differentially throttled to provide attitude control in pitch and yaw.

2.2.1.6 Approach Television

The approach television group (part of the television subsystem) consists of an approach television camera and television auxiliary (shared with the survey television group) to provide pictures of the lunar landing site during terminal descent. This equipment was carried but not used on the SC-1 mission.

2.2.1.7 Engineering Instrumentation

Engineering instrumentation strategically placed on the basic bus and engineering payload provides data on the performance of the spacecraft and its response to the environment. The engineering instrumentation consists of the following:

1) Resistance thermal sensors
2) Mechanical switches
3) Current shunts
4) Position potentiometers
5) Pressure sensor potentiometers
6) Accelerometers (with one accelerometer amplifier)
7) Spin motor running detectors
8) Microdiode thermal sensor
9) Strain gages

For telemetry configuration see Table 2-1.

2.2.2 Engineering Payload

The engineering payload consists of the following:

1) Survey television camera (with two TV photometric charts)
2) Television auxiliary (shared with the approach television group)

TABLE 2-1. SURVEYOR SC-1 TELEMETRY ASSIGNMENTS

DATA LINK

CHAN	NAME	DIGITAL	MODE 1 WORDS	MODE 2 WORDS	MODE 3 WORDS	MODE 4 WORDS	MODE C (5) WORDS	MODE T (6) WORDS	SCO FREQ
D-1	OMNI A TRANSMITTED POWER					1	87		
D-2	TRANSMITTER A FILAMENT ON	6,10(5)							
D-3	OMNI B TRANSMITTED POWER					11	117		
D-4	TRANSMITTER B FILAMENT ON	6,10(6)							
D-5	TRANSPONDER A PHASE LOCKED	6,10(3)							
D-6	TRANSPONDER B PHASE LOCKED	6,10(4)							
D-7	STATIC PHASE ERROR A					3,23,43,63,83	17		
D-8	STATIC PHASE ERROR B					13,33,53,73,93	27		
D-9	RECEIVER A AGC					5,25,45,65,85	3		
D-10	RECEIVER B AGC					15,35,55,75,95	33		
D-11	MESSAGE REJECT	5,6,10,12(2)							2.3KC
D-12	CENTRAL DECODER A ON	6,10(8)							
D-13	TRANSMITTER A TEMP.					2	10	10	
D-14	TRANSMITTER B TEMP.					12	30	30	
D-15	MESSAGE ENABLE	5,6,10,12(1)							2.3KC
D-16	RECEIVER A AFC					7	37		
D-17	RECEIVER B AFC					17	41		
D-18	CENTRAL DECODER B ON	6, 10(7)							

ELECTRICAL POWER

CHAN	NAME	DIGITAL	MODE 1 WORDS	MODE 2 WORDS	MODE 3 WORDS	MODE 4 WORDS	MODE C (5) WORDS	MODE T (6) WORDS	
EP-1	29-VOLT NON-ESSENTIAL VOLTAGE					27	39	39	
EP-2	UNREGULATED BUS VOLTAGE		66	86		86	69	69	
EP-3	MAIN BATTERY MANIFOLD PRESSURE					81	63		
EP-4	UNREGULATED OUTPUT CURRENT		22	22		22	9	9	
EP-5	MAIN BATTERY VOLTAGE			66		66	79	79	
EP-6	BATTERY CHARGE CURRENT		32	32		32	15		
EP-7	BOOST REG. DIFFERENCE CURRENT			69		69	19	19	
EP-8	MAIN BATTERY TEMP.					4	42		
EP-9	BATTERY DISCHARGE CURRENT		72	72		72	29	29	
EP-10	SOLAR CELL ARRAY VOLTAGE					47	67		
EP-11	SOLAR CELL ARRAY CURRENT		59	59		59	23		
EP-12	SOLAR CELL ARRAY TEMP.					8	36		
EP-13	BOOST REGULATOR TEMP.					10	30	20	
EP-14	REGULATED OUTPUT CURRENT		42	42		42	39	39	
EP-15	SPARE								
EP-16	OPTIMUM CHARGE REG. OUTPUT CURRENT		79	79		79	35		
EP-17	RADVS AND SQUIB CURRENT			89		89	49	49	
EP-18	FULL SCALE CURRENT CALIB. (ESP)		92	92		92			
EP-19	MID-SCALE CURRENT CALIB. (ESP)		39	39		39			
EP-20	ZERO SCALE CURRENT CALIB. (ESP)		19	19		19			
EP-21	COMPARTMENT A HEATER CURRENT					9	45		
EP-22	COMPARTMENT B HEATER CURRENT					29			
EP-23	AUXILIARY BATTERY VOLTAGE					57	16	88	
EP-24	SOLAR CELL STRING 4 CURRENT					49	53		
EP-25	SOLAR CELL STRING 6 CURRENT						65		
EP-26	AUXILIARY BATTERY TEMP.			78			96		
EP-27	FULL SCALE CURRENT CALIB. (AESP)						75		
EP-28	MID-SCALE CURRENT CALIB. (AESP)						85		
EP-29	ZERO SCALE CURRENT CALIB. (AESP)						95		
EP-30	BOOST REG. PRIMER. VOLTAGE		64	21		21	93		
EP-31	AUXILIARY BATTERY MODE ON	7,11(5)							
EP-32	HIGH CURRENT MODE OFF	7,11(6)							
EP-33	BMA RADVS PYRO SWITCHES	7,11(8)							
EP-34	BATTERY CHARGE REG. TEMP.					78	46		

FLIGHT CONTROL

CHAN	NAME	DIGITAL	MODE 1 WORDS	MODE 2 WORDS	MODE 3 WORDS	MODE 4 WORDS	MODE C (5) WORDS	MODE T (6) WORDS	SCO FREQ
FC-1	ROLL GYRO SPEED								5.4KC
FC-2	PITCH GYRO SPEED								5.4KC
FC-3	YAW GYRO SPEED								5.4KC
FC-4	NITROGEN GAS PRESSURE		20	30			89	89	
FC-5	PRIMARY SUN SENSOR PITCH ERROR		1,21,41,61,81				71		
FC-6	PRIMARY SUN SENSOR YAW ERROR		3,23,43,63,83				77		
FC-7	SECONDARY SUN SENSOR CELL A		10,60	27			99		
FC-8	SECONDARY SUN SENSOR CELL B		20,70	35			101		
FC-9	SECONDARY SUN SENSOR CELL C		28,78	47			105		
FC-10	SECONDARY SUN SENSOR CELL D		38,88	55			107		
FC-11	SPARE								
FC-12	CANOPUS ERROR		7,27,47,67,87				109		
FC-13	CANOPUS LOCK-ON	10(6)							
FC-14	STAR INTENSITY SIGNAL		9,29,49,69,89				113		
FC-15	ACCELERATION ERROR		11,31,51,71,91	11	11			6,36,66,96	
FC-16	PITCH GYRO ERROR		13,33,53,73,93	13,73	13		1	1,31,61,91	
FC-17	YAW GYRO ERROR		17,37,57,77,97	17,77	17		3	3,33,63,93	
FC-18	MAGNITUDE REGISTER READOUT	2							
FC-19	PROGRAMMER ROLL SIGNAL	3(1)							
FC-20	SPARE								
FC-21	PROGRAMMER PITCH SIGNAL	3(3)							
FC-22	SPARE								
FC-23	PROGRAMMER YAW SIGNAL	3(5)							
FC-24	SPARE								
FC-25	THRUST CMD TO VERNIER ENGINE 1		18,68	9, 18	9,18,19,29,39			8,38,68,98	
FC-26	THRUST CMD TO VERNIER ENGINE 2		12,62	1, 12,	1,12,21,31,41			15,45,75,105	
FC-27	THRUST CMD TO VERNIER ENGINE 3		8,38	2, 8	2, 8, 22, 32, 42			36,46,76,106	
FC-28	VERNIER IGNITION SIGNAL	3(10), 4(1)							
FC-29	RETRO IGNITION SIGNAL	4(6)							
FC-30	RETRO BURNOUT SIGNAL	4(5)							
FC-31	RETRO EJECT SIGNAL	4(6)							
FC-32	RETRO ACCELEROMETER			7,57	24			17,47,77,107	
FC-33	RELIABLE OPERATION - RADAR ALTIMETER	9(9)							
FC-34	RELIABLE OPERATION - DOPPLER RADAR	9(10)							
FC-35	RADAR ALTIMETER RANGE SIGNAL			49, 74	44			28,48,78,108	
FC-36	TEN FEET PER SECOND MARK	4(9)							
FC-37	ONE THOUSAND FOOT MARK	4(8)							
FC-38	THIRTEEN FOOT MARK	4(10)							
FC-39	DOPPLER VELOCITY V_x			51,63	38			24,54,84,114	
FC-40	DOPPLER VELOCITY V_y			43, 52	34			25,55,85,115	
FC-41	DOPPLER VELOCITY V_z			3,53	3,23,33,43			26,56,86,116	
FC-42	START VERNIER ENGINE THRUST	4(7)							
FC-43	ROLL ACTUATOR SIGNAL		48,98	48,91	7,27,37,47,48			27,34,47,67,117	
FC-44	FLIGHT CONTROL E/U TEMP. 1					94			
FC-45	FLIGHT CONTROL E/U TEMP. 2		24				40	40	
FC-46	ROLL GYRO TEMP.			60			64		
FC-47	CANOPUS SENSOR TEMP.		44				69		
FC-48	NITROGEN GAS TANK TEMP.					18	92		
FC-49	ROLL PRECESSION COMMAND		14,34,54,74,94	14	14		3	5,35,65,95	
FC-50	PITCH PRECESSION COMMAND			75			7	7,37,67,97	
FC-51	YAW PRECESSION COMMAND			17			11	11,41,71,101	
FC-52	NOMINAL ENGINE THRUST BIAS	9(8)							
FC-53	SECONDARY SUN SENSOR CENTER CELL			29					
FC-54	PITCH GYRO TEMP.			20			110	110	
FC-55	YAW GYRO TEMP.			80			98		
FC-56	MANUAL DELAY MODE ON	3(2)							
FC-57	GAS JET AMPLIFIERS INHIBITED	1(8)							
FC-58	BATE MODE ON	9(1)							
FC-59	SUN MODE ON	9(2)							
FC-60	STAR MODE ON	9(3)							
FC-61	CRUISE MODE ON	9(4)							
FC-62	RETRO SEQUENCE MODE ON	6(1)							
FC-63	INERTIA SWITCH SIGNAL	9(5)							
FC-64	ALTITUDE MARKING RADAR SIGNAL	4(2)							
FC-65	MIDCOURSE VELOCITY CORRECTION SIGNAL	3(9)							
FC-66	THRUST PHASE POWER ON	3(4)							
FC-67	PROGRAMMER POS. ANGLE MANEUVER SIGNAL	1(7)							
FC-68	SPARE								
FC-69	PRIMARY SUN SENSOR CENTER CELL LOCK-ON	10(5)							
FC-70	ATTITUDE GAS JET 2 TEMP.						102		
FC-71	ROLL ACTUATOR TEMP.						104		
FC-72	SPARE								
FC-73	MANUAL LOCK-ON (SUN OR STAR)	9(1)							
FC-74	PITCH GYRO HEATER CONTROLLER ON	1(9)							
FC-75	ROLL GYRO HEATER CONTROLLER ON	10(9)							
FC-76	ACQUISITION SUN SENSOR ILLUMINATED	1(7)							

MECHANISMS

CHAN	NAME	DIGITAL	MODE 1 WORDS	MODE 2 WORDS	MODE 3 WORDS	MODE 4 WORDS	MODE C (5) WORDS	MODE T (6) WORDS	
M-1	OMNI ANTENNA A EXTENDED	7,11(9)							
M-2	OMNI ANTENNA B EXTENDED	7,11(10)							
M-3	SOLAR PANEL POSITION					71	57		
M-4	POLAR AXIS POSITION			98		98	61		
M-5	SPARE								
M-6	ELEVATION AXIS POSITION					77			
M-7	ROLL AXIS POSITION					87	91		
M-8	PLANAR ARRAY TEMP.					14	38		
M-9	VEHICLE SEPARATION	1(4)							
M-10	SOLAR PANEL STEPPING MOTOR TEMP.					58	64		
M-11	SOLAR PANEL LOCKED IN TRANSIT POSITION	7,11(3)							
M-12	ELEVATION AXIS STEPPING MOTOR TEMP.					64			
M-13	ROLL AXIS LOCKED IN TRANSIT POSITION	7,11(4)							
M-14	SOLAR PANEL LAUNCH LOCK UNLOCKED	7,11(2)							
M-15	SOLAR PANEL DEPLOYMENT LOGIC ON	7,11(7)							

PROPULSION

CHAN	NAME	DIGITAL	MODE 1 WORDS	MODE 2 WORDS	MODE 3 WORDS	MODE 4 WORDS	MODE C (5) WORDS	MODE T (6) WORDS	
P-1	HELIUM PRESSURE		86	25			21	21	
P-2	OXIDIZER PRESSURE 3		88	41			51	51	
P-3	UPPER RETRO CASE TEMP.			68					
P-4	VERNIER LINES 2 TEMP.		2				6		
P-5	VERNIER FUEL TANK 2 TEMP.			66					
P-6	VERNIER OXIDIZER TANK 3 TEMP.			86			56		
P-7	VERNIER ENGINE 1 TEMP.			34			70	70	
P-8	VERNIER LINES 1 TEMP.		32				88		
P-9	VERNIER LINES 3 TEMP.		82				84		
P-10	VERNIER ENGINE 2 TEMP.			34			30	30	
P-11	VERNIER ENGINE 3 TEMP.			44			60	60	
P-12	LOWER RETRO CASE TEMP.			88			28		
P-13	VERNIER FUEL TANK 1 TEMP.			56			4		
P-14	VERNIER FUEL TANK 3 TEMP.			76			54		
P-15	VERNIER OXIDIZER TANK 1 TEMP.			82			92		
P-16	VERNIER OXIDIZER TANK 2 TEMP.			84			2		
P-17	HELIUM TANK TEMP.					20	86		
P-18	VERNIER ENGINE 1 STRAIN GAGE		15,35,55,75,95	15				4,44	
P-19	VERNIER ENGINE 2 STRAIN GAGE		16,36,56,76,96	37				14,74	
P-20	VERNIER ENGINE 3 STRAIN GAGE		98	90				28,88	
P-21	SPARE								
P-22	RETRO NOZZLE TEMP.		80				100	100	

RADAR

CHAN	NAME	DIGITAL	MODE 1 WORDS	MODE 2 WORDS	MODE 3 WORDS	MODE 4 WORDS	MODE C (5) WORDS	MODE T (6) WORDS	
R-1	ALTITUDE MARKING RADAR ON	5,12(7)							
R-2	RADVS-A AMPLITUDE			26	26			43	
R-3	RADVS-D_1 AMPLITUDE			28	28			44	
R-4	RADVS-D_2 AMPLITUDE			36	36			56	
R-5	RADVS-D_3 AMPLITUDE			46	46			94	
R-6	AMR ANTENNA TEMP. NO. 1			54					
R-7	AMR ELECTRONICS TEMP.			64			26		
R-8	ALTIMETER & DOPPLER KLYSTRON UNIT TEMP.			38			18		
R-9	RADAR SIGNAL DATA CONVERTER TEMP.			62			22		
R-10	DOPPLER RADAR SENSOR TEMP.			94			76		
R-11	AMR ENABLED	5,12(8)							
R-12	AMR POWER OUTPUT (IMAG. CURRENT)			23				99	
R-13	ALTIMETER RADAR SENSOR TEMP.			96			24		
R-14	ALTITUDE MARKING RADAR AGC			33				104	
R-15	RADVS - D_1 TRACKER LC CK	8,13(1)							
R-16	RADVS - D_2 TRACKER LOCK	8,13(10)							
R-17	RADVS - D_3 TRACKER LOCK	5,12(2)							
R-18	RADVS - R TRACKER LOCK	5,12(6)							
R-19	RADVS - D_1 GAIN 1	8,13(2)							
R-20	RADVS - D_1 GAIN 2	8,13(3)							
R-21	RADVS - D_2 GAIN 1	8,13(4)							
R-22	RADVS - D_2 GAIN 2	8,13(5)							
R-23	RADVS - D_3 GAIN 1	8,13(6)							
R-24	RADVS - D_3 GAIN 2	8,13(7)							
R-25	RADVS - R GAIN 1	8,13(8)							
R-26	RADVS - R GAIN 2	8,13(9)							
R-27	AMR ANTENNA TEMP. NO. 2		26				80	80	
R-28	RADVS ON SIGNAL	3(6)							
R-29	AMR LATE GATE SIGNAL			71					

SIGNAL PROCESSING

CHAN	NAME	DIGITAL	MODE 1 WORDS	MODE 2 WORDS	MODE 3 WORDS	MODE 4 WORDS	MODE C (5) WORDS	MODE T (6) WORDS	
S-1	REFERENCE VOLTAGE			67		67			
S-2	REFERENCE RETURN			97		97			
S-3	COMMUTATOR SELECT F/F R500 (ESP MODE 2 OR B)	5,6(10)							
S-4	COMMUTATOR SELECT F/F R501 (ESP MODE 3 OR A)	5,6(9)							
S-5	COMMUTATOR UNBALANCE CURRENT (ESP)			31		31			
S-6	COMMUTATOR SELECT F/F R100 (AESP MODE C)	10(10)							
S-7	COMMUTATOR UNBALANCE CURRENT (AESP)						47		

SURVEY TV CAMERA NO. 3

CHAN	NAME	DIGITAL	MODE 1 WORDS	MODE 2 WORDS	MODE 3 WORDS	MODE 4 WORDS	MODE C (5) WORDS	MODE T (6) WORDS	TV
TV-1	CAMERA NUMBER								2
TV-2	MIRROR AZIMUTH								3,11
TV-3	MIRROR ELEVATION								7
TV-4	LENS FOCAL LENGTH SETTING								12
TV-5	LENS FOCUS SETTING								5
TV-6	LENS IRIS SETTING								13
TV-7	LENS IRIS SERVO ON								15
TV-8	FILTER WHEEL POSITION								10
TV-9	VIDICON FACEPLATE TEMP.								8
TV-10	CAMERA ELECTRONICS TEMP.								4
TV-11	SHUTTER MODE (OPEN OR NORMAL)								9
TV-12	CALIBRATE VOLTAGE								6,14
TV-13	MULTIPLE STEP FOCUS ON								16
TV-14	COMPOSITE VIDEO								CARR
TV-15	SPARE								
TV-16	SURVEY CAMERA 3 ELECTRONICS TEMP.					16			
TV-17	SURVEY CAMERA 3 MIRROR ASSEMBLY TEMP.						116		

APPROACH TV CAMERA NO. 4

CHAN	NAME	DIGITAL	MODE 1 WORDS	MODE 2 WORDS	MODE 3 WORDS	MODE 4 WORDS	MODE C (5) WORDS	MODE T (6) WORDS	TV
T-1	APPROACH VIDICON 4 FACEPLATE TEMP.			10			97		
T-2	APPROACH VIDICON 4 THERMAL CONTROL ON	7,11(1)							
T-3	APPROACH CAMERA 4 ELECTRONICS TEMP.			70			16		
T-4	APPROACH CAMERA 4 POWER ON	5,12(4)							
T-5	VIDEO								CARR

VEHICLE

CHAN	NAME	DIGITAL	MODE 1 WORDS	MODE 2 WORDS	MODE 3 WORDS	MODE 4 WORDS	MODE C (5) WORDS	MODE T (6) WORDS	SCO FREQ
V-1	LANDING GEAR 1 EXTENDED	1(1)							
V-2	LANDING GEAR 2 EXTENDED	1(2)							
V-3	LANDING GEAR 3 EXTENDED	1(3)							
V-4	RETRO NOT EJECTED	5,12(5)							
V-5	LANDING GEAR 1 DEFLECTION			93					
V-6	LANDING GEAR 2 DEFLECTION			95					
V-7	LANDING GEAR 3 DEFLECTION			83					
V-8	VEH. ACCELEROMETER 1, COLUMN BASE LEG 1								52.5KC
V-9	VEH. ACCELEROMETER 2, COLUMN BASE LEG 2								70KC
V-10	VEH. ACCELEROMETER 3, COLUMN BASE LEG 3								90KC
V-11	VEH. ACCELEROMETER 4, FCSG								110KC
V-12	SHOCK ABSORBER 1 STRAIN GAGE								1.7KC
V-13	SHOCK ABSORBER 2 STRAIN GAGE								2.0KC
V-14	SHOCK ABSORBER 3 STRAIN GAGE								5.4KC
V-15	COMPART. A TEMP.-THERMAL TRAY TOP					24	66		
V-16	COMPART. A TEMP.-LOWER SUPPORT					26	78		
V-17	COMPART. A TEMP.-INSULATED RETAINER					28			
V-18	COMPART. A TEMP.-CANISTER					30	64		
V-19	COMPART. A TEMP SW 3 IN CONTACT RING					34			
V-20	COMPART. A TEMP SW 5 IN FACE RADIATOR					36	32		
V-21	COMPART. B TEMP.-TRAY TOP CENTER					44	58		
V-22	COMPART. B TEMP.-LOWER SUPPORT					46	74		
V-23	COMPART. B TEMP.-CANISTER					48			
V-24	COMPART. B TEMP SW 4 IN FACE RADIATOR					52	34		
V-25	COMPART. A TEMP SW 8 IN FACE RADIATOR					38	94		
V-26	COMPART. B TEMP SW 4 IN CONTACT RING					54			
V-27	UPPER SPACEFRAME TEMP., NO. 1					56	12		
V-28	LOWER SPACEFRAME TEMP., UNDER COMPART B					62	14		
V-29	WIRING HARNESS TEMP.-THERMAL TUNNEL					66	62		
V-30	SHOCK ABSORBER 1 TEMP.					68			
V-31	LEG 2 UPPER WEB TEMP.						52		
V-32	SHOCK ABSORBER 2 TEMP.				38		8		
V-33	SHOCK ABSORBER 3 TEMP.					76			
V-34	ASPP TEMP.					82			
V-35	UPPER SPACEFRAME TEMP., NO. 2					74			
V-36	LOWER SPACEFRAME TEMP., UNDER COMPART A					96			
V-37	RETRO ATTACH POINT 1 TEMP.					84			
V-38	RETRO ATTACH POINT 2 TEMP.					86	72		
V-39	RETRO ATTACH POINT 3 TEMP.					88			
V-40	VEH. ACCELEROMETER 5, ASPP								130KC
V-41	VEH. ACCELEROMETER 6, VEL. SENSING ANT.								130KC
V-42	VEH. ACCELEROMETER 7, COMPART. A								150KC
V-43	VEH. ACCELEROMETER 8, COMPART. B								150KC
V-44	CRUSHABLE BLOCK TEMP.		46				90	90	
V-45	COMPART B TEMP SW 1 IN FACE RADIATOR						108		
V-46	COMPART B TEMP SW 5 IN FACE RADIATOR						112		
V-47	COMPART. A TEMP SW 2 IN FACE RADIATOR						114		
V-48	AUXILIARY BATTERY COMPART TEMP.						106		

COMMUTATOR WORDS

DIGITAL WORD	MODE 1	MODE 2	MODE 3	MODE 4	MODE C (5)	MODE T (6)
1	40	40	---	40	23	23
2	50	50	---	50	53	53
3	5, 25, 45, 65, 85	65	---	---	13, 43, 73, 103	13
4	---	5, 45, 85	5, 10, 15 20, 25, 30, 35, 40, 45	---	---	7, 12, 22, 32, 42, 52, 62, 72, 82, 92, 102, 112
5	---	6	6	---	---	---
6	6	---	---	6	---	---
7	---	---	---	30	---	---
8	---	16	16	---	---	---
9	4	4	4	---	83	83
10	---	---	---	---	111	111
11	---	---	---	---	113	113
12	---	---	---	---	---	73
13	---	---	---	---	---	103

3) Auxiliary engineering signal processor

4) Auxiliary battery and battery control

The survey television which provides pictures of the lunar surface, portions of the spacecraft, and free space is used during lunar operations. The auxiliary engineering signal processor provides a redundant mode of processing engineering data for telemetry to the DSIF. The auxiliary battery and battery control provide a backup nonchargable battery to increase the probability of a successful transit and landing mission.

2.3 FLIGHT CONFIGURATION

The spacecraft, at launch, was made up of the control items listed in Table 2-2. Also shown in this table is the alpha-numeric designator for each telemetry channel that is contained or originates in that control item. For the identification of these alpha-numeric designators, see Table 2-1.

TABLE 2-2. SC-1 FLIGHT CONFIGURATION AND TELEMETRY SOURCES

Control Item Name	Control Item	Serial Number	Associated Analog Telemetry Signals	Associated Digital Telemetry Signals
Transmitter A	263220-4	14	D-1, D-13	D-2
Transmitter B	263220-4	20	D-3, D-14	D-4
Command receiver and transponder A	231900-3	13	D-7, D-9, D-16	
Command receiver and transponder B	231900-3	14	D-8, D-10, D-17	D-6
Receiver buffer A	290780		D-7	
Receiver buffer B	290780		D-8	
Battery charge regulator	274100-3	11	EP-2, EP-10, EP-11, EP-16 EP-34	
Main battery	237900	49	EP-3, EP-8	
Boost regulator	274200-96	12	EP-1, EP-7, EP-13, EP-14 EP-30	
Fixed wire wound meter shunt resistor – unregulated output	988645-3	778012	EP-4	
Auxiliary battery control unit	273000-2	15	EP-5, EP-23	EP-31
Fixed wire wound meter shunt resistor – battery current	988645-2	778004	EP-6, EP-9	
Fixed wire wound meter shunt resistor – RADVS	988647-1	2	EP-17	
Thermal control and heater assembly – compartment A	232210-1	20	EP-21	

Table 2-2 (continued)

Control Item Name	Control Item	Serial Number	Associated Analog Telemetry Signals	Associated Digital Telemetry Signals
Thermal control and heater assembly – compartment B	232210-2	14	EP-22	
Auxiliary battery	237921	44	EP-26	
Solar panel	237760-3	1	EP-12, EP-24; FC-7, FC-8 FC-9, FC-10, FC-53	
Engineering signal processor	233350-7	2	EP-18, EP-19, EP-20; S-1, S-2, S-5; V-8, V-9, V-10, V-11	
Auxiliary engineering signal processor	264900-3	1	EP-27, EP-28, EP-29; S-7; V-12, V-13, V-14, V-40, V-41, V-42, V-43	
Flight control sensor group	235000-8	2	FC-5, FC-6, FC-12, FC-14, FC-15, FC-16, FC-17, FC-25, FC-26, FC-27, FC-32, FC-35, FC-39, FC-40, FC-41, FC-43, FC-44, FC-45, FC-46, FC-47, FC-49, FC-50, FC-51, FC-54, FC-55	FC-13, FC-18, FC-19, FC-21, FC-23, FC-28, FC-29, FC-31, FC-33, FC-36, FC-37, FC-38, FC-42, FC-52, FC-56, FC-58, FC-59, FC-60, FC-61, FC-62, FC-63, FC-64, FC-65, FC-66, FC-67, FC-69, FC-72, FC-73, FC-74, FC-75, FC-76
Attitude jet 2	235700-3	1	FC-70	
Attitude gas jet supply	235600-2	1	FC-4, FC-48	
Roll actuator	235900-3	2	FC-43, FC-71	M-13
RADVS signal data converter	(AM-4) 232908-2	6	FC-35, FC-39, FC-40, FC-41; R-2, R-3, R-4, R-5, R-9	R-15, R-16, R-17, R-18, R-19, R-20, R-21, R-22, R-23, R-24, R-25, R-26
Planar array antenna	232300	11	M-8	
Antenna and solar panel positioner	287550	1	M-3, M-4, M-6, M-7, M-10, M-12; V-34	M-11, M-14
Fuel tank 1	287000-2	4	P-13	
Fuel tank 2	287001-3	3	P-5	
Fuel tank 3	287000-2	3	P-14	
Oxidizer tank 1	287002-2	2	P-15	
Oxidizer tank 2	287004-2	2	P-16	
Oxidizer tank 3	287003-3	2	P-6	
Thrust chamber assembly 1	285063-1	545	P-7	
Thrust chamber assembly 2	285063-2	541	P-10	
Thrust chamber assembly 3	285063-3	539	P-11	
Spaceframe subassembly (vernier engines 1, 2, and 3 strain gages)	264178	2	P-18, P-19, P-20	
Retro rocket engine	238612	A21-26	P-3, P-12, P-22	
Strain gage amplifier assembly – leg 3	238930	1	P-18, P-19, P-20; V-12, V-13, V-14	
Helium tank and valve assembly	262789-1	4	P-1, P-17	

Table 2-2 (continued)

Control Item Name	Control Item	Serial Number	Associated Analog Telemetry Signals	Associated Digital Telemetry Signals
Transducer (oxidizer pressure No. 3)	262609	–	P-2	
Thermostat heater and temperature assembly, leg 1 (vernier lines 1 temperature)	238673-1	–	P-8	
Thermostat heater and temperature assembly, leg 2 (vernier lines 2 temperature)	262556-1	–	P-4	
Thermostat heater and temperature assembly, leg 3 (vernier lines 3 temperature)	262557-1	–	P-9	
Altitude marking radar	283827	12	R-6, R-7, R-12, R-14, R-27, R-29	R-1, R-11, R-28
Altimeter and doppler klystron unit	(AM-5) 232909	7	R-8	
Altimeter radar sensor	(AM-1) 232910	3	R-13	
Doppler radar sensor	(AM-1) 232911-1	3	R-10	
Approach television camera 4	284302	11	T-1, T-3	T-2, T-4
Survey television camera 3	284312-3	12	TV-2, TV-3, TV-4, TV-5, TV-6, TV-8, TV-9, TV-10, TV-16, TV-17	TV-1, TV-7, TV-11, TV-13
Accelerometer 1 – leg 1	239002-1	9	V-8	
Accelerometer 2 – leg 2	239002-2	10	V-9	
Accelerometer 3 – leg 3	239002-3	11	V-10	
Accelerometer 4 – FCSG	239002-4	12	V-11	
Accelerometer amplifier	239011	2	V-8, V-9, V-10, V-11, V-40, V-41, V-42, V-43	
Thermal resistor – compartment A	988653-2	–	V-15	
Thermal resistor – compartment A	988653-2	–	V-16	
Thermal resistor – compartment A	988653-2	–	V-17	
Thermal resistor – compartment A	988653-2	–	V-18	
Thermal resistor – compartment A	988654-10	–	V-19	
Thermal resistor 1 – compartment A thermal switch 5	988653-2	–	V-20	
Thermal resistor 2 – compartment A thermal switch 8	988653-2	–	V-25	
Thermal resistor – compartment B	988653-2	–	V-21	

Table 2-2 (continued)

Control Item Name	Control Item	Serial Number	Associated Analog Telemetry Signals	Associated Digital Telemetry Signals
Shock absorber – leg 1	264300-1	4	V-12, V-30	
Shock absorber – leg 2	264300-1	7	V-13, V-32	
Shock absorber – leg 3	264300-1	4	V-14, V-33	
Thermal resistor – compartment B thermal switch 1	988653-2	–	V-45	
Thermal resistor – compartment B thermal switch 5	988653-2	–	V-46	
Thermal resistor – compartment A thermal switch 2	988653-2	–	V-47	
Thermal resistor – auxiliary battery compartment	988653-2	–	V-48	
Thermal resistor – compartment B	988653-2	–	V-22	
Thermal resistor – compartment B	988653-2	–	V-23	
Thermal resistor – compartment B thermal switch 4	988653-2	–	V-24	
Thermal resistor – compartment B thermal switch 4	988654-10	–	V-26	
Thermal resistor – upper spaceframe 1	988654-2	–	V-27	
Thermal resistor – upper spaceframe 2	988654-2	–	V-35	
Thermal resistor – compartment B lower spaceframe 1	988653-2	–	V-28	
Thermal resistor – lower spaceframe	988653-2	–	V-36	
Thermal resistor – landing gear 2	988653-2	–	V-31	
Thermal resistor – retro 1	988653-2	–	V-37	
Thermal resistor – retro 2	988653-2	–	V-38	
Thermal resistor – retro 3	988653-2	–	V-39	
Thermal resistor – harness tunnel	988657-1	–	V-29	
Landing gear 1 deflection	988684-1	914	V-5	
Landing gear 2 deflection	988684-1	915	V-6	
Landing gear 3 deflection	988684-1	916	V-7	
Accelerometer 5 – antenna/ solar panel positioner mast	239002-5	13	V-40	

Table 2-2 (continued)

Control Item Name	Control Item	Serial Number	Associated Analog Telemetry Signals	Associated Digital Telemetry Signals
Accelerometer 6 – velocity sensor antenna (RADVS)	239002-6	14	V-41	
Accelerometer 7 – compartment A	239002-7	15	V-42	
Accelerometer 8 – compartment B	239002-8	24	V-43	
Antenna mechanism – omnidirectional antenna A	287300	2		M-1
Antenna mechanism – omnidirectional antenna B	273880	2		M-2
Retro rocket release mechanism	230069-1	1, 2, 3		V-4
Central command decoder	232000-5	1		D-12
Main power switch	254112	4		EP-32
Landing gear 1	261278	3		V-1
Landing gear 2	261279	2		V-2
Landing gear 3	261280	3		V-3
Central signal processor	232200-8	1		
Signal processor auxiliary	232540-1	5		
Low data rate auxiliary	264875-2	5		
Engineering mechanism auxiliary	263500-2	3		
TV auxiliary	232106-5	19		
Jet, attitude 1	235700-2			
Jet, attitude 3	235700-2			
Secondary solar sensor	235450-1	1		
Coax., engineering measurement sensors	239013-1 through -8	9, 10, 11, 12, 13, 14, 15, 24		
Antenna – omnidirectional A	232400	17		
Antenna – omnidirectional B	232400	6		
Low pass filter A	233466	9		
Low pass filter B	233466	20		
Auxiliary battery compartment	263730	–		
RF SPDT switch	283983	12		
RF transfer switch	283984	14		
Waveguide assembly (RADVS)	(AM1) 232912	3		
Separation sensing and arm devise – (3)	293000	13, 14, 15		

Table 2-2 (continued)

Control Item Name	Control Item	Serial Number	Associated Analog Telemetry Signals	Associated Digital Telemetry Signals
TV photometric chart – antenna B	231051	11		
TV photometric chart – leg 2	230992	11		
Fixed meter shunt resistor (2)	988645-1	1, 2		
Pin puller cartridge actuator – legs 1, 2, and 3	263390-3	–		
Pin puller cartridge actuator (2)	263390-1	–		
Pin puller cartridge actuator (7)	263390-2	–		
Thermal shell assembly, compartment A	263997	–		
Thermal shell assembly, compartment B	230134	–		
Thermal switch compartment A	238810 and 238810-3	5, 6, 14, 17, 52 and 19, 8, 24		
Thermal switch compartment B	238811	11, 13, 15, 34, 37, 38		
Thermal tray assembly, compartment A	264344-1	1		
Thermal tray assembly, compartment B	276935	2		
Wire harness basic bus 1	286473	4		
Wire harness basic bus 2	286398	1		
Wire harness compartment A	276951	5		
Wire harness compartment B	264094	1		
Wire harness auxiliary battery	264100	2		
Wire harness retro rocket	286390	1		
Wire harness TV 3 (survey)	276979	4		
Wire harness A/SPP	286417	4		

3.0 MISSION PERFORMANCE SUMMARY

3.1 INTRODUCTION

Following a successful prelaunch systems readiness test (SRT) and countdown, Surveyor I was launched into a near perfect lunar trajectory from pad 36A by the A/C 10 at 1441 GMT (0741 PDT) on Memorial Day, 30 May 1966. Sixty-three hours and 36 minutes later (at 0617 on 2 June GMT or 2317 on 1 June PDT), after a nearly ideal transit phase, marred only by a failure in the omnidirectional antenna A mechanism, Surveyor I landed softly on the lunar surface within a few kilometers of the prescribed landing spot and without even a momentary loss in the transmission of telemetry data from the spacecraft to the earth.

Shortly after landing, the historic first TV picture transmitted from the surface of the moon was received on the earth and displayed for the world to see via commercial TV and the Hughes "Early Bird" communication satellite. During the remaining 12 days of lunar daylight operation, over 10,000 TV pictures, requiring more than 86,000 commands, were transmitted to the earth. In addition, several other special tests were performed.

At the onset of lunar night, the spacecraft was put into a quiescent condition to minimize power drain and maximize the probability of night survival. Twenty days later, after 14 days of lunar night and 6 days of lunar daylight, the spacecraft was successfully commanded on (after trying unsuccessfully to do so for 3 days), and approximately 100 additional TV pictures were taken before contact with the spacecraft was lost upon going into the second lunar night.

3.2 TRANSIT PHASE DESCRIPTION

The transit phase of the mission proceeded in an almost text book fashion. A listing of the major milestones and when they occurred is given in Table 3-1, and a complete event history including all major and minor sequences that resulted in the 288 commands sent during transit is given in Table 3-2. A brief description of each mission phase is given below.

TABLE 3-1. SC-1 MISSION MILESTONES–TRANSIT PHASE

Event	Date	Time (To Nearest Second)	
		GMT, hr:min:sec	Time After Launch, hr:min:sec
Launch	30 May 1966	14:41:01	0
Injection	30 May 1966	14:52:30	11:29
Separation	30 May 1966	14:53:38	12:37
Automatic sun acquisition completed	30 May 1966	15:00:34	19:33
Automatic solar panel deployment completed	30 May 1966	15:03:54	22:53
Spacecraft visibility at Johannesburg begins	30 May 1966	15:04:31	23:30
Initial DSIF acquisition (two-way lock) confirmed	30 May 1966	15:08:41	27:40
First ground command sequence initiated	30 May 1966	15:20:42	39:41
Canopus verification started	30 May 1966	18:53:39	4:12:38
Canopus acquisition completed	30 May 1966	19:13:20	4:32:19
First premidcourse attitude maneuver initiated	31 May 1966	06:30:13	15:49:12
Midcourse thrust executed	31 May 1966	06:45:03	16:45:03
Sun reacquired	31 May 1966	06:54:51	16:13:51
Canopus reacquired	31 May 1966	07:00:55	16:19:54
First terminal descent attitude maneuver initiated	2 June 1966	05:36:46	62:55:45
Retro thrust direction properly positioned	2 June 1966	05:43:47	63:02:46
Altitude marking radar mark generated	2 June 1966	06:14:41	63:33:40
Vernier engine ignition	2 June 1966	06:14:48	63:33:47
Retro engine ignition	2 June 1966	06:14:49	63:33:48
Retro separation	2 June 1966	06:15:40	63:34:39
Radar control initiated	2 June 1966	06:15:42	63:34:41
Touchdown	2 June 1966	06:17:36	63:36:35

TABLE 3-2. SC-1 EVENT/TIME HISTORY—TRANSIT PHASE

Time		Command Sequence**		
Mission (Time After Launch), hr:min:sec	GMT,* hr:min:sec	Major	Minor	Event
Mission Phase: Launch to Separation				
0	14:41:01 (5/30/66)	–	–	Launch
11:56	14:52:57	–	–	"Extend landing gears" commanded by Centaur
12:06	14:53:07	–	–	"Extend omnidirectional antennas" commanded by Centaur
12:25	14:53:26	–	–	"Transmitter high voltage on" commanded by Centaur
12:32	14:53:33	–	–	Spacecraft/Centaur electrical disconnect
12:37	14:53:38	–	–	Separation
16:49	14:57:50	–	–	Sun acquisition cell illuminated (after 100.5-degree roll)
18:19	14:59:20	–	–	Solar panel locked in transit position
19:33	15:00:34	–	–	Sun lockon achieved (primary sun sensor cell illuminated after 82-degree yaw)
22:19	15:03:20	–	–	Roll axis locked in transit position
27:59	15:09:00	–	–	Initial DSIF acquisition completed (two-way lock)
Mission Phase: DSIF Acquisition Through Star Acquisition				
		0040		Initial spacecraft operations
39:58	15:20:59		0552	1) Turn off transmitter high power
			0050	2) Turn off basic bus accelerometer amplifiers and solar panel deployment logic
			0454	3) "Rock" solar panel back and forth to seat locking pin
46:56	15:27:55		0455	4) "Rock" roll axis back and forth to seat locking pin
53:14 to 1:46:56	15:34:15 to 15:56:04		0051, 0052, 0055, 0251, 0056, 0550	5) Perform interrogation of all engineering signal processor data modes at 1100 bits/sec
1:40:20 to 1:45:07	16:21:21 to 16:26:08	Nonstandard sequence for attempting to extend omnidirectional antenna A	0601 sent 6 times	Attempt to extend omnidirectional antenna A by ground command
				Star verification/acquisition
3:50:53	18:31:54	0247	0250, 0251, 0252	1) 1100 bits/sec engineering interrogation of modes 4, 2, and 1
4:01:20	18:42:21	0247	0652, 0653	2) Transmitter high power turnon prior to star verification (high voltage on at 18:44:24 GMT)

*Subtract 7 hours from GMT values to obtain Pacific Daylight Times.

**Sequence numbers are from EPD-180 except where noted.

Table 3-2 (continued)

Time		Command Sequence		
Mission (Time After Launch), hr:min:sec	GMT, hr:min:sec	Major	Minor	Event
Mission Phase: DSIF Acquisition Through Star Acquisition (cont)				
4:08:33	18:49:34	Unscheduled sequence for selecting coast mode commutator for use in star verification to obtain additional telecommunication telemetry data for possible confirmation of omnidirectional antenna A failure to extend	0550	3) Selection of coast mode commutator
4:09:43	18:50:44	0642	0654	4) Execution of positive roll (roll begun at 18:53:39 GMT)
4:32:19	19:13:20	Unscheduled sequence	Commands 0704, 0716	5) Manual star lock achieved
4:40:03	19:21:04	0044		6) Return to low-power operation
Mission Phase: Coast I				
6:13:01 to 9:10:09	20:54:02 to	0342	0354, 0054	Gyro drift check
10:57:18	01:38:19 (5/31/66)	0141	0151	Bit rate reduction from 1100 to 550 bits/sec
11:59:00 to 12:06:08	02:40:01 to 02:47:09	0447	0250, 0251, 0550	Low power engineering interrogation of modes 4 and 2
13:33:04 to 13:37:02	04:14:05 to 04:20:03	0247	0250, 0251, 0252	Engineering interrogation at 1100 bits/sec; made with low power
13:45:03 to 13:49:16	04:26:04 to 04:30:17	0341	0350, 0351, 0215	Gyro speed check and return to 550 bits/sec telemetry data
13:52:36 to 13:52:43	04:33:37 to 04:33:44	0546	0550	Return to coast mode commutator data
14:14:35	04:55:36	Nonstandard command to manually lock to star	0716	Achieve manual lockon to Canopus to null out star error signal prior to midcourse execution
Mission Phase: Midcourse Correction				
				Midcourse correction sequence
15:20:14 to 15:25:45	06:01:15 to 06:06:46	0247	0250, 0251, 0252	1) Engineering interrogation of modes 4, 2, and 1 at 1100 bits/sec conducted with transmitter low power
15:25:45	06:06:46	0247	0652, 0653	2) Turnon of high power transmitter (high voltage on at 06:08:25 GMT)
15:29:22	06:10:23	0440	0253	3) Increase telemetry rate from 550 to 4400 bits/sec
15:38:07	06:19:08	0740	0750	4) Pressurize vernier system (helium)
15:39:22	06:20:23	1140	1150	5) Command desired roll maneuver magnitude and direction (minus roll – 86.5 degrees)

Table 3-2 (continued)

Time		Command Sequence		
Mission (Time After Launch), hr:min:sec	GMT, hr:min:sec	Major	Minor	Event
Mission Phase: Midcourse Correction (cont)				
15:49:12	06:30:13	1140	1251	6) Execute roll
15:53:13	06:34:14	1141	1151	7) Command desired yaw maneuver magnitude and direction (minus yaw – 57.99 degrees)
15:53:47	06:34:48	1141	1253	8) Execute yaw
15:57:03	06:38:05	0741	0751	9) Propulsion strain gage powered
15:58:06	06:39:07	0741	0157	10) Unlock engine 1 to permit roll control
16:02:04	06:43:05	0741	0752	11) Thrust phase power on
16:02:41	06:43:42	0741	0753	12) Command desired thrust duration (20.8 seconds)
16:04:02	06:45:03	0742	0754	13) Execute midcourse thrust
16:04:25	06:45:26		0737	14) Turn off thrust phase power
16:05:21	06:46:22		0754	15) Turn off propulsion strain gage power
16:08:01 to 16:09:36	06:49:02 to 06:50:37	Unscheduled sequence to obtain coast phase commutator data at 550 bits/sec during reverse maneuvers	0503, 0204, 0220, 0215, 0232, 0506	16) Operations to obtain coast mode data at 550 bits/sec (for obtaining receiver A AGC data, in an attempt to verify condition of omnidirectional antenna A)
16:10:45	06:51:46	1240	1252	17) Command reverse yaw maneuver magnitude and direction (plus 57.99 degrees)
16:11:54	06:52:55	1240	1253	18) Execute yaw (sun reacquired at 06:54:51 GMT)
16:16:03	06:57:04	1244	1250	19) Command reverse roll maneuver magnitude and direction (plus 86.5 degrees)
16:47:01	06:58:02	1244	1251	20) Execute roll (Canopus "reacquired" at approximately 07:00:55 GMT)
16:23:29 to 16:30:52	07:04:30 to 07:11:53	1245	0051	21) Postmidcourse engineering interrogation of modes 1, 2, and 4
16:31:42	07:12:43	0547	0552	22) Return to transmitter low-power operation
16:45:38	07:26:39	Unscheduled sequence to ensure turn off auxiliary accelerometer amplifier and touchdown strain gage power	0512, 0516	23) Sequence to turn off auxiliary accelerometer amplifier and touchdown strain gage power (if they were inadvertently turned on when propulsion strain gage power on was commanded)
Mission Phase: Coast Phase II				
17:51:01	08:32:02	0447	0250, 0251, 0550	Low power interrogation of modes 4 and 2 to obtain thermal data
18:49:13 to 21:49:15	09:30:14 to 12:30:16	0342, 0343	0354, 0054	Gyro drift check

Table 3-2 (continued)

Time		Command Sequence		
Mission (Time After Launch), hr:min:sec	GMT, hr:min:sec	Major	Minor	Event
Mission Phase: Coast Phase II (cont)				
22:55:16	13:36:17	Unscheduled sequence	0702	Start drift check of roll axis only
25:32:27 to 25:46:20	16:13:28 to 16:27:41	0447	0250, 0251, 0550	Low power interrogation of modes 4 and 2 to obtain thermal data
29:51:41 to 30:02:43	20:32:42 to 20:43:44	0447	0250, 0251, 0550	Low power interrogation of modes 4 and 2 to obtain thermal data
32:56:37	23:37:38	Unscheduled sequence	0716, 0702	Terminate roll drift check and null out accumulated error produced by drift
37:24:54 to 37:30:53	04:05:55 to 04:11:54 (6/1/66)	0447	0250, 0251, 0550	Low power interrogation
37:37:38 to 39:34:56	04:18:39 to 06:25:57	0342	0354	Gyro drift check for pitch and yaw gyros; roll gyro drift check allowed to continue
39:50:16	06:31:17	Unscheduled sequence	Command 0601	Attempt to extend omnidirectional antenna A
Mission Phase: Coast Mode II				
40:53:14 to 43:11:58	07:34:15 to 09:52:59	0342	0354 plus commands 0702, 0716	Gyro drift check (roll gyro drift check also terminated)
43:14:41	09:55:42	Unscheduled sequence	0354	New gyro drift check initiated
43:17:44 to 43:26:22	09:58:45 to 10:07:23	0447	0250, 0251, 0550	Low-power interrogation of modes 4 and 2
45:05:33 to 45:36:56	11:46:34 to 12:17:57	1741	2053	Start power mode cycling remaining in auxiliary battery mode to check rate of temperature rise of auxiliary battery
45:36:56	12:17:57	1741	2053	"Hi" current mode on – both batteries directly on line
45:56:57	12:37:58	1341	1350	Vernier tanks' thermal control on
46:24:02	13:05:03	Unscheduled sequence	Command 0702	Terminate yaw and pitch gyro drift check, but allow roll check to continue
49:06:13	15:47:14	Unscheduled sequence	Command 0317	Return to auxiliary battery mode to increase rate of temperature rise of auxiliary battery
49:07:19 to 49:21:36	15:48:20 to 16:02:37	0447	0250, 0251, 0550	Low-power interrogation of modes 2 and 4
49:48:44 to 49:53:17	16:29:45 to 16:34:18	1742	2054	Power mode cycling, with return to auxiliary battery (to insure proper auxiliary battery temperature rise)
52:03:15 to 52:20:19	18:44:16 to 19:01:20	0447	0254, 0251, 0550	Low-power interrogation of modes 4 and 2
52:34:13	19:15:14	Unscheduled sequence	Command 0716	Terminate roll gyro drift check and null accumulated error

Table 3-2 (continued)

Time		Command Sequence		
Mission (Time After Launch), hr:min:sec	GMT, hr:min:sec	Major	Minor	Event
Mission Phase: Coast Mode II (cont)				
52:39:42	19:20:43	Unscheduled sequence (0342)	Command 0700	Begin new gyro drift check
55:00:50	21:41:51	Unscheduled sequence	Command 0702	Terminate yaw and pitch drift check and null out accumulated errors
56:38:52 to 56:54:06	23:19:53 to	0447	0250, 0251, 0550	Low-power interrogation of modes 4 and 2
57:29:40 to 57:43:03	00:10:41 to 00:24:04 (6/2/66)	1742	2054	Power mode cycling, with return to auxiliary battery mode (to ensure proper auxiliary battery temperature rise)
58:35:41	01:16:42	1740	1750	Turn on survey TV electronic thermal control power
58:41:59	01:23:00	Unscheduled sequence	0320	Restore main battery, placing both batteries on line in preparation for terminal descent
59:10:22	01:51:23	Unscheduled sequence	Command 0716	Terminate roll gyro drift check and null accumulated error
59:14:23 to 59:19:22	01:55:24 to 02:00:23	0446	0250	Low-power interrogation of mode 4 only
60:26:59 to 60:35:53	03:08:00 to 03:16:54	0446	0250	Low-power interrogation of mode 4 only
61:14:23 to 61:20:06	03:55:24 to 04:01:07	0247	0250, 0251	Engineering interrogation of modes 4, 2, 1 (accomplished with low power at 550 bits/sec)
61:24:41 to 61:28:14	04:05:42 to	0344	0550, 1050, 1053	VCXO check
	No time confirmation (communication line out)	Special sequence	Command 1133	Vidicon temperature control on survey camera
Mission Phase: Terminal Descent				
62:37:06 to 62:44:36	05:18:07 to 05:25:37	1646	0250, 0652, 0653, 0255, 2057, 0056, 0252	Terminal descent 1) Interrogation of modes 4, 2, and 1 and turn on of high power transmitter (at 05:20:18 GMT) and adjustment of telemetry rate to 1100 bits/sec (at 05:21:27); summing amplifiers off (to turn off presumming amplifier) and turn on of phase summing amplifier
62:44:36	05:25:37	1345	1755	2) Propulsion strain gage power turned on
62:45:13	05:26:14	1345	1756	3) Touchdown strain gage power and SCOs turned on

Table 3-2 (continued)

Time		Command Sequence		
Mission (Time After) Launch), hr:min:sec	GMT, hr:min:sec	Major	Minor	Event
Mission Phase: Terminal Descent (cont)				
62:48:46 to 62:51:08	05:29:47 to 05:32:09	1040	1050	4) Transponder power turned off and one-way lock achieved
62:51:08	05:32:09	1144	1154	5) Roll maneuver magnitude and direction commanded (plus 89.3 degrees)
62:55:45	05:36:46	1144	1251	6) Execute roll
62:59:43	05:40:44	1145	1155	7) Yaw magnitude and direction commanded (plus 59.9 degrees)
63:00:46	05:41:47	1145	1253	8) Execute yaw (retro thrust direction aligned properly at approximately 05:43:47 GMT)
63:03:28	05:44:29	1147	1157	9) Roll maneuver magnitude and direction commanded (plus 94.1 degrees)
63:04:16	05:45:17	1147	1257	10) Roll executed
63:09:22	05:50:23	1640	1751, 1656	11) Vernier thrust level (200 pounds) for retro phase and delay between AMR mark and vernier ignition (7.85 seconds) commanded
63:19:33	06:00:34	1644	0251	12) Command on mode 2 data
63:25:26	06:06:27	1644	1657	13) Retro sequence mode on commanded
63:25:51	06:06:52	1644	1752	14) Vernier lines and tanks thermal control commanded off
63:28:56	06:09:57	1644	1753	15) AMR on
63:29:56	06:10:57	1644	1754	16) Thrust phase power on
63:31:56.8	06:12:57.8	1644	2051	17) AMR enabled
63:33:37.3	06:14:38.3	1644	2052	18) Backup AMR mark commanded
63:33:38.7	06:14:39.7‡	–	–	19) AMR mark
63:33:46.6	06:14:47.6	–	–	20) Vernier ignition
63:33:47.7	06:14:48.7	–	–	21) Retro ignition
63:33:49.2	06:14:50.2‡	–	–	22) RADVS on
63:34:19	06:14:20‡	–	–	23) RODVS
63:34:28	06:15:29‡	–	–	24) RORA
63:34:26.9	06:15:27.9	–	–	25) Retro burnout
63:34:38.9	06:15:39.9	–	–	26) Retro eject
63:34:39.1	06:15:40.1	–	–	27) Retro separation
63:34:41.1	06:15:42.1	–	–	28) Enable doppler control
63:34:43	06:15:44‡	–	–	29) Beam 3 loses lock
63:34:45	06:15:46‡	–	–	30) Beam 3 regains lock

‡Time telemetry data was received in the Performance Analysis Area at SFOF (i.e., includes transit time from spacecraft to ground, SFOF processing delay, and commutation delay).

Table 3-2 (continued)

Time		Command Sequence		
Mission (Time After Launch), hr:min:sec	GMT, hr:min:sec	Major	Minor	Event
Mission Phase: Terminal Descent (cont)				
63:35:00	06:16:01	1644	0056	31) Mode 3 commanded
63:35:01	06:16:02	1644	1252	32) Presumming amplifier on commanded (to get touchdown strain gage data)
63:36:19.5	06:17:10.5	–	–	33) 1000-foot mark
63:36:28.7	06:17:28.7	–	–	34) 10-ft/sec mark
63:36:34.2	06:17:34.2	–	–	35) 14-foot mark
63:36:35.7	06:17:35.7	–	–	36) Touchdown indicated by retro accelerometer (Note: could be off by 0.5 seconds due to commutation delay)

3.2.1 Prelaunch Countdown

The prelaunch countdown which started at 2000 PDT on 29 May 1966 consisted of two separate spacecraft testing phases, the launch pad systems readiness test (Procedure No. 2271381E), which ran from 2000 PDT on 29 May to 0150 PDT on 30 May, followed by the countdown procedure (Procedure No. 227391D), which started at 0515 PDT on 30 May and terminated at launch at 0741 PDT on 30 May. In both these phases, the spacecraft performed properly with no significant anomalies.

The launch pad SRT was run with some difficulty, as the interface between the ground test equipment (STEA) and the computer data processing system (CDS) was excessively noisy, producing numerous erroneous outputs on the computer printouts of the spacecraft telemetry. Each of these erroneous outputs had to be investigated to ensure that it was definitely a ground data processing problem and not a spacecraft problem.

During the RF silence period from 0154 to 0515 PDT, this interface was worked on and, in the ensuing countdown, the performance of the entire system (spacecraft, STEA, and CDS) was exemplary. The countdown went without incident, and the spacecraft was launched at 0741 PDT on 30 May. The only spacecraft anomalies evident during this period are described briefly as follows:

1) The regulated output current (EP-14) read slightly higher and noisier than in the same configurations in other test environments (the ESF or the AO Buildings) (see TFR 45905). This condition has not been conclusively explained to this time. The most

probable explanation is that the increased readings are actually the correct ones and that earlier readings were slightly low due to an unknown ground or noise loop that was eliminated when the spacecraft was placed in the actual flight configuration.

2) During the countdown, the Centaur air conditioning temperature was allowed to get to 100°F, above the upper limit of 90°F, but all spacecraft temperatures were back within their launch limits at the time of launch.

3.2.2 Launch, Injection, and Separation

The boost phase was normal and resulted in SC-1 being injected properly on a trajectory that insured a landing in the near vicinity of the target area. Subsequent to injection and just prior to its separation from the spacecraft, the Centaur issued the preprogrammed commands for accomplishing spacecraft operations required for the postseparation phase, namely, "extend landing gears" (at L + 11M55.5S), "extend omni-antennas" (at L + 12M5.7S), and "transmitter high power on" (at L + 12M25.4S). Normal response to the first and third commands was verified from telemetry data received by the downrange ships, but only omnidirectional antenna B extension in response to the second command was confirmed (i.e., telemetry indicated that omnidirectional antenna A has not extended). Separation was initiated by the Centaur at L + 12M32.3S and was accomplished satisfactorily at L + 12M37S.

Following separation, the spacecraft automatically executed the sequences it was designed to perform as soon as separation occurred. By using its cold-gas jets, which were now enabled, the flight control subsystem nulled out the rotational rates imparted by the separation springs and initiated a roll-yaw sequence to acquire the sun. At L + 19M33S, after a minus roll of approximately 87 degrees and a plus yaw of 99 degrees, the acquisition and lockon to the sun by the spacecraft sun sensors were complete. Concurrently with the sun acquisition sequence, the antenna/solar panel positioner (A/SPP) initiated its solar-panel-axis and roll-axis deployment, and at L + 22M, the solar panel was in its proper transit position. All these operations were confirmed in real time by the telemetry received by the downrange ships.

3.2.3 DSIF Acquisition

At approximately L + 24M, the spacecraft became visible to DSS 51 (Johannesburg), and the initial DSIF acquisition procedure for establishing the communication and tracking link between the spacecraft and the ground station was initiated. In less than 4 minutes (L + 27M40S), the acquisition was completed when two-way lock was established between DSS 51 and the spacecraft.

The first ground-controlled sequence (initial spacecraft operations) was initiated at approximately L + 40M, and consisted of commands for turning off equipment required only for the launch-to-DSIF acquisition phase (i.e., deploy logic off, "transmitter high power off," "accelerometer

amplifiers off," etc.), for seating the solar panel and roll axis locking pins securely (i.e., commands for "rocking" the axes back and forth), for increasing the telemetry bit rate to 1100 bits/sec, and for initially interrogating all telemetry commutator modes so that the spacecraft overall condition could be assessed. All spacecraft responses to the commands were normal. However, the telemetry still indicated that omnidirectional antenna A was not extended. An attempt was made to command the extension of omnidirectional antenna A at L + 1H40M, but the spacecraft did not respond. Since the spacecraft was using omnidirectional antenna B and the spacecraft-to-DSS vector was located on the best part of this antenna pattern, there was no need to use omnidirectional antenna A.

3.2.4 Coast Phase I (Including Canopus Acquisition)

The spacecraft continued to coast normally with its pitch-yaw attitude controlled to track the sun and with its roll axis held inertially fixed. Tracking and telemetry data was obtained by using transponder B and transmitter B in low power.

At L + 4H9M, a spacecraft roll sequence was initiated for making a star map and for acquiring Canopus in order to fix the roll attitude of the spacecraft to a precise position from which the midcourse maneuvers could be initiated. During the first revolution of the maneuver, star intensity signals from 10 stars, in addition to Canopus, were identified with Canopus being observed and identified after 220 degrees of roll. It was also noticed that a Canopus lockon signal was not obtained as the star sensor swept past Canopus, since the Canopus intensity signal was above the upper threshold of the lockon range. As the vehicle continued to roll, the time for sending the proper command to achieve manual lockon to Canopus (when the vehicle rolled around to the proper position) was computed. This command was sent at the computed time, and manual lockon was successfully achieved at L + 4H32M after 580 degrees of roll.

The vehicle continued to coast as before, but with its roll attitude controlled so that the star sensor remained locked to Canopus. During this coasting phase, which continued until the execution of the midcourse correction sequence, continuous telemetry was received from the spacecraft (at 1100 bits/sec until approximately L + 11H and at 550 bits/sec subsequently). Three engineering interrogations (including the two interrogations scheduled to be done with transmitter high power) plus a 3-hour check of the drift of the three gyros (roll, pitch, and yaw) were performed during this period of low power transmitter operation. Performance of all spacecraft subsystems was satisfactory.

3.2.5 Midcourse Correction

All midcourse operations were performed normally. With the spacecraft visible to and controlled by DSS 11 (Goldstone), the maneuver sequence for applying the midcourse thrust in the proper direction was initiated, with the first maneuver (a minus roll of 86.5 degrees) starting at L + 15H49M.

The second maneuver (a minus yaw of 57.9 degrees) was executed at L + 15H54M. With the vehicle thrusting direction now positioned properly, the midcourse thrust was applied by igniting the vernier engines and controlling their thrust to achieve a constant spacecraft acceleration of 0.1 g for 20.8 seconds (a correction of 20.34 m/sec). Analog recorder data verified that the thrust duration was correct (i.e., time actually measured was 20.75 seconds, which is well within the accuracy of the recorder).

Following the midcourse thrusting, the reverse maneuvers were performed successcully, with the sun and Canopus sensors being illuminated properly. Thus, confirmation that the gyros had retained their inertial reference during the vernier engine shutdown was obtained, and the need for performing a postmidcourse star verification was eliminated.

Of special interest is the spacecraft injection accuracy, the midcourse correction, and resulting landing point accuracy. These items are summarized in the data below showing lunar latitude and longitude for the initial aim point, the unbraked impact point if no midcourse correction was made, the revised aim point for which the midcourse correction was computed, and the actual soft landing point as determined from postmidcourse orbit determination and descent trajectory analyses.

	Latitude, °S	Longitude, °W
Initial aim point	3.25	43.83
Uncorrected impact point	11.43	54.15
Final aim point	2.33	43.83
Actual landing point	2.411	43.345

In terms of miss, the spacecraft injection errors would have resulted in only a 264-mile miss on the moon. After midcourse correction, the miss was less than 9 miles.

3.2.6 Coast Phase II

The postmidcourse coasting phase (Coast Phase II) was begun and continued until the time of terminal descent maneuver initiation. Throughout this period, a telemetry rate of 550 bits/sec was obtained, and during this interval, five additional gyro drift measurements and ten engineering interrogations were made. The results of the gyro drift measurements were consistent and indicated that the drift of all gyros was below their specified upper limit (i.e., zero for the pitch gyro, 0.2 deg/hr for the roll gyro, and 0.75 deg/hr for the yaw gyro), and the interrogations confirmed that the temperature data channels which were not being sampled continuously were indicating normal performance.

Also during Coast Phase II, power mode cycling checks were made to help predict the percentage of the electrical load which would be supplied by the main and auxiliary batteries during the terminal descent when both batteries are placed directly on the bus. To ensure that the auxiliary battery would be at the desired temperature (>60°F) at the time of terminal descent, a slight change was made in the procedure which called for placing both batteries directly on the line following these checks. The auxiliary battery was

used to supply most of the load (auxiliary battery mode) so that its rate of temperature rise would be increased from 1 to 2 deg/hr to 3 deg/hr.

3.2.7 Terminal Descent

The terminal descent sequence was initiated at L + 62H37M with the turnon of the high power transmitter and the performance of the last engineering interrogation. Three attitude maneuvers were then performed — the first two for orienting the retro engine thrust direction properly and the last maneuver forensuring optimum telecommunication performance during the retro and vernier descent sequences. The first maneuver (a plus roll of 89.3 degrees) was executed at L + 62H55M45S, and the second maneuver (a plus yaw of 59.9 degrees) was performed at L + 63H0M46S. The last maneuver (a plus roll of 94.1 degrees) was executed at L + 63H4M16S.

The altitude marking radar (AMR) was turned on at L + 63H28M56S and was enabled at L + 63H31M57S. Except for two commands for turning on the touchdown strain gage data and for obtaining the optimum sampling rate for the flight control telemetry data, the remaining operations were automatically performed by the spacecraft.

The automatic descent sequence was initiated by the AMR mark, the generation of which was confirmed on the ground at L + 63H33M38.7S. The automatic sequence of events (including vernier ignition, retro ignition, RADVS on, retro burnout and separation, enable doppler control, 1000-foot mark, 10-ft/sec mark, and finally the 14-foot mark) occurred normally as indicated on the last page of Table 3-2. Quick-look analysis of the telemetry data indicates that touchdown occurred between 1 and 2 seconds following the occurrence of the 14-foot mark at approximately L + 63H36M35.7S. Confirmation of the soft landing was provided by the DSIF receiver retaining its lockon to the spacecraft transmitter signal and by the low magnitude of the force telemetered by the shock absorber strain gages (< 1600 pounds indicating touchdown velocities on the order of 10 ft/sec).

3.3 FIRST LUNAR DAY DESCRIPTION

Following the successful soft landing at 06:17:35.7 GMT on 2 June 1966, the standard postlanding lunar preparation sequences were completed (see Table 3-3). This consisted of the following:

1) Shutting off the radar and flight control subsystems
2) Shutting off the landing gear and vernier engine strain gages
3) Locking the landing gear
4) Switching the auxiliary battery off the line
5) Dumping the helium system
6) Switching telemetry to the coast mode commutator for thermal and power assessment

TABLE 3-3. SC-1 MISSION MILESTONES – LUNAR PHASE

Event	Date	Time (To Nearest Minute)	
		GMT, day:hr:min	After Touchdown, day:hr:min
Touchdown	2 June 1966	153:06:18	0
Spacecraft secured		06:27	0:00:09
First 200 line TV picture		06:52	0:00:34
Solar panel positioning complete		08:56	0:02:38
Planar array positioning complete		09:19	0:03:01
First 600 line TV picture		09:40	0:03:22
A/SPP repositioning		12:52	0:06:34
Gas jet test	4 June	155:12:55	2:06:37
A/SPP repositioning		17:03	2:10:45
A/SPP repositioning	5 June	156:18:29	3:12:11
Special telecommunications test		22:12	3:15:54
A/SPP repositioning	6 June	157:07:07	4:00:49
Gas jet test		09:46	4:03:28
A/SPP repositioning	7 June	158:01:03	4:18:45
Lunar noon		06:27	5:00:09
A/SPP positioning for lunar noon		09:04	5:02:46
A/SPP positioning		11:03	5:04:45
Strain gage experiment	8 June	159:13:15	6:06:57
Planar array mapping		16:59	6:10:41
A/SPP stepping	9 June	160:12:55	7:06:37
Data link threshold test		17:02	7:10:44
A/SPP positioning	10 June	161:17:49	8:11:31
A/SPP positioning	11 June	162:15:56	9:09:38
A/SPP positioning	12 June	163:10:11	10:03:53
A/SPP positioning		18:27	10:12:09
A/SPP positioning	13 June	164:11:25	11:05:07
Voice relay test		18:15	11:11:57
A/SPP positioning		23:55	11:17:37
A/SPP positioning	14 June	165:02:13	11:19:55
Day-night terminator		16:32	12:10:14
A/SPP positioning		17:33	12:11:15
Final shutdown for lunar night	16 June	167:20:32	14:14:14

The engineering assessment was successfully conducted with no anomalies, and all compartment temperatures were well within operating limits. The survey television camera had been heated to operational temperatures and was ready for immediate use. Within 34 minutes of touchdown, the first TV picture had been taken.

Sun and earth acquisition by the solar panel and planar array, respectively, were completed with transmitter temperatures well within operational range. It was then possible to send 600 line TV pictures and transmit high bit rate (1100 bits/sec) telemetry in transmitter low power.

During the remainder of the lunar day, operations consisted of television operation or engineering experiments during the Goldstone tracking periods (see Table 3-4) and continuous engineering data transmission during the overseas DSS periods. The most important operational events are summarized in Table 3-5. During the midlunar day interval, the survey camera was conservatively shaded by either the planar array or the solar panel, resulting in the loss of planar array earth tracking during one Goldstone pass. Although the planar array could have been positioned to provide 600 line TV capability, the decision was made to assign the entire above Goldstone period (8 June) and the next following period (9 June) for engineering experiments.

TABLE 3-4. GOLDSTONE VISIBILITY DURING LUNAR PHASE

Event	Time (GMT), day:hr:min	Rise (GMT), day:hr:min	Set (GMT), day:hr:min
Touchdown	153:06:17	153:02:30	153:11:26
		154:03:22	154:12:08
		155:04:30	155:12:50
		156:05:31	156:13:42
		157:06:22	157:14:44
Lunar noon	158:06:27	158:07:04	158:15:50
		159:07:37	159:16:58
		160:08:07	160:18:02
		161:08:34	161:19:02
		162:09:03	162:19:58
		163:09:32	163:20:55
		164:10:02	164:21:45
Sunset	165:16:32	165:10:32	165:22:40
		166:11:02	166:23:35
Spacecraft shutdown	167:20:32	167:11:32	168:00:30

TABLE 3-5. LUNAR OPERATIONS SEQUENCES* – FIRST LUNAR DAY

2 June 1966 (day 153)
Soft landing at 06:17:36 GMT
Post-touchdown standard sequence for turning off power to systems used during terminal descent
First pictures (200 line) using standard sequence (survey of pads 2 and 3)
Solar panel and high-gain antenna erection
First 600 line pictures (360-degree constant range survey)
Wide-angle survey of one sector (54 degrees)
Narrow-angle survey of two sectors (18 degrees each)
3 June 1966 (day 154)
Wide-angle survey of five sectors (54 degrees each – 360 degrees total)
Survey of pad 2 area
Narrow-angle surveys of 14 sectors (18 degrees each)
Color survey of pad 2
4 June 1966 (day 155)
DSS 51 video training survey (three pictures)
Surveys of pads 2 and 3 and crushable block 1 and 2 imprints
Color survey
DSS 42 video training survey
Nitrogen jet/surface reaction study
5 June 1966 (day 156)
Surveys of pad 2 color test chart, pads 2 and 3, and crushable block 3 imprint
Narrow-angle survey of 10 sectors (18 degrees each)

*Other than routine engineering interrogations. All picture sequences are 600 line unless other wise noted.

Table 3-5 (continued)

5 June 1966 (day 156) (continued)
Color survey of rock A
Wide-angle survey of four sectors (54 degrees each)
Mapping survey of star Sirius
Survey of pads 2 and 3
DSS 42 200 line TV thermal study
6 June 1966 (day 157)
Surveys of pad 2 color test chart; pads 2 and 3, crushable block 1 and 3 imprints
Nitrogen gas jet/surface reaction study
Wide-angle color survey (360 degrees total)
Mapping survey of stars Sirius and Canopus
Wide-angle color survey (360 degrees total)
Survey for earth search
7 June 1966 (day 158)
(Lunar noon 06:17 GMT)
Surveys of pad 2 color test chart, and pads 2 and 3
Wide-angle survey (360 degrees total)
Narrow-angle color survey of six sectors (18 degrees each)
Surveys of pad 2 color test chart, and pads 2 and 3
8 and 9 June 1966
No TV pictures taken during lunar noon

Table 3-5 (continued)

9 June 1966 (day 160)
Standard spacecraft interrogations
Repositioned solar panel and planar array
Switched transmitter A from omni to planar array
Telecommunications experiment: used and checked all telemetry telecommunications system components except FM summing amplifier B
Spacecraft receiver threshold experiment
10 June 1966 (day 161)
Surveys of pad 2 color test chart
Wide-angle survey (360 degrees total)
Surveys of rocks A and B (color), helium bottle (color), focus ranging profile, and crushable block 1 imprint
Narrow-angle survey of nine sectors (18 degrees each)
Search survey of planet Venus
11 June 1966 (day 162)
Survey of pad 2 color test chart
Wide-angle survey (360 degrees total)
Narrow-angle survey (360 degrees total)
Survey of crushable block 1 imprint, omnidirectional antenna B lacking strut and auxiliary battery
Search survey of star Arcturus
Survey of compartment A top, and omnidirectional antenna B color test chart
Narrow-angle color survey of one sector
Color survey of compartment B top
Surveys of landing legs 2 and 3
Mapping survey of star Sirius

Table 3-5 (continued)

12 June 1966 (day 163)

- Survey an omnidirectional antenna B color test chart
- Wide-angle survey (300 degrees total)
- Narrow-angle survey (330 degrees total)
- Narrow-angle color survey of pads 2 and 3
- Three focus ranging profiles
- Horizon scan and wide- and narrow-angle azimuth scans

13 June 1966 (day 164)

- Wide- and narrow-angle horizontal surface scan
- Survey of crushable block 3 imprint
- Narrow-angle surveys of two sectors
- Survey of omnidirectional antenna B color test chart
- Wide-angle survey (300 degrees total)
- Narrow-angle survey (270 degrees total)
- Voice experiment: Surveyor used for voice communication between California and Canberra

14 June 1966 (day 165)

- Survey of omnidirectional antenna B color test chart
- Wide-angle survey (360 degrees total)
- Narrow-angle survey of five sectors (18 degrees each)
- Horizon scans at sunset
- (Start lunar night at 15:12 GMT)
- Survey of solar corona
- Pad 2 earth-shine picture (14-minute exposure)

15 and 16 June 1966

- Engineering interrogations only

16 June 1966 (day 167)

- Spacecraft telemetry commanded off at 20:32 GMT

Each of the engineering experiments or tests will be discussed in detail by the appropriate subsystem in Section 5. At this point, then, only a brief summary of these operations will be given.

3.3.1 Gas Jet/Surface Reaction Experiment

For the gas jet experiment, the nitrogen in gas jet 2 was exhausted in a counterclockwise direction (down), with TV pictures taken before, during, and after the gas jet thrusting. Commands 0710 and 0713 (positive yaw maneuver) were used to generate an error signal that would cause downward exhaust from gas jet 2 when gas jet amplifiers were enabled. The sequence was performed three times on day 155 and again on day 157, but no dust was observed in any picture.

3.3.2 Strain Gage Experiment

On day 159, the solar panel was stepped 30 times to determine if the motion could be detected by the spacecraft strain gages. No effect could be detected, however.

3.3.3 Spacecraft Shading (Thermal) Experiment

The planar array and the solar panel were utilized as umbrellas for spacecraft shading during the entire high-sun period. For most of this time, spacecraft and earth-sun orientations were such that normal tracking yielded both optimum communication and compartment shading. However, on day 158 (0500 GMT), both panels were put normal to the spacecraft Z axis for maximum shading of compartment B for a thermal experiment. On day 159, 1600 GMT, the planar array was elevated to 92.6 degrees and the solar panel to 242.5 degrees to shade the TV camera.

3.3.4 Antenna Mapping Experiment

During the panel erections for TV shading shortly after lunar noon (day 159), the broad vertical arm of the planar array antenna pattern was mapped over two profiles. Excellent agreement was obtained for predicted sidelobe gains and positions, except for several of the bottom sidelobes which were displaced by 2 degrees.

3.3.5 Special Telecommunication Tests

On day 160, all functions of the telecommunication system (telemetry modes, bit rates, SCOs, etc.) were selected and observed. All were operating properly.

3.3.6 Voice Relay Experiment

The Surveyor telecommunications system was used to transmit voice messages by audio modulation of the carrier between Goldstone and Canberra on day 164. The result was successful, although no special effort was made for audio quality and much distortion existed.

Normal operation during the first lunar day consisted of periodic commutator assessments (see Table 3-6) at all times, with TV sequences up to 1 hour each during Goldstone visibility periods (see Table 3-7). Statistics on the number of commands sent and TV pictures taken will be found in Section 5.1.

A mission plan was prepared and executed to maximize lunar night survival. The battery was charged to near maximum capacity by float charging (reduced rate) prior to the start of the Goldstone pass at sunset. The spacecraft was to be kept operational for 100 hours after sunset to avoid drastic battery discharge. However, due to failure of some of the compartment thermal switches, actual shutdown occurred 52 hours after sunset. Battery charge was estimated to be 80 amp-hr, with a predicted drain during the rest of the night of 0.205 amps (290 hours remained until lunar sunrise). The solar panel had been placed close to vertical in order to cast a maximum shadow for possible detection by the Lunar Orbiter spacecraft. This orientation would also permit gradual battery charging during the next lunar day when power units regained minimum operating temperatures.

3.4 SECOND LUNAR DAY DESCRIPTION

The historic SC-1 spacecraft revival was successfully accomplished by the Hughes Canberra (DSIF 42) team on 6 July with the following observations:

1) Initial acquisition at 11:29:10 GMT (04:29 PDT)

2) Narrow band transmitter VCXO at 22.193825 mc

3) Receiver VCXO X3 at 70.147013 mc

4) DSIF receiver AGC at -147 dbm

5) Telemetry mode 4 at 137.5 bits/sec

6) First good data frame at 11:36:26 GMT (see Table 3-8)

At 12:25 GMT, a decision was made to go to two-way lock. Instructions were then given to Canberra to turn nothing off until solar panel stepping had at least been started. The battery discharge current was 1.5 amps, and pressure was 15 psi. Solar panel stepping was initiated with main battery voltage at 17 volts, with occasional loss of up- and downlinks. Two-way lock was obtained at 13:15 GMT, followed by solar panel sun acquisition and planar array earth acquisition. The battery was then charging at 1 amp, and 1100 bits/second data was generated at a final signal strength of -117.4 dbm.

It was determined that, due to an available battery charge rate of only 1 amp when transmitting in low power, the spacecraft would be shut down for 2-hour periods to allow charging in the blind. Short interrogations would

TABLE 3-6. SUMMARY OF LUNAR DAY ENGINEERING INTERROGATIONS

(From: Command Confirmation Record)

From (GMT), hr:min:sec	To (GMT), hr:min:sec	Modes
	Day 153	
07:17:41	07:27:53	4
07:51:17	08:06:52	4 and 5
09:00:44	09:32:35	4 and 5
11:37:19	12:13:09	1, 2, 4, 5
15:12:41	15:33:16	4 and 5
17:48:04	18:27:28	2, 4, and 5
19:30:12	20:02:02	2, 4, 5
21:02:07	21:24:16	2, 4, 5
22:33:45	22:52:38	2, 4, 5
	Day 154	
00:00:00	00:54:57	2, 4, 5
02:37:00	02:46:45	2, 4, 5
04:17:33	04:31:09	1, 2, 4, 5
05:47:21	05:53:56	2, 4, 5
06:41:41	06:47:35	2, 4, 5
07:22:52	07:28:27	2, 4, 5
08:26:04	08:34:43	2, 4, 5
11:06:12	11:10:10	2, 4, 5
12:16:52	16:48:58	2, 4, 5
19:01:03	19:13:21	2, 4, 5
21:17:47	21:41:59	2, 4, 5
	Day 155	
00:03:48	00:17:42	2, 4, 5
02:48:00	04:08:03	2, 5
04:35:34	05:08:28	2, 4, 5
05:56:03	06:10:05	2, 4, 5
06:15:36	06:18:43	2, 4, 5
07:04:18	07:13:49	2, 5
08:09:13	08:27:42	2, 4, 5
09:21:49	09:38:10	2, 4, 5
10:13:49	10:20:59	2, 4, 5
?	?	2, 4, 5
13:01:13	13:07:33	2, 4, 5
15:31:25	15:58:55	2, 4, 5
20:09:23	20:09:29	2, 4, 5
21:47:58	22:01:09	2, 4, 5

Table 3-6 (continued)

From (GMT), hr:min:sec	To (GMT), hr:min:sec	Modes
	Day 156	
00:17:22	00:25:27	2, 4, 5
02:34:30	03:01:19	2, 4, 5
04:36:02	04:42:46	2, 4, 5
04:59:44	05:26:52	4
05:53:09	06:01:38	2, 4, 5
06:51:39	07:07:32	2, 4, 5
07:44:19	08:05:49	2, 4, 5
08:46:33	09:11:26	2, 4, 5
09:48:08	10:11:48	2, 4, 5
10:51:31	11:03:54	2, 4, 5
11:53:40	12:17:03	2, 4, 5
13:03:11	13:10:58	2, 4, 5
15:12:38	17:12:30	2, 4, 5
18:28:30	18:35:09	4, 5
?	?	1, 2, 4, 5
22:11:58	22:53:58	2, 4, 5
	Day 157	
01:22:59	01:14:50	2, 4, 5
03:35:21	03:38:16	2, 4, 5
05:57:42	06:12:34	2, 4, 5
07:11:39	07:18:07	2, 4, 5
08:01:51	08:07:46	2, 4, 5
08:49:01	09:11:48	2, 4, 5
09:48:26	10:05:38	2, 4, 5
10:52:17	11:00:41	2, 4, 5
12:00:15	12:24:34	2, 4, 5
13:17:24	13:40:12	2, 4, 5
14:35:46	14:53:15	2, 4, 5
16:33:10	16:28:11	2, 4, 5
18:48:41	20:47:44	2, 4, 5
20:57:04	22:47:05	2, 4, 5
22:53:53	01:03:01	2, 4, 5
	Day 158	
01:11:46	01:15:34	2, 5
03:13:53	03:26:11	2, 4, 5
09:08:33	09:36:18	2, 4, 5
10:26:14	10:59:28	2, 4, 5

Table 3-6 (continued)

From (GMT), hr:min:sec	To (GMT), hr:min:sec	Modes
	Day 158 (continued)	
12:04:09	12:27:33	2, 4, 5
13:33:00	13:55:42	2, 4, 5
15:01:15	15:09:21	2, 4, 5
15:42:47	16:10:59	2, 4, 5
	Day 159	
08:21:21	10:23:55	2, 4, 5
10:26:33	10:28:28	2, 5
12:13:59	13:05:56	2, 5
15:03:36	15:23:53	2, 4, 5
	Day 160	
08:41:22	10:50:14	2, 4, 5
10:56:12	12:17:28	2, 4, 5
13:02:41	13:07:34	2, 5
14:20:06	14:27:28	1, 2, 3, 4, 5
	Day 161	
08:52:31	09:12:18	2, 4, 5
?	?	1, 5, 4
10:17:28	10:30:18	2, 4, 5
11:26:31	11:41:50	2, 4, 5
13:24:02	13:31:44	2, 4, 5
15:15:27	15:21:22	2, 4, 5
16:45:07	17:29:01	2, 4, 5
18:43:00	18:59:25	2, 4, 5
	Day 162	
09:22:22	09:37:01	2, 4, 5
11:20:58	11:35:19	2, 4, 5
12:49:08	13:09:15	2, 4, 5
15:20:05	15:39:46	2, 4, 5
17:16:48	17:22:27	2, 5

Table 3-6 (continued)

From (GMT), hr:min:sec	To (GMT), hr:min:sec	Modes
	Day 163	
09:51:29	09:58:33	2, 4, 5
11:56:23	12:10:48	2, 4, 5
14:05:00	14:17:45	2, 4, 5
15:27:30	15:40:56	2, 4, 5
16:47:44	16:53:10	2, 4, 5
17:13:55	18:21:44	2, 4, 5
19:00:13	19:04:38	2, 4, 5
	Day 164	
10:25:10	11:08:44	2, 4, 5
12:54:20	13:11:30	2, 4, 5
14:28:28	15:09:14	2, 4, 5
16:09:49	16:23:13	2, 4, 5
17:39:48	18:34:18	2, 4, 5
20:02:47	20:09:07	2, 4, 5
21:52:00	23:55:10	2, 4, 5
	Day 165	
23:58:48	01:07:23	2, 4, 5
02:80:02	03:28:49	2, 4, 5
03:45:00	04:49:21	2, 4, 5
05:10:53	06:15:34	2, 4, 5
06:19:28	07:22:59	2, 4, 5
07:45:28	08:51:58	2, 4, 5
09:02:41	10:59:29	2, 4, 5
12:37:42	12:55:59	2, 4, 5
14:23:53	14:26:43	2, 4, 5
16:22:27	16:27:07	2, 4, 5
17:33:16	18:11:42	2, 4, 5
19:28:24	19:48:22	2, 4, 5
20:50:48	21:06:52	2, 4, 5
?	22:26:41	2, 4, 5
23:39:29	23:50:38	2, 4, 5
	Day 166	
00:51:00	01:04:09	4, 5
02:06:16	02:20:27	2, 4, 5
03:22:11	03:29:28	4, 5
04:31:31	04:40:09	4, 5
05:54:08	06:07:08	4, 5
07:13:03	07:24:30	4, 5

Table 3-6 (continued)

From (GMT), hr:min:sec	To (GMT), hr:min:sec	Modes
	Day 166 (continued)	
08:30:31	08:43:50	4, 5
09:46:00	09:54:15	4, 5
10:56:10	11:03:58	4, 5
12:07:01	12:27:19	4, 5
13:28:35	13:40:22	4, 5
14:40:18	14:48:16	4, 5
16:51:24	17:03:01	4, 5
17:58:18	18:06:12	4, 5
20:08:10	20:19:00	4, 5
22:15:00	22:25:53	4, 5
23:29:12	23:38:01	4, 5
	Day 167	
00:15:27	00:22:44	4, 5
01:19:00	01:24:57	4, 5
03:05:33	03:16:01	4, 5
04:13:17	04:22:41	4, 5
06:11:59	06:26:12	4, 5
07:22:48	07:40:17	4, 5
09:05:57	09:13:29	4, 5
10:07:40	10:13:06	4, 5

TABLE 3-7. SUMMARY OF FIRST LUNAR DAY TV SEQUENCES

Day	Start Time (GMT), hr:min	Completed (GMT), hr:min	Remarks
153	06:52		200 line
	07:29	07:51	200 line
	09:36	10:05	
	10:20	10:53	
	11:02	11:12	
154	03:39	04:17	
	04:32	05:35	
	06:02	06:37	
	06:52	07:18	
	07:39	08:20	
	08:38	09:39	
	11:14	11:59	
155	04:09	04:31	
	05:12	05:55	
	06:21	07:03	
	07:35	08:09	
	08:30	09:21	
	09:42	10:13	
	10:35	11:05	

Table 3-7 (continued)

Day	Start Time (GMT), hr:min	Completed (GMT), hr:min	Remarks
156	06:06	06:49	
	07:10	07:43	
	08:08	08:44	
	09:12	09:46	
	10:14	10:47	
	11:15	11:51	
	12:24	13:02	
	14:09	14:47	200 line
157	07:22	07:59	
	08:15	08:48	
	09:15	09:36	
	09:41	09:45	During gas jet experiment
	10:08	10:50	
	11:08	11:59	
	12:28	13:16	
	13:44	14:34	
158	09:40	10:25	
	11:03	12:03	
	12:31	13:27	
	14:00	14:56	
	15:18	15:42	
161	09:16	10:16	
	10:34	11:25	
	11:46	13:12	
	13:37	15:09	
	15:28	16:44	
	17:49	18:42	
162	09:46	11:20	
	11:41	12:48	
	13:14	15:00	
	15:56	17:16	
163	10:19	11:55	
	12:14	13:36	
	14:22	15:26	
	15:45	16:47	
	18:26	18:59	
164	11:25	12:53	
	13:22	14:28	
	15:12	16:09	
	16:38	17:36	
	18:38	19:59	
	20:10	21:34	
165	11:06	12:33	
	12:58	14:22	
	14:29	16:20	
	16:29	16:40	

TABLE 3-8. LUNAR OPERATION SEQUENCES – SECOND LUNAR DAY

28 June to 6 July 1966

Spacecraft did not respond to commands

6 July 1966 (day 187)

Spacecraft acquired by DSS 42 (Canberra)
Solar panel positioning for increased charge rate

7 July 1966 (day 188)

Camera status verification at -54 degrees azimuth (24 pictures)

8 July 1966 (day 189)

Surveys of pad 2, compartment A top, and crushable block imprint
Attempt to fire vernier engines
Horizon scans at three azimuths
Surveys of pad 3, crushable block 3 imprint, and auxiliary battery
Approach TV camera turnon (no video transmitted)

9 to 11 July 1966

No camera operation owing to excessive battery temperature

12 July 1966 (day 193)

Survey of rock B
Horizon scan
Wide-angle survey (360 degrees total)
Repeated surveys of compartments A and B tops
Repeated surveys of advancing spacecraft shadow
Repeated surveys of crushable block 3 imprint
Survey of pads 2 and 3
Survey of omnidirectional antenna B color test chart

13 July 1966 (day 194)

DSS 42 and DSS 51 surveys of spacecraft shadow at hourly intervals
Surveys of omnidirectional antenna B color test chart, and pads 2 and 3
Mirror/filter wheel dust determination
Narrow-angle survey of four sectors
Survey of compartment A top
Narrow-angle survey of two sectors
Survey of pad 3

14 July 1966 (day 195)

DSS 51 solar corona survey attempt (200 line)

be scheduled, then, at 2-hour intervals, and battery charge rate would hopefully be nearly doubled by the load reduction. The spacecraft was consequently shut down at approximately 00:02 GMT on 7 July, but could not be reactivated by Johannesburg. Finally, at 08:25 GMT on 7 July 1966, the spacecraft was detected by Goldstone at a -165 dbm level (extremely weak) after some 2 hours of search. (This level was some 46 db lower than anticipated for low power planar array operation.) Transmitter A was commanded off and the signal disappeared. Transmitter B was commanded on and Surveyor I returned to its more usual "all systems OK" condition at expected dbm levels.

Several complete engineering assessments were performed, and all signals indicated the spacecraft was nominal and the battery was charging at a rate in excess of 1.0 amp. Since the upper plateau (approximately 50 amp-hr) was indicated by EP-2 at 08:34 GMT on 8 July 1966, a residual charge of 10 to 15 amp-hr may have been available in the battery at time of acquisition.

SC-1 did not respond to the thrust phase power on commands at 10:45 GMT 8 July which attempted to fire the vernier engines.

As of 00:00 GMT, 9 July, the spacecraft status was as follows:

	Telemetry Signal	Value
EP-3	Battery pressure	14 psi
EP-2	Battery voltage	25 volts
EP-8	Main battery temperature	135°F
V-15	Compartment A top temperature	100°F
V-16	Compartment A bottom temperature	116°F
V-21	Compartment B top temperature	116°F
V-22	Compartment B bottom temperature	122°F

A severe problem was developing with the main battery as its temperature was increasing toward its survival limit of 142 degrees at a rate of 1°F/hr. At 05:00 on 9 July, the spacecraft was put in a noncharging quiescent mode, i.e., only the receivers were left on. Main battery temperature at this time was 139.8°F. After several hours, it became apparent that main battery temperature was stabilizing.

By 16:00 on 9 July, with main battery voltage of about 19.5 volts and main battery temperature of 137°F, battery recharging was commenced at a quiescent charge rate of about 1.25 amps. Twelve hours later, the charge rate was increased to about 2 amps in the quiescent mode. Main battery temperature continued to drop and stabilized at about 112°F on 11 July. It appeared that the battery would now sustain TV operation again, provided care was used to avoid sustained loads.

The survey TV camera was operated periodically throughout the Goldstone visibility for a total of eight TV interrogation periods of approximately 1 hour each. The solar panel and planar array were repositioned so that the planar array was looking at the earth and the solar panel was normal to the sun.

The transfer from Goldstone to Canberra took place between 20:46 and 20:56 GMT. During the Canberra visibility, the spacecraft performance seemed to be normal. Battery pressure was 37 psi, battery voltage was approximately 21.8 volts, and battery temperature was 106°F. However, the inability of the battery to hold any amount of charge was demonstrated at 22:00 GMT when the solar panel was stepped away from the sun (zero solar panel current), and the bus voltage decreased to approximately 15.7 volts with a 1.4-amp battery discharge current.

Johannesburg and Canberra stations TV picture taking sequences were such that spacecraft shadow effects could be observed. The spacecraft performance seemed to be normal. The battery pressure now was 42 psi, battery voltage was between 22 and 25 volts (depending on whether TV pictures were being taken or the battery was being charged), and battery temperature was 106°F.

As of 10:00 GMT on 13 July 1966, Goldstone was taking TV pictures. Battery pressure was 39 psi, battery temperature was 113.6°F, and battery voltage in the unloaded state was 26.3 volts and in the loaded state was 20.5 volts. The solar panel was in a near-vertical position, being tilted approximately 3 degrees toward the west. Just prior to lunar night, the solar panel was stored in a 20-degree tilt from the vertical toward the west to cast a long shadow for Lunar Orbiter at NASA's request.

At approximately 02:45 GMT on 13 July 1966, communications with Surveyor I failed. Nine pictures of the sunset sequence were taken. Upon the start of the tenth TV frame, no response was received to the start command. The Johannesburg station sent the following commands to attempt to bring the spacecraft out of TV mode:

1104 – Survey power off

0107 – High voltage off

0130 – Transfer switch to low power

At this point, all contact was lost and a frequency search of ±20 kc was started, but no response was received.

Interrogation was made with transmitter B in low and then high power with B on omni in NBVCXO. The transponder mode and wide band VCXO were used for search, but still there was no response. At 08:32 GMT on 14 July 1966, all DSIF stations ceased to support SC-1 lunar operations.

3.5 SUMMARY OF SIGNIFICANT ANOMALIES

The anomalies occurring during flight and first lunar day postlanding phases are summarized in Table 3-9. For the purposes of this report, an anomaly is defined as any unexpected occurrence that might be indicative of a spacecraft trouble or failure. The anomalies are discussed in detail in the sections noted in Table 3-9.

3.6 SUMMARY OF TRANSIT DEVIATIONS FROM EPD 180

The significant changes in the transit sequence from the preprepared standard transit mission sequence as documented in EPD 180 (Reference 1) are summarized in Table 3-10. Also included in this table are the reasons for the deviations. No such table has been prepared for the lunar phase as that phase of the mission is not as "standard" as the transit phase and is full of many options. Briefly, these transit sequence changes resulted from the following:

1) Failure of omnidirectional antenna A to extend during the preseparation phase, thus causing the implementation of nonstandard sequences for attempting to extend this antenna.

2) Performance of all high-power interrogations (except for the one conducted as part of the terminal descent sequence) in low power because of the good telecommunication signal strength operating margin.

3) Use of manual lockon (instead of automatic lockon) for Canopus acquisition, due to high signal level produced by all stars, including Canopus.

4) Additional gyro drift checks obtained during Coast Phase II to obtain the best estimate of the drift of each gyro for use in the terminal descent computations.

5) Additional use of auxiliary battery mode (instead of high current mode) to increase the rate of temperature rise of the auxiliary battery so that the desired auxiliary battery temperature was achieved during terminal descent.

6) Three attitude maneuvers performed during terminal descent because of the constraint of not using omnidirectional antenna A, with the first maneuver being initiated 38 minutes prior to retro ignition (instead of 33 minutes – due to lower-than-specified gyro drift).

TABLE 3-9. SUMMARY OF SIGNIFICANT ANOMALIES

Time of Occurrence		Description	Effect on Mission	TFR Number
GMT, day:hr:min	Mission			
150:14:53	L + 12M	Omnidirectional antenna A extension not confirmed by telemetry. Boom apparently did not extend, although squib was fired. Sometime during terminal descent and landing, boom did extend and lock (see Sections 5.4 and 5.12).	Mission was flown entirely on a transmitter B, transponder B, and omnidirectional antenna B combination. Required one additional maneuver at terminal descent. Overall mission effect was negligible although spacecraft operations were effected.	18233
150:14:53	L + 12M	Postmission processed data indicated that omnidirectional antenna deployment took place at nearly the same time as leg extension instead of delayed 10 seconds (see Section 5.12).	None – this is a data processing problem, not a spacecraft problem. Extension timing was actually correct, but postmission processing "threw out" 3 bcd data frames and mistime tagged the following one which made omnidirectional antenna extension appear to take place 7.2 seconds earlier than it actually did.	27627
150:15:21	L + 40M	After first DSIF acquisition, the "auto solar panel deploy logic off" was sent to the spacecraft without effect. The command was repeated and was effective the second time.	Preliminary investigation indicates that although the proper command was initiated at the CDC, the proper command modulation was not transmitted from the DSIF due to a glitch on the command SCO output caused by a phone jack being removed. No effect on mission.	18238 18239
150:18:54	L + 4H 13M	During the star verification maneuver, an extra "star" was evident which did not repeat on subsequent maneuvers (see Section 5.6).	Apparently a "Canopus particle" interference. No effect on mission. Did not repeat on any subsequent star map or roll maneuvers.	
151:06:20	L + 15H 39M	A short transient appeared on the Canopus error signal just after the vernier pressurization squib was blown prior to the premidcourse maneuvers (see Section 5.6).	Probably caused by "Canopus particles" liberated by the squib firing. No effect on mission.	
152:06:41	L + 40H 0M	Auxiliary battery temperature fell below desired minimum during transit. Temperature was raised to desired level at terminal descent by operating in auxiliary battery mode instead of high current mode for last 15 hours of transit (see Sections 5.2 and 5.3).	Changed sequence to operate last 15 hours in auxiliary battery mode instead of high current mode.	18237
157:15:00	TD + 4D 9H	After many hours of lunar operation at temperatures above the design temperatures for the unit, the oxidizer pressure relief valve popped at 865 psia and failed to properly reseat itself (see Section 5.7).	No effect on design mission as the "life" of the unit was over by this time. Would preclude any subsequent prolonged firing of vernier engines.	

Table 3-9 (continued)

Time of Occurrence		Description	Effect on Mission	TFR Number
GMT, day:hr:min	Mission			
		Spacecraft receiver threshold test indicated that spacecraft receiver AGC telemetry voltage preflight calibration does not give the proper values for the actual environment (see Section 5.4).	No effect on real-time mission. For postmission analyses, telemetry was "in-flight" calibrated using data from the special spacecraft receiver threshold test. Telemetry accuracy somewhat degraded.	27628
Throughout lunar operations		Excessive sunlight reflected into survey TV camera under certain lighting condition. In worst case, approximately 50 percent of narrow angle picture reached saturation (see Section 5.13).	In worst-case lighting conditions (2 June) 130 degrees out of the full 360 degrees of narrow angle survey was eliminated. ECA 111769 redesigns hood for SC-5 and subsequent spacecraft.	27503
163:07:48	TD + 10D	Survey camera elevation potentiometer opened causing loss of all mirror elevation position information (see Section 5.13).	Mirror elevation position had to be tracked by keeping track of steps and checking periodically with known position pictures. ECA 111769 changes potentiometer lubricant on SC-5 and subsequent spacecraft.	27504
165:05:07	TD + 12D	Intermittent failure of TV mirror elevation to step up (see Section 5.13).	Complicates the lunar picture taking operation as content of each picture must be examined to verify that mirror did respond to up commands. ECA 111769 corrects this on SC-5 and subsequent spacecraft.	27505
165	TD + 12D	Compartment A thermal switches 2 and 5 did not open at day/night terminator until the temperature fell significantly below the design actuating temperature (see Section 5.2).	Caused compartment A to reach its quiescent lunar night temperature a little sooner than if the switches had opened at the proper temperature.	18234
165	TD + 12D	Five compartment B thermal switches did not open at their design actuating temperature on spacecraft cooldown. It is not known when or if all switches finally opened (see Section 5.2).	Would cause compartment B to reach a lower temperature during lunar night and might affect survivability if switches never opened. If they did open (as indicated by subsequent compartment temperatures), would only cause temperature to reach quiescent level a little sooner.	18235
		SSAC could not use approximately 5 percent of the TV frame identification data throughout the mission due to intermittent false synch words in TV PCM data (TFR 27561 for SC-2 TV). (See Section 5.13.)	Increased operational difficulties.	27509

TABLE 3-10. SUMMARY OF SIGNIFICANT TRANSIT DEVIATIONS FROM EPD 180

Mission Phase	Mission Time	Event/Deviation	Reason for Deviation
DSIF acquisition through star verification	L + 44 M 33 S	Repeat of command to turn automatic solar panel deployment logic off.	CDC command tape printout indicates that the command was improperly transmitted the first time that it was sent.
DSIF acquisition through star acquisition	L + 1 H 40 M	Unscheduled attempt to extend omnidirectional antenna A via ground command following completion of "initial spacecraft operations" sequence.	Telemetry indication of failure of omnidirectional antenna A to extend during the preseparation period.
DSIF acquisition through star acquisition	L + 3 H 48 M	1100-bits/sec engineering interrogation preceding star acquisition conducted with low-power transmitter instead of high-power.	High-power-transmitter operation not required to obtain 1100 bits/sec telemetry data.
DSIF acquisition through star acquisition	L + 4 H 09 M	Unscheduled selection of coast mode commutator for use in star verification maneuver (instead of scheduled commutator mode 1).	Coast mode commutator selected to obtain receiver AGC telemetry signals during the spacecraft roll maneuver used for star verification/acquisition so that possible verification of failure of omnidirectional antenna A to extend could be made.
DSIF acquisition through star acquisition	L + 4 H 32 M	Unscheduled use of manual lockon to achieve lock to Canopus instead of automatic star acquisition mode.	Intensity of Canopus above upper limit of automatic lockon range, due to intentional high setting of intensity channel for ensuring that sufficient signal strength would be obtained if the sensor window had experienced "fogging" such as that observed in SC-2 STV testing.
Coast phase I	L + 13 H 33 M and L + 15H 20M	Premidcourse engineering interrogations conducted with low power.	Telecommunication signal strength margin was sufficient to obtain data rate of 550 bits/sec with low-power operation of the transmitter.
Midcourse	L + 15H 40M 15S	Unscheduled commanding of manual lockon.	To null out star channel transients.
Midcourse	L + 16H 8M	Selection of coast phase commutator for use during postmidcourse maneuvers (instead of mode 1).	To obtain receiver A AGC data which is not on mode 1 (attempt to confirm condition of omnidirectional antenna A).
Midcourse	L + 16H 23M	Addition of mode 1 sampling postmidcourse maneuver engineering interrogation.	Since coast mode commutator was used for reverse maneuvers instead of mode 1, mode 1 data was sampled in addition to modes 2 and 4.
Midcourse	L + 16H 45M	Additional commands sent to turn off the auxiliary accelerometer amplifiers and touchdown strain gages following midcourse.	Signature list item indicates that turnon of propulsion strain gages for midcourse might possibly turn on the other amplifiers.
Coast phase II	L + 39H 50M 16S	Additional command sent to extend omnidirectional antenna A.	Attempt to extend omnidirectional antenna A based on possibility that midcourse correction may have had some effect.
Coast phase II	L + 43H 14M, L + 52H 34M	Additional gyro drift checks.	To obtain as much gyro drift data as possible for use in terminal descent computations.
Coast phase II	L + 49H 06M	Return to auxiliary battery mode (instead of use of high current mode).	To ensure proper temperature rise of auxiliary battery so that it would be correct at time of terminal descent.
	L + 49H 49M, L + 57H 30M	Return to auxiliary battery mode (instead of high current mode following all proper cycling checks).	To ensure proper temperature rise of auxiliary battery so that it would be correct at time of terminal descent.

Table 3-10 (continued)

Mission Phase	Mission Time	Event/Deviation	Reason for Deviation
Coast phase II	L + 58H 42M	Both batteries placed on bus.	Since auxiliary battery mode was being used at this time (instead of preplanned use of high current mode which places both batteries directly on the bus), the main battery had to be placed directly on the bus.
	L + 61H 14M	Engineering interrogation conducted with transmitter low power.	Telecommunication signal strength margin sufficient to obtain 550 bits/sec with low power.
	≈ L + 62H 41M	Mode 2 not sampled during pre-terminal descent engineering interrogation.	To conserve time since attitude maneuvers were initiated earlier than scheduled. Mode 2 was not sampled at this time, but terminal descent following attitude maneuvers and until last part of vernier descent utilized mode 2.
	= L + 62H 56M	Initiation of first maneuver at 38 minutes prior to retro ignition (instead of 33 minutes prior to retro ignition).	Since three maneuvers had to be performed, and since gyro drift measurements showed that gyro drift was less than specified upper limit, first maneuver was initiated early.

3.7 MISSION EVENT TIME HISTORY

A complete tabulation of all commands sent to the spacecraft (excluding the survey TV commands) is given in Volume II of Reference 2. This tabulation is over 250 pages long and thus will not be repeated here. A summary of the significant major events can be seen in Tables 3-1 through 3-3 and 3-7.

4.0 SYSTEM SUMMARY AND CONCLUSIONS

4.1 SUMMARY OF SYSTEM PERFORMANCE PARAMETERS

Performance parameters that could be determined through post-mission analysis of spacecraft telemetry data are summarized in tables near the beginning of each subsection in Section 5. For the reader's convenience, the major or significant system performance parameters are summarized in Table 4-1. Also included in this summary for comparison purposes are the required or predicted values for these parameters.

TABLE 4-1. SUMMARY OF SYSTEM PERFORMANCE PARAMETERS

Parameter	Required	Source	Predicted	Source	Actual	Reference
Overall						
1. Injected weight	<2250 pounds	30240			2192.86 pounds	
Actual landed weight	587 to 645 pounds	224510			644.68 pounds	
2. Mission payload weight	>62.5 pounds	30240			64.10 pounds	
3. Transit time	66-hour nominal	30240			63 hours 36 minutes	
4. Goldstone visibility at landing	2 hours before 3 hours after	30240 30240			4 hours before 5 hours after	
5. Landing location accuracy (excluding tracking errors)	100 km for a 50 m/sec midcourse ΔV	30240			<14 km (including tracking errors)	
6. Landing approach angle	0 to 25 degrees	30240	5.87 degrees		6.13 degrees	5.15.3
7. Touchdown conditions						
Vertical velocity	<15 ft/sec	30240			13 ft/sec	
Lateral velocity	<5 ft/sec	30240			<2 ft/sec	
Vertical shock (rigid body)	<30 earth g	30240			≈6.5 g (estimated)	
Lateral shock (rigid body)	<12 earth g	30240			≈1.5 g (estimated)	
Stable	Yes		Yes		Yes	
8. Lunar operating life	1 lunar day +150 hours of nonoperating mode postsunset operation	30240	Yes		2 lunar days and 1 lunar night	
9. Midcourse ΔV capability	Up to 50 m/sec	30240	Up to 50 m/sec		Actually used 20 m/sec	5.4
10. Telemetry during transit	Continuous at bit rate ≥17 bits/sec				Continuous at bit rate of ≥550 bits/sec	

Table 4-1 (continued)

Parameter	Required	Source	Predicted	Source	Actual	Reference
11. Nitrogen gas used	<4.7 pounds		0.546	Calculated	0.68 pound	5.6.7.13
12. Total vernier fuel used			137.3 pounds	Calculated	139 pounds	5.15.6.4
13. Battery energy remaining at touchdown			72.7 amp-hours	Calculated	72 amp-hours	5.3.3.2
Launch to injection						
1. Launch time	Between 1440 and 1527 GMT on day 150				150-14:41:00.990	
2. Spacecraft angular rates during boost	<5.0 deg/sec	224510			1.72 deg/sec (pitch)	5.6.7.1
3. Spacecraft angular rates at separation	<3.0 deg/sec	30240	<3.0 deg/sec		0.38 deg/sec (pitch)	5.6.7.2
4. Time to null separation rates	<50 seconds	224510			15 seconds	5.6.7.2
5. Angular motion during rate stabilization						
Roll	None		<75 degrees	Calculated	≈0 degree	5.6.7.2
Pitch	None		<75 degrees	Calculated	≈2.3 degrees	5.6.7.2
Yaw	None		<75 degrees	Calculated	≈0 degree	5.6.7.2
Separation to acquisition						
1. Solar panel deployment time			10M24S	STV test	10 minutes 17 seconds	5.12.6.2
2. Sun acquisition time	<18 minutes	224510			6 minutes 12 seconds	5.6.7.3
3. Required maneuvers to acquire sun						
Roll			<360 degrees	Calculated	-87 degrees	5.6.7.3
Yaw			<180 degrees	Calculated	+99 degrees	5.6.7.3
4. Time of first DSS 11 visibility; Delta time to:			150-15:04:31		150-15:04:20	5.4.7.3
One-way lock	<12 minutes	224510			-11 seconds	5.4.7.3
Two-way lock	<30 minutes	224510			4 minutes 14 seconds	5.4.7.3
Transmission of first command	<18 minutes	224510			16 minutes 24 seconds	5.4.7.3
5. Time of initiation of Canopus acquisition	2 hours prior to midcourse	224510	Launch +6 hours	EDP 180	Launch +4H12M (midcourse – 11H52M)	5.6.7.4
6. Time required to acquire Canopus	<38 minutes	224510			19 minutes 40 seconds	5.6.7.4
7. Roll angle from beginning of maneuver to Canopus			<360 degrees		220.6 degrees	5.6.7.4
8. Total roll angle from beginning of maneuver to Canopus lockon			<1080 degrees		580.6 degrees	5.6.7.4

PRECEDING PAGE BLANK

Table 4-1 (continued)

Parameter	Required	Source	Predicted	Source	Actual	Reference
Coast phases						
1. Attitude orientation						
Mean error from sun line	<0.2 degree	224510			-0.058 degree (pitch)	5.6.7.5
					-0.053 degree (yaw)	5.6.7.5
Mean error from Canopus	<0.2 degree	224510			-0.055 degree (roll)	5.6.7.5
2. Limit cycle – optical mode						
Roll – average amplitude	<0.6 degree	224510	0.44		0.441 degree	5.6.7.5
Pitch – average amplitude	<0.6 degree	224510	0.44		0.470 degree	5.6.7.5
Yaw – average amplitude	<0.6 degree	224510	0.44		0.457 degree	5.6.7.5
Average period (time between gas jet pulses)	–		80 sec/pulse		65 sec/pulse	5.6.7.5
3. Gyro drift						
Roll	<1 deg/hr	224510			0.2 deg/hr average	5.6.7.5
Pitch	<1 deg/hr	224510			0 deg/hr average	5.6.7.5
Yaw	<1 deg/hr	224510			0.75 deg/hr average	5.6.7.5
4. Mean solar panel output	89 ± 5 watts	224510			≈86 watts	5.3.3
5. Mean OCR output					≈69 watts	5.3.3
Midcourse correction						
1. Premidcourse maneuver angles						
Roll	Not available		-86.5 degrees command		-86.585 degrees	5.6.7.6
Yaw	Not available		-57.99 degrees command		-57.900 degrees	5.6.7.6
2. Pointing accuracy	<0.7 degree error	224510	–		0.313 degree	5.6.7.8
					0.221 degree	5.14.2.1
3. Midcourse engine burn time	Not available		20.85 seconds command		20.815 seconds	5.6.7.8
4. Midcourse ΔV	Not available		20.347 m/sec command		20.365 m/sec	5.6.7.8
					20.266 m/sec	5.14.2.1
5. Midcourse ΔV error	<0.4 m/sec	224510			0.018 m/sec	5.6.7.8
					-0.081 m/sec	5.14.2.1
6. Peak attitude transient at engine ignition						
Roll					-0.43 degree	5.6.7.8
Pitch					0	5.6.7.8
Yaw					-0.08 degree	5.6.7.8

Table 4-1 (continued)

Parameter	Required	Source	Predicted	Source	Actual	Reference
7. Mean attitude error during burning	<0.10 degree	224510				
Roll					-0.33 degree	5.6.7.8
Pitch					+0.01 degree	5.6.7.8
Yaw					-0.01 degree	5.6.7.8
8. Roll actuator position:						
Peak at ignition					+0.9 degree	5.6.7.8
Mean during burn			0.75 degree		+0.65 degree	5.6.7.8
9. Engine shutoff impulse	<5 lb/sec per engine with a dispersion between engines of <0.66 lb/sec	224510				
Engine 1					0.27 lb/sec	5.6.7.8
Engine 2					-0.37 lb/sec	5.6.7.8
Engine 3					0.10 lb/sec	5.6.7.8
10. Postmidcourse maneuvers						
Yaw			+86.5 degrees command		≈86.5	5.6.7.7
Roll			+57.99 degrees command		≈57.9	5.6.7.7
Terminal descent						
1. Preretro maneuvers						
Roll	Not available		+89.30 degrees command		+89.27 degrees	5.6.7.9
Yaw	Not available		+59.90 degrees command		+59.98 degrees	5.6.7.9
Roll	Not available		+94.10 degrees command		+94.42 degrees	5.6.7.9
2. Time of initiation of first maneuver	<33 before AMR mark time	224510			38 minutes before AMR mark time	5.6.7.9
3. Preretro pointing error	<0.7 degree	Calculated			0.34 degree (-yaw) 0.00 degree (pitch)	5.6.7.10
4. Thrust to velocity vector misalignment during retro burn	<1 degree	224510			0.26 degree (+pitch) 0.08 degree (yaw)	5.15.3
5. Approach angle (velocity vector to lunar vertical)	<25 degrees		5.87 degrees		6.13 degrees	5.15.3
6. AMR mark altitude			59.62 miles		No data	5.9.6.2
7. Time between AMR mark and vernier ignition			7.85 seconds command		7.85 seconds	5.15.3
8. Retro thrust to center of gravity offset during burning	<0.18 inch	224510			<0.02 inch	5.6.7.10
9. Retro burn time (ignition to 3500 pounds thrust)			38.5 seconds		38.9 seconds	5.8.4
10. Maximum retro thrust	<10,000 pounds	224510	9800 pounds		≈9900 pounds	5.15.6.2 5.8.4

Table 4-1 (continued)

Parameter	Required	Source	Predicted	Source	Actual	Reference
11. Peak attitude transient at vernier ignition						
Roll					Not determined	
Pitch					-0.13 degree	5.6.7.10
Yaw					-0.89 degree	5.6.7.10
12. Peak roll error during burning	<1 degree				<0.5 degree	5.6.7.10
13. Retro burnout conditions					153-06:15:27.7	5.15.3
Slant range					27,820 feet	5.15.3
Longitudinal velocity, V_z					425 ft/sec	5.15.3
Lateral velocity, V_x					71.3 ft/sec	5.15.3
Lateral velocity, V_y					-4.1 ft/sec	5.15.3
Flight path angle (angle between Z axis and velocity vector)						
14. Descent segment intercept at time:					153-06:16:05.9	5.15.3
Slant range					18,000 feet	5.10.4.9
Velocity					442 ft/sec	
15. Vernier engine shut-off conditions at time:					153-06:17:34.2	5.15.3
Altitude (from foot pads)					13 feet	5.15.3
Vertical velocity					5 ft/sec	5.15.3
Lateral velocity					≈0	5.15.3
Angle to local vertical					≈0.3 degree	5.15.3
16. Touchdown conditions (based on descent trajectory)					153-06:17:35.678	5.15.3
Vertical velocity					12.2 ft/sec	5.15.3
Lateral velocity					≈0.6 ft/sec	5.15.3
Angle to local vertical					≈0	5.15.3
Time of free fall					1.5 seconds	5.15.3
17. Touchdown conditions (based on interpretation of TD strain gage data)					153-06:17:35.559	5.11.2
Vertical velocity					≈10 ft/sec	5.11.2
Lateral velocity					≈2 ft/sec	5.11.2
Angle to local vertical					≈1 degree	5.11.2
18. Spacecraft roll orientation after touchdown	Not available				-X axis 1 degree West of North	

4.2 CONCLUSIONS AND RECOMMENDATIONS

4.2.1 Conclusions

It is concluded that the Surveyor I lunar flight, landing, and post-landing operations were truly remarkable. With the few, almost trivial, exceptions noted in Section 3.5, all spacecraft subsystems performed as designed or better. Those "uncertainties" in the design (such as lunar radar reflectivity, attitude control during retro burn, etc.) due to the impracticality of testing in the earth environment all proved to operate almost exactly as predicted. The resultant nearly perfect soft landing within a few kilometers of the target attests to the proper operation of all subsystems and launch vehicle as well as the space flight operations activities.

4.2.2 Recommendations

Numerous operational and procedural recommendations are made in each of the subsections in Section 5. These recommendations are summarized very briefly below.

4.2.2.1 Spacecraft Design Change Recommendations

1) Redesign the omnidirectional antenna boom extend mechanism to assure more positive deployment (see Section 5.12). This change has already been accomplished on SC-2 and following spacecraft.

2) Revise calibration methods for spacecraft receiver AGC telemetry signals. Also make study to determine stability of this calibration. Commutators should be changed to include AGC signals in every mode (see Section 5.4).

3) Review Canopus window fogging data and, if no fogging is expected, change Canopus sensor gain calibration to 1 X Canopus. If fogging is still a potential occurrence, use a Canopus sensor gain calibration of approximately 1.25 X Canopus instead of 1.5 X Canopus (see Section 5.6).

4) Revise paint pattern on auxiliary battery to provide a higher temperature at time of terminal descent (see Section 5.2).

4.2.2.2 Operational Recommendations

1) Delete the gyro speed measurements from the sequence until the gyro signal processing channels are improved (see Section 5.6).

2) Postlanding TV picture sequences should use mirror scanning techniques that make better use of the azimuth drive life while conserving the more limited elevation drive life (see Section 5.13).

3) DSIF station reports should include phase jitter measurements every hour and AGC levels going into or out of high power (see Section 5. 4).

4. 2. 2. 3 Postmission Data Processing Recommendations

1) Except for mission phases where absolute or relative time is critical (such as terminal descent), SFOF digitized tapes should be used in lieu of DSIF tapes for economy and earlier accessibility reasons.

2) Full 66-hour transit phase averaged plots need not be made for all telemetry channels. Those signals listed in Table 4-2 should not be routinely plotted on subsequent missions as such plots are not useful.

3) More use should be made of real-time SFOF data, especially for lunar operations. A copy of all teletype data and bulk printer data should be made immediately available to postmission analysis personnel.

4) Excessive duplication of efforts both at Hughes and JPL should be minimized on subsequent missions as follows:

   a) There should be closer coordination and exchange of data between Hughes and JPL to assure proper telemetry processing techniques are being used and to make reduced data available to both activities.

   b) SPAC and FPAC activities should publish early Quick Look Reports (within 2 weeks of touchdown for the transit phase, for example), thus eliminating any need for a postmission analysis Quick Look Report.

5) When processing telemetry data, continuous frame by frame corrections for the current differential amplifier calibration based on telemetered data should be eliminated as they are unnecessary and wasteful of computer processing time. The current amplifier gain is sufficiently stable that corrections can be based on one set of calibration coefficients and only changed when periodic samplings of the current calibration telemetry show a change greater than some preset threshold (see Sections 5. 3 and 5. 5).

6) Automatic unbalance current corrections to all telemetry channels having a capacitive output impedence should be eliminated. Provision should be added for an additional correction to each signal for unbalance current depending on the commutator switch used (see Sections 5. 1 and 5. 5).

TABLE 4-2. TELEMETRY ANALOG CHANNELS FOR WHICH FULL 66-HOUR TRANSIT PHASE AVERAGED PLOTS ARE NOT USEFUL

Telemetry Number	Signal Name	Reason
T-1	TV 4 vidicon temperature	Not meaningful during transit
R-2	RADVS R amplitude	Important only at touchdown, and then unaveraged plots are required
R-3	RADVS D_1 amplitude	
R-4	RADVS D_2 amplitude	
R-5	RADVS D_3 amplitude	
R-12	AMR power out	
R-14	AMR AGS	
R-29	AMR late gate	
D-1	Omnidirectional antenna A transmitter power	Continuous plots unnecessary
D-3	Omnidirectional antenna B transmitter power	
FC-15	Acceleration error	Important only at mid-course and touchdown, and then unaveraged plots are required
FC-25	Vernier engine 1 thrust command	
FC-26	Vernier engine 2 thrust command	
FC-27	Vernier engine 3 thrust command	
FC-32	Retro accelerometer	Important only at touchdown, and then unaveraged plots are required
FC-35	RADVS range	
FC-39	RADVS V_x	
FC-40	RADVS V_y	
FC-41	RADVS V_z	
FC-43	Roll actuator signal	Important only at mid-course and touchdown, and then unaveraged plots are required
P-18	Vernier engine 1 strain gage	
P-19	Vernier engine 2 strain gage	
P-20	Vernier engine 3 strain gage	
EP-17	Radar and squib current	Important only at touchdown
EP-21	Compartment A heater current	Not used during transit
EP-22	Compartment B heater current	

7) Greater care should be taken when digitizing the raw telemetry tapes to assure that "end of file" marks are always placed at the proper place, and that the discriminators are properly adjusted so that "bit slip" does not occur (see Sections 5. 1 and 5. 4).

8) The Reformatter program should be modified to eliminate the feature of "saving" telemetry data when the time coding on the digitized tape is noisy by adding a fictitious time tag delayed a fixed amount of time after the last good frame. This feature, in conjunction with that of throwing out bad telemetry frames, has resulted in wrong conclusions being made based on erroneous time information (see Sections 5. 1 and 5. 12).

9) The following data (from DSIF or JPL processing) should be made available to postmission analysis personnel in a more timely manner (it has not yet been received on SC-1):

   a) All station telecommunication parameters including receiver AGC, dynamic phase error, transmitter power, etc. (see Section 5. 4)

   b) Frequency of all SCOs, when used during the mission, both maxima and minima (see Section 5. 5)

   c) TV data (full set of contact strip pictures, command summary, and all frame identification data) to fully evaluate the survey camera performance (see Section 5. 13)

4. 2. 3 Test and Performance Prediction Model Recommendations

1) The solar intensity in the Hughes STV test chamber should not be changed based on this mission's thermal data. The range of variation of actual flight solar intensity at all thermal sensors, due to seasonal and positional differences, is 87 to 97 percent solar constant. Use of present 105 percent maximum STV sun will permit marginal testing (see Section 5. 2).

2) Battery parameters should be further investigated to permit a more accurate model of the state of charge to be made (see Section 5. 3).

3) The vibration levels used during flight acceptance tests should be reduced to more nearly approximate the actual Centaur vibration environment (see subsection 5. 11-4).

4) The reliability model should be changed to allow for nonstandard procedures and lessened boost vibration effects (see Section 5. 16).

5) A revised A/SPP thermal prediction model should be used on all subsequent spacecraft. This model has already been developed based on actual SC-1 performance data (see subsection 5. 2. 3. 3).

6) The survey TV thermal model for prediction of postlanded thermal performance needs revision in order to give results consistent with SC-1 performance. Further studies are required to develop these revisions (see subsection 5.2.3.18).

4.2.4 Acknowledgements

This report reflects the efforts of many individuals and activities at the Hughes Aircraft Company. Those individuals making major contributions to the various subsystem sections in Section 5 are identified there. In addition, the following people also had a major part in preparing this report:

System coordinating, editing, preparation: K. C. Beall, R. H. Leuschner

Development and checkout of postmission data processing programs: S. Volansky, J. Berger, D. Partridge

Providing data handling, logging, reduction of all postflight data: S. McCormick, D. Brackney, B. Levy

Editing and publication of the report, coordinating the art work: B. Godwin, N. Redmond, W. Scott

4.2.5 References

The following reference material was used without specific acknowledgement in the preparation of many parts of Sections 2, 3, and 4:

1. Spaceflight Operations Plan – Surveyor Mission A, JPL EPD 180 Revision 5, February 1966.

2. "Surveyor Mission A Spaceflight Operations Report," Hughes Aircraft Company, SSD 64189R, August 1966.

3. Surveyor Spacecraft System Specification, JPL Specification 30240 (latest revision).

4. Surveyor Mission A Flight Test Objectives, JPL Report PO 32-S/MA Revision 1, 19 May 1966.

5. "Surveyor I Flight Performance Preliminary Report," Hughes Aircraft Company, SSD 68152 I, 27 June 1966.

6. "Surveyor I Mission Report, Part 1," JPL Technical Report 32-1023, 31 August 1966.

5.0 PERFORMANCE ANALYSIS

5.1 SYSTEM

5.1.1 INTRODUCTION

The operation of the spacecraft as a system was thoroughly discussed under mission phase in Section 3. Included here, therefore, are those items of additional information needed to set the stage for the detailed analyses of each spacecraft subsystem that will follow.

5.1.2 MISSION STATISTICS

In Tables 5.1-1 through 5.1-4, statistics are given on total commands sent to the spacecraft, number of TV pictures taken, and high power load intervals. Most of this data has been taken from "Surveyor I Mission Report, Part 1," JPL Technical Report 32-1023, August 31, 1966.

TABLE 5.1-1. COMMANDS TRANSMITTED BY PRIME TRACKING STATIONS (NOT INCLUDING SECOND LUNAR DAY OPERATIONS)

Pass Number	Date, 1966 GMT	Event	Commands Transmitted		
			DSS 51	DSS 11	DSS 42
1	May 30/31	Midcourse commands sent by DSS 11	77	88	3
2	May 31/June 1		10	8	28
3	June 1/2	Soft landing, 06:17:37 GMT (June 2)	13	66	590
4	June 3		30	4,833	6
5	June 3/4		60	1,080	680
6	June 4/5		5	4,372	988
7	June 5/6		20	7,876	300
8	June 6/7	Lunar noon, 06:17 GMT (June 7)	1,656	9,345	67
9	June 7/8		30	3,158	18
10	June 8/9		20	4,000	15
11	June 9/10		15	12,000	17
12	June 10/11		22	10,100	71
13	June 11/12		237	10,611	35
14	June 13		64	7,614	444
15	June 14/15	Start lunar night, 15:12 GMT (June 14)	25	5,000	109
16	June 15/16		73	96	30
17	June 16	Spacecraft power turned off by DSS 11, 167: 20:31:00 GMT	80	100	N/A
		Station Total	2,435	80,333	3,399
		Grand Total		86,177	

Note: Of 86,177 commands transmitted, only one (sequence 0316) was rejected by the spacecraft.

TABLE 5.1-2. TV PICTURES MADE BY COMMANDS FROM PRIME TRACKING STATIONS (NOT INCLUDING SECOND LUNAR DAY OPERATIONS)

Pass Number	Date, 1966 GMT	Event	Number of TV Pictures		
			DSS 51	DSS 11	DSS 42
3	June 2	Soft landing 06:17:37 GMT (June 2)		145 (includ-13 200-line)	
4	June 3			863	
5	June 3/4		3	395	
6	June 4/5			646	13
7	June 5/6			867	263*
8	June 6/7	Lunar noon, 06:17 GMT (June 7)		1,048	
9	June 7/8				
10	June 8/9				
11	June 9/10			1,759	
12	June 10/11			1,373	
13	June 11/12			1,363	
14	June 13			1,321	
15	June 14/15	Start lunar night, 15:12 GMT (June 14)		520**	
16	June 15/16				
17	June 16	Spacecraft power turned off by DSS 11, 20:31:00 GMT (June 16)			
		Station Total	3	10,300	13
		Grand Total		10,316	

*Received during DSS 11 transmission and DSS 11/42 mutual view period.

**Last picture was of pad 2 by earth light (after lunar sunset). Exposure was f4.0 at 4 minutes.

TABLE 5.1-3. TRANSMITTER HIGH POWER INTERVALS

Day	Time On, GMT, hr:min:sec	Time Off, GMT, hr:min:sec	Total Interval On, hr:min:sec	Event
150	14:53:26	15:20:46	27:20	DSIF acquisition
150	18:44:25	19:21:05	36:40	Canopus verification
151	06:08:25	07:12:44	1:04:19	Midcourse
153	05:20:17	09:03:05	3:42:48	Terminal descent and TV sequence
Total			5:51:07	

TABLE 5.1-4. THRUST POWER ON INTERVALS

Day	Time On, GMT, hr:min:sec	Time Off, GMT, hr:min:sec	Total Interval On, min:sec	Event
151	06:43:05	06:46:09	3:04	Midcourse
153	06:10:57	06:18:16	7:19	Terminal descent
Total			10:23	

5.1.3 COMMANDS TO THE SPACECRAFT IN FLIGHT

A total of 293 commands were sent to the spacecraft from DSIF stations from initial acquisition to touchdown. Not included are commands that came directly from the Centaur programmer. All the flight commands are listed in Table 5.1-5, along with an indication of the source of time data used to get the most accurate value. The command data sources are listed in order of accuracy, with the DSIF magnetic tape being most accurate.

TABLE 5.1-5. SC-1 FLIGHT-TIME COMMAND LOG

Command Number	Description	Most Accurate Time From All Available Data, Day 150, hr:min:sec	Source			
			Magnetic DSIF Tape	CDS at ETR	CDC Printer Tape	SPAC Command Confirmation Record
0110	XMTR filament power off	15:20:44.020	X			
0130	Transfer B low power	15:20:44.520	X			
0623	Basic bus accelerator amplifier off	15:21:08.019	X			
0316	Solar panel deploy logic off	15:21:08.519	X			
0623	Basic bus accelerator amplifier off	15:25:34.003	X			
0316	Solar panel deploy logic off	15:25:34.503	X			
0402	Step solar panel minus	15:26:52.499	X			
0402	Step solar panel minus	15:26:53.001	X			
0402	Step solar panel minus	15:26:53.499	X			
0402	Step solar panel minus	15:26:54.001	X			
0402	Step solar panel minus	15:26:54.499	X			
0402	Step solar panel minus	15:26:55.001	X			
0402	Step solar panel minus	15:26:55.499	X			
0402	Step solar panel minus	15:26:56.001	X			
0402	Step solar panel minus	15:26:56.499	X			
0402	Step solar panel minus	15:26:57.001	X			
0401	Step solar panel plus	15:26:57.499	X			
0401	Step solar panel plus	15:26:58.001	X			
0401	Step solar panel plus	15:26:58.498	X			
0401	Step solar panel plus	15:26:58.998	X			
0401	Step solar panel plus	15:26:59.498	X			
0405	Step roll axis plus	15:27:55.495	X			
0405	Step roll axis plus	15:27:55.995	X			
0405	Step roll axis plus	15:27:56.495	X			
0405	Step roll axis plus	15:27:56.995	X			
0405	Step roll axis plus	15:27:57.495	X			
0405	Step roll axis plus	15:27:57.995	X			
0405	Step roll axis plus	15:27:58.495	X			
0405	Step roll axis plus	15:27:58.995	X			
0405	Step roll axis plus	15:27:59.495	X			
0405	Step roll axis plus	15:27:59.995	X			
0406	Step roll axis minus	15:28:00.495	X			
0406	Step roll axis minus	15:28:00.995	X			
0406	Step roll axis minus	15:28:01.495	X			
0406	Step roll axis minus	15:28:01.995	X			
0406	Step roll axis minus	15:28:02.495	X			
0510	AESP off	15:34:14.974	X			X
0226	Mode 1 on	15:34:23.973	X			X
0237	Low modulation index SCO on	15:39:29.995	X			X
0216	7.35 kc A/D SCO on	15:39:30.455	X			X

Table 5.1-5 (continued)

Command Number	Description	Most Accurate Time From All Available Data, Day 150-151, hr:min:sec	Source			
			Magnetic DSIF Tape	CDS at ETR	CDC Printer Tape	SPAC Command Confirmation Record
0205	Rate 1100 bits/sec on	15:39:30.955	X			X
0231	Mode 4 on	15:42:38.445	X			X
0227	Mode 2 on	15:48:21.425	X			X
0230	Mode 3 on	15:54:37.404	X			X
0232	AESP off	15:55:56.399	X			X
0506	Mode C on	15:56:04.899	X			X
0601	Extend omnidirectional antenna	16:21:21.812	X			X
0601	Extend omnidirectional antenna	16:21:50.310	X			X
0601	Extend omnidirectional antenna	16:22:11.309	X			X
(3737)	Modulation interrupt	16:24:53				X
0601	Extend omnidirectional antenna	16:25:05.299	X			X
0601	Extend omnidirectional antenna	16:25:32.798	X			X
0601	Extend omnidirectional antenna	16:25:51.297	X			X
(3737)	Modulation interrupt	16:26:08				X
0510	AESP off	18:31:54.365	X			X
0231	Mode 4 on	18:32:03				X
0227	Mode 2 on	18:34:32.356	X			X
0226	Mode 1 on	18:39:09.840	X			X
0105	XMTR B filament on	18:42:21.329	X			X
0127	Transfer B high power	18:44:24.322	X			X
0106	XMTR B high volt on	18:44:24.822	X			X
0232	Mode 2 on	18:49:34.804	X			X
0506	Mode C on	18:49:47.304	X			X
0704	Cruise mode on	18:50:44.300	X			X
0715	Manual delay mode on	18:50:44.800	X			X
0710	Positive angle maneuver	18:50:45.300	X			X
0714	Sun and roll	18:53:39.290	X			X
0704	Cruise mode on	19:12:57.224	X			X
0716	Manual lockon sun/star	19:13:20.723	X			X
0110	XMTR filament power off	19:21:04.696	X			X
0130	Transfer B low power	19:21:05.196	X			X
0700	Inertial mode on	20:54:02.376	X			X
0704	Cruise mode on	23:51:10				X
0503	Rate 550 bits/sec on	01:38:19				X
0204	A/D coast phase clock rates	(01:38:19.5)				X
0220	A/D SCO and isolation amplifier off	(01:38:20)				X
0215	3.9 kc A/D SCO on	(01:38:20.5)				X
0510	AESP off	02:40:01.216		X	X	X

Table 5.1-5 (continued)

Command Number	Description	Most Accurate Time From All Available Data, Day 151, hr:min:sec	Source			
			Magnetic DSIF Tape	CDS at ETR	CDC Printer Tape	SPAC Command Confirmation Record
0231	Mode 4 on	02:40:08.715		X	X	X
0227	Mode 2 on	02:44:53.680		X	X	X
0232	ESP off	02:47:02.165		X	X	X
0506	Mode C on	02:47:09.164		X	X	X
0510	AESP off	04:14:05.038		X	X	X
0231	Mode 4 on	04:14:13.037		X	X	X
0227	Mode 2 on	04:17:11.516		X	X	X
0226	Mode 1 on	04:20:03.495		X	X	X
0220	A/D SCO and isolation amplifier off	04:26:04.451		X	X	X
0221	Gyro speed signal processing on	04:26:04.951		X	X	X
0222	Select next gyro speed channel	04:27:48.438		X	X	X
0222	Select next gyro speed channel	04:28:30.933		X	X	X
0222	Select next gyro speed channel	04:29:04.929		X	X	X
0223	Gyro speed signal processing off	04:30:03.922		X	X	X
0215	3.9 kc A/D SCO on	04:30:16.920		X	X	X
0232	ESP off	04:33:37.078	X	X	X	X
0506	Mode C on	04:33:44.577	X	X	X	X
0716	Manual lockon sun/star	04:55:35.948	X	X	X	X
0510	AESP off	06:01:15.559	X	X	X	X
0231	Mode 4 on	06:01:21.559	X	X	X	X
0227	Mode 2 on	06:04:08.042	X	X	X	X
0226	Mode 1 on	06:05:27.035	X	X	X	X
0105	XMTR B filament power on	06:06:46.527	X	X	X	X
0127	Transfer B high power	06:08:25.017	X	X	X	X
0106	XMTR B high volt on	06:08:25.517	X	X	X	X
0220	A/D SCO and isolation amplifier off	06:10:23,006	X	X	X	X
0217	33 kc A/D SCO on	06:10:23.506	X	X	X	X
0206	Rate 4400 bits/sec on	06:10:24.006	X	X	X	X
3617	Interlock	06:19:07.954	X	X	X	X
0607	Pressurize vernier system (helium)	06:19:08.454	X	X	X	X
0704	Cruise mode on	06:20:22.947	X	X	X	X
3617	Interlock	06:20:39.945	X	X	X	X
1521	Magnitude (0433) (86.6 degrees)	06:20:40.445	X	X	X	X
0716	Manual lockon sun/star	06:22:08.436	X	X	X	X
0714	Sun and roll	06:30:12.888	X	X	X	X
3617	Interlock	06:34:13.865	X	X		X

Table 5.1-5. (continued)

Command Number	Description	Most Accurate Time From All Available Data, Day 151, hr:min:sec	Source			
			Magnetic DSIF Tape	CDS at ETR	CDC Printer Tape	SPAC Command Confirmation Record
1102	Magnitude (0290) (58.0 degrees)	06:34:14.365	X	X		X
0713	Yaw	06:34:48.861	X	X		X
0521	Propulsion strain gage power on	06:38:05 342	X	X		X
0700	Inertial mode on	06:38:05.842	X	X	X	X
0720	Reset set 4 output	06:38:14.341	X	X	X	X
0605	Unlock roll actuator	06:39:07.836	X	X	X	X
0605	Unlock roll actuator	(06:39:08.336)		X	X	X
0727	Thrust phase power on	06:43:05.312	X	X	X	X
3617	Interlock	06:43:42.809	X	X	X	X
1501	Magnitude (0417) (20.85 seconds)	06:43:43.309	X	X	X	X
3617	Interlock	06:45:03.301	X	X	X	X
0721	Vernier ignition	06:45:03.801	X	X	X	X
0735	Emergency purge vernier engine	06:45:26.299	X	X	X	X
0735	Emergency purge vernier engine	06:45:26.798	X	X	X	X
0735	Emergency purge vernier engine	06:45:27.298	X	X	X	X
0737	Thrust phase power off	06:46:09.794	X	X	X	X
0522	Propulsion strain gage power off	06:46:22.293	X	X	X	X
0503	Rate 550 bits/sec on	06:49:02.277	X	X	X	X
0204	A/D coast phase clock rates	06:49:08.277	X	X	X	X
0220	A/D SCO and isolation amplifier off	06:49:14.276	X	X	X	X
0215	3.9 kc A/D SCO on	06:49:20.776	X	X	X	X
0232	ESP off	06:50:28.769	X	X	X	X
0506	Mode C on	06:50:37.268	X	X	X	X
0710	Positive angle maneuver	06:51:46.261	X	X	X	X
3617	Interlock	06:52:00.760	X	X	X	X
1102	Magnitude (0290)	06:52:01.260	X	X	X	X
0713	Yaw	06:52:55.754	X	X	X	X
0702	Sun acquisition mode on	06:56:28.234	X		X	X
0710	Positive angle maneuver	06:57:04.230	X		X	X
3617	Interlock	06:57:19.229	X		X	X
1521	Magnitude (0433)	06:57:19.728	X		X	X
0714	Sun and roll	06:58:02.224	X		X	X
0510	Auxiliary command off	07:04:30.186	X	X	X	X
0226	Mode 1 on	07:04:38.685	X	X	X	X
0227	Mode 2 on	07:07:06.671	X	X	X	X
0231	Mode 4 on	07:09:12.158	X	X	X	X
0232	ESP off	07:11:53.143	X	X	X	X

Table 5.1-5 (continued)

Command Number	Description	Most Accurate Time From All Available Data, Day 151-152, hr:min:sec	Source			
			Magnetic DSIF Tape	CDS at ETR	CDC Printer Tape	SPAC Command Confirmation Record
0506	Mode C on	07:11:59.142	X	X	X	X
0110	XMTR filament power off	07:12:43.638	X	X	X	X
0130	Transfer B low power	07:12:44.138	X	X	X	X
0512	Auxiliary accelerometer amplifiers off	07:26:39.055	X	X	X	X
0516	Touchdown strain gage power off	07:26:56.054	X	X	X	X
0510	AESP off	(08:32:02.170)		X	X	X
0231	Mode 4 on	(08:32:09.669)		X	X	X
0227	Mode 2 on	(08:36:50.640)		X	X	X
0232	ESP off	(08:41:20.115)		X		X
0506	Mode C on	(08:41:27.115)		X		X
0700	Inertial mode on	09:30:14			X	X
0704	Cruise mode on	12:30:16			X	X
0702	Sun acquisition mode on	13:36:17			X	X
0510	AESP off	16:13:28			X	X
0231	Mode 4 on	16:13:39			X	X
0227	Mode 2 on	16:18:08.491	X		X	X
0323	ESP off	16:27:30.959	X		X	X
0506	Mode C on	16:27:40.959	X		X	X
0510	AESP off	20:32:42.618	X			X
0231	Mode 4 on	20:32:53.617	X			X
0227	Mode 2 on	20:40:01.093	X			X
0232	ESP off	20:43:34.581	X			X
0506	Mode C on	20:43:44.578	X			X
0716	Manual lockon sun/star	23:37:37.984	X			X
0702	Sun acquisition mode on	23:40:56.973	X			X
0510	AESP off	04:05:55.104	X	X	X	X
0231	Mode 4 on	04:06:04.603	X	X	X	X
0227	Mode 2 on	04:08:23.589	X	X	X	X
0232	ESP off	(04:11:45.069)		X	X	X
0506	Mode C on	(04:11:54.069)		X	X	X
0700	Inertial mode on	04:18:39.028	X	X	X	X
0702	Sun acquisition mode on	06:25:57.276	X		X	X
0601	Extend omnidirectional antennas	06:31:17.244	X		X	X
0700	Inertial mode on	07:34:15			X	X
0702	Sun acquisition mode on	07:52:16			X	X
0716	Manual lockon sun/star	09:52:59			X	X
0700	Inertial mode on	09:55:42			X	X
0510	AESP off	09:58:45			X	X
0231	Mode 4 on	09:58:54			X	X
0227	Mode 2 on	10:02:44			X	X

Table 5.1-5 (continued)

Command Number	Description	Most Accurate Time From All Available Data, Day 152-153, hr:min:sec	Source			
			Magnetic DSIF Tape	CDS at ETR	CDC Printer Tape	SPAC Command Confirmation Record
0232	ESP off	10:07:12			X	X
0506	Mode C on	10:07:23			X	X
0317	Auxiliary battery mode on	11:46:34			X	X
0322	High current mode on	12:17:57.166	X		X	X
0320	Restore main battery mode	12:18:31.164	X		X	X
0612	Vernier fuel tank No. 2 thermal control power on	12:37:58.117	X		X	X
0615	Vernier oxidizer tank No. 2 thermal control power on	12:37:58.617	X		X	X
0620	Vernier oxidizer tank No. 3 thermal control power on	12:37:59.117	X		X	X
0702	Sun acquisition mode on	13:05:03.050	X		X	X
0317	Auxiliary battery mode on	15:47:14.150	X		X	X
0510	AESP off	15:48:20.647	X		X	X
0231	Mode 4 on	15:48:30.147	X		X	X
0227	Mode 2 on	15:53:53.634	X		X	X
0232	ESP off	16:02:25.613	X		X	X
0506	Mode C on	16:02:37.113	X		X	X
0323	High current mode off	16:29:45.546	X		X	X
0320	Restore main battery mode	16:32:01.040	X		X	X
0322	High current mode on	16:33:03.038	X		X	X
0317	Auxiliary battery mode on	16:34:18.034	X		X	X
0510	AESP off	18:44:16.028	X		X	X
0231	Mode 4 on	18:44:27.527	X		X	X
0227	Mode 2 on	18:54:04.995	X		X	X
0232	ESP off	19:01:10.471	X		X	X
0506	Mode C on	19:01:19.970	X		X	X
0716	Manual lockon sun/star	19:15:14.424	X		X	X
(3737)	Modulation interrupt	19:20:18.625	X			X
0700	Inertial mode on	19:20:42.905	X		X	X
(3737)	Modulation interrupt	19:20:55.623	X			X
(3737)	Modulation interrupt	19:23:50			X	X
(3737)	Modulation interrupt	19:25:44			X	X
(3737)	Modulation interrupt	19:27:10			X	X
0702	Sun acquisition mode on	21:41:50.932	X		X	X
0510	AESP off	23:19:53.102	X		X	X
0231	Mode 4 on	23:20:01			X	X
0227	Mode 2 on	23:25:43.083	X		X	X
0232	ESP off	23:34:56.552	X		X	X
0506	Mode C on	23:35:07.551	X		X	X
0323	High current mode off	00:10:40.932	X		X	X

Table 5.1-5 (continued)

Command Number	Description	Most Accurate Time From All Available Data, Day 153, hr:min:sec	Source			
			Magnetic DSIF Tape	CDS at ETR	CDC Printer Tape	SPAC Command Confirmation Record
0320	Restore main battery mode	00:12:07.927	X		X	X
0322	High current mode on	00:18:11.406	X		X	X
0317	Auxiliary battery mode on	00:24:04.387	X		X	X
1136	Electronic temperature control on survey camera on	01:16:42.710	X		X	X
0320	Restore main battery mode	01:23:00.189	X		X	X
0716	Manual lockon sun/star	01:51:23.093	X		X	X
0510	AESP off	01:55:24.580	X		X	X
0231	Mode 4 on	01:55:41.579	X		X	X
0232	ESP off	02:00:12.064	X		X	X
0506	Mode C on	02:00:23.063	X		X	X
0510	AESP off	03:13:04			X	
0231	Mode 4 on	03:13:19.145	X		X	
0232	ESP off	03:16:41			X	X
0506	Mode C on	03:16:54.623	X		X	X
0510	AESP off	03:55:23.896	X	X	X	X
0231	Mode 4 on	03:55:33.895	X	X	X	X
0227	Mode 2 on	03:58:55.375	X	X	X	X
0226	Mode 1 on	04:01:07.862	X	X	X	X
0232	ESP off	04:05:42.835	X	X	X	X
0506	Mode C on	04:05:53.833	X	X	X	X
0124	Transponder power off	04:07:13.826	X	X	X	X
0123	Transponder B power on	04:09:15.314	X	X	X	X
1133	Vidicon temperature control survey camera on	05:04:07.989	X	X	X	
0510	AESP on	05:18:06.906	X	X	X	X
0231	Mode 4 on	05:18:14.405	X	X	X	X
0105	XMTR B filament power on	05:18:38.903	X	X	X	X
0127	Transfer B high power	05:20:17.893	X	X	X	X
0106	XMTR B high volt on	05:20:18.393	X	X	X	X
0220	A/D SCO and isolation amplifier off	05:21:08.888	X	X	X	X
0216	7.35 kc A/D SCO on	05:21:19.387	X	X	X	X
0205	Rate 1100 bits/sec on	05:21:27.386	X	X	X	X

Table 5.1-5 (continued)

Command Number	Description	Most Accurate Time From All Available Data, Day 153, hr:min:sec	Source			
			Magnetic DSIF Tape	CDS at ETR	CDC Printer Tape	SPAC Command Confirmation Record
0214	Summing amplifier off	05:21:54.383	X	X	X	X
0211	Phase summing amplifier B on	05:21:54.883	X	X	X	X
0230	Mode 3 on	05:22:11.882	X	X	X	X
0226	Mode 1 on	05:23:02.377	X	X	X	X
0521	Propulsion strain gage power on	05:25:37.861	X	X	X	X
0515	Touchdown strain gage power on	05:26:14.358	X	X	X	X
0517	Touchdown strain gage data channel on	05:26:14.858	X	X	X	X
0124	Transponder power off	05:29:47.838	X	X	X	X
0710	Positive angle maneuver on	05:32:09.823	X	X	X	X
3617	Interlock	05:32:24.321	X	X	X	X
1537	Magnitude (0447) (89.4 degrees)	(05:32:24.821)			X	X
0714	Sun and roll	05:36:46.295	X	X	X	X
3617	Interlock	05:40:44.272	X	X	X	X
1114	Magnitude (0300) (60.0 degrees)	(05:40:44.772)			X	X
0713	Yaw	05:41:47.766	X	X	X	X
3617	Interlock	05:44:29.250	X	X	X	X
1627	Magnitude (0471) (94.2 degrees)	(05:44:29.750)			X	X
0711	Roll	05:45:17.745	X	X	X	X
0723	Reset normal thrust bias	05:50:23.715	X	X	X	X
3617	Interlock	05:51:43.207	X	X	X	X
0435	Magnitude (0157) (7.85 seconds)	(05:51:43.707)			X	X
0227	Mode 2 on	06:00:34			X	X
0720	Reset set 4 output	06:02:14			X	X
3617	Interlock	06:06:27			X	X
0724	Retro sequence mode on	06:06:28			X	X
0613	Vernier lines No. 2 and vernier fuel tank No. 2 thrust chamber power off	06:06:52			X	X
0616	Vernier lines No. 1 and vernier oxidizer tank No. 2 thrust chamber power off	06:06:53			X	X
0621	Vernier lines No. 3 and vernier oxidizer tank No. 3 thrust chamber power off	06:06:53.5			X	X
0625	AMR power on	06:09:57			X	X
0727	Thrust phase power on	06:10:57			X	X
0626	Enable AMR	06:12:57.684		X	X	X
0730	Emergency AMR signal	06:14:38.175		X	X	X
0230	Mode 3 on	06:15:57.667		X	X	X
0207	Presumming amplifier on	06:16:02.666		X	X	X

5.1.4 POSTMISSION DATA PROCESSING

5.1.4.1 Data Flow

All pertinent data originally received from the spacecraft or generated at the DSIF stations is recorded on the multiple channels of FR-1400 magnetic tapes. JPL's telemetry processing system (TPS) operates on the FR-1400 tapes in non-real time to produce a digitized PDP-4 magnetic tape. An alternate method for generating PDP-4 tapes is to transmit information directly to the JPL SFOF area from a DSIF station over a microwave link. This so called SFOF data has been found to be less accurate in time code information and to contain periods of bad data. The DSIF-derived PDP-4 tapes are the most complete input to the Hughes data processing system.

The incoming data is always processed first by the reformatter (RFM) program (Figure 5.1-1), which redesigns the data format and outputs the result on tape. Miscellaneous information such as commands, gyro speed counts, and ground instrumentation samples is separated from the commutated telemetry data. At this point, telemetry data may be run through the special signal processor (SSP) which calibrates all data points to engineering units, tabulates the results, and produces corresponding plots. Alternatively, the data may be processed by the engineering data reduction (EDRS) program. Basically, EDRS averages all analog signals over a time period corresponding to 30 telemetry frames. Calibration and appropriate corrections are applied to each signal. The mean and variance are computed, and noisy samples (values outside a preset interval about the mean) are discarded, in addition to bad parity words. The number of samples eliminated are recorded as an indication of data quality. Then the mean and variance are recomputed.

The individual EDRS output data tapes may be combined into one tape by the MERGE program for ease of handling. If further averaging or algebraic manipulation of the signals of a general nature is desired, the postmission processor (POMP) may be used. The MPLOT program is capable of taking the EDRS or POMP-supplied values and driving a Calcomp plotter to obtain graphs of any signals.

The QUAL program provides a statistical summary of parity error rate from the EDRS information. The effectiveness of power and thermal models may be verified by using the PWR and THM programs on the EDRS data.

5.1.4.2 Detailed Description of Data and Programs

JPL PDP-4 Tape

The PDP-4 tape contains a digital representation of the following types of information:

1) Commands – All commands transmitted to the spacecraft are time coded to the millisecond. Each command and its complement are recorded in command octal.

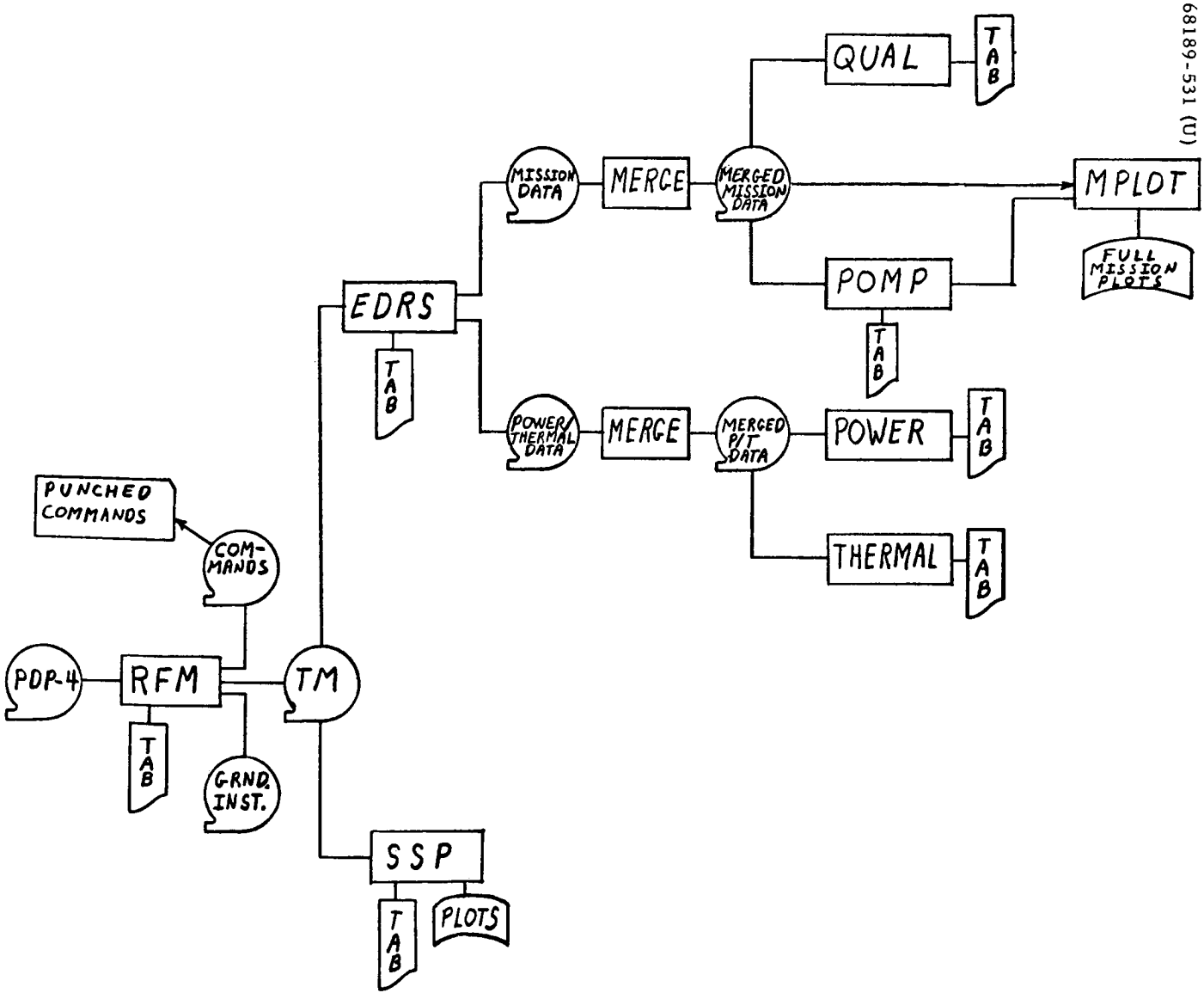


Figure 5.1-1. Postmission Data Processing Flow

2) Gyro speed count data – The gyro speed data, telemetered at certain times with its own SCO, is processed by counting the number of cycles that occur in a fixed-time interval. This count is made every ten seconds.

3) Ground instrumentation data – DSIF receiver parameters (AGC, phase error) are available on the FR-1400 tapes. Every 2 seconds, one of the DSIF parameters or a test voltage is digitized and stored on the PDP-4 tape. For five parameters, the total cycle would require 10 seconds. No time code is provided, however.

4) Telemetry data – All data frames returned from the spacecraft engineering commutators are recorded. Each signal value appears in raw BCD count format, including the transmitted sync words. The frames are individually time coded, with the last word time, to the millisecond, of receipt at the DSIF station. An interesting feature of the time code is that since only five bits are available for the day code, the maximum time that can be recorded is 32 days. This means that a reference base for days must be supplied later on in the data processing.

Reformatter (RFM) Program

The RFM program operates on the PDP-4 tape to produce the following outputs:

RFM-TM Tape. Each record written on the RFM-TM tape corresponds to one frame of telemetry data. The first word in the record contains mode information, as determined from digital status bits. The second and third words contain the start time of the frame in days, hours, minutes, seconds and milliseconds. The remainder of the record is filled with the telemetry values in frame sequence. These raw count values and a parity indicator bit are packed three to a word in command octal format.

A frame of telemetry data found on the PDP-4 tape may be rejected by the RFM program and not written on the RFM-TM tape for the following reasons:

1) Excessive parity errors. This rejection criterion was set at 50 per frame.

2) Incorrect number of words for the indicated mode.

3) Improper sync pattern.

4) Excessive time gap since previous accepted frame. This rejection criterion was set at 30 minutes.

If three successive frames fail to meet the time gap test, the RFM program compares the next frame with the time of the last frame rejected,

instead. If a frame time is less than the one preceding, the data is not rejected. The regressive time is ignored, and the frame is tagged with the preceding frame time plus 1 millisecond.

RFM Tabulations. All rejected frames are printed out with their frame time and rejection cause. A summary of rejection causes and frame acceptance rate is tabulated. The bit rate, inferred by the time between frames, and the telemetry mode are tabulated with times of change. Each of the DSIF ground instrumentation frames is tabulated. All gyro speed count data is printed out. All commands and their complements are tabulated, and written on a tape that may be used to punch cards if desired.

Special Signal Processor (SSP) Program

The SSP program calibrates, processes, and plots data from the RFM-TM tape. Only specifically requested signals, over a fixed time period, are processed. The SSP program extracts all values of the selected signals, including multiple values in a frame, for processing. The time code of a signal is extrapolated from the frame start time to the word of occurrence, using the given nominal bit rate.

Analog signals are converted from raw BCD counts to engineering units, with a fifth order polynomial. Each value of the signal is then tabulated with its extrapolated time (to the millisecond), BCD counts, and engineering value. Bad parity words are displayed with negative BCD counts. Every-point Calcomp plots of either BCD or engineering unit values may be generated.

Digital status bits are examined for changes of state and a change tabulation is formed. Each line of the tabulation contains all the states of the requested digital status bits, to a maximum of 19. A line is generated each time any bit changes, with the time of the word in which the bit occurs. Bad parity is indicated by signal values of 100 or 101, instead of the normal 0 or 1.

Engineering Data Reduction (EDRS) Program

The EDRS program averages, calibrates, and processes telemetry data from the RFM-TM tape. A mean, a variance, and various accuracy and quality tags for each telemetry signal are tabulated. The time periods during which the data is processed are determined primarily from the command sequence.

Normally, the number of frames (N) averaged is 30. However, if a command occurs before a group of 30 frames has been completed, the interval will end there and a new interval will start. For each individual signal which is in mode during the averaging interval, the EDRS program functionally selects specific calibration, correction, and processing subroutines to be performed.

Signal values are converted from raw BCD counts to engineering units by using a fifth order polynomial. The coefficients of the fifth order polynomial generally include a correction to compensate for bias caused by the return harness drop of the subunit involved. In cases where a data channel is temperature sensitive, the nominal set of coefficients is used.

To achieve the highest level of accuracy, various corrections are applied selectively to appropriate data channels. The corrections are as follows:

1) Current calibration – The true value of signals representing spacecraft currents is determined by using the telemetered current calibration channels.

2) Potentiometer calibration – The true value of signals representing positional data is determined by using the telemetered reference voltage value.

3) Unbalanced current calibration – The value of signals on data channels that are affected by unbalanced current flowing at the commutator is determined by using the telemetered unbalanced current value.

4) Quantization – The addition of one-half bit to all data is made so that the quantization error is shifted from +0/-1 bit to ±1/2 bit.

Prior to the computation of means and variances, all samples with bad parity are discarded. The number of samples discarded (P) is tabulated for each signal. The initial means and variances of the data are then computed. Samples whose value is outside a preset interval (2.5σ) about the calculated mean are considered noisy and eliminated. The number of samples thus eliminated is recorded as a quality tag (Q) for the signal. The mean and variance are then recomputed. A statistical measure (AI) of accuracy of the mean is computed using the percent difference between the mean and each sample value in comparison with the expected percent difference for each signal. Also, each mean is compared to predetermined upper and lower limits. Signal mean values falling outside the predetermined range are indicated on the output tabulation.

For data channels containing digital status words, a count of the state of each of the ten bit positions over the interval determines the most likely value (D) of each bit position. If the ratio of the most likely value of the bit is greater than a predetermined amount (3:1), the bit position error indicator (I) is set to zero; if not, the error indicator is set to a one.

As an option, a frame by frame data tabulation may be printed out. This tabulation displays the raw BCD counts of each signal in matrix form, the frame time (to the nearest second) and data mode.

In addition, the EDRS program generates two tapes: a mission data tape, and a power and thermal data tape. The mission data tape contains all the mean, variance, accuracy, quality, and time interval information already discussed. The power and thermal tape contains the required subset of this information for the power and thermal programs.

MERGE Program

Two separate but similar versions of the MERGE program are utilized, each operating on its appropriate input. One program provides the capability for combining the power/thermal tapes; the other version combines the mission data tapes. This consolidation of consecutive tapes permits ease of handling and facilitates the use of the Calcomp to provide continuous and complete mission plots.

Quality Program

Information on the data quality is provided by tabulating statistics on the parity error rate.

MPLOT Program

The function of the MPLOT program is to drive the Calcomp plotter to produce graphs. The formats of the mission data tape, power thermal data tape, and postmission processor (POMP) output tape are compatible with the MPLOT program. Complete transit mission plots for all SC-1 analog signals were generated using the 30 frame averaged mission data tapes.

POMP Program

Several specialized operations performed on the EDRS data by the POMP program are as follows:

1) Additional averaging – Signal parameters may be averaged to any extent desired.

2) Tabulations – Selected groups of signals may be printed out.

3) Algebraic manipulation – Signals may be combined according to any selected algebraic equation. The output will be tabulated and stored on tape, for plotting.

Power and Thermal Management Programs

The power and thermal management programs are used to verify the effectiveness of prediction models in the power and thermal areas.

5.1.4.3 Problems in Processing SC-1 Data

When using the previously mentioned programs on actual SC-1 mission data, some problems were encountered. They are as follows:

1) PDP-4 tape anomalies – On some earlier tapes, the end of file mark was omitted. Very few ground instrumentation frames were found to be on any of the tapes.

2) SSP program faults – The plots were generated without eliminating bad parity points. This proved to be misleading and was remedied by a program change, but not in time to re-do the plots in this report.

3) EDRS program faults – Bad parity on the unbalanced current signals caused a gross miscalculation of the unbalanced current correction applied to some signals. When this was discovered, a program fix was made. Most of the data calculated incorrectly has been run through the corrected version of the EDRS program, but some isolated bad points may still remain on mission plots.

   Another similar problem occurred on signals using a current correction. A number of current signals, namely, EP-4, EP-7, EP-9, EP-11, and EP-16, appear to have negative current spikes just prior to the terminal descent period (approximately day 153:05:16). The cause of this problem was found to be a gross miscalculation of the current calibration correction, due to improper processing of bad-parity current calibration signals.

   Some signals, mostly in the power subsystem, were calibrated using outdated coefficients for the terminal descent period only. This interval thus appears at the wrong level on mission plots.

4) MERGE program problems – After plotting the transit mission graphs, it was discovered that a 5 hour period of coast phase II data from 152:03:00 to 152:08:00 had not been properly merged. The signals for which the gap was most critical were corrected and replotted. The MERGE program now prints out the number of records merged, giving an immediate indication of missing data.

5.1.4.4 Summary of Available Data

Predicted station view periods are given in Table 5.1-6. Table 5.1-7 shows how the magnetic tapes were processed. The primary purpose of the processing was to make the mission plots, plus certain shorter plots of selected signals from the SSP program. Now that this has been accomplished, the tapes used to do this have been released (the master DSIF tapes are still on file at JPL, and any data could be retrieved by processing these again). However, a few tapes have been retained for possible future investigations.

TABLE 5.1-6. PREDICTED VIEW PERIOD SUMMARY

Station	Event	May-June 1966	GMT, hr:min:sec	Station	Event	May-June 1966	GMT, hr:min:sec
DSS 51, Johannesburg	5-degree elevation rise	30	15:04:30	DSS 42, Tidbinbilla	5-degree elevation rise	1	06:29:44
DSS 11, Goldstone	5-degree elevation rise	31	02:08:40	DSS 11, Goldstone	5-degree elevation set	1	11:08:04
DSS 51, Johannesburg	90-degree hour angle set	31	02:16:36	DSS 51, Johannesburg	270-degree hour angle rise	1	15:14:32
DSS 42, Tidbinbilla	5-degree elevation rise	31	05:59:23	DSS 42, Tidbinbilla	5-degree elevation set	1	19:36:12
DSS 11, Goldstone	5-degree elevation set	31	10:33:47	DSS 11, Goldstone	5-degree elevation rise	2	02:25:13
DSS 51, Johannesburg	270-degree hour angle rise	31	15:00:04	DSS 51, Johannesburg	90-degree hour angle set	2	03:09:12
DSS 42, Tidbinbilla	5-degree elevation set	31	19:25:16	DSS 42, Tidbinbilla	5-degree elevation rise*	2	06:38:55
DSS 11, Goldstone	5-degree elevation rise	1	02:23:28	DSS 11, Goldstone	5-degree elevation set*	2	11:25:08
DSS 51, Johannesburg	90-degree hour angle set	1	02:58:45				

*View periods of moon's center.

The merged mission tape (No. 3932) contains all EDRS data for the entire flight. Any RFM output tapes listed in Table 5.1-6 have been retained, including those for launch, midcourse, and terminal descent. Experience will determine what amount of data should be saved and at what level in the processing.

5.1.4.5 Calibration Coefficients

Various sets of coefficients were used to convert telemetry information to engineering units. A tabulation of counts-to-engineering-units type coefficients is included in the "Surveyor SC-1 Spacecraft, Telemetry Calibration Handbook, 17 June 1966." The EDRS program operated exclusively on the fifth order coefficients shown in the handbook. Where more than one set of coefficients is applicable to a signal, the EDRS program used only the set specified in Table 5.1-8, which gives the coefficient parameter associated with that set.

The SSP program is not limited to one particular set of coefficients per signal. Therefore, some signals were calibrated at different times, using different sets of coefficients. For the most part, the fifth order coefficients in the handbook were used. In addition, the coefficients in Table 5.1-9 were also used at appropriate times by the SSP program.

TABLE 5.1-7. SURVEYOR I PDP-4 TAPES

Station	Start Time, day:hr:min	End Time, day:hr:min	Number of Frames	Percent Good	RFM Output Tape Number	EDRS Run Available
Transit Phase						
SFOF	150:13:50	150:19:15	6,396	93.4	765	
Antigua	150:14:47	150:14:53	127	90.0		
Yankee	150:14:54	150:14:59	–	–		
DSS 51, Johannesburg	150:15:00	150:18:44	10,288	99.3	252	
DSS 51, Johannesburg	150:18:09	150:22:07	12,007	99.4		
DSS 51, Johannesburg	150:21:40	151:01:33	11,617	99.4		
DSS 51, Johannesburg	151:00:58	151:02:18	2,953	98.1		
DSS 11, Goldstone	151:02:14	151:04:57	3,900	98.0		
DSS 11, Goldstone	151:04:32	151:08:19	14,027	99.5	4093	
SFOF	151:05:46	151:07:02	10,139	99.8	3930	
DSS 42, Canberra	151:08:10	151:12:10	5,981	99.2		
DSS 42, Canberra	151:11:46	151:15:30	5,712	99.8		
DSS 51, Johannesburg	151:14:59	151:17:05	3,170	99.3		
DSS 51, Johannesburg	151:16:51	151:20:50	5,904	99.0		
DSS 51, Johannesburg	151:20:24	152:00:12	5,623	98.6		
DSS 51, Johannesburg	151:23:45	152:02:57	4,646	98.2		
DSS 11, Goldstone	152:02:24	152:04:50	2,570	72.9		
DSS 11, Goldstone	152:04:24	152:08:05	4,875	85.7		
DSS 42, Canberra	152:08:42	152:12:30	5,504	97.8		
DSS 42, Canberra	152:12:06	152:15:56	5,698	98.5		
DSS 42, Canberra	152:15:37	152:19:35	5,909	97.3		
DSS 51, Johannesburg	152:17:27	152:21:07	5,175	91.7		
DSS 51, Johannesburg	152:20:46	153:00:31	5,284	91.5		
DSS 51, Johannesburg	153:00:08	153:03:09	4,128	89.6		
DSS 11, Goldstone	153:02:23	153:04:36	2,467	41.1		
DSS 11, Goldstone	153:04:48	153:05:55	2,740	87.4		

Table 5. 1-7 (continued)

Station	Start Time, day:hr:min	End Time, day:hr:min	Number of Frames	Percent Good	RFM Output Tape Number	EDRS Run Available
SFOF	153:05:17	153:07:30	7,285	83.3	312	
DSS 14, Goldstone (210 minutes)	153:05:20	153:06:19	3,696	98.8		
DSS 11, Goldstone	153:05:20	153:06:22	3,938	99.6	SUR-2	
DSS 42, Canberra	153:06:45	153:08:08	1,494	98.9		
DSS 42, Canberra	153:08:08	153:11:52	8,404	92.2		
Lunar Phase						
DSS 11, Goldstone	154:06:05	154:10:03	3,269	18.0	973	X
DSS 11, Goldstone	155:07:35	155:11:34	4,147	77.7	726	X
DSS 42, Canberra	155:11:06	155:14:53	10,679	99.4	3391	X
DSS 42, Canberra	155:14:22	155:18:18	12,589	99.4	3121	X
DSS 42, Canberra	156:14:06	156:18:03	10,933	99.0	3099	X
DSS 42, Canberra	156:17:36	156:21:33	12,378	99.9	2597	X
DSS 51, Johannesburg	157:03:04	157:06:40	10,902	99.6	3402	
DSS 11, Goldstone	157:06:21	157:09:19	5,294	98.8	651	
DSS 11, Goldstone	157:09:24	157:13:26	4,100	97.4	3847	
DSS 51, Johannesburg	158:04:27	158:07:32	1,286	98.2	2499	X
DSS 11, Goldstone	158:07:05	158:10:11	2,142	96.5	2136	X
DSS 11, Goldstone	159:10:03	159:13:59	9,570	–	2950	X
DSS 11, Goldstone	159:13:33	159:16:59	1,600	–	2741	
DSS 11, Goldstone	160:14:03	160:17:58	10,738	99.2	1283	X
DSS 11, Goldstone	161:15:40	161:19:06	4,514	99.0	3030	X
DSS 11, Goldstone	162:10:03	162:14:00	11,460	–	1875	
DSS 11, Goldstone	163:09:32	163:12:45	2,483	99.0	2406	X
DSS 42, Canberra	164:20:02	165:00:00	7,723	99.3	2294	
DSS 11, Goldstone	165:14:16	165:18:02	1,483	94.9	2223	
DSS 42, Canberra	166:20:10	167:04:24	323	86.1	1945	
DSS 51, Johannesburg	167:02:45	167:11:16	736	88.6	4075	

TABLE 5.1-8. DESIGNATION OF NOMINAL COEFFICIENTS USED BY EDRS PROGRAM

Signal	Coefficient Parameter
D-1	75° F
D-3	75° F
D-7	75° F
D-8	75° F
D-9	75° F
D-10	75° F
D-16	75° F
D-17	75° F
FC-14	1.0 Canopus
FC-35	40,000 feet maximum (above 1000 feet)
FC-49	deg/sec
R-2	40.0 db
R-3	40.0 db
R-4	40.0 db
R-5	40.0 db
R-14	3.0 microseconds
R-29	3.0 microseconds

TABLE 5. 1-9. VOLTS-TO-ENGINEERING-UNITS COEFFICIENTS

Signal	A0	A1	A2	A3	A4	A5	Parameter
D-9	-0. 172425E2	-0. 145614E3	0.868166E2	-0. 161035E2	-0. 197193E1	0	90° F
D-10	-0. 450110E2	-0. 744651E2	0. 264766E1	0. 360043E2	-0. 154552E2	0	90° F
R-2	-0. 105001E3	0. 106448E3	-0. 104431E3	0. 539346E2	-0. 136441E2	0. 133269E1	40. 0 db
R-2	-0. 107752E3	0. 498909E2	-0. 367542E2	0. 163145E2	-0. 383114E1	0. 364400E0	60. 0 db
R-2	-0. 159821E3	0. 162208E3	-0. 178748E3	0. 980371E2	-0. 256522E2	0. 256245E1	80. 0 db
R-3	-0. 929737E2	0. 651452E2	-0. 482618E2	0. 193637E2	-0. 384293E1	0. 296973E0	40. 0 db
R-3	-0. 127217E3	0. 937583E2	-0. 831543E2	0. 392711E2	-0. 910559E1	0. 813034E0	65. 0 db
R-3	-0. 156490E3	0. 981440E2	-0. 822293E2	0. 363283E2	-0. 790503E1	0. 667161E0	90. 0 db
R-4	-0. 917969E2	0. 585020E2	-0. 403973E2	0. 153563E2	-0. 292476E1	0. 219493E0	40. 0 db
R-4	-0. 114616E3	0. 490261E2	-0. 289041E2	0. 934719E1	-0. 150852E1	0. 956364E1	65. 0 db
R-4	-0. 157749E3	0. 985046E2	-0. 783135E2	0. 322805E2	-0. 649889E1	0. 506474E0	90. 0 db
R-5	-0. 956234E2	0. 664903E2	-0. 489977E2	0. 196649E2	-0. 392885E1	0. 305915E0	40. 0 db
R-5	-0. 123502E3	0. 749514E2	-0. 571207E2	0. 228524E2	-0. 443122E1	0. 329324E0	65. 0 db
R-5	-0. 133013E3	0. 241055E2	-0. 707758E0	-0. 464249E1	0. 165037E1	-0. 170174E0	90. 0 db

5.2 THERMAL SUBSYSTEMS

5.2.1 INTRODUCTION

The Surveyor thermal control system provides the proper temperature environment for the various units and subsystems throughout the transit and lunar phases of operation. The thermal control systems are unique in that the spacecraft requirements of soft landing and a jettisonable retro engine dictate an "open" rather than the conventional closed thermal system. Rather than encapsulate the Surveyor in a temperature-controlled shroud during transit from which the base temperatures of all units are biased, each unit is exposed to the deep space environment and must be individually temperature controlled. Thus the concept evolved of multiple closed thermal systems mounted on a skeletal tubular spaceframe. The spacecraft, in addition, was required to survive the lunar day environment with maximum surface temperatures of 260° F in conjunction with solar irradiation and the lunar night environment with surface temperatures of -245° F.

Four types of thermal control systems are employed on the vehicle as well as thermal systems which are combinations of the basic types. The four kinds of temperature control systems are as follows:

1) The passive thermal system controls temperatures exclusively with wavelength selective finishes that exhibit the desired solar absorptance and infrared emittance properties. This method of temperature control is used for the most part on spacecraft subsystems which dissipate little or no electrical energy and which are illuminated by the sun.

2) The active thermal control system employs electrical heaters to maintain desired temperature levels. This type of thermal control is used on systems that cannot rely solely on solar energy for temperature control.

3) The main retro and the vernier propellant tanks make use of a large heat capacity in solid and liquid propellant in conjunction with radiation and conduction isolation to reduce energy losses. These subsystems continually cool down during transit but so slowly that temperatures are above the lower limit at the end of transit.

PRECEDING PAGE BLANK

4) Various methods of temperature control are used on subsystems that dissipate electrical energy in the form of heat. Compartments A and B use a mechanical device, the thermal switch, in conjunction with superinsulation to control temperature. The bimetallically-operated switch controls the primary heat conduction path.

   The television system uses a combination of a passive system for survival, an active system for preconditioning prior to use, and a passive heat capacity system during transient operation for temperature control. The RADVS system uses a passive thermal technique to maintain temperatures in the desired range at the time of electrical activation and heat capacity for thermal control during operation.

Temperature control throughout all phases of the mission was excellent. Preflight transit temperature predictions agreed very closely with flight results. Unlimited operation of the spacecraft was possible throughout the first lunar day. Judicious use was made of the solar panel and planar array antenna to achieve shadowing of critical telecommunications compartments simultaneously with the performance of their prime functions of battery charging and high gain radio transmission.

Sole anomalies were the less than optimum auxiliary battery storage temperature during transit and some of the thermal switches not opening prior to spacecraft shutdown during the first lunar night. Modifications to the prescribed mission sequence in real time allowed the auxiliary battery to be brought within the required temperature range at the start of the terminal descent.

The flight temperatures in transit have allowed a calibration of the solar thermal vacuum facility in which the final vehicle flight acceptance test is performed. The integrity of all the thermal control systems was verified and demonstrated in all environmental phases of the mission. Experiments were performed from which it was possible to estimate the infrared emission of the lunar surface and to compare these results with ground based measurements. Finally, vital thermal information was gathered from which a liftoff and translation on the lunar surface could be planned.

5.2.2 SUMMARY OF THERMAL EVENTS AND RESULTS

The thermal control system has been divided into a number of areas for analysis, as follows:

1) Compartments A and B

2) Auxiliary battery

3) Antenna and solar panel positioner

4) Spaceframe and crushable block 3 heat shield

5) Legs

6) Shock absorbers

7) Thrust chamber assemblies

8) Vernier propellant tanks

9) Propellant lines

10) Helium tank

11) Main retro engine

12) Flight control electronics and Canopus sensor

13) Roll actuator

14) Nitrogen tank

15) Attitude gas jet

16) RADVS system

17) Altitude marking radar

18) Television system

19) Determination of lunar surface temperature

20) Surveyor liftoff and translation

21) Calibration of STV test facility for flight conditions

Each of these will receive detailed treatment in Section 5.2.3.

In Table 5.2-1, times for Mission A events which have a major effect on the thermal systems are given. Table 5.2-2 shows a comparison between predicted and actual transit coast phase temperatures and maximum and minimum temperatures on the spacecraft in the first lunar day. Temperature histories in transit for all spacecraft sensors are shown in Figures A-1 through A-64 and are given for the first lunar day in Figures B-1 through B-23.

TABLE 5.2-1. MISSION A MAJOR EVENTS AND TIMES

A. Transit

Day	GMT, hr:min:sec	Day	PDT, hr:min	From Launch, hr:min	Event
150	14:41	150	7:41	00:0	Launch
5/30/66	14:53	5/30/66	7:53	00:12	XMTR B high power on (HP-on)
	15:00		08:00	00:19	Spacecraft sun acquisition
	15:20		08:20	00:39	XMTR B high power off (HP-off) (DSIF acquired)
	18:44		11:44	04:03	XMTR B HP-on (star verification)
	18:54		11:54	04:13	Sun and roll
	19:21		12:21	04:40	XMTR B HP-off
	20:54		13:54	06:13	Gyro drift check
	23:51		16:51	09:10	End gyro drift check
151	04:26:4		21:26	13:45	Gyro speed check
5/31	04:30:4		21:30	13:49	End gyro speed check (midcourse phase)
	06:08		23:08	15:27	XMTR B HP-on
	06:19		23:19	15:38	Vernier pressurization
	06:30		23:30	15:49	Premidcourse sun and roll
	06:34		23:34	15:53	Premidcourse yaw (-58 degrees)
	06:45:3		23:45	16:04	Midcourse thrust
	06:45:26		23:45	16:04	End midcourse thrust (20.8 seconds)
	06:52		23:52	16:11	Postmidcourse yaw (58 degrees)
	06:58		23:58	16:17	Postmidcourse sun and roll
	07:12	151 5/31	00:12	16:31	XMTR B HP-off (end midcourse)
	09:30		02:30	18:49	Gyro drift check
	12:30		05:30	21:49	End gyro drift check

Table 5.2-1 (continued)

Day	GMT, hr:min:sec	Day	PDT, hr:min	From Launch, hr:min	Event
152	04:19	151	21:19	37:38	Gyro drift check
6/1	06:25	5/31	23:26	39:45	End gyro drift check
	7:34	152	00:34	40:53	Gyro drift check
	9:52	6/1	02:52	43:11	End gyro drift check (power mode cycling phase)
	12:17:57		05:18	45:37	Auxiliary battery high current mode on
	12:18:31		05:19	45:38	Main battery mode
	12:38		05:38	45:57	Vernier thermal control on
	16:33:3		09:33	49:52	Main battery high current on
	16:34:18		09:34	49:53	Auxiliary battery on
	19:21		12:21	52:40	Gyro drift check
	21:42		14:42	55:01	End gyro drift check
153	00:12		17:12	57:31	Main battery mode, high current off
6/2	00:18		17:18	57:37	High current mode on
	00:24		17:24	57:43	Auxiliary battery mode on
	01:17		18:17	58:36	Survey TV electronics, thermal control on
	01:23		18:23	58:42	Main battery mode on
	05:04		22:04	62:23	Survey TV vidicon, thermal control on (terminal descent)
	05:20		22:20	62:39	XMTR B HP-on
	05:37		22:37	62:56	Sun and roll (89.3 degrees)

Table 5.2-1 (continued)

Day	GMT, hr:min:sec	Day	PDT, hr:min	From Launch, hr:min	Event
153	05:42	152	22:42	63:01	Yaw (60 degrees)
6/2	05:45	6/1	23:45	63:04	Roll (94 degrees)
	06:07		23:07	63:26	Thermal control power off for: vernier lines 2, 1, 3, vernier fuel tank 2, vernier oxidizer tanks 2, 3
	06:09:57		23:10	63:29	AMR power on
	06:10:57		23:11	63:30	Thrust phase power on
	06:12:57		23:13	63:32	AMR enable
	06:17:37		23:18	63:37	Touchdown

B. Lunar Operations

Day	GMT, hr:min:sec	Day	PDT, hr:min	From Touch-down, hr:min	Event
153	06:18:15	152	23:18	0:0	Thrust phase power off
6/2	06:18:49	6/1	23:19	00:01	RADVS power off
	06:18:49		23:19	00:01	Flight control power off
	06:27		23:27	00:09	Dump helium
	06:27		23:27	00:09	AMR heaters off
	06:41		23:41	00:23	Auxiliary battery mode on, high current mode off
	06:45		23:45	00:27	Survey camera power on
	06:48		23:48	00:38	Survey camera power off
	07:08	153	00:08	00:50	XMTR B HP-on
	07:19	6/2	00:19	01:01	XMTR B HP-off
					XMTR A HP-on
	08:10		01:10	01:52	Step panels to postlanding configuration
	08:58		01:58	2:40	Main battery mode
	09:03		02:03	2:45	XMTR A HP-off
	09:17		02:17	2:59	Reposition A/SPP
	09:19		02:19	3:01	

Table 5.2-1 (continued)

Day	GMT, hr:min:sec	Day	PDT, hr:min	From Touch-down, hr:min	Event
153	09:33	153	02:33	3:15	Picture taking phase
6/2	11:18	6/2	4:18	5:00	
	12:13		05:13	5:55	Reposition A/SPP
	12:53		05:53	6:35	
	13:15		06:15	6:57	Reposition A/SPP
	13:17		06:17	6:59	
	13:41		06:41	7:23	Survey TV electronics thermal control off
	13:54		06:54	7:36	Survey TV vidicon thermal control off
154	03:37		20:37	21:19	Picture taking phase – XMTR A on high power periodically
6/3	thru		thru	thru	
	11:59	154	4:59	29:41	
155	02:58	6/3	19:58	44:40	Reposition A/SPP
6/4	04:06		21:06	45:48	Picture taking phase
	04:32		21:32	46:14	
	04:50		21:50	46:32	Reposition A/SPP
	05:10		22:10	46:52	Begin picture taking phase
	06:12		23:12	47:54	Survey camera power on
	11:04	155	04:04	52:46	End picture taking phase
	11:04	6/4	04:04	52:46	Survey camera power off
	11:36		04:36	53:18	Flight control power on
	11:40		04:40	53:22	Yaw
	11:42		04:42	53:24	Picture taking phase
	11:48		04:48	53:30	
	11:49		04:49	53:31	Flight control power off

Table 5.2-1 (continued)

Day	GMT, hr:min:sec	Day	PDT, hr:min	From Touch-down, hr:min	Event
155	12:01	155	05:01	53:43	Flight control power on
6/4	12:03	6/4	05:03	53:45	Yaw
	12:03 }		05:03 }	53:45	Picture taking phase
	12:11 }		05:11 }	53:53	
	12:11		05:11	53:53	Flight control power off
	12:54		05:54	54:36	Flight control power on
	12:56		05:56	54:38	Yaw
	12:58		05:58	54:40	All flight control power off
	15:58 }		08:58 }	57:40	Reposition A/SPP
	16:52 }		09:52 }	58:34	
156	6:05 }		23:05 }	71:47	Picture taking phase
6/5	13:01 }	156	06:01 }	78:43	
	17:12 }	6/5	10:12 }	82:54	Reposition A/SPP
	18:29 }		11:29 }	84:11	
157	06:41 }		23:41 }	96:23	Reposition A/SPP
6/6	07:07 }	157	00:07 }	96:49	
	07:21 }	6/6	00:21 }	97:03	Picture taking phase
	09:36 }		02:36 }	99:18	
	09:37		02:37	99:19	Flight control power on
	09:39		02:39	99:21	Yaw
	09:40		02:40	99:22	XMTR A HP-on

Table 5.2-1 (continued)

Day	GMT, hr:min:sec	Day	PDT, hr:min	From Touch-down, hr:min	Event
					(TV Gas Jet Experiment)
157 6/6	09:45	157 6/6	02:45	99:27	All flight control power off
	09:46		02:46	99:28	XMTR A HP-off
	10:06		3:06	99:48	Picture taking phase
	14:34		7:34	104:16	
	22:56		15:56	111:38	Reposition A/SPP
	23:05		16:05	111:47	
158 6/7	04:40		21:40	117:22	Reposition A/SPP
	05:54		22:54	118:36	
	06:28		23:28	119:10	LUNAR NOON first day
	07:46	158 6/7	00:46	120:28	Reposition A/SPP
	09:04		02:04	121:46	
	09:20		02:20	122:02	Reposition A/SPP
	09:36		02:36	122:18	
	09:38		02:38	122:20	Picture taking phase
	10:25		03:25	123:07	
	10:38		03:38	123:20	Reposition A/SPP
	10:51		03:51	123:33	
	11:02		04:02	123:44	Picture taking phase
	15:42		08:42	128:24	
	16:11		09:11	128:53	Reposition solar panel
159	13:07	159	06:07	149:49	Reposition solar panel
6/8	13:28	6/8	06:28	150:10	Reposition A/SPP
	16:40		09:40	153:22	
160 6-9	11:45	160 6/9	04:45	172:27	Reposition A/SPP
	12:55		05:55	173:37	(Lunar telecommunications test phase to 17:02 GMT)

Table 5.2-1 (continued)

Day	GMT, hr:min:sec	Day	PDT, hr:min	From Touch-down, hr:min	Event
160	14:16	160	07:16	174:58	XMTR A HP-on
6/9	14:31	6/9	07:31	175:13	Basic bus accelerometer amps and channels on
	14:36		07:36	175:18	Basic bus accelerometer amps and channels off
	14:36		07:36	175:18	XMTR A HP-off
	14:48		07:48	175:30	XMTR A HP-on
	14:58		07:58	175:40	XMTR A HP-off
161	09:15	161	2:15	193:57	Picture taking phase
6/10	16:43	6/10	9:43	201:25	
	17:00		10:00	201:42	Reposition A/SPP
	17:41		10:41	202:23	
	17:48		10:48	202:30	Picture taking phase
	18:42		11:42	203:24	
162	09:44	162	02:44	218:26	Picture taking phase
6/11	15:00	6/11	08:00	223:42	
	15:10		08:10	223:52	Reposition A/SPP
	15:20		08:20	224:02	
	15:55		08:55	224:37	Picture taking phase
	17:16		10:16	225:58	
	22:23		15:23	231:05	Reposition solar panel
163	00:39		17:39	233:21	Reposition solar panel
6/12	03:49		20:49	236:31	Reposition solar panel
	07:22	163	00:22	240:04	Reposition solar panel

Table 5.2-1 (continued)

Day	GMT, hr:min:sec	Day	PDT, hr:min	From Touch-down, hr:min	Event
163	10:00	163	03:00	242:42	Reposition solar panel
6/12	10:11	6/12	03:11	242:53	
	10:17		03:17	242:59	Picture taking phase
	16:56		09:56	249:38	
	16:59		09:59	249:41	Reposition A/SPP
	17:09		10:09	249:51	
	18:26		11:26	251:08	Picture taking phase
	18:59		11:59	251:41	
	22:27		15:27	255:09	Reposition solar panel
164	00:19		17:19	257:01	Reposition solar panel
6/13	01:59		18:59	258:41	Reposition solar panel
	03:53		20:53	260:35	Reposition solar panel
	05:00		22:00	261:42	Reposition solar panel
	10:33	164	03:33	267:15	Survey camera power on
	10:34	6/13	03:34	267:16	Survey camera power off
					Survey camera video temperature control on
	11:07		04:07	267:49	Survey camera video temperature control off
	11:13		04:13	267:55	Reposition solar panel
	11:16		04:16	267:58	
	11:22		04:22	268:04	Begin picture taking phase
	11:23		04:23	268:05	Survey camera video temperature control on
	17:36		10:36	274:18	End picture taking phase
	18:30		11:30	275:12	Reposition solar panel
	18:37		11:37	275:19	Picture taking phase
	21:34		14:34	278:16	
	21:52		21:52	278:34	Survey camera electronics temperature control on
	22:13		15:13	278:55	Reposition A/SPP
	22:18		15:18	279:00	

Table 5.2-1 (continued)

Day	GMT, hr:min:sec	Day	PDT, hr:min	From Touch-down, hr:min	Event
165	01:46	164	18:46	282:28	Compartment A heater on
6/14	01:57	6/13	18:57	282:39	Reposition solar panel
	02:13		19:13	282:55	
	10:48	165	03:48	291:30	Compartment A heater off
	11:05	6/14	04:05	291:47	Picture taking phase—lunar
	16:40		09:40	297:22	Sunset occurred about 16:38 GMT
	16:57		09:57	297:39	Reposition A/SPP
	17:06		10:06	297:48	
	17:09		10:09	297:51	Survey camera video temperature control and electronics temperature control off
	17:10		10:10	297:52	
	17:33		10:33	298:15	Reposition A/SPP
	18:12		11:12	298:54	Non-essential loads off
					(Begin SIESTA Phase)
	21:10		14:10	301:52	Compartment B heater on
166	01:01		18:01	305:43	Compartment B heater off
6/15	05:57		22:57	310:39	Compartment B heater on
	07:16	166	00:16	311:58	Compartment B heater off
	09:47	6/15	02:47	314:29	Compartment B heater on
	10:57		03:57	315:39	Compartment B heater off
	13:33		06:33	318:15	Compartment B heater on
	14:43		07:43	319:25	Compartment B heater off
	17:00		10:00	321:42	Compartment B heater on
	17:58		10:58	322:40	Compartment B heater off
	22:26		15:26	327:08	Compartment B heater on
	22:31		15:31	327:13	Compartment B heater off

Table 5.2-1 (continued)

Day	GMT, hr:min:sec	Day	PDT, hr:min	From Touch-down, hr:min	Event
167	00:21	166	17:21	329:03	Compartment B heater on
6/16	01:22	6/15	18:22	330:04	Compartment B heater off
	03:11		20:11	331:53	Compartment B heater on
	04:13		21:13	332:55	Compartment B heater off
	06:22		23:22	335:04	Compartment B heater on
	07:24	167	00:24	336:06	Compartment B heater off
	08:50	6/16	01:50	337:32	Compartment B heater and XMTR A HP-on
	08:52		01:52	337:34	Compartment B heater and XMTR A HP-off
	08:54		01:54	337:36	Compartment B heater and XMTR A high power on
	08:56		01:56	337:38	Compartment B heater and XMTR A high power off
	08:57		01:57	337:39	Compartment B heater and XMTR A high power on
	08:59		01:59	337:41	Compartment B heater and XMTR A high power off
	09:00		02:00	337:42	Compartment B heater and XMTR A high power on
	09:02		02:02	337:44	Compartment B heater and XMTR A high power off
	09:03		02:03	337:45	Compartment B heater and XMTR A high power on
	09:05		02:05	337:47	Compartment B heater and XMTR A high power off
	11:02		04:02	339:44	Compartment B heater on
	11:34		04:34	340:16	Compartment B heater off
	13:16		06:16	341:58	Compartment B heater on
	14:14		07:14	342:56	Compartment B heater off
	16:32		09:32	345:14	Compartment B heater on
	17:30		10:30	346:12	Compartment B heater off
	20:24)		13:24)	349:06	LUNAR NIGHT shutdown
	20:31)		13:31)	349:13	
180	About	180	About		Second LUNAR DAY
6/29	10:58	6/29	03:58	651:40	sunrise (approximately)

TABLE 5.2-2. SC-1 THERMAL CONTROL SUBSYSTEM FLIGHT PERFORMANCE

Subsystem/Element	Sensor Code	Mission A Steady-State Transit Temperature, °F		Maximum Lunar Phase Temperature[1]	
		Preflight Prediction	Actual	°F	Time[2], day:hr:min:sec
Vehicle					
Compartment A					
Transmitter A	D-13	76	68	185	153:08:56:39
Transmitter B	D-14	78	68	106	153:08:56:39
Main battery	EP-8	98	97	118	153:12:31:59
Battery charge regulator	EP-34	125	123	142	153:10:11:20
Top thermal tray	V-15	78	70	110	153:08:56:39
Bottom thermal tray	V-16	98	93	118	153:10:11:20
Radiator 5	V-20	36	42	78	153:08:56:39
Radiator 2	V-47	30	35		
Radiator 8	V-25	30	44	88	153:08:56:39
Outer canister (outboard)	V-18	-110	- 85		
Shell (inside)	V-17	102	92		
Thermal switch (inside)	V-19	79	66		
Compartment B					
Boost regulator	EP-13	110	115	132	160:08:48:40
Top thermal tray	V-21	97	93	118	160:08:48:40
Botton thermal tray	V-22	102	98	124	160:08:48:40
Radiator 4	V-24	75	67	99	160:08:48:40
Radiator 1	V-45	71	73	104	160:08:18:30
Radiator 5	V-46	71	66	96	160:08:18:30
Outer canister (outboard)	V-23	- 78	- 70	111	159:08:22:48
Thermal switch 4 (inside)	V-26	93	88		
Auxiliary battery	EP-26	60	35	155	156:12:00:52
A/SPP mechanism					
Solar panel	EP-12	118	109	217	158:01:07:14
Planar array	M-8	- 60	- 50	228	158:07:02:10
Solar panel axis motor	M-10	40	60	218	158:07:02:10
Elevation axis motor	M-12	- 86	1	190	158:07:02:10
Mast	V-34	-114	- 84	130	160:12:28:29
Landing system					
Crushable block 3	V-44	- 50	- 62	189	154:06:45:52
Leg 2	V-31	85	83	148	158:03:29:53
Shock 1	V-30	90	84	193	159:15:50:02
Shock 2	V-32	88	72	171	157:12:07:44
Shock 3	V-33	90	82	175	157:12:20:38
Spaceframe					
Upper spaceframe near leg 1	V-27	73	60	138	160:15:38:13
Lower spaceframe under compartment B	V-28	46	48	190	162:11:26:12
Upper spaceframe near leg 2	V-35	- 70	- 79	125	158:13:42:40
Lower spaceframe under compartment A	V-36	- 21	- 27	166	160:15:38:15

Table 5.2-2 (Continued)

Subsystem/Element	Sensor Code	Mission A Steady-State Transit Temperature, °F		Maximum Lunar Phase Temperature[1]	
		Preflight Prediction	Actual	°F	Time[2], day:hr:min:sec
Retro attach point 1	V-37	46	39	222	162:09:24:49
Retro attach point 2	V-38	-21	-36	175	155:19:51:03
Retro attach point 3	V-39	46	44	185	156:06:51:35
Flight control					
Flight control electronics					
Electronic board 1	FC-44	100	90	192	158:01:07:41
Electronic board 2	FC-45	135	124	200	155:13:12:00
Canopus sensor	FC-47	90	78	180	156:12:00:34
Inertial reference unit gyros					
Roll gyro	FC-46	178*	170*	167	155:13:12:00
Pitch gyro	FC-54	175*	175*	188	155:13:12:00
Yaw gyro	FC-55	177*	180*	170	155:13:12:00
Roll actuator	FC-71	98	79	224	160:16:56:45
Attitude control nitrogen tank					
Lower inboard	FC-48	71	45	173	155:06:20:17
Gas jet	FC-70	87	88	205	155:12:03:51
Propulsion					
Thrust chamber assemblies					
1	P-7	76	59	244	160:08:50:52
2	P-10	81	72	229	158:16:00:36
3	P-11	62	59	227	156:15:15:18
Helium tank	P-17	75	60	145	160:08:47:40
Propellant lines					
Oxidizer line 1	P-8	35	23 to 29	221	161:08:44:38
Oxidizer line 2	P-4	20 to 27	21 to 26	203	157:18:26:08
Oxidizer line 3	P-9	30	21 to 26	184	157:18:26:09
Propellant tanks		Launch	Launch		
Oxidizer tank 1	P-15	74 45**	75 41**	173	162:15:25:47
Fuel tank 1	P-13	73 48**	76 52**	190	162:17:21:49
Oxidizer tank 2	P-16	74 35**	77 24**	166	157:01:26:05
Fuel tank 2	P-5	74 30**	75 34**	164	158:16:00:36
Oxidizer tank 3	P-6	73 45**	79 40**	154	157:10:55:52
Fuel tank 3	P-14	73 51**	76 53**	171	158:12:14:55
Main retro	P-3	74 67**	74 64**		
	P-12	74 36**	74 43**		
	P-22	74-222**	74-124**		

Table 5.2-2 (Continued)

Subsystem/Element	Sensor Code	Mission A Steady-State Transit Temperature, °F		Maximum Lunar Phase Temperature[1]	
		Preflight Prediction	Actual	°F	Time[2], day:hr:min:sec
Radar					
KPSM	R-8	22	12	225	162:09:21:55
SDC	R-9	53	56	149	160:09:52:09
V/S preamplifier	R-10	32	22	235	161:18:50:55
A/V preamplifier	R-13	45	33	214	161:09:01:44
Altitude marking radar					
Electronics platform	R-6	0	-12		
Electrical conversion unit	R-7	20 to 22	14 to 16		
Antenna	R-27	-160	-185		
Televisions					
Survey					
Electronics	TV-16	-150	-134	127	158:15:16:00
Hood	TV-17	-162	-120	124	155:12:03:16
Approach electronics	T-3	-140	-124	186	155:12:03:16

*For telemetry bit rates of 17.2 and 137 bits/sec, i.e., without error due to bit rate.

**Launch +62 hours.

(1)Temperatures based on following locations and times at touchdown:

Landing point = 2.36 degrees south latitude and 43.36 degrees west longitude

Time (GMT) = 153:06:17:37

Sun elevation = 28.5 degrees

Spacecraft landed attitude: +X axis within 1 degree of south

Overall slope < 1 degree

North – south slope = 0.85 degrees south

(2)Times indicate when maximum temperature occurred initially; length of time maximum temperature remained or times of secondary peaks not indicated.

5.2.3 ANALYSIS OF THERMAL CONTROL SYSTEM

5.2.3.1 Compartment System Thermal Performance

Introduction

The compartment system thermal performance depends primarily upon the following parameters: 1) thermal switch conductance, 2) thermal switch radiator properties (α = 0.12 and ε = 0.79), 3) thermal dissipation within each compartment, and 4) total thermal energy incident on the radiators. These parameters cannot be evaluated individually with a high degree of accuracy; however, there are definite indicators that would appear in the data if any of these parameters was largely different from that expected during the mission.

The limited number of thermal sensors complicates the analysis particularly in the case of the compartment A and B thermal switches since only three of the nine thermal switch radiators on compartment A and three of the six on compartment B are instrumented. Conclusions about some of the compartment system thermal parameters that are linked directly to radiator temperatures therefore must be based upon the performance observed on only one-third of the compartment A thermal switches and on one-half of the compartment B switches. This limitation in instrumentation does not limit the conclusions about the resulting overall system performance which is clearly indicated by the two thermal tray temperature sensors in each compartment and the sensors within the electronics.

Similarly, limitations in the number of power measurements make it necessary to estimate portions of the thermal dissipation within each compartment. The primary area of uncertainty in thermal dissipation appears to be in the main battery which is housed in compartment A. Due to the uncertainty in main battery thermal dissipation, any parameter that could be evaluated using data from either compartment was evaluated using compartment B data. The internal power dissipation is believed to be more accurately known for that compartment.

Transit

Discussion. A brief scan of the compartment system temperature data (Table 5.2-2 and Figures A-1 through A-6 and A-39 through A-50) shows a consistent tendency toward flight temperatures well below those predicted during the first 20 hours of the mission whereas good correlation between flight and predicted temperatures is shown during the last half of the transit mission. This flight data characteristic is easily explained when a comparison is made between the actual SC-1 spacecraft operational sequence and that shown in EPD-180, Revision 5C, on which the temperature predictions were based. The reduction in spacecraft high power operations during the actual flight clearly explains the lower than predicted temperatures early in the mission. Table 5.2-3 is a comparison of the high power operations specified in EPD-180, Revision 5C, with those actually performed during flight.

TABLE 5.2-3. SC-1 ACTUAL HIGH POWER OPERATION DURATIONS COMPARED WITH THAT SPECIFIED IN EPD-180, REVISION 5C

Per EPD 180, Revision 5C			Actual SC-1 Missions		
Launch Plus Time, hr:min:sec	High Power Duration, minutes	Event	Launch Plus Time, hr:min:sec	High Power Duration, minutes	Event
00:12:18	24	Initial acquisition	00:12:00	28	Initial acquisition
5:56:00	63	High power interrogation	4:03:00	37	Star verification
10:37:30	27	High power interrogation	15:15:00	64	Midcourse
13:42:00	20	High power interrogation	62:14:00	55	Terminal descent
15:04:00	74	Midcourse	Total high power time during actual SC-1 flight	184	
19:15:30	53	Star verification			
60:38:00	34	High power interrogation			
62:04:00	49	Terminal descent			
Total high power time per EPD-180, Revision 5C	334				

After reaching equilibrium conditions during the long coast phase II, excellent agreement between flight temperatures and predicted temperatures was demonstrated in compartment B as temperatures were all within ±5°F of prediction.

Compartment A transit equilibrium temperature data also correlated well with prediction; however, the correlation was not as close as that of compartment B since the thermal tray and most components operated at temperatures up to 10°F cooler than predicted. The main battery, however, reached an equilibrium temperature of 98°F which was the predicted value. The maximum temperature on the main battery during transit (103°F) was reached at about L + 17 hours. Had all the high power operations specified

in EPD-180, Revision 5C, been performed, the battery temperature would perhaps have reached its predicted maximum of 116° F; therefore, it appears that the reduction in high power operations resulted in a 13° F reduction in peak battery temperature.

The transient response of each compartment and electronics was as predicted. Table 5.2-4 lists some of the transient thermal characteristics during high power operations for each compartment and electronics starting from transit equilibrium conditions.

TABLE 5.2-4. TRANSIENT RESPONSE TO HIGH POWER MODES – TRANSIT

Temperature Sensor	Location	Temperature Increase During Event – ° F			
		Initial Acquisition (28-minutes High Power)	Star Verification (37-minutes High Power)	Midcourse (1 hour, 4 minutes High Power)	Terminal Descent (55-minutes High Power)
D-13	XMTR A TWT	4	11	18	*
D-14	XMTR B TWT	38	51	58	*
EP-8	Main battery	3	5	7	9
EP-13	Boost regulator	15	16	20	*
EP-34	Battery charge regulator	*	3	7	*
V-15	Compartment A upper tray	12	23	31	*
V-16	Compartment A lower tray	7	4	8	8
V-21	Compartment B upper tray	5	6	9	*
V-22	Compartment B lower tray	6	4	6	*

*Data was not available because no engineering interrogations were made during or immediately following the high power event or the loss of sun lock influenced data to a high degree in the case of the battery charge regulator.

The compartment radiators' thermal environment was evaluated to verify the adequacy of analytical methods used in analyzing the thermal environment. The results indicate that the total thermal energy absorbed from the external environment by a fully illuminated compartment radiator is about 19.7 watts/ft^2, assuming a solar constant of 126 watts/ft^2 at the time of the SC-1 mission. The design value determined analytically was 20.4 watts/ft^2 based on the same solar intensity; therefore, the environment indicated by flight data agrees well with analytical solutions.

The average thermal switch conductance was analyzed on compartment B, and the value was 0.53 Btu/hr-°F per switch at 45° F over closure temperature. The compartment B thermal switch conductance therefore exceeded the minimum requirement of 0.50 Btu/hr-°F per switch at 50°F over closure temperature. The thermal switch conductance could not be accurately evaluated on compartment A due to the limited instrumentation coupled with the fact that the thermal switches on compartment A were not all set at the same closure temperature; however, the data did not indicate any anomalous switch performance during transit.

Conclusions. The SC-1 mission data verified the adequacy of the compartment system thermal control during transit. The average thermal switch conductance exceeded the minimum specified value, and the thermal environment of the compartment radiators agreed well with analytically determined values. All temperatures were well within specified tolerances, and no anomalous performance was evident during the transit portion of the mission.

Lunar Day

Introduction. The lunar day thermal performance of the compartment system is a function of the same parameters listed in the transit performance discussion. The one major difference between transit and lunar day is that the external thermal environment is much more severe, at least during midday, and that parameter becomes the major single factor for determining performance. Due to the importance of the thermal environment of the radiators, an extensive effort was made to define this environment as a function of time during the lunar day. Various approaches were used in evaluating the thermal environment to compare results and arrive at a reliable definition of the environment based on the mission data. Temperatures of the compartments and enclosed electronics throughout the first lunar day and into the lunar night are presented in Figures B-1 to B-10.

Discussion. The most accurate method of evaluating the thermal environment of a compartment radiator is to find a point in the mission where a thermal switch was open, thereby decoupling the radiator from the inside of the compartment. Such data will lead directly to the total energy absorbed by a radiator (both solar and infrared energy) by simply calculating $q = \sigma \epsilon A T^4_{Rad}$. Fortunately, some points did exist during portions of the lunar day where the thermal tray reached a temperature low enough to cause a thermal switch to open. These data points were utilized in arriving at the environment definition presented in Figure 5.2-1. Several other data points were also utilized throughout the lunar day by resorting to other methods of

68189-383 (U)

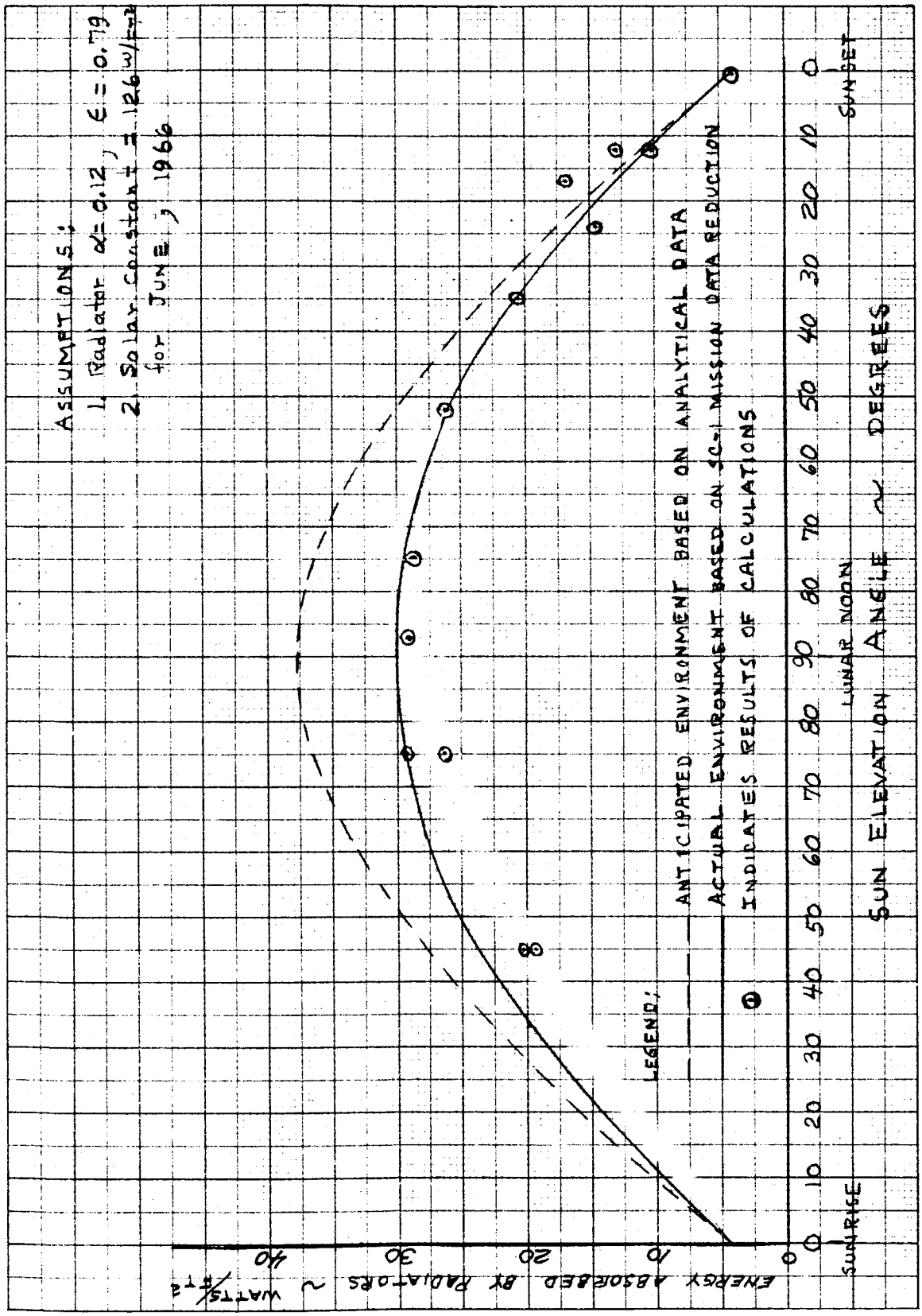


Figure 5.2-1. Compartment A and B Radiator Thermal Environment During Lunar Day

analysis. The resulting thermal environment definition is presented in Figure 5. 2-1. Compartment B data was used most extensively since it was fully illuminated throughout most of the lunar day, and the uncertainty in main battery dissipation which existed in compartment A was eliminated from the calculations. In addition, compartment A was partially shadowed during a large portion of the lunar day, thereby adding the uncertainty of the shadow line location to compartment A analysis.

Figure 5. 2-1 compares the apparent thermal environment definition determined from the SC-1 data analysis with that calculated by analytical methods prior to the flight of SC-1 for fully illuminated radiators. SC-1 data indicates a thermal environment about 25 percent less severe than expected throughout most of the lunar day. The cooler environment increased the thermal dissipating capability of each compartment considerably. The apparent thermal dissipating capabilities with a maximum thermal tray temperature of 125° F are shown in Figure 5. 2-2 as a function of time of lunar day.

The apparently cooler than anticipated compartment thermal environment was due primarily to lower than expected temperatures on the upper spaceframe, solar panel, and planar array antenna. The solar panel was not positioned normal to the sun's rays throughout the day since it was desired to reduce the charging rate; therefore, the solar panel temperature was less than assumed in the predicted thermal environment definition.

Approximately 50 percent of the difference between predicted and actual thermal environment intensity can be explained by the reduced temperatures of the environment surrounding the radiators; however, the remaining 50 percent of that difference is not clearly explainable.

The spacecraft was operated in a low power mode throughout most of the lunar day with the exception of those periods during TV sequences. The compartment A and B thermal dissipations during low power operation are approximately 13 and 15 watts, respectively. Both compartments operated throughout the lunar day without exceeding their upper thermal tray temperature limit of 125° F. The thermal dissipating capability of the compartment system was calculated as a function of the sun elevation angle (Figure 5. 2-3), based on the apparent actual thermal environment shown in Figure 5. 2-1. The resulting compartment A and B dissipating capability for the SC-1 spacecraft is shown in Figure 5. 2-2. The marked improvement in thermal dissipating capability over that previously predicted results from the thermal environment being less severe than anticipated (Figure 5. 2-1).

The only anomalies associated with the compartment system thermal control were the thermal switches that stuck in the closed position and failed to open upon entering lunar night. Switch 2 on compartment A stuck until the compartment thermal tray reached about 15° F (Figures B-4 and B-6). The switch should have opened when the thermal tray reached 40 ±5° F. At least one additional thermal switch on compartment A is believed to have temporarily stuck, but, since all radiators did not have temperature sensors on their radiators, such conclusions had to be based on the slope changes observed in the lunar night cooldown rate.

68189-384 (U)

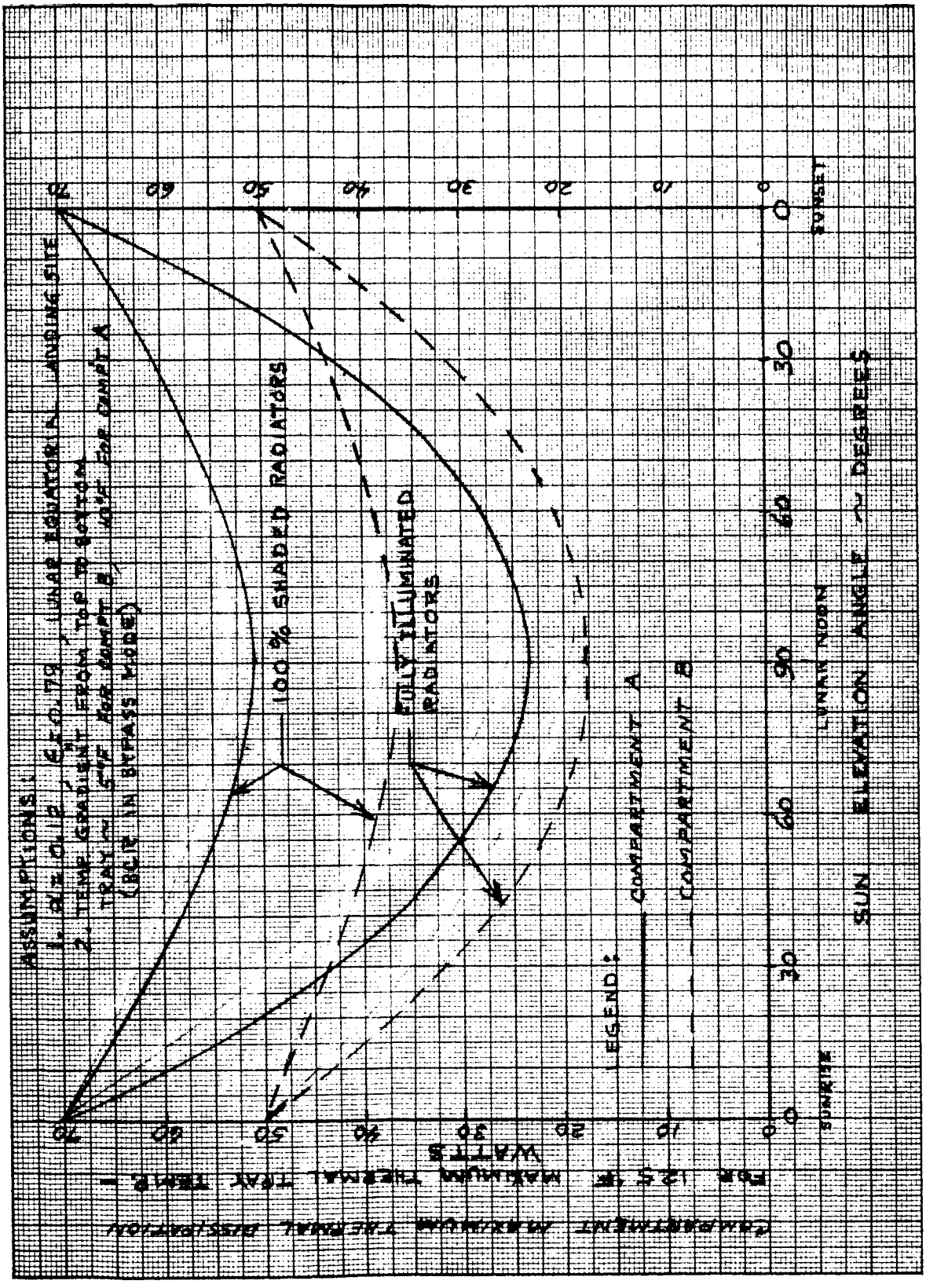
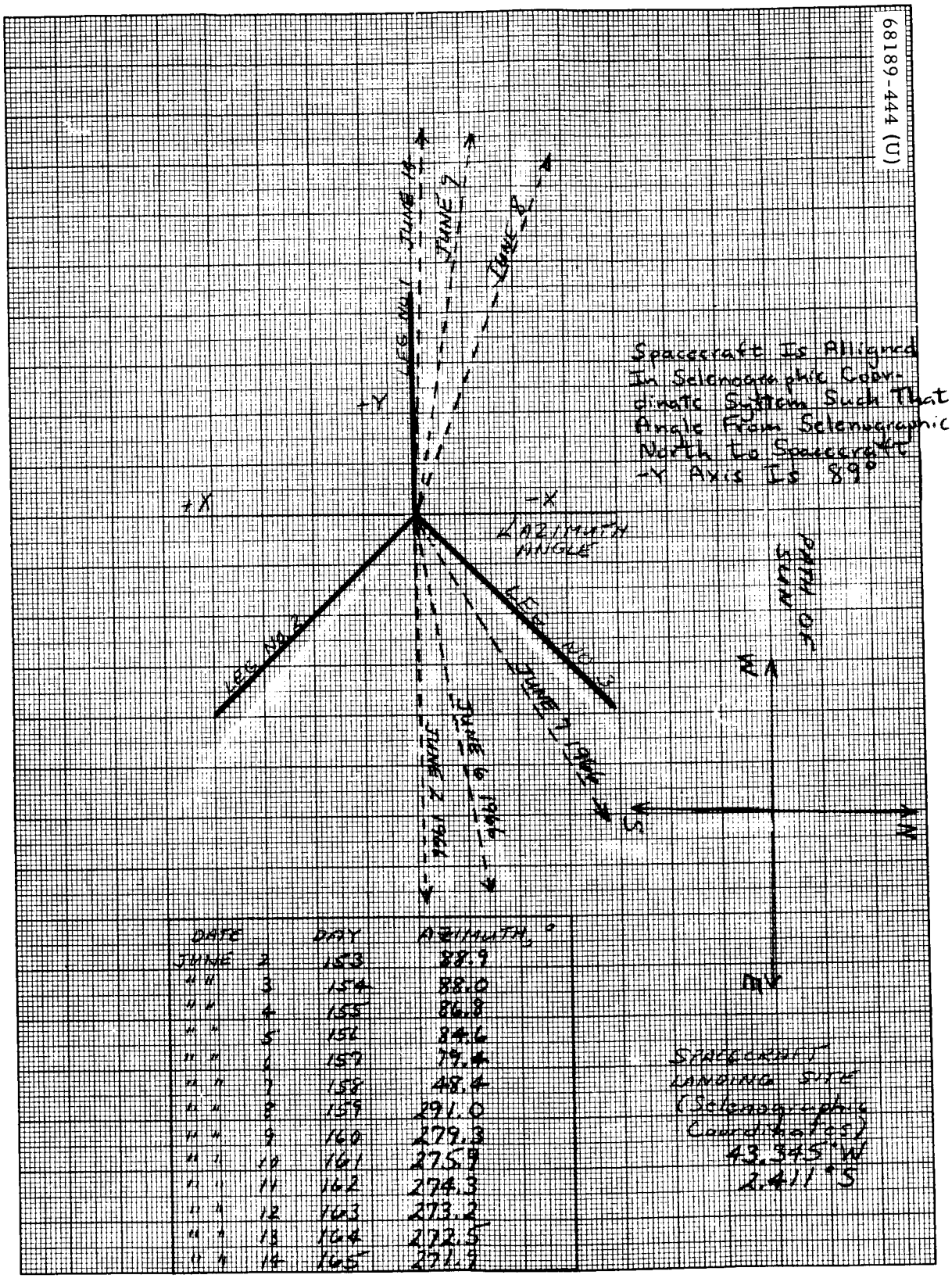


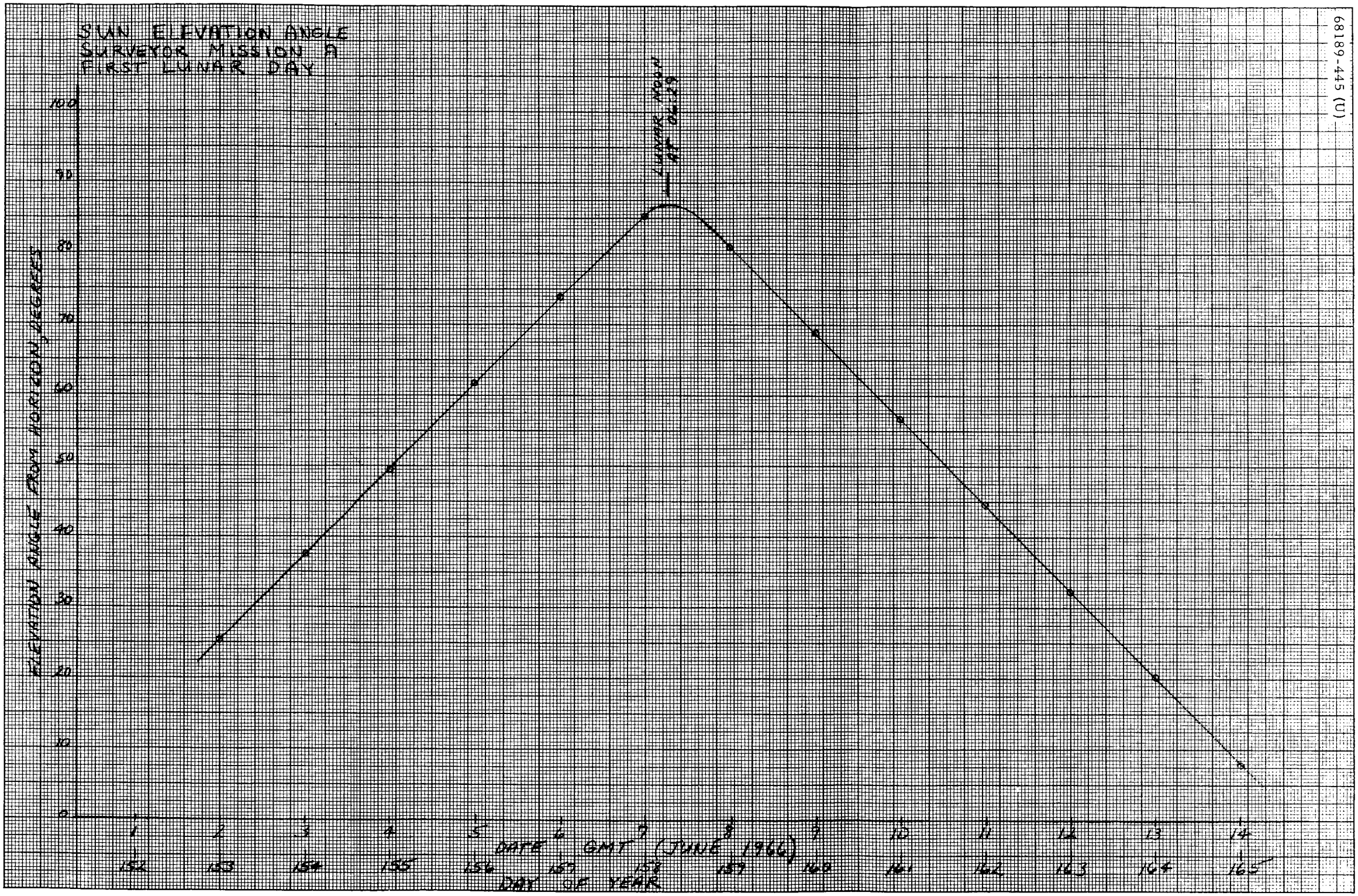
Figure 5.2-2. Compartment A and B Lunar Day Thermal Dissipating Capability



DATE		DAY	AZIMUTH, °
JUNE	2	153	89.9
"	3	154	88.0
"	4	155	86.8
"	5	156	84.6
"	6	157	79.4
"	7	158	48.4
"	8	159	291.0
"	9	160	279.3
"	10	161	275.9
"	11	162	274.3
"	12	163	273.2
"	13	164	272.5
"	14	165	271.9

a) Azimuth

Figure 5.2-3. Sun Angle on First Lunar Day



68189-445 (U)

b) Elevation

Figure 5.2-3 (continued). Sun Angle on First Lunar Day

FOLDOUT FRAME

5.2-25-1

FOLDOUT FRAME

FOLDOUT FRAME

FOLDOUT FRAME

5.2-25-2

It is believed that four of the compartment B thermal switches initially stuck in the closed position. Two of the three thermal switches with temperature sensors definitely stuck (Figure B-10). The remaining switches believed to have stuck were not instrumented, and conclusions had to be drawn from calculated heat loss data. Each stuck switch appeared to dissipate about 4.5 watts. Each of the stuck instrumented switches maintained a thermal conductance of 0.5 Btu/hr-°F or greater. The sticking problem is more prevalent when a high pressure and high temperature combination exists. The compartment B thermal switches were exposed to temperatures up to about 120°F during the lunar noon interval, whereas the compartment A switches were exposed to temperatures no greater than 100°F. The one compartment A switch that remained stuck the longest had a 40°F closure point; therefore, it had higher contact pressures developed than the remaining two instrumented switches which were set to close at 65°F.

Due to the thermal switches sticking, lunar night heat losses could not be accurately evaluated; however, it is believed that the lunar night heat losses determined analytically and verified by tests will prove to be relatively accurate.

Conclusions. The thermal environment as seen by the compartment system radiators during the lunar day is about 25 percent less severe than anticipated. This is due partially to lower than anticipated temperatures on the planar array antenna, solar panel, and upper spaceframe tubes. However, some additional factors appear to be involved and are not clearly understood at this time. The less severe lunar day thermal environment resulted in compartment system thermal dissipating capabilities far in excess of those anticipated.

The only thermal anomalies observed during the lunar portion of the mission involved several thermal switches that stuck in the closed position upon entering the lunar night.

5.2.3.2 Auxiliary Battery

Temperatures, as measured by the sensor inside the battery, cooled to levels below both those predicted for the unit and the 40°F defined lower temperature limit of the unit. The auxiliary battery temperature history (Figure A-5), indicates a long cooldown period until steady-state temperatures are reached approximately 30 hours into the mission, which is normal for the thermal design of this unit. The fact that the battery equilibrated at 35°F (40°F is the lower limit) is a thermal anomaly even though the battery performed its function after it started to supply power to the spacecraft at hour 45 in the mission. A warmup period to the desired 70°F operating temperature is normal, and the actual warmup profile followed the predicted value very closely although it was displaced below the predicted curve by 20°F (Figure A-5). Examination of available data reveals the following factors as contributory to the cause of the observed low temperatures. Review of ground-based STV test data indicates a 25°F battery temperature during the SC-1 phase 6A low intensity (87 percent solar constant) tests followed by a 67°F temperature during the phase 6B high intensity

(112 percent solar constant) test for comparable equilibrium states. A single steady-state point of 47°F was obtained in phase 2 of SC-1 STV at an equivalent one solar constant.

Interpolation from the high and low intensity data and the nominal one solar constant data both suggest that the predicted steady-state nominal value for Mission A should have been 47°F instead of 60°F. Using this as a point of departure, the corrected discrepancy is 12°F instead of 25°F.

There are two additional reasons to explain the remaining discrepancy of 12°F: 1) Mission A was flown when the solar constant was low by 3 percent due to seasonal variation which alone accounts for 5°F of the 12°F, and 2) spacecraft temperatures were 10 to 15°F lower in flight compared to predicted nominals on many passive systems. This appears to be a general condition applicable to the system rather than a single unit.

The thermal design of the SC-2 auxiliary battery thermal point pattern has been modified. The objective of this thermal finish change was to improve battery voltage performance by raising the coast phase equilibrium temperature to 60 ± 15°F and temperature at TD-5 to 95°F ± 15°F. The validity of the design was verified during SC-3 STV testing.

5.2.3.3 Antenna Solar Panel Positioner Performance

The A/SPP system provides support and positioning capability for the solar panel and planar array. The system is controlled by four different drive motors: polar axis, roll axis, elevation axis, and solar axis motors. These four motors and the solar panel are the primary thermal considerations in this system.

A thermal model for the A/SPP system was developed analytically and then modified to predict test results. The transit phase temperature predictions for the five A/SPP flight sensors were made by adjusting the boundary conditions in the thermal model to space conditions.

With one exception, the elevation axis motor temperature, the A/SPP system performed within the predicted temperature limits (Figures A-3, A-15, A-16, A-17, and A-57). The elevation axis motor (F/S M-12) was approximately 86°F (steady state) warmer than predicted. For several reasons the temperature prediction for the elevation axis motor was the most fallible (±50°F temperature tolerance) of the five predictions made. The fallibility of that prediction was due primarily to the uncertainty of the value of the contact conductance across the sector gear. Other factors contributing to the reliability of the prediction were 1) the uncertainty of the amount of energy reflected from the rest of the spacecraft to the elevation axis housing, and 2) the uncertainty of spacecraft boundary temperatures.

With the data obtained from the SC-1 flight and from the temperature gradients of prior tests on the A/SPP, the thermal model was revised. The following is a brief explanation of this revision.

In order to evaluate the existing thermal model, a new computer program was written using node temperatures, boundary temperatures, radiation coefficients, conduction coefficients, and heat inputs. By inputing these parameters, the following information was found: 1) individual amounts of radiation heat transfer between each node in the system, 2) individual amounts of conduction heat transfer between each node in the system, 3) net amount of radiation heat transfer to or from each node, 4) net amount of conduction heat transfer to or from each node, and 5) heat balance for each node in the system.

Transit steady-state temperatures of the A/SPP were represented by using the actual flight sensor temperatures from SC-1; then, using temperature gradients from STV tests done on the A/SPP, node temperatures not indicated by flight sensors were calculated. These temperatures, the existing radiation and conduction coefficients, and heat inputs were input to the new computer program. After consideration of the resulting output, several changes were made in the computer model, including 1) a more reliable value for the contact conductance across the sector gear, 2) upgraded reflected energy terms, 3) two separate spacecraft boundaries, a conduction boundary, and a radiation boundary, 4) adjusted conduction coefficients, and 5) radiation coefficients based on SC-1 geometry and surface properties. These changes resulted in a revised computer model that yields the actual flight temperatures of SC-1 as well as the assumed temperature gradients (Figure 5.2-4).

The temperatures experienced by the A/SPP during the first lunar day were well within the temperature ranges expected. Figures 5.2-5 through 5.2-9 show preflight temperature expectations compared to the actual flight temperatures. As can be seen from the graphs, the maximum temperature reached by each of the flight sensors was either very close to or slightly lower than expected maximum temperatures. The lunar surface A/SPP temperatures were developed using the A/SPP thermal model with lunar surface parameters substituted for transit parameters.

The thermal response of the A/SPP both during transit and during the first lunar day was within the temperature range considered necessary for reliable operation. The elevation axis motor was significantly warmer than predicted, but the warmer temperature was more favorable for A/SPP operation than the predicted temperature would have been.

Although the transient flight data during midcourse and terminal descent are scattered, it can be seen from Figures 5.2-5 through 5.2-9 that the anticipated thermal transient response was very close to the actual response. From Figure A-4 (solar cell array), it can be seen that during midcourse the solar panel returned to its steady-state temperature at the anticipated time. The limited transient data seems to verify the validity of the transient thermal model.

Before flight it was noted that during transit the solar panel flight sensor (EP-12) would be 16° F cooler than the actual temperature of the solar

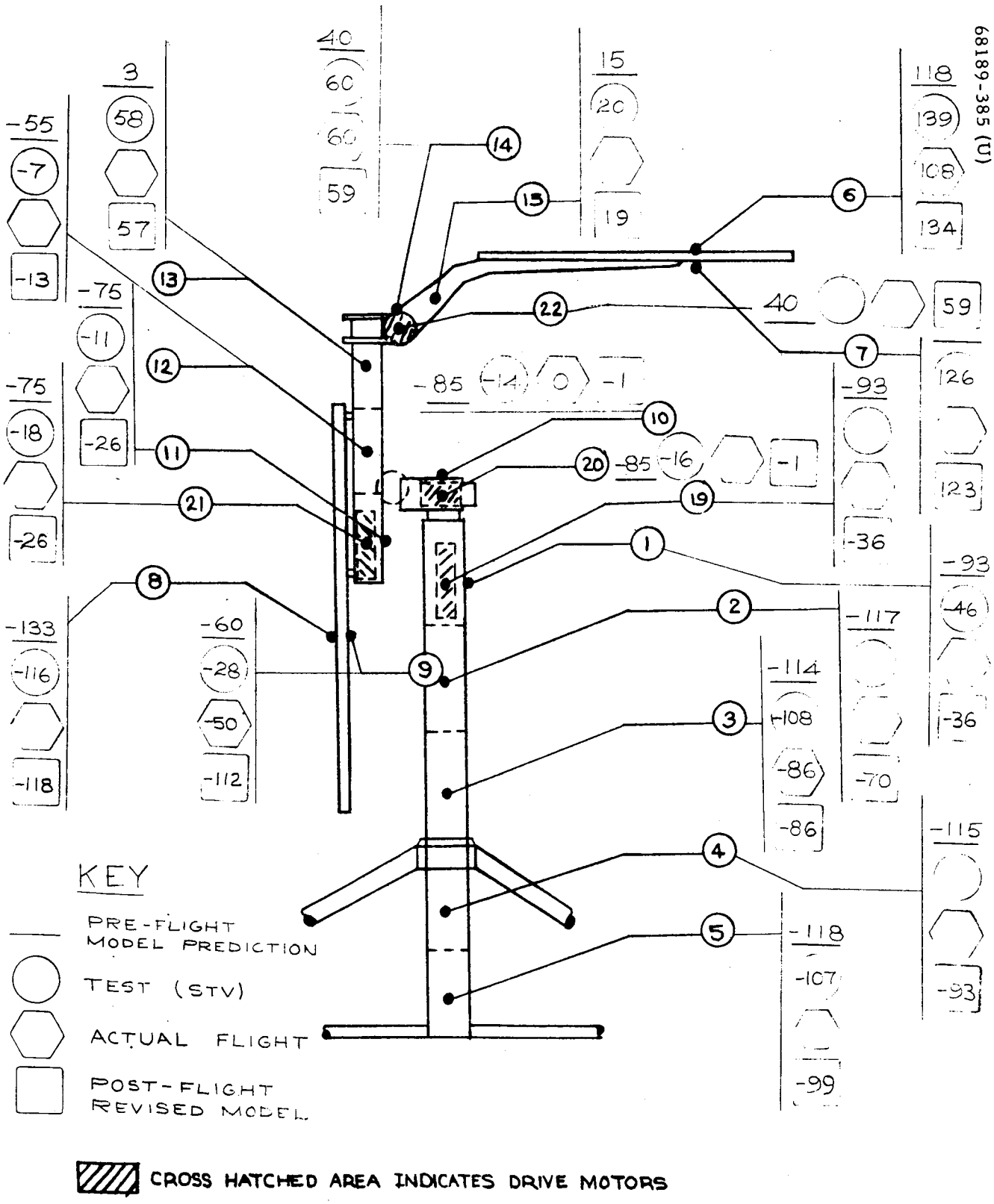


Figure 5.2-4. SC-1 A/SPP Transit Analysis

panel. The flight sensor (EP-12) is located under the secondary sun sensor and not on the solar cells; a 16° F difference results. What this temperature difference is during lunar surface operation has not been determined.

Flight sensor M-8 is located on a support at the back of the planar array and is in such a position (away from the planar array) that the indicated temperature is not an accurate recording of the planar array temperature. In transit it is estimated that the bulk temperature of the planar array was approximately -120°F; this is in contrast to the flight sensor indication of -50°F. This observation is based on data from STV tests on the A/SPP system. During the tests, thermocouples were located on the planar array and at the flight sensor location. With the A/SPP in the transit orientation, the planar array flight sensor receives direct solar illumination, whereas the planar array does not receive direct solar illumination. On the lunar surface, the difference in temperature between the flight sensor and the planar array has not been evaluated; consequently, the plot of expected temperature of the planar array on the lunar surface is not included in Figure 5.2-9.

A revised thermal model of the A/SPP system with a higher degree of reliability was made possible by the data received from SC-1. This revised model has already been modified to do thermal analysis on the model 500 A/SPP (jackscrew). SC-2, -3, and subsequent spacecraft flight temperature predictions will be made using the revised model and adjusting those parameters that change from spacecraft to spacecraft.

5.2.3.4 Spaceframe and Crushable Block Heat Shield No. 3

The Surveyor spaceframe is a skeletal structure of aluminum tubing on which various compartments and components are mounted. Seven sensors are employed to monitor spaceframe temperatures at selected sites. While most other units are mounted on the spaceframe with low conductance hardware, they are still coupled to the spaceframe conductively and radiatively. Although the spaceframe will survive a wider range of thermal conditions than many other components, it is important that it does not compromise the thermal integrity of other vehicle subsystems.

In consideration of the spaceframe's complexity, it was decided to make predictions for the SC-1 mission based on test data as shown in Figures A-50, A-51, A-58, and A-59. Predictability was ±30°F or ±50°F, depending upon specific flight sensor location. No predictions were made for the post-touchdown period. Flight data was found to correlate well with predictions. Temperature deviations were from 2 to 18° F below predicted temperatures as shown in Figure 5.2-10. The mean deviation from predicted values was 9° F. Figure 5.2-11 displays an extensive temperature distribution in the spaceframe based on results of various tests and modified to reflect SC-1 flight data.

Maximum temperatures recorded during lunar day ranged from 110 to 225° F for the several sensors. It is interesting to note that by observing the trends of temperature history curves shown in Figures 5.2-12 and 5.2-13, one can determine approximately the movement of shadow patterns over the spacecraft. The clearest example of this is V-37, which obviously was

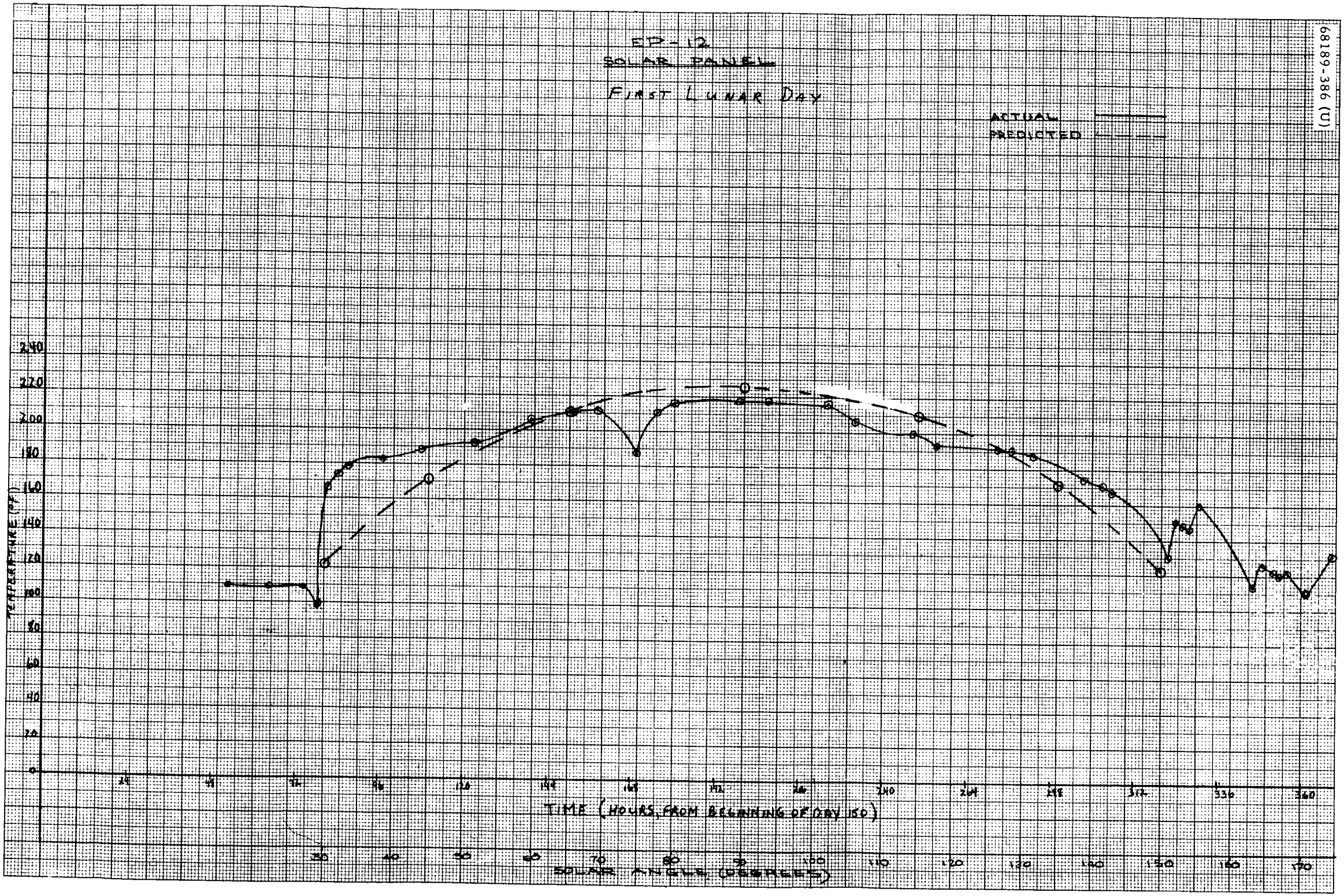


Figure 5.2-5. Solar Panel (EP-12) on First Lunar Day

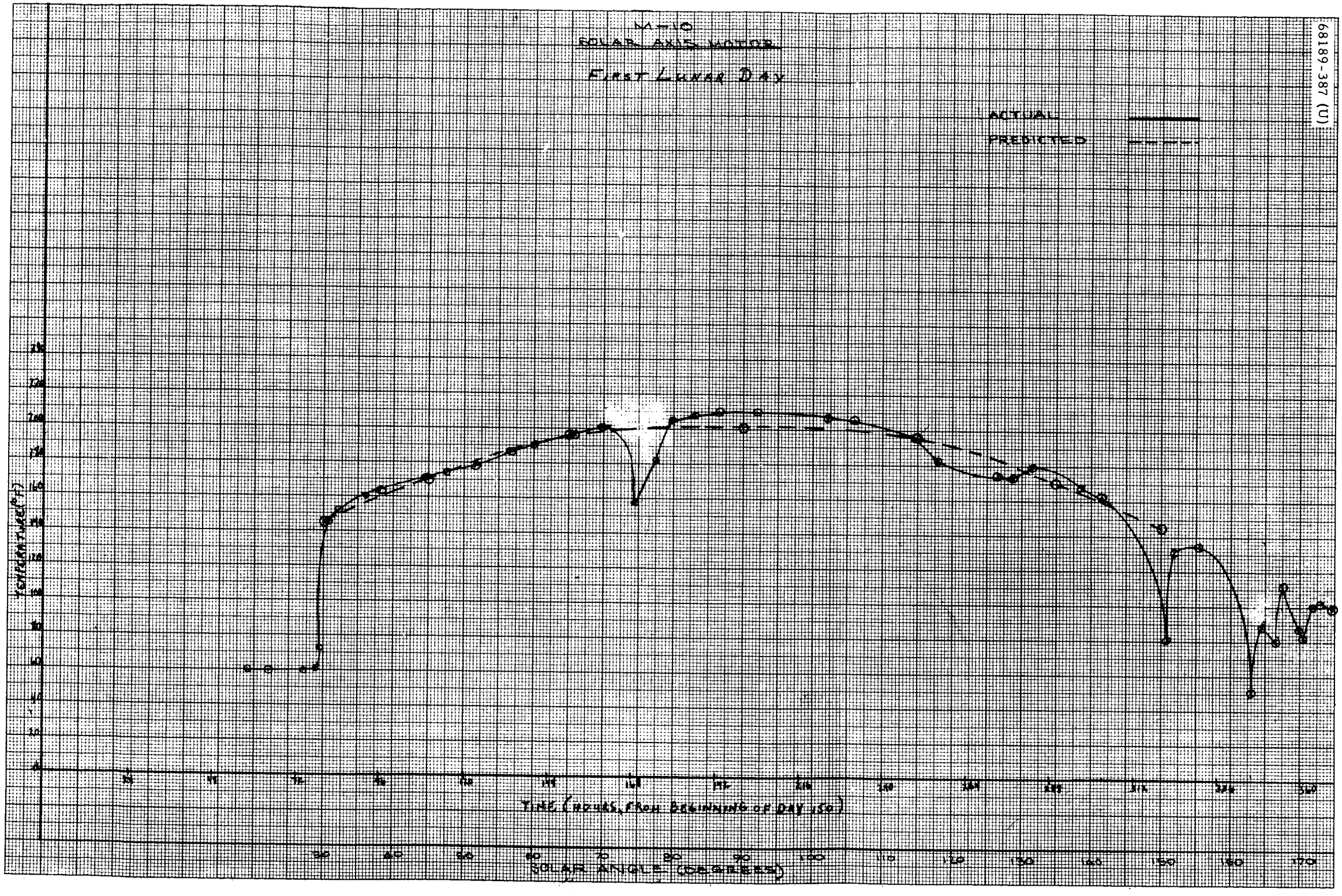


Figure 5.2-6. Solar Panel Axis Motor (M-10) on First Lunar Day

FOLDOUT FRAME
FOLDOUT FRAME

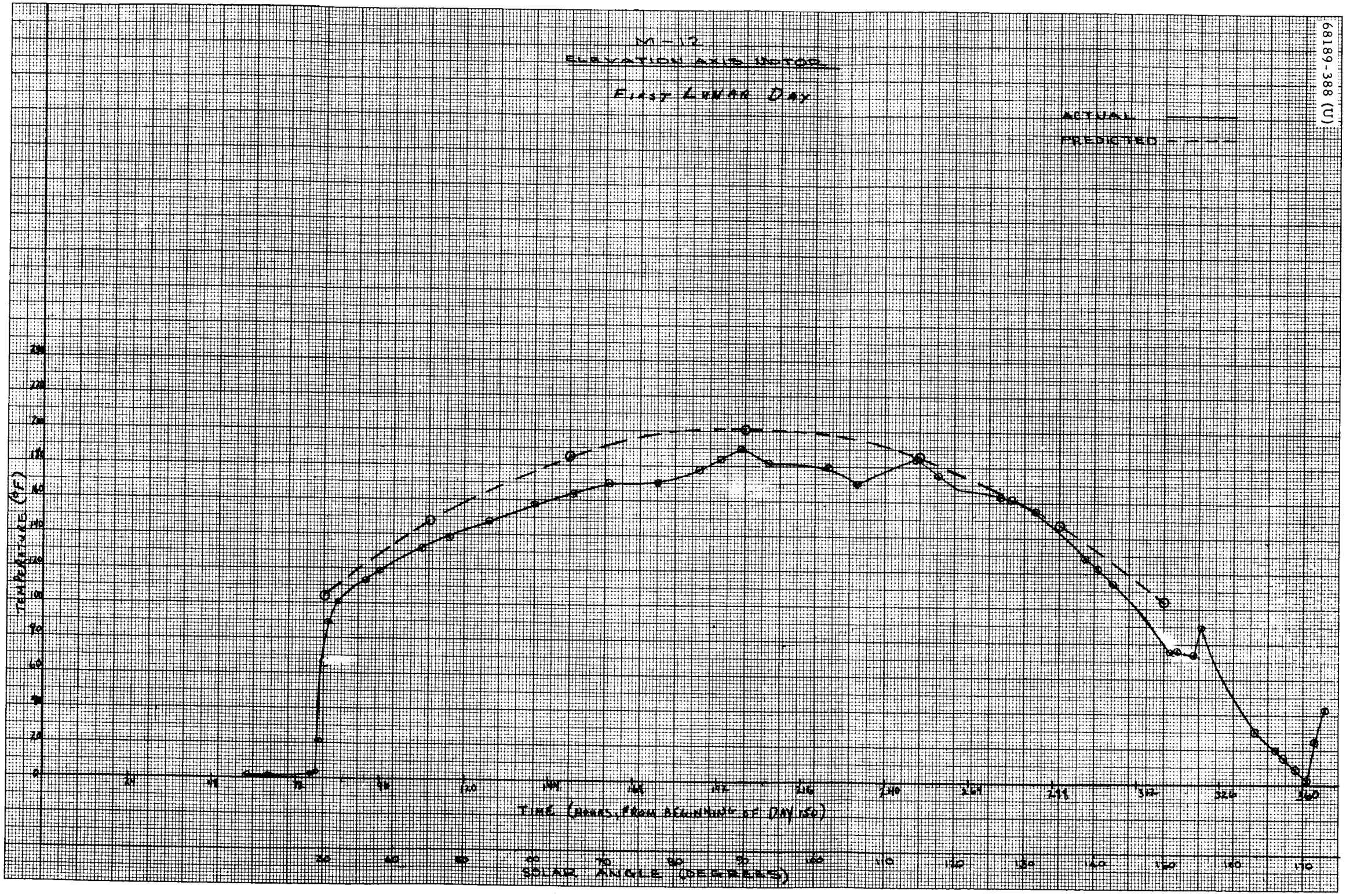


Figure 5.2-7. Elevation Axis Motor (M-12) on First Lunar Day

FOLDOUT FRAME

FOLDOUT FRAME

5-2-36

Figure 5.2-8. Lower Mast (V-34) on First Lunar Day

FOLDOUT FRAME

FOLDOUT FRAME

5-2-38

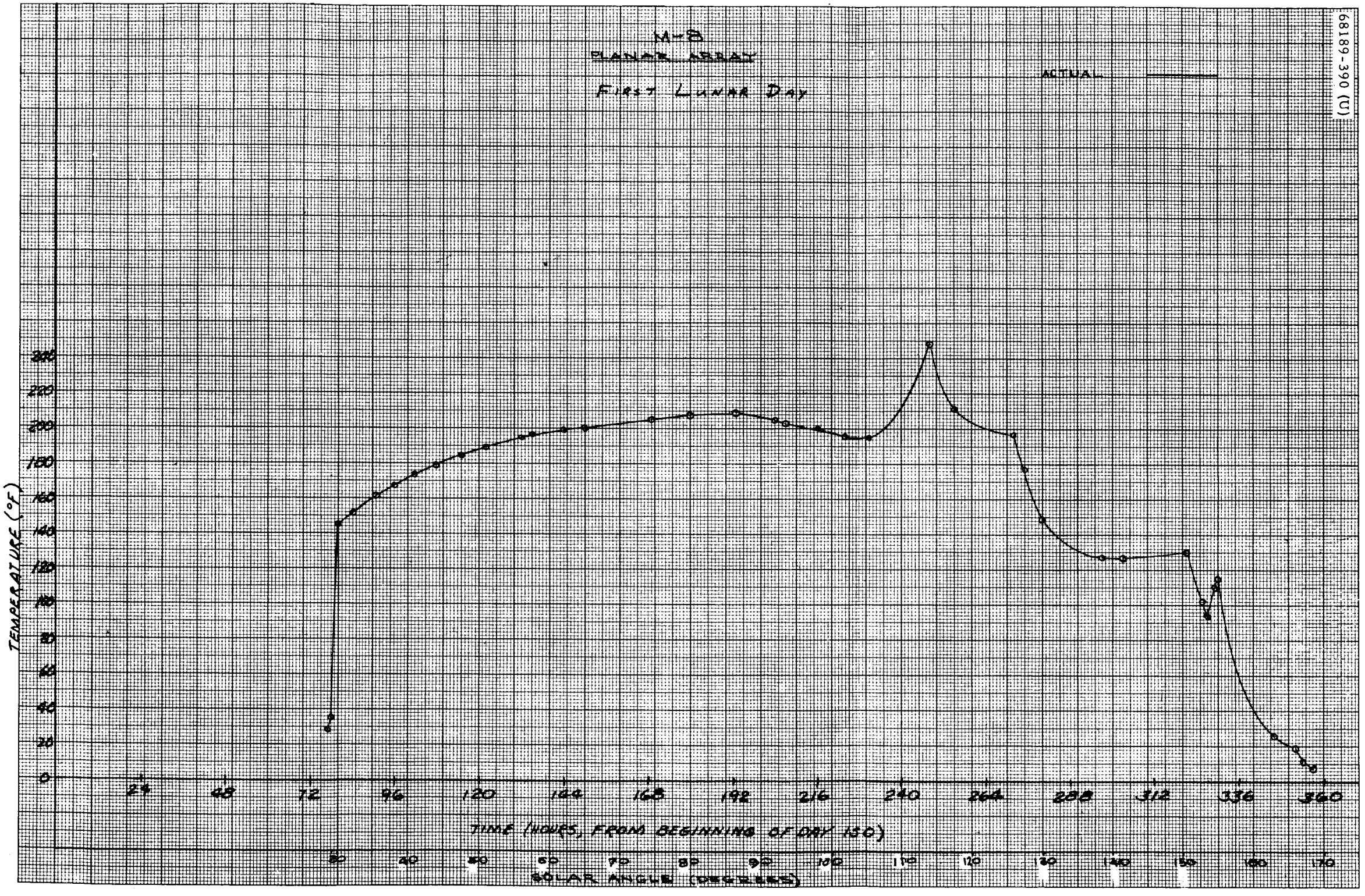


Figure 5.2-9. Planar Array (M-8) on First Lunar Day

FOLDOUT FRAME

FOLDOUT FRAME

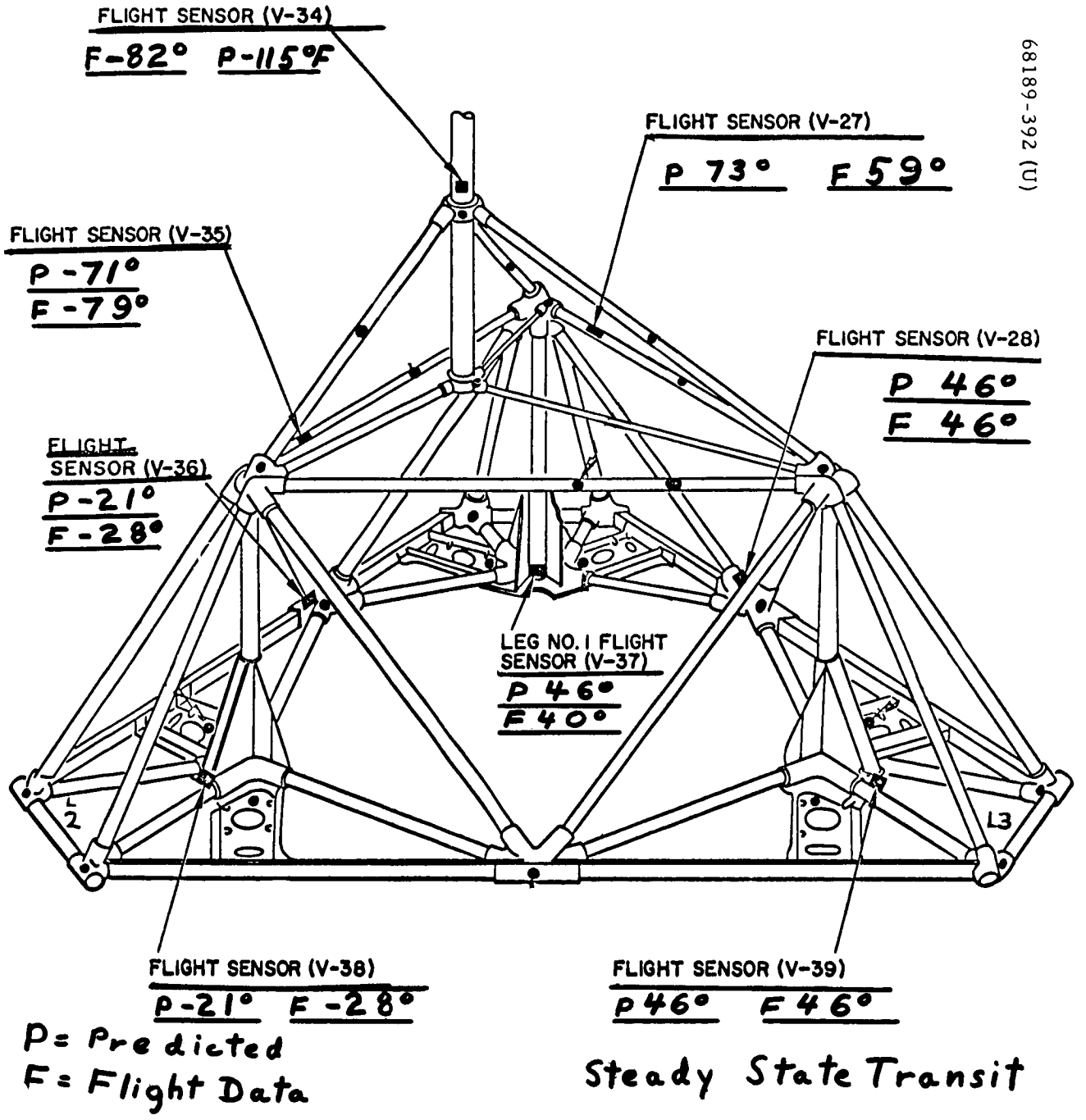


Figure 5.2-10. SC-1 Spaceframe Flight Data Compared with Predictions Steady-state transit

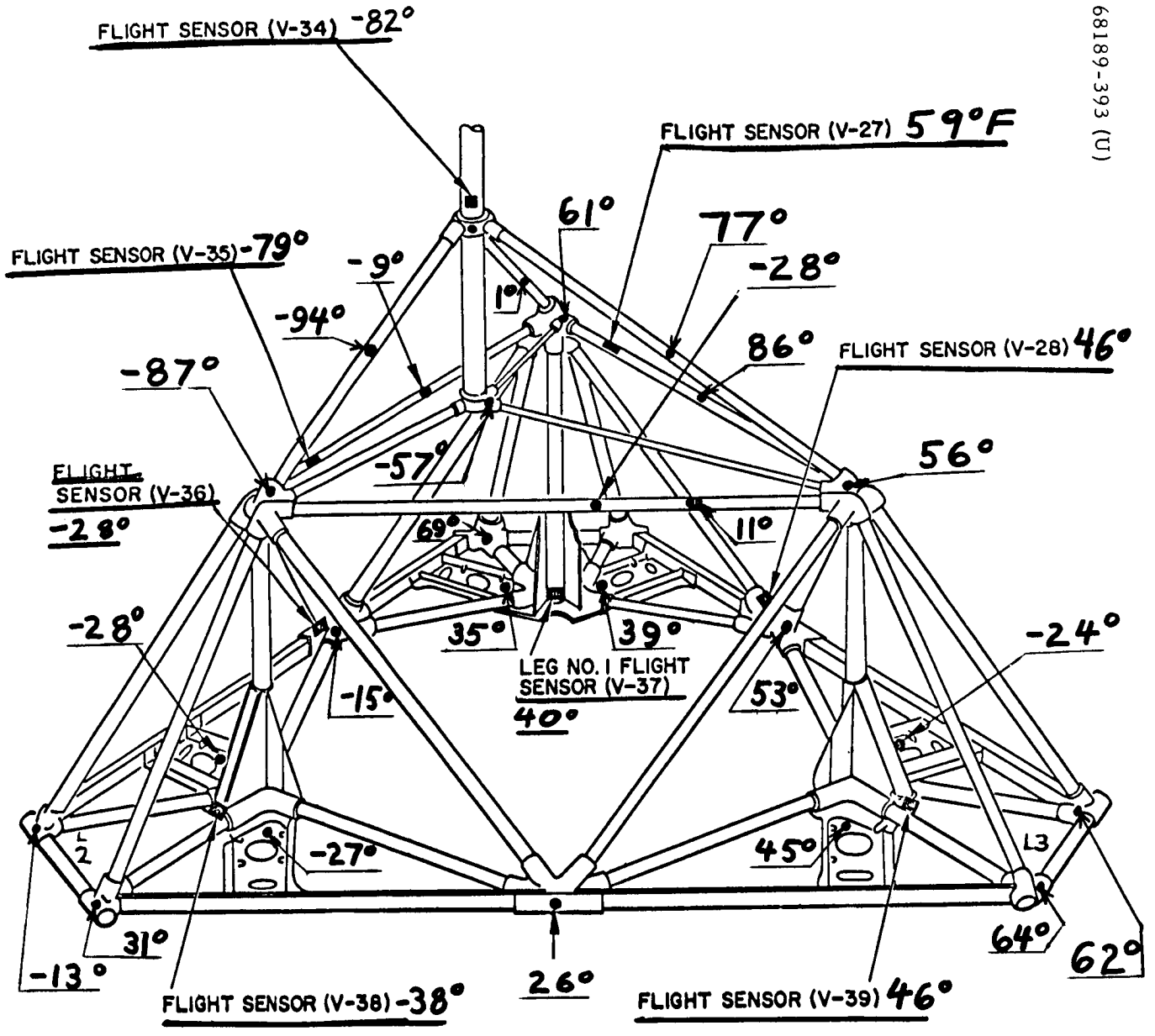


Figure 5.2-11. Spaceframe Temperature Distribution on Test Data and SC-1 Flight Data Survey Transit Coast Phase

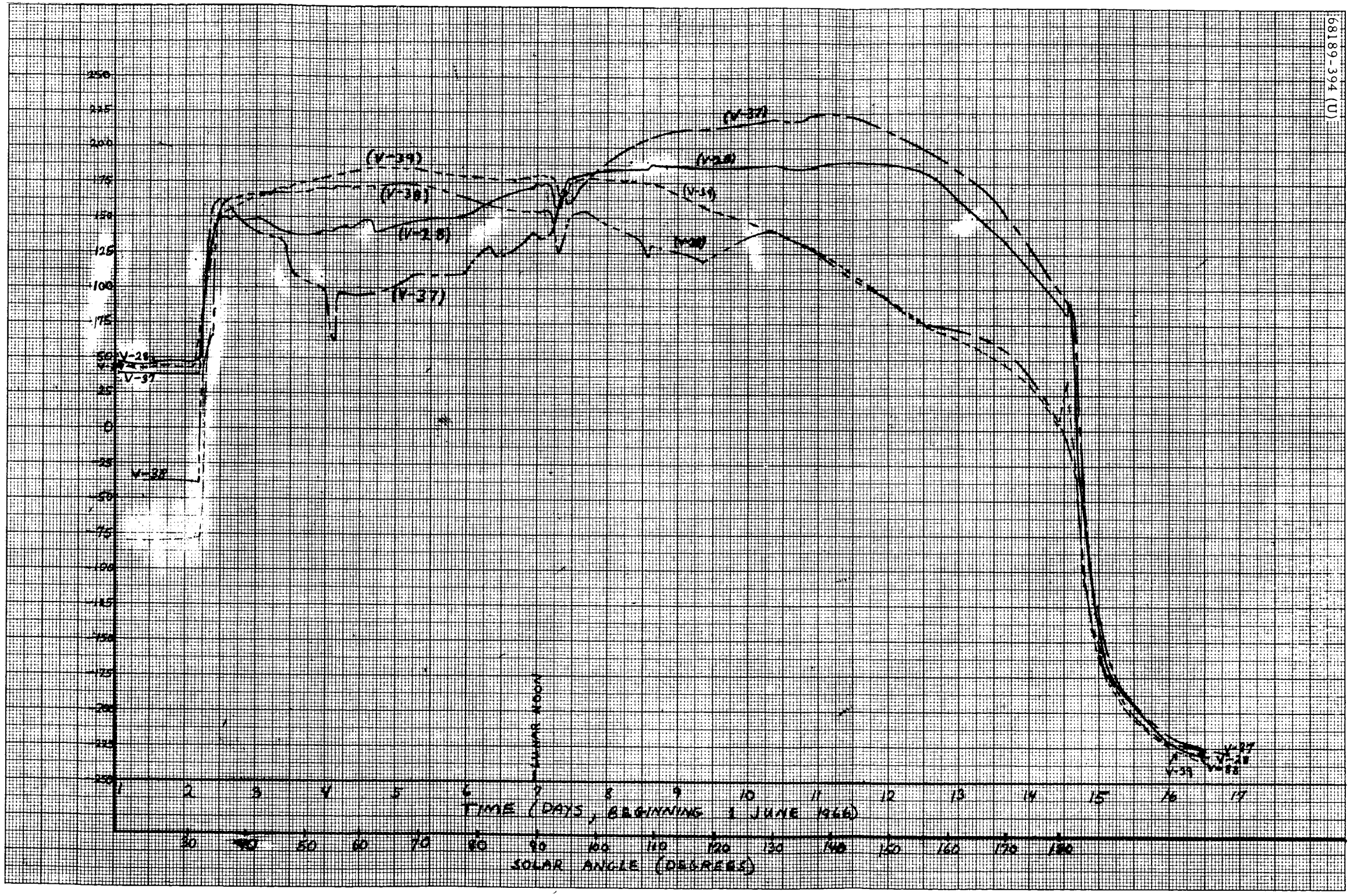


Figure 5.2-12. Spaceframe Lunar History (V-28, V-37, V-38, and V-39)

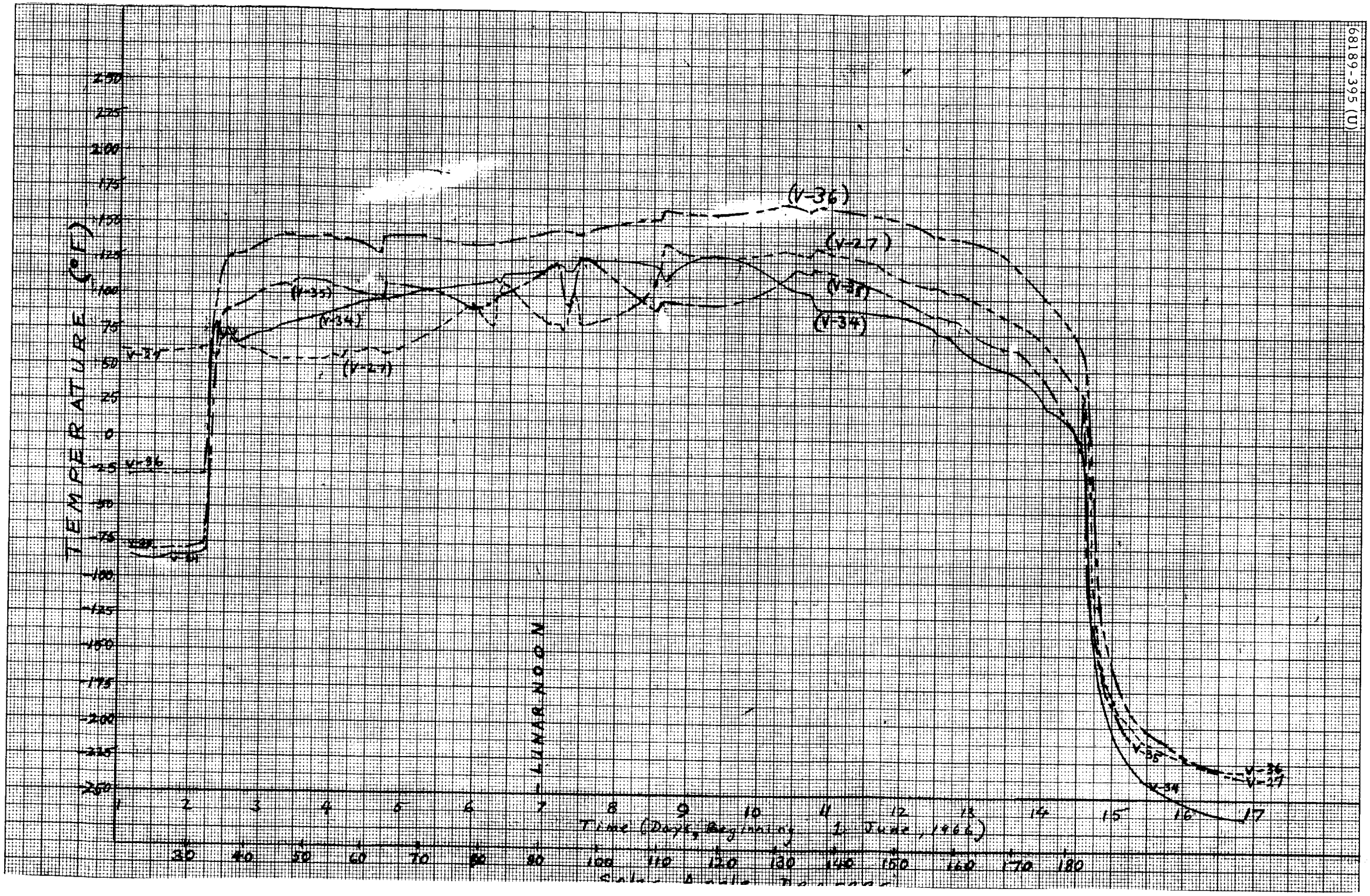


Figure 5.2-13. Spaceframe Lunar History (V-27, V-34, V-35, and V-36)

FOLDOUT FRAME

FOLDOUT FRAME

shaded during lunar forenoon and in sunlight during lunar afternoon. (See Figures 5.2-10 and 5.2-11 for sensor locations.) The sun was moving easterly as the lunar day progressed from the auxiliary battery along the Y axis to leg 1. For V-38 and V-39, the opposite trend to that of V-37 is indicated. V-27 and V-28 behave similarly to V-37.

Crushable Block No. 3 Heat Shield

The crushable block No. 3 heat shield steady-state temperature was -62° F during transit, 12 degrees cooler than the preflight prediction of -50° F. The crushable block and not the heat shield is of prime interest, and, although no sensor was located in this area, analysis and test data indicate that the block bulk temperature is 80° F higher than the heat shield temperature. Therefore, the crushable block No. 3 bulk temperature may be assumed to have been at 18° F when the shield was at -62° F.

The transient temperature cooldown rate after launch was much greater than predicted (Figure A-60). This rapid temperature drop indicated that the calculated heat capacity in the region of the flight sensor was too large by a multiple of three. This region is comprised of the heat shield itself (a 0.020-inch thick laminated glass cloth bonded with phenolic resin), an aluminum powder filled epoxy resin on the back of the corrugated shield (which provides a flat area for mounting the temperature sensor), and the temperature sensor. The heat capacity parameters (specific heat, density, thickness, and area) were reexamined. The changes are shown in Table 5.2-5. The main error was in the original calculation of the temperature sensor heat capacity.

The radiation heat transfer was calculated for a 1 in^2 area of the heat shield. The actual area of the temperature sensor is 0.25 in^2, but 1 in^2 was used in the original calculation of the sensor heat capacity. Also, the actual area of the filler material surface is 0.7 in^2, but 1 in^2 was used in the original calculation of its heat capacity.

Table 5.2-6 shows the changes made in the radiation parameters, the surface emittance values, and view factors to space. These parameters were changed to increase the calculated temperature drop rate after launch but to keep the steady-state coast phase temperature at -62°F.

The midcourse flight data and the revised thermal model with the reduced heat capacity were used to calculate the midcourse convection heat flux on the heat shield. The convection flux needed to match the actual temperature response at midcourse was 0.76 Btu/sec-ft^2 for 21 seconds. This compares with a predicted convection flux of 0.2 Btu/sec-ft^2 for 17 seconds. Unfortunately, there is no data for the temperature rise from vernier engine operation at terminal descent. The data (Figure A-60) shows a 32°F temperature rise after the yaw maneuver but before engine operation at terminal descent.

TABLE 5.2-5. CRUSHABLE BLOCK SHIELD NO. 3 HEAT CAPACITY

	Heat Capacity		Reason for Change
	Preflight, Btu/°F	Postflight, Btu/°F	
Shield	0.0005	0.0004	Changed C_p (specific heat) from 0.25 to 0.2 Btu/lb-°F
Filler material (aluminum filled epoxy)	0.002	0.0009	Changed ρ (density) from 0.1 to 0.064 lb/in^3 Changed A (heat transfer area) from 1 to 0.7 in^2 Changed t (thickness) from 0.125 to 0.10 inch Changed C_p from 0.25 to 0.2 Btu/lb-°F
Temperature sensor	0.002	0.00015	Changed A from 1 to 0.25 in^2 Changed t from 0.1 to 0.06 inch Changed C_p from 0.2 to 0.1 Btu/lb-°F
Totals	0.0045	0.00145	

TABLE 5.2-6. SC-1 CRUSHABLE BLOCK SHIELD NO. 3 RADIATION PROPERTIES

	Preflight Values	Postflight Values
Outside surface		
Emittance	0.04	0.07
View factor to space	0.7	0.7
Inside surface*		
Emittance	0.8	0.85
View factor to space	0.1	0.28

*Filler material and temperature sensor.

Table 5.2-7 shows the calculated convection heat flux values on crushable block shield No. 3, the AMR antenna heat shield, and the retro nozzle. In each case, the allowable flux is larger than the maximum flux determined from the flight temperature data. The lunar day data for the crushable block heat shield is shown in Figure 5.2-14.

TABLE 5.2-7. SC-1 VERNIER ENGINE EXHAUST CONVECTION HEAT FLUX

	Calculated Flux* During 20.8-second Engine Operation, Btu/sec-ft^2	Allowable Flux for 200-second Burn, Btu/sec-ft^2
Crushable block No. 3	0.76	> 1
AMR dish heat shield	3.7 maximum	7
Retro nozzle	0.32 ± 0.15	> 4

*From flight temperature rise data.

5.2.3.5 Legs

Transit Phase

The leg 2 steady-state temperature of 80° F occurred approximately 90 minutes after launch and compared favorably to the predicted value of 85° F. The leg temperature gradually increased throughout the flight and at 60 hours after launch had risen to 85° F (Figure A-54). This increase in temperature can be attributed to continued degradation of the organic white paint on the leg. Analysis based on test data indicates that the increase in solar absorptance of the white paint necessary to produce the higher temperature at the end of the flight was approximately 0.02. Legs 1 and 3 are not instrumented in flight, but are known to be warmer than leg 2 because of the absence of the partial shadowing on leg 2 by the solar panel. It is estimated that the temperatures of the uninstrumented legs 1 and 3 were 100° F at launch, increasing to 105° F near touchdown.

PRECEDING PAGE BLANK NOT FILMED.

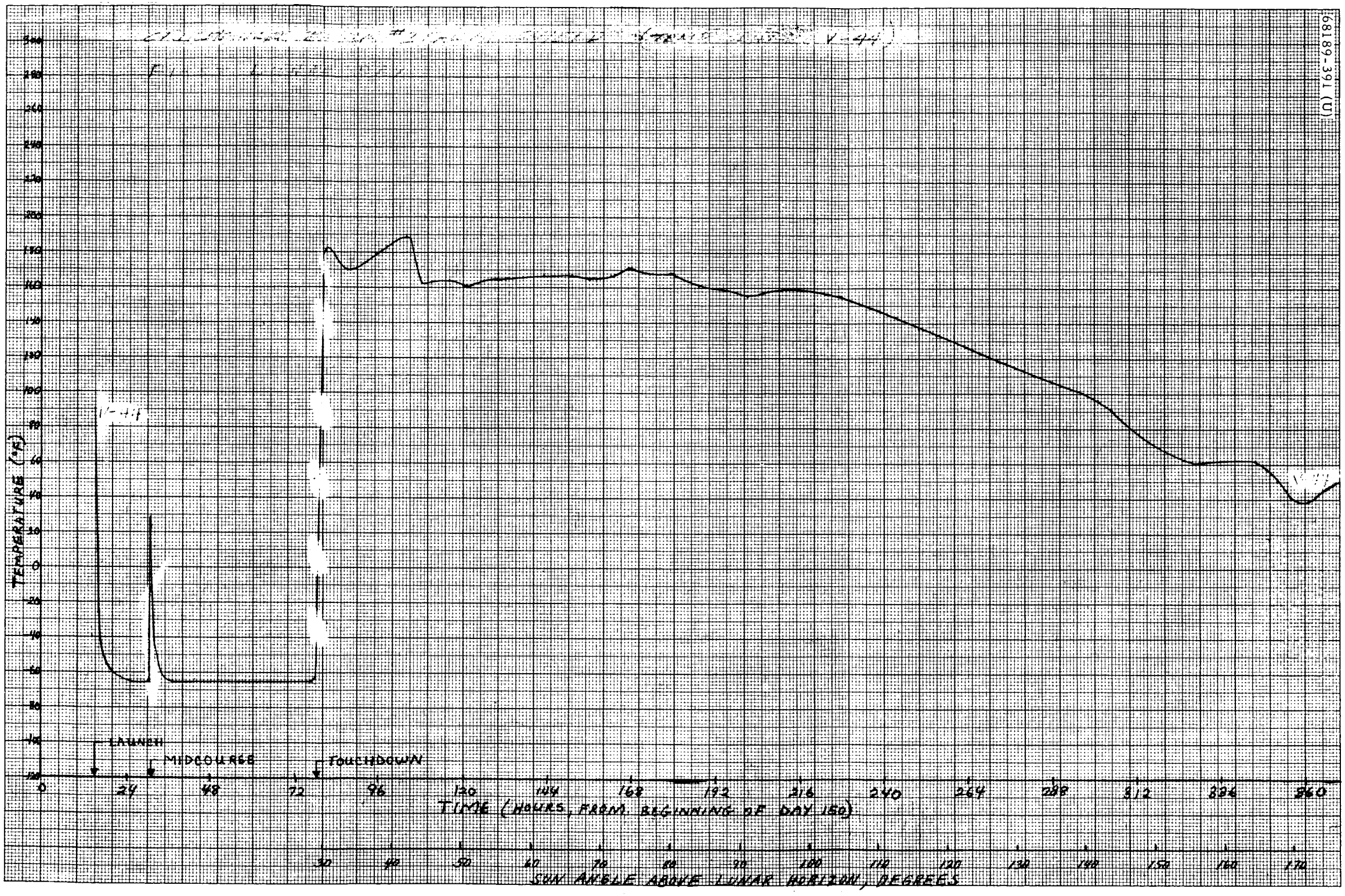


Figure 5.2-14. Crushable Block 3 Heat Shield (V-44) on First Lunar Day

Legs 1 and 3 would have similar peak temperatures, but the thermal response of leg 1 to the lunar environment would be different because of shadowing from the solar panel and planar array during the day.

5.2.3.6 Shock Absorbers

Transit

Steady-state temperatures on all three shocks were obtained approximately 4 hours after launch. Flight data indicated temperatures 6 to 16 degrees lower than the predicted temperatures, as shown in Table 5.2-2 and Figures A-53, A-55, and A-56.

The 2-degree temperature increase in shock No. 2 coupled with the 2-degree decrease in shock No. 3 during the gyro drift checks was as expected and confirms the positive yaw drift. Temperature perturbations in shock absorber one, which were not sampled during this time period, were expected to be negligible during these checks.

During the midcourse maneuver, the flight sensor on shock No. 2 recorded a 30-degree drop as compared to an expected 36-degree cooldown. No temperature perturbation was expected on shock No. 3 during this maneuver because the shock absorber projected area to the sun remained approximately the same. The flight sensor on shock No. 1 probably experienced an increase in temperature, increasing from a steady-state value of 84° F to a peak temperature of about 88° F before the midcourse maneuver was completed. The reason for this is that shock No. 1 projects a larger surface area to the sun vector for the negative yaw maneuver employed for the midcourse correction. It should be noted that during transient responses of the shocks, the temperature of the enclosed fluid, which is the most critical part thermally, lags approximately 15 degrees behind the temperatures recorded by the flight sensors.

During the terminal descent, the shock No. 2 flight sensor recorded a 12-degree increase. This agrees well with the predicted increase of 11 degrees for a warm lunar landing. Shock No. 1 probably decreased in temperature while shock No. 3 probably increased several degrees. Data from shocks 1 and 3 was lacking during the maneuvers, and therefore the response of these units during this period can only be estimated.

Lunar Phase

At touchdown, all three shocks were within their required temperature limits for landing. However, after touchdown, flight sensor V-30 (shock No. 1) exhibited interesting fluctuations. It appeared at first that the temperature perturbation recorded indicated that the flight sensor had broken free of the shock. It was determined, however, that shadowing from the solar panel and planar array during this period would produce such thermal perturbations. Not until near lunar noon did the shock exhibit a response similar to that of shocks 2 and 3. As was expected, shock No. 1 was warmer in the lunar

It is anticipated that leg temperatures will be 25° F cooler during transit coast phase conditions on subsequent vehicles as compared to SC-1. On the SC-1 spacecraft legs, the optical properties of the paint were severely degraded by prolonged ultraviolet exposure during STV tests. It was not possible to restore these properties during the refurbishing of the thermal coatings prior to launch with the usual procedure of sanding off the yellowed surface layer. Previous sanding of the legs made the paint too thin for continued abrasion to be feasible. On all subsequent vehicles, the legs are protected during the STV phase to prevent ultraviolet paint degradation.

The several gyro drift checks performed during the flight clearly influenced the temperature on the legs. Leg 2 increased about 3° F after each drift check, indicating a positive yaw drift. Theoretical calculations support the 3-degree temperature rise for a 2-degree angle drift. Legs 1 and 3, on the other hand, would be expected to decrease by about 3 degrees since in a positive yaw drift the illuminated surface area of these legs decreases by about the same amount that the leg 1 area increases.

The cooldown rate of leg 2 during the midcourse maneuver was similar to its cooldown rate during a solar eclipse performed in STV tests. This indicates, therefore, that the negative yaw maneuver (-58 degrees) probably put leg 2 into a position where illumination of the leg from the sun and/or reflections was considerably reduced. Although legs 1 and 3 remained illuminated during this maneuver, they should have experienced a cooldown similar to leg 2 but at a much slower rate. Cooldown of legs 1 and 3 is attributed to the decreased surface area normal to the sun which results in a lower heat load.

During terminal descent, temperatures of all three legs probably decreased. This decrease is the result of the smaller projected surface areas of the legs to the sun vector resulting from the terminal maneuvers. Leg 1, in particular, probably experienced a cooldown rate similar to that recorded on leg 2 during the midcourse maneuver because of a similar orientation with respect to the sun vector. Finally, it should be noted that vernier engine firing during the midcourse and terminal maneuvers appeared to have no thermal effects on the legs.

Lunar Phase

Leg 2 appeared to be illuminated continuously throughout the lunar day and, therefore, its temperature time history resembles that of the lunar surface but at a lower temperature level. The maximum temperature of 148° F on the leg occurred at around lunar noon and then cooled at a rate similar to its warmup rate after touchdown (Figure B-20). The suppressed peak of 148° F can be attributed to the white paint on the top surface of the leg and the small view this surface had of the flat terrain of the lunar surface, which is characteristic of this landing site. Higher leg temperatures would be expected for lunar terrain that is not flat.

afternoon than shocks 2 and 3 because of its continuous illumination from noon throughout the rest of the lunar phase.

Shocks 2 and 3 were expected to exhibit identical responses to the lunar environment because of their similar positions with respect to the sun. Confirmation of this is displayed in Figure B-21.

5.2.3.7 Thrust Chamber Assembly (TCA) Temperatures

The basic thermal control design for the thrust chamber assemblies consists of a gold-plated thrust chamber, injector, and propellant valve assembly attached to a molybdenum nozzle extension cone coated with green pyrochrome thermal paint. Additional thermal paints were placed on sunlit sections of the TCAs to produce the desired heating or cooling effect. TCA-2 and TCA-3 are partially shadowed by the solar panel and omnidirectional antenna boom B mounting bracketry, respectively; solar energy reflectors are mounted in the proximity of engines 2 and 3 to increase the energy input into the bottom of the engines, reduce thermal gradients through the thrust chamber and injector assembly, and increase engine total temperature levels.

A thermal assessment of the SC-1 flight data indicates that TCA temperatures were, in general, lower than predicted. TCA temperature predictions were based on the results of analytical studies and data obtained during the SC-1 STV flight acceptance test. Prior to making flight predictions, thermal analytical models were upgraded through data correlation studies to duplicate the results obtained in STV tests.

A comparison of flight predictions and flight results for TCA-1, TCA-2, and TCA-3, respectively, is shown in Table 5.2-2 and in Figures A-22 and A-24a. Figure A-22 indicates that the flight temperature of TCA-1 was approximately 17° F lower than predicted. This temperature difference is attributable partly to errors in the analytical model and partly to discrepancies in the test/flight solar intensity correspondence. The results of STV test data and analytical model correlation studies indicate that the temperature discrepancy between flight sensor P-7 and the corresponding nodal location in the thermal model is 5° F; this discrepancy was not reflected in the flight predictions since it was considered to be small. Hence, TCA-1 was actually predicted within 12° F.

Figure A-24a indicates that the flight temperature of TCA-2 was approximately 10° F lower than predicted. This temperature difference is attributable to discrepancies in the test/flight solar intensity correspondence.

The thermal effects of gyro drift check maneuvers on the temperature control of TCA-2 can be seen clearly from Figure A-24a. Figure 5.2-15 shows the location of the vertical projection of the outboard edge of the solar panel across TCA-2 used for thermal design purposes. One of the critical thermal design parameters associated with temperature controlling TCA-2 is the location of the outboard edge of the solar panel with TCA-2 directly underneath. Solar panel location affects TCA-2 temperatures because the edge of the solar panel casts a shadow on TCA-2 during the transit phase.

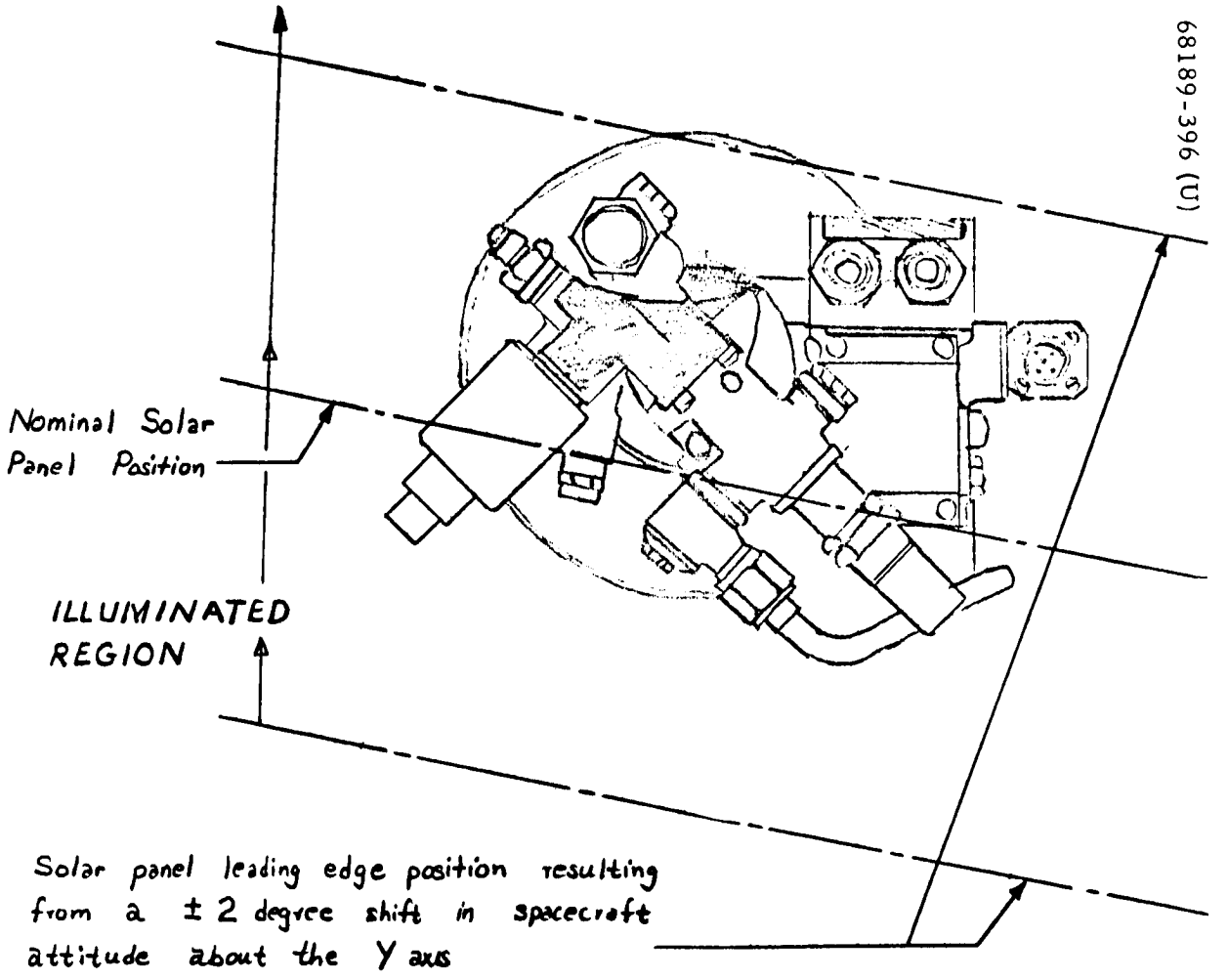


Figure 5.2-15. Thrust Chamber Assembly Illumination Pattern Resulting From Attitude Shifts

Movement of this shadow occurs when the nominal spacecraft-sun attitude is misaligned; misalignment occurs during the gyro drift check maneuvers. The actual magnitude and direction of the temperature perturbations, occurring during gyro drift check, are directly related to the spacecraft attitude and rate of change of the spacecraft attitude.

The temperature of TCA-2 increased by as much as 24° F during one gyro drift check maneuver. Positive TCA temperature perturbations occur during positive yaw maneuvers, and negative temperature perturbations occur during negative yaw maneuvers. Figure A-24 indicates that the spacecraft attitude always shifted in a positive yaw direction, exposing TCA-2 to increased solar insolation.

Figure A-24b indicates that the TCA-3 flight temperature was approximately 4° F lower than predicted. However, when considering possible solar intensity discrepancies between STV tests and flight, it seems reasonable to expect that TCA-3 should have experienced similar temperature perturbations as TCAs 1 and 2. Hence, the thermal analytical model for TCA-3 is probably biased on the high side. Small, but finite, temperature perturbations were expected during the gyro drift check maneuvers; however, the TCA-3 data does not clearly reflect any definable temperature perturbations. TCA-3 temperature perturbations would result from the shift in the shadow line cast over the engine by the omnidirectional antenna boom mounting bracketry.

Midcourse Maneuver

During the midcourse correction, the Surveyor SC-1 spacecraft performed a minus 86.5-degree roll maneuver followed by a minus 58-degree yaw maneuver. Spacecraft roll maneuvers do not disturb the normal transit solar insolation pattern on the vehicle because the vehicle-sun attitude alignment is not affected during roll maneuvers. However, yaw maneuvers result in spacecraft orientations whereby the nominal transit coast phase vehicle-sun attitude is misaligned. Increased shadowing and illumination of the vehicle subsystems occur during pitch and yaw maneuvers. The degree of shadowing and illumination of individual subsystems, resulting from pitch and yaw attitude changes, is a function of the maneuver angle.

The spacecraft-sun attitude following the midcourse minus 58-degree yaw turn may be determined by fixing the spacecraft attitude and moving the sun off normal toward the plus X axis. The sun vector now intercepts the spacecraft Z axis at a 58-degree angle when measured from the minus Z axis toward the plus X axis.

The SC-1 vernier engines operated at approximately two-thirds full thrust for 20.7 seconds during the midcourse correction maneuver. The maximum temperatures indicated by the thermal sensor for the vernier engines were 322, 272, and 252° F for TCA-1, TCA-2 and TCA-3, respectively. However, test data indicates that the radiation-cooled nozzle extension cones probably reached temperatures as high as 1850° F. The thrust chamber barrel decay following engines shutoff was significantly more rapid than predicted for all engines.

Midcourse thermal transient predictions were based on extrapolations of vernier engine operating data obtained from a series of firing tests (DD 107, 108, 109, 110) performed by JPL during May and June of 1965. These tests were conducted at Edwards Air Force Base at a simulated altitude of 100,000 feet. A comparison of the predicted and actual thermal transients for the vernier engines resulting from the midcourse burn for vernier engines 1, 2, and 3, respectively, is shown in Figures A-22 and A-24. Attempts to correlate engine firing test data with thermal analytical models were at best crude and approximate because of the inherent difficulties in defining the test environment and thermal parameters associated with the environment. Therefore, conservative analytical techniques were employed in predicting the thermal behavior of the thrust chamber assemblies during the midcourse and terminal descent operational phases.

Terminal Descent Maneuver

The nominal transit temperatures of TCA-1 and TCA-2 decreased by 6 and 4° F, respectively, following the initiation of the spacecraft plus yaw attitude maneuver. These temperature perturbations result from off-axis illumination. The maximum temperatures recorded by the thermal sensors for the vernier engines during the terminal descent mission phase were 364, 318, and 298° F for engines 1, 2, and 3, respectively. TCA-1, TCA-2, and TCA-3 were predicted to reach peak temperatures of 376, 358, and 340° F, respectively. The vernier engines operated for approximately 166 seconds.

SC-1 flight data will be particularly useful in upgrading the thermal analytical models used to predict the thermal behavior of the regenerative cooled thrust chamber assemblies during engine operation and subsequent to engines shutoff.

Lunar Surface

Lunar surface thermal behavior of TCAs 1, 2, and 3, respectively, is illustrated in Figure B-17. The thermal sensors indicated a peak temperature of 245° F for the vernier engines; however, calculations show that the vernier engines exhibit large thermal gradients when subjected to the lunar surface thermal environment. Analysis has shown a 50° F gradient between the flight sensor location and the top of the barrel/valve assembly; therefore, the maximum temperature for the TCAs can be projected to be approximately 295° F for the SC-1 landed orientation.

Calculations indicated that the TCAs could reach a peak temperature of 390° F subsequent to vehicle touchdown on the lunar surface (Reference 1). The maximum predicted temperature is based on conservative assumptions because of the complex nature of the thermal environment. However, it must be observed that lunar surface data is available for only one spacecraft location and vehicle orientation, and, further, that the SC-1 landed orientation probably is not indicative of the limiting case.

Reference 1 indicates that TCA-2 probably would be the hottest vernier engine on the lunar surface, assuming maximum solar insolation and no shadowing from vehicle subsystems. However, TCA-1 was hottest for the SC-1 touchdown orientation. Analyses showed that TCA-2 would reach a higher temperature on the lunar surface than TCA-1 for vehicle orientations, exposing each engine to maximum solar insolation because of the following reasons:

1) TCA-1 has approximately 4.5 square inches of Hughes organic white thermal paint on its head end; TCA-2 has approximately 2.8 square inches of 3M black velvet paint on its head end. While both paints are good infrared energy absorbers, the 3M black velvet paint absorbs three to four times as much solar energy per unit area as does the Hughes organic white paint.

2) Direct solar insolation on TCA-2 will be greater than that on TCA-1 because of the solar reflector placed in the proximity of vernier engine 2 to increase coast phase incident solar energy.

The SC-1 touchdown sun-spacecraft orientation is probably a good representation of a limiting case for TCA-1 and TCA-3 because of the proximity of the vehicle to the lunar equator and because the spacecraft Y axis is almost parallel to the lunar equator. TCA-3 received near maximum solar insolation during the lunar morning, and TCA-1 received maximum solar insolation during the lunar evening.

5.2.3.8 Vernier Propellant Tanks

Transit

From launch to L + 5 hours, high cooldown rates (recorded by the sensors) were observed on all vernier tanks (Figures A-20, A-26, and A-27b). This rate does not correlate with data obtained in SC-1 STV tests, but it does agree with temperature time histories observed in SC-2 STV. The difference is attributed to the rapid chilldown (51 minutes) employed in SC-2 STV as compared to the slow chilldown (5 hours) used in SC-1 STV. The rapid chilldown more closely simulates the actual environment experienced by the tanks during the flight. The rapid cooldown rates observed early in the flight represent the response of the tanks rather than the response of the propellants. Not until the tank temperatures approach a value where the heat transferred from propellant to tank very nearly equals the heat transferred from tank to thermal blanket and mount does the cooldown rate of the tanks decrease and become constant. This usually occurs about 5 hours after launch.

Analysis of oxidizer tank 2 indicated that, during the cooldown which occurs in transit, the oxidizer bulk temperature would run approximately 15 degrees warmer than the tank at the location of the flight sensor. This difference in temperature was confirmed after the midcourse maneuver when flight sensor P-16 (oxidizer tank 2) increased 16 degrees. Until

this time, the propellant that had stratified isothermally was mixed, resulting in a higher propellant temperature (probably the bulk temperature) in the vicinity of the flight sensor. The rapid rise of the flight sensor is a result of the increased heat transfer between the propellant and tank caused by the induced mixing. However, once the midcourse maneuver is completed, isothermal layers will reform in the propellant and remain in this thermal state until terminal descent. The other five propellant tanks performed similarly during the midcourse maneuver, increasing in temperature a minimum of 6 degrees (fuel tank 1) to a maximum of 16 degrees (oxidizer tank 3) and, after midcourse, cooling once again at approximately the same rate experienced immediately after launch. However, about 5 hours later, the cooldown rates again decreased and appeared to be the same as before midcourse. This again confirms the fact that the flight sensors are recording tank and not propellant temperatures.

The lowest tank temperature observed during transit was 24°F. As expected (from STV tests and analysis), oxidizer tank 2 recorded this reading. However, the temperature was not low enough to cause the tank heater to come on.

During thermal maneuvers, tank temperatures increased about the same amount they increased during the midcourse maneuver. Reference to Figures A-20, A-21, A-26, and A-27 will confirm this.

Lunar Phase

As expected, the temperature rise rate of oxidizer tank 2 (after touchdown) was considerably greater than any of the other vernier tanks. An expected 65-degree rise per day on this tank correlates well with the 63-degree rise per day recorded by flight sensor P-16. Although fuel tanks 2 and 3 and oxidizer tank 3 did not experience the same temperature rise rate as oxidizer tank 2, their warmup rates were considerably greater than the warmup rates of oxidizer tank 1 and fuel tank 1. This is to be expected since the area of the spacecraft around vernier tanks is not illuminated probably until nearly noon.

On day 157 (June 6) at around 1400 GMT, it appeared that the helium value on the oxidizer side may not have completely reseated itself, permitting depressurization of all three oxidizer tanks to occur. Response of the oxidizer tanks at this time show a rapid cooldown (Figure B-16). It is conjectured that depressurization of the oxidizer tanks permitted expansion and evaporation to occur, which would account for this cooling effect.

The maximum tank temperature was recorded on flight sensor P-13 (fuel tank 1). Because of the shadowing effect of the solar panel and planar array during the lunar day, vernier No. 1 tanks, not the expected vernier No. 2 tanks, recorded the highest temperatures for this particular spacecraft touchdown orientation. Also, the oxidizer tank and not the fuel tank was expected to be warmer. It is conjectured that the depressurization and resulting cooling of the oxidizer tanks on day 157 prevented this from occurring.

At sunset, vernier No. 1 tanks were still very warm, showing 170°F for the fuel tank and 125°F for the oxidizer tank. This is attributed to the large thermal inertia and low thermal conductance associated with vernier tanks.

5.2.3.9 Propellant Lines Temperature

The thermal response of the SC-1 propellant lines for vernier propellant lines 1, 2, and 3, respectively, is shown in Table 5.2-2 and in Figures A-19 and A-23. Vernier lines 1 and 3 temperatures were lower than predicted. Figure A-23 shows that engine 1 lines cycled between 24 and 31°F and engine lines cycled between 21 and 26°F. Cycling of vernier lines 1 and 3 was not anticipated. Nominal flight predictions were based upon the results obtained during SC-1 STV flight acceptance tests. Test data did not predict vernier lines 1 and 3 cycling at the nominal intensity level; line cycling is attributable to the discrepancy in the test/flight solar intensity correspondence. Vernier line 2 cycled as anticipated.

Flight data (Figures A-19 and A-23) indicated that the duty cycles for vernier lines 1, 2, and 3 were 17, 77, and 67 percent, respectively. Hence, the heaters for vernier lines 2 and 3 drew current from most of the transit mission phase, while the heater for vernier line 1 drew current for only 17 percent of the transit mission phase.

The maximum temperatures reached by the vernier propellant lines during the midcourse maneuver were 66, 65, and 61°F for lines connecting engines 1, 2, and 3, respectively. Propellant line temperature perturbations resulted primarily from the warmer storage propellants flowing through the lines during engine operation and not from radiation interchange and exhaust gas impingement from the vernier engines and their exhaust plumes. Radiative and convective heating from the vernier engines and the exhaust plumes, while present, has been determined to be small. An investigation of the Surveyor S-10 (thermal control model test phase 1, March 1966) thermal data indicates little or no radiative heating on the lines as a result of radiation interchange.

During engine operation, the cool stagnant propellant flows from the vernier lines, and warm propellants from the storage tanks flow through to the engines. The propellant lines attempt to equilibrate at the mean bulk temperature of the flowing propellants, giving rise to the maximum temperatures observed on lines 1, 2, and 3. The lunar surface thermal behavior of the SC-1 vernier propellant lines is illustrated by Figure B-15. The vernier lines reached a peak temperature of 221°F subsequent to vehicle touchdown on the lunar surface. Maximum temperatures were not calculated for the propellant lines for a lunar surface thermal environment.

5.2.3.10 Helium Tank Temperatures

Figure A-28 indicates that the flight temperature of the helium tank (P-17) was approximately 17°F lower than predicted. This temperature difference is attributable partly to the fact that predictions are based on a semidegraded white thermal finish and partly to discrepancies in the test/flight solar intensity correlations.

The helium tank temperature, as indicated by the thermal sensor, decreased 9°F during the midcourse maneuver. Localized shadowing by spacecraft subsystems and structural members resulted in decreased solar insolation on the tank. Hence, tank temperatures dropped following the initiation of the yaw maneuver.

The nominal transit temperature of the helium gas supply tank decreased by 23°F following the initiation of the terminal positive yaw maneuver. The helium tank temperature perturbation is attributed to the off-axis heating of the tank and decreased solar insolation on the tank resulting from shadowing by spacecraft subsystems and structural support members.

The lunar surface thermal behavior of the Surveyor SC-1 helium tank is shown by Figure B-14. The helium tank reached a peak temperature of 145°F during the lunar day. Calculations indicate that the helium tank could reach a peak temperature of 205°F subsequent to spacecraft touchdown on the lunar surface (Reference 2). The maximum predicted temperature assumes prior ultraviolet degradation of the inorganic white thermal finish, maximum solar insolation, and no shadowing from vehicle subsystems.

5.2.3.11 Main Retro Engine

The thermal behavior of the retro propellant is monitored by two flight sensors located on the retro case. Flight sensor P-3, representative of the upper propellant temperatures, dropped 11°F during transit, measuring 75°F at launch and 64°F just prior to retro firing as shown in Figure A-18. The temperatures for P-3 showed a maximum deviation of 2°F from prediction. Temperatures of the middle and lower propellant, as indicated by sensor P-12, were as much as 10°F higher than prediction as shown in Figure A-25. This sensor read 76°F at launch and was 43°F just prior to retro firing. The discrepancy, while within the prediction accuracy of ±15°F, is attributed to basing the predictions on a STV test phase (S-10 vehicle, phase 2, 15 March 1966) in which the spaceframe and nozzle were artificially cooled, thereby suppressing lower case temperatures. Predictions took this suppressed case temperature into account, but did not compensate for it sufficiently.

The propellant bulk temperature at ignition was predicted to be 54°F based on real time data and was calculated by arithmetically averaging flight sensors P-3 and P-12. This correlation was based on the results of STV

tests of an inert engine with thermal properties nearly identical to those of actual propellant. These STV tests, which provided sufficient data to determine the bulk temperature accurately, agreed with the correlation within 5°F. The prediction of 38.5 seconds for the burn time of the propellant, which is a function of the bulk temperature, was 1 percent lower than the estimated burn time of 38.9 seconds in the SC-1 flight. If the entire error in predicted burn time, which is a function of several variables, is assumed to occur solely due to error in temperature, the actual bulk temperature would have had to be 10°F lower than the predicted value of 54°F.

Nozzle sensor P-22 achieved a steady-state temperature of -124°F during the SC-1 flight as compared to its predicted steady-state value of -222°F. The deviation is accounted for by an error in the analytical model. The analytical program did not include any radiation coupling with the spacecraft but did predict nozzle sensor temperatures in the -200°F range. Temperatures in the -200°F range were further substantiated by STV testing of the thermal control model (S-10) where similar temperatures were encountered. In S-10 phase 2 testing, a shroud was placed over the nozzle, thereby eliminating any radiative coupling to the spacecraft. Based on the SC-1 flight results, the analytical program was revised accordingly with a steady-state temperature of -120°F resulting. SC-1 STV tests (phases 6A and 6B) indicated sensor temperatures of -98°F and -84°F, respectively, the difference from the -120°F being due to the test chamber environment. It should be emphasized that the temperature of the nozzle cone has little or no influence on the survival capabilities of the retro propellant. The sensor is used primarily to monitor vernier engine exhaust impingement during thrusting.

Retro preconditioning with the onstand air conditioning system results in propellant bulk temperatures in the desired 70 ± 5°F range at launch. During the last 2 hours prior to launch, the conditioning air temperature was raised to 85 ± 5°F. A 2°F increase in propellant bulk temperature resulted during this period. The flight sensors read 75°F (P-3) and 76°F (P-12) at launch, while they were predicted to start at 73°F. Test data from a previous test on the retro, in which the retro assembly was exposed to an ambient temperature 15 ± 5°F higher than the initial bulk temperature of the propellant, indicated that the outer propellant temperatures, and therefore case temperatures, rose 4 to 6°F during the first 2 hours of the test. The bulk temperature rose 2°F in this time. Because the flight sensor temperatures in the SC-1 preconditioning were consistent with data recorded in the simulated retro prelaunch environmental test, a correlation is believed to exist between the test and the actual preconditioning. Projecting into future Surveyor flights where the 85°F Centaur environment may last as long as 6 hours for a flight in which the Centaur is boosted into a parking orbit, the flight sensors on the case may be expected to register as much as a 10°F increase, whereas the bulk temperature would increase by 4°F during this period.

During the midcourse maneuver, nozzle sensor P-22 rose to a temperature of -53°F, 71°F above its coast phase steady-state temperature of -124°F. This rise in nozzle temperature was due to a combination of two events, the midcourse yaw and the vernier engine firing.

During midcourse, SC-1 yawed -58 degrees, exposing half the nozzle to direct sunlight (Figure 5.2-16). The region of the nozzle near the sensor was exposed to solar radiation. An analysis of the nozzle was conducted to verify the rate of temperature increase due to incident sunlight. The analysis showed that the 29°F rise in nozzle sensor temperature prior to vernier engine firing was consistent with the nozzle temperature rise expected for the position of the sensor in relation to the sun vector. However, the noisy flight data (Figure 5.2-17) for P-22 during midcourse tends to decrease the certainty that can be associated with interpretation of P-22 midcourse data.

As a by-product of the analysis of off-angle insolation on the nozzle, it was found that the maximum possible temperature gradients occur on the nozzle when any combination of pitching or yawing maneuvers produces an angle of 75 degrees between the negative Z axis of the spacecraft and the sun vector. After 1/2 hour of solar irradiation at this 75 degree orientation, the element of the nozzle normal to the sun vector, having started at steady-state temperatures, will experience temperatures varying from 105°F at the nozzle closure to 129°F at the exit plane. Elements of the nozzle 180 degrees away, however, will not have changed from steady-state temperatures which range from 5°F at the closure to -170°F at the exit plane.

The P-22 temperature-time plot experienced a noticeable change of slope during midcourse vernier firing (Figure 5.2-17 with midcourse events annotated). The vernier engines fired for 20.75 seconds, and the temperature rose 15°F in this time. Bounding calculations indicate that the incident heat flux due to vernier engine firing was between 0.162 and 0.485 Btu/sec-ft^2. A conservative analysis of the vernier plume predicts flux values below 0.100 Btu/sec-ft^2 at the sensor. Hence, a discrepancy exists between the prediction and data-based calculation of the heat flux due to vernier firing. Error is possibly in the somewhat limited midcourse data of P-22 or in the assumptions of the analysis of the vernier plume.

5.2.3.12 Flight Control Electronics and Canopus Sensor

The flight control electronics chassis boards, numbers 1 and 6 (sensors FC-44 and FC-45), and the Canopus sensor interior (FC-47) were 10 to 12°F lower than the predicted temperatures for the coast phase (Figures A-7, A-8, and A-10a).

The calculation of the predicted temperatures included consideration of all factors that would cause the in-flight temperature to be different than in the STV tests. These factors are the effects of the test chamber walls, the divergence of the simulated sunlight, the spectral mismatch of the simulated sunlight, and the seasonal variation in the actual sun intensity.

Temperatures of the flight control electronics boards and the Canopus interior while on the lunar surface are shown in Figures 5.2-18 and 5.2-19. After the spacecraft was on the moon for about 56 hours, the flight control

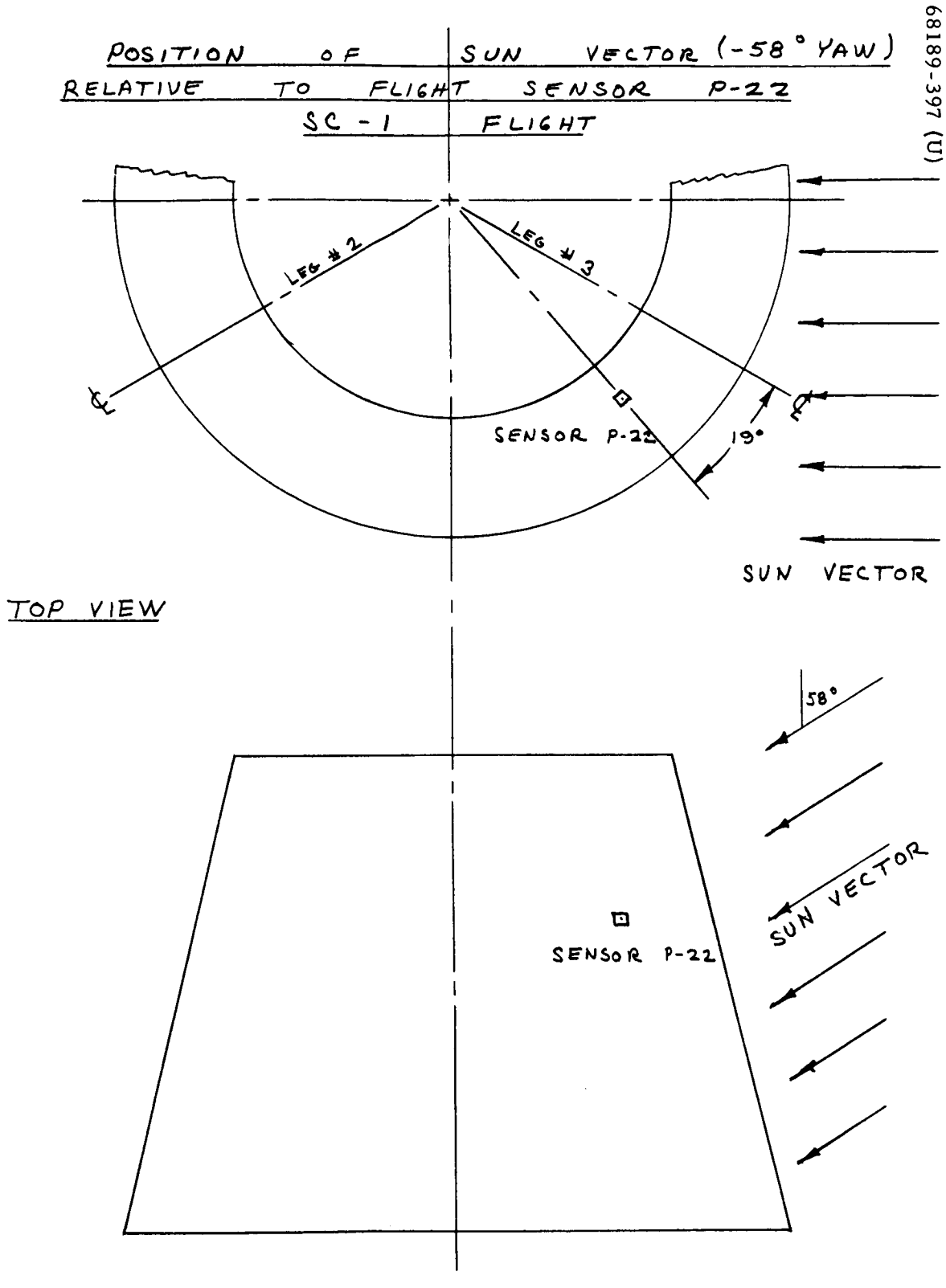


Figure 5.2-16. Position of Sun Vector (-58 degree Yaw) Relative To Flight Sensor P-22

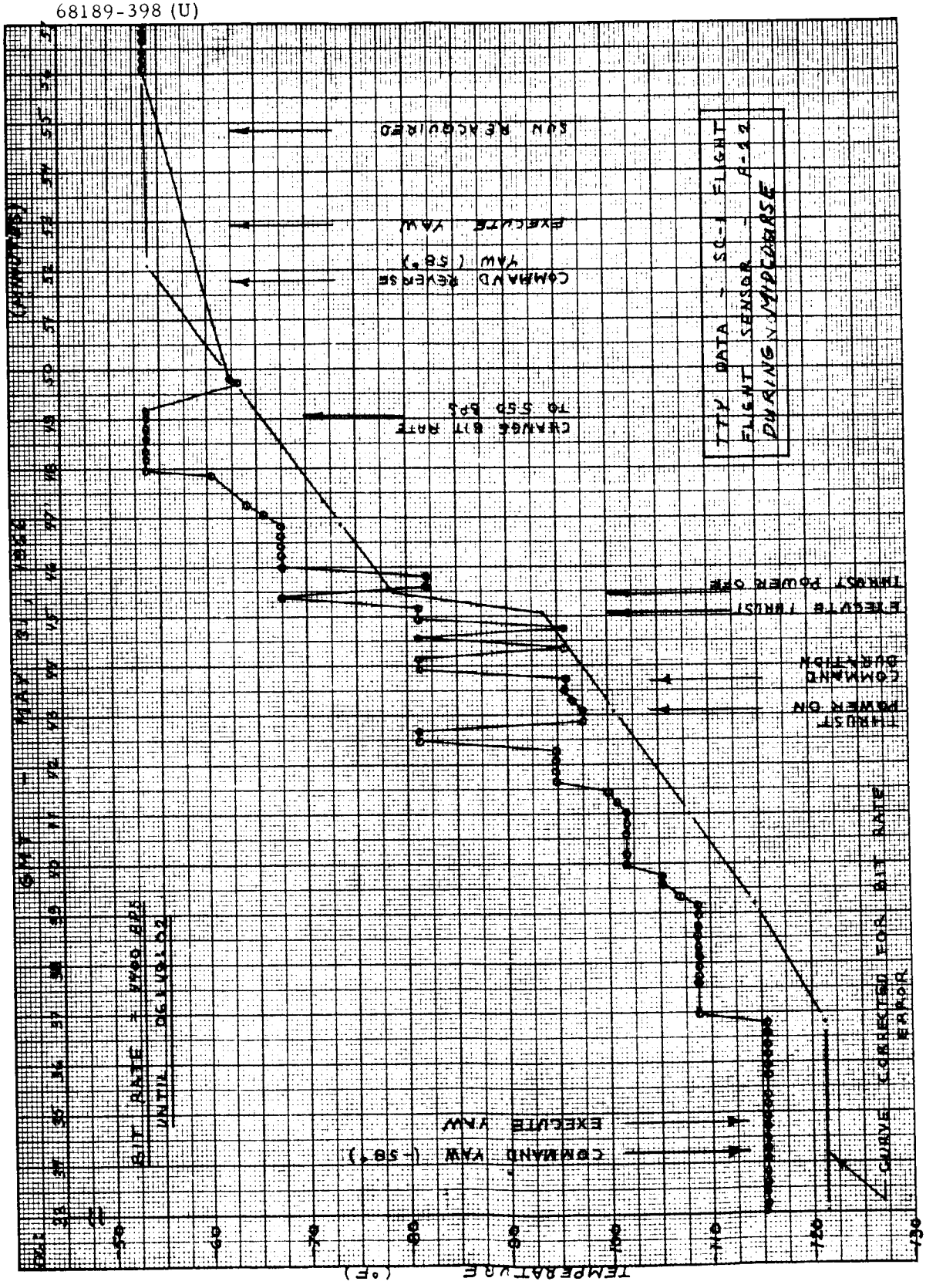


Figure 5.2-17. SC-1 Flight Sensor P-22 (Retro Nozzle) During Midcourse

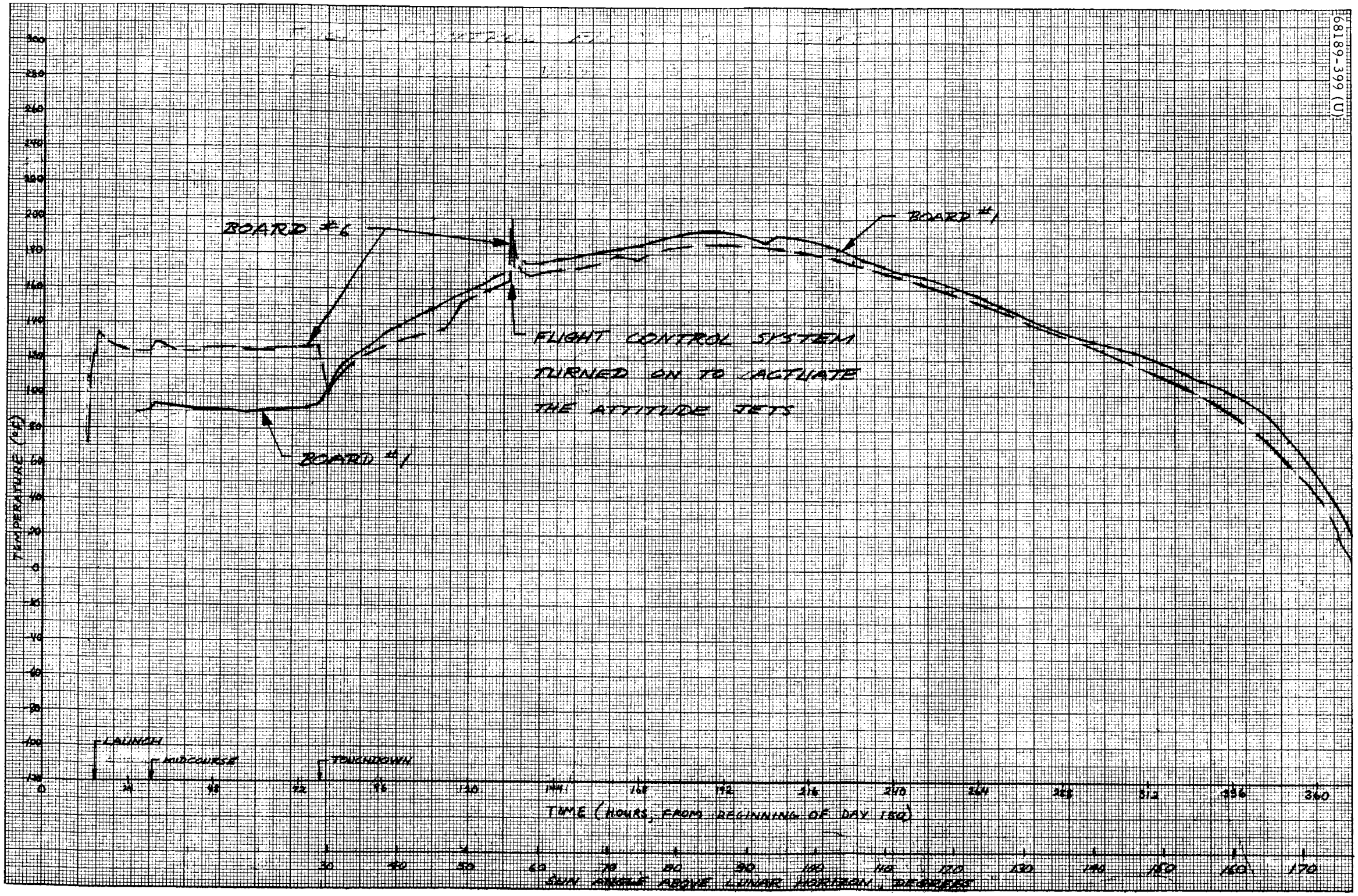


Figure 5.2-18. Flight Control Electronics Boards (FC-44 and FC-45) on First Lunar Day

FOLDOUT FRAME

FOLDOUT FRAME

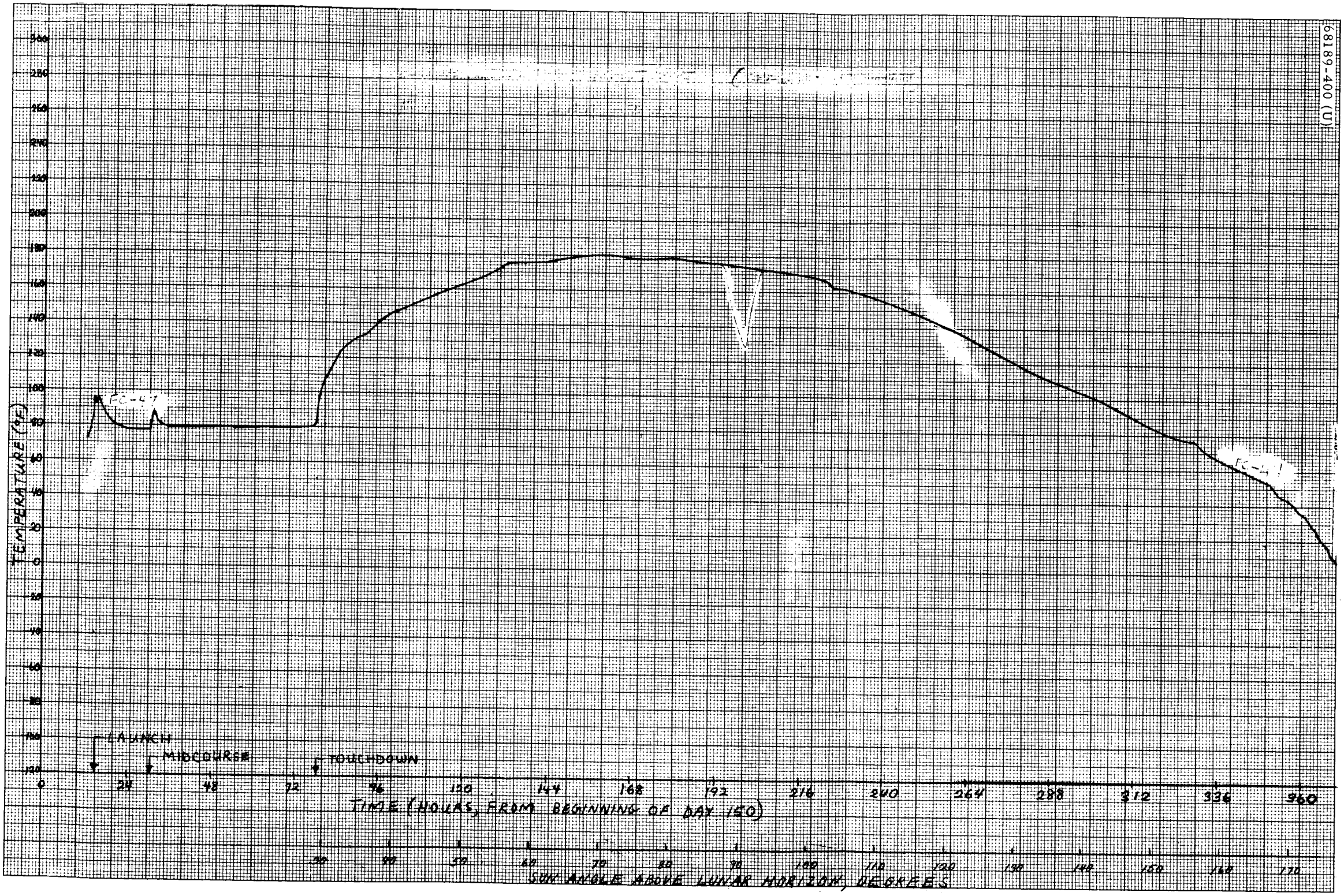


Figure 5.2-19. Canopus Temperature (FC-47) on First Lunar Day

system was turned on to actuate the attitude jets to see if the lunar dust would be disturbed. At that time, the sun angle was 56 degrees above the lunar horizon, and the initial temperature of flight control electronics board 6 was 164°F. The temperature rise rate of flight control electronic board 6 was 32°F in 12.5 minutes or 144°F per hour (Figure 5.2-20). The temperature response data is valuable for the studies of the lunar liftoff capability of forthcoming Surveyor spacecrafts.

Inertial Reference Unit

The inertial reference unit consists of the roll, pitch, and yaw gyros, three temperature controllers, and three heaters. The temperature control system keeps the inside of the gyros at 180 ± 1°F. The flight temperature data is derived from temperature sensors located on the outside of the gyro cases and is independent of the temperature control system.

The temperature readings of the high accuracy gyro temperature sensors are influenced by the telemetry bit rate. At 550 bits/sec, the gyro temperature sensors read 2.7°F higher than at 17.2 or 137 bits/sec. At 1100 and 4400 bits/sec, the gyro temperature sensors read 7 to 11°F higher than at 17.2 or 137 bits/sec. The bit rate was 1100 bits/sec from 1 to 11 hours after launch, and then it was changed to 550 bits/sec. The pitch and yaw gyro temperatures were within 3°F of the predicted temperatures (Figure A-12).

The roll gyro was 8°F lower than predicted (Figure A-9). The duty cycle of the roll gyro heater was normal, and therefore the temperature inside the gyro probably was 180 ± 1°F. The reason for the 8°F-error in the predicted temperature of the roll gyro is not known, but it might be due to a change in the contact conductance in the gap between the support ring and the gyro case. The heater is located on the gyro support ring, and the temperature sensor for the flight data is on the gyro case. Vacuum grease will be used between the support rings and the gyro cases (on SC-5 and up) to make the contact conductance less variable.

The roll, pitch, and yaw gyro temperature curves for the first lunar day are shown in Figures 5.2-21 through 5.2-23. The flight control system was turned on to actuate the attitude jets on the lunar surface. The temperature rise of the gyros can be seen in Figures 5.2-20 through 5.2-23. The temperature rise rate of the pitch gyro was 25°F in 10 minutes or 150°F per hour. The temperature rise rate and drop rate is very useful for evaluation of the lunar liftoff capability of future Surveyor spacecraft.

5.2.3.13 Roll Actuator

The steady-state temperature of the roll actuator in the transit phase was 81°F compared to a preflight prediction of 98°F. The calculation of the predicted temperature included consideration of all the factors that could

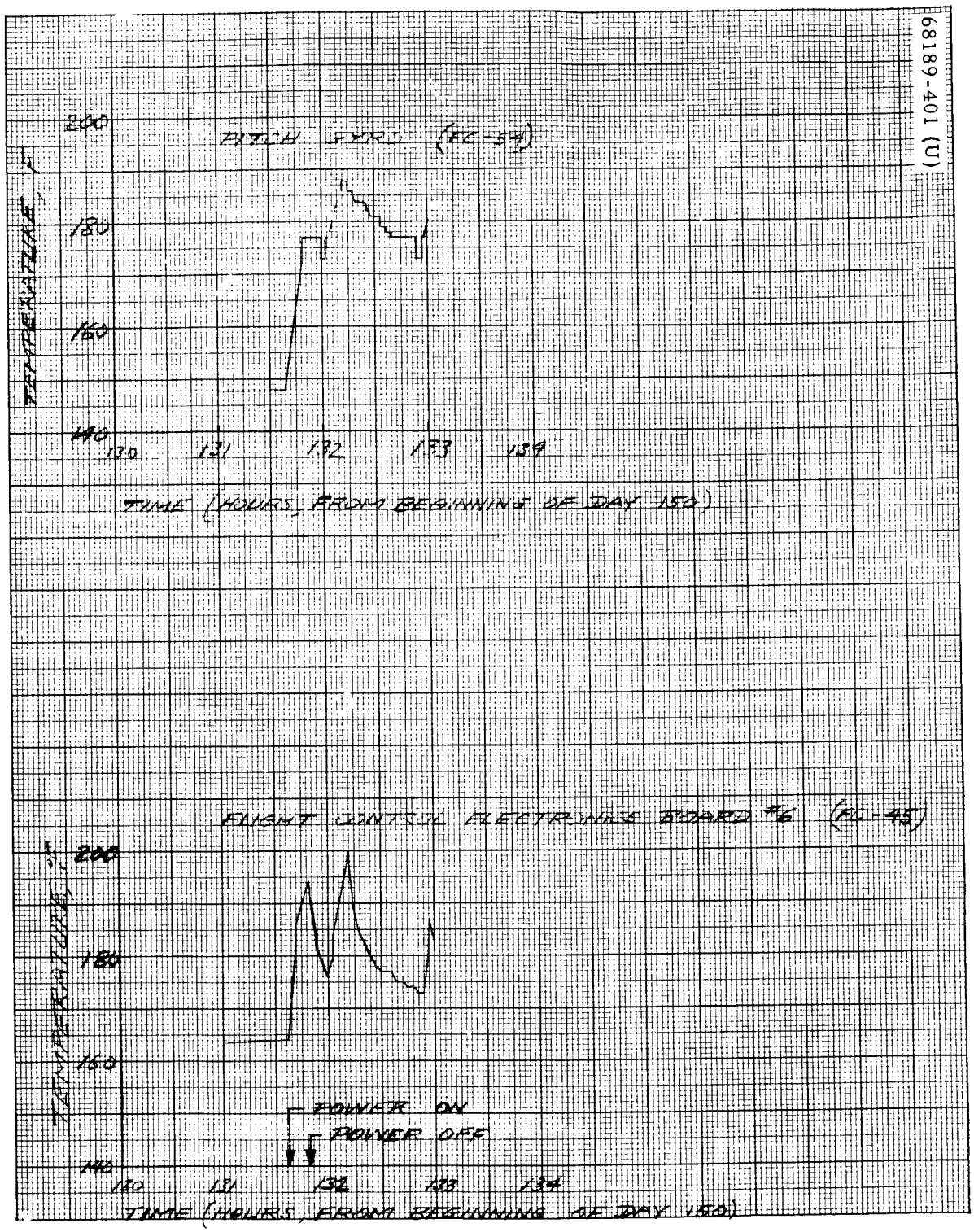


Figure 5.2-20. Temperature Rise of Pitch Gyro (FC-54) and Flight Control Electronics Board 6 (FC-45) When Flight Control System Operated on Moon

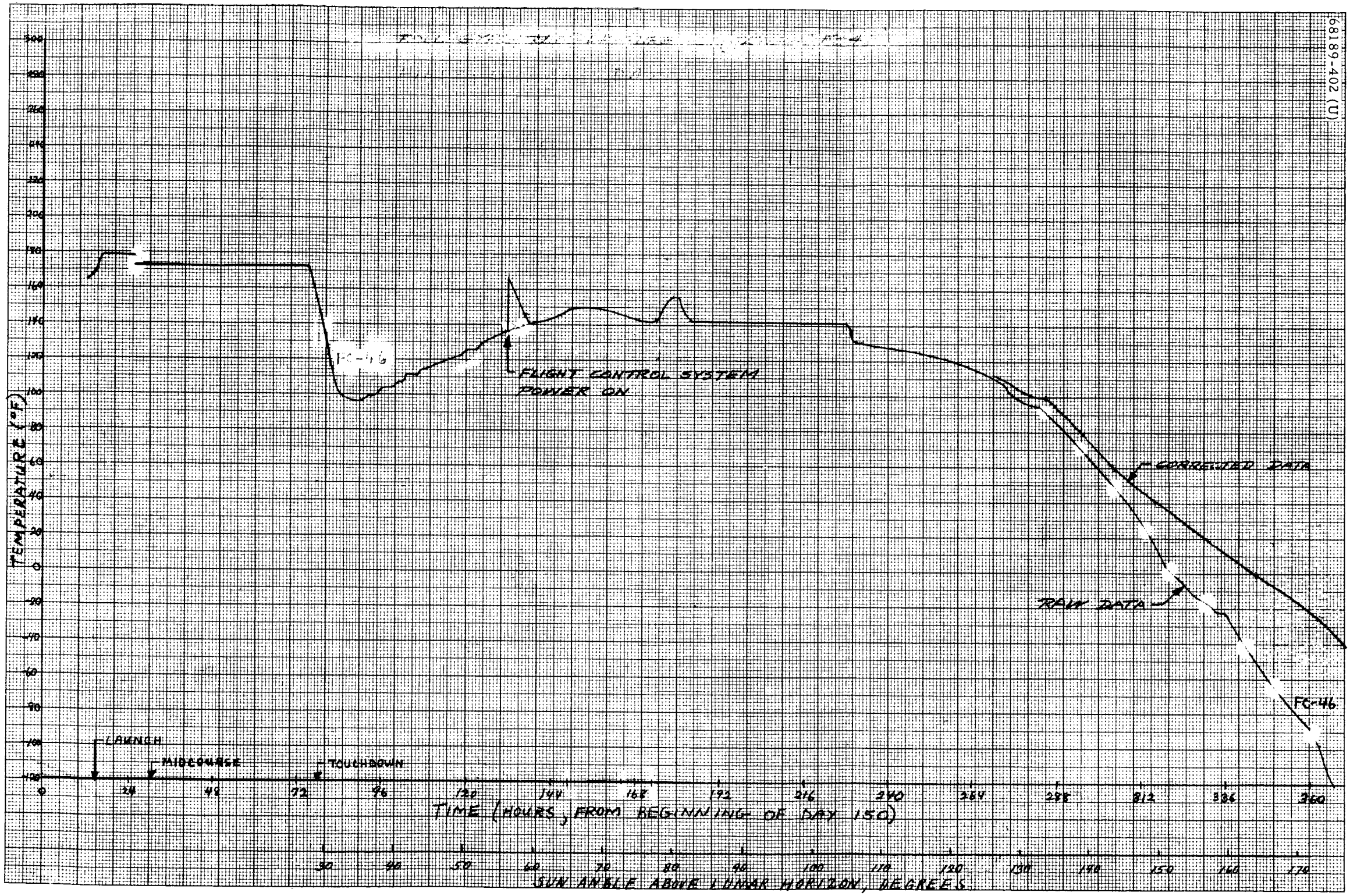


Figure 5.2-21. Roll Gyro Temperatures (Sensor FC-46) on First Lunar Day

FOLDOUT FRAME

FOLDOUT FRAME

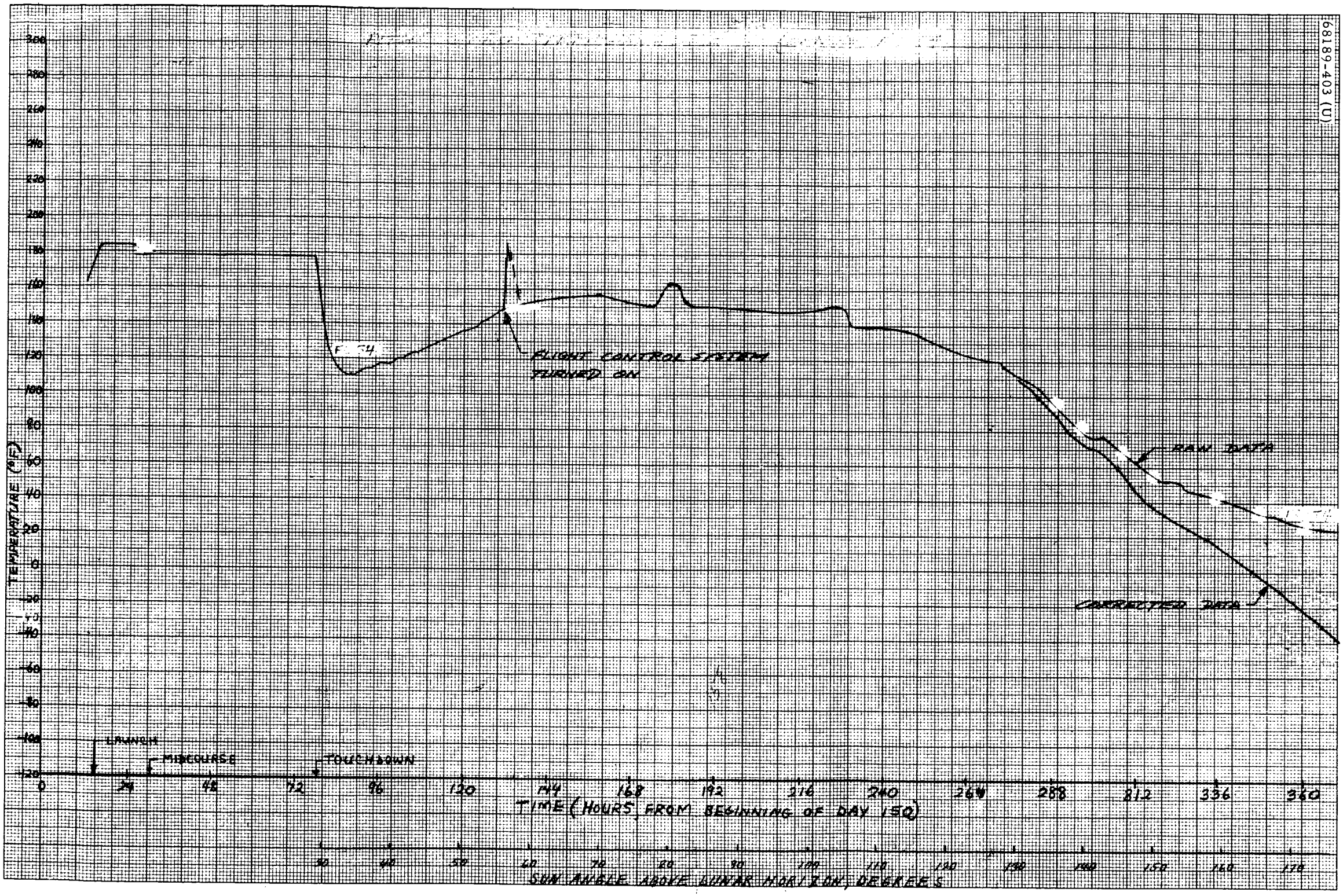


Figure 5.2-22. Pitch Gyro Temperature (Sensor FC-54) on First Lunar Day

FOLDOUT FRAME

FOLDOUT FRAME

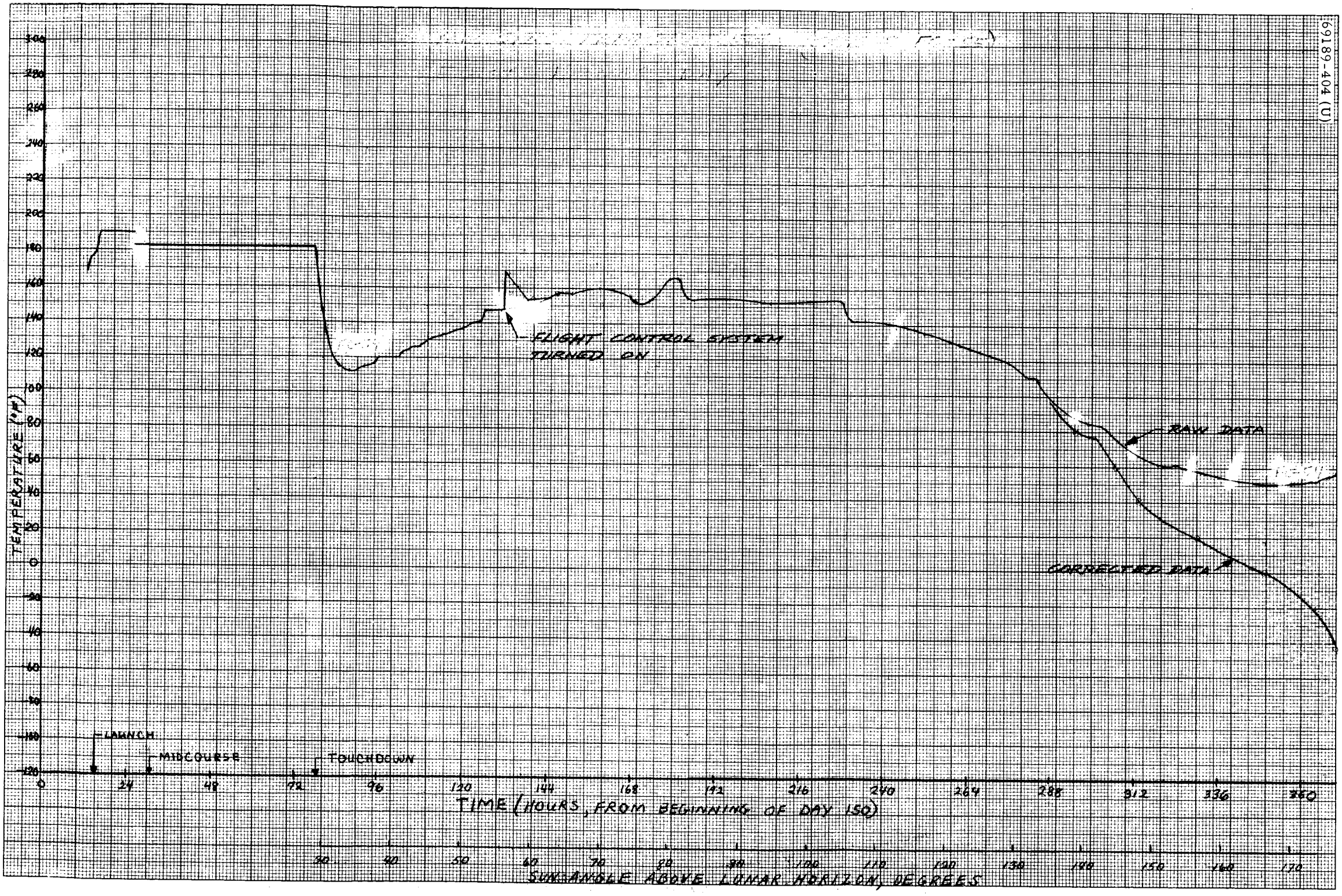


Figure 5.2-23. Yaw Gyro Temperature (Sensor FC-55) on First Lunar Day

FOLDOUT FRAME

FOLDOUT FRAME

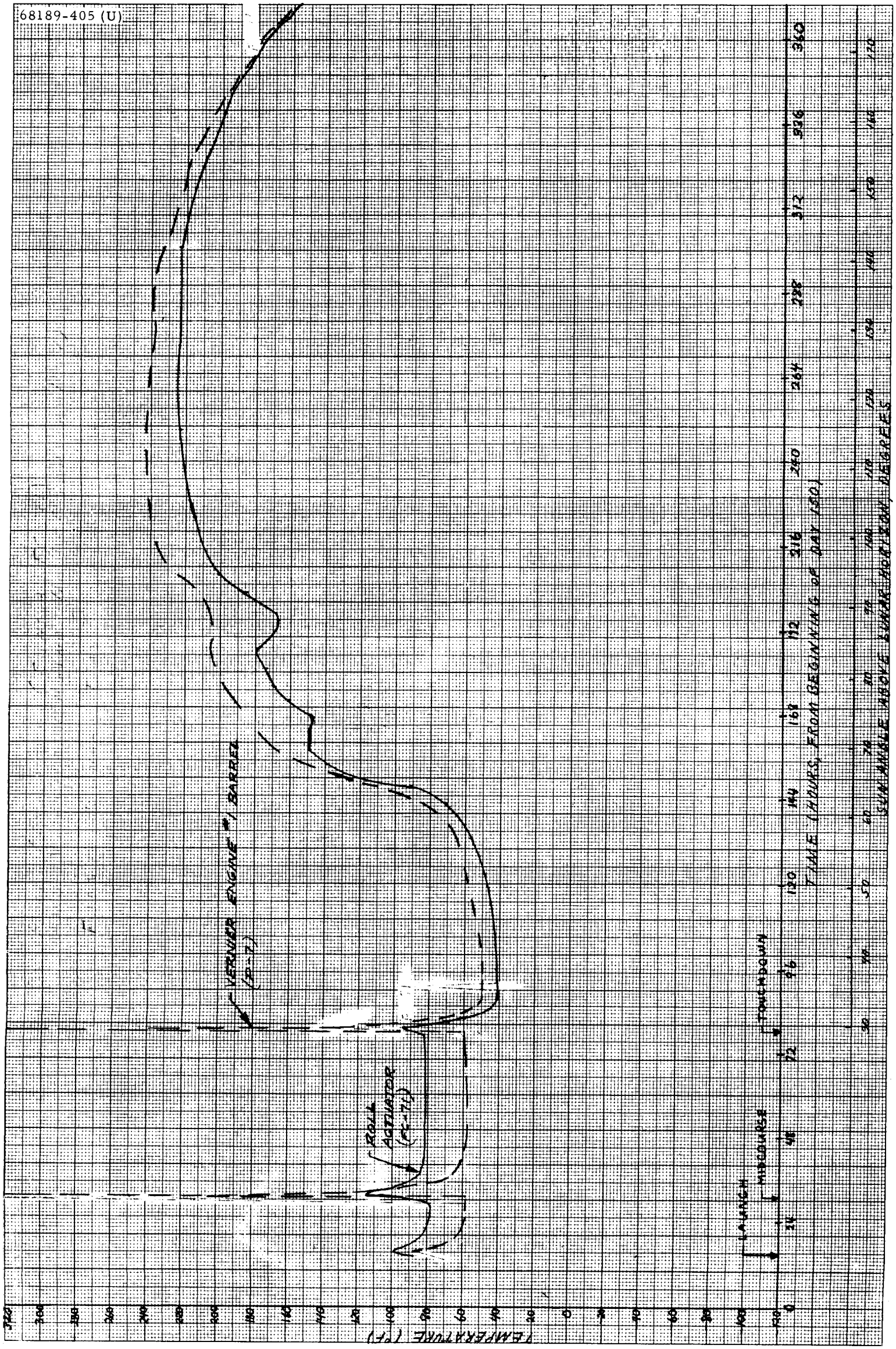
cause the temperature in STV tests to be different than in the actual flight environment. The calculated steady-state temperature for flight was based on the simulated sun intensity indicated by the Eppley radiometer. If the black plate radiometer sun intensity had been used, the predicted temperature would have been 12°F lower, and the error would have been only 5°F instead of 17°F. (The difference between the Eppley radiometer and the black plate radiometer is 7 percent, and this makes a difference of 12°F in the roll actuator temperature.) It appears that the black plate radiometer used in the STV tests gives a more accurate value of the simulated sun intensity than the intensity indicated by the Eppley radiometer.

The roll actuator temperature rise at midcourse due to the vernier engine operation was 2.5 times greater than predicted. (The predicted temperature rise was 15°F, and the actual temperature rise was 38°F.) The predicted temperature rise was for engine operation at 67 pounds thrust for 16.7 seconds while the actual SC-1 engine operation at midcourse was 72.5 pounds average thrust for 20.8 seconds. The predicted temperature rise was proportional to engine operating duration; it was one-third of the roll actuator temperature rise seen in test number DD-107 at Edwards Air Force Base on 14 May 1965. This test was conducted for 51 seconds of engine operation at 78 pounds thrust. However, the roll actuator temperature rise after the 20.8-second midcourse engine operation was approximately the same as seen after the 51-second engine test. This rise probably occurs because the roll actuator is adjacent to the vernier engine barrel, and the barrel temperature rise is almost independent of the engine operating duration. The engine 1 barrel temperature rise due to the 20.8-second midcourse firing duration at 72.5 pounds thrust was 262°F, and the barrel temperature rise due to the 51-second duration test at 78 pounds thrust was 290°F. A comparison of the temperatures of the roll actuator (FC-71) and vernier engine 1(P-7) throughout the transit and lunar phases of the mission is shown in Figure 5.2-24.

5.2.3.14 Nitrogen Tank

The nitrogen tank steady-state temperature in the transit phase was 46°F while the predicted temperature was 71°F (see Figure A-11). The predicted temperature was based on STV test data (with degraded white paint on the tank) plus a correction for the combined effect of the test chamber walls and the spectral mismatch of the simulated sun. No correction was made for the seasonal variation in the solar constant. If the 3 percent reduction in the sun intensity had been included, the predicted temperature would have been 5°F lower. The white paint on the nitrogen tank was cleaned before launch, and this effect on the temperature (a 15°F reduction) was not included in the prediction. If the effect of the seasonal variation in sun intensity and the effect of cleaning the nitrogen tank had been included in the prediction, the error would have been only 5°F. The nitrogen tank temperatures on the lunar surface are shown in Figure 5.2-25.

PRECEDING PAGE BLANK NOT FILMED.



FOLDOUT FRAME

5.2-82

Figure 5.2-24. Roll Actuator (FC-71) and Vernier Engine 1 (P-7) Temperature History

FOLDOUT FRAME

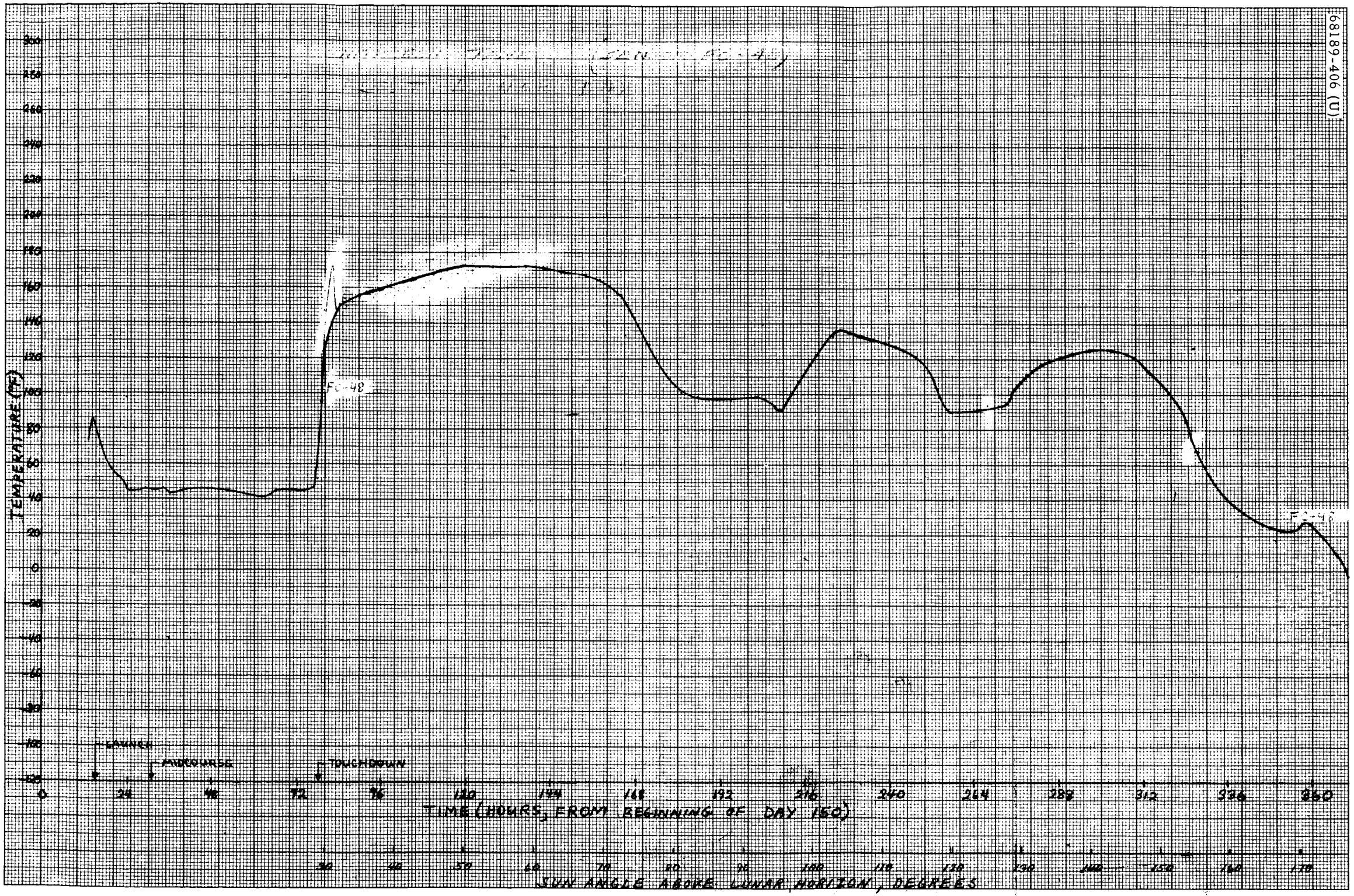


Figure 5.2-25. Nitrogen Tank (FC-48) on First Lunar Day

FOLDOUT FRAME

FOLDOUT FRAME

5.2.3.15 Attitude Gas Jet

Flight Summary

The No. 2 gas jet's temperature increased about 5 degrees about 30 minutes into the flight. This temperature rise rate is representative of a gas jet illuminated normal to its length, such as gas jet 1 was illuminated during transit. The data obtained during this period correlates well with posteclipse warmup data obtained from STV testing.

The gas jet 2 steady-state temperature (88°F) occurred approximately 3 hours after launch (Figure A-13 and Table 5.2-2). However, the jet temperature increased slowly throughout the flight and, at L plus 60 hours, had risen to 91°F. This condition is to be expected since the leg to which the jet is mounted increased in temperature during the flight because of the continued degradation of its white paint. This increase of 3 degrees in gas jet 2, for an increase in leg temperature of 5 degrees during the flight, agrees with the value extracted from STV tests.

During the midcourse maneuver, gas jet 2 increased in temperature, confirming the negative yaw maneuver. After the execution of the reverse yaw, the jet cooled to 80°F and then rewarmed to its coast phase temperature of 88°F in about 3 hours. The dip in jet temperature below 88°F after the reverse yaw is attributed to the much cooler leg temperature which, at the time of the reverse yaw, had cooled to 80°F.

No visual response of the gas jet to gyro drift tests was observed, although an increase of about 1 degree was expected.

During the terminal maneuvers, gas jet 2 probably decreased in temperature after the plus 59.9-degree yaw; then it increased in temperature (after the plus 94.1 degree roll) to about 105°F at touchdown. However, flight data for this period is unavailable.

Gas jet 3 was expected to be about 10 degrees warmer than gas jet 2, 98°F near launch with the spacecraft in a stabilized transit attitude and increasing slowly to 101°F late in transit. Although jets 2 and 3 are attached to their respective legs in a similar manner, the jet on leg 3 is probably warmer because that leg has a higher temperature. However, this cannot be confirmed because gas jet 3 did not have a flight sensor.

Gas jet 1 was expected to be the warmest of all jets (about 145°F) because of its orientation with respect to the sun vector during transit. This jet is mounted with its length normal to the sun, while gas jets 2 and 3 are illuminated on one end only. Gas jet 1 had no flight sensor.

During the midcourse maneuver, gas jet 3 probably increased in temperature to about 105°F, while gas jet 1 decreased to about 130°F. As a result of the terminal maneuver, gas jet 3 probably increased to about 111°F, and gas jet 1 decreased to about 120°F at touchdown.

Lunar Phase

Approximately 4 hours after touchdown, gas jet 2 increased in temperature to 175°F. This rapid increase was due to the low elevation angle of the sun at this time, illuminating the jet along its length in addition to reflected energy off the lunar surface. The recorded 175°F agrees well with the calculated 150°F, the major difference in temperature being attributable to conductance errors between the jet and the leg to which it is attached.

The maximum temperature (206°F) of gas jet 2 occurred about 2-1/2 days before lunar noon when the sun angle above the lunar horizon was 60 degrees (Figure B-20). The conductance between the gas jet and leg prevented jet temperatures from exceeding 300°F during this period. After lunar noon, the gas jet and leg cooled at the same rate.

It is conjectured that gas jet 3 behaved similarly to gas jet 2 after touchdown, but that gas jet 1 responded differently. This is due to the different orientation of the jets with respect to the sun vector, coupled with the different jet/leg conductances. Gas jet 1 was expected to reach a maximum temperature of about 190°F near lunar noon and then exhibit a cooldown rate similar to the cooldown rate of the leg to which it is attached. It is interesting to note that, because of the orientation of gas jet 1 with respect to its environment, as well as its conductance to leg 1, a gas jet/leg temperature difference of about 30 degrees is maintained from around lunar noon to terminator.

5.2.3.16 RADVS System

As can be seen in Table 5.2-8, the RADVS system flight temperatures varied from 12°F cooler to 3°F warmer than predicted. If STV test data had been used instead of analytical techniques to determine the temperature decrement associated with the higher than nominal intensity at the elevation of the signal data converter compared to the test plane, a flight temperature prediction of 58 instead of 53°F would have resulted. Then all the predictions would have been consistently higher in temperature than the resulting flight temperatures.

During midcourse maneuvers, the yawing of the spacecraft caused the altitude/velocity (A/VS) preamplifier to be shadowed and the velocity sensor (VS) preamplifier to be fully illuminated by solar irradiation. The A/VS preamplifier cooled 10°F at a rate somewhat less than its STV eclipse rate.

TABLE 5.2-8. COMPARISON OF RADVS FLIGHT AND STV TEMPERATURE

Unit	Sensor	Flight Prediction, °F	Actual Flight, °F	Phase 6C "Plugs Out," °F	Minimum-Maximum Operating Limits, °F
KPSM	R-8	22	12	12	-22 to 100
SDC	R-9	53	56	58	18 to 118
VS Preamp	R-10	45	33	30	-58 to 122
A/VS Preamp	R-13	32	22	19	-58 to 122

The slower cooling effect was caused by partial illumination of the preamplifier by reflected solar energy and by hotter bounding spacecraft temperatures. The VS preamplifier increased 14°F during off-angle solar heating. This temperature rise was less than the maximum possible temperature rise due to off-angle solar heating because the solar vector was not in the maximum heating orientation. Comparisons of flight temperature with predictions for the RADVS system are shown in Figures A-32 through A-35.

The temperature history of the RADVS subsystem during the first lunar day is presented in Figure 5.2-26. If the RADVS subsystem is to be used for a future "hopping" experiment on the lunar surface, the temperature of each unit should not exceed its maximum operating temperature. Therefore, if the sun's vector is in the direction of leg 1, as it was in the lunar afternoon for SC-1, the klystron power supply modulator (KPSM), A/VS preamp, and VS preamp would all exceed their maximum operating temperature even at a solar elevation angle of 0 degree. However, if the sun's vector is between legs 2 and 3, as in the lunar morning for SC-1, all RADVS units would be below their maximum operating limits for a solar elevation angle below 35 degrees.

It was assumed in the previous discussion that maximum operating temperature at the time of RADVS turnon was the same as during terminal descent. If the RADVS were turned on for a shorter period of time during lunar "hopping" than during terminal descent, a higher starting temperature would be permissible, thereby allowing a greater range of times (solar angles) which could be used for the "hopping" experiment.

PRECEDING PAGE BLANK NOT FILMED.

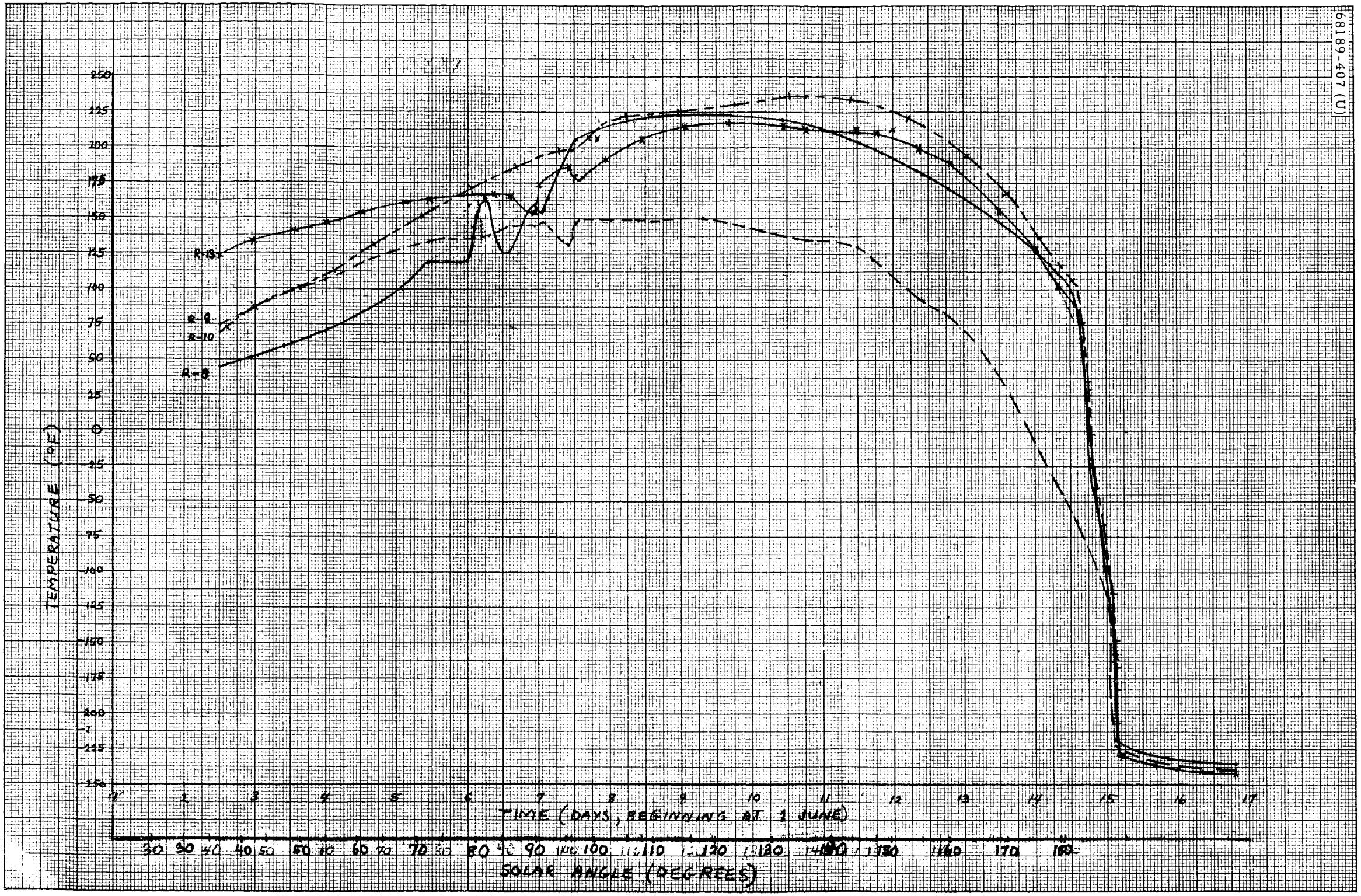


Figure 5.2-26. RADVS Temperature on First Lunar Day

FOLDOUT FRAME

FOLDOUT FRAME

5.2-89-1

5.2-89-2

5.2.3.17 Altitude Marking Radar

AMR flight temperatures were lower than predicted although well within allowable tolerances as shown in Table 5.2-2 and Figures A-30, A-31, and A-36. The electronics (sensor R-7) were 5°F lower than predicted, the electronics mounting platform (sensor R-6) is 12 degrees lower, and the antenna dish edge (sensor R-27) is 20°F lower. The increased temperature gradient in the direction from inside the electronics compartment to the antenna indicates larger heat losses in flight by this path than in the STV qualification tests upon which the predictions were based. These results are consistent with the space environments being colder than the test chamber environment.

Figure 5.2-27 shows a high resolution plot of the response of the AMR electronics temperature to the cycling of the thermostatically controlled heater during SC-1 flight. The data indicated the heaters are operating at a 68 percent duty cycle. The AMR nominal heater capability is 5 watts, and the average heater dissipation is 3.41 watts for stabilized transit temperature conditions. The energy expenditure was 198 watt-hr for the 58-hour period in transit in which the heater was cycling. This compares to the 60 percent duty cycle and 3 watt heater dissipation during the STV test phase. The increased power consumption of the thermostatically controlled heaters in space is in agreement with the greater heat loss from the AMR compartment to the antenna dish associated with the larger temperature gradients.

Figure 5.2-28 presents the temperature of the AMR antenna dish during the midcourse maneuver. The temperature response of the flight sensor to the change in attitude (-58 degrees yaw) is 2.5°F/min, and the temperature response due to the vernier exhaust impingement is 9.4°F/min. The temperature response to the maneuver in which the edge of the antenna becomes illuminated by the sun lags the attitude change by 3 minutes. This is because the sensor is covered by an insulation batt that delays the transfer of solar energy to the sensor and/or is remotely located relatively to the sun vector.

5.2.3.18 Television System

Introduction

This subsection is a summary of the thermal information so far extracted from SC-1 data pertaining to television camera 3.

Prior to the mission, extensive thermal analyses were made to assist in the thermal design of the camera and also to attempt to determine any specific thermal problems that might arise either in transit or upon the lunar surface.

These studies were initiated in May 1964 along the lines laid down in Reference 3. In all these studies, the camera's thermal environment was assumed to be that as predicted in Reference 4 for transit and as predicted in Reference 2 for the lunar surface. The technique employed in making the

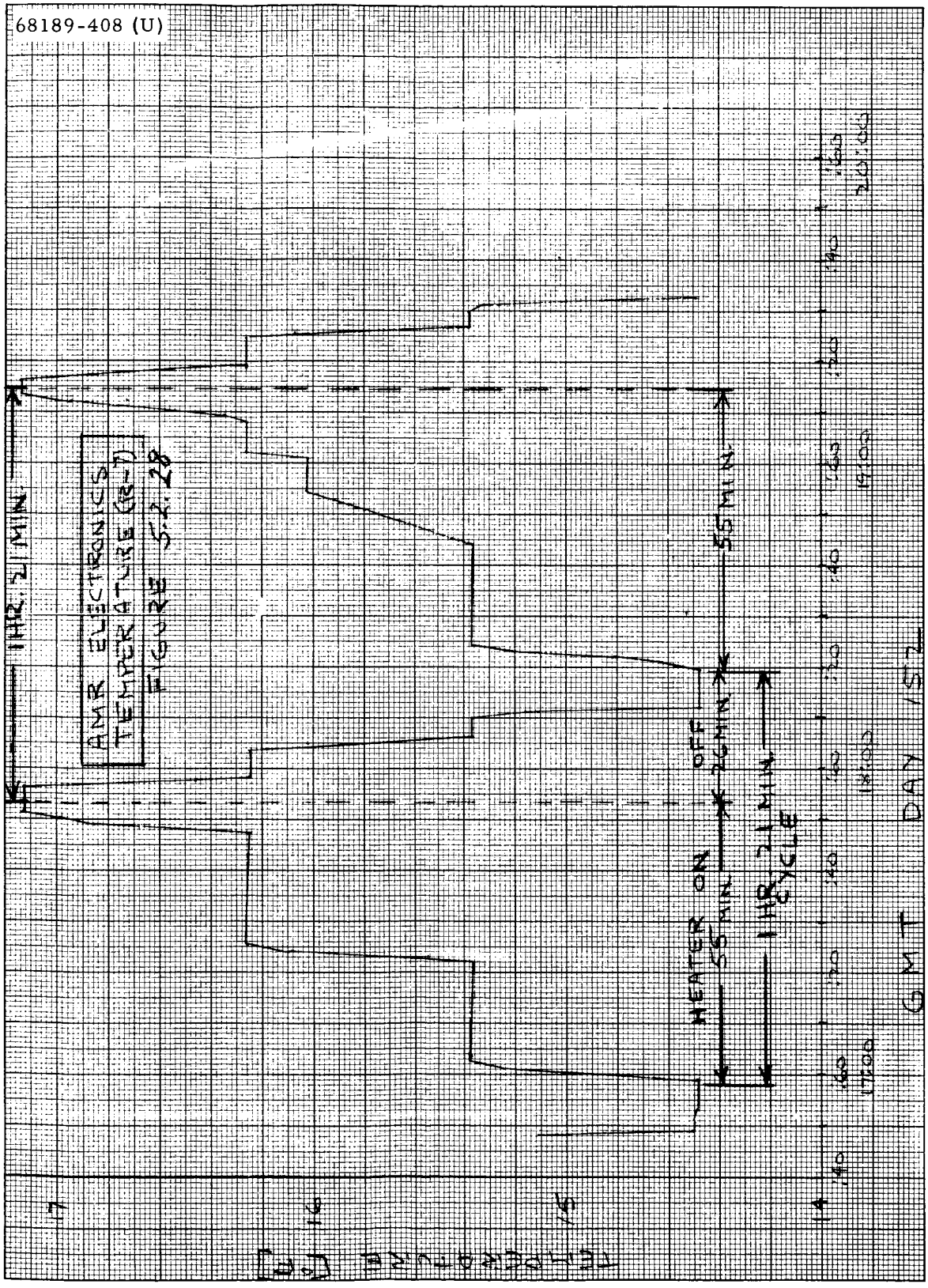


Figure 5.2-27. AMR Electronics Temperature (R-7)

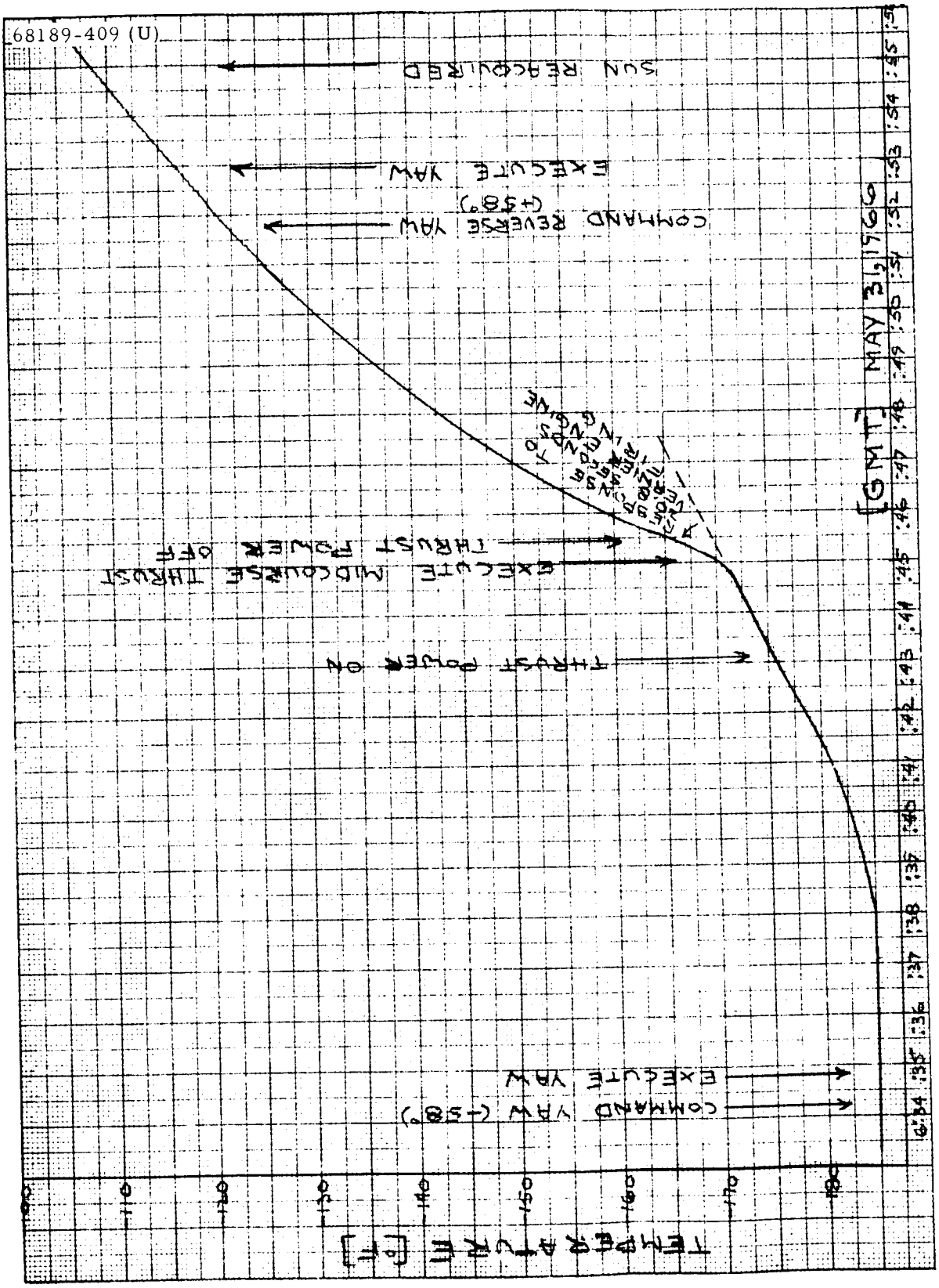


Figure 5.2-28. AMR Antenna (R-27) During Midcourse

camera temperature predictions for the various environments to which it would be subjected is outlined in Reference 5. This reference gives predictions for the steady-state transit temperatures, points out the inadequacy of the then current heater design for in-transit heating, and shows predictions for transit heatup based upon a revised heater design that was adopted for all the cameras. These predictions, supported by STV test data, formed the basis for the transit heating sequence used for SC-1.

Lunar day thermal analyses were also made and reported upon in Reference 6. It was in this area that the greatest discrepancies between predicted and measured thermal response were discovered. This has emphasized the requirement for updating the thermal model of the camera for future missions. Hopefully, the data will permit a resolution of the discrepancies into those due to environmental definition and those due to shortcomings within the camera model per se.

In addition to these two primary studies, many other analyses were undertaken, the results of which are summarized in References 7 through 14.

Comparisons of the measured data with the preflight predictions have been made at or during some selected times in the mission. These include steady-state transit and lunar nonoperating temperatures, temperatures at or close to touchdown, and temperature-time profiles during periods of operation on days 154 and 158.

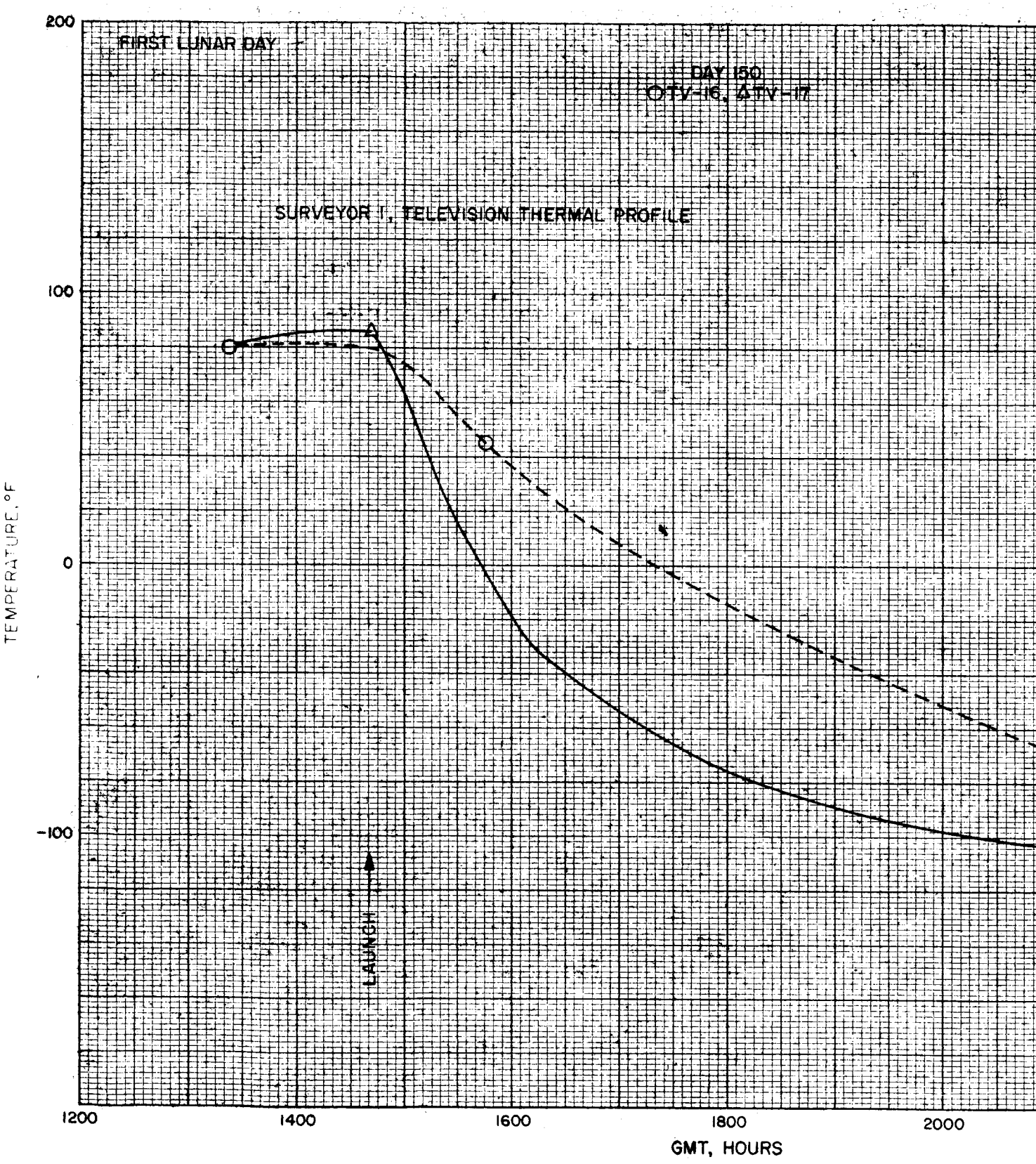
Observed Results

The data obtained from the sensors is presented in Figure 5.2-29, covering the first and second lunar days, respectively. Note that solar angles shown in these figures are measured from the horizontal, not from zenith.

Transit. During this phase of the mission, data was obtained from sensors TV 16 and 17 located on electronics chassis 3 and the mirror baseplate, respectively. TV 17 was monitored almost continuously during transit, which meant that very little data was obtained from TV 16. A 13°F rise in TV 17 was recorded during the midcourse correction. The temperature stabilized at -118°F at 26 hours after launch and exhibited some minor fluctuations between 38 and 59 hours after launch with the lowest temperature being -126°F. TV 16 stabilized at -133°F.

Electronics thermal control was commanded on at 5 hours 1 minute before touchdown and vidicon thermal control at 1 hour 13.5 minutes before touchdown. TV 17 measured 14°F at 6 minutes after touchdown, and TV 16 measured 8°F at 18 minutes after touchdown. Following initialization of the spacecraft and camera turnon, the interrogation mode changes so that data is obtained from two different temperature sensors. These are TV 9 and TV 10 located within the boron nitride collar surrounding the vidicon tube and upon the electrical conversion unit (ECU) chassis, respectively. The first readouts from these showed TV 9 and TV 10 to be 59.5°F and 22.5°F, respectively, at 29 minutes after touchdown.

PRECEDING PAGE BLANK NOT FILMED.

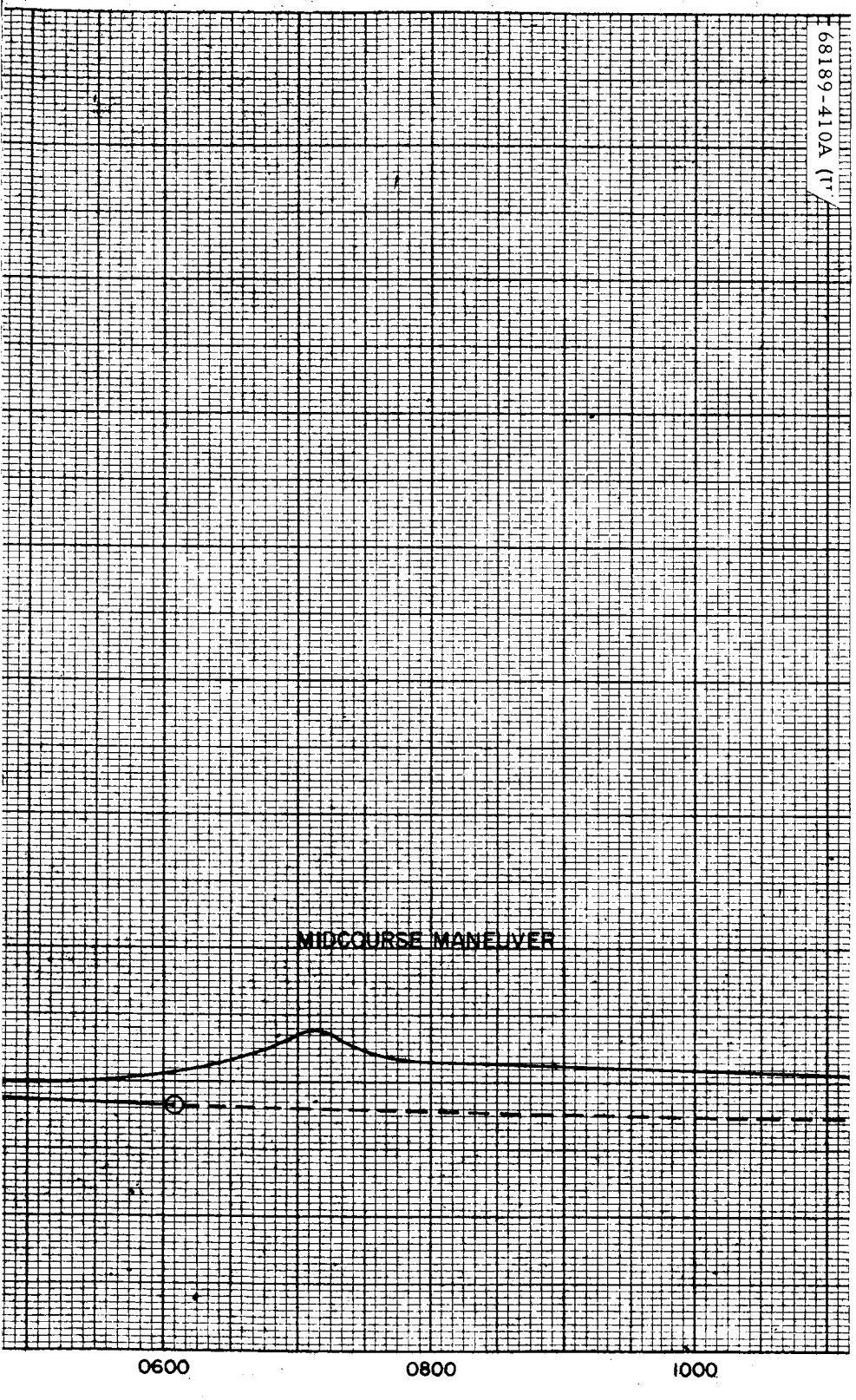


a) First Lunar Day

Figure 5.2-29. Surveyor Television Thermal Profile



5.2-96-1


68189-410A (1)
MIDCOURSE MANEUVER
0600
0800
1000

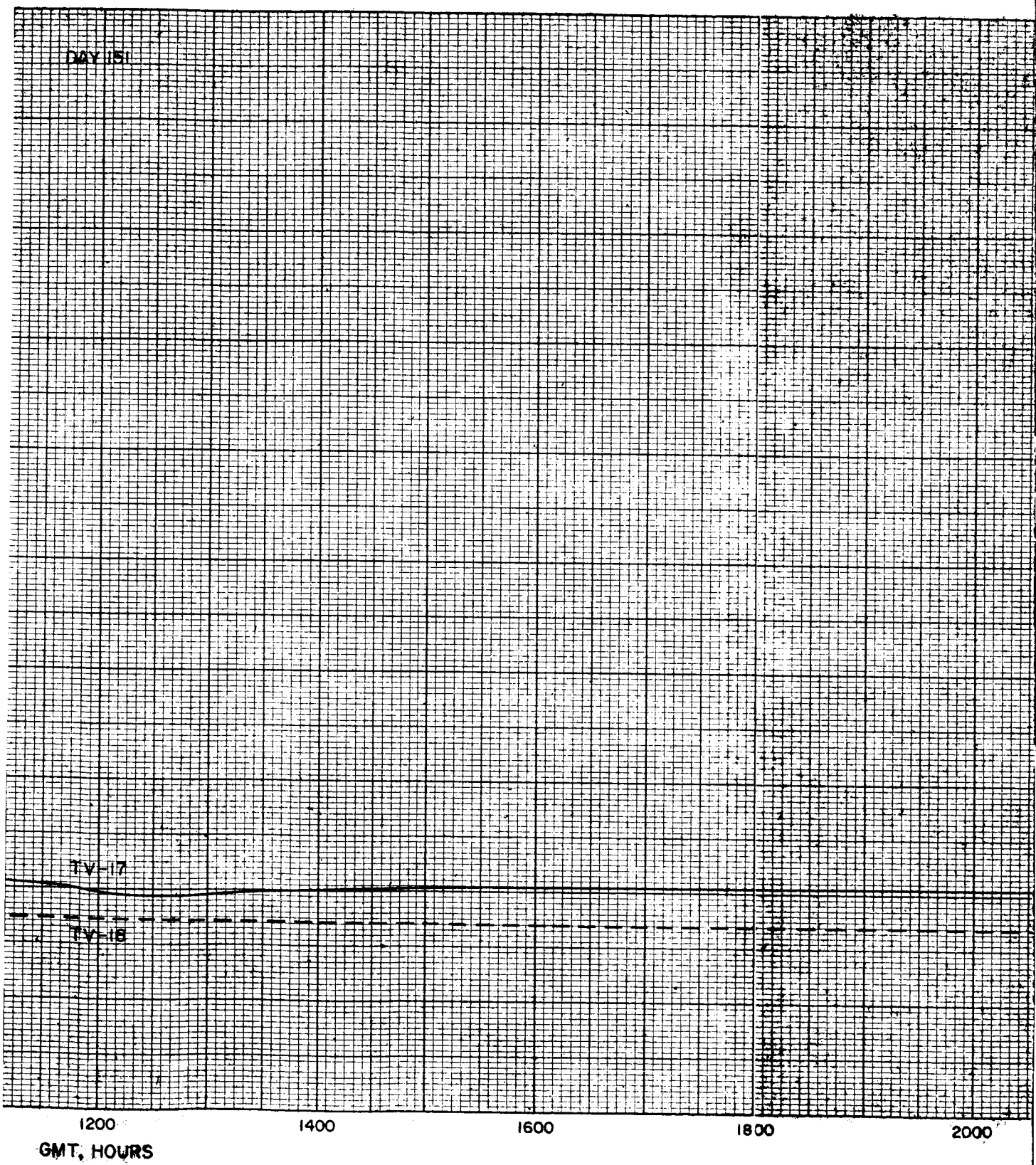
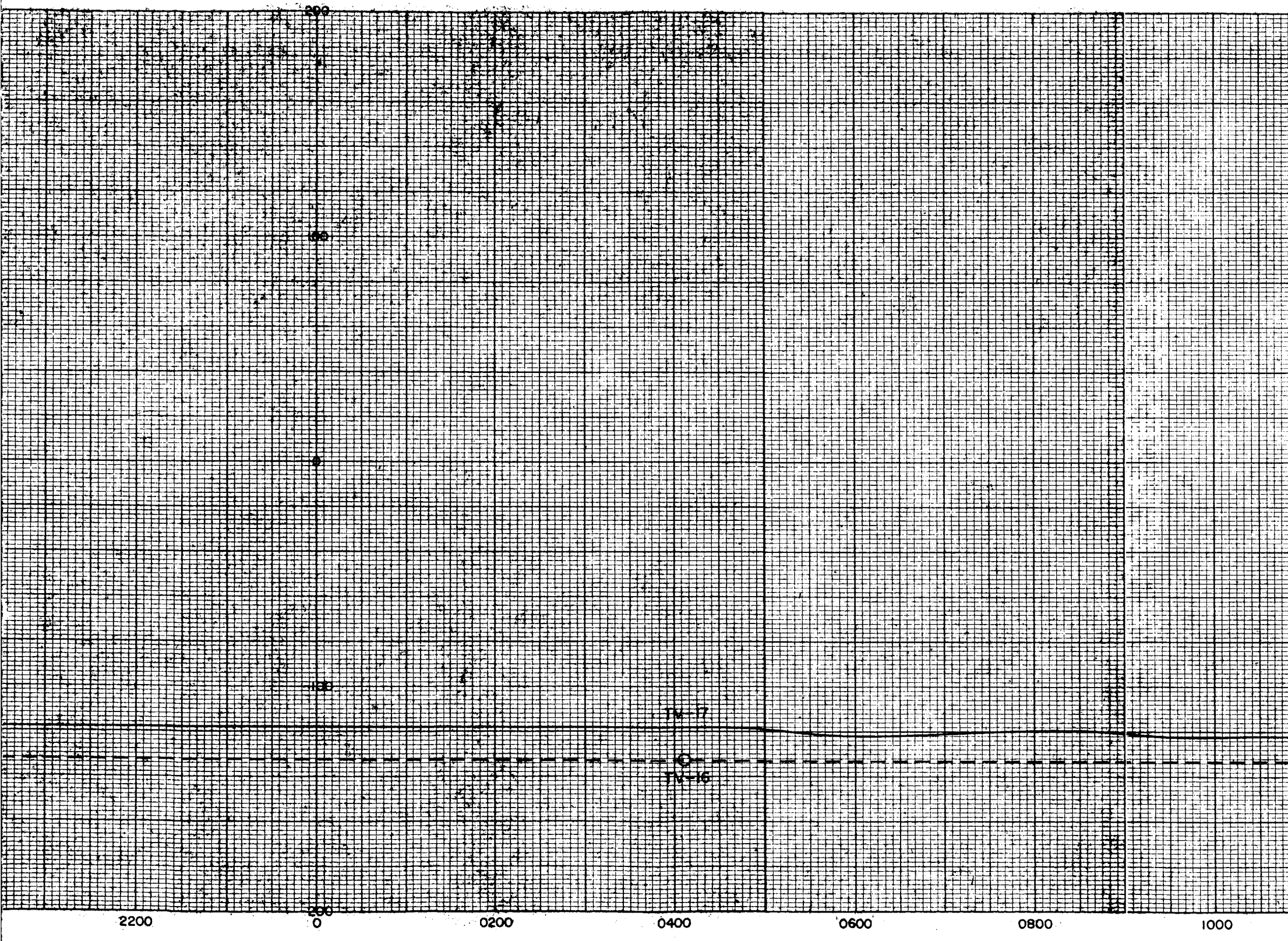


Figure 5.2-29a (continued). Surveyor Television Thermal Profile, First Lunar Day

FOLDOUT FRAME



FOLDOUT FRAME

FOLDOUT FRAME

5-2-97-2

5-2-97-3

DAY 152

TV-10

TV-9

1200 1400 1600 1800 2000 2200

GMT, HOURS

FOLDOUT FRAME

5.3-98-1

FOLDOUT FRAME

5.3-98-2

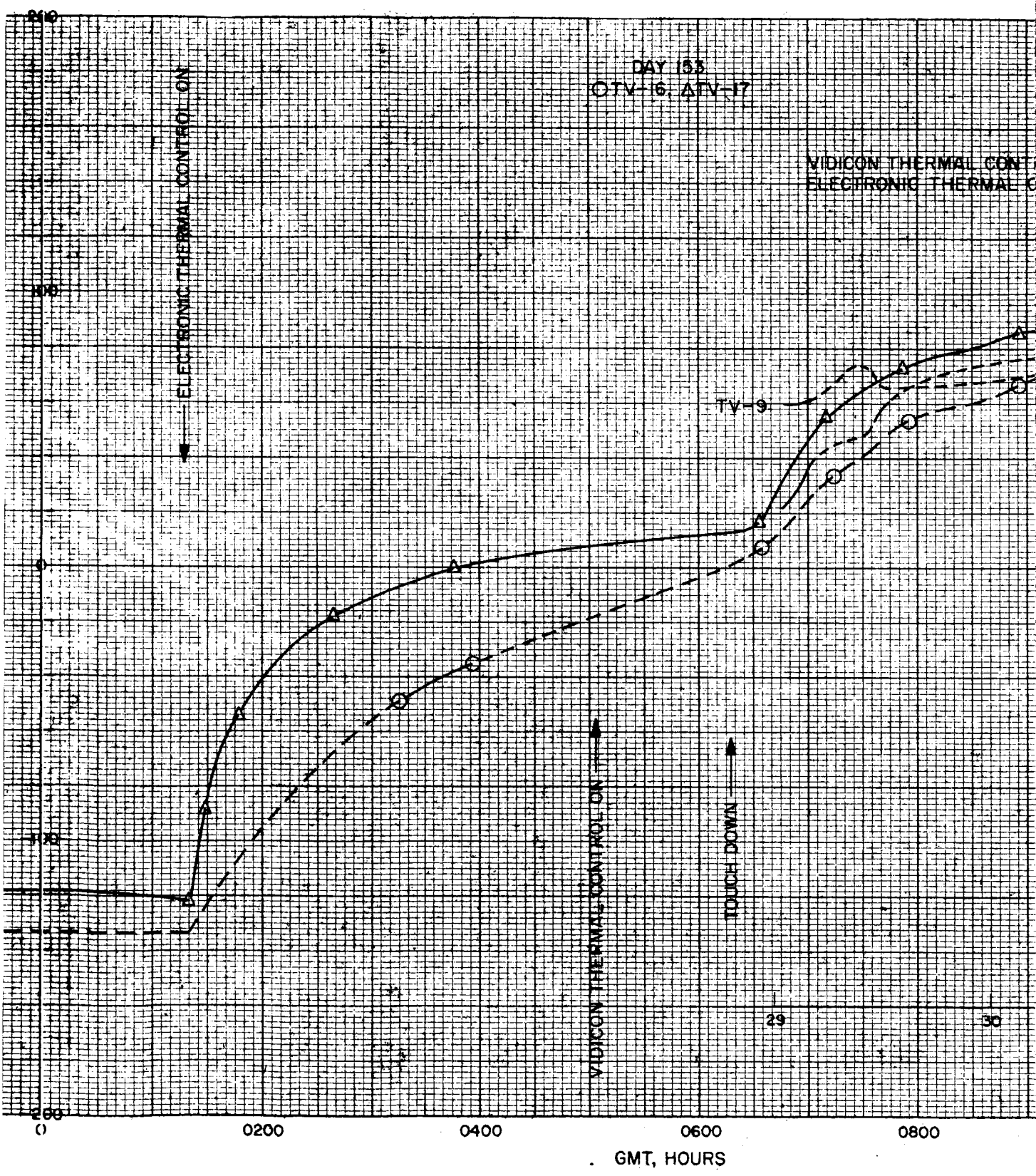
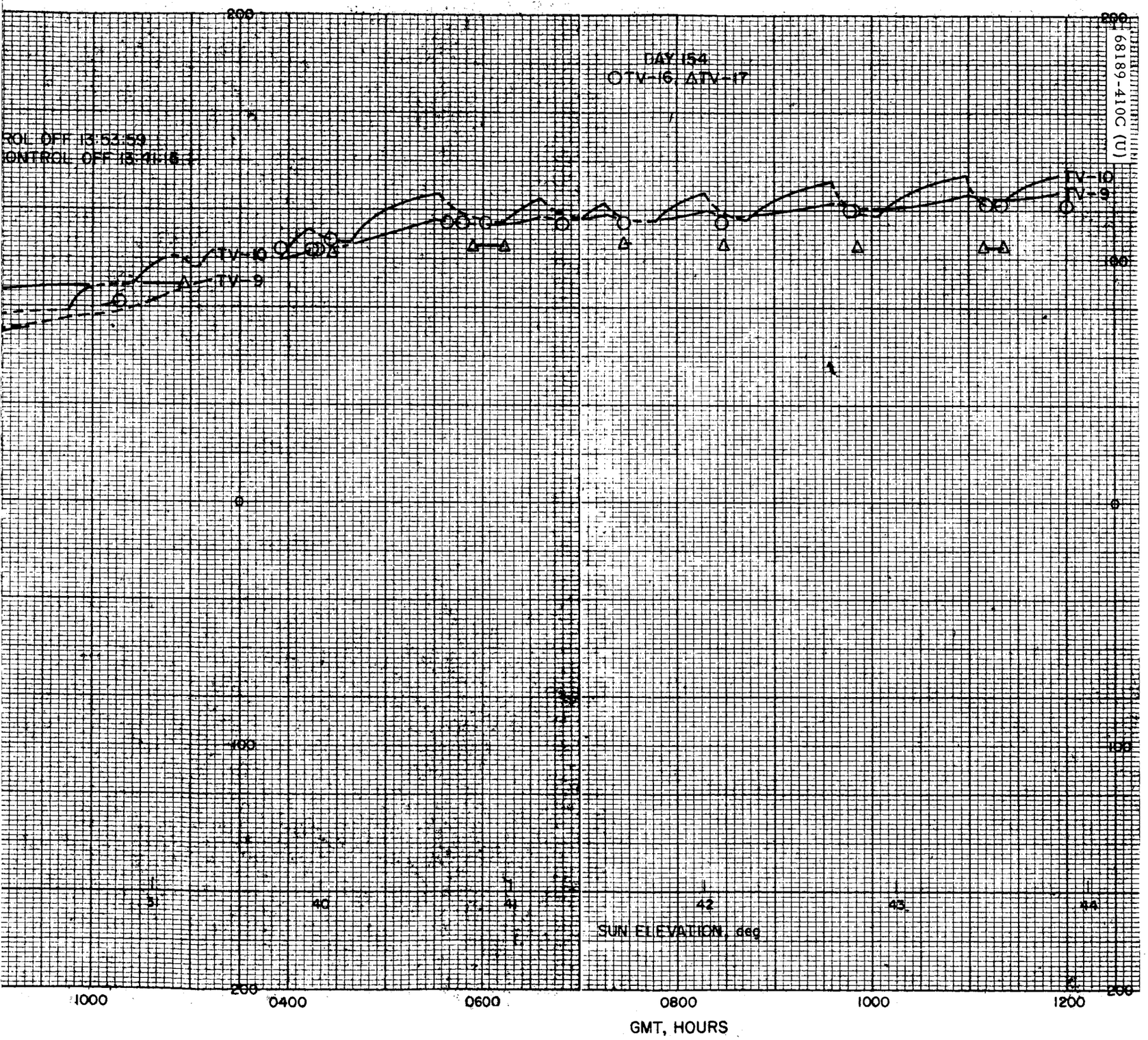


Figure 5.2-29a (continued). Surveyor Television Thermal Profile, First Lunar Day

FOLDOUT FRAME



68189-410C (U)

FOLDOUT FRAME

5.0-100-1

FOLDOUT FRAME

5.0-100-2

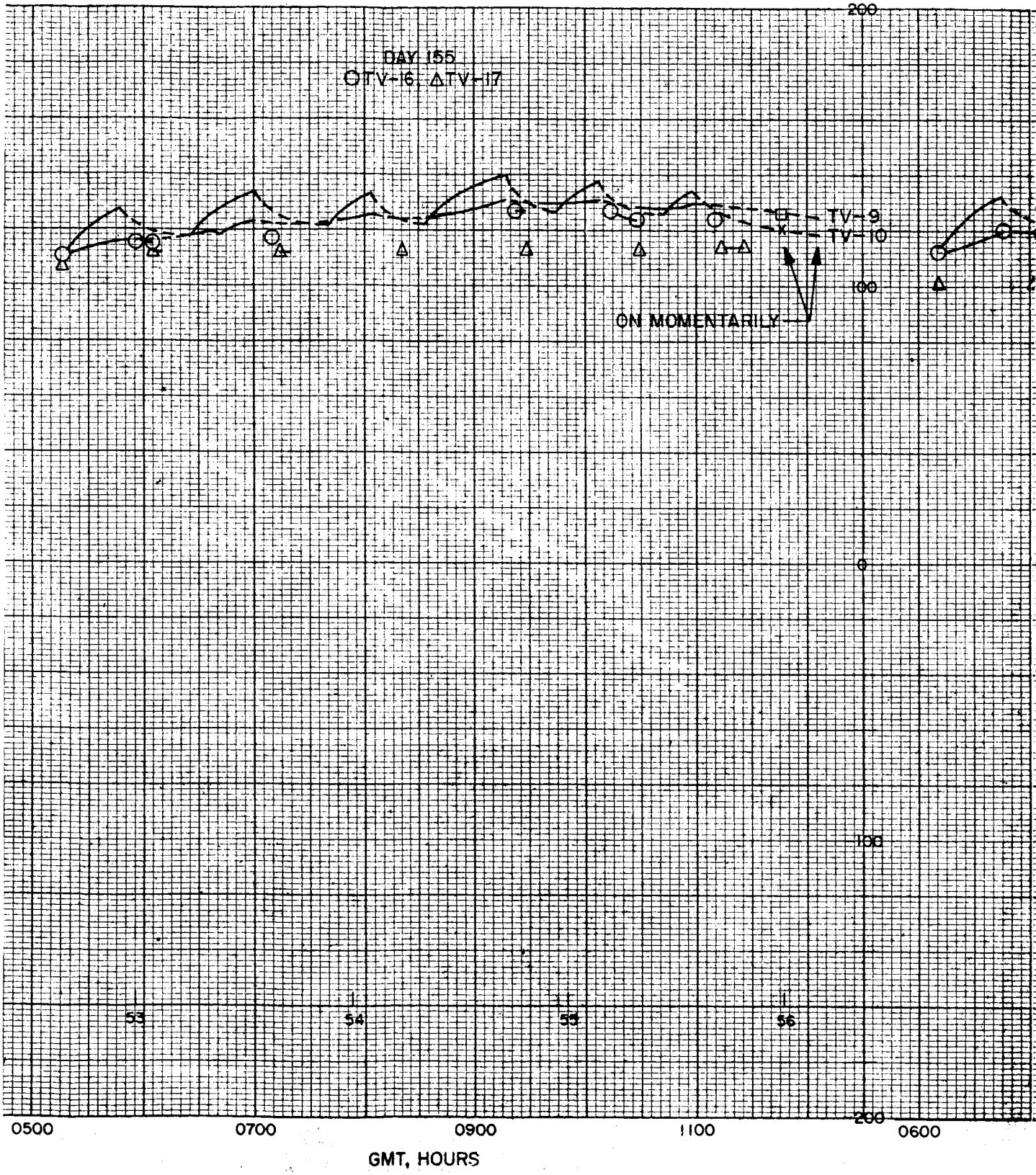
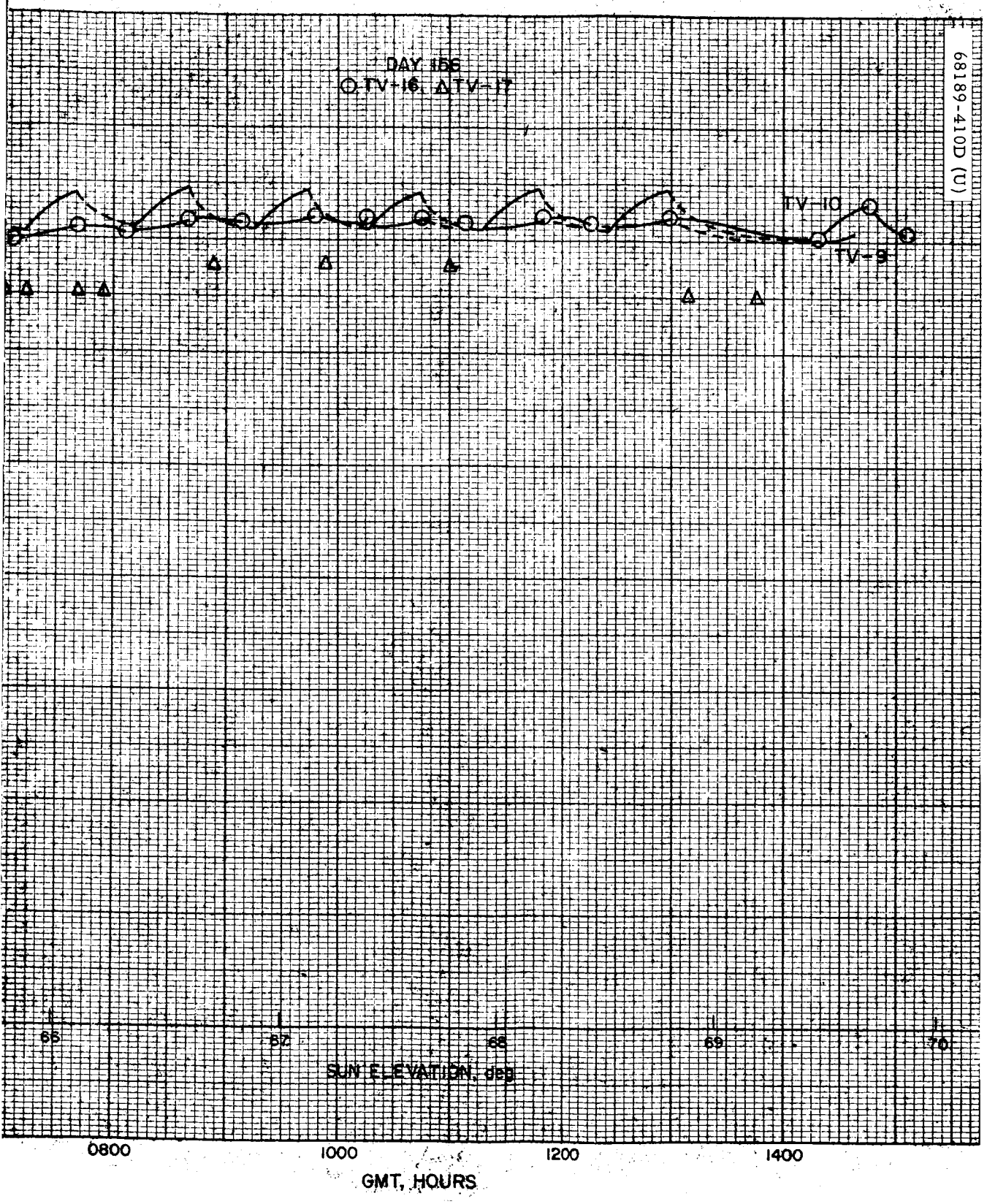


Figure 5.2-29a (continued). Surveyor Television Thermal Profile, First Lunar Day

FOLDOUT FRAME



FOLDOUT FRAME

5-2-102

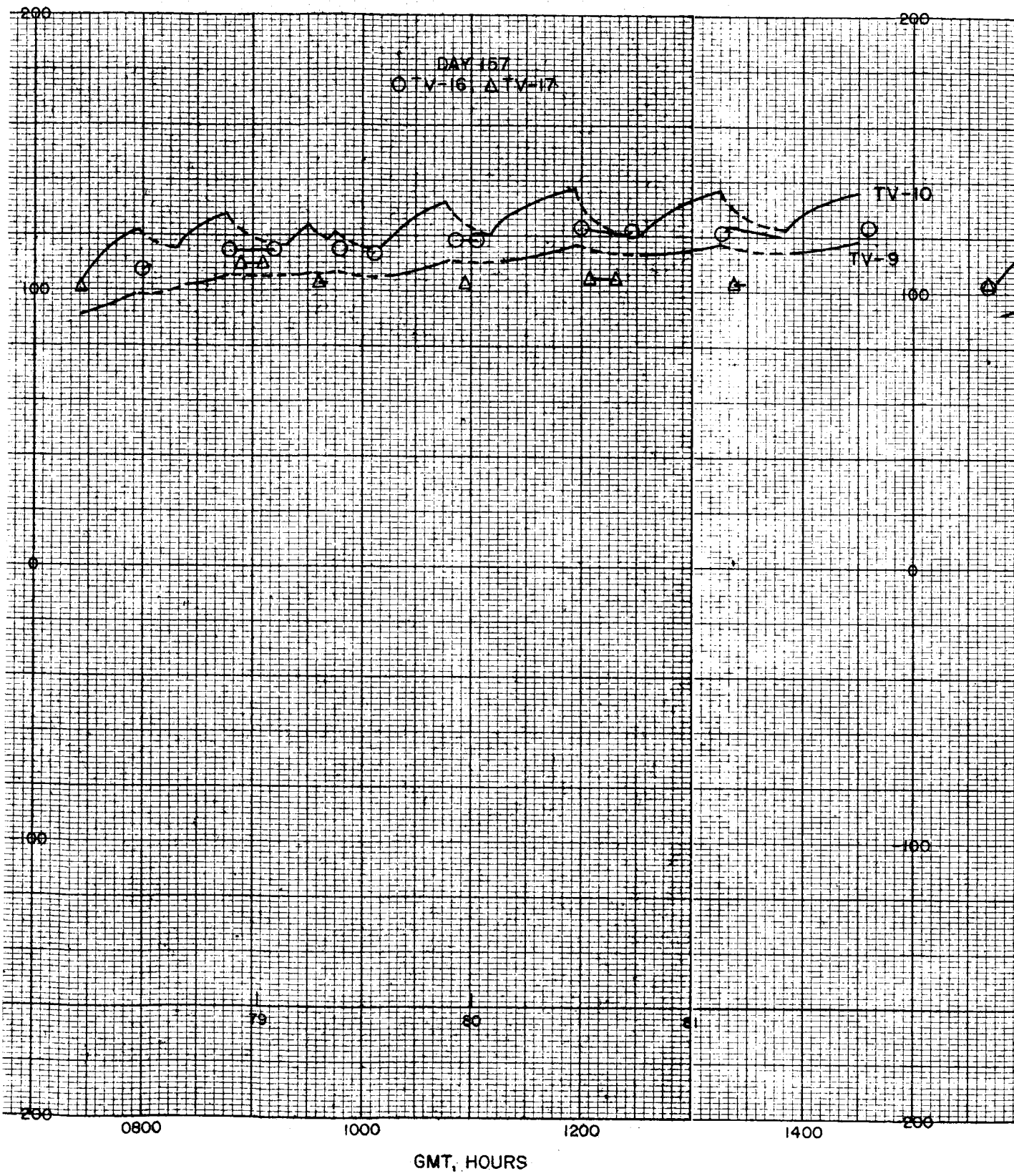
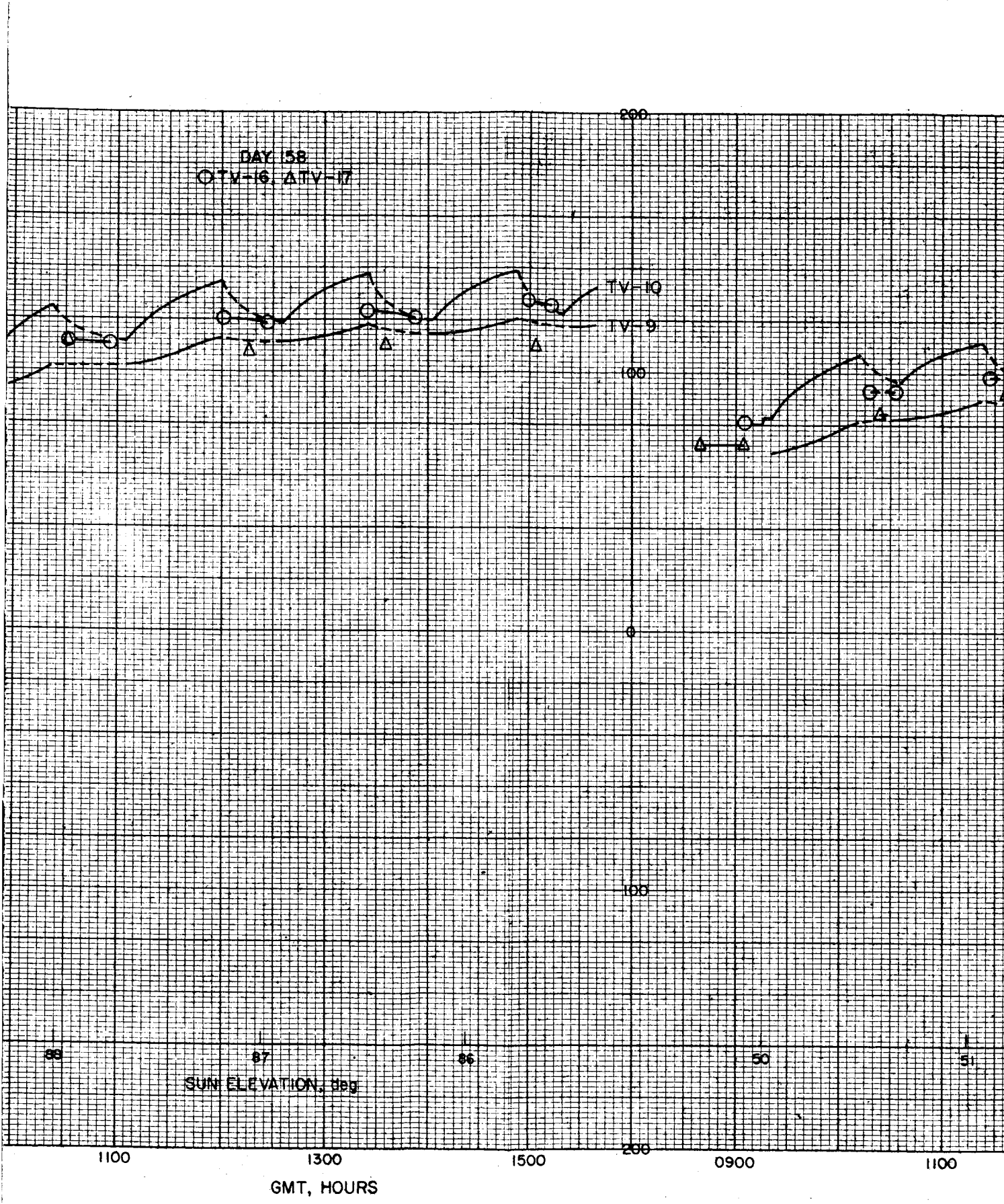


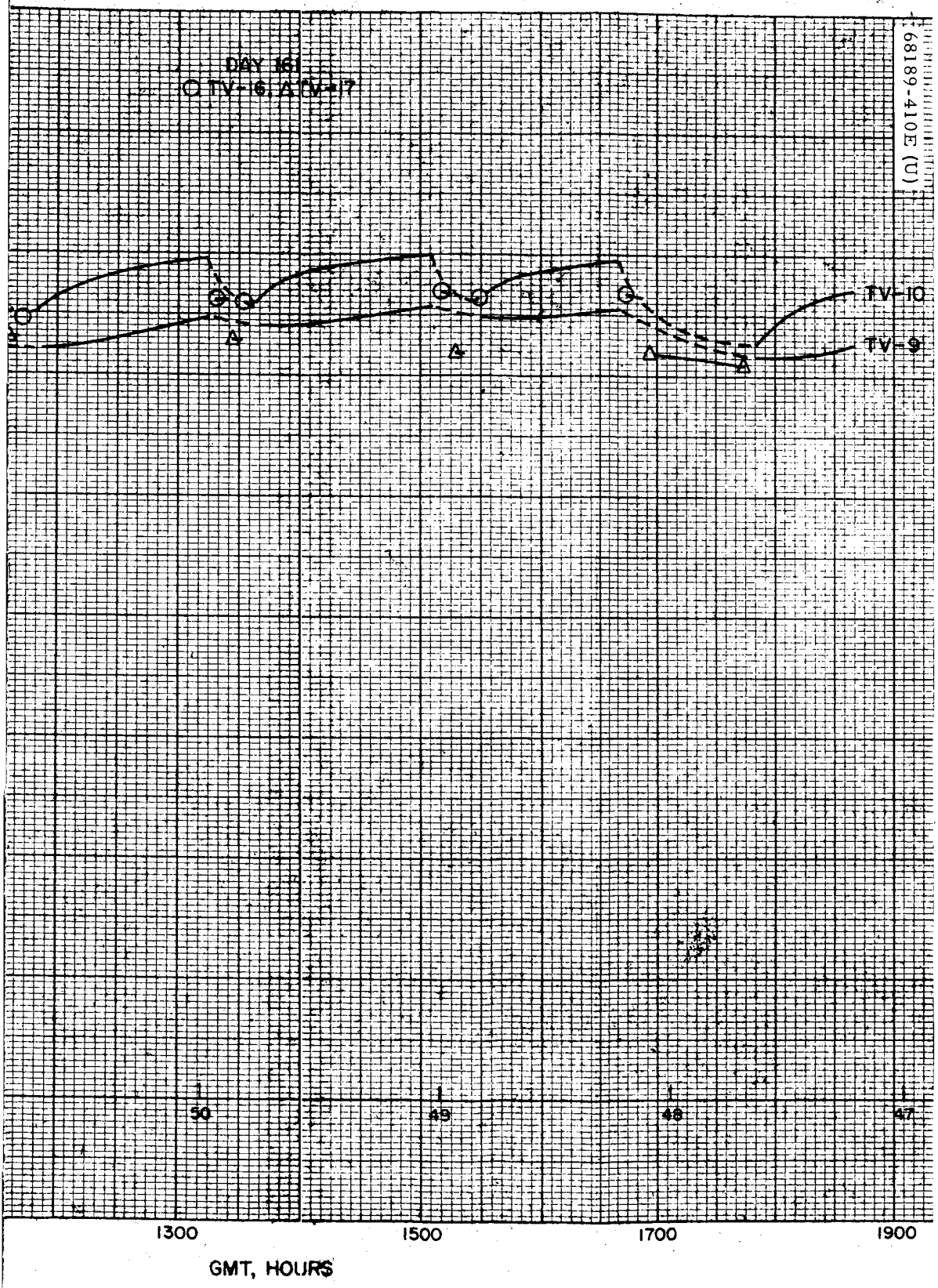
Figure 5.2-29a (continued). Surveyor Television Thermal Profile, First Lunar Day

FOLDOUT FRAME



FOLDOUT FRAME

S. 7.103-2



68189-410E (U)

FOLDOUT FRAME

5.2 124

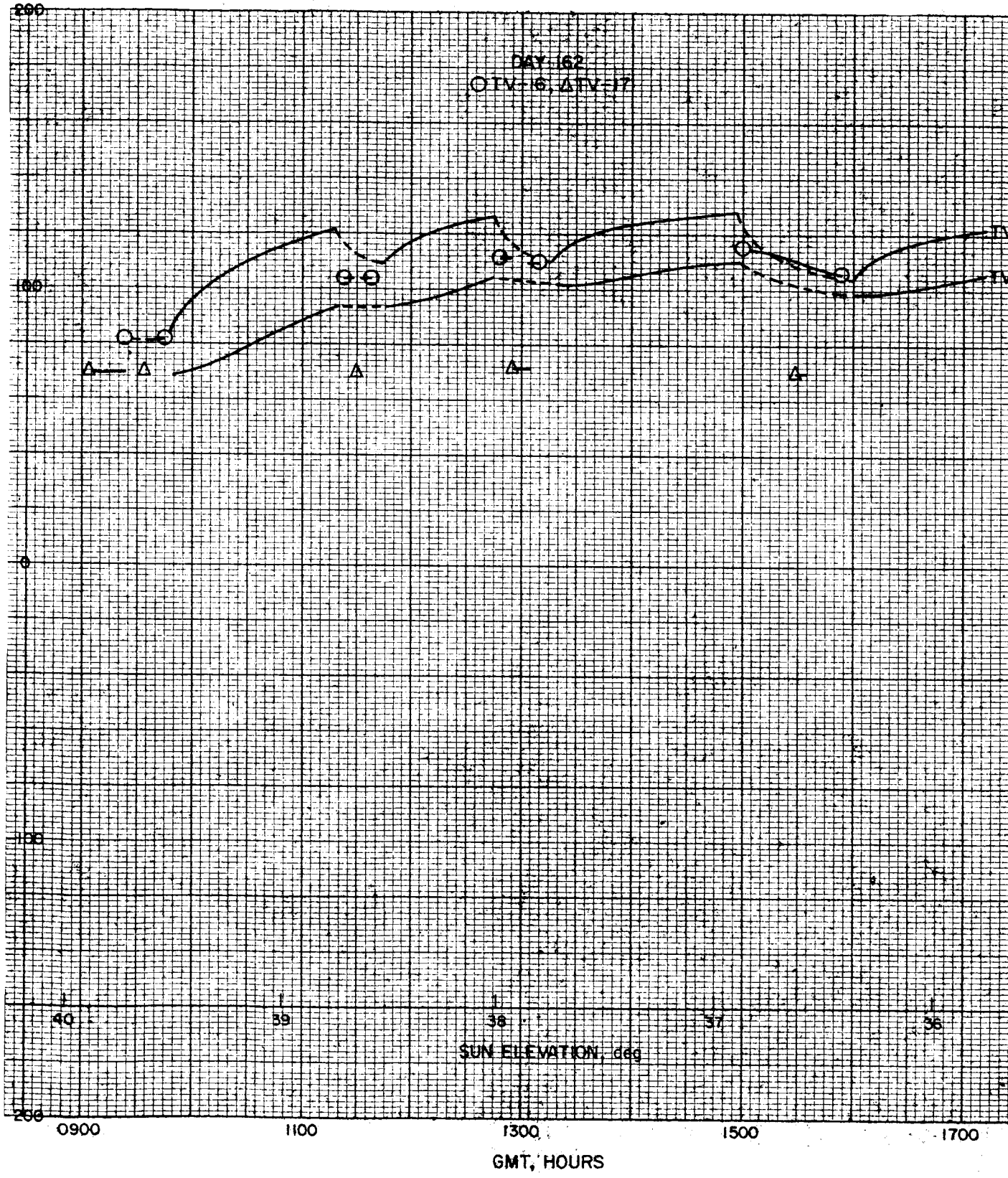
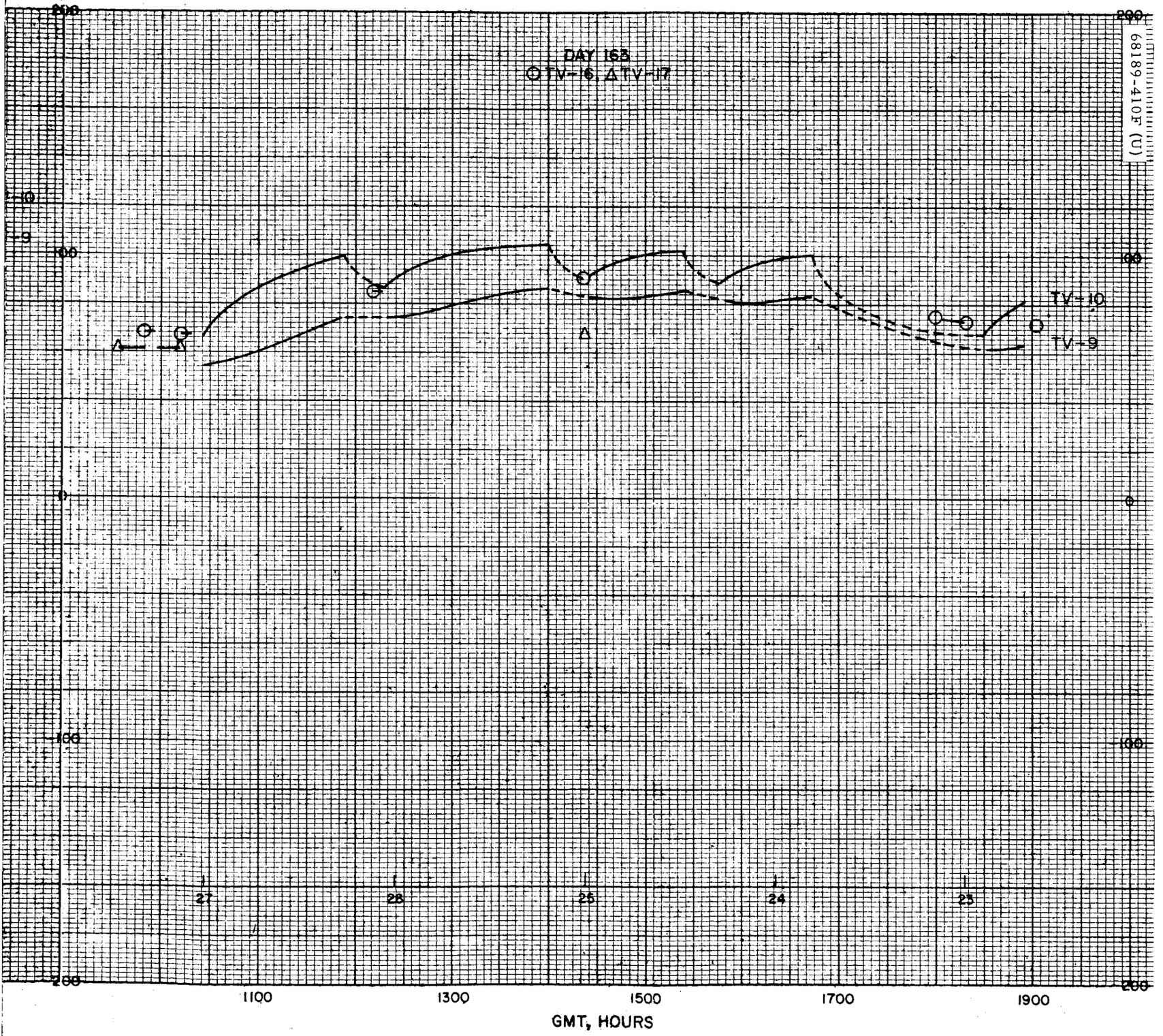


Figure 5.2-29a (continued). Surveyor Television Thermal Profile, First Lunar Day

FOLDOUT FRAME



68189-410F (U)

FOLDOUT FRAME

5.2-105-2

5.2-106

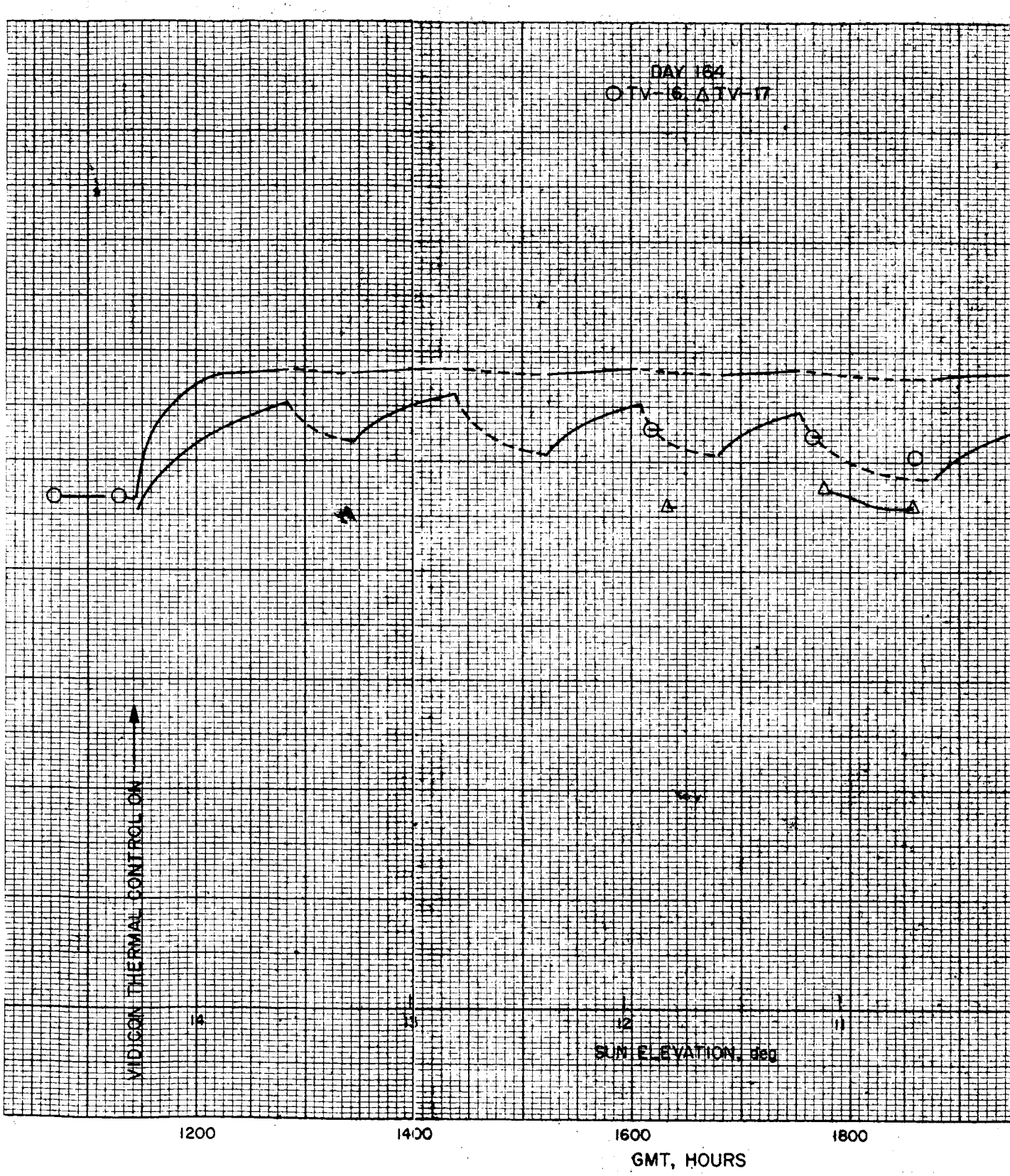
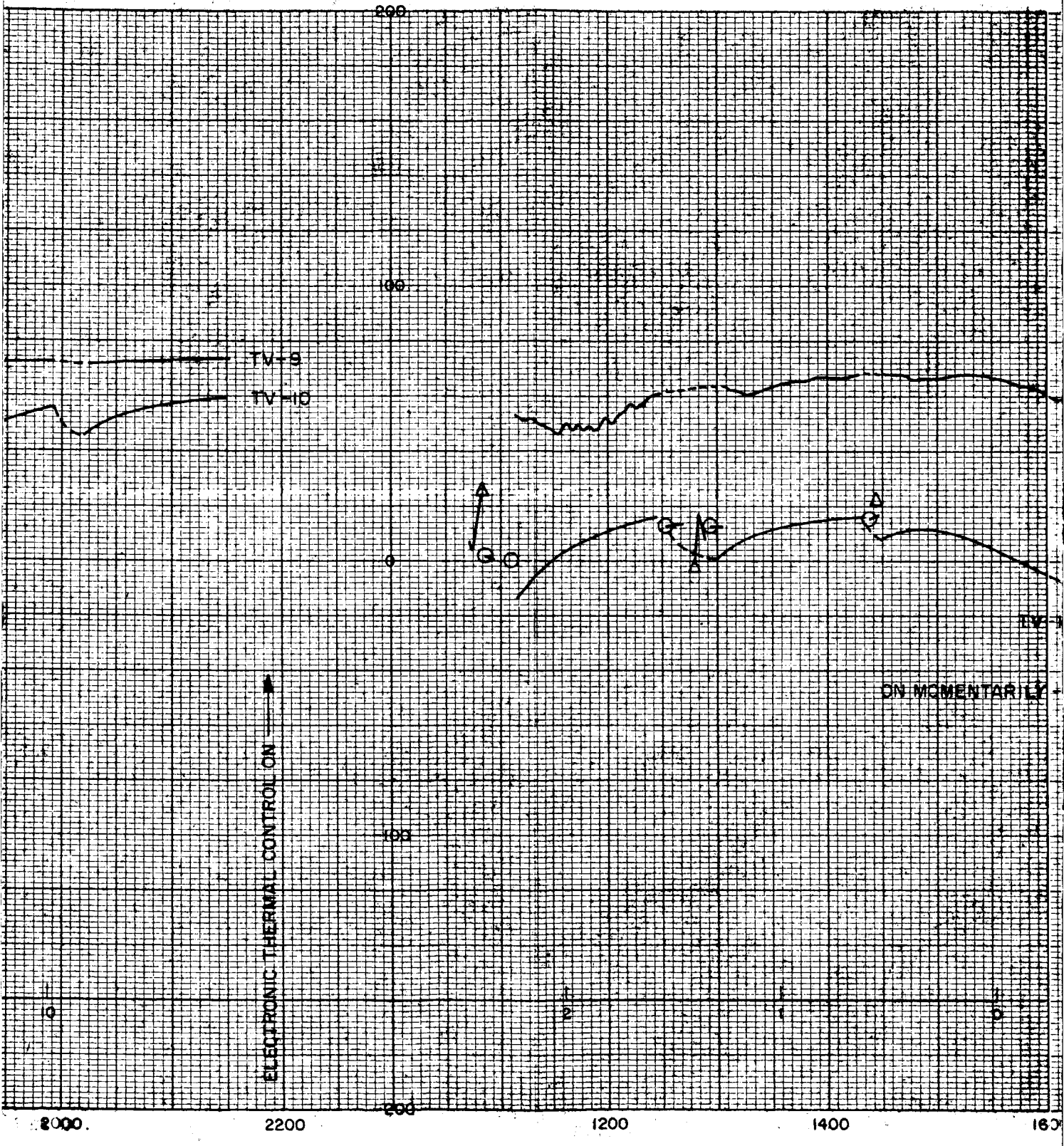


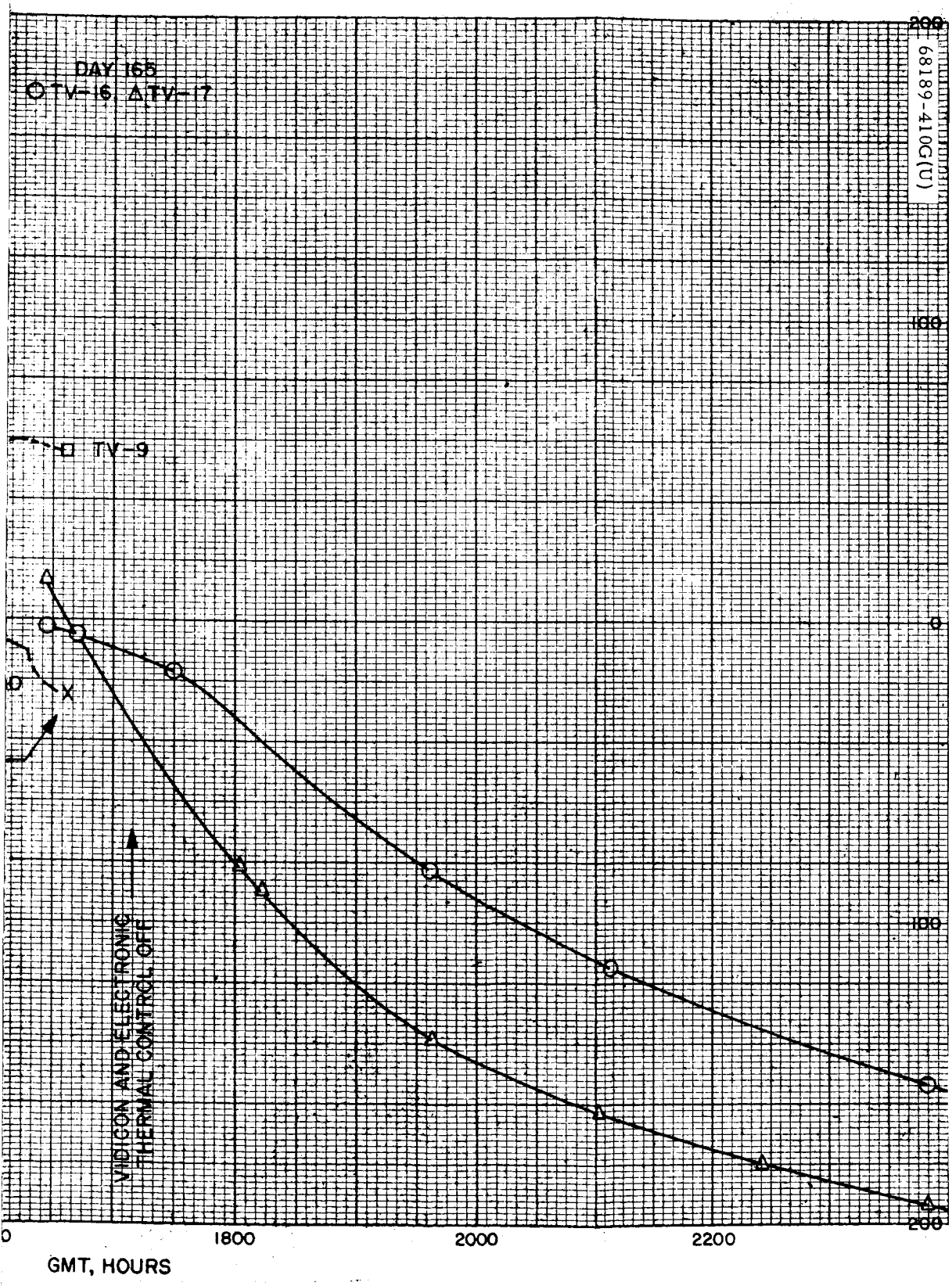
Figure 5.2-29a (continued). Surveyor Television Thermal Profile, First Lunar Day

FOLDOUT FRAME



5.2-17-2

FOLDOUT FRAME



FOLDOUT FRAME

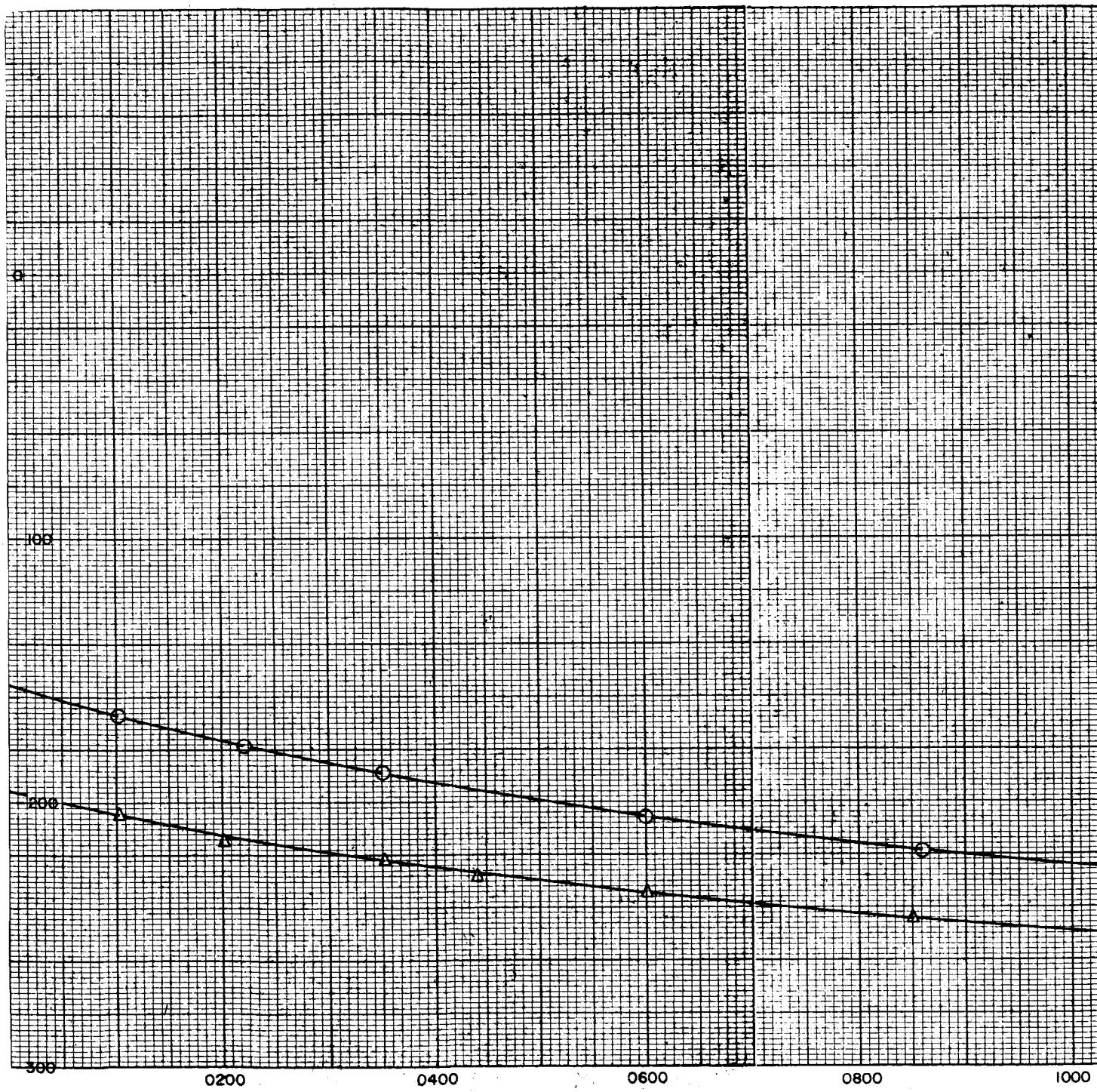


Figure 5.2-29a (continued). Surveyor Television Thermal Profile, First Lunar Day

DAY 168

TV-16

TV-17

1200 1400 1600 1800 2000 2200 0 0200 0400

GMT, HOURS

FOLDOUT FRAME

5.2-109-2

FOLDOUT FRAME

5.2-110-1

DAY 167

FIRST LUNAR DAY

SURVEYOR . TELEVISION THERMAL PROFILE

68189-410H (U)

TV-16

TV-17

0

-100

-200

-300

TEMPERATURE, °F

0600 0800 1000 1200 1400 1600 1800 2000

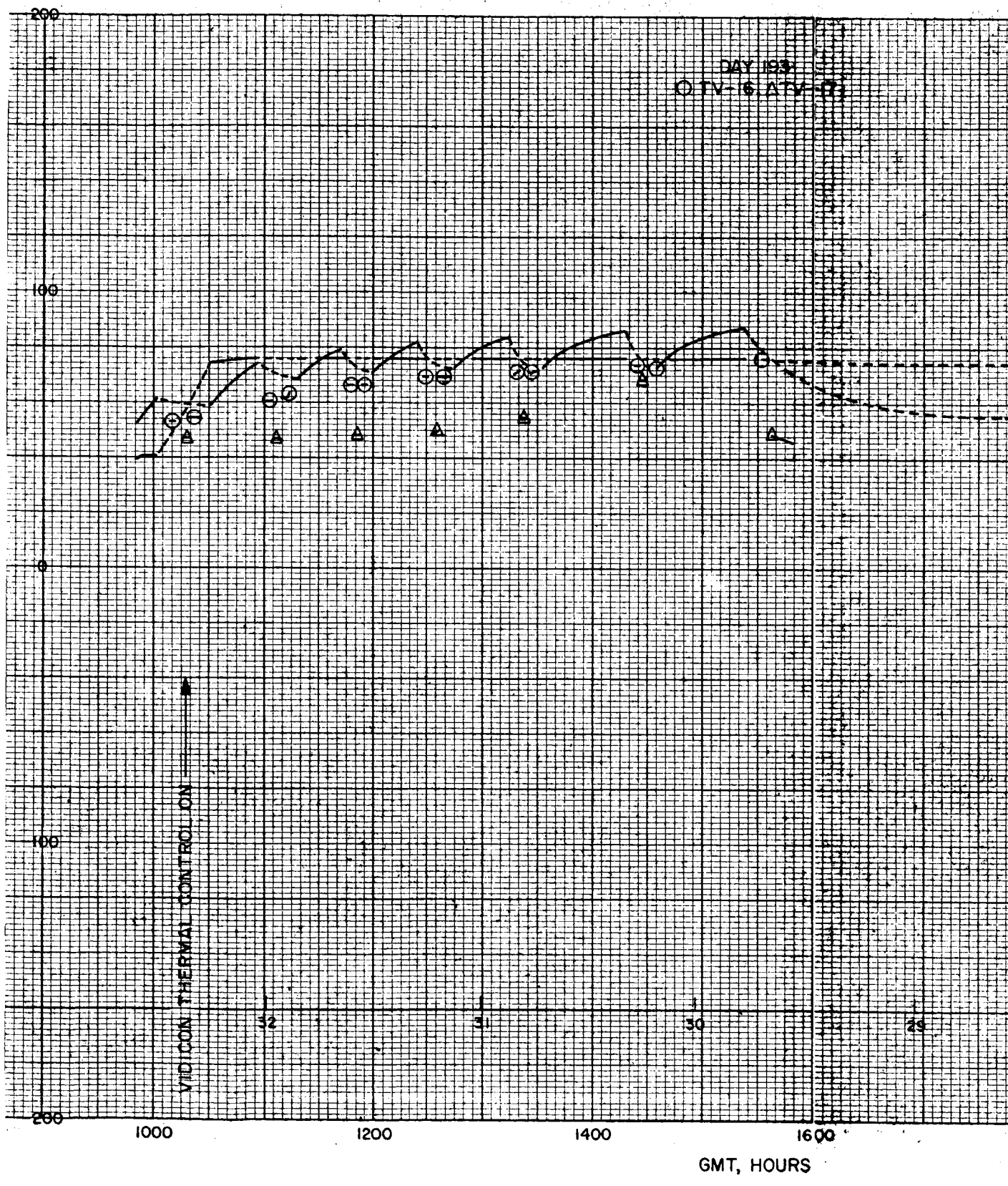
GMT, HOURS

FOLDOUT FRAME

S.D-110-2

FOLDOUT FRAME

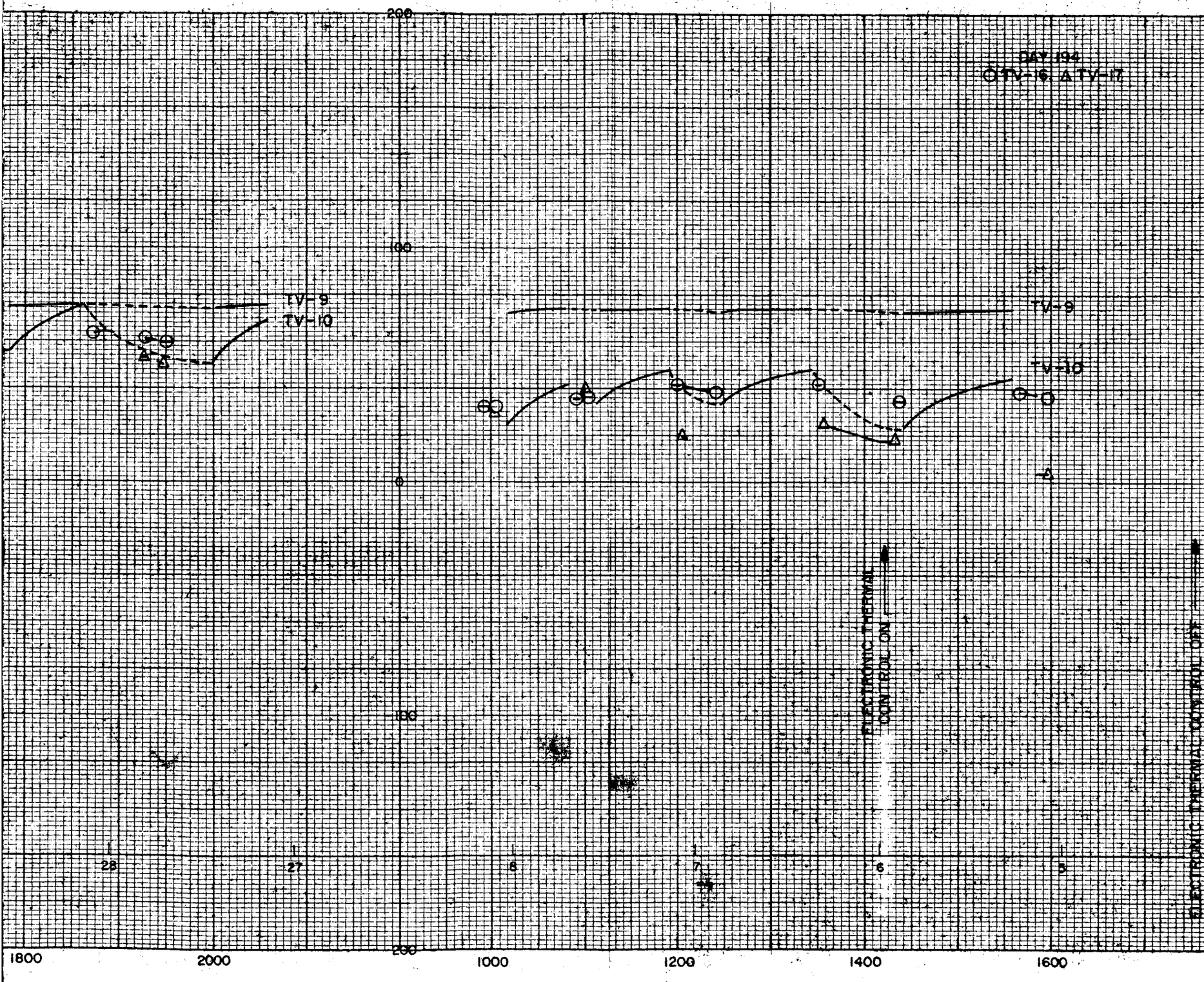
S.D-110-3



b) Second Lunar Day

Figure 5.2-29. Surveyor Television Thermal Profile

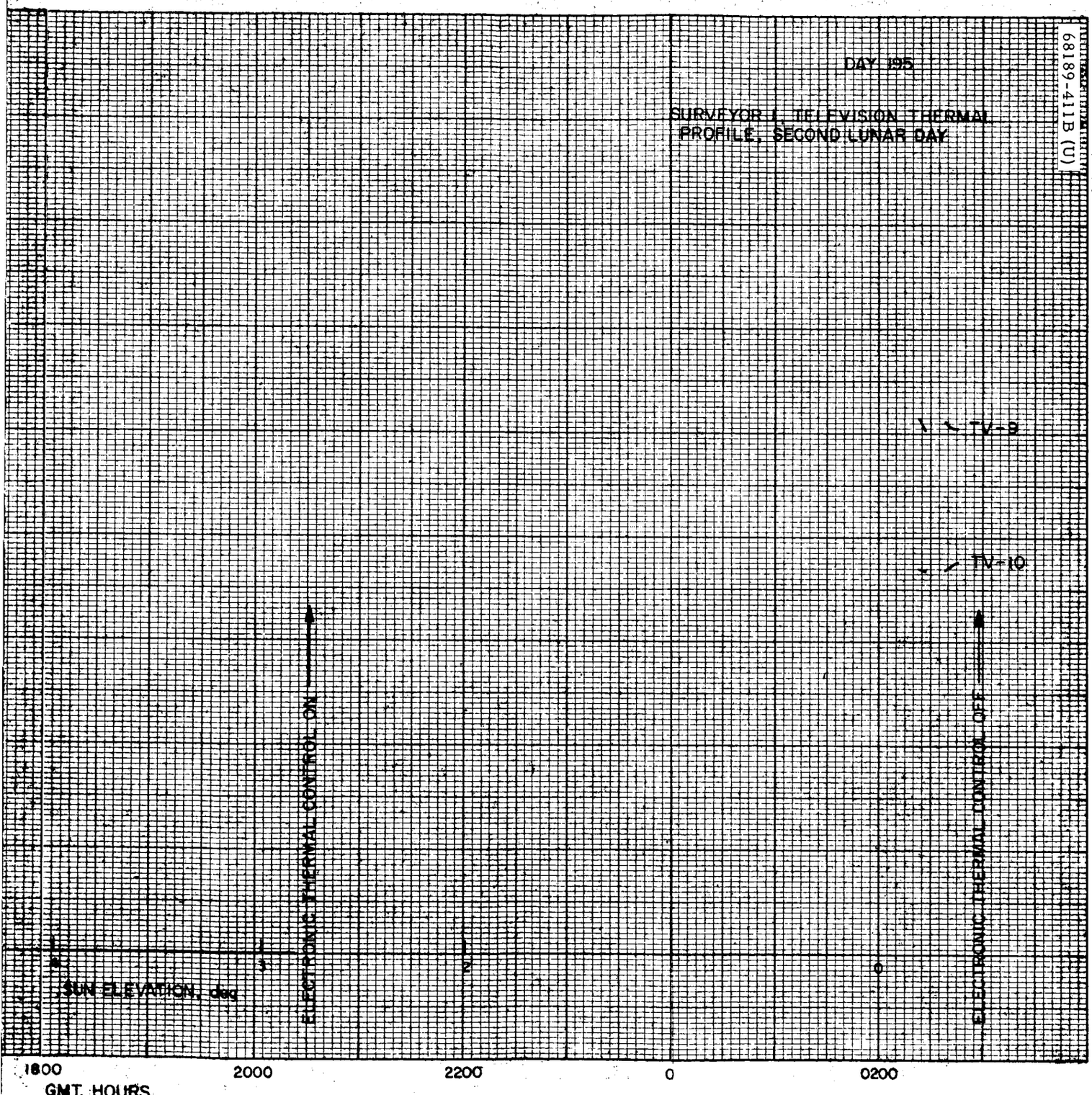
FOLDOUT FRAME



5.2-111-2

5.2-112-1

FOLDOUT FRAME



5.2-112-2

5.2-112-3

FOLDOUT FRAME

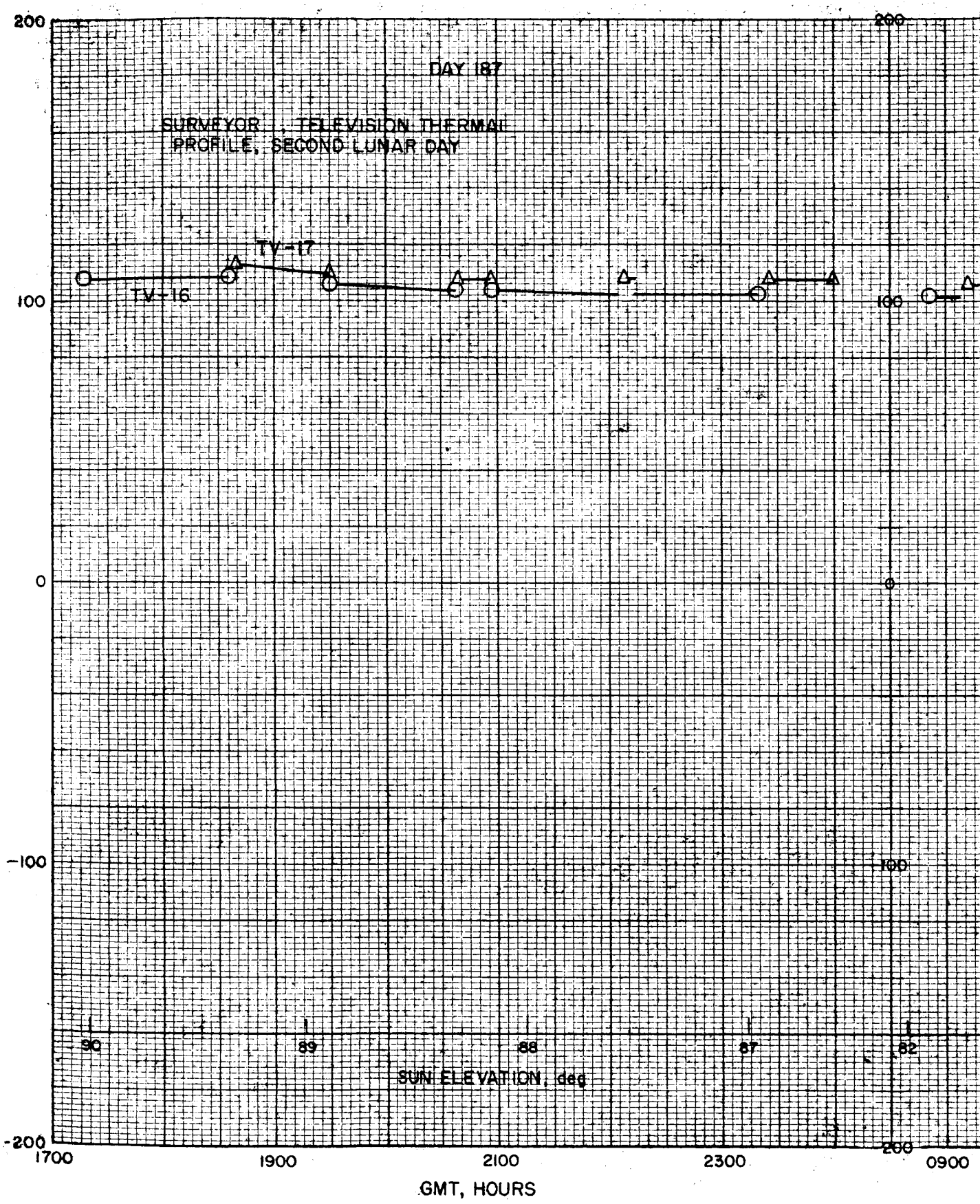


Figure 5.2-29b (continued). Surveyor Television Thermal Profile, Second Lunar Day

DAY 188

DAY 189 AND 190
○ TV-16, Δ TV-17

TV-10

TV-9

TV-10

TV-9

200

100

0

100

200

81 80 79 78 84 83 82

SUN ELEVATION, deg

1100 1300 1500 1700 2000 2200 0

GMT, HOURS

GMT, HOURS

68189-411A (U)

FOLDOUT FRAME

5.2-113-2

FOLDOUT FRAME

5.2-113-3

Thus it can be concluded that the objective of the in-transit heating, namely, to raise the electronics chassis and the vidicon tube faceplate above their minimum operating temperature of -20°F and the azimuth and elevation drive motors above -50°F, had been achieved.

First Lunar Day. The first lunar day encompasses days 153 through 165. The camera was operated for varying periods of time on all days except 159 and 160. At no time during this period was camera operation restricted by any thermal constraints. The relevant thermal data and summary of camera performance is given in Table 5.2-9. Since TV 16 and TV 17 data was received only when the camera was off and not during operation, information on these sensors has been excluded from this table.

The electronics thermal control was commanded on throughout the viewing periods of days 153 and 165. The vidicon thermal control was commanded on throughout the viewing periods of days 153, 164, and 165. Details of the thermal control operation are shown in Table 5.2-10.

The highest temperatures were recorded on day 155 when the camera was operating fully exposed to direct sunlight and the solar angle was approximately 35.4 degrees from zenith. These maxima were 140°F for TV 10 and 130.7°F for TV 9. The upper operating temperature for the electronics chassis is 165°F and for the vidicon faceplate, 150°F; consequently, it was felt that a good margin for safety was being used when TV 10 did not exceed 140°F.

However, analyses reported upon Reference 6 indicated that, under most circumstances, the rate of increase of temperature on chassis 4 might exceed that of the ECU. There is no sensor on chassis 4, but the 1.6 watts dissipated thereon during operation in the 600 line mode is transferred to chassis 3 in the 200 line mode. Furthermore, TV 16 is located on this chassis. At the end of day 156, the camera was operated in the 200 line mode for approximately 25.5 minutes, and the response of sensors TV 10 and TV 16 were compared. It was very reasonable to assume that the response of chassis 3 in this mode would be equivalent to the response of chassis 4 in the 600 line mode. The thermal responses of TV 10 in the 600 line mode and TV 16 in the 200 line mode were almost identical, from which it was deduced that the differences in temperature between the ECU chassis and chassis 4 during operation were not significant. This enhanced confidence in using TV 10 data as the criterion for determining camera on and off times. On subsequent days, the temperatures did not reach the levels attained on day 155, however, and the operating cycles were determined by factors other than camera thermal constraints.

Excluding days 159 and 160 when the camera was not used, and if the 165 and 150°F upper temperature limits for the electronics and vidicon had to be enforced, the temperature-time profiles indicate that practically unlimited continuous operation of the camera could be attained when it is not exposed to direct sunlight. The same would appear to hold true for a camera exposed to direct sunlight for solar angles greater than 40 degrees from zenith. No conclusions can be made regarding cases in which the solar angle would be less than 40 degrees since no data is available.

TABLE 5.2-9. SUMMARY OF SC-1 TV CAMERA PERFORMANCE DURING FIRST LUNAR DAY

Day	Solar Angle From Zenith at 0 Hour, GMT	Approximate Percentage of Camera in Direct Sunlight	Total Time On, minutes	Total Time for Cooling, minutes	Maximum Time On Continuously, minutes	Temperatures			
						Initial (= minimum),* °F		Maximum, °F	
						TV 9	TV 10	TV 9	TV 10
153	64.4	100	61.7	49.0	29.4	59.5	22.5	90.8	102.6
154	52.2	100	282.8	199.2	54.0	100.0	99.0	127.0	134.7
155	40.0	100	173.5	240.5	45.0	110.0	110.0	130.0	140.0
156	27.7	5	231.6	285.2	35.0	112.0	112.0	127.5	138.5
157	15.5	0	241.8	184.2	45.7	90.7	103.0	118.0	137.0
158	4.5	0	214.8	143.7	55.3	91.0	102.0	119.5	138.0
159	9.2		0						
160	21.1		0						
161	33.1	0	390.1	170.0	86.2	69.1	81.8	102.5	120.0
162	45.6	72	306.0	132.3	88.5	69.0	91.2	110.2	127.8
163	57.7	90	327.4	181.6	102.0	55.0	67.0	86.6	105.0
164	69.9	100	291.5	215.5	69.0	41.5	27.3	74.2	64.4
165	82.1	100	258.7	44.0	106.9	52.0	-13.2	68.5	16.0

*With the exception of day 165 which encompassed the initial phases of the lunar night cooldown.

Lunar Night Cooldown Following First Lunar Day. Both the electronics and vidicon thermal controls were commanded on throughout day 165. TV 9 held steady until approximately 152300 hours GMT and then commenced falling at about 8.4°F/hr until the heater was turned off. TV 10 held steady until approximately 145800 hours GMT and then fell at about 16°F/hr. During these initial periods of cooling, the camera was operating. Also, the electronics thermal control was still cycling so that full heater power was not being delivered to the camera. If the camera had been turned off but the heaters kept on, the rate of temperature fall would probably have been arrested since both STV data and preflight analyses had shown that the thermostat duty cycle is reduced during camera operation by the 1.6 watts dissipated continuously on chassis 4 upon which the thermostat is situated.

At the end of this initial cooldown period, both the camera and heater powers were commanded off, and this terminated TV 9 and TV 10 data. The final picture was taken with TV 9 at 56°F and TV 10 at -24°F. The subsequent data from TV 16 and TV 17 showed that the camera temperature then fell very rapidly. TV 16 exhibited an initial fall at approximately 32°F/hr and TV 17 at 63°F/hr. From the time that the heaters were turned off, data was received from TV 16 and TV 17 for approximately 51.5 hours. At the end of this period, TV 16 was -276°F and TV 17 was -290°F, with both still falling at about 0.5°F/hr.

TABLE 5.2-10. SURVEY CAMERA THERMAL CONTROL HEATER OPERATION DURING SC-1

Day	Time, GMT	Electronic Thermal Control	Vidicon Thermal Control
153	011642	On	–
153	050414	–	On
153	134115	Off	–
153	135359	–	Off
164	112312	–	On
164	215159	On	–
165	170855	–	Off
165	170909	Off	–
193	101618	–	On
194	141300	On	–
194	173230	Off	–
194	203137	On	–
195	025827	Off	–

Second Lunar Day. Operation of the camera was far less extensive than on the first day. No data was received from the camera until approximately lunar noon on day 187. The camera was not turned on until 1517 hours GMT on day 188 and was operated for 3 short cycles and finally turned off at 1636 hours GMT. At this time, the highest temperatures for the entire second lunar day were recorded: TV 10, 130°F; TV 9, 108°F; and TV 16, 116°F. The camera was operated subsequently on days 189, 190, 193, and 194, with a final brief sequence on day 195 at terminator. The vidicon thermal control was on from the start of operations on day 193 through the final sequence on day 195. The electronics thermal control was on for the final 1 hour 23 minutes of camera operation on day 194 and was turned off approximately 1 hour 56 minutes after the final sequence on that day. It was turned on again approximately 6 hours before the ultimate operation on day 195. Thus, as on the first lunar day, the ability of the heaters to maintain the camera operational close to terminator had been demonstrated. The final pictures were taken on day 195 with TV 10 at approximately -10°F and TV 9 at 43°F.

On days 187 through 195 as terminator was approached, the general level of the camera temperature decreased. Again, camera operation was not restricted by any thermal constraints, and no temperature anomalies were seen to exist on the basis of comparison with the data obtained during the first lunar day.

Comparison of Data with Predictions

Transit. All transit analyses were based upon the camera thermal environment as predicted in Reference 4. At the time transit analyses were being performed, this was the only information available. Subsequently, a more detailed breakdown of the spacecraft view factors to camera 3 was made for both transit and the lunar surface and, in addition, predictions for the transient cooldown of the spacecraft had been made. This information was published in Reference 2.

This breakdown was utilized for all the lunar analyses, but the transit analyses were never updated to include the more refined model nor were any predictions made for the transient phase of the cooldown following launch. This decision was made on the basis of the fact that priority was being given to the lunar studies, and the agreements between measured and predicted temperatures during T-21 STV testing did not justify any modifications to the transit thermal model at that time (Reference 15).

Consequently, only comparisons with respect to the transit steady-state temperatures and the response to heating prior to touchdown can be made.

For the steady-state transit temperatures the following comparisons are made:

	Predicted	Measured
TV 16	-129 ± 19°F	-133°F
TV 17	-133 ± 18°F	-120 to -126°F

During the transient phase of the transit heatup, comparisons only for TV 16 and TV 17 can be made. The comparison between predicted and measured values are shown in Figure 5.2-30. The predictions during the transit heatup were all based upon the minima of the predicted spacecraft temperature ranges. Since no data from the other two sensors became available until after touchdown, only spot comparisons can be made for these as follows:

	Predicted	Measured	
TV 9	33°F	59°F	At touchdown +29 minutes
TV 10	6°F	22°F	At touchdown +29 minutes

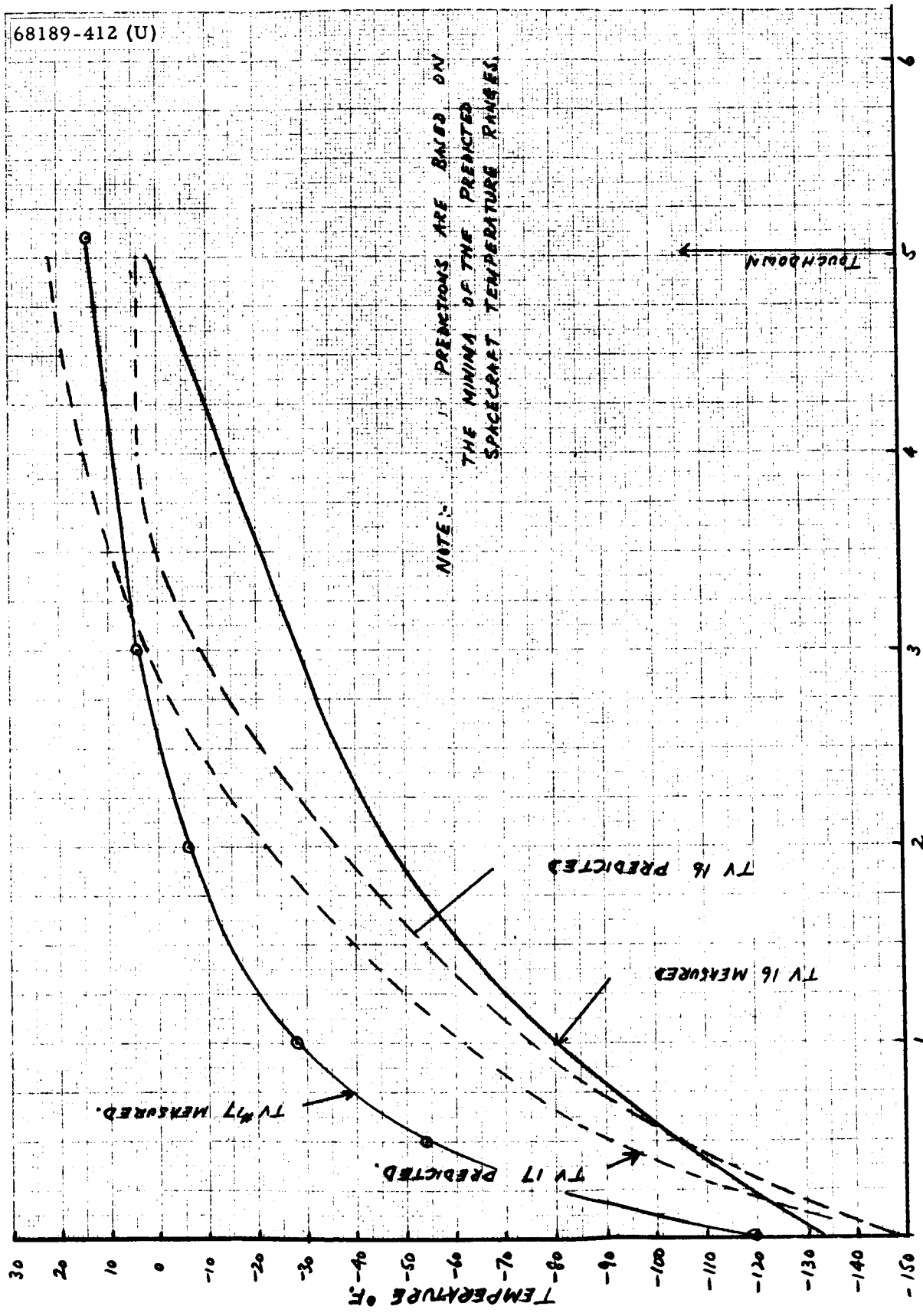


Figure 5.2-30. Transit Heatup of Camera 3
Comparison of measured and predicted values

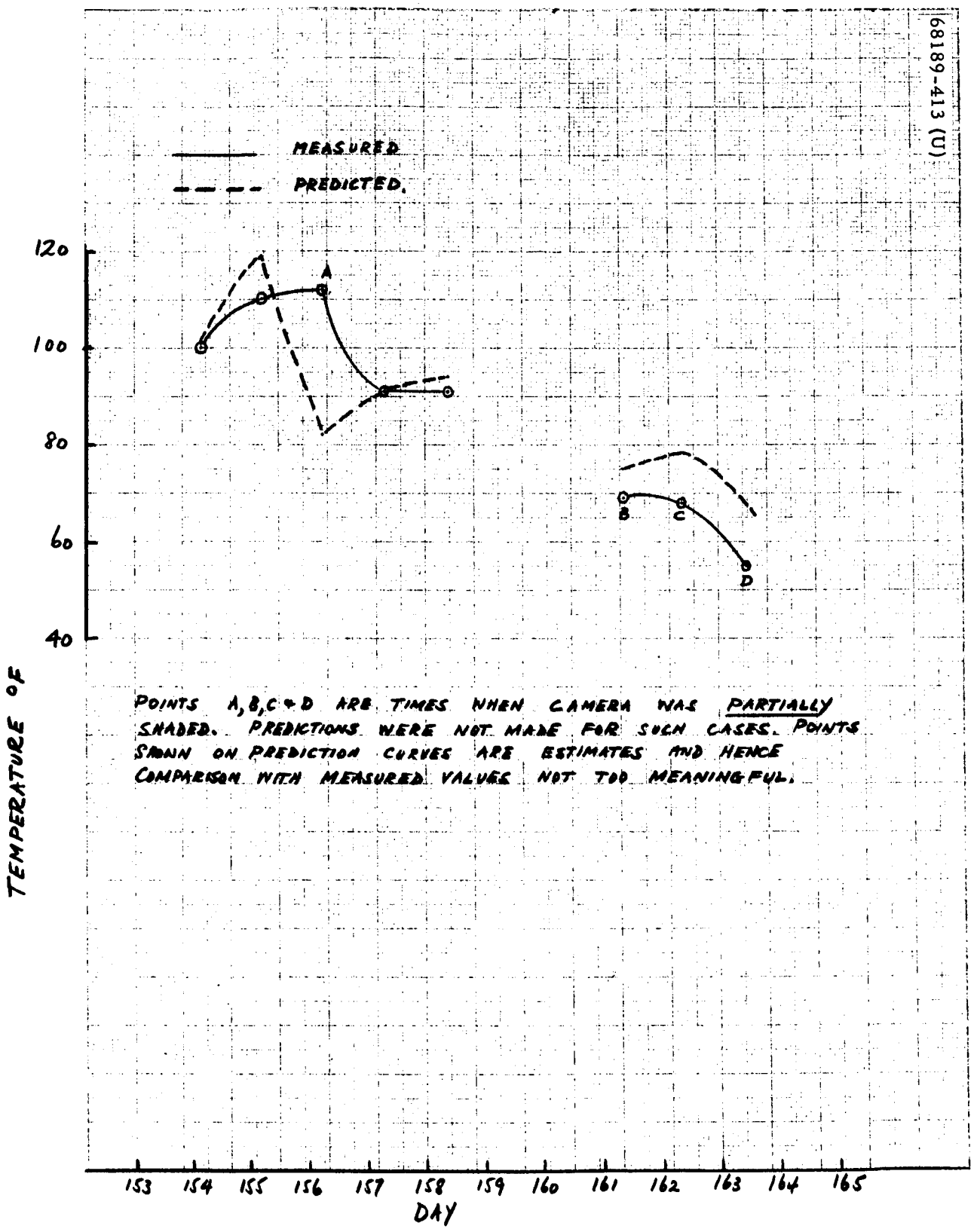
	Predicted	Measured	
TV 16	-2°F	8°F	At touchdown +18 minutes
TV 17	20°F	14°F	At touchdown +6 minutes

In the analyses, no perturbations due to reorientation of or changes in the spacecraft during terminal descent were considered; 20 volts at the heaters were assumed. As stated above, the minima of the predicted spacecraft temperature ranges were used, and it was assumed that no direct or reflected sunlight impinged upon the camera throughout transit. All these assumptions involve varying degrees of uncertainty. However, no serious discrepancies are present which could jeopardize future missions. The thermal model employed does require updating but updating may not be justified on the grounds that transit conditions will not be significantly different for future missions. Therefore, a transit heating sequence based upon these same predictions, will, if adhered to, ensure an operational camera at touchdown.

First Lunar Day – Steady-State Nonoperating Temperatures. Insufficient data was available from TV 16 to make the comparison. However, Figure 5.2-31 shows the comparisons for TV 9, TV 10, and TV 17, respectively. Except for one anomaly occurring for TV 9 on day 156, the predicted temperatures exceeded the measured values. Preflight analyses were made using the thermal environment as predicted in Reference 2. Predictions of steady-state nonoperating temperatures were made as a function of solar angle for both a shaded and unshaded camera. For the shaded case, minimum spacecraft temperatures were used and, for the unshaded case, the maxima of the predicted range for the appropriate solar angle were used. No analyses were made for partially shaded cases, so that the comparisons made for days 156, 161, 162, and 163 are based upon estimates of what the camera temperature would be, rather than direct comparison of an analysis for the specific partly shaded case with measured data. Work is currently underway to determine from the data, as precisely as possible, the temperatures of those sections of the spacecraft utilized in determining the boundary nodes for the camera lunar thermal model. Until this is done and the analyses rerun utilizing this new information, further comment on the discrepancies would be meaningless.

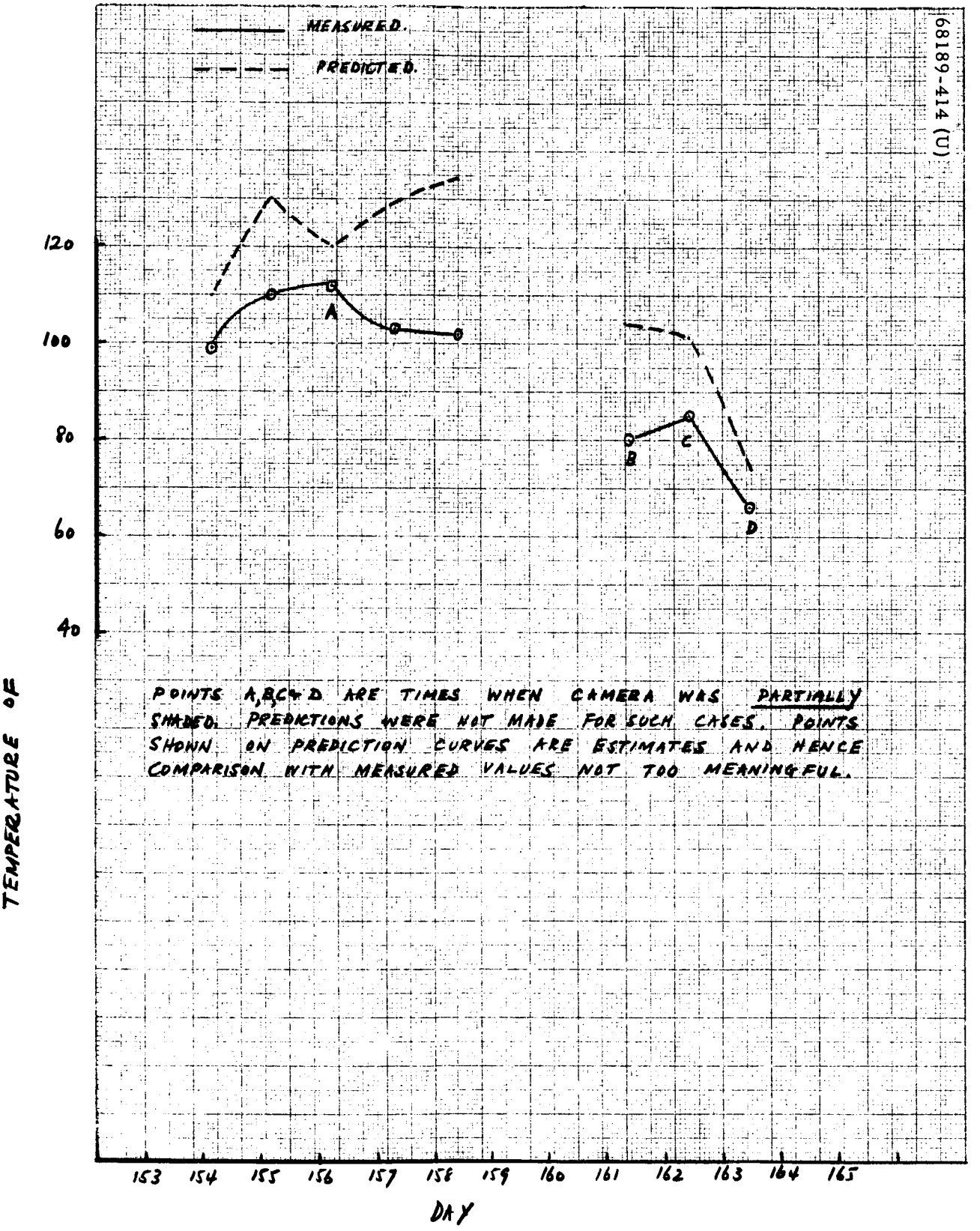
First Lunar Day – Camera Operation on Day 154. Day 154 was selected as one of the viewing periods within which to make comparisons between predictions and measured data as the camera was fully exposed to direct sunlight.

It would have been too time consuming to collect all the relevant information and prepare the computer run for the entire period; consequently, the first three operating cycles only, covering 188 minutes, were compared.



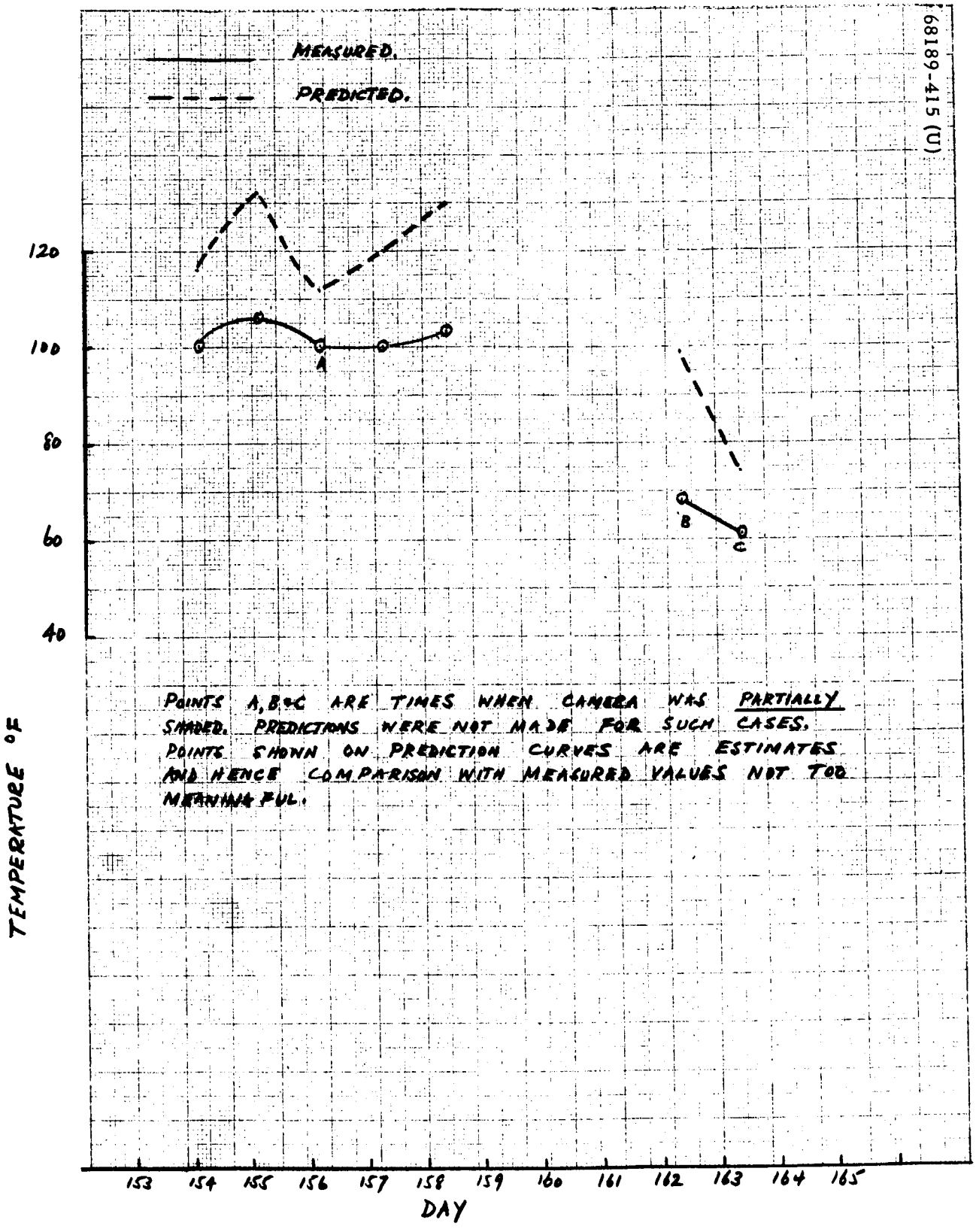
a) TV-9

Figure 5.2-31. Comparison of Predicted and Measured Temperatures — Steady-State Nonoperating



b) TV-10

Figure 5.2-31 (continued). Comparison of Predicted and Measured Temperatures – Steady-State Nonoperating



c) TV-17

Figure 5.2-31 (continued). Comparison of Predicted and Measured Temperatures — Steady-State Nonoperating

During the period the following surveys were made:

1) 360 degrees wide angle 120 frames

2) Pad 2 narrow angle 40 frames

3) Sectors 1 and 9 narrow angle 98 frames

These surveys yielded a total of 258 frames encompassing 175 azimuth and 489 elevation steps, 342 focus steps, and, of course, 258 shutter operations. The appropriate power dissipations within the electromechanical components and the chassis were computed from this data and used to perform the analysis, the results of which are compared with the measured data in Figures 5.2-32 and 5.2-33 for TV 9 and TV 10, respectively.

The predicted temperatues were initially higher, as already discussed, and remained higher throughout the 188-minute period. Both the predicted rates of rise during operation and the rates of fall during the cooldown periods were higher than the measured rates.

First Lunar Day – Camera Operation on Day 158. Day 158 was selected because it was representative of a completely shaded case. Again, comparisons were made only for the first three operating periods covering 260.5 minutes. During this period the following surveys were made:

1) 360 degrees wide angle 120 frames

2) Sector 18 narrow angle 3 filters 129 frames

3) Sector 19 narrow angle 3 filters 129 frames

4) Sector 1 narrow angle 3 filters 129 frames

5) Sector 2 narrow angle 3 filters 138 frames

These surveys yielded a total of 645 frames encompassing 308 azimuth and 1241 elevation steps, 1953 focus steps, and 645 shutter operations. Using the power dissipations appropriate to these sequences, the analysis was performed, and the comparison between predicted and measured values for TV 9 and TV 10 are shown in Figures 5.2-34 and 5.2-35, respectively.

Again, the predicted values were initially higher and remained higher. Also, the predicted rates of rise during operation and fall during cooldown were higher than the measured rates.

Discussion. The thermal performance of the camera throughout the SC-1 mission was highly satisfactory. The prescribed transit warmup schedule, which called for electronics and vidicon thermal control to be commanded on at 5 hours and at 1 hour before touchdown, respectively, warms the camera so that it is operational at touchdown. There would appear to be no reason to change this schedule for future missions.

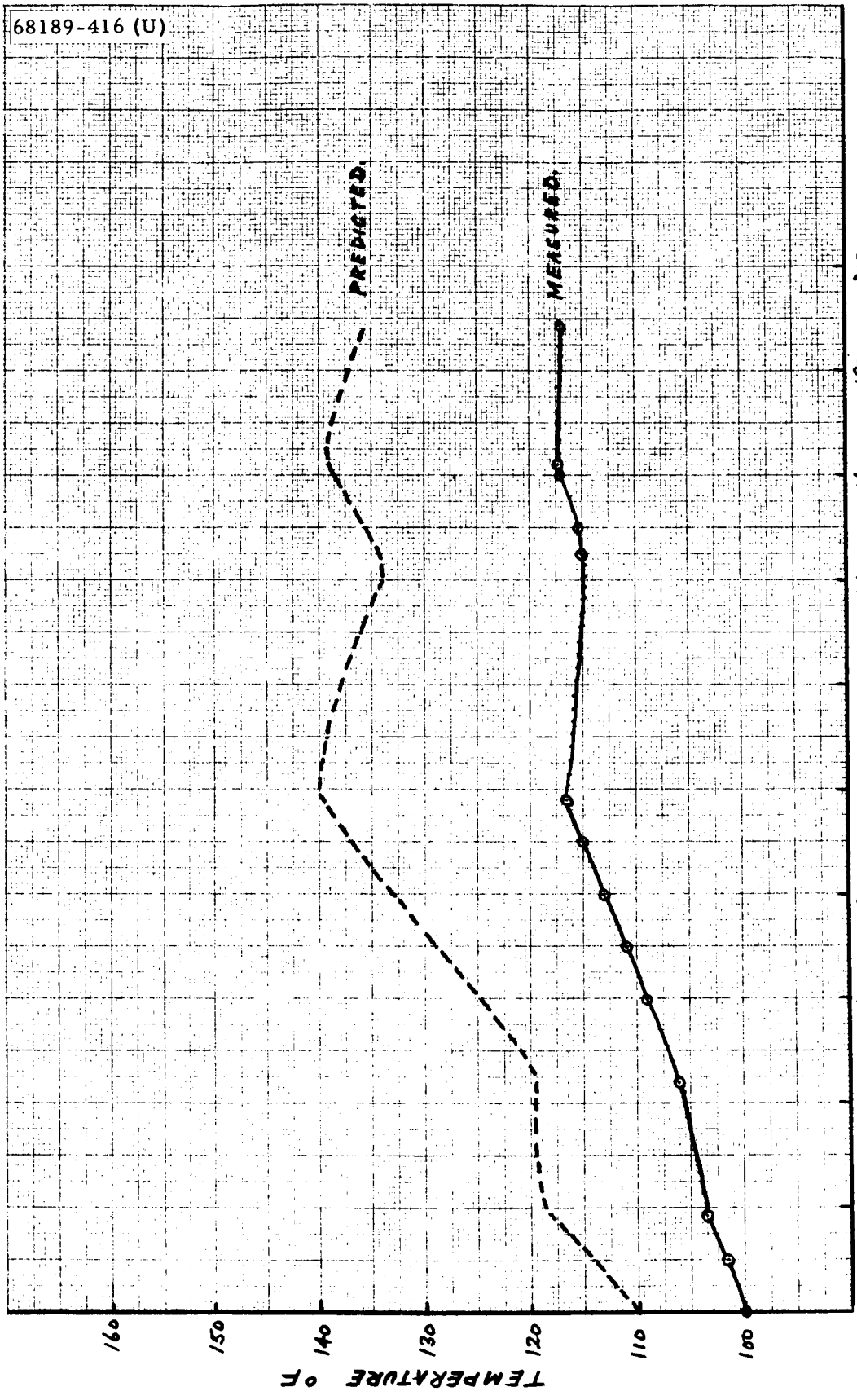


Figure 5.2-32. TV-9: Vidicon Collar

Comparison of predicted and measured temperatures for first three camera operating duty cycles on day 154

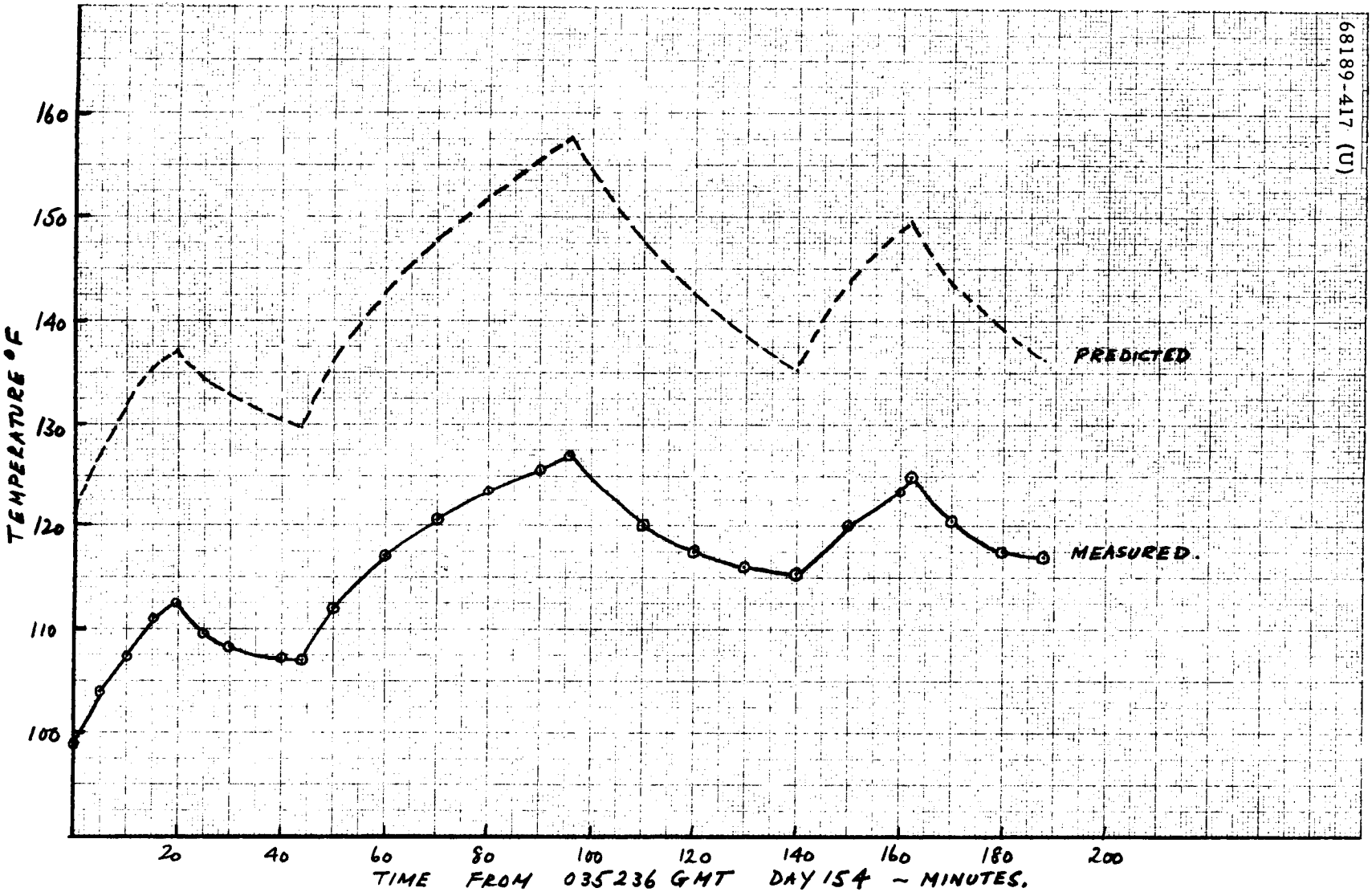


Figure 5.2-33. TV-10: ECU Chassis

Comparison of predicted and measured temperatures for first three camera operating cycles on day 154

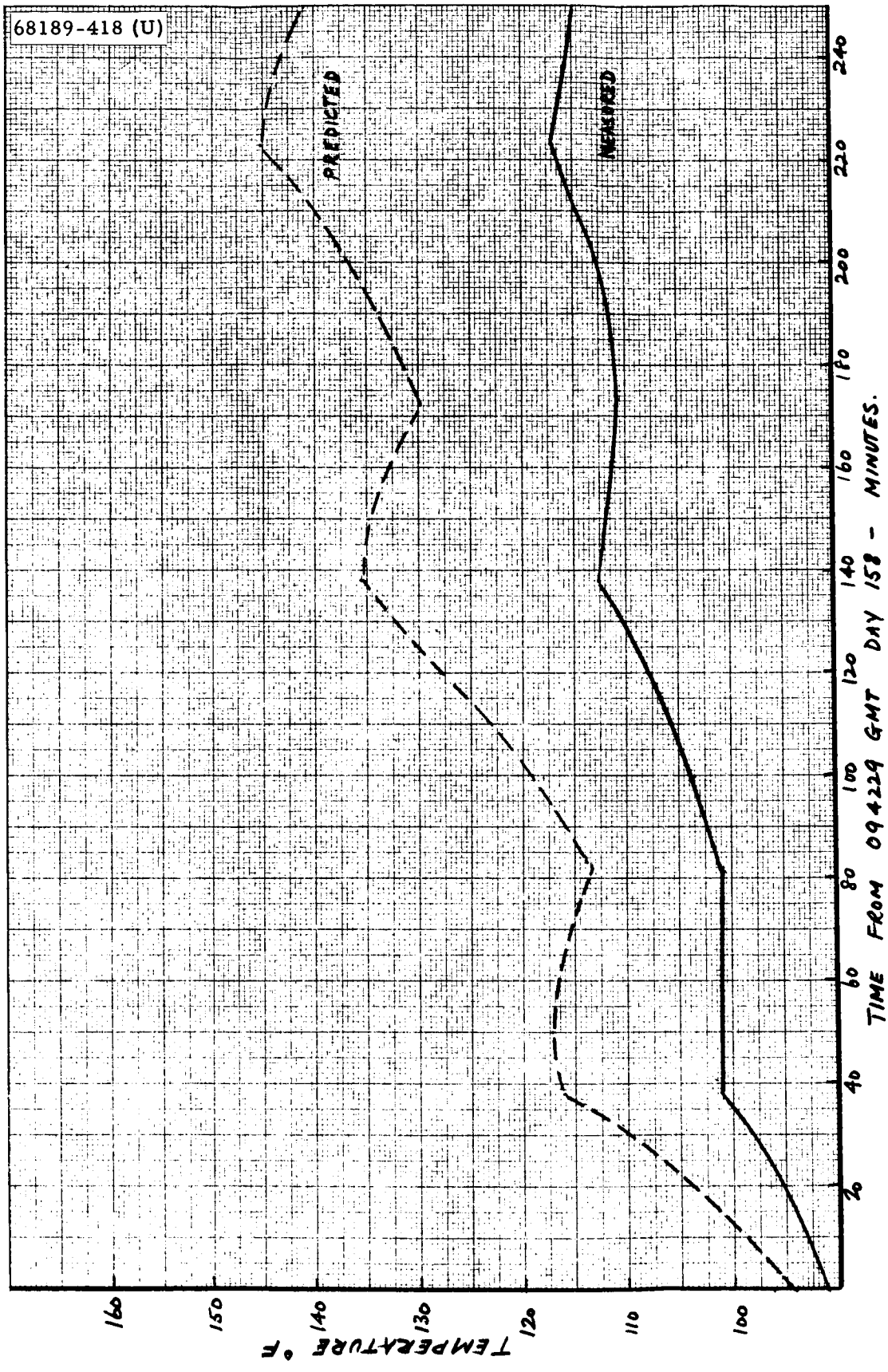


Figure 5.2-34. TV-9: Vidicon Collar
Comparison of predicted and measured temperatures for first three camera operating cycles on day 158

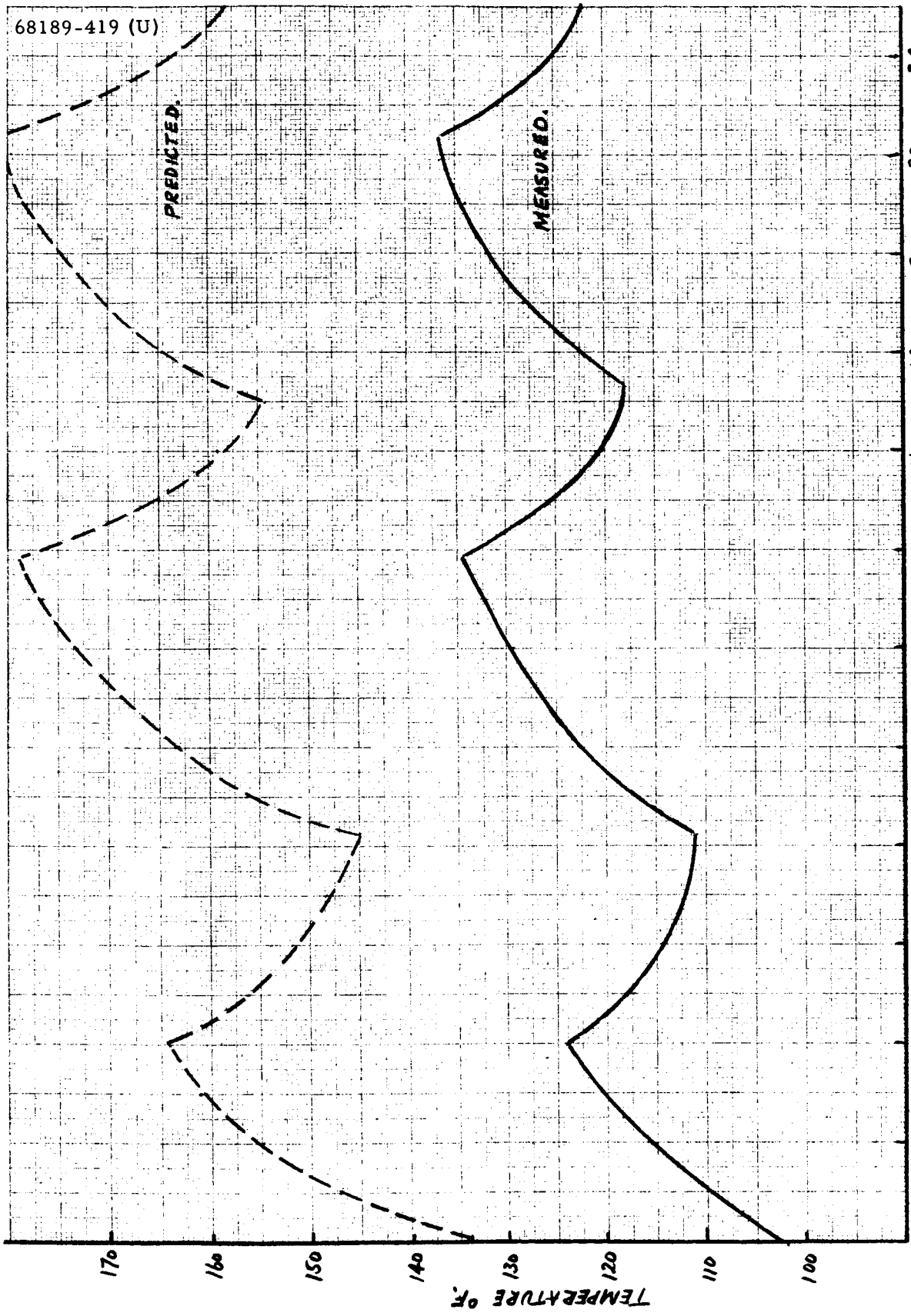


Figure 5.2-35. TV-10: ECU Chassis

Comparison of predicted and measured temperatures for first three camera operating cycles on day 158

Provided the camera is shaded, either by the planar array or the solar panel, it would appear that unlimited continuous operation of the camera would be possible regardless of the time of lunar day if 165 and 150°F were adhered to as the upper temperature limits for TV 10 and TV 9, respectively. The same would pertain if the camera were exposed to direct sunlight, certainly for solar angles of 40 degrees or greater from zenith. Closer to lunar noon, operation may become limited.

These findings regarding lunar operation were quite unexpected on the basis of the preflight analyses. These had shown that operation would be restricted for solar angles less than approximately 50 and 67 degrees for the shaded and exposed camera, respectively. This discrepancy can be explained by two factors. First, the initial temperatures prior to camera operation were lower than predicted for all viewing periods. This infers a cooler camera environment than that assumed in the analyses. The spacecraft temperature data must be examined in detail before this question can be resolved; this task is currently under way. Also of significance may be the fact that areas of the lunar surface shaded by the planar array and solar panel could have temperatures considerably less than nearby exposed areas (Reference 16).

The thermal load upon the camera contributed by the lunar surface, even when exposed to direct sunlight, has been estimated to account for 68 percent of the total for a solar angle of 45 degrees, increasing to 85 percent at lunar noon (Reference 7). Thus, any perturbation in the surface temperature of any areas having significant view factors to the camera could conceivably reduce predicted temperature values. This will, however, be a more difficult problem to resolve.

Second, the power dissipation is a function of the camera operating sequence. When the camera is merely turned on but not operating (the quiescent mode), the dissipation is 8.9 watts. The dissipation increases during operation due to added power expenditure in the drive motors and associated logic circuitry and in the 22-volt switch within the ECU. Furthermore, this added dissipation is a function of temperature due to the thermal coefficient of resistance of the coils in the drive motors. All preflight analyses were based upon the operating sequence prescribed in Reference 3. For comparison, the number of steps, or operations, performed per minute in the electromechanical elements for such a sequence is compared with the average number during the operating sequences analyzed on days 154 and 158. This comparison is shown in Table 5.2-11.

These reduced frequencies mean less dissipation within the motors, in the associated circuitry, and, in particular, within the 22-volt switch in the ECU. The latter is most significant because its dissipation reflects the combined duty cycles of the electromechanical elements. In addition, sensor TV 10 is located very close to this 22-volt switch, in fact within the same node in the nodal breakdown of the camera thermal model. Consequently, any predictions for the thermal response of TV 10 would be quite sensitive to the camera operating sequence assumed in the analysis.

TABLE 5.2-11. FREQUENCY OF OPERATION OF DRIVE MOTORS

(Steps per Minute)

	Assumed in Preflight Analyses per Reference 3	Mean Actual, First Three Cycles for Days 154 and 158
Mirror azimuth	16	2
Mirror elevation	16	7
Focus drive	16	10
Shutter drive	8	4

Table 5.2-12 shows the effect of these factors upon the dissipation. The dissipations shown for days 154 and 158 were those actually used in the postmission analyses, the results of which are shown in Figures 5.2-32 and 5.2-33.

TABLE 5.2-12. CAMERA POWER DISSIPATION

Comparison of Dissipations Used for Preflight Analyses With Best Estimates of Actual Average Dissipations During First Three Cycles of Operation on Days 154 and 158

	Dissipation, watts		
	Used for Preflight Analyses	Estimation Used in Postmission Analysis	
		Day 154	Day 158
Chassis 1 through 6	5.15	5.13	5.13
Vidicon tube	1.40	1.40	1.40
ECU*	3.78	3.78	3.78
22-volt switch	1.68	0.71	1.09
Azimuth drive	1.01	0.31	0.21
Elevation drive	1.01	0.11	0.64
Lens assembly	1.24	0.26	0.83
Shutter drive	1.07	0.36	0.75
Totals	16.34	12.06	13.83

*Excluding 22-volt switch which is listed separately.

The comments regarding the discrepancies between predicted and measured temperatures are presented here merely to emphasize the fact that additional studies of the data and modifications to the thermal model which may be dictated by this data are necessary.

Conclusions. From the thermal standpoint, the following conclusions regarding camera 3 and its performance during the SC-1 mission can be drawn:

1) The thermal response of the camera during transit, including the warmup phase prior to touchdown, was very close to the anticipated response and instills confidence in this phase of the mission for future operations.

2) Camera operation was not restricted by any thermal constraints during the periods it operated on lunar surface. This was not as anticipated; however, the preflight predictions at least had the dubious virtue of being conservative.

3) Further studies of the camera thermal model based upon the SC-1 data are necessary not only to increase knowledge of the lunar thermal environment but also to enhance confidence in preflight predictions for an additional survey camera which may be on subsequent Surveyor spacecraft.

The temperature of the approach camera during the transit phase of the mission is shown in Figure A-37a.

5.2.3.19 Determination of Lunar Surface Temperature

Summary

Lunar surface temperatures based on an emissivity value of the moon of 1.00 are calculated from the thermal data obtained from SC-1 on the moon. Temperature sensors located on the outboard sides of compartments A and B were used to arrive at the lunar surface temperatures. The results are presented in Figure 5.2-36. The unpublished predicted lunar surface temperatures of J.M. Saari of Boeing Aircraft Company are given as a comparison in the same figure. The temperatures obtained from the two temperature sensors agree reasonably well, being within 10° F of each other, and fall within the range of predicted results. When the emissivity of the lunar surface is established, the lunar surface temperature can be modified by Equation 2 below.

Method of Analysis

The successful landing of SC-1 on the moon makes the measurement of the lunar surface temperature more direct and more reliable than ground-based observations. Upon examination of the locations of the various temperature sensors, the two sensors located at the two outboard sides of compartments A and B were found most satisfactory for determining the

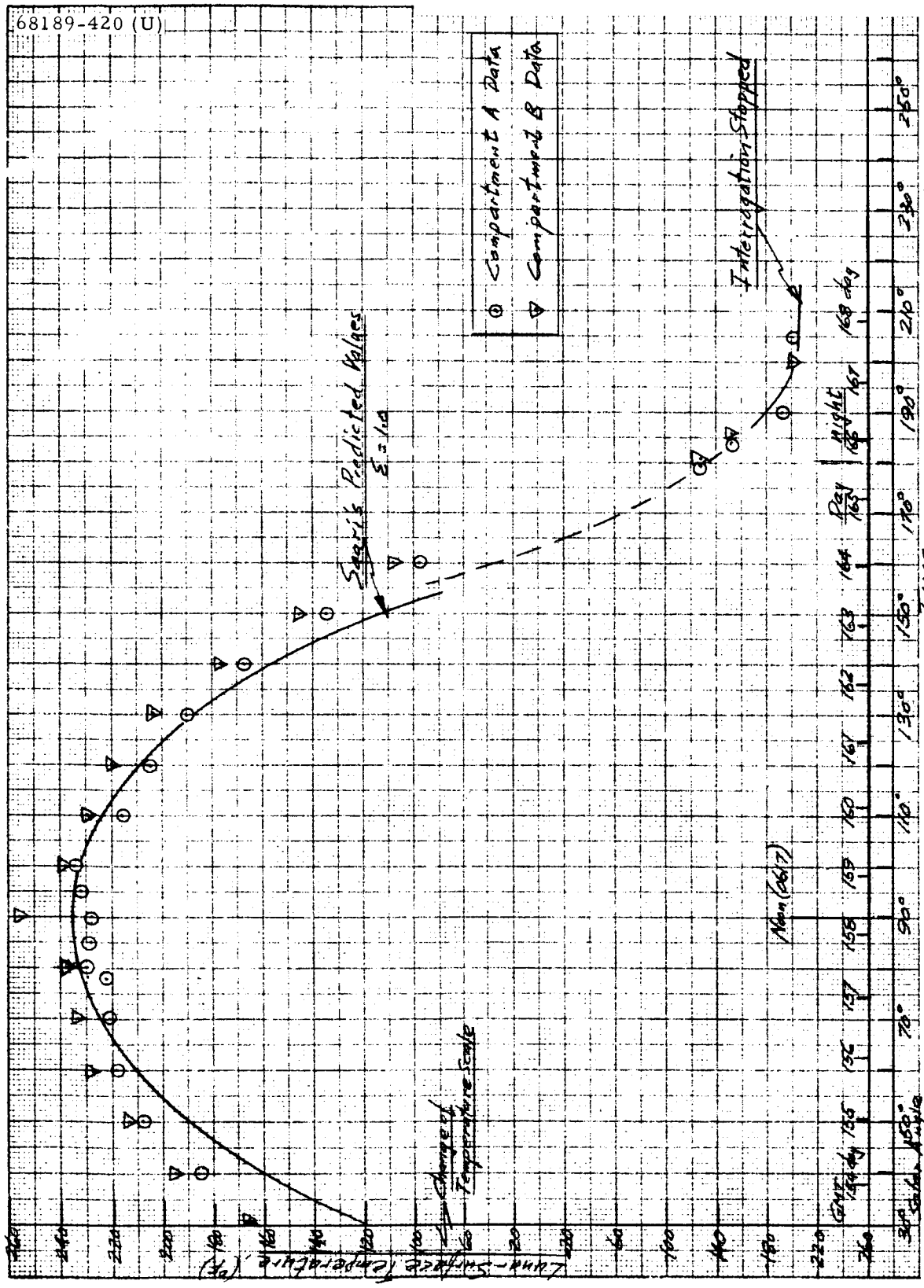


Figure 5.2-36. Lunar Surface Temperature (Based on $\varepsilon_{moon} = 1.0$) Obtained from SC-1

lunar surface temperature. The surfaces are radiantly and conductively decoupled from the remainder of the spacecraft, have a well-defined view factor to the moon, and are of relatively low heat capacity. The relatively slow rate of change of the lunar surface temperature allows a quasi steady-state temperature to be defined. An energy balance is made on the outboard sides using the sensors' temperatures. It is assumed that the surface is isothermal and that the temperature is indicated by the respective sensors. The resulting equation from the energy balance is as follows:

$$T_{Lunar}^4 = \frac{-Q + S_1 (T_{Sensor}^4 - T_{Comp}^4) + S_3 T_{Sensor}^4 + S_2 T_{Sensor}^4}{S_3} \quad (1)$$

where

T_{Lunar} = lunar surface brightness temperature, °R

T_{Sensor} = sensor temperature, °R

T_{Comp} = inside compartment temperature, °F

T_{Space} = space temperature = 0°R

Q = solar energy, $\frac{Btu}{hr}$

S_1, S_2, S_3 = $\sigma F A \varepsilon$ = grey body, radiation heat transfer constant, $\frac{Btu}{hr\ °R^4}$

The radiation heat transfer constants differ from each other by their appropriate view factors, F, the surface area, A, and the emissivity, ε. It is observed that $S_1 (T_{Sensor}^4 - T_{Comp}^4) \ll$ other numerator terms during the lunar day. Equation 1 can be simplified to the following:

$$T_{Lunar} = \left[\frac{-Q + (S_3 + S_2) T_{Sensor}^4}{S_3} \right]^{1/4} \quad (2)$$

The values of S_2 and S_3 can be obtained readily. The hemispherical emissivity of the outboard sides is 0.87, and a value of 1.00 for the lunar surface was used. The view factor between the outboard side and the lunar surface is computed by

$$F_{out\text{-}lunar} = \frac{1}{2} (1 + \cos \gamma) \quad (3)$$

wnere γ is the intersecting angle between the outboard side and the lunar surface. The view factor between the outboard side and space is $(1 - F_{out\text{-}lunar})$. The solar energy to the outboard side is calculated by

$$Q = \alpha I A_{proj} \Psi \tag{4}$$

where

α = absorptivity = 0.20

I = solar intensity = $430 \pm 1 \frac{Btu}{hr\text{-}ft^2}$ (average value for 2 through 14 June 1966)

A_{proj} = projected area of the outboard side to the sun

Ψ = fraction of the projected area which is not shadowed

The projected area is given by

$$A_{proj} = A_{total} \cos \theta \tag{5}$$

where θ is the angle between sun rays and the normal to the plane area of interest. It can be shown by vector analysis that the projected areas (in square inches) of the two outboard sides are

for compartment A:

$$A_{proj} = 144 \cos \varphi - 120 \sin \varphi + 13 \tag{6}$$

and

for compartment B:

$$A_{proj} = 110 \cos \varphi - 84 \sin \varphi - 9.2 \tag{7}$$

where φ is the solar elevation angle.

Thus, the lunar surface can be calculated by Equation 2 using the inputs of sensors' temperatures, shadow plots, projected areas, and view factors. The sensor temperatures and the shadow plots are presented in Figures 5.2-37 and 5.2-38 for compartments A and B outboard sides, respectively. Their respective projected areas are given in Figures 5.2-39 and 5.2-40 in terms of θ.

PRECEDING PAGE BLANK NOT FILMED.

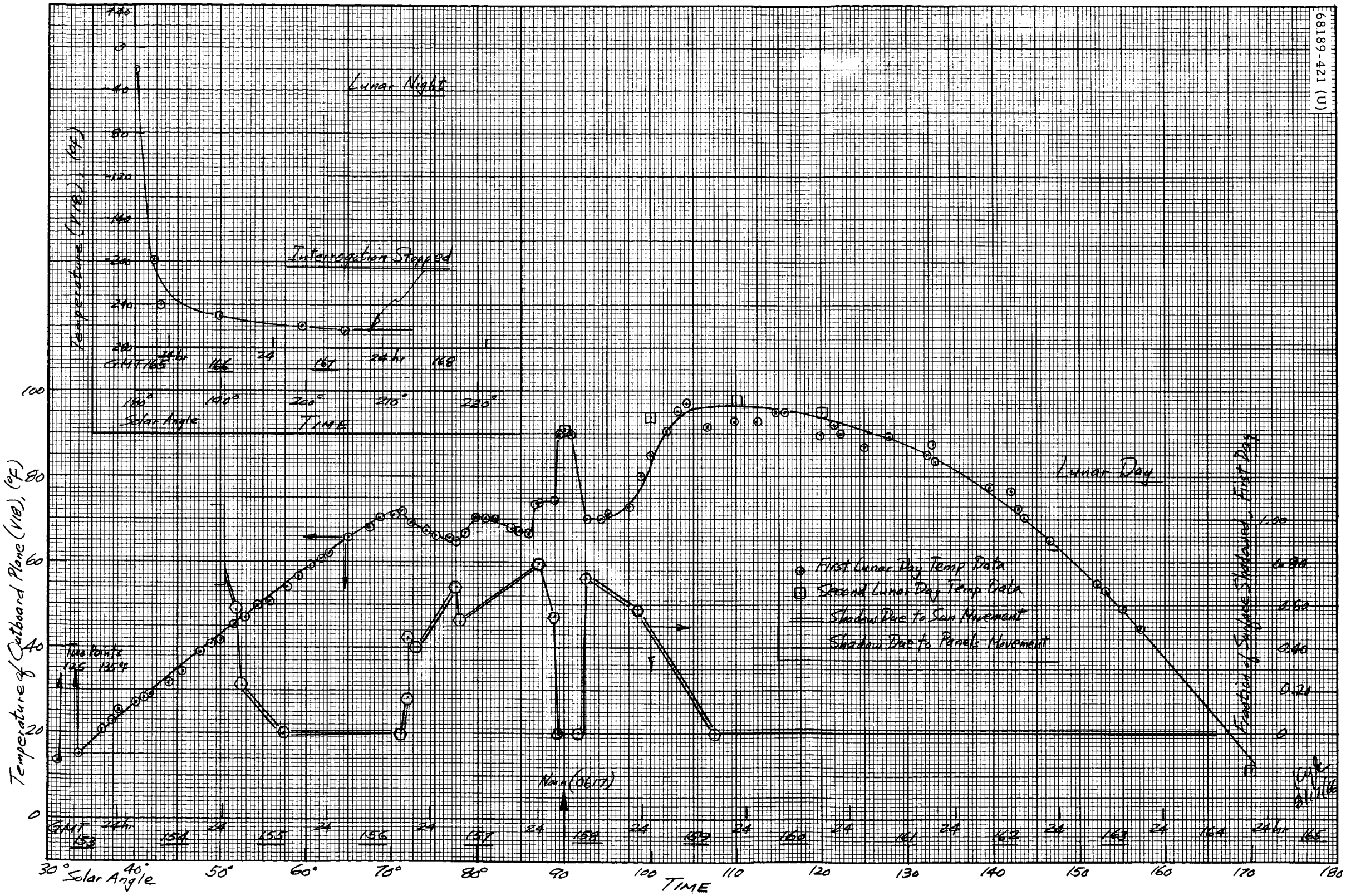


Figure 5.2-37. Temperature and Shadow of Outboard Side of Compartment A During First Lunar Day and Night

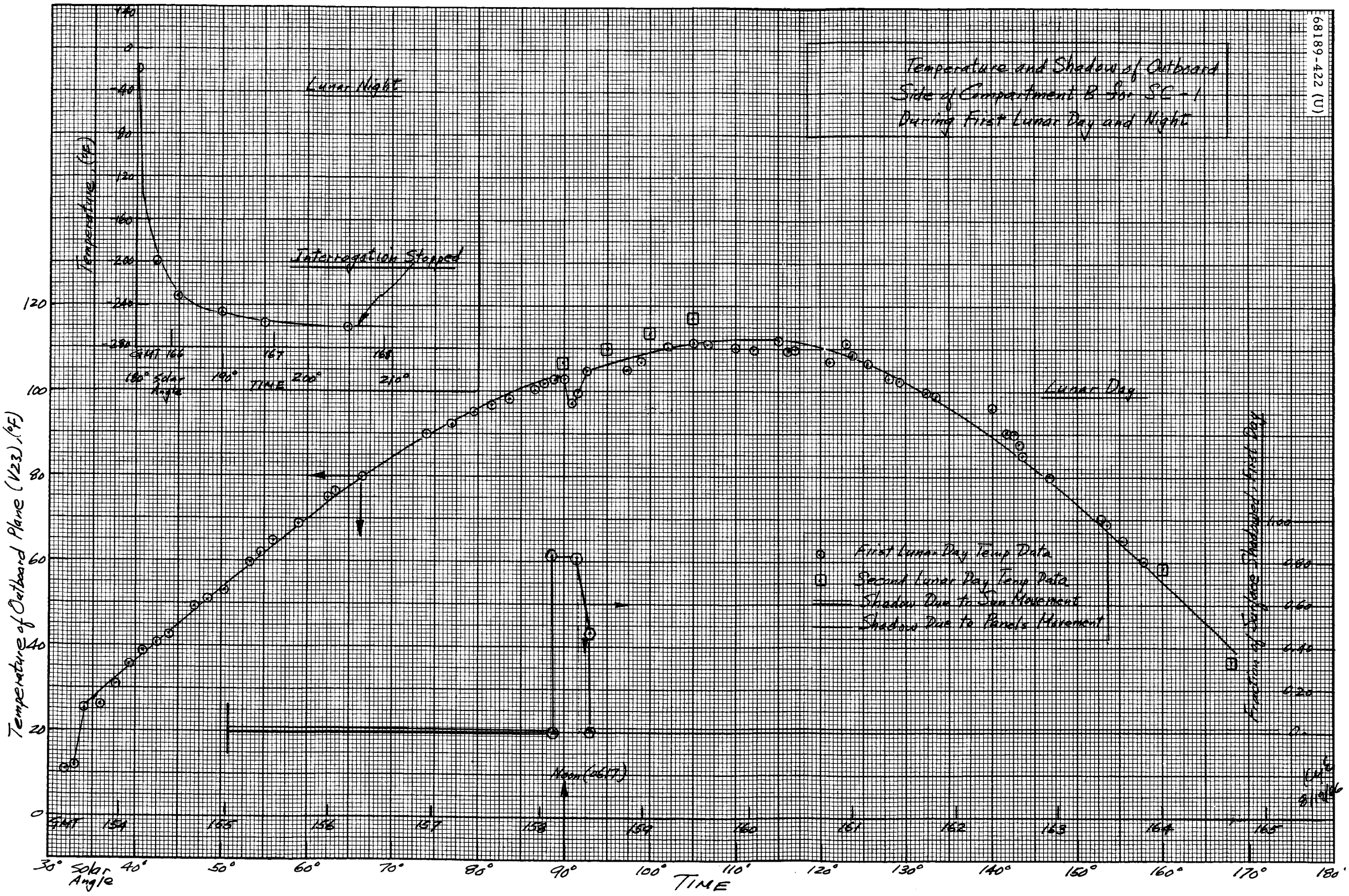


Figure 5.2-38. Temperature and Shadow of Outboard Side of Compartment B During First Lunar Day and Night

5.2-137

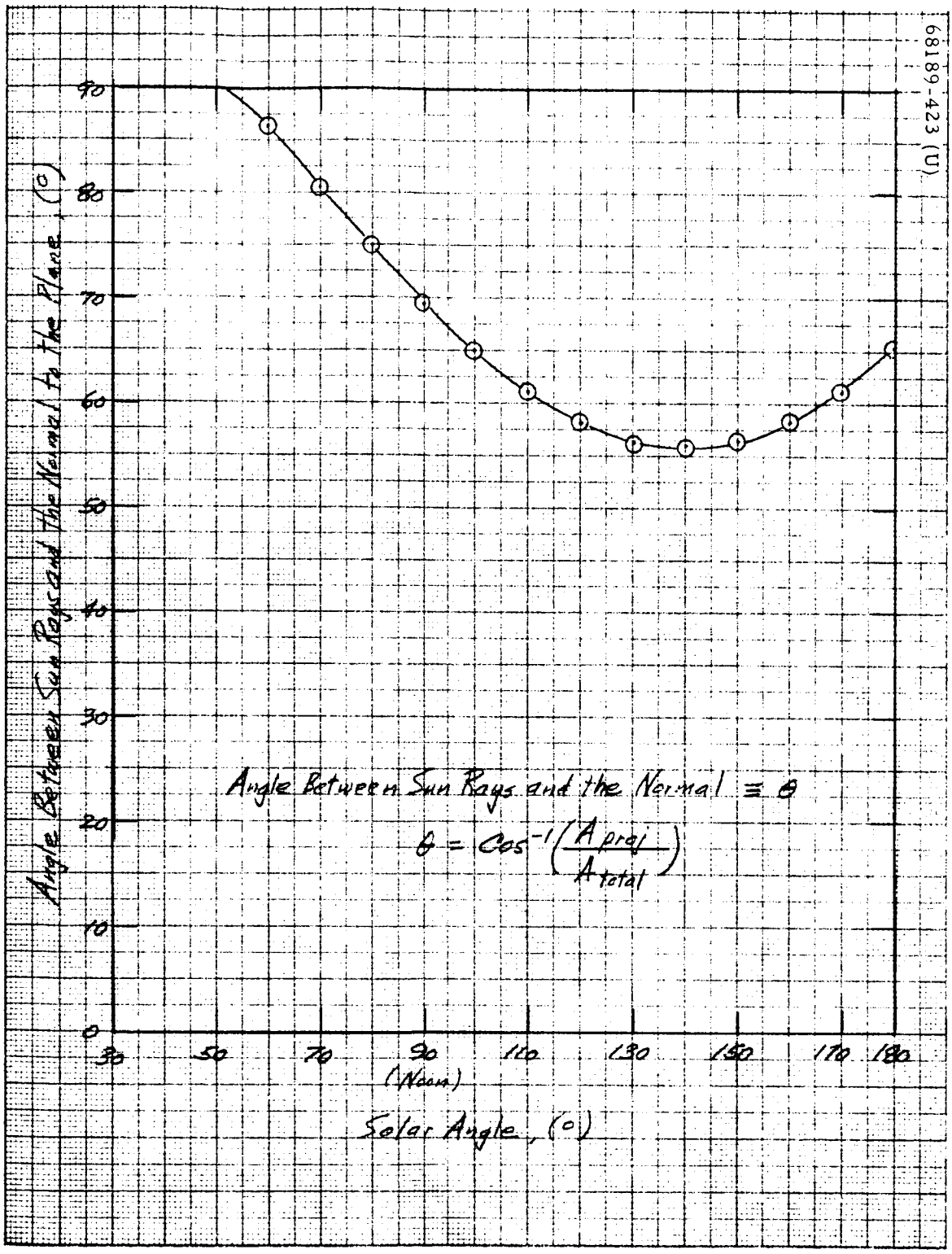


Figure 5.2-39. Angle Between Sun Rays and the Normal to Outboard Side of Compartment A During First Lunar Day

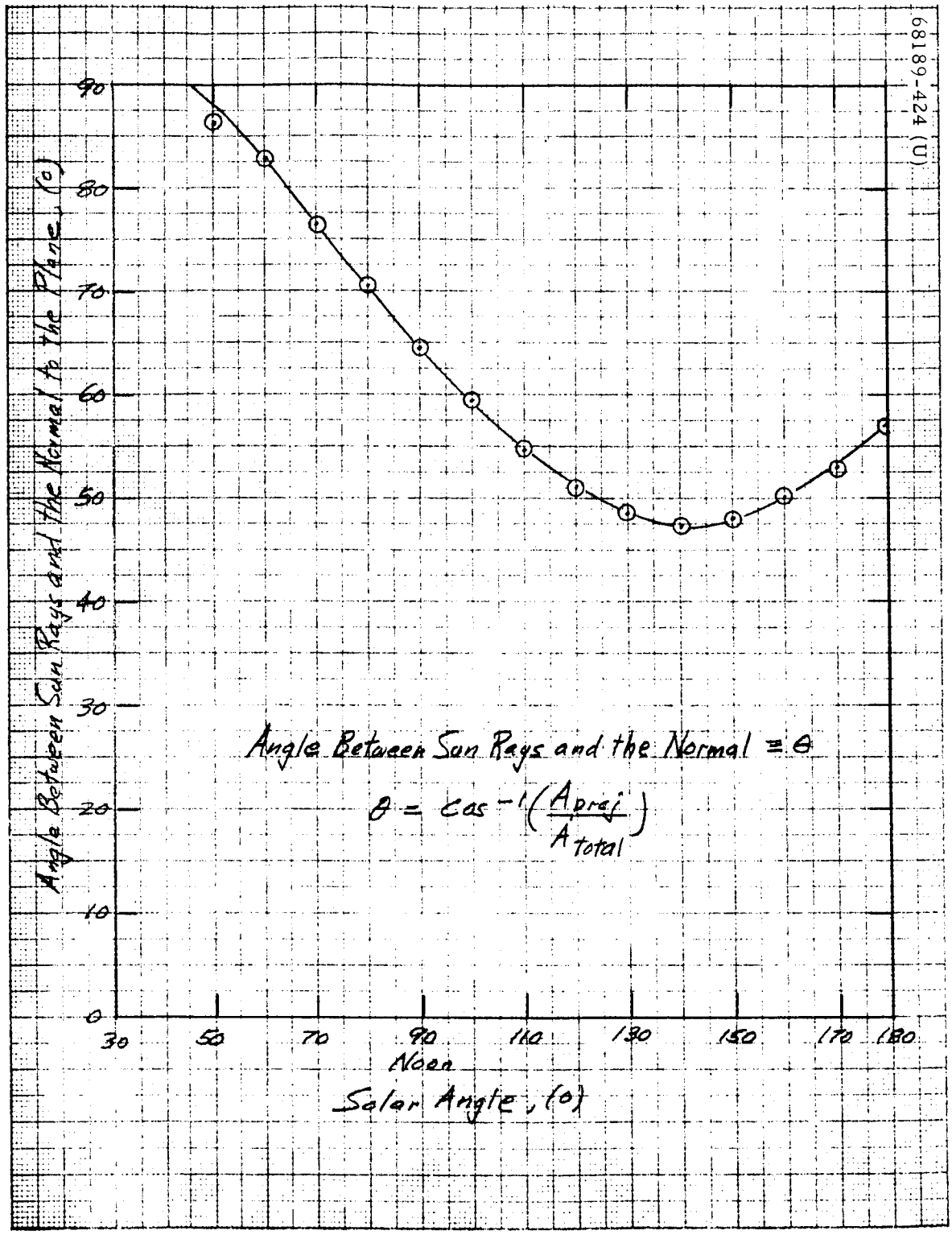


Figure 5.2-40. Angle Between Sun Rays and the Normal to Outboard Side of Compartment B During First Lunar Day

Discussion of Results

The results seem to have some anomalies. In the morning, before $\varphi = 50$ degrees, the lunar surface temperature obtained is higher than the predicted values. This may be due to some physical phenomenon on the moon that the predicted values did not consider, and also to the solar reflected energy from the lunar surface and other components of the spacecraft not having been included in this calculation. The results near noon are more scattered than at other times of the day. This may be attributed to the low resolution in the calculated shadow plots or other factors that have not been investigated. According to the shadow plots at lunar noon, the shadows on compartments A and B outboard sides are zero and 82 percent, respectively. In order to bring the results closer to each other, the approximate percentage of shadows should be 40 to 60 for both sides. During the lunar night, the heat transferred from the inside of the compartments is significant, in which case Equation 1 must be used to obtain the lunar surface temperature. The amount of heat transferred from the compartments is not exactly known. Bounding values of heat loss of zero and 1.0 Btu/hr yielded night lunar surface temperatures of -215 and -200°F.

The parameter that affects the lunar surface temperature most importantly is the view factor between the outboard side and the lunar surface. The slope of the outboard side, which nominally is 21 degrees with respect to the vertical, consists of spacecraft tilt, construction tolerances, and alignment of the compartments. These conditions can affect the lunar surface temperature by 10°F near noon if the compartment slope should be off by 1 degree. The slope uncertainty is about 1 degree due to the construction and alignment without considering the uncertainty in the tilt of the landing site. The uncertainty in the range of ±10 percent in emissivity and absorptivity for the outboard side does not affect the lunar surface temperature appreciably.

Conclusions and Recommendations

The lunar surface temperatures obtained (based on $\epsilon_{moon} = 1.0$) can be concluded as precise and fall within predicted values. The precision between the results obtained from the two sensors is within 10°F, which is reasonable considering the method of analysis and the uncertainties in the thermal data. It is recommended that: 1) efforts should be continued to obtain lunar surface temperature when additional thermal data becomes available, 2) an alternate and better method of measurement should be used in the future instead of the sensors used, and 3) more precise shadow plots should be made and other smaller heat sources and sinks should be included if additional analysis is done using SC-1 data.

5.2.3.20 Surveyor Liftoff and Translation

The large quantity of post-touchdown spacecraft temperature data gives a firm baseline from which to predict spacecraft lunar surface performance and on which to base test verification plans. The temperature data from SC-1 is extremely valuable because of the complexity of the

analytical approach to determining the spacecraft temperatures on the lunar surface. The lunar surface thermal environment and variable solar illumination of the spacecraft together produce complex shadowing and solar reflection interactions on spacecraft subsystems.

Figures 5.2-41 through 5.2-50 show the SC-1 lunar surface temperature profiles for those subsystem units required for liftoff and translation. The flight data is available for only one post-touchdown spacecraft orientation and solar azimuthal angle. An extensive study of the thermal behavior of all subsystems required for post-touchdown, liftoff, and translation maneuvers for all solar azimuthal angles and post-touchdown spacecraft orientations is a prerequisite to establishing the spacecraft total post-touchdown thermal capabilities for future missions.

Lunar surface thermal requirements are presented in Table 5.2-13 for all subsystem units required for the maneuver. The information presented in this table is based on a relaxation of transit thermal requirements for the lunar surface mission phase. Temperature requirements for RADVS are applicable only to missions involving RADVS.

Because of the subsystem temperature limits shown in Table 5.2-13, the spacecraft liftoff and translation maneuvers should be restricted to solar incidence angles approximately in the range of 15 degrees $\leq \eta \leq$ 50 degrees. η = 90 degrees defines the subsolar point, commonly referred to as lunar noon. It is desirable that the initial spacecraft touchdown occur with the spacecraft Y axis parallel to the lunar equator. Specific touchdown orientations should be selected to minimize solar insolation on the RADVS (for those missions when it is used) and the flight control sensor group.

An evaluation of the SC-1 post-touchdown thermal data indicates that the vernier propellant tanks, the limiting subsystem on high temperature operation, will exceed their upper temperature limits of 130°F for oxidizer and 120°F for fuel at some time subsequent to lunar touchdown. Tank temperatures may reach 200°F during the course of the lunar day. For morning landings, oxidizer tank temperatures will exceed the upper operational limit of 130°F at a solar elevation angle of approximately 50 degrees. Because of the long thermal time constant of the tanks, tank temperatures will not have decreased to the upper operational limits until the solar angle is 165 degrees. Therefore, the liftoff and translation maneuver must be accomplished before the tanks reach the upper operational temperature limit. The implications here are that morning landings followed by evening liftoff and translation maneuvers probably are not feasible. Following vehicle liftoff from the lunar surface, the remainder of the spacecraft translation and touchdown maneuver does not pose an obvious thermal problem.

The maximum liftoff solar angle of approximately 50 degrees is derived by using the data shown in the figures along with limited analyses. The maximum liftoff solar angle is a function of several parameters: vehicle orientation at touchdown, solar elevation and azimuth angles, thermal coupling of the subsystem units with their environment, and the translation maneuver to be performed. Therefore, the maximum liftoff angle can be

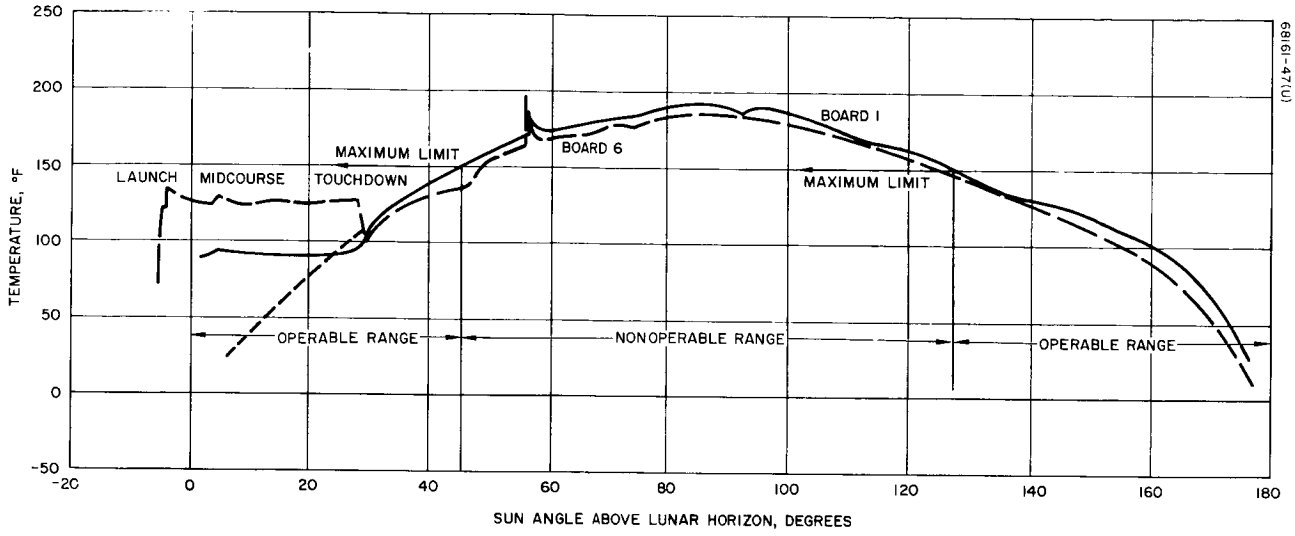


Figure 5.2-41. SC-1 Flight Data for Flight Control Electronics

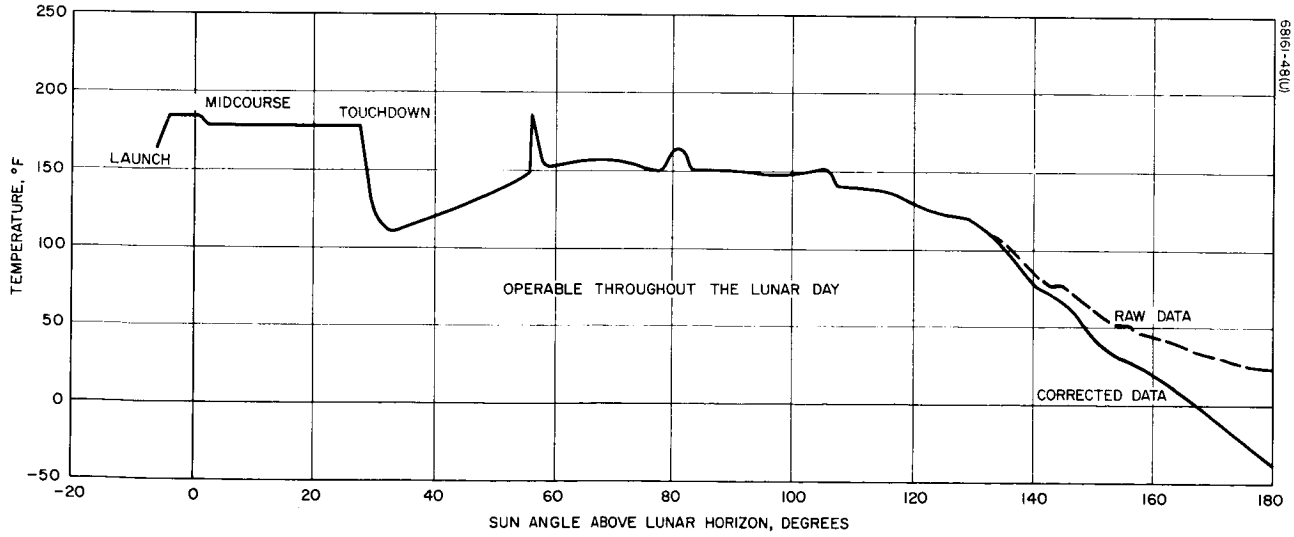


Figure 5.2-42. SC-1 Flight Data for Pitch Gyro

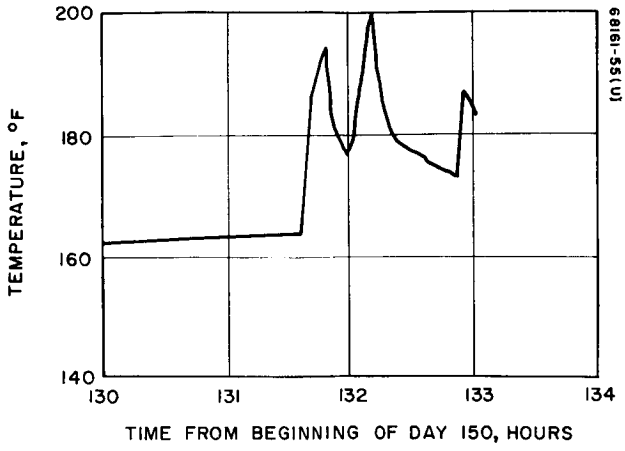


Figure 5.2-43. SC-1 Flight Data for Pitch Gyro Temperature Rise When Flight Control System Operated

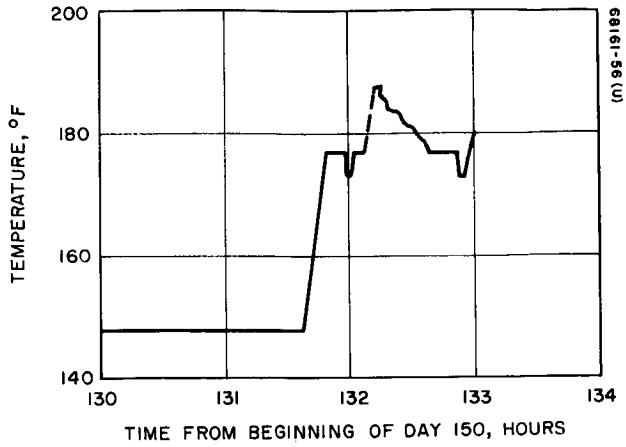


Figure 5.2-44. SC-1 Flight Data for Flight Control Electronics Board 6

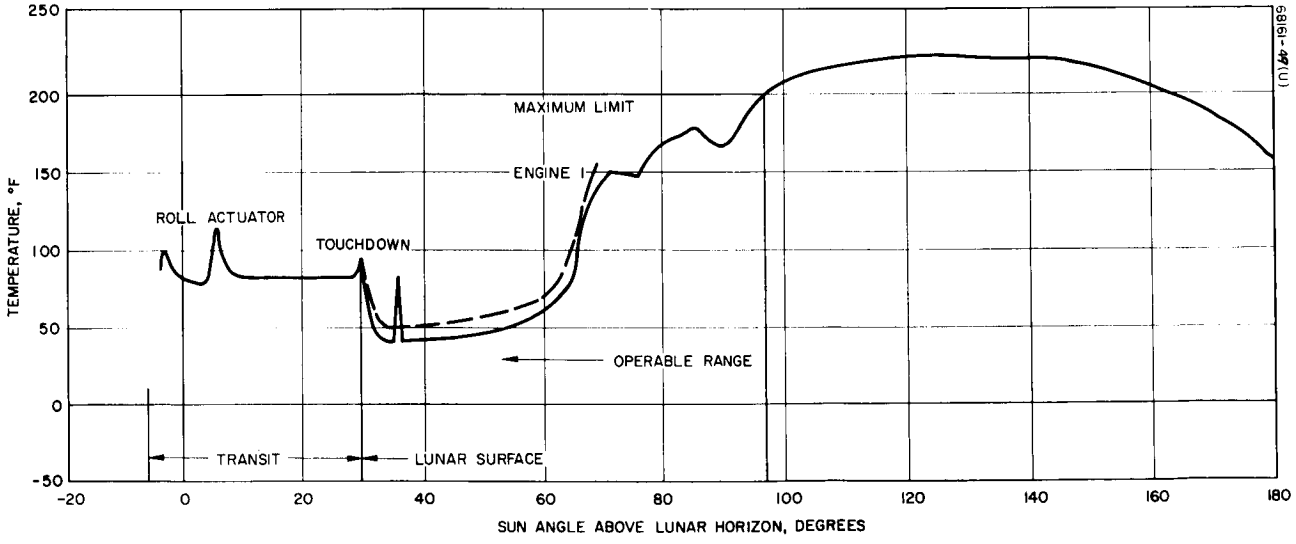


Figure 5.2-45. Thermal Response of SC-1 Roll Actuator

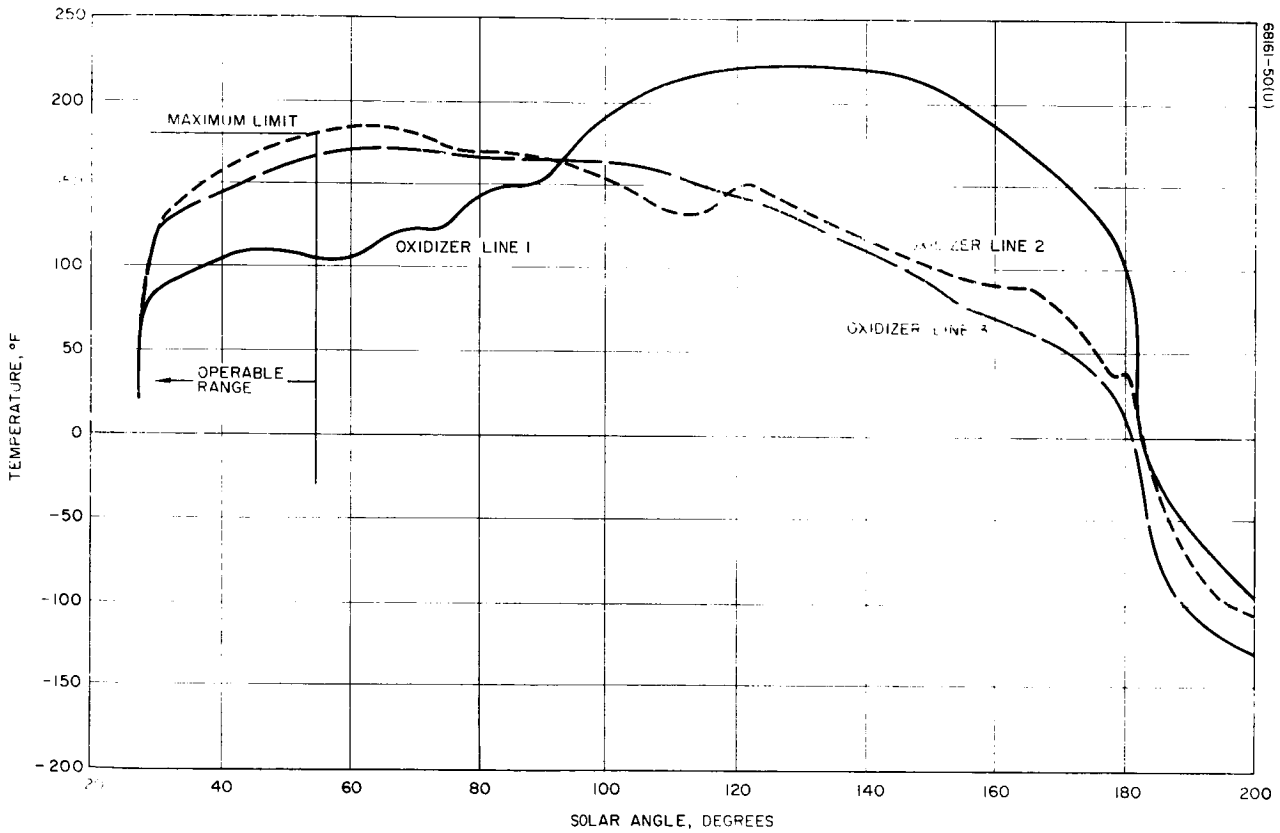


Figure 5.2-46. Thermal Response of Propellant Lines on Lunar Surface

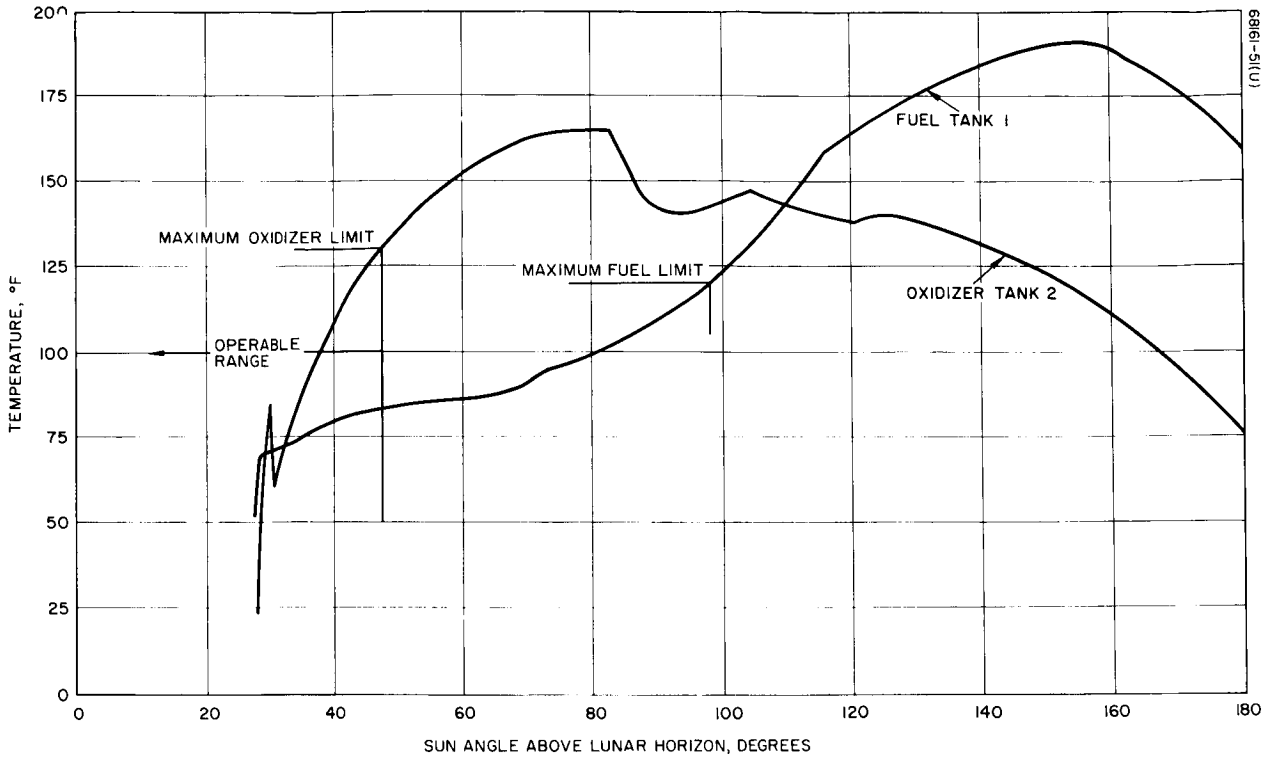


Figure 5.2-47. Thermal Response of Propellant Tanks on Lunar Surface

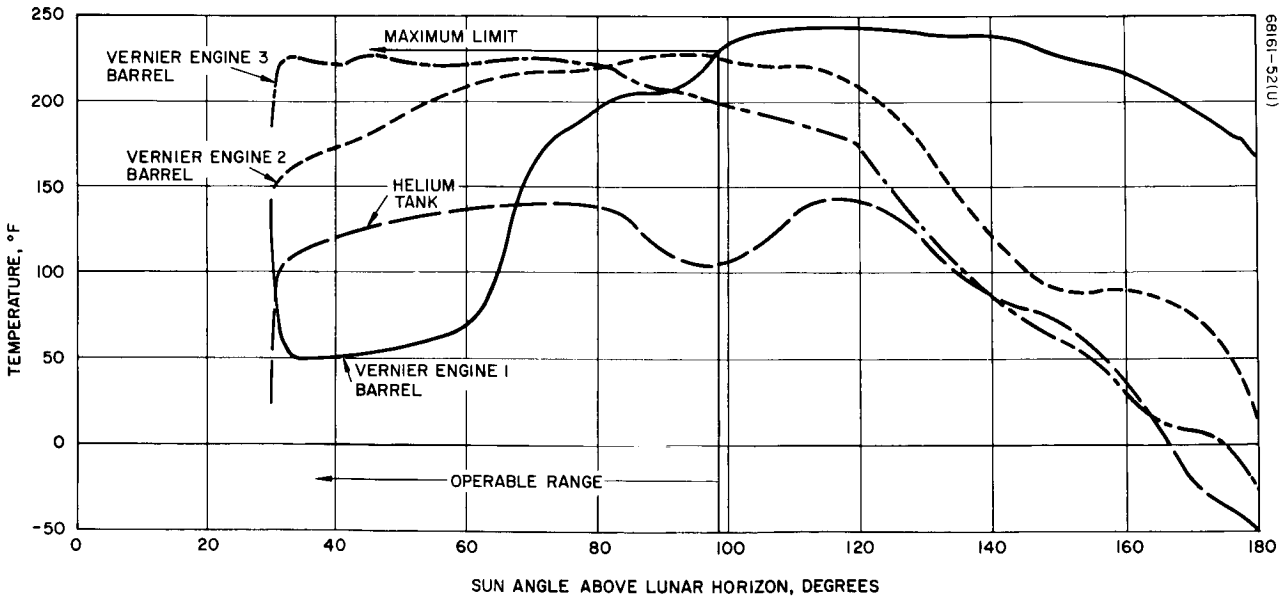


Figure 5.2-48. Thermal Response of Vernier Engines and Helium Tank on Lunar Surface

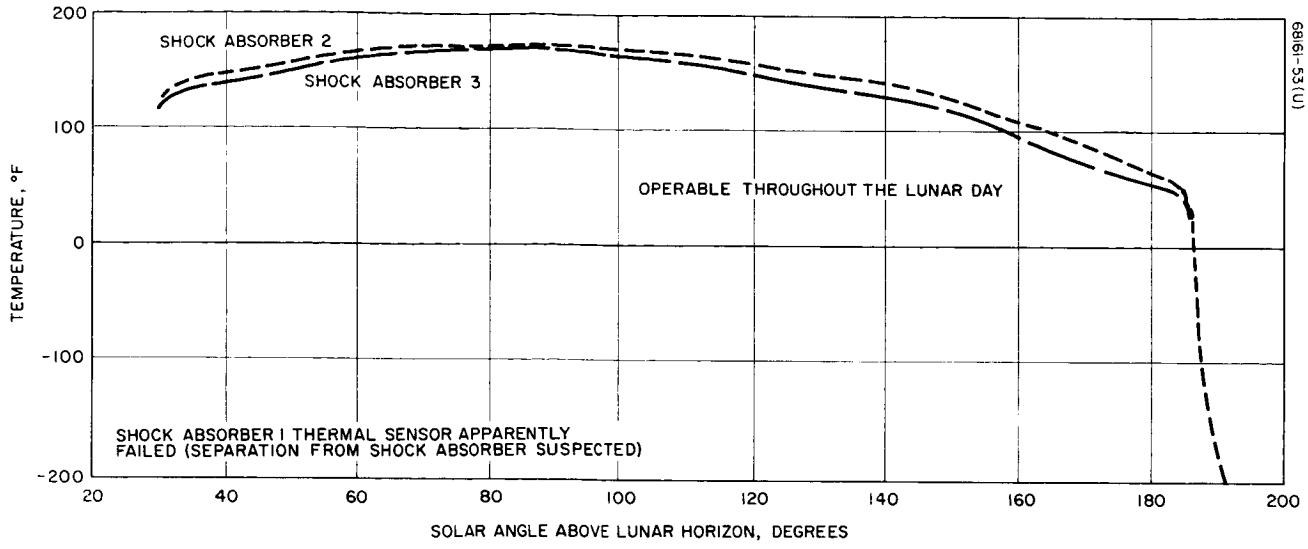


Figure 5.2-49. Thermal Response of Shock Absorber on Lunar Surface

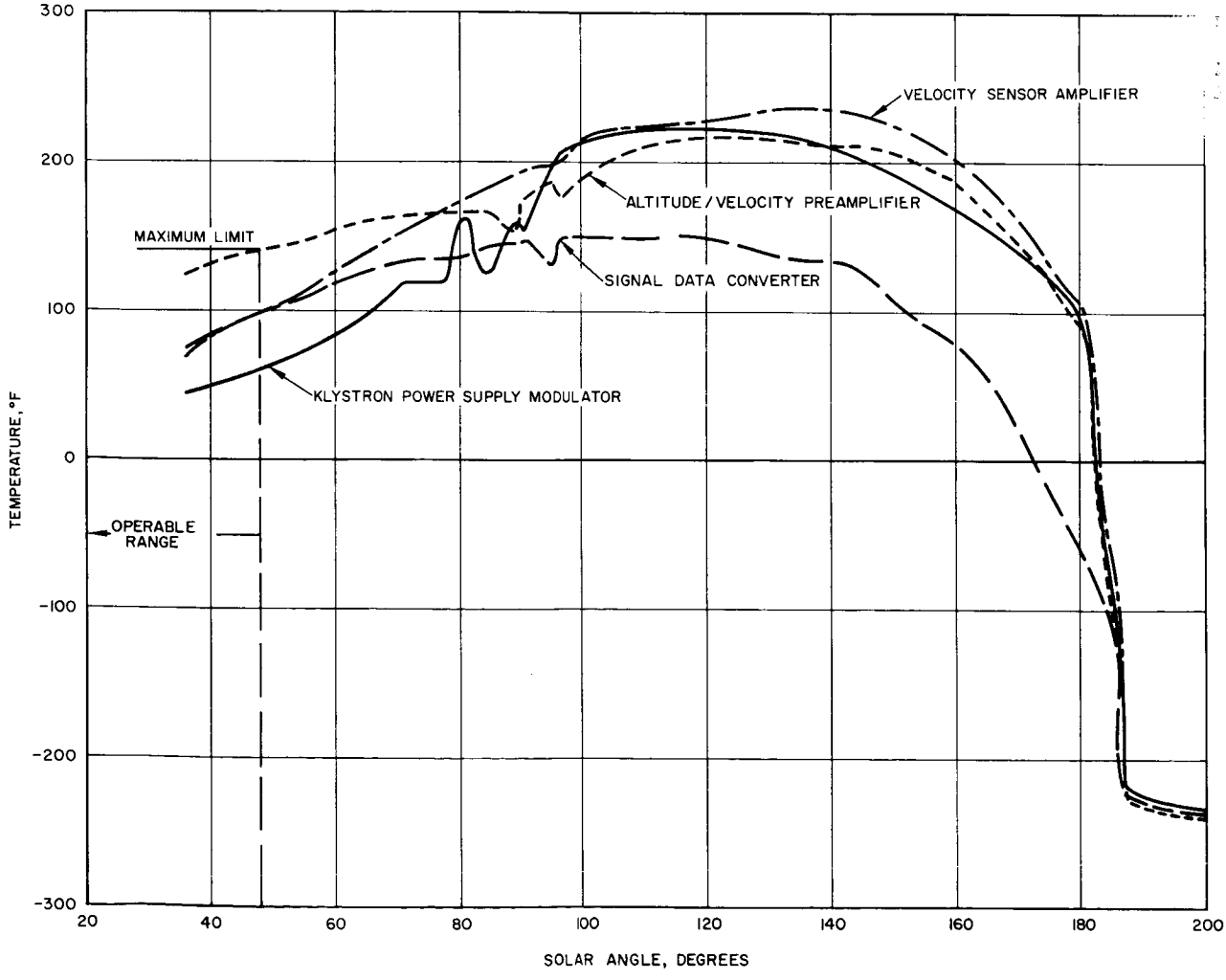


Figure 5.2-50. Thermal Response of SC-1 RADVS Units on Lunar Surface

TABLE 5.2-13. PROPOSED LUNAR SURFACE TEMPERATURE REQUIREMENTS PRIOR TO LIFTOFF

Subsystems Required for Maneuver Liftoff and Translation	Temperature Limits, °F	
	Operational	Survival
Compartment-housed telecommunication and power subsystems	0 to 125	140
Vernier propulsion system		
Propellant tanks		
Fuel	0 to 120	260
Oxidizer	0 to 130	260
Lines	0 to 180	230
Vernier engines	0 to 230	250
Helium supply	0 to 160	180
Flight control		
RADVS		
KPSM	-22 to 140	
SDC	15 to 140	
A/VS and VS preamplifiers	-60 to 140	
IRU	$120 < T < 180$	190
FCE	190	210
Programmer	158	
Landing system		
Leg structure	-165 to 300	300
Footpads (3)*	-50 to 200	300
Shock absorbers (3)	20 to 180	300
Crushables (3)*	-50 to 150	300

*Not of concern for secondary landing; the operational limits are for the first touchdown.

determined only after lunar touchdown for any given spacecraft and will require continuous thermal data monitoring to arrive at the required real time decision. It may also be observed that the low temperature capability of the spacecraft subsystems at grazing solar angles, particularly the vernier propellant lines, makes it inadvisable to consider liftoff and translation maneuvers at elevation angles below about 15 degrees.

Thus, it may be concluded that for morning landings the spacecraft will be thermally constrained to perform liftoff and translation maneuvers only between solar elevation angles of 15 to 50 degrees. For evening landings, capability will similarly exist for solar angles from approximately 130 to 165 degrees, although the exact thermal constraints for landings occurring at angles less than 130°F have not been defined and will require further study.

IRU Warmup for Liftoff

In the existing design, the flight control electronics must be on at the coast phase power level to warm up the IRU gyros to some minimum temperature between 120 to 165°F before liftoff. (The actual minimum temperature required can be determined in laboratory tests in the near future.) Flight control electronics board 6 had an upper temperature limit of 190°F for the transit coast phase to the moon. This limit might be increased for the liftoff from the moon. However, the SC-1 data from the moon shows that it is not necessary to increase the maximum allowable temperature of flight control electronics board 6 above 190°F or reduce the gyro minimum allowable temperature below 165°F to have some liftoff capability.

Useful SC-1 temperature data is available for the time when the flight control system was operated on the moon to actuate the attitude jets to see if the lunar dust could be disturbed. At that time, the sun angle was 56 degrees above the lunar horizon, and the initial temperatures of flight control electronics board 6 and the pitch gyro were 164°F and 148°F, respectively. The temperature rise rate of flight control electronics board 6 was 30°F in 12.5 minutes or 150°F per hour (Figures 5.2-43 and 5.2-44). Therefore, the gyros can be warmed to 165°F without overheating flight control electronics board 6.

Another restriction on the flight control system is that the programmer (part of the flight control electronics) must be cooler than approximately 160°F. This means that the sun angle must be less than approximately 50 degrees above the lunar horizon for SC-1 orientation. The maximum allowable sun angle depends on the temperature rise rate of the programmer as well as its maximum allowable temperature. The temperature rise rate and maximum allowable temperature can be determined in laboratory tests.

The IRU gyros were 30 to 70°F colder than flight control electronics board 6 when the sun was 10 to 45 degrees from sunset. Therefore, in this orientation, flight control electronics board 6 would be heated to a temperature above its present coast phase upper limit of 190°F if the gyros had to be heated to their present lower limit of 165°F, assuming the heating was

continuous. It might be possible to warm up the gyros faster than the flight control electronics by turning the flight control system on and off several times. Data from tests in the vacuum chamber and from SC-1 on the moon shows that the gyros cool off at about one-fourth the rate of flight control electronics board 6. Therefore, turning the flight control system on and off several times should give a net result of heating the gyros at a faster rate than the electronics. This stepped heating technique could be used after a lunar night landing. Alternatively, changes to provide gyro preheat independent of the flight control electronics unit could be implemented. However, it probably will not be necessary to preheat the gyros if their performance is satisfactory at 120°F.

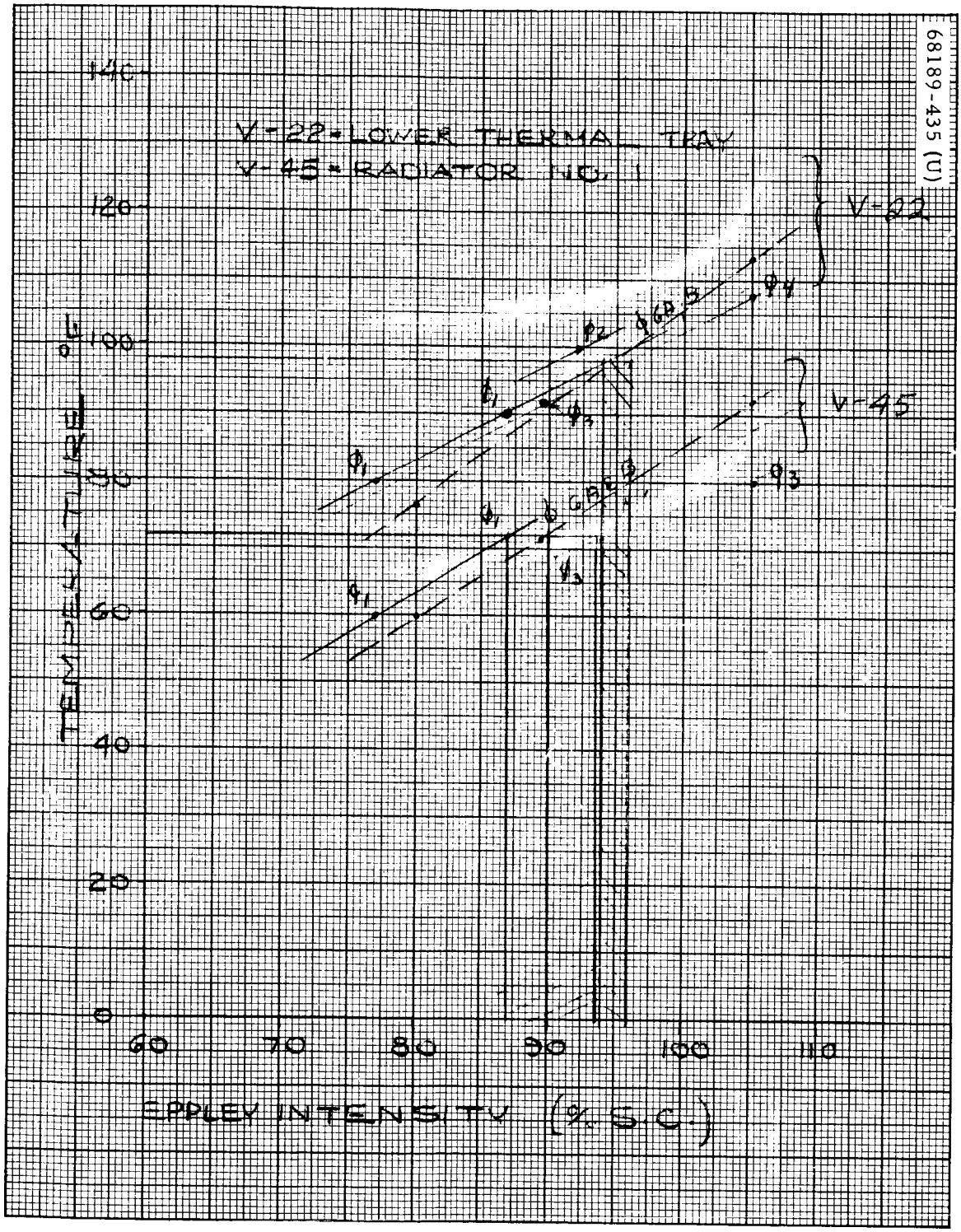
5.2.3.21 Calibration of STV Test Facility for Flight Conditions

Introduction

A study directed primarily toward the examination of problems related to spacecraft simulation applications was initiated. The desired results of this study are to provide the extremes of the solar intensity range for STV testing which will encompass all possible flight temperatures, and to determine, if possible, a chamber intensity equivalent to one solar constant in space.

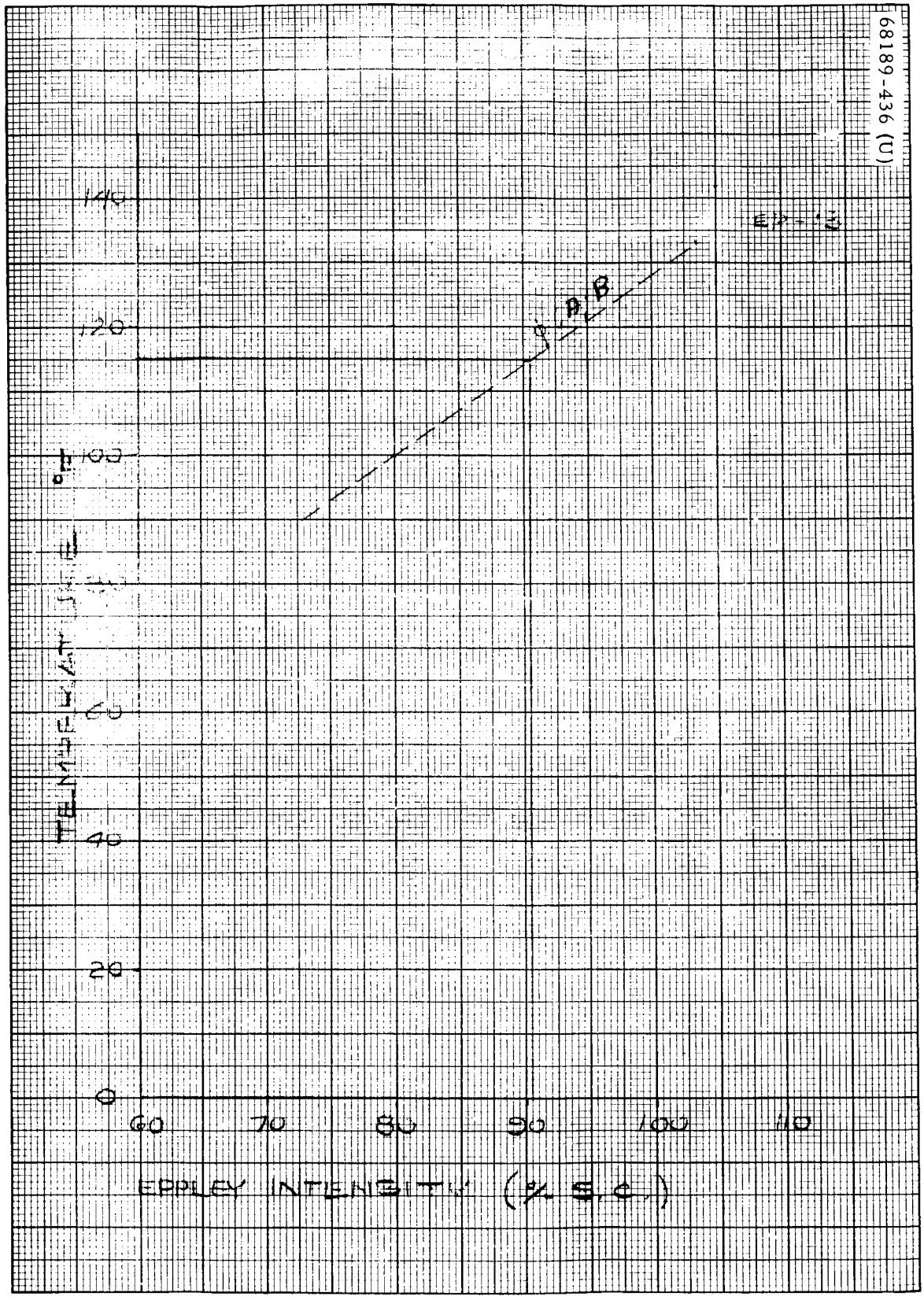
Figure 5.2-51 shows spacecraft temperatures versus the average integrated solar intensity at the test plane as indicated by Eppley radiometer No. 7120. SC-1 transit flight temperatures are superimposed to determine the equivalent test intensity corresponding to the measured temperature in flight. It is necessary to be mindful of the fact that the solar intensity during the SC-1 transit was 97.3 percent of a solar constant due to the seasonal variation.

Time does not permit inclusion of the details of the study here, but the conclusions are presented. A nominal solar intensity that will subject all spacecraft units to their flight environment simultaneously does not exist. The test intensity corresponding to flight temperatures varies for each of the spacecraft sensors. Furthermore, this intensity changes as the properties of the thermal coatings become degraded from prolonged exposure to ultraviolet irradiation. Adjusting for the seasonal variation, the nominal test intensity correspondence for nondegraded thermal surfaces varied from 87 to 97 percent of a solar constant for the 20 temperature sensors included in this study. The average value for this range was 91-1/2 percent of a solar constant (see Table 5.2-14). Testing of SC-1 at intensities of 80 and 100 percent of a solar constant would have included all values of temperatures measured in flight. However, selecting these intensities at which to test does not allow those units whose intensity correspondence determines the extremes to function in an environment in excess of their flight temperatures. Compartment B thermal trays set the upper bound of the 80 to 100 percent solar constant range. In view of the importance of the power and signal processing systems housed in this compartment, it was felt that the existing 105 percent solar constant should be retained for STV testing to preserve the concept of margin



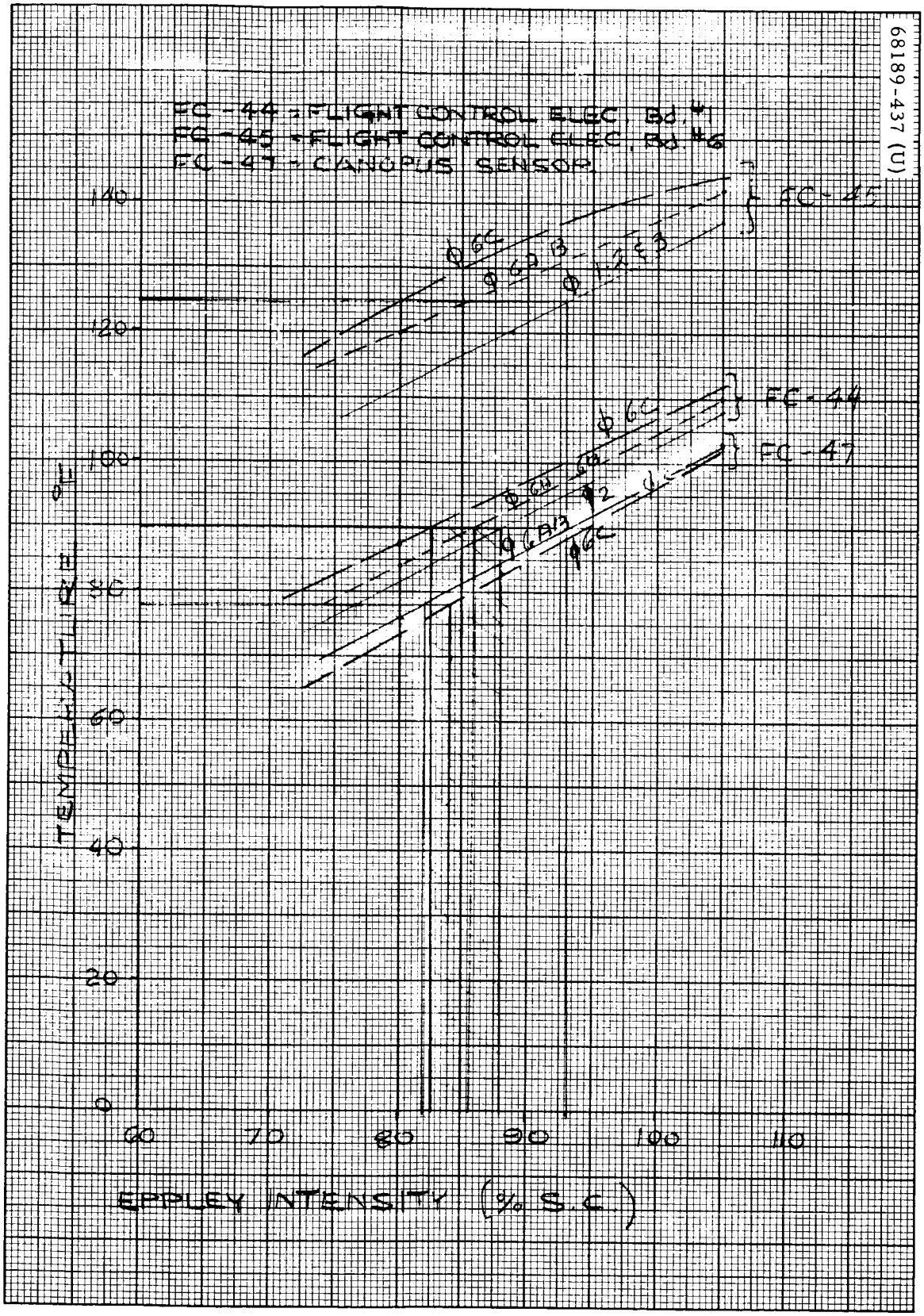
a) Compartment B

Figure 5.2-51. Temperature Versus Eppley Solar Intensity



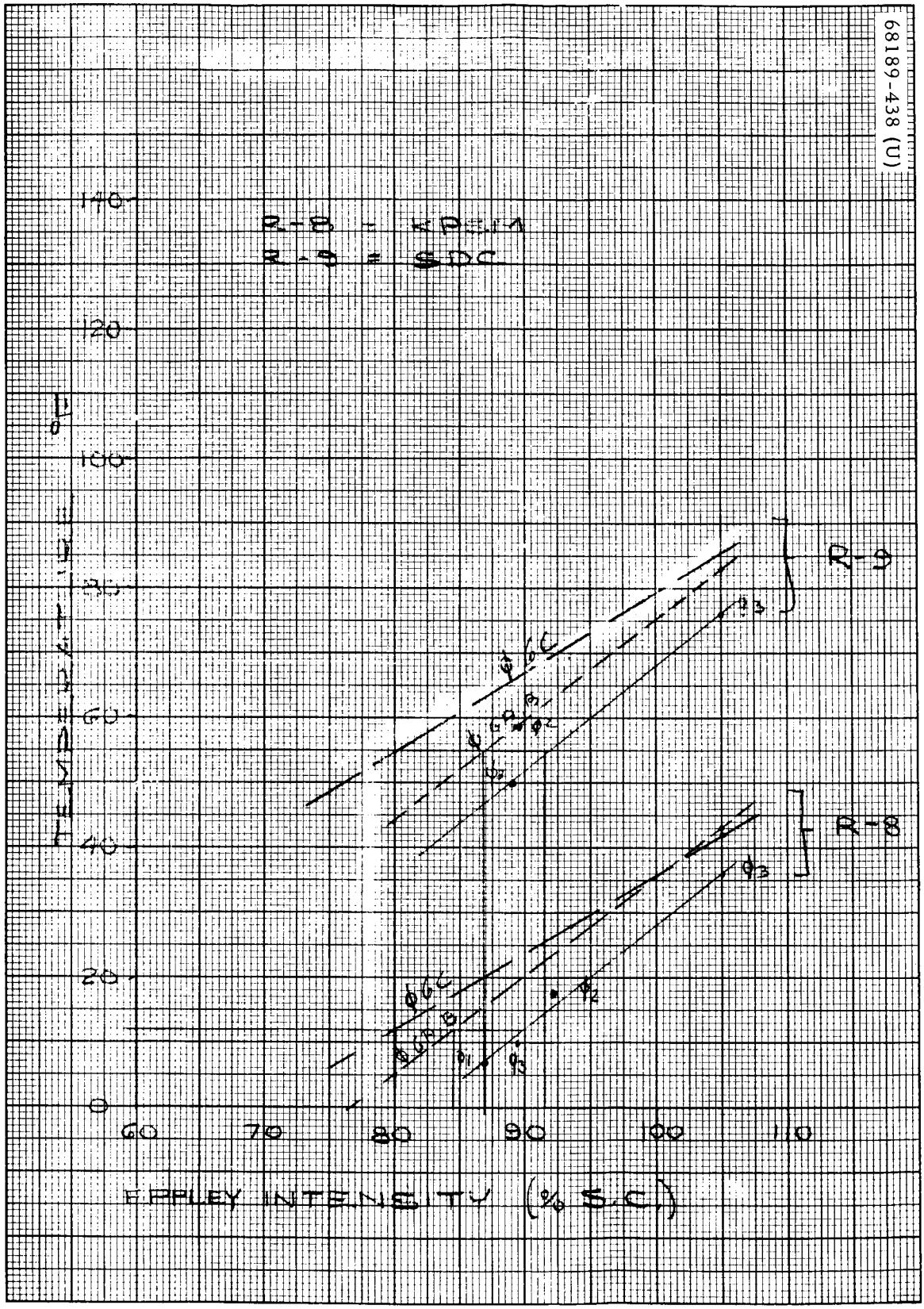
b) Boost Regulator

Figure 5.2-51 (continued). Temperature Versus Eppley Solar Intensity



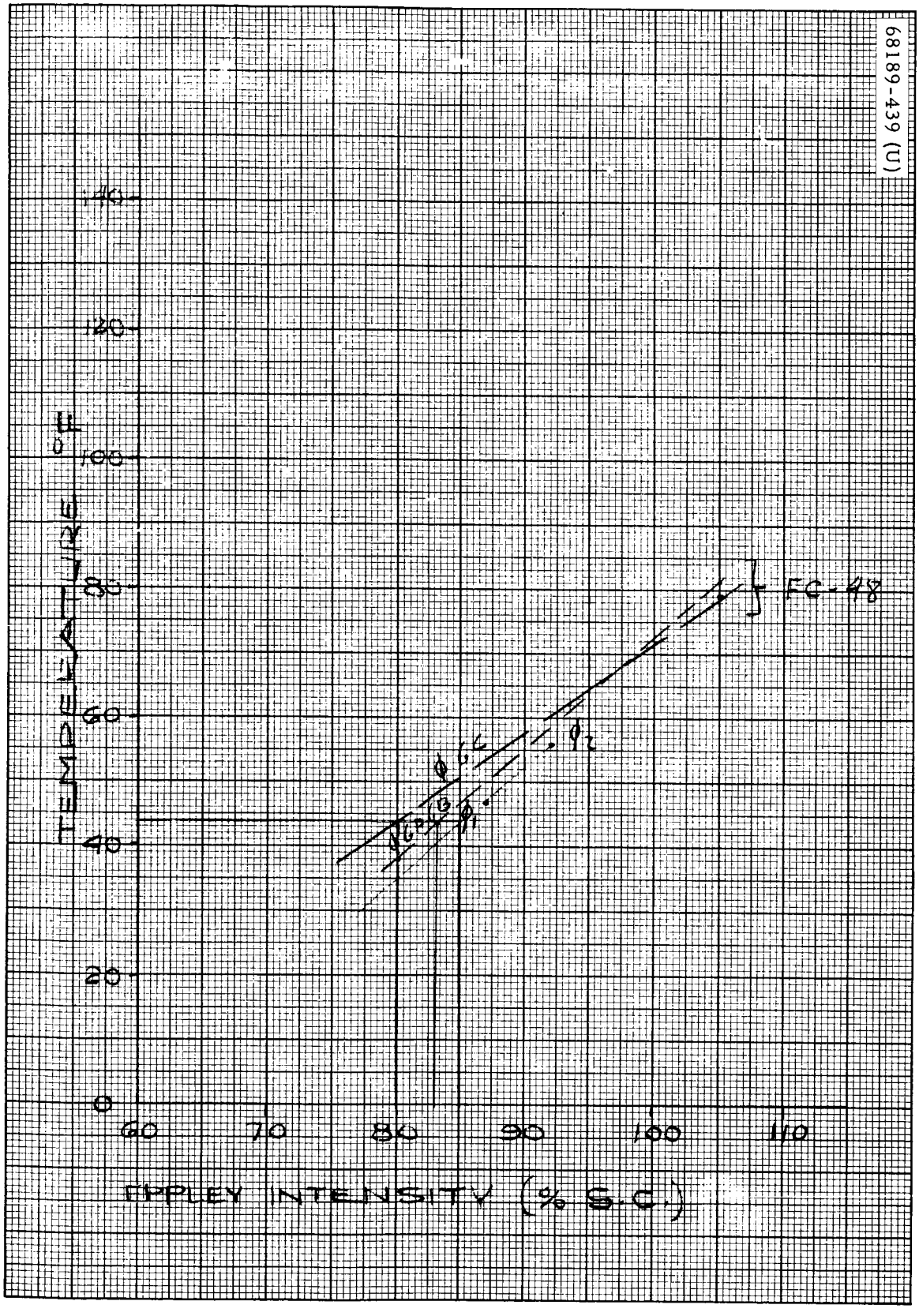
c) Flight Control Sensor Group

Figure 5.2-51 (continued). Temperature Versus Eppley Solar Intensity



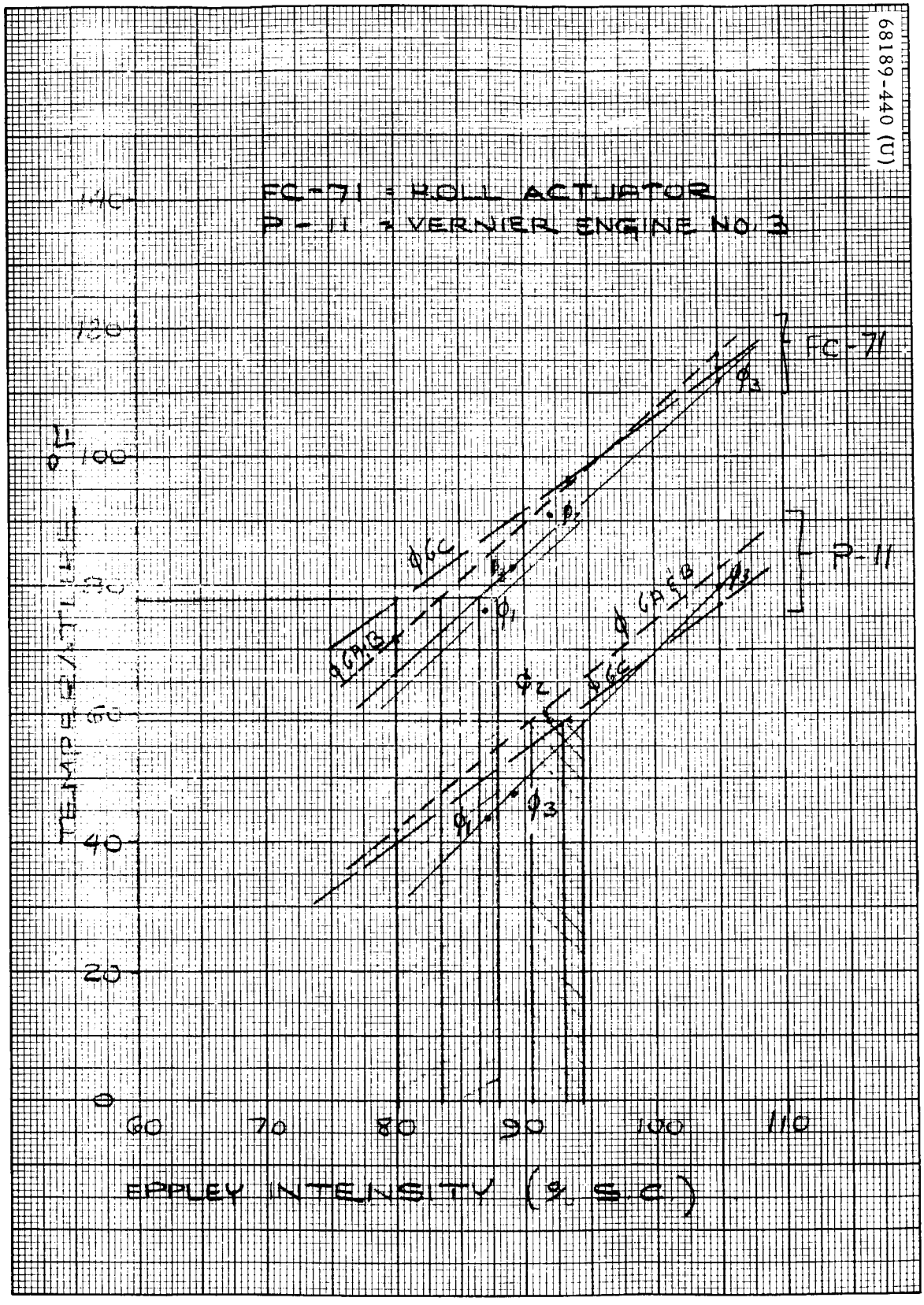
d) RADVS

Figure 5.2-51 (continued). Temperature Versus Eppley Solar Intensity



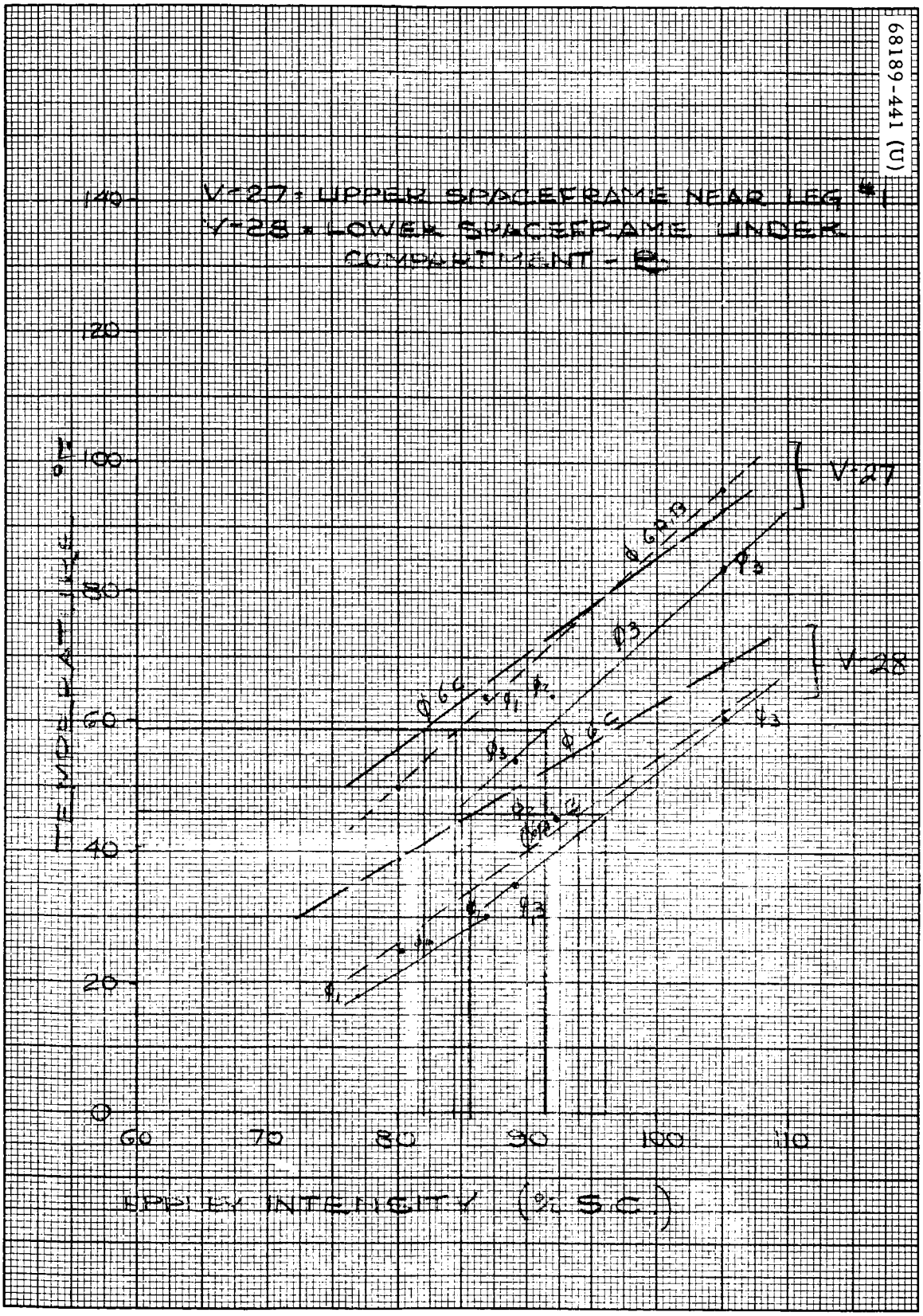
e) Nitrogen Tank

Figure 5.2-51 (continued). Temperature Versus Eppley Solar Intensity



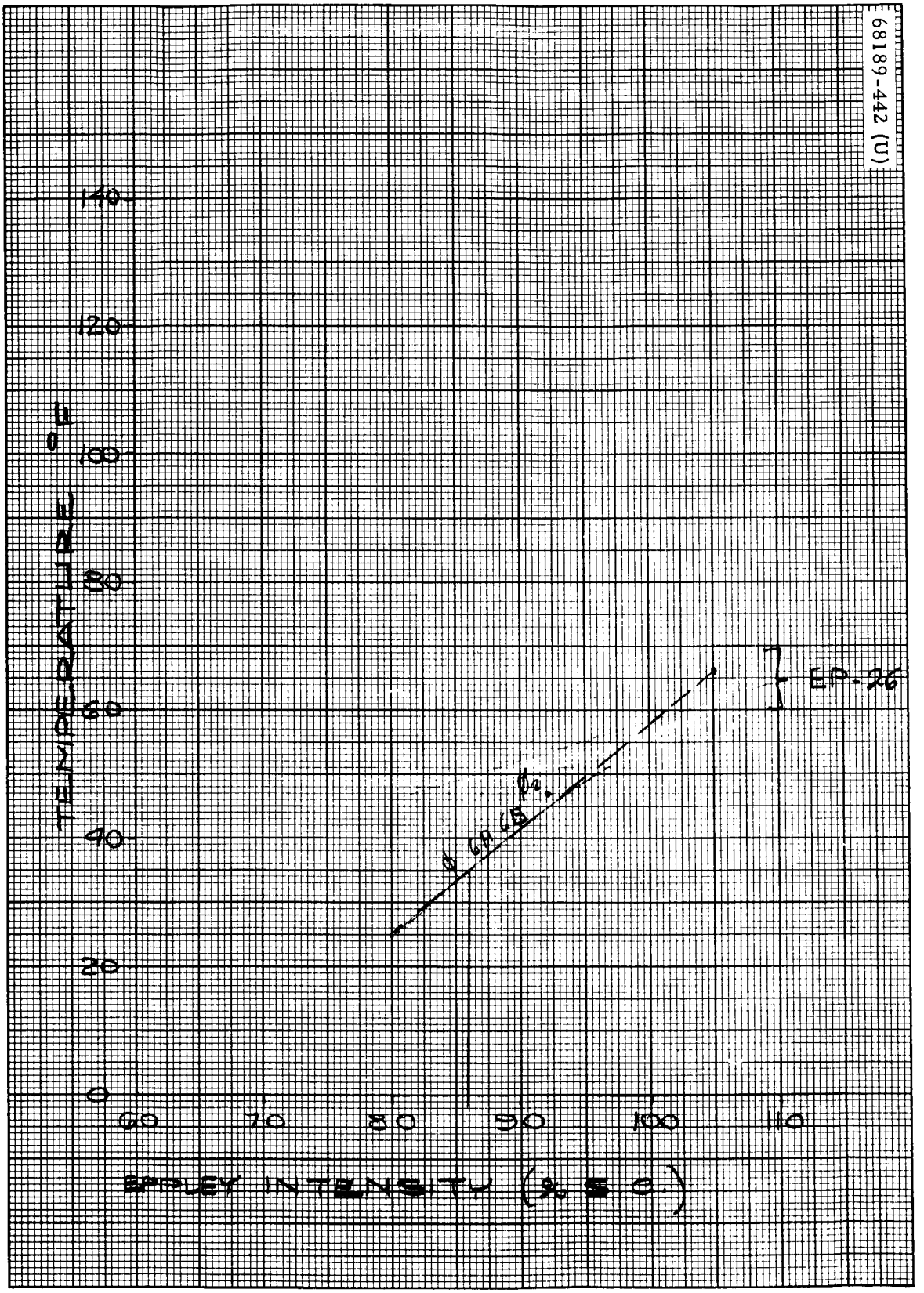
f) Propulsion

Figure 5.2-51 (continued). Temperature Versus Eppley Solar Intensity



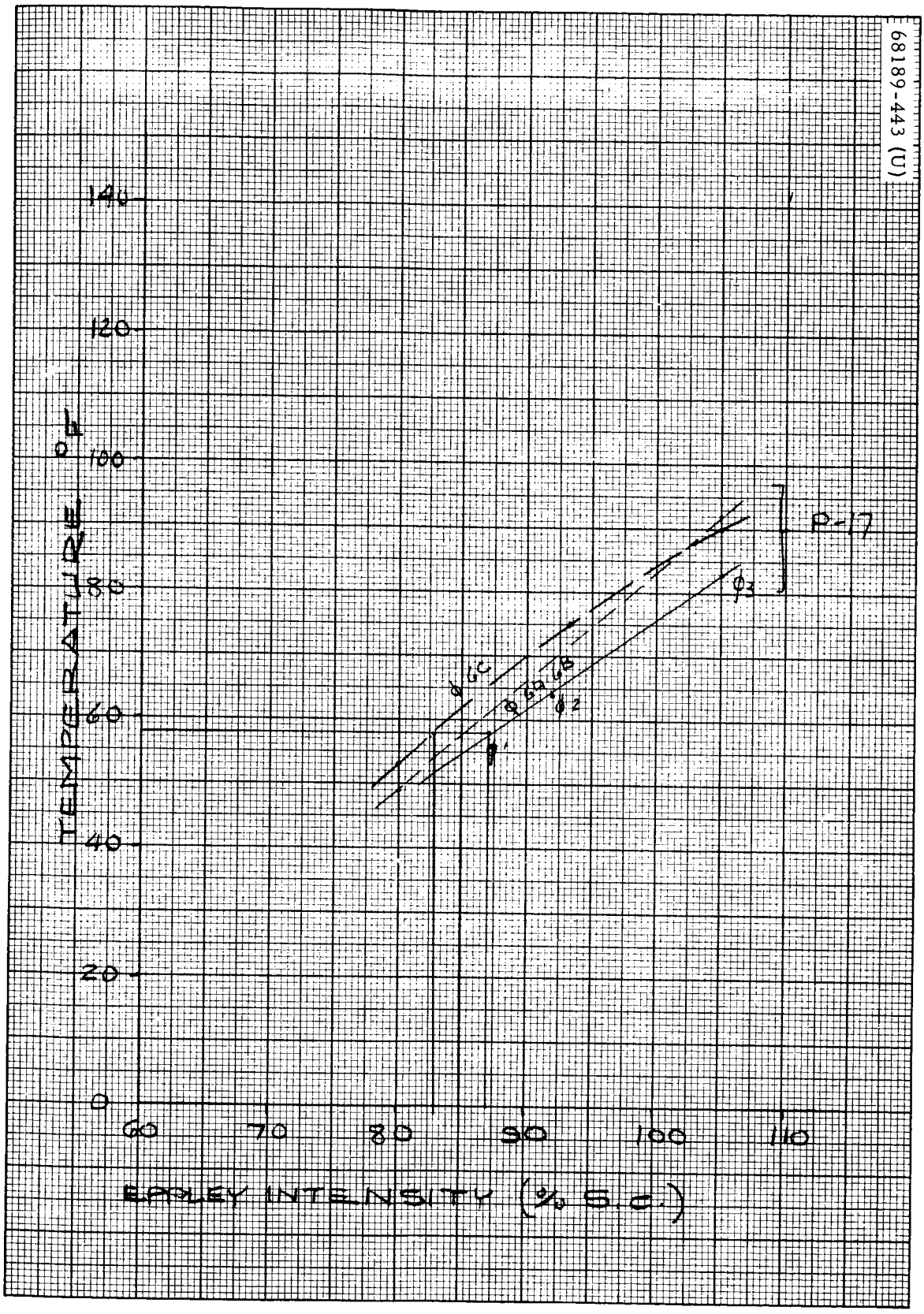
g) Spaceframe

Figure 5.2-51 (continued). Temperature Versus Eppley Solar Intensity



h) Auxiliary Battery

Figure 5.2-51 (continued). Temperature Versus Eppley Solar Intensity



i) Helium Tank

Figure 5.2-51 (continued). Temperature Versus Eppley Solar Intensity

TABLE 5.2-14. FLIGHT TO STV PHASE INTENSITY CORRESPONDENCE

	Phase 1	Phase 2	Phase 3	Phases 6A and 6B	Phase 6C	Range
Flight control						
FC-44	Bad data	87.5	—	85	82	82-87.5
FC-45		93		84.5	79.5	79.5-93
FC-47	Bad data	85	Bad data	82	Bad data	82-85
Miscellaneous						
EP-26	Bad data	86	—	86		86
FC-48		85	—	83	80	80-85
P-17	—	87.5	—	85	83	83-87.5
RADVS						
R-8	—	90	—	84	80	80-90
R-9	Bad data	87	92	87	80	80-92
R-10	—	93	Bad data	93	81	81-93
R-13				90.5	82	82-90.5
Spaceframe						
V-27	85.5	88.5	91.5	84.5	82	82-91.5
V-28	Bad data	93.5	Bad data	94	85.5	85.5-94
V-37	—	90.5	—	90	83	83-90.5
V-39	—	94	—	93	89	89-94
Compartment B						
V-21	90	—	—	94.5	—	90-94.5
V-22	90.5	—	—	94.5	—	90.5-94.5
V-45	—	87	—	90	Not steady state	87-90
V-46	90	Bad data	90	90	90	90
EP-13	—	—	—	90.5	—	90.5
Propulsion						
FC-71	Bad data	84	80.5	84	80	80-84
P-7	—	—	89	Bad data	87.5	87.5-89
P-10	—	86	86	86	90.5	86-90.5
P-11	94	92.5	94	90.5	92.5	90.5-94

testing for these systems. No change to the solar intensity values used for the STV test phase is recommended at this time.

5.2.4 ANOMALY/DISCREPANCY DESCRIPTION

The anomalies and/or discrepancies in the thermal performance given below were observed during Mission A. Only item 1, the cold auxiliary battery design, and item 5, the closed thermal switches during lunar night, were considered serious enough to require nonstandard action during the mission. The remaining discrepancies are of an academic nature and are recorded to reflect an understanding of them resulting from postflight evaluation. The auxiliary battery thermal design has been modified to provide the desired transit storage temperatures for Mission B. Unit level testing has indicated that electronics can be exposed to colder temperatures than were allowed in Mission A in the event that thermal switches might stick closed during lunar night.

The anomalies are as follows:

1) The auxiliary battery was predicted to cool to a steady-state unenergized temperature of 60° F. The flight data indicated a steady-state temperature of 35° F. Nonstandard operation of the auxiliary battery was required to increase the internal heat generation to warm the battery to the desired level for terminal descent. Review of the SC-1 STV data under the lower solar intensity shows a steady-state battery temperature of 25° F. It is therefore apparent that the thermal performance of the auxiliary battery is also indicative of a nominal solar intensity of less than that simulated in test. The paint pattern on the SC-2 battery has been modified to give a steady-state coast mode temperature of 60 ± 15° F.

2) The elevation axis of the A/SPP was 1°F in flight compared to a prediction of -86°F. The flight temperatures, in addition to being more desirable from an operational standpoint, are more indicative of the temperatures experienced during STV test. The data indicated deficiencies in the analytical model. Upgrading of the model has taken place, and the flight temperature has been reproduced analytically.

3) The nitrogen tank was predicted to run 26°F higher than the flight temperature indicated. The predictions were based on the data obtained during STV testing; however, before launch the tank finishes were refurbished to return them to their original thermal properties (i.e., the 400 hours of STV testing had significantly degraded the white paint).

4) The main retro nozzle was predicted to run at -222°F. Flight data indicated a steady-state temperature of -124°F. While the flight data shows a large variation from prediction, the effect is

inconsequential. The nozzle had no effect on the thermal control of the propellant, and the sensor is used to monitor temperatures during vernier engine firing when the exhaust impinges on the nozzle. Based on flight experience, the analytical thermal model has been updated, and accurate predictions can be made for future missions.

5) With the onset of lunar night, anomalous thermal switch performance was observed. One compartment A switch did not open until the thermal tray was 40°F below the designed opening temperature. Calculations indicate that four of the compartment B switches had not opened when the compartment was 60°F below the designed opening temperature. The last data before shutdown of the spacecraft for lunar night (approximately 50 hours into the night) indicated all compartment A switches open and possibly three compartment B switches still closed. Second lunar day temperature data indicates that all switches eventually opened; however, the conclusion is based on analysis and is therefore subject to verification.

6) Television inspection of the spacecraft during the second lunar day showed that one quadrant of a thermal switch radiator on compartment A was shattered. (There are 36 quadrants on compartment A and 24 on B.) The glass was apparently broken during the extremely low temperatures (-300°F) experienced during the lunar night. However, the damaged radiator had no noticeable effect on the compartment's performance.

5.2.5 CONCLUSIONS AND RECOMMENDATIONS

Spacecraft thermal performance throughout the transit and lunar phases of the mission was excellent. The anomalies of a lower than desired auxiliary battery temperature in transit prior to operation and compartment B thermal switches failing to open prior to spacecraft shutdown during the lunar night had only a minor effect on the mission. The SC-2 auxiliary battery thermal design has been modified to provide a temperature of 60°F during the nonoperating part of transit phase. The latter anomaly did prevent the obtaining of lunar night heat loss data, which is valuable engineering information for compartments A and B.

The thermal environment of compartments A and B is 25 percent less severe (i.e., externally absorbed energy is 25 percent less) than had been anticipated in preflight analysis. The convective heat flux on the retro nozzle, crushable block shields, and AMR antenna due to vernier exhaust impingement is higher than predicted but within design limits. Response of TCA 2 to gyro drift maneuvers was as predicted. Unlimited use of the television camera on the lunar surface was possible from a thermal standpoint for most of the lunar day even without shadowing. A comparison of flight data with that of STV testing indicates that the solar intensity levels employed for margin testing are valid and do not require modification. Determination of lunar surface emission using spacecraft temperature data agrees well with

earth-based measurements. A liftoff and translation maneuver on the lunar surface is possible without exceeding temperature limits if performed between sun elevation angles of 15 to 50 degrees when the spacecraft is on or near to the lunar equator.

Based on the experience of the SC-1 mission and this report, the following is recommended. Postmission data reduction should be accomplished more rapidly to facilitate the writing of the report. Power dissipation data reduction for compartments A and B should be more timely. For Mission A, this data was made available too late to be used in the thermal evaluation. An economical way of reducing the lunar phase telemetry should be developed. Much of the potential engineering information is lost because the data is too extensive for detailed hand plotting. The transit phase plots should be extended to include the 12-hour period subsequent to touchdown. This initial response of spacecraft temperature to the lunar environment is of great value. The main retro engine and AMR temperature plots should be terminated just short of retro ignition. These parameters go to full scale, and the resulting machine plots have poor resolution. The transit temperature plots should include the 3-hour period prior to launch. The data during this period is required to determine exact response of spacecraft temperatures to Centaur air conditioning temperature changeover from 70 to 85°F. In Mission A, a troublesome air conditioning temperature overshoot was observed which requires additional study. A detailed log of A/SPP positioning should be kept in real time to facilitate the generation of shadow plots. A polaroid picture and a standard black and white picture should be taken of each panel configuration during lunar operation using the 1/6 scale model in spacecraft performance/analysis/command. The camera angle should be consistent with the sun angle so that additional monitoring of shadow patterns is provided.

5.2.6 REFERENCES

1. R. Welsh, "Maximum Temperature of the RMD Vernier Engines in the Lunar Surface: A-21 Surveyor Spacecraft," IDC 2222.6/54, 20 September 1965.

2. J. Lewis and R. J. McGrath to P. F. Taylor and F. Wolf, "Definition of Surveyor A-21 Television Camera's Thermal Environment," IDC 2222.2/241, 13 April 1965.

3. F. J. Wolf to R. L. Quandt, "Statement of Work for Thermal Analysis of the Survey and Approach TV Cameras," IDC 2256.4/74, 27 May 1964.

4. H. E. Knudsen to R. L. Quandt, "Surveyor Model A-21 Television System Thermal Environmental Definition," IDC 2222.2/52, 20 August 1964.

5. F. Charles and P. F. Taylor to R. L. Quandt, L. R. Shrum, and E. E. St. John, "Progress Report on the Thermal Study of the Surveyor Television Cameras," IDC 2710.2/37, 24 March 1965.

6. F. Charles and P. F. Taylor to R. L. Quandt and F. J. Wolf, "Survey Camera No. 3, Lunar Day Thermal Analysis," IDC 2710.2/51, 13 September 1965.

7. F. Charles and P. F. Taylor to R. L. Quandt, L. R. Shrum, and E. E. St. John, "Surveyor TV Camera No. 3, Preliminary Data on the Effects of Increased Solar Absorptance by the Camera in the Lunar Day Environment," IDC 2710.2/40, 30 April 1965.

8. F. Charles and P. F. Taylor to R. L. Quandt, L. R. Shrum, and E. E. St. John, "Capability of Camera No. 3 Heaters Close to Terminator, SC-1 Mission," IDC 2710.2/45, 27 May 1965.

9. F. Charles and P. F. Taylor to R. L. Quandt, "Thermal Design of the Star Mode and Filter Wheel Chassis," IDC 2710.2/52, 16 September 1965.

10. F. Charles and P. F. Taylor to R. L. Quandt, "Surveyor Televsion Camera No. 3 Cryogenic Survival of the Vidicon Tube," IDC 2711.10/148, 21 September 1965.

11. P. F. Taylor to R. L. Quandt, "Thermal Considerations in the Design of the Mirror Assembly," IDC 2710.2/54, 27 September 1965.

12. F. Charles and P. F. Taylor to R. L. Quandt and F. J. Wolf, "Surveyor TV Camera No. 3, Temperature-Time Profile Following Lunar Landing," IDC 2721/34, 4 November 1965.

13. P. F. Taylor to R. L. Quandt and F. J. Wolf, "Surveyor TV Camera No. 3, Independent Control of the Mirror Baseplate Heater Power," IDC 2721/51, 16 March 1966.

14. P. F. Taylor to F. J. Wolf, "Surveyor SC-1 Mission, Thermal Control of Camera No. 3," IDC 2721/58, 5 May 1966.

15. F. Charles and P. F. Taylor to R. L. Quandt and E. E. St. John, "Surveyor Television Cameras, Comparison of Preliminary T-21 STV Test Temperature Data with Theoretical Predictions – Phase II," IDC 2711.10/96, 9 March 1965.

16. T. A. Harvey, Jr. to R. R. Garipay, "A Study of Lunar Surface Temperatures in a Shadow," IDC 2221.19/34, 5 July 1966.

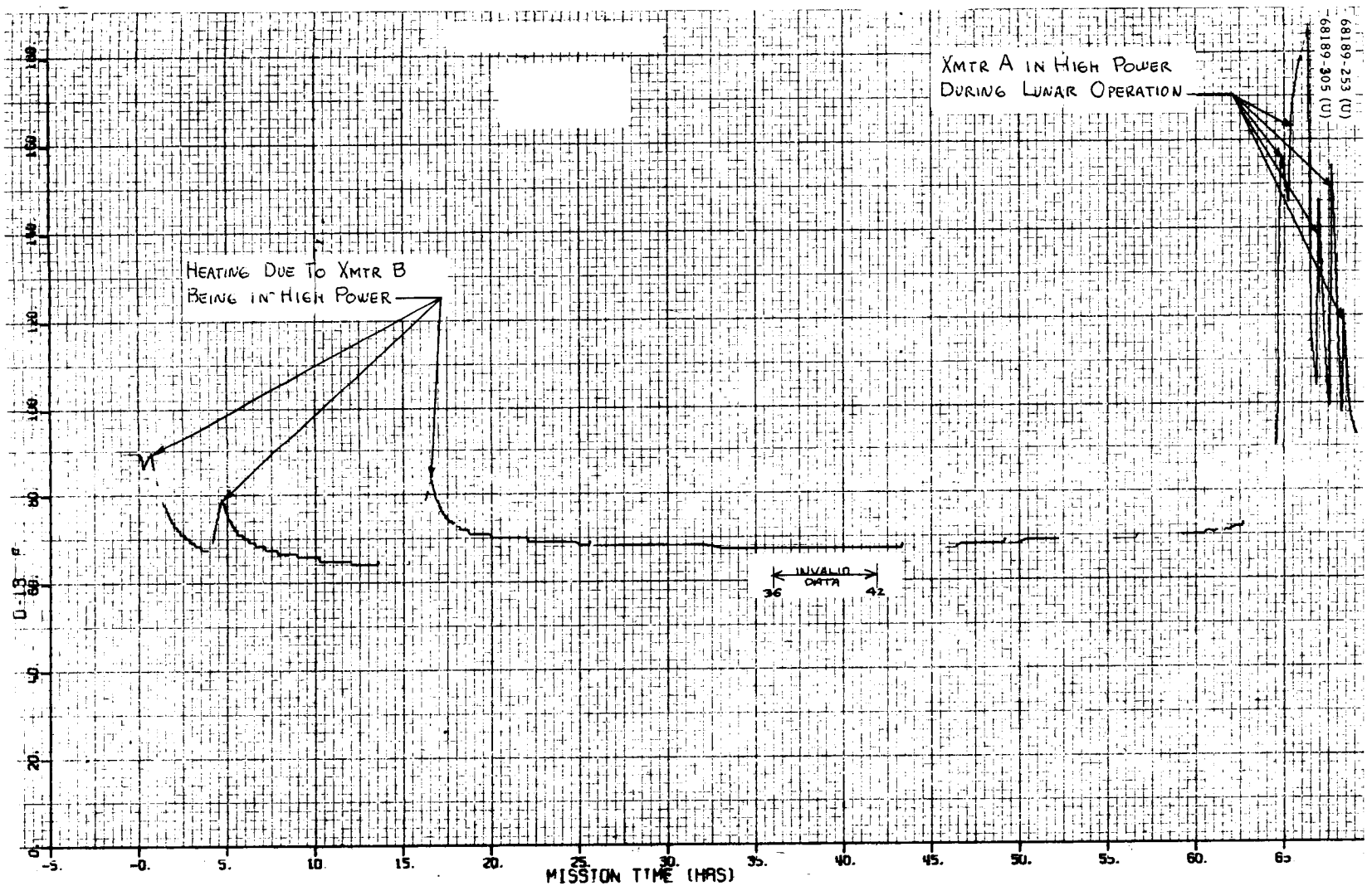
5.2.7 ACKNOWLEDGEMENTS

The SC-1 postflight thermal performance report was prepared by the Hughes Aircraft Company Surveyor Thermal Control Section with the exception of the television system thermal analysis which was prepared by the Surveyor Electronics Department. The graphs of lunar phase temperature data given

in Appendix B were prepared by the JPL Surveyor Thermal Control Section. The efforts of the following individuals are greatly appreciated for their respective contributions to this report:

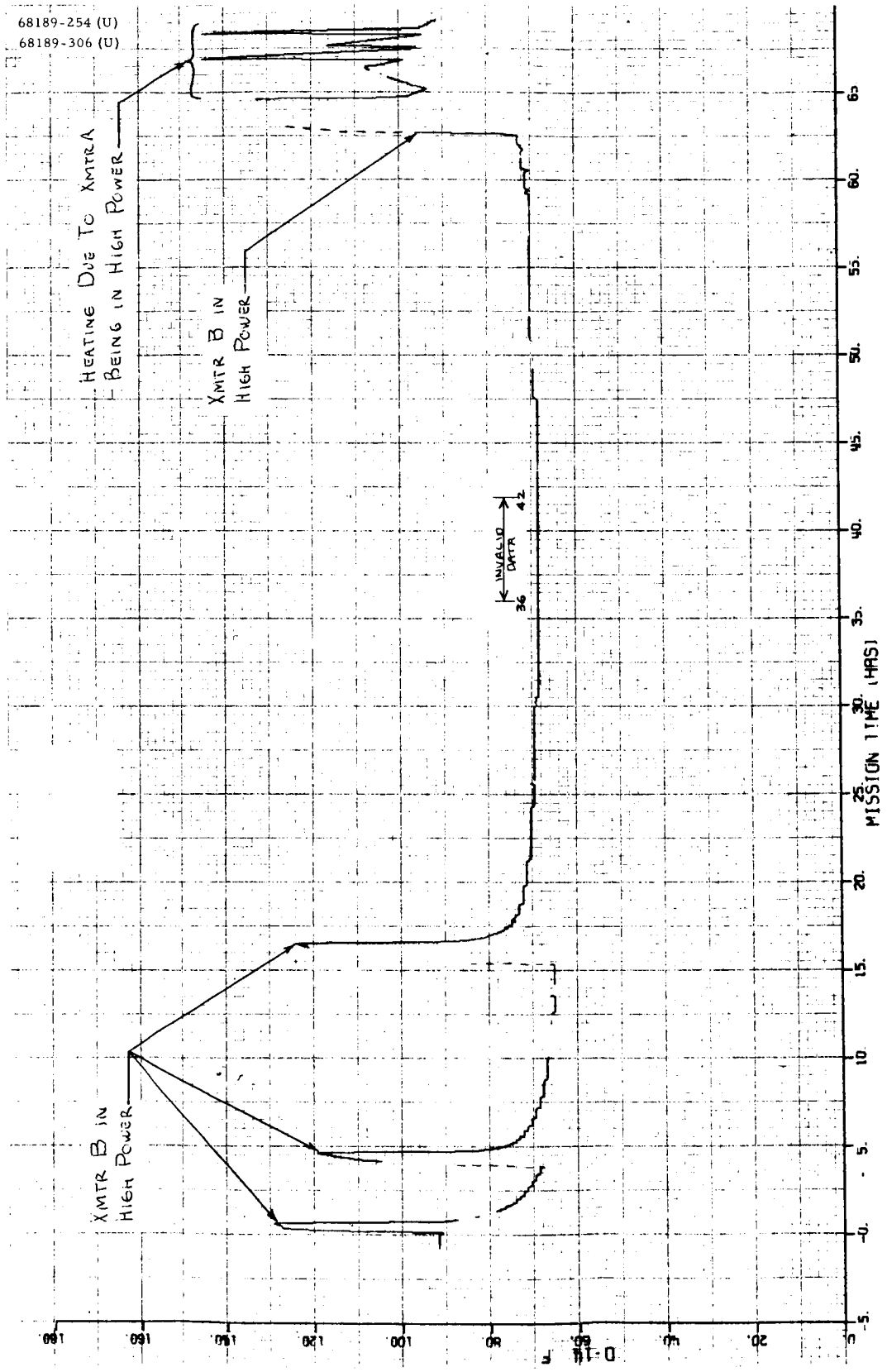
J. Duckworth	—	A/SPP, solar panel, planar array
K. Eng	—	Lunar surface emission
A. Friedman	—	Propellant tanks, legs, shock absorbers, gas jet
M. Goldstein	—	AMR
J. Goodblatt	—	Spareframe and sequence of events
T. Harvey	—	RADVS
H. Knudson	—	Compartments A and B
L. Krajewski	—	Main retro engine
J. Lebental	—	Solar simulator evaluation
J. Lewis	—	Vernier engines, vernier lines, helium tank
P. Taylor	—	Television system
J. Tuchscher	—	Technical coordinator
R. Welsh	—	Flight control sensor group, nitrogen tank crushable block, roll actuator, liftoff and translation
W. Williams	—	Auxiliary battery
M. Vickers (JPL Thermal Control)	—	Lunar phase temperatures graphs

APPENDIX A



a) Transmitter A

Figure A-1. Transmitter Traveling-Wave Tubes



b) Transmitter B

Figure A-1 (continued). Transmitter Traveling-Wave Tubes

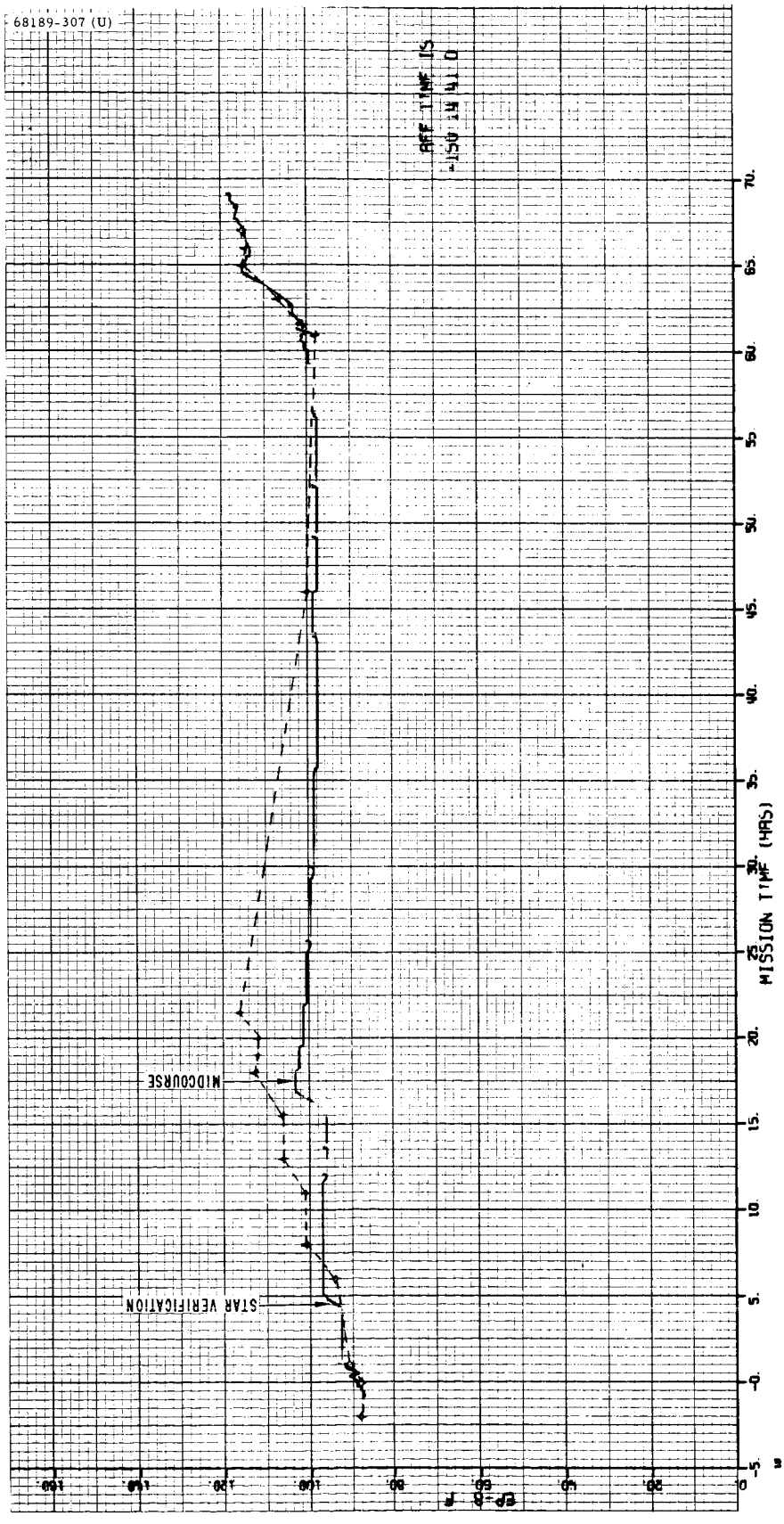


Figure A-2. Main Battery

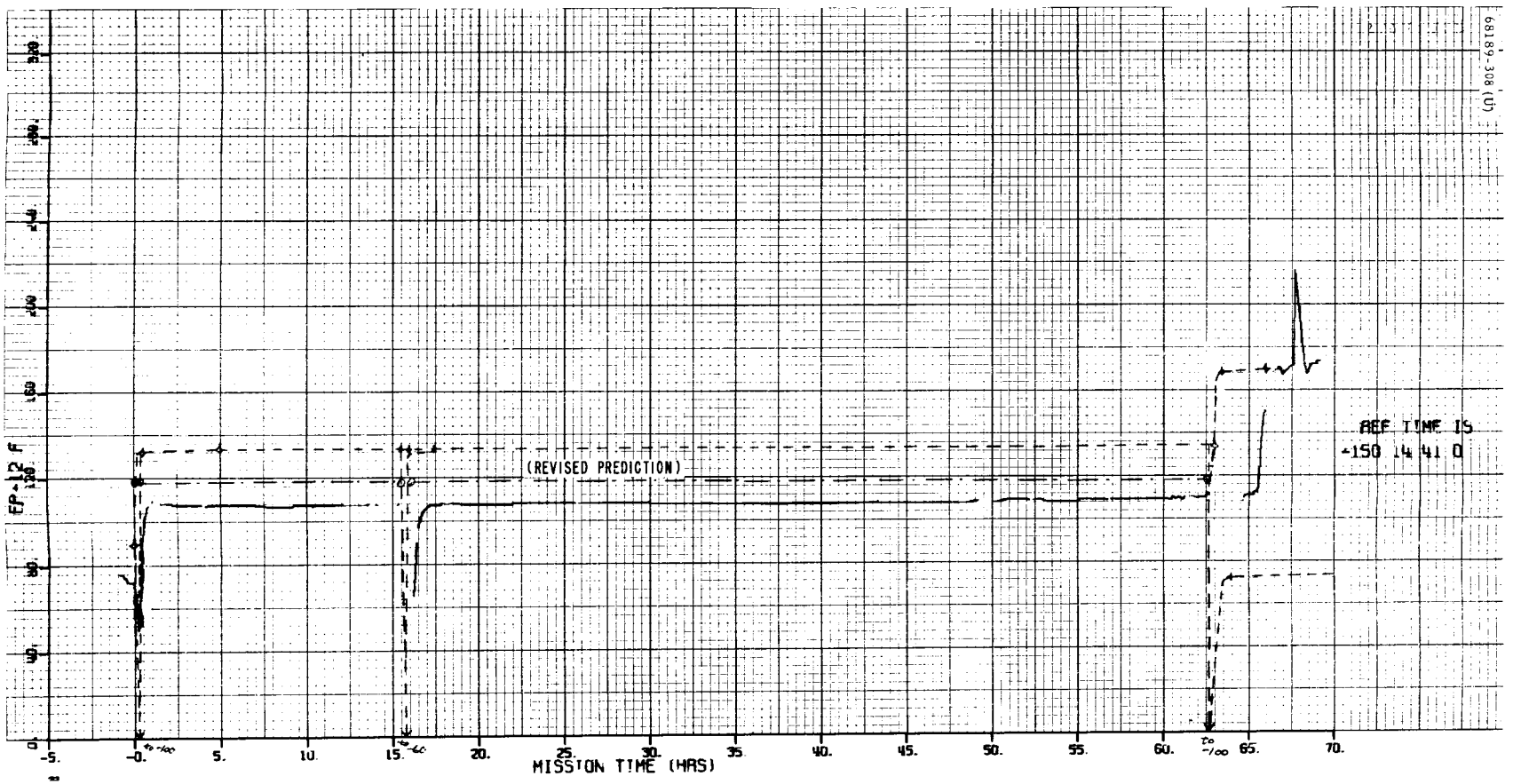


Figure A-3. Solar Cell Array

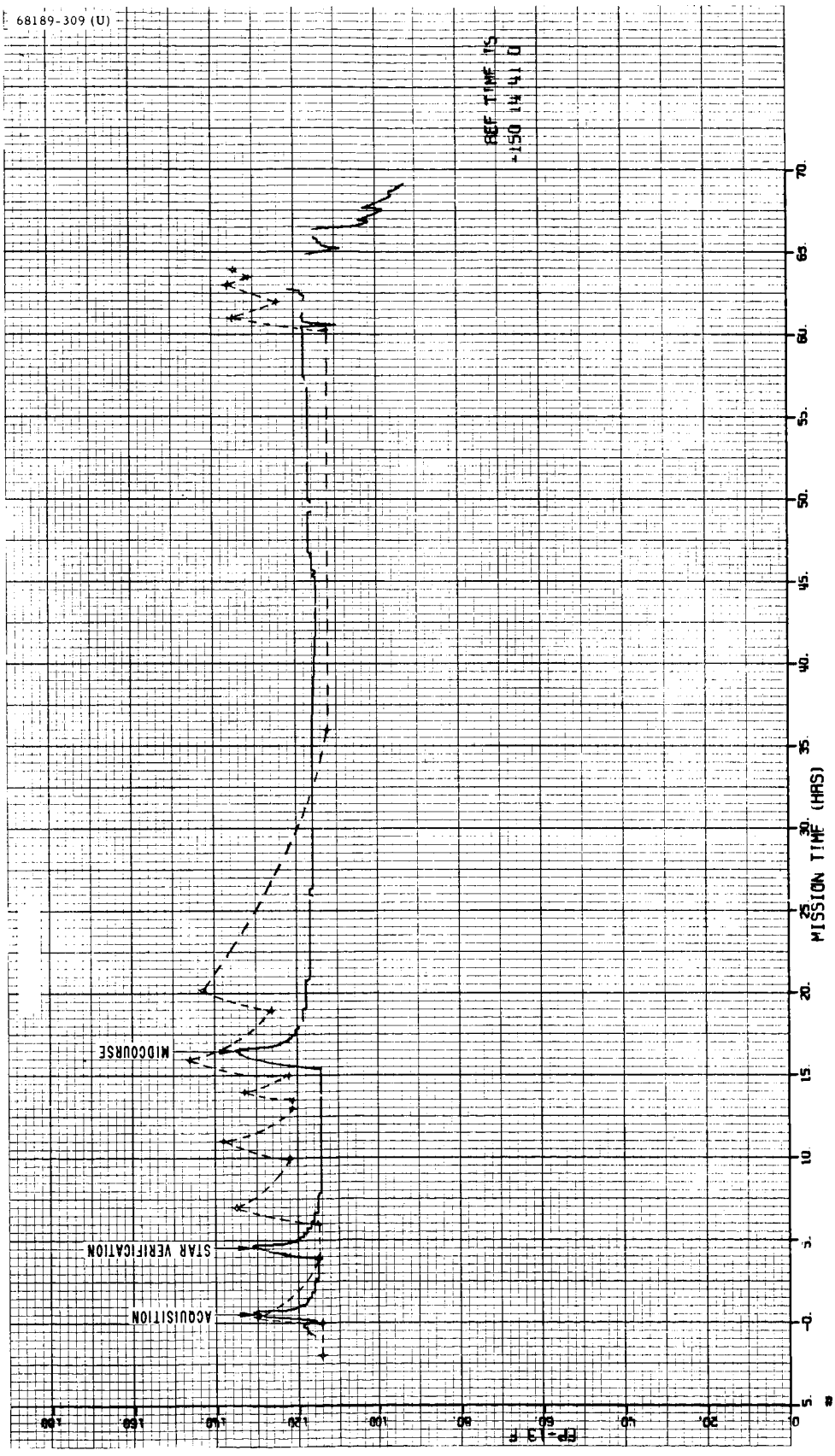


Figure A-4. Boost Regulator

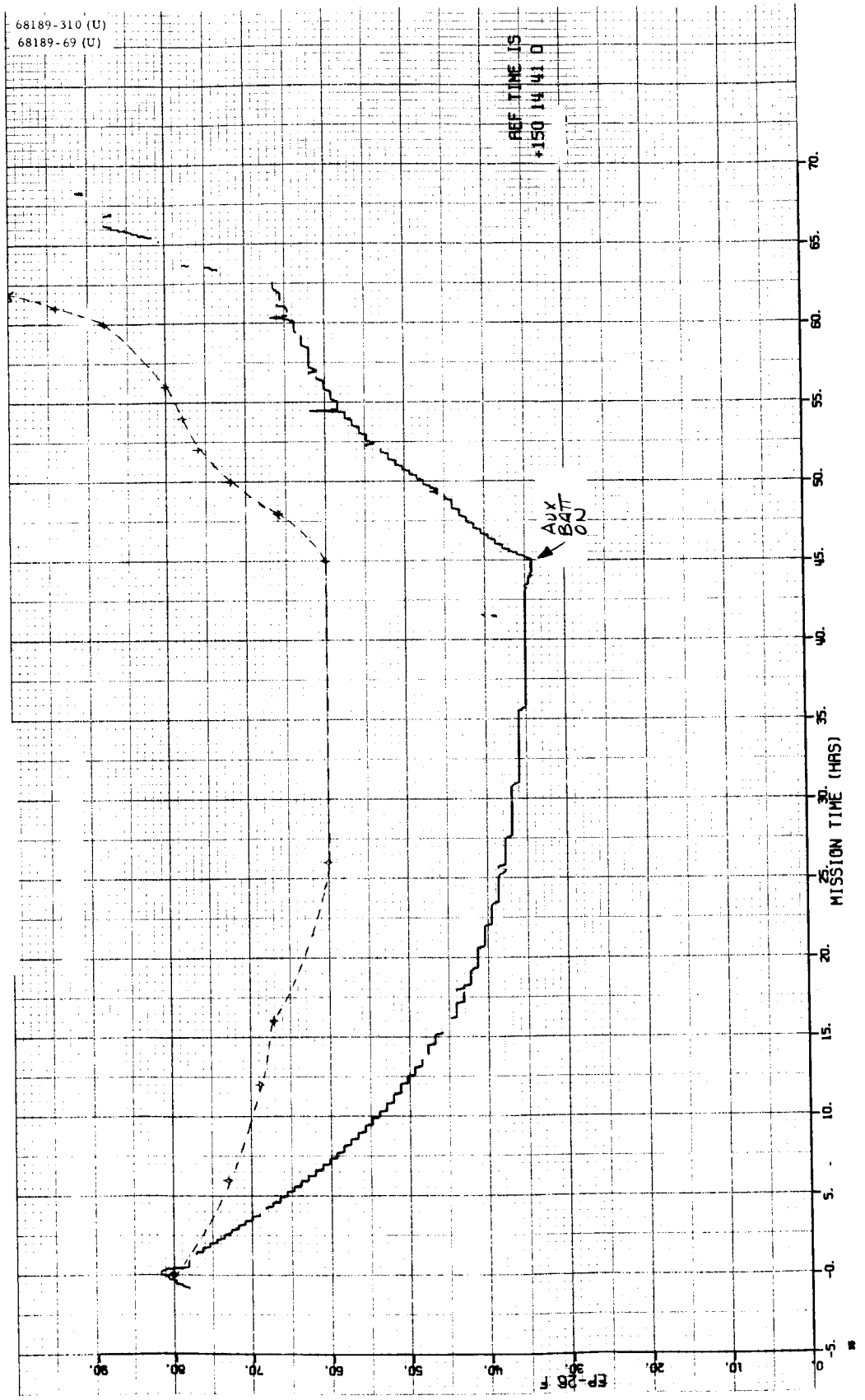


Figure A-5. Auxiliary Battery

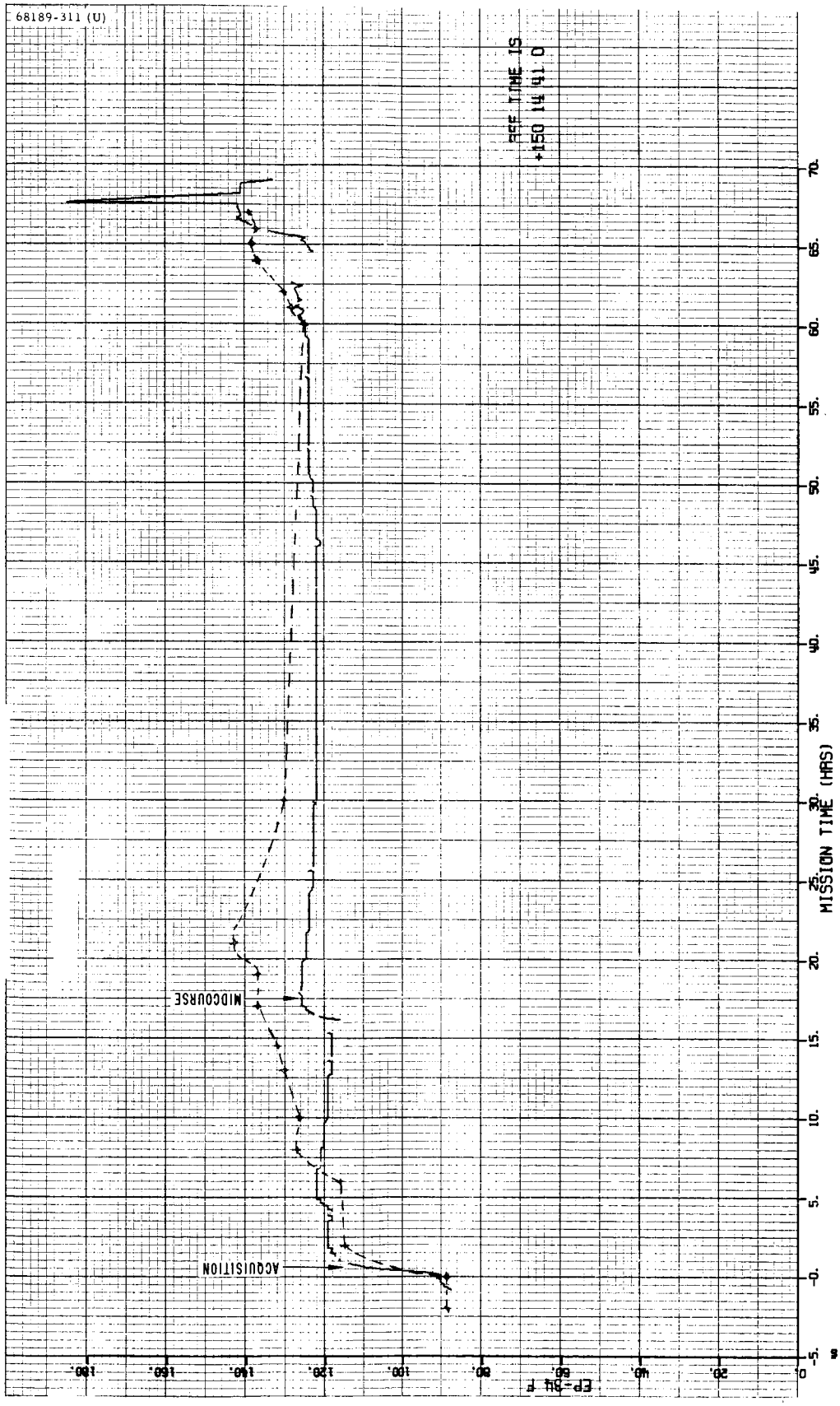


Figure A-6. Battery Charge Regulator

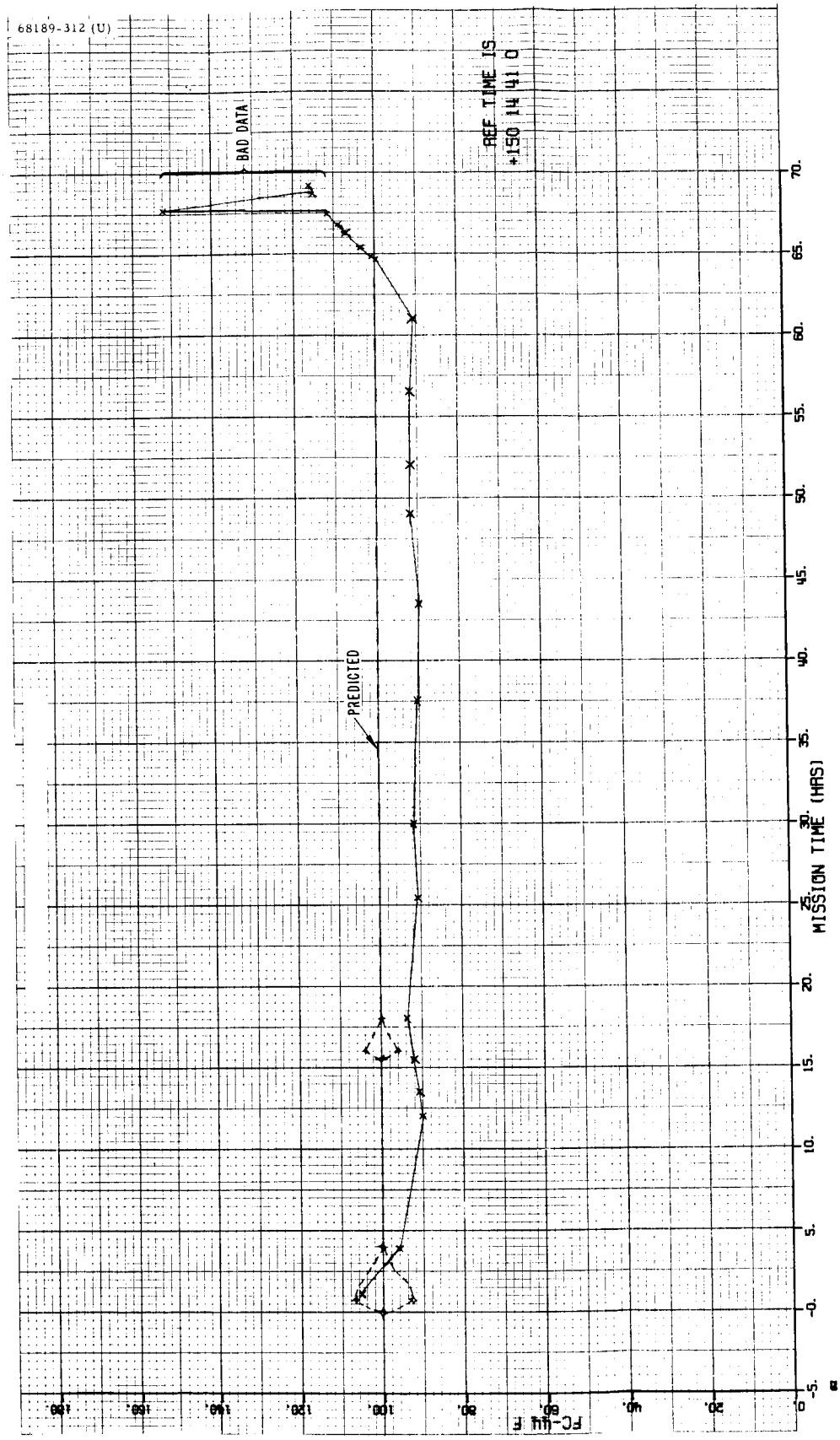
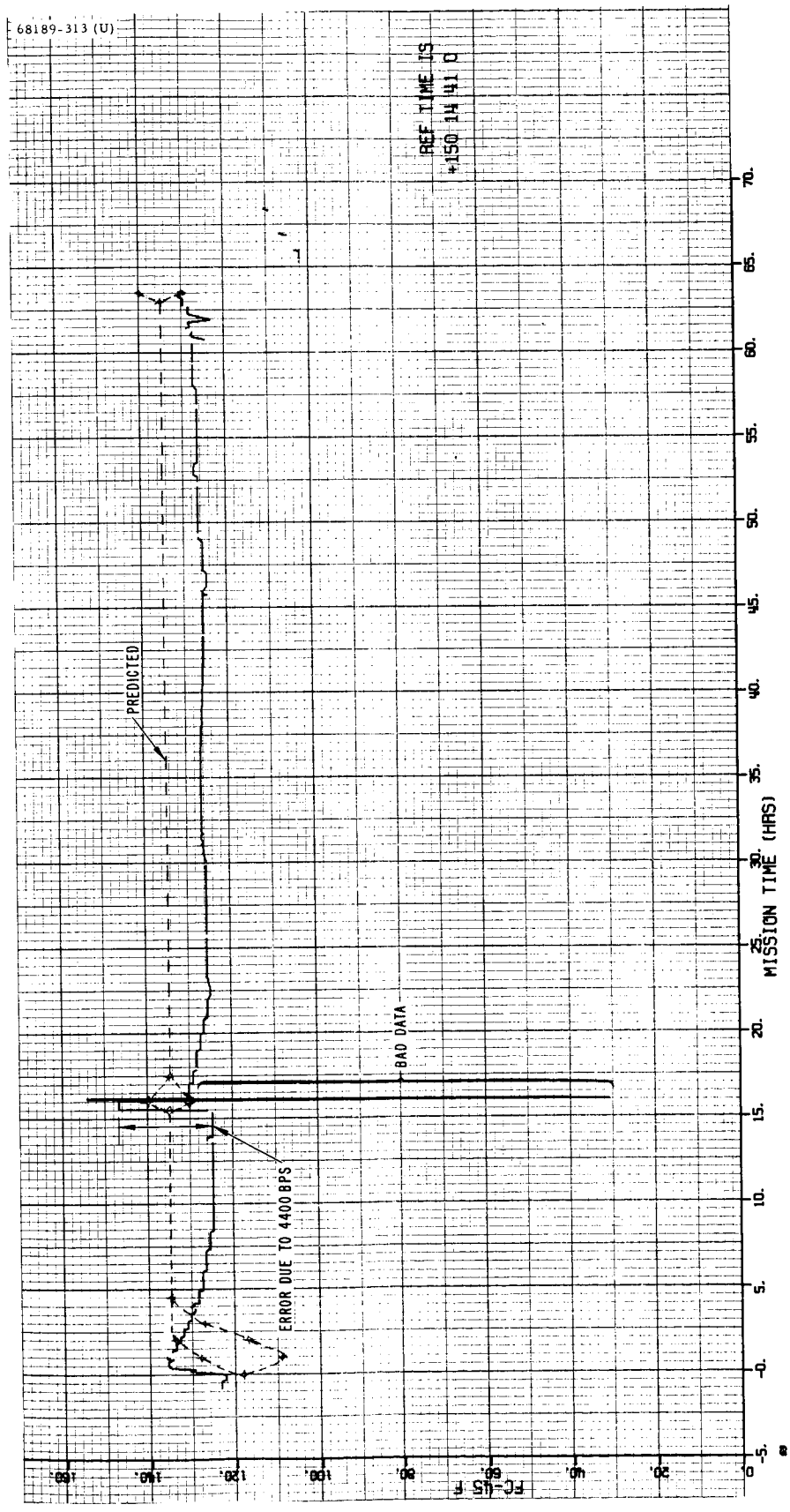
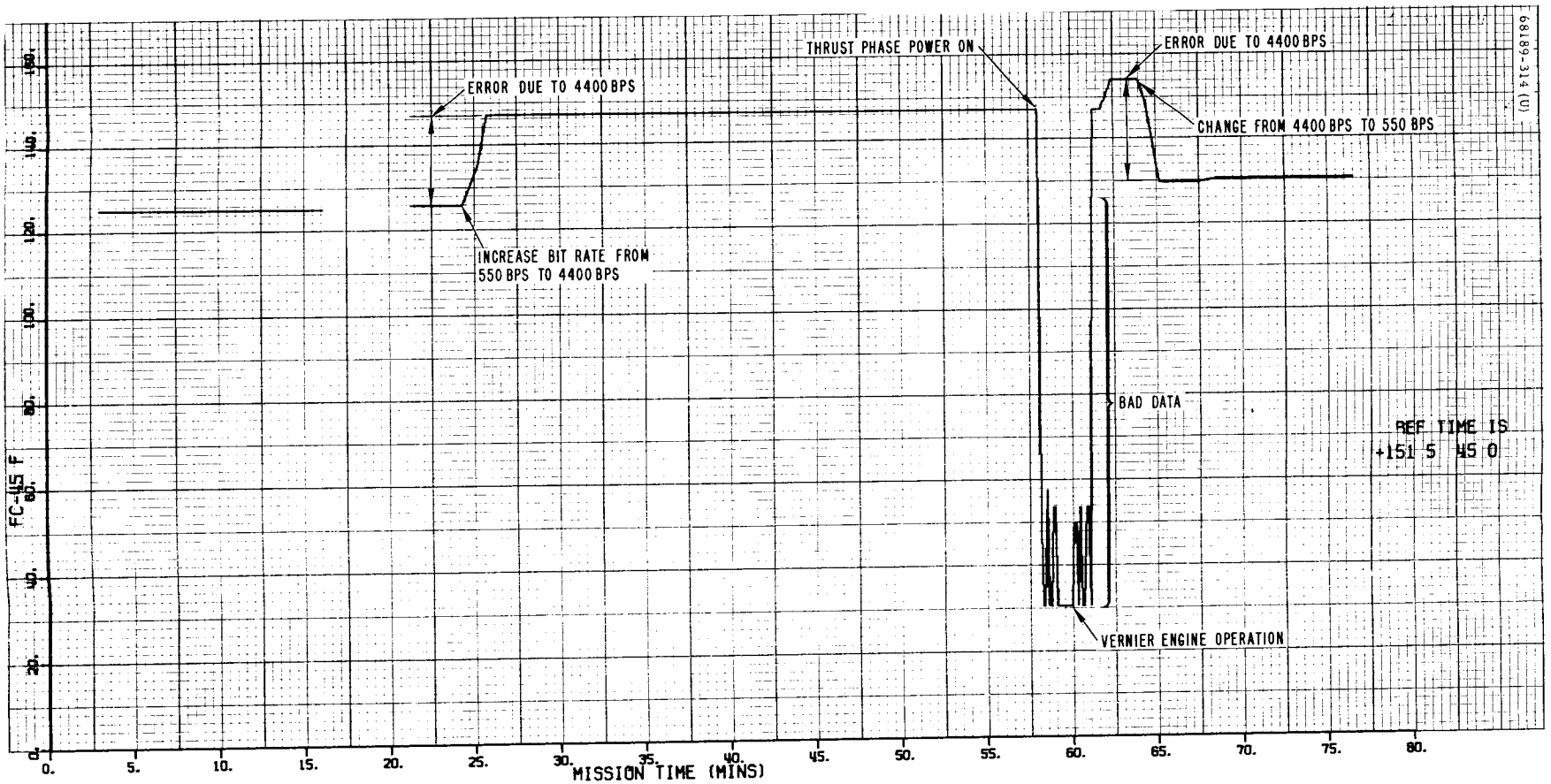


Figure A-7. Flight Control Electronics



a) Mission Plot

Figure A-8. Flight Control Electronics



b) Midcourse

Figure A-8 (continued). Flight Control Electronics

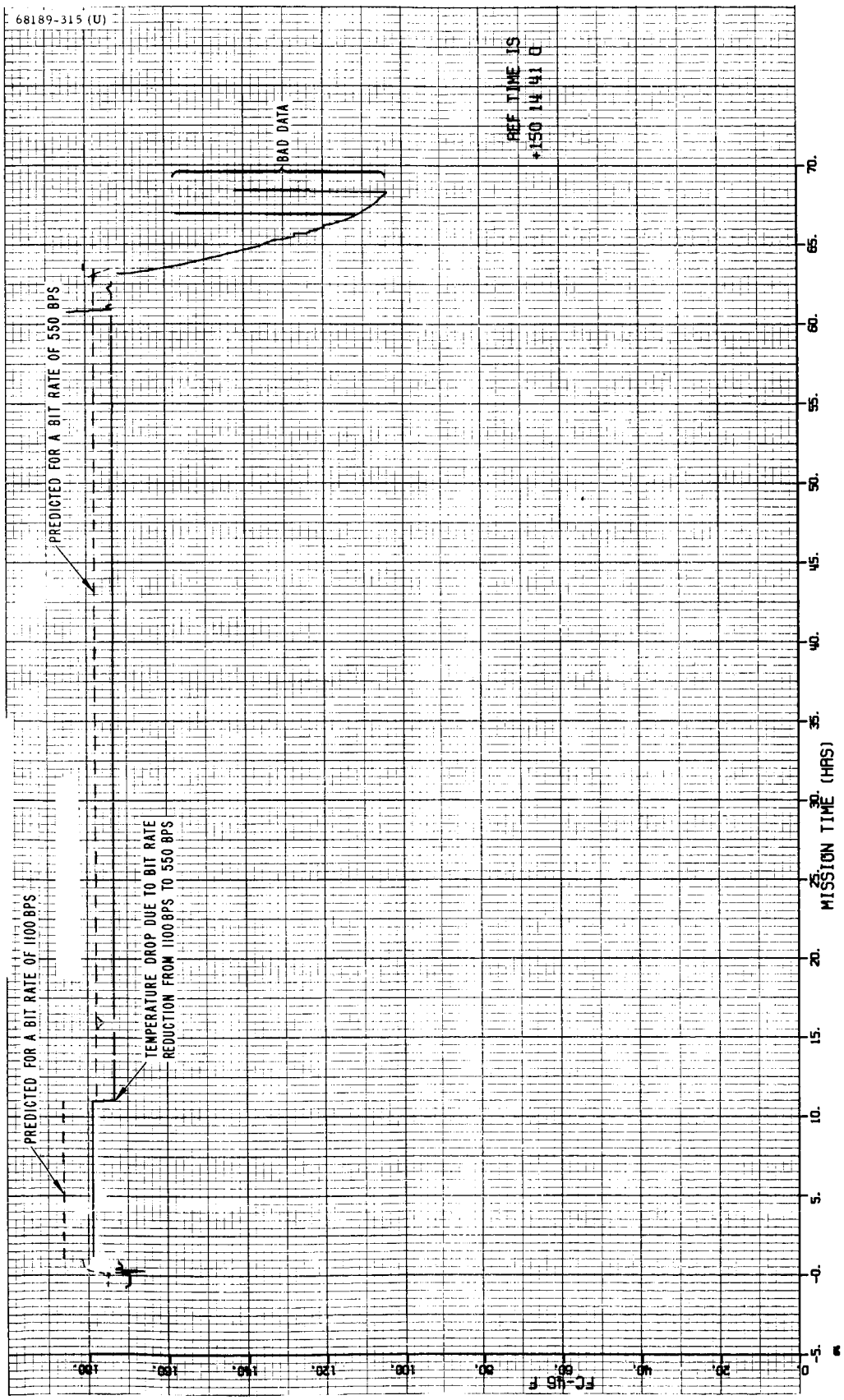
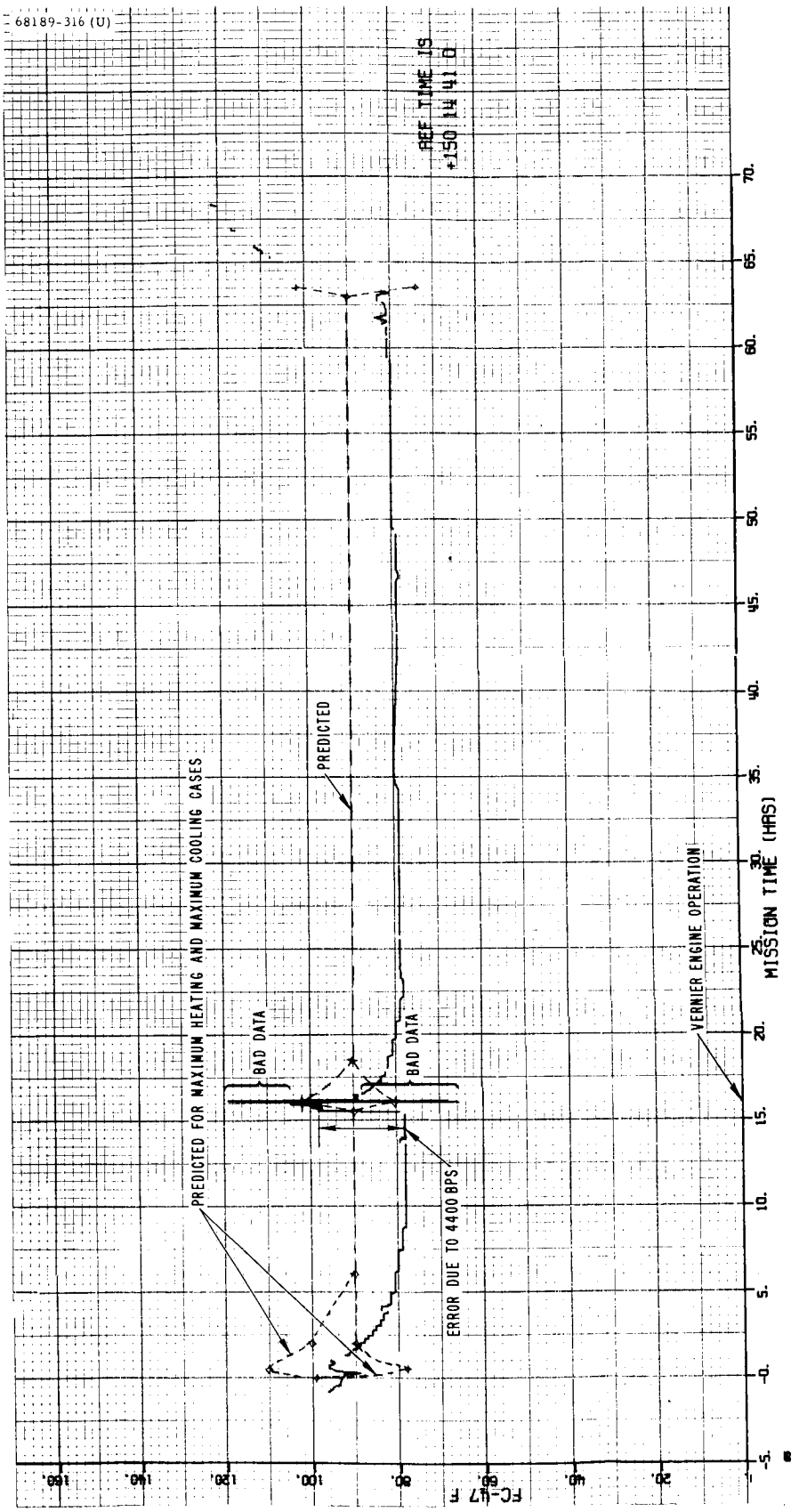
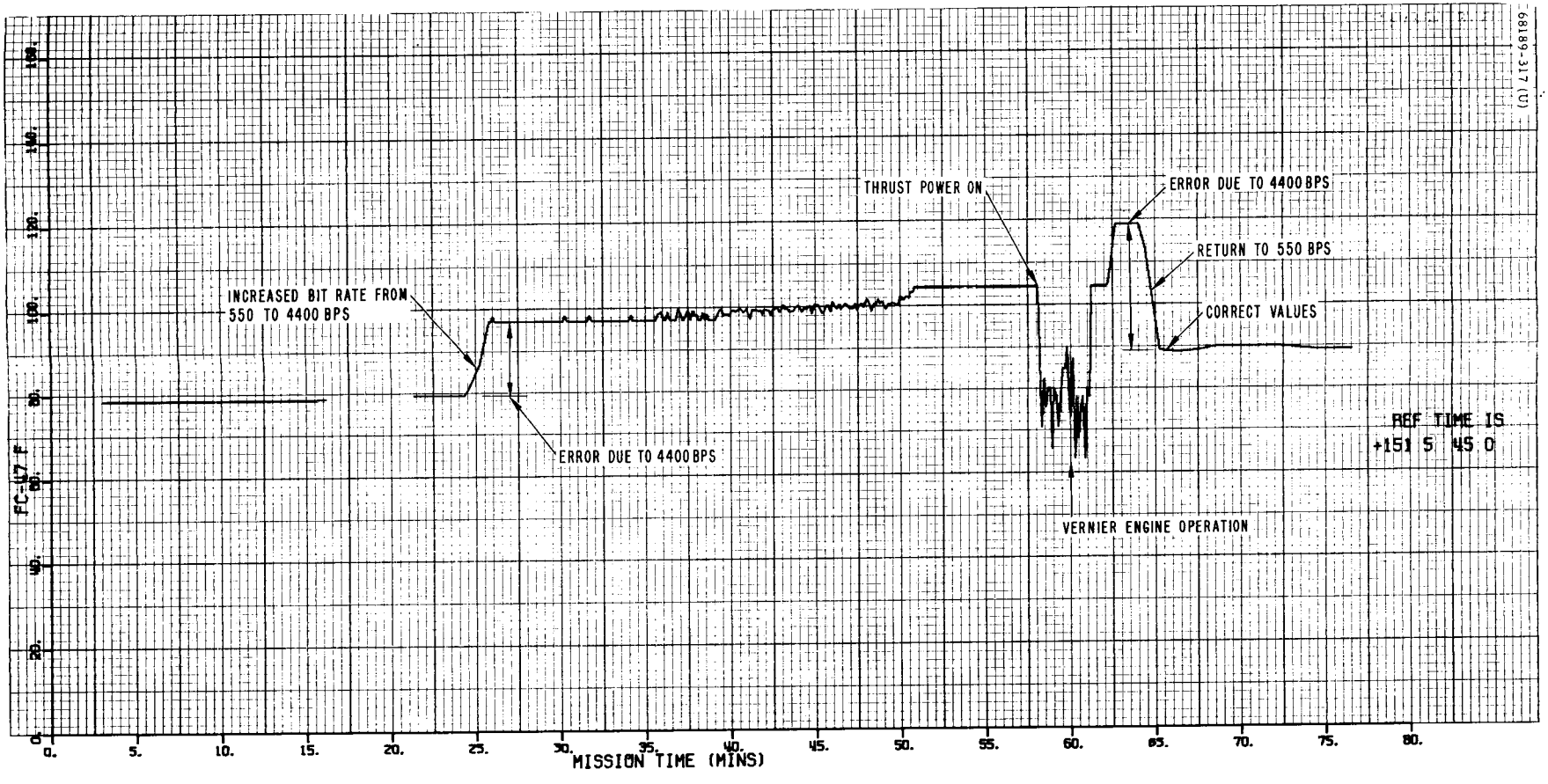


Figure A-9. IRU Roll Gyro



a) Mission Plot

Figure A-10. Canopus Sensor



b) Midcourse

Figure A-10 (continued). Canopus Sensor

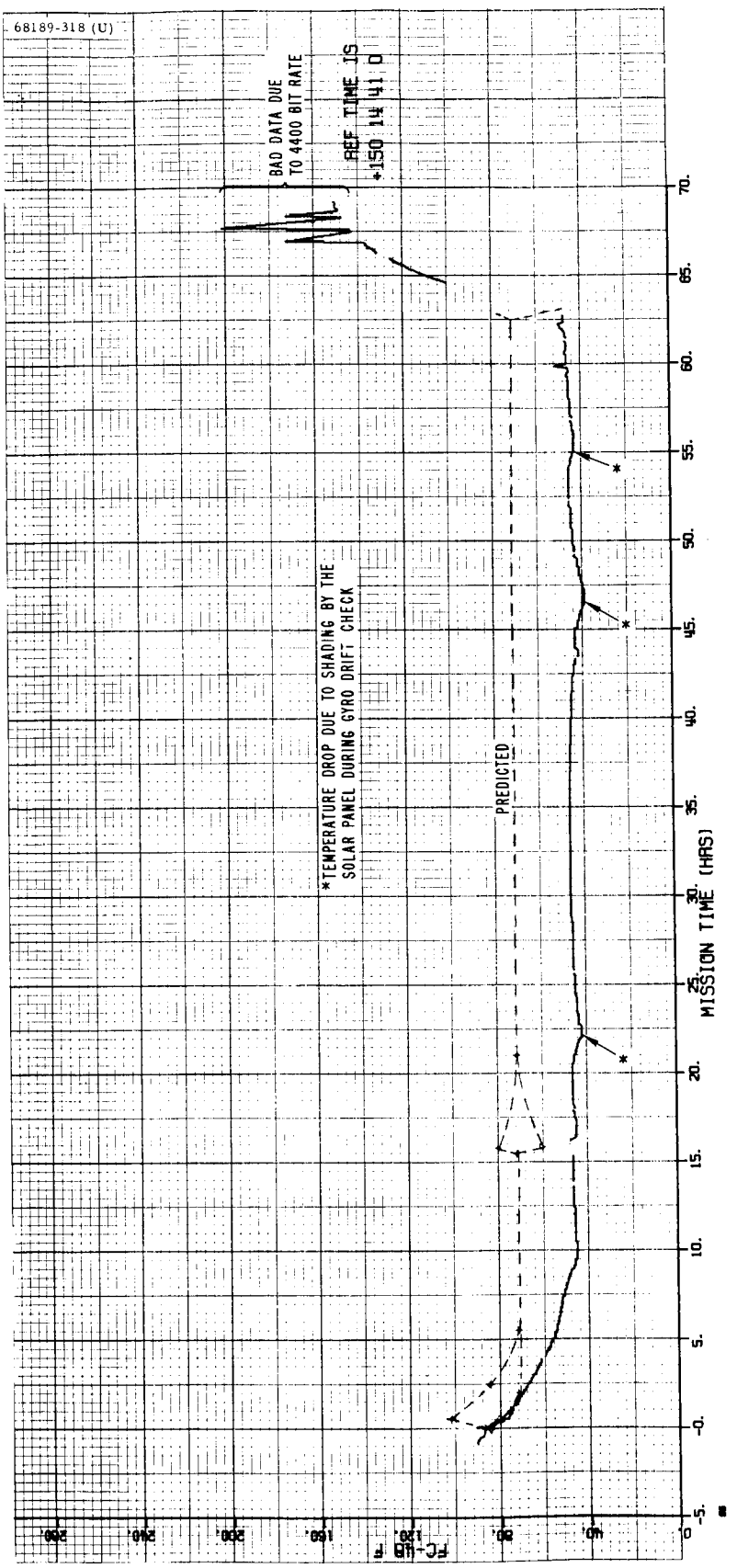
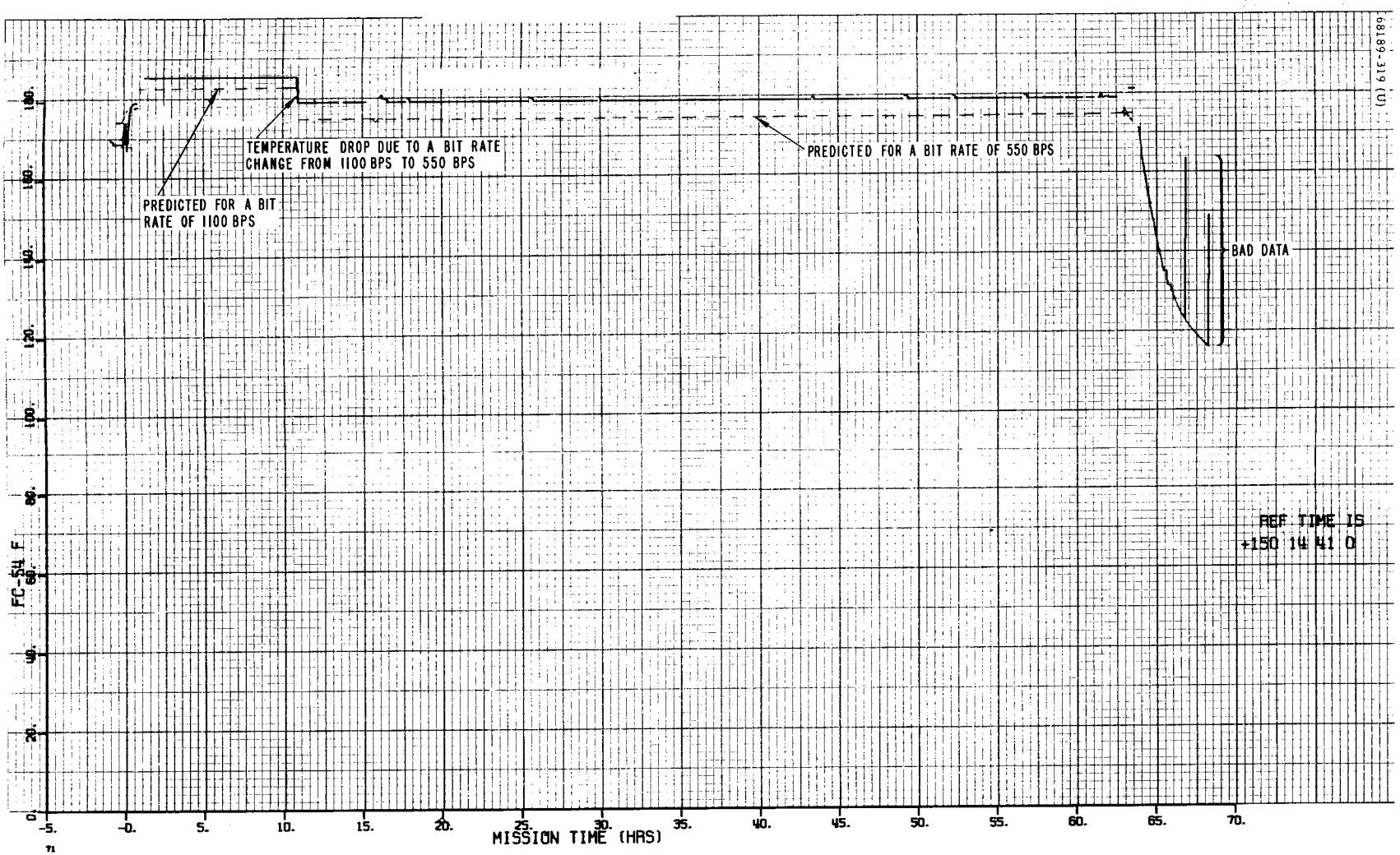
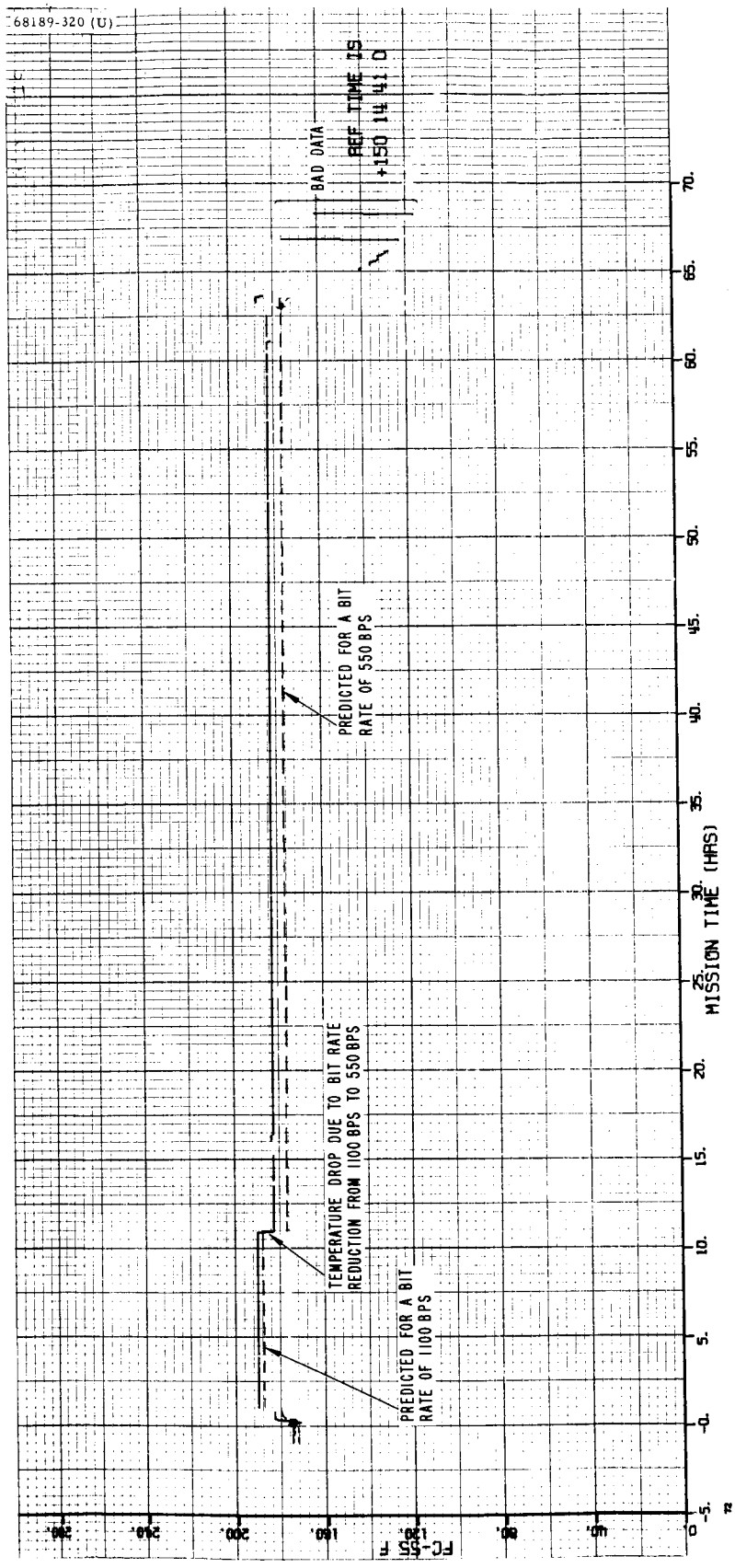


Figure A-11. Nitrogen Tank



a) Pitch

Figure A-12. IRU Gyros



b) Yaw

Figure A-12. (continued). IRU Gyros

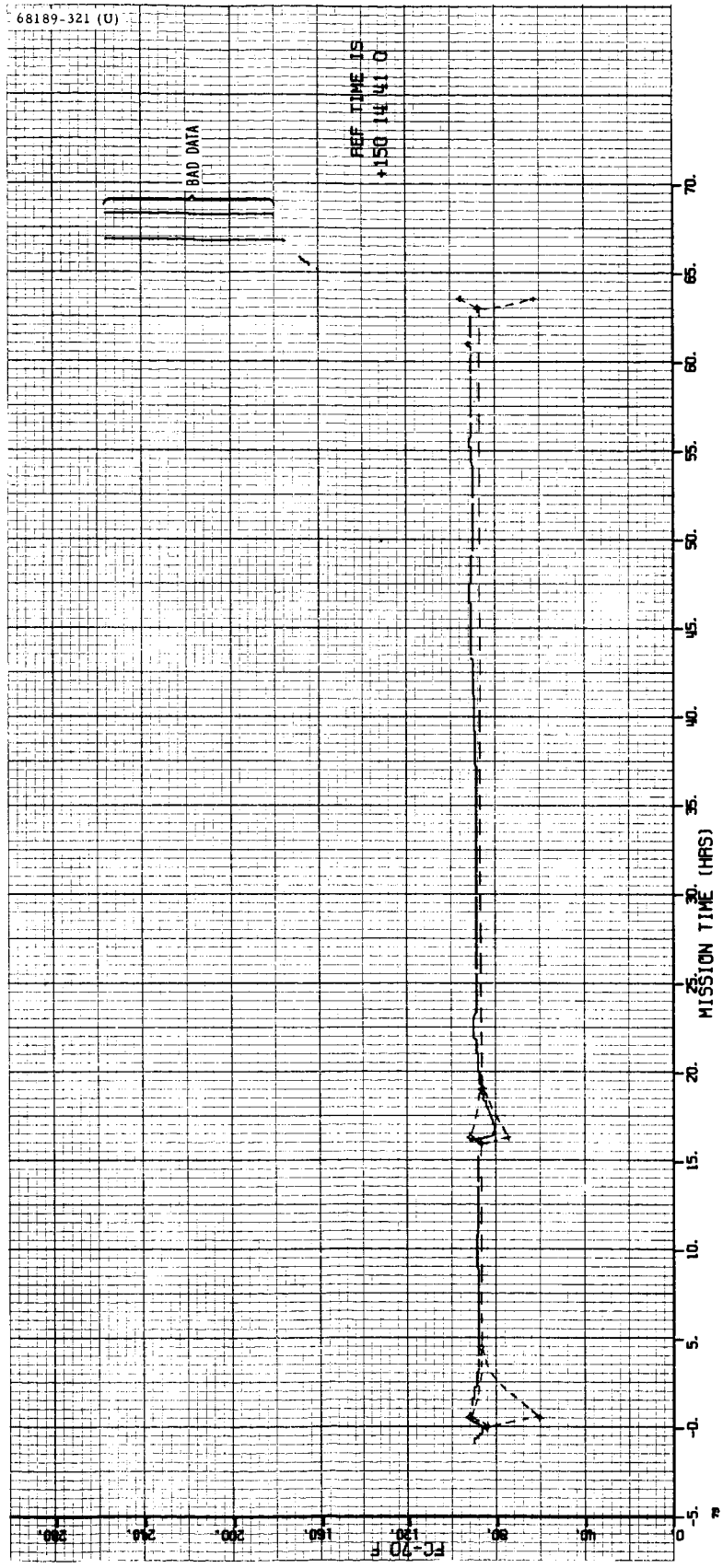


Figure A-13. Attitude Jet 2

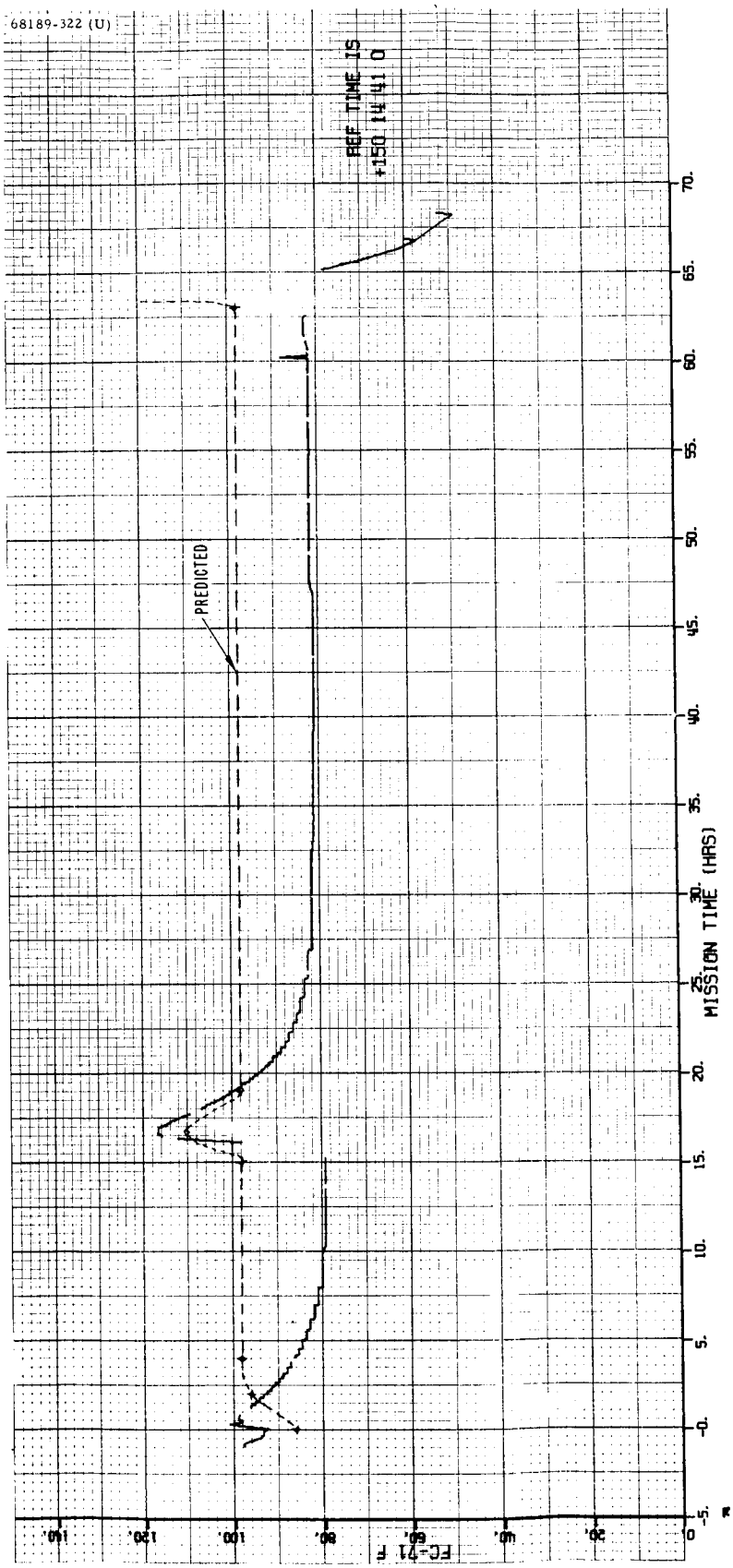


Figure A-14. Roll Actuator

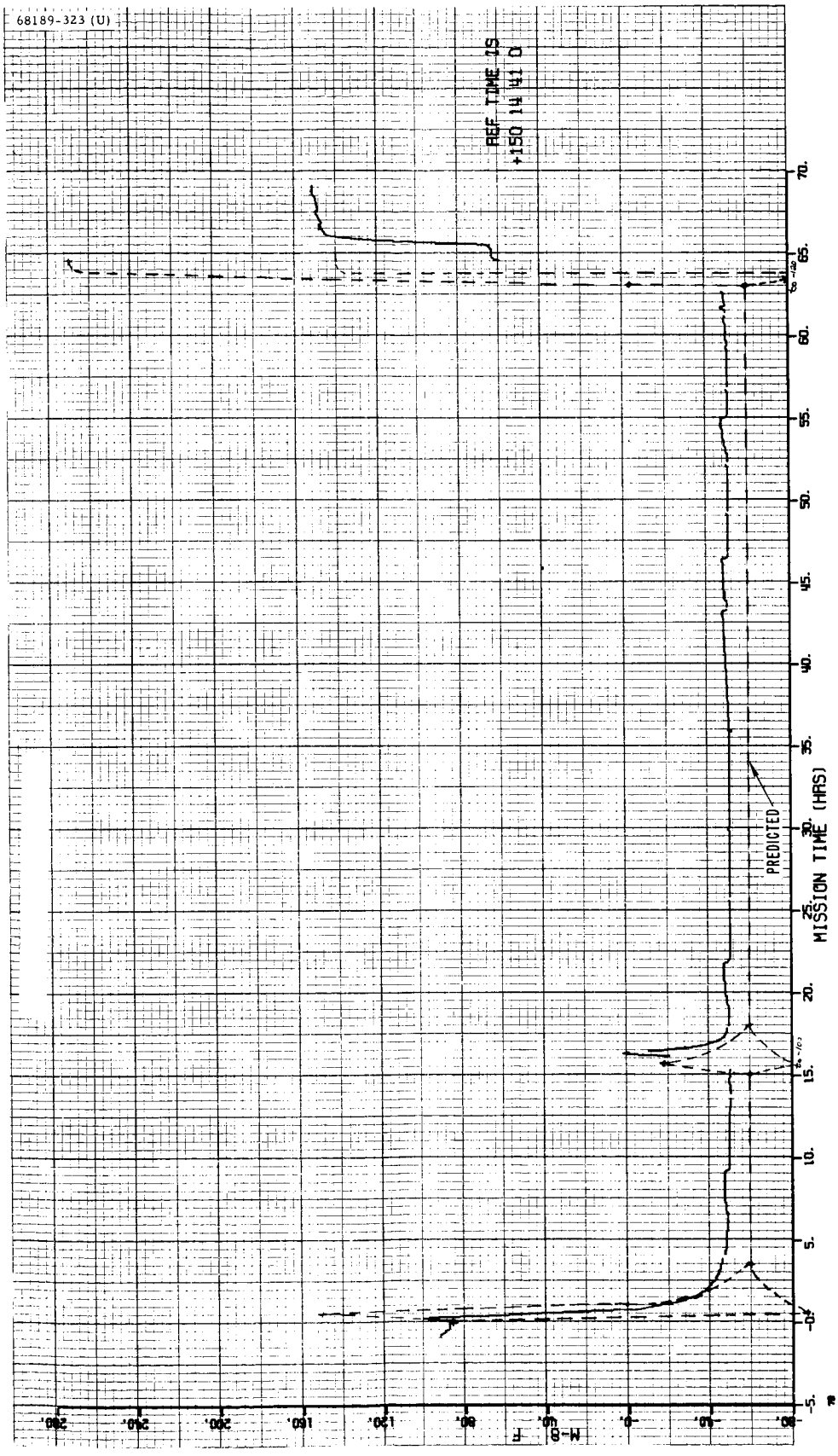


Figure A-15. Planar Array

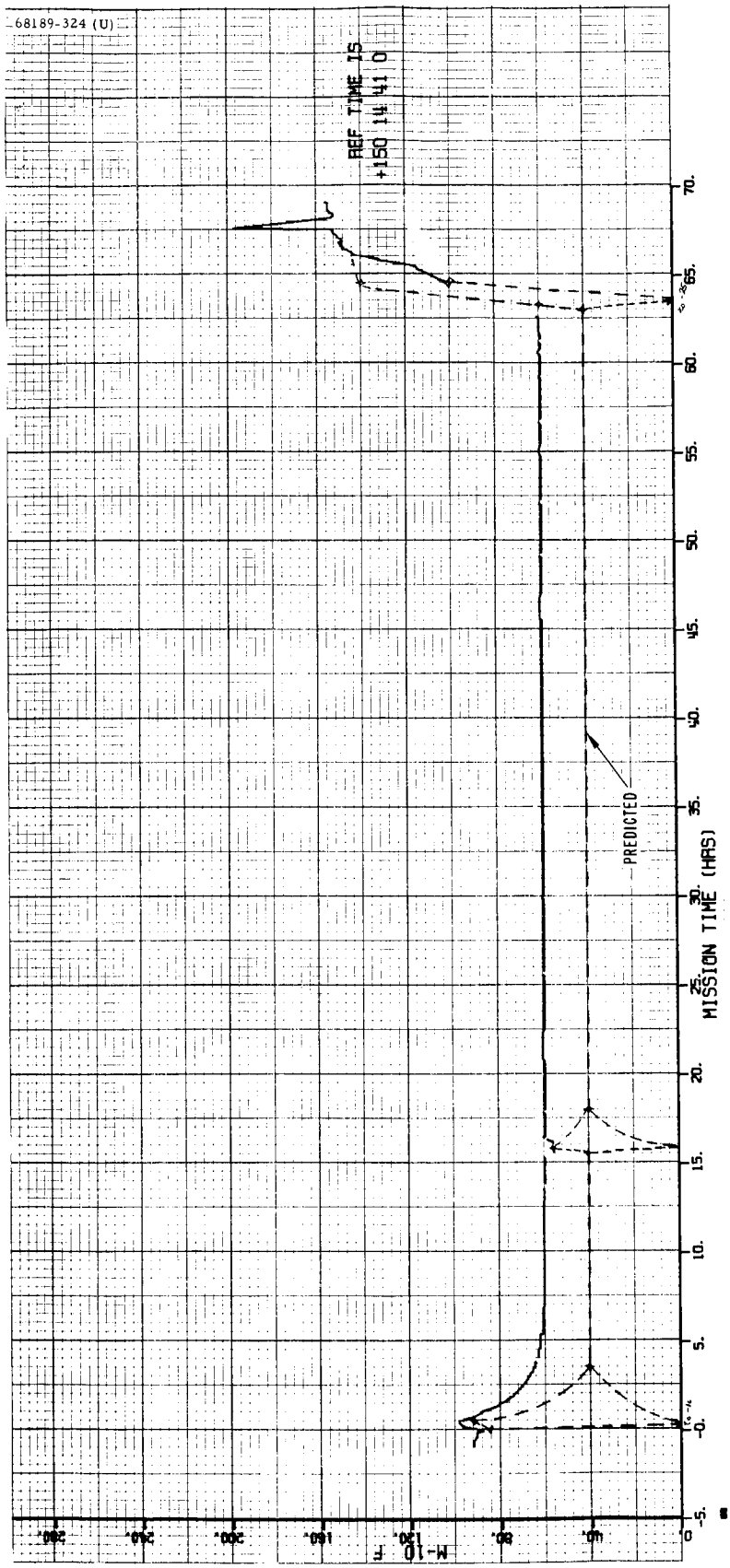


Figure A-16. Solar Panel Axis Motor

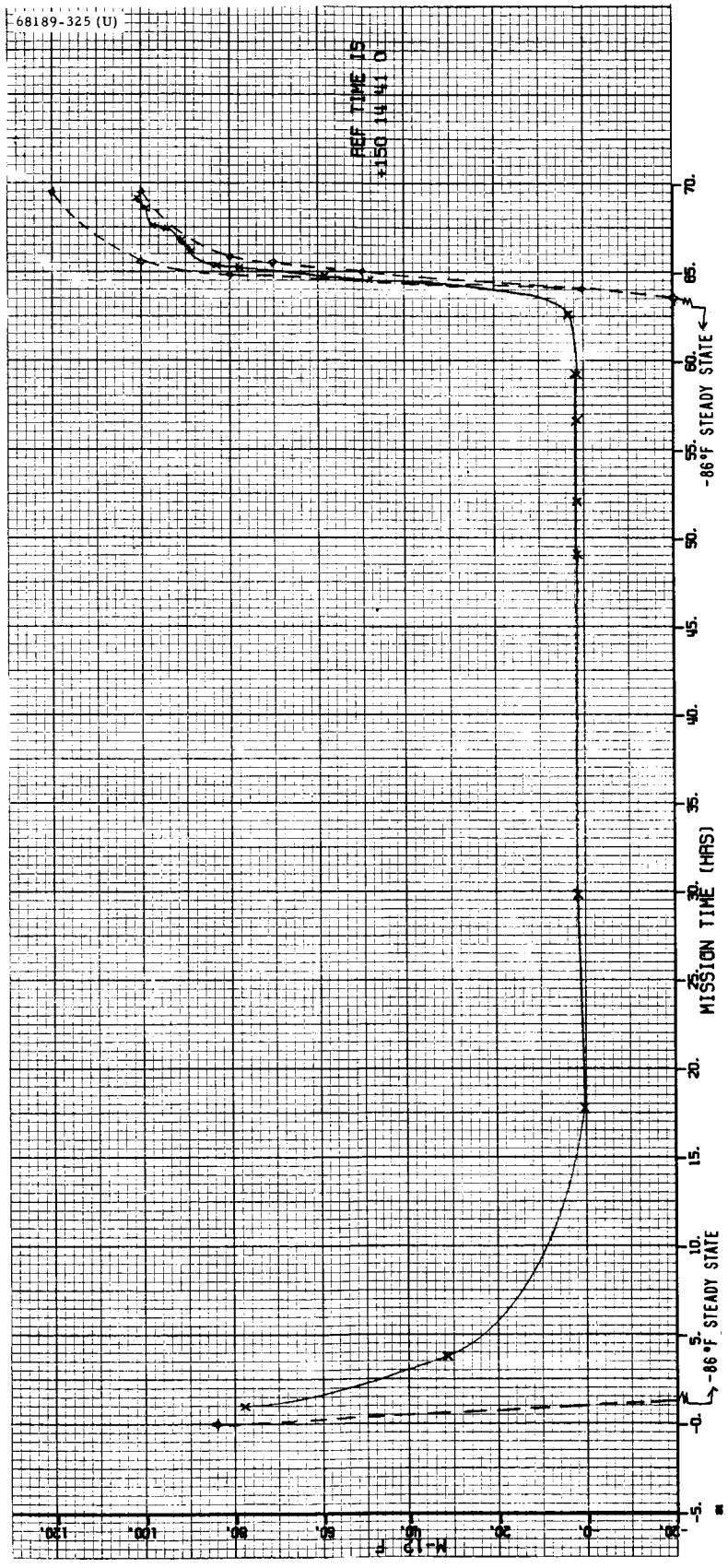


Figure A-17. Elevation Axis Motor

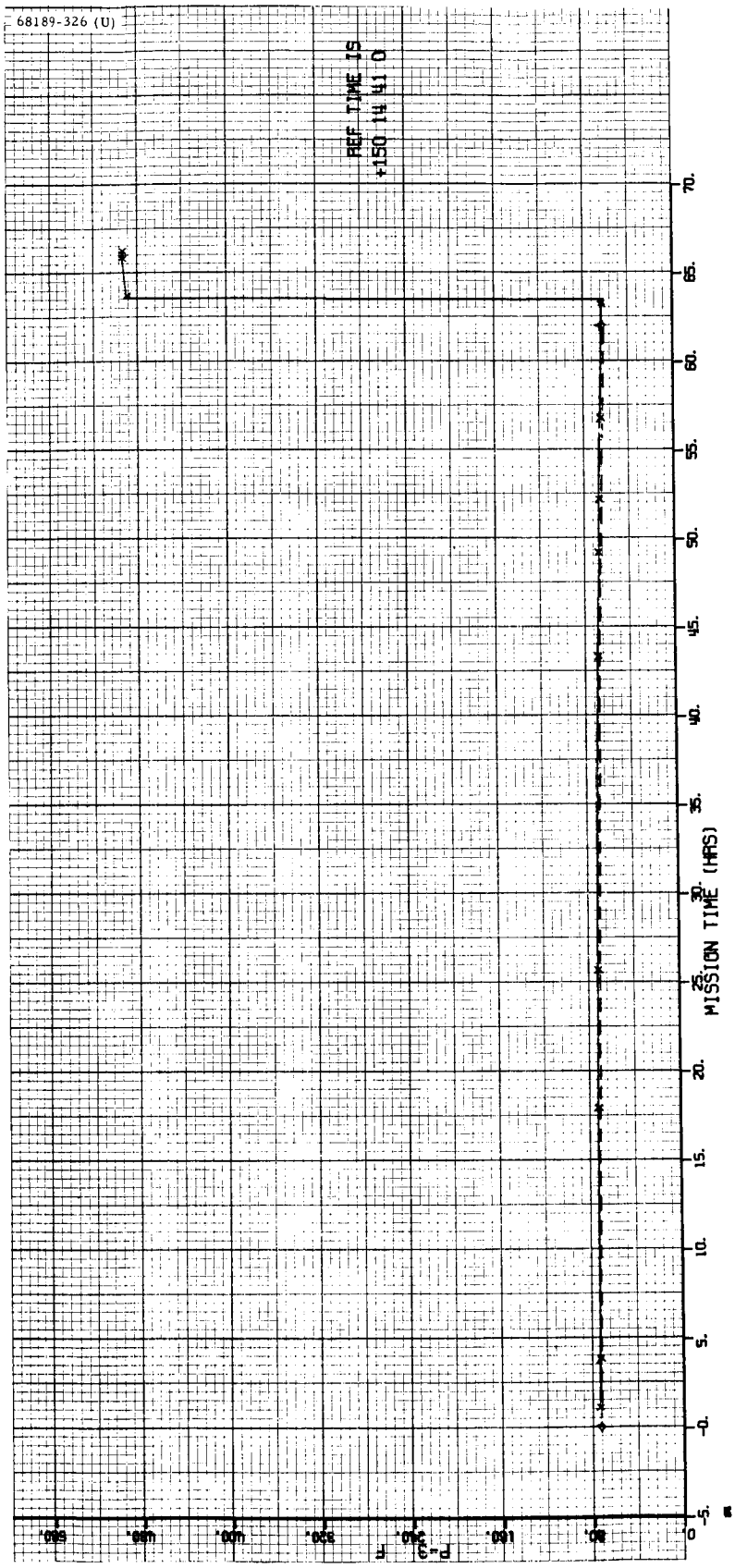


Figure A-18. Retro Engine Upper Case

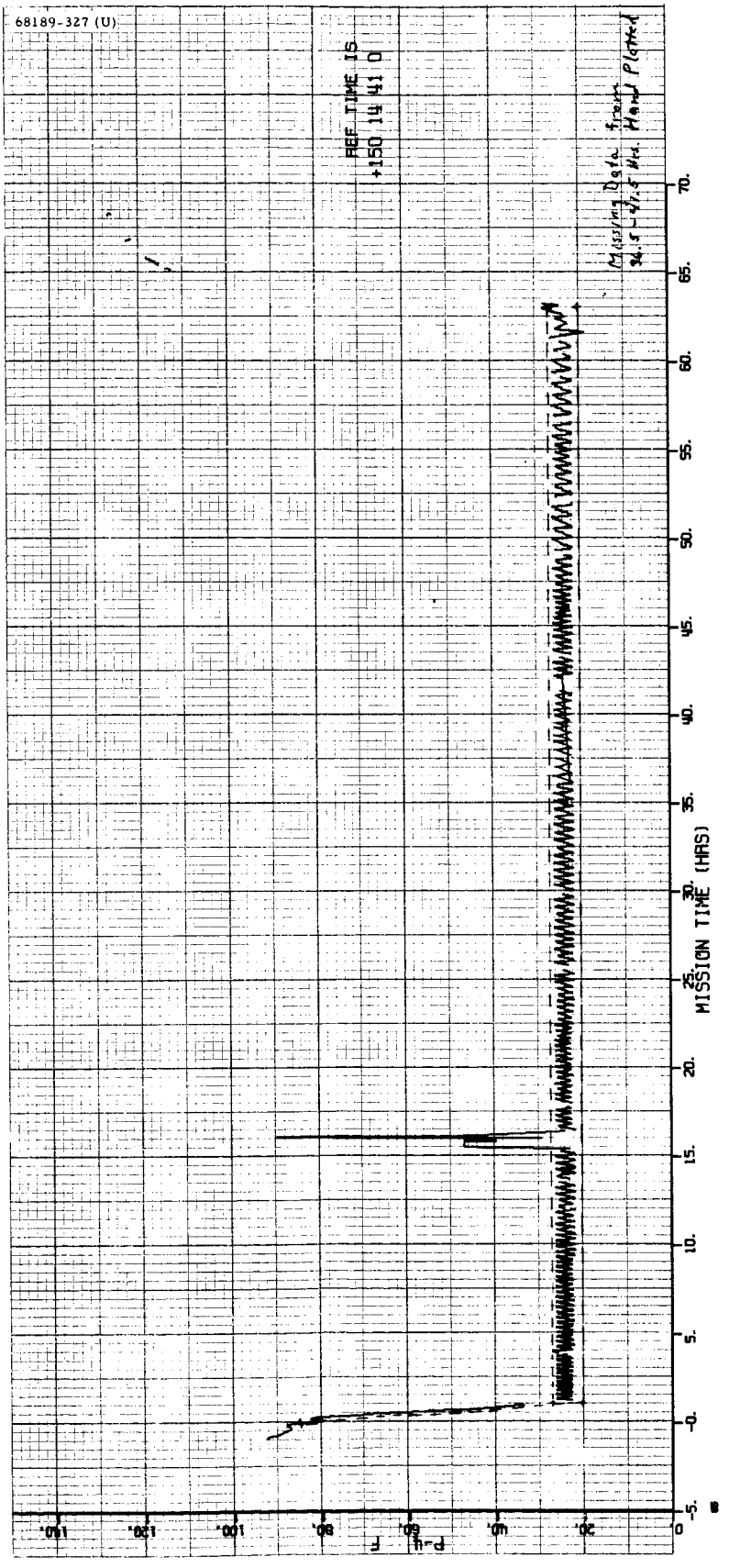


Figure A-19. Oxidizer Line Near Engine 2

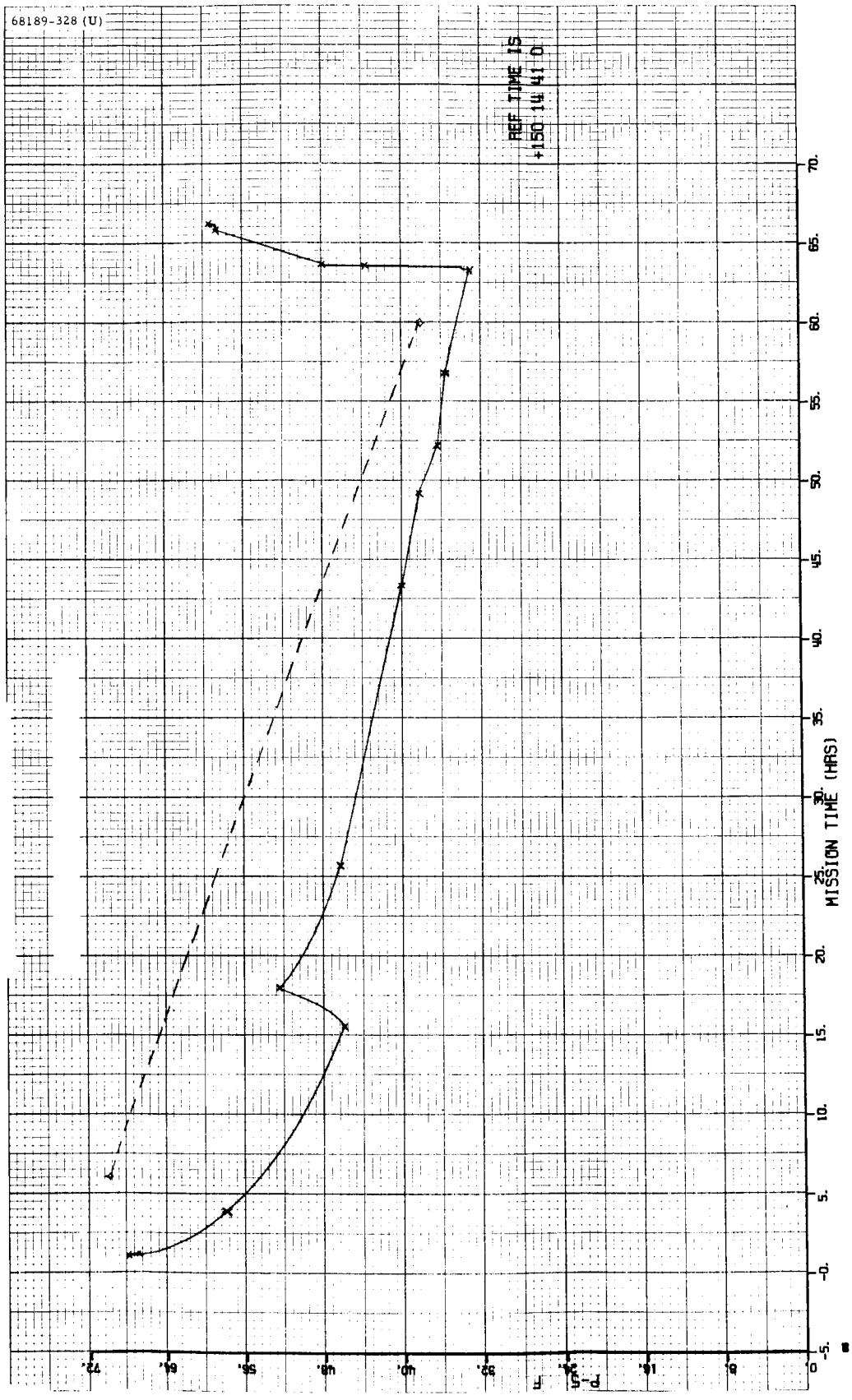


Figure A-20. Fuel Tank 2

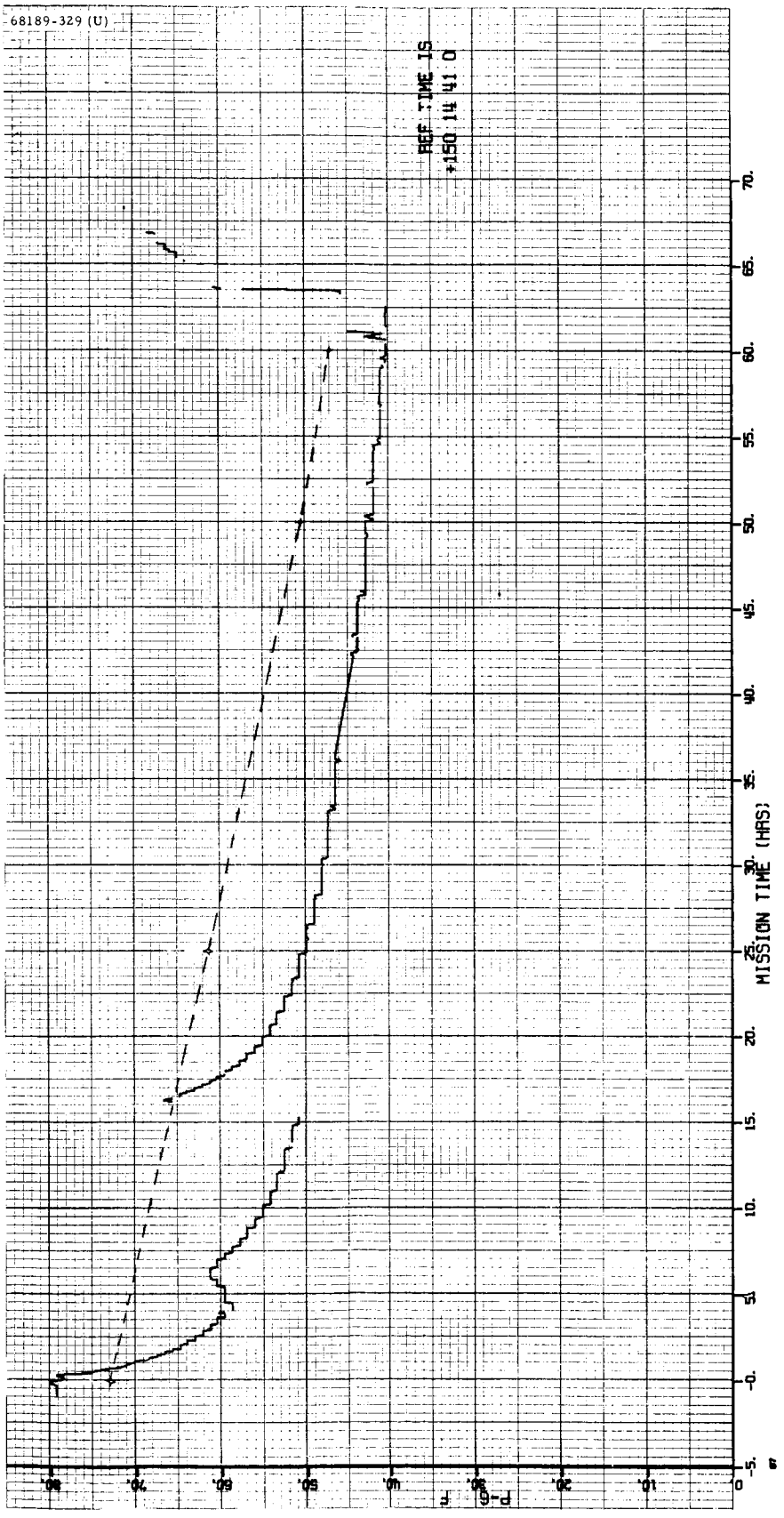


Figure A-21. Oxidizer Tank 3

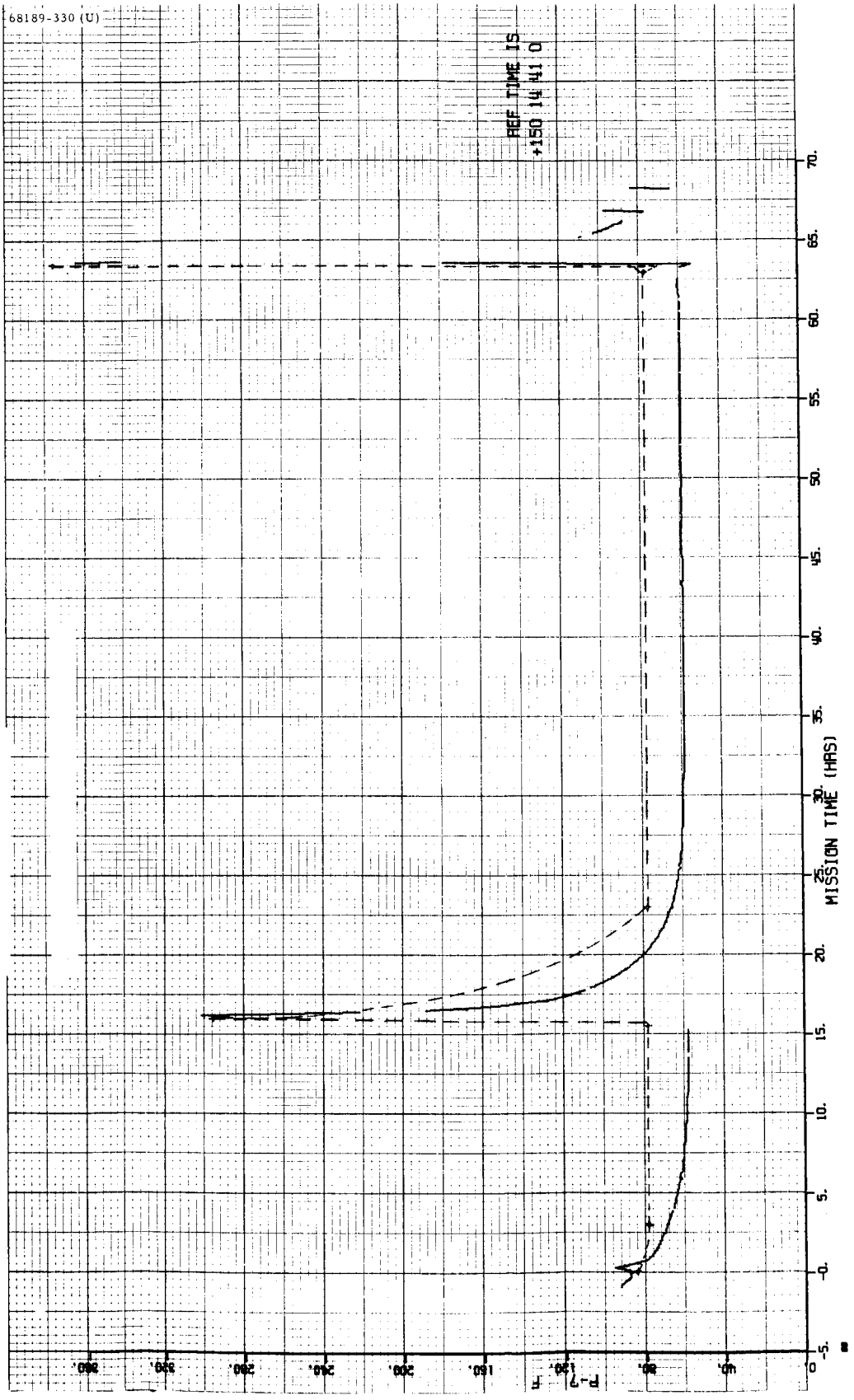


Figure A-22. Vernier Engine 1

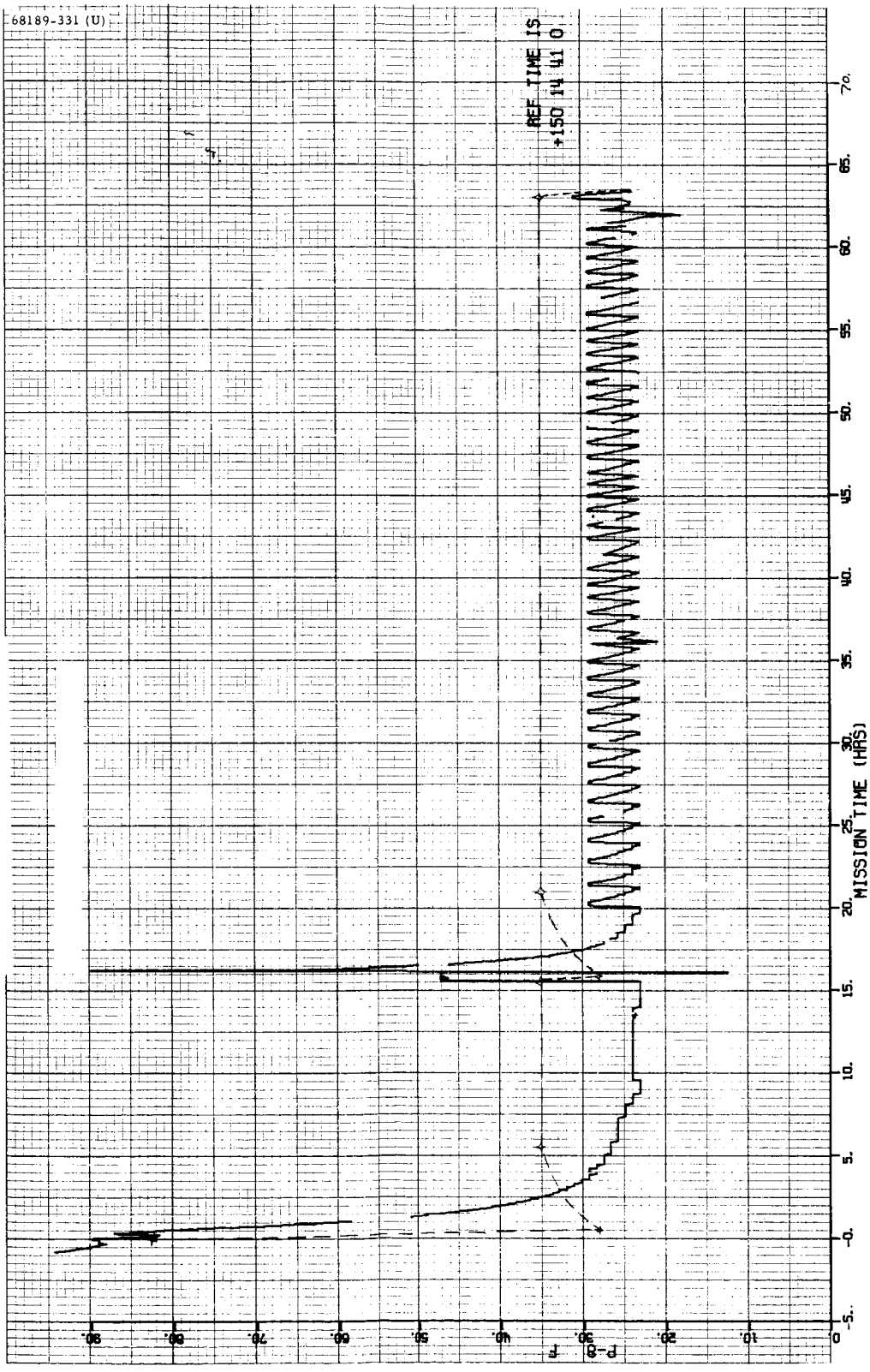


Figure A-23. Oxidizer Line Near Engine 1

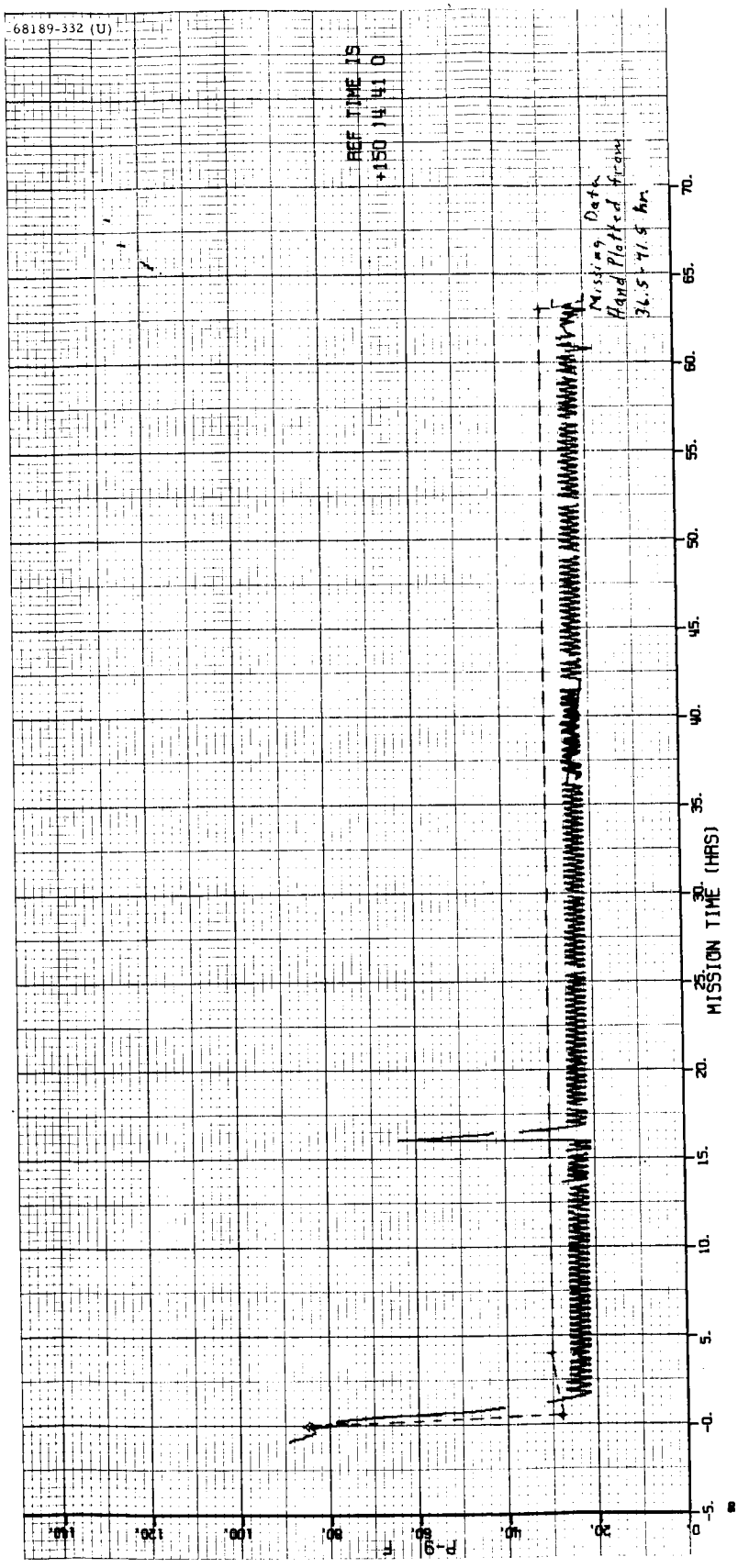
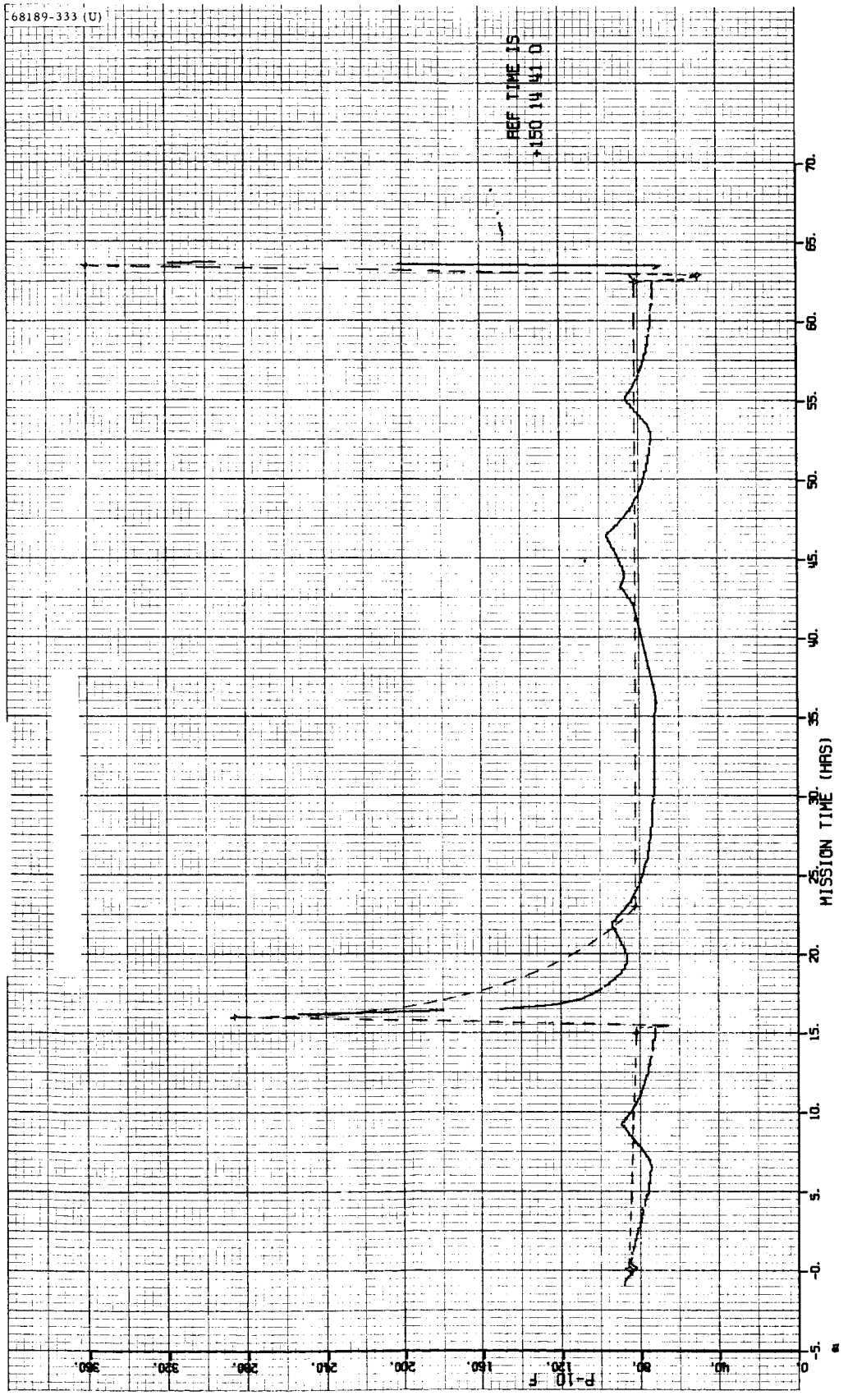
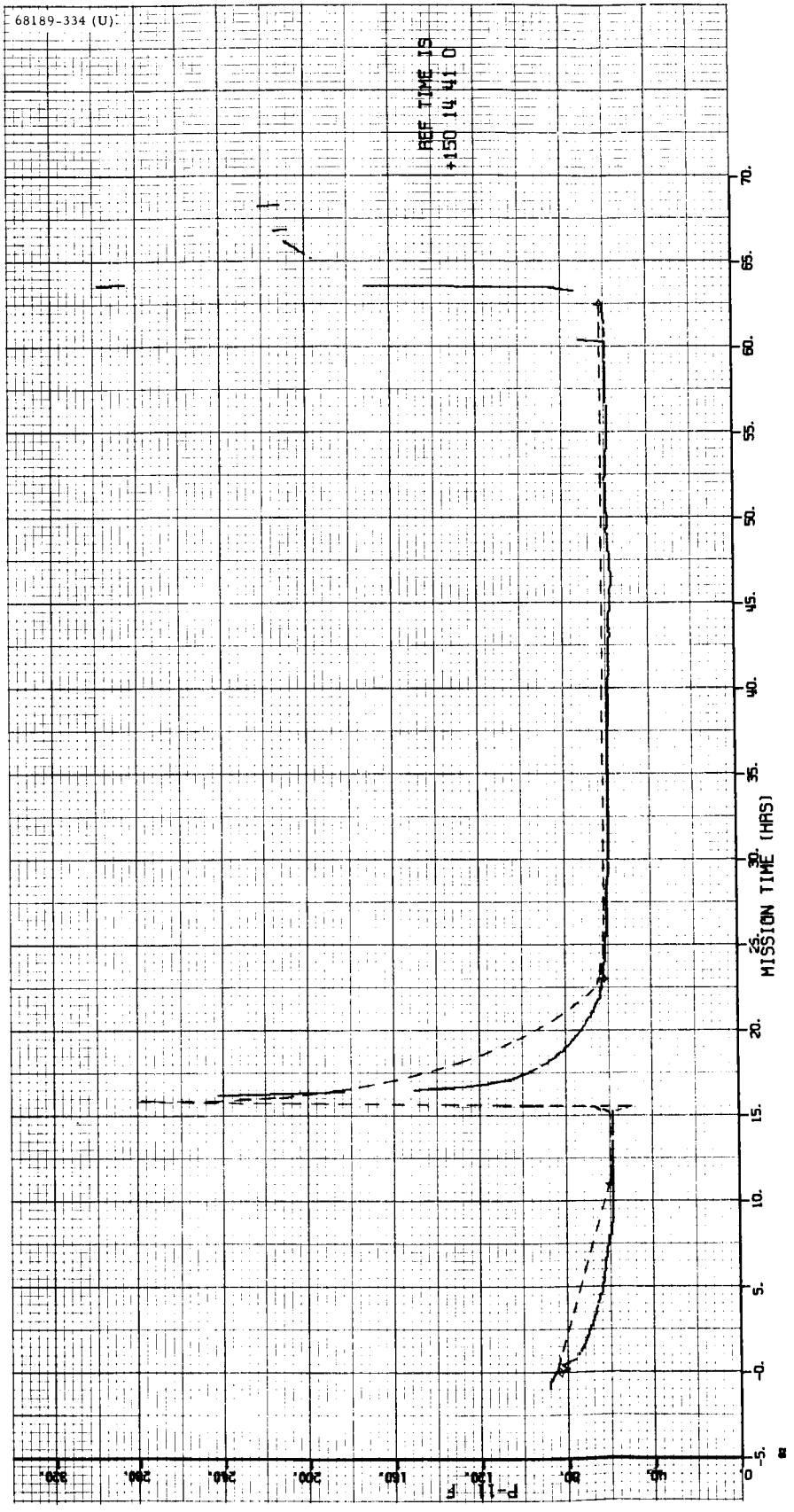


Figure A-23 (continued). Oxidizer Line



a) Engine 1

Figure A-24. Vernier Engines



b) Engine 2

Figure A-24 (continued). Vernier Engines

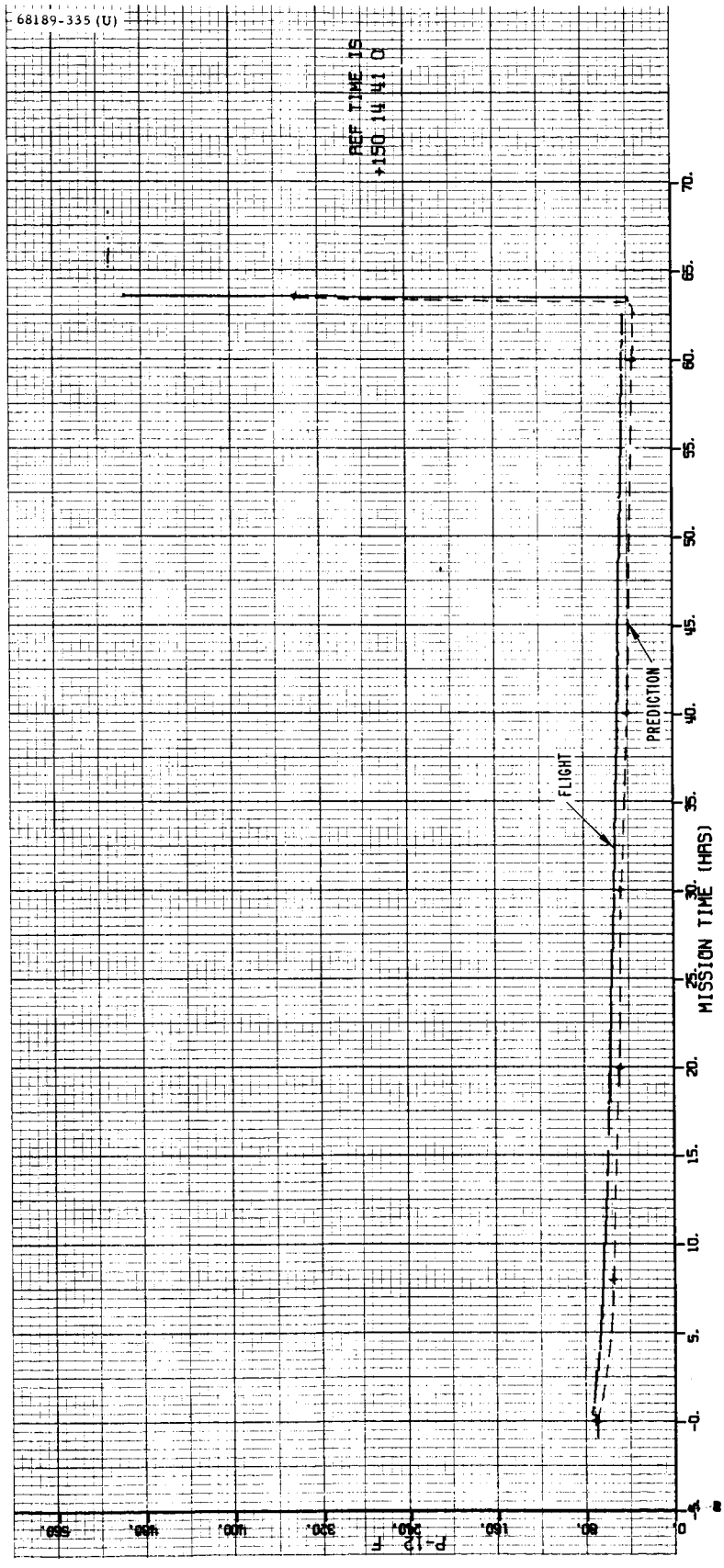
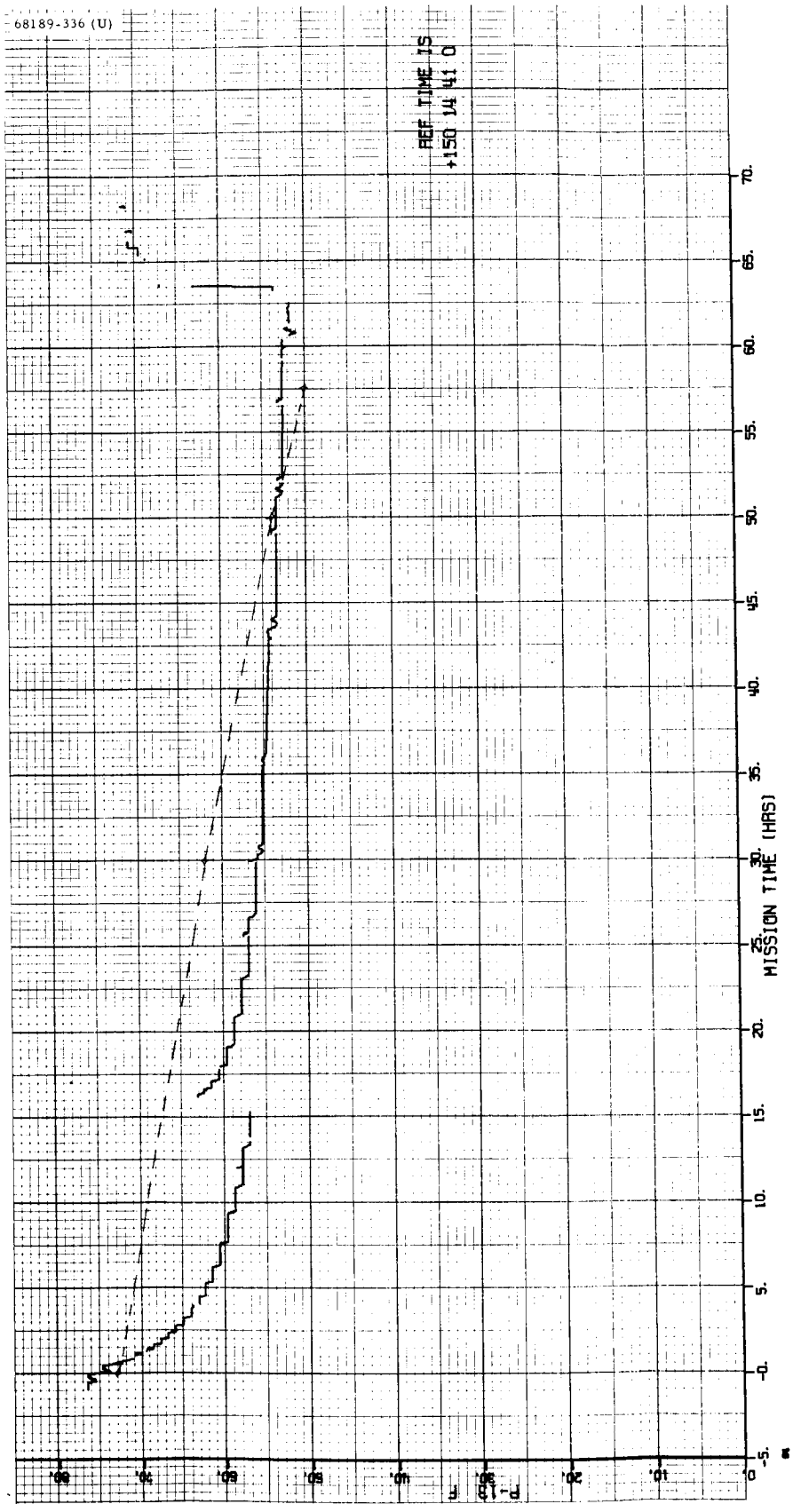
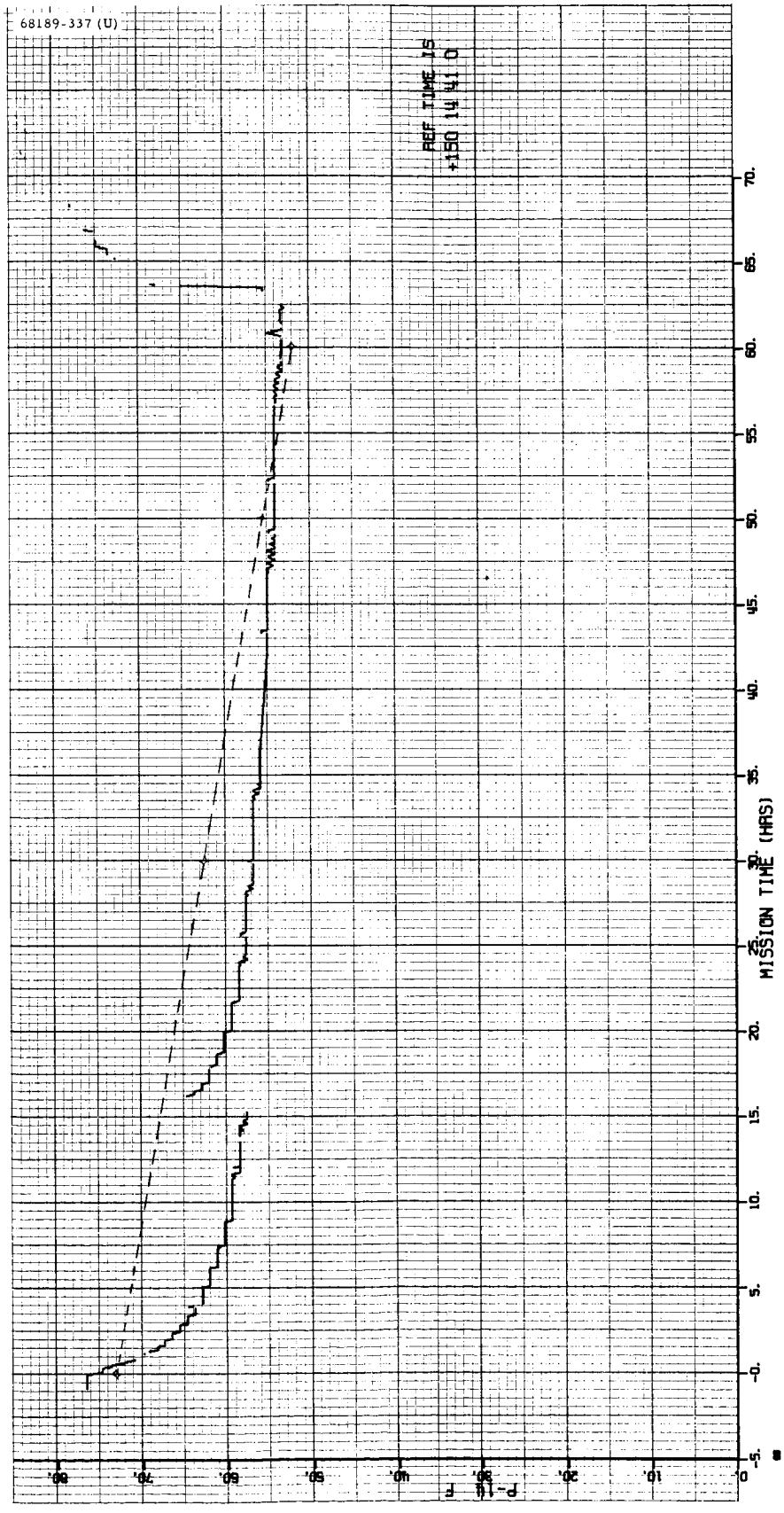


Figure A-25. Retro Engine Lower Case



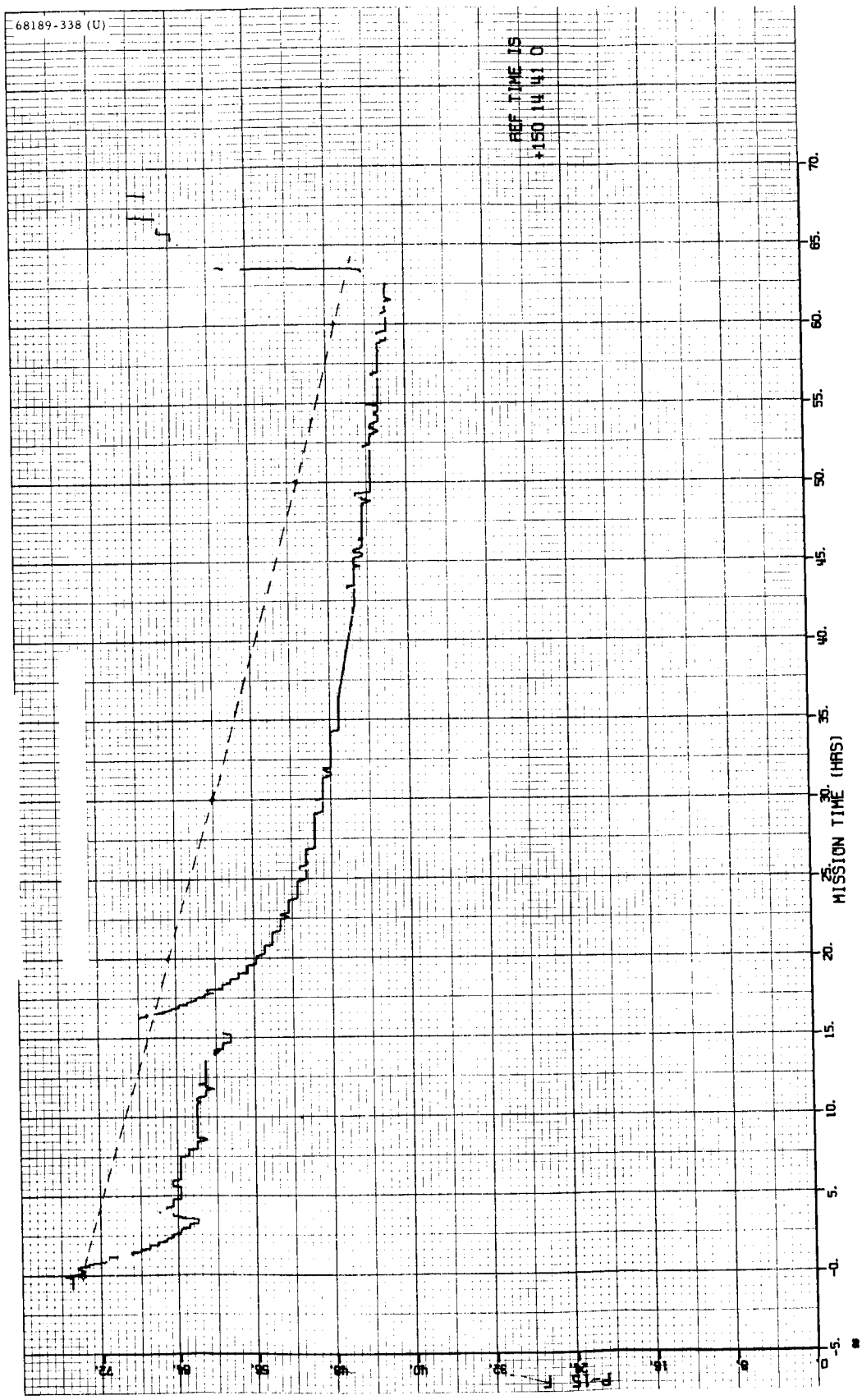
a) Tank 1

Figure A-26. Fuel Tanks



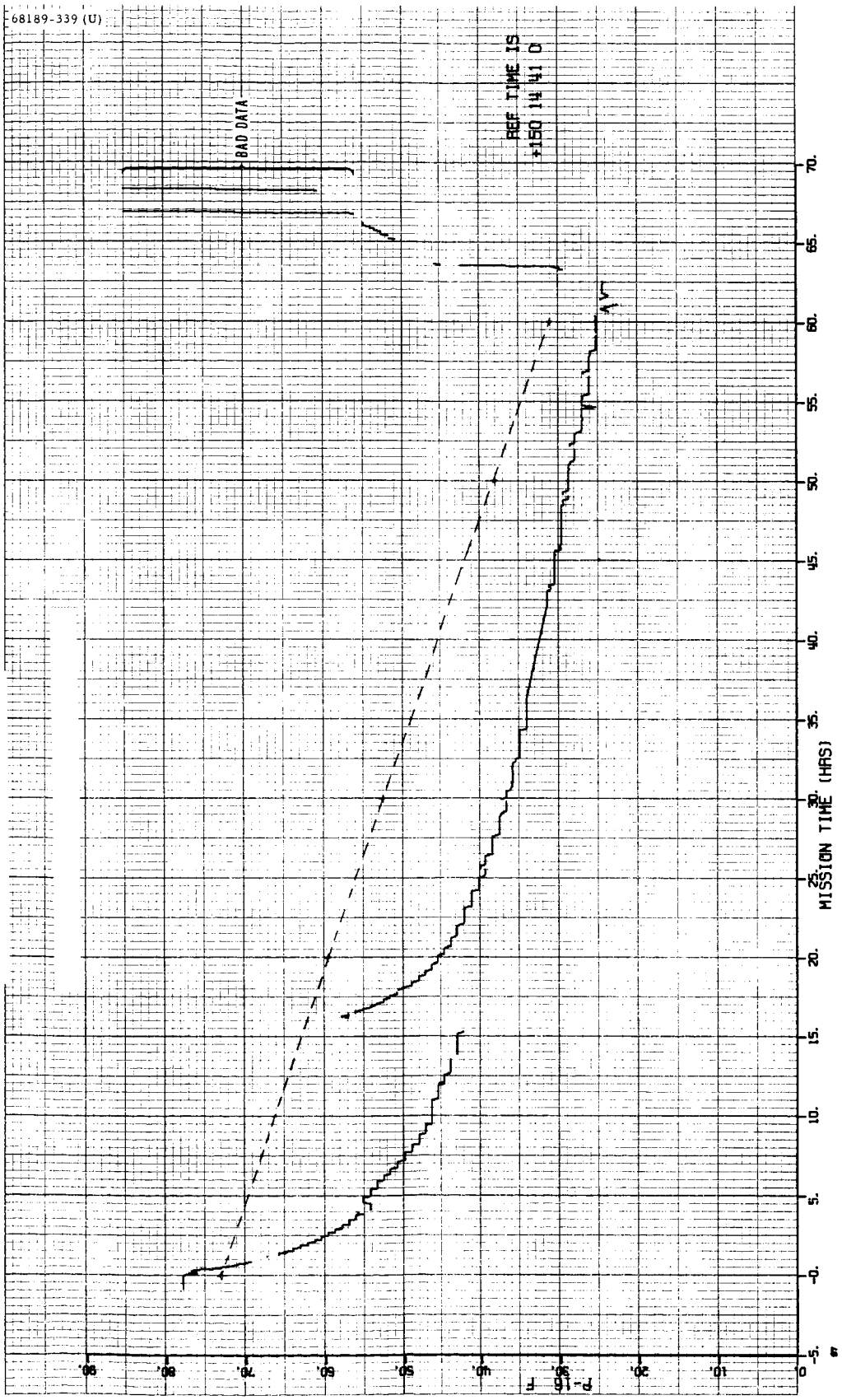
b) Tank 2

Figure A-26 (continued). Fuel Tanks



a) Tank 1

Figure A-27. Oxidizer Tanks



b) Tank 2

Figure A-27 (continued). Oxidizer Tanks

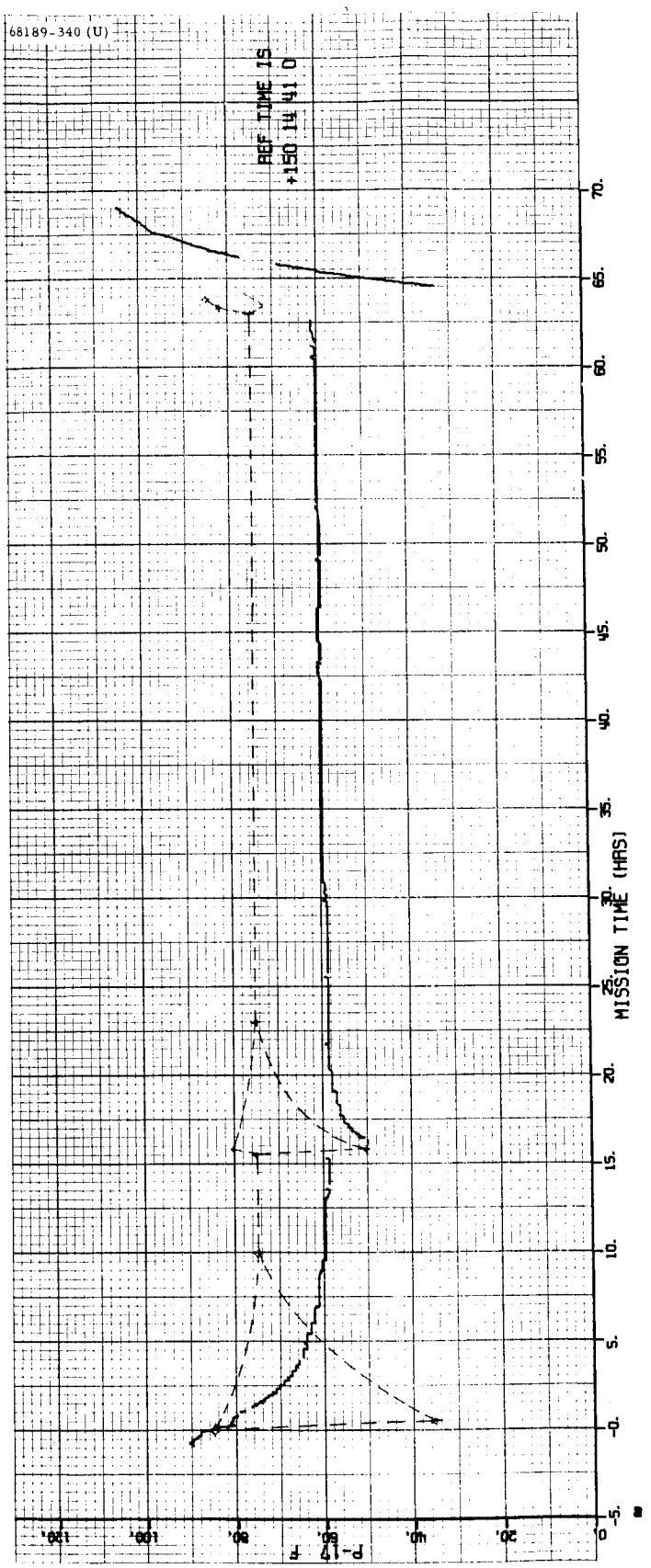


Figure A-28. Helium Tank

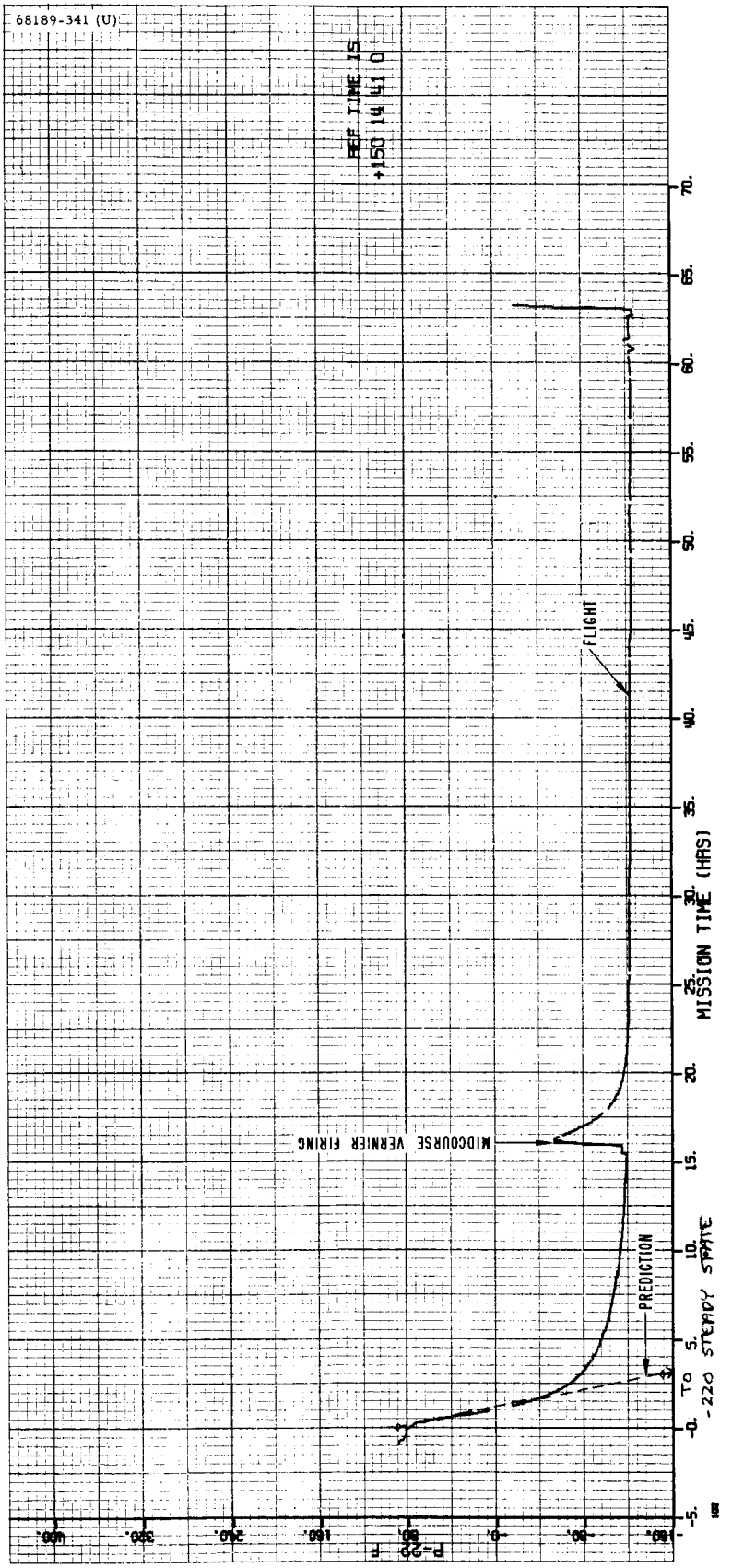


Figure A-29. Retro Engine Nozzle

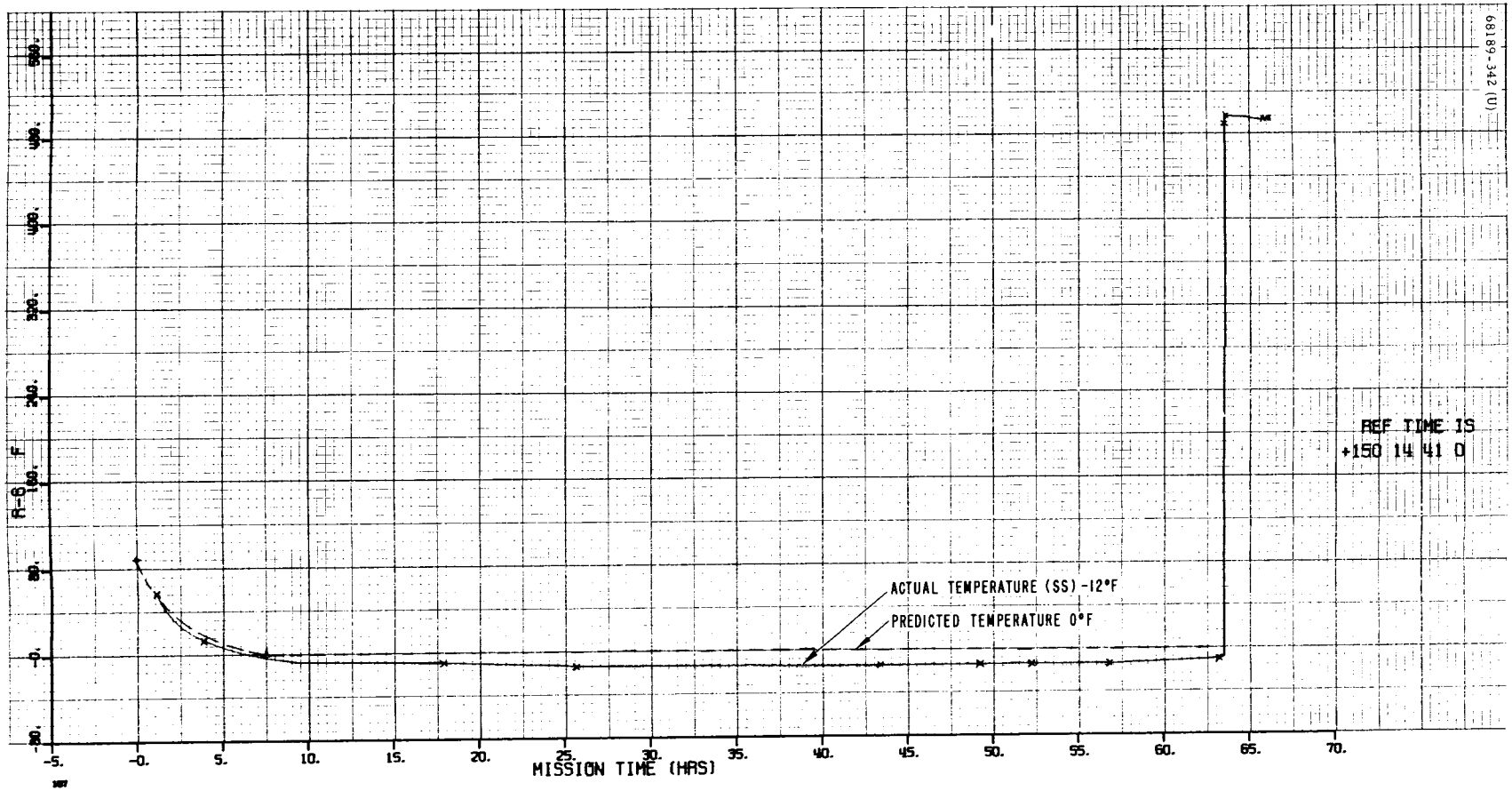


Figure A-30. AMR Electronics Platform

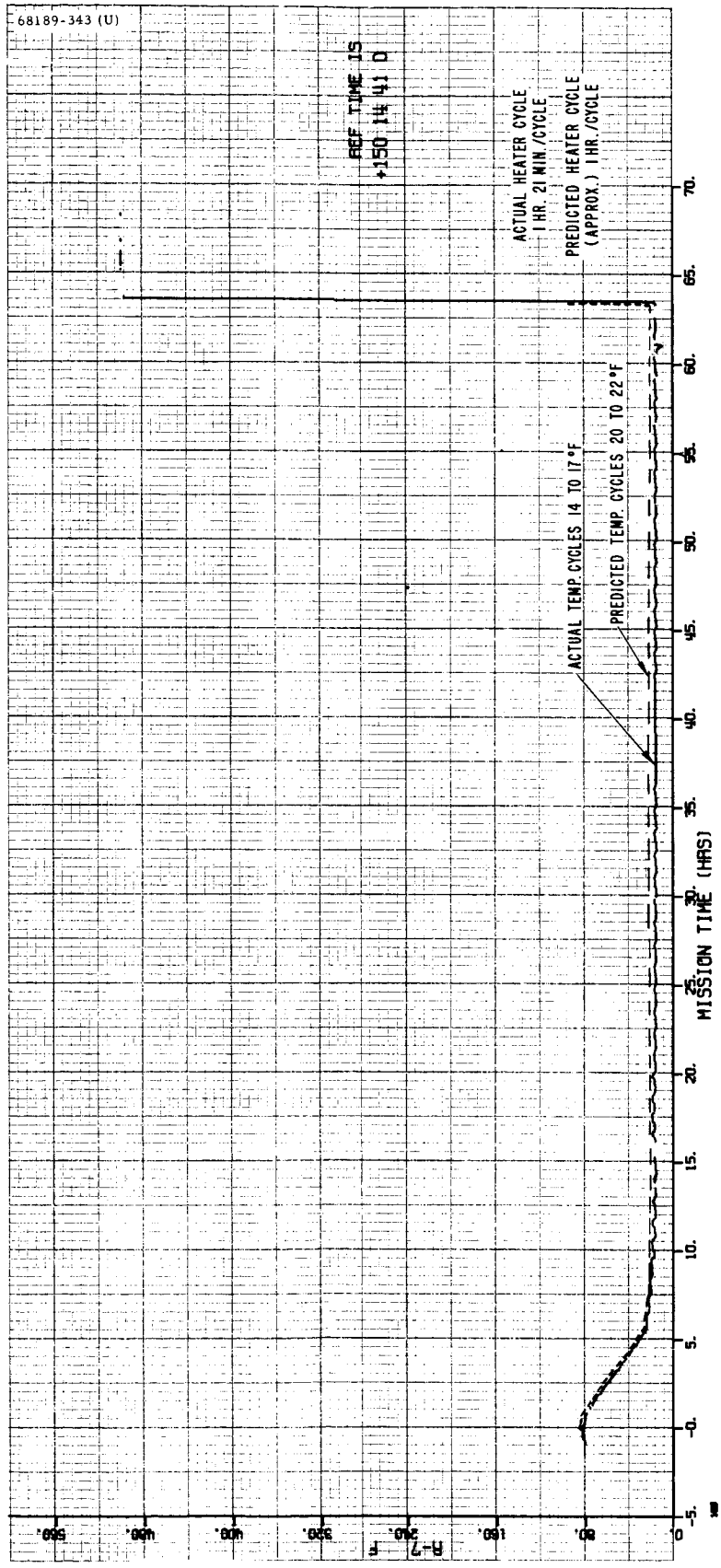


Figure A-31. AMR ECU Heat Sink

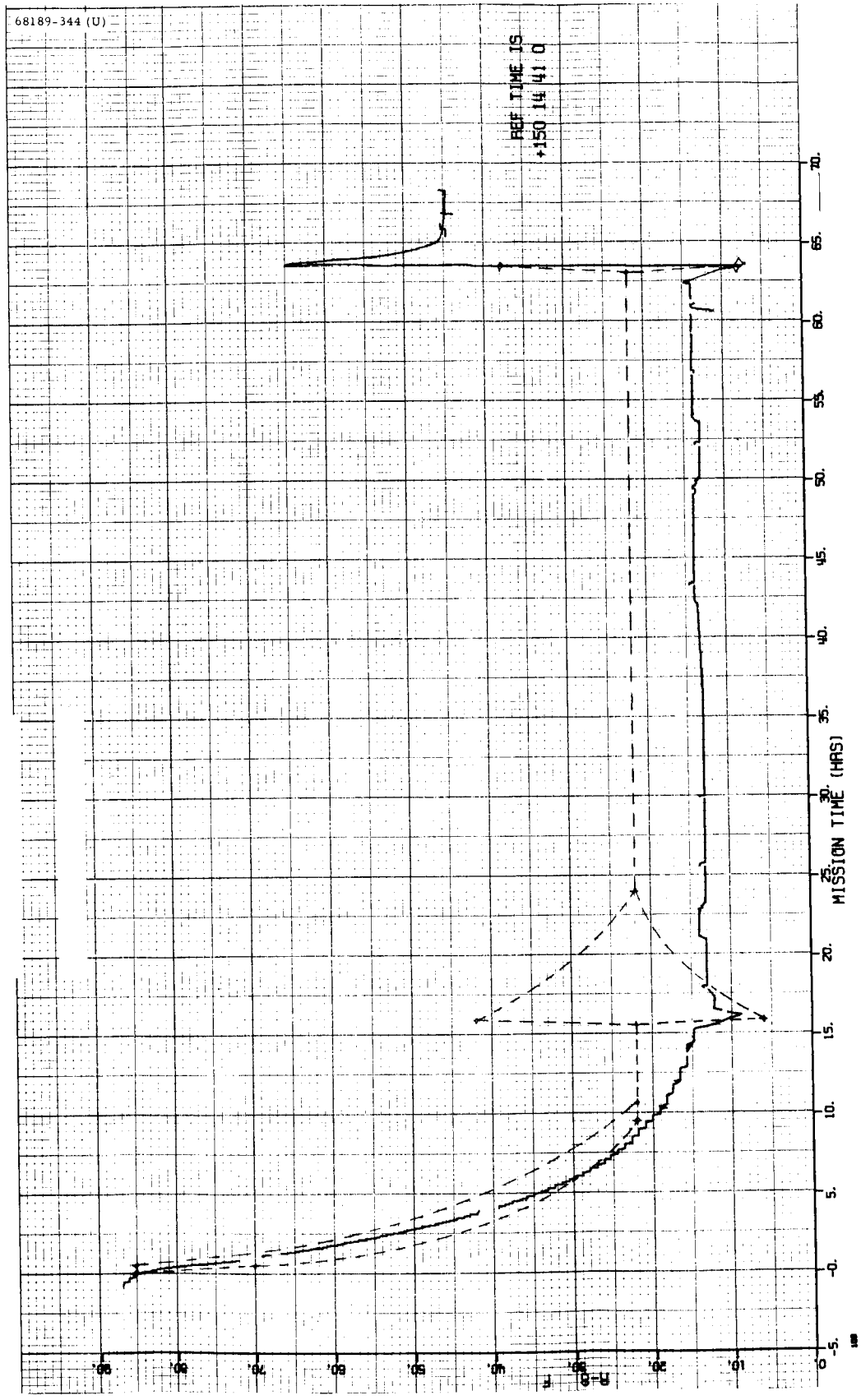


Figure A-32. RADVS Klystron Unit

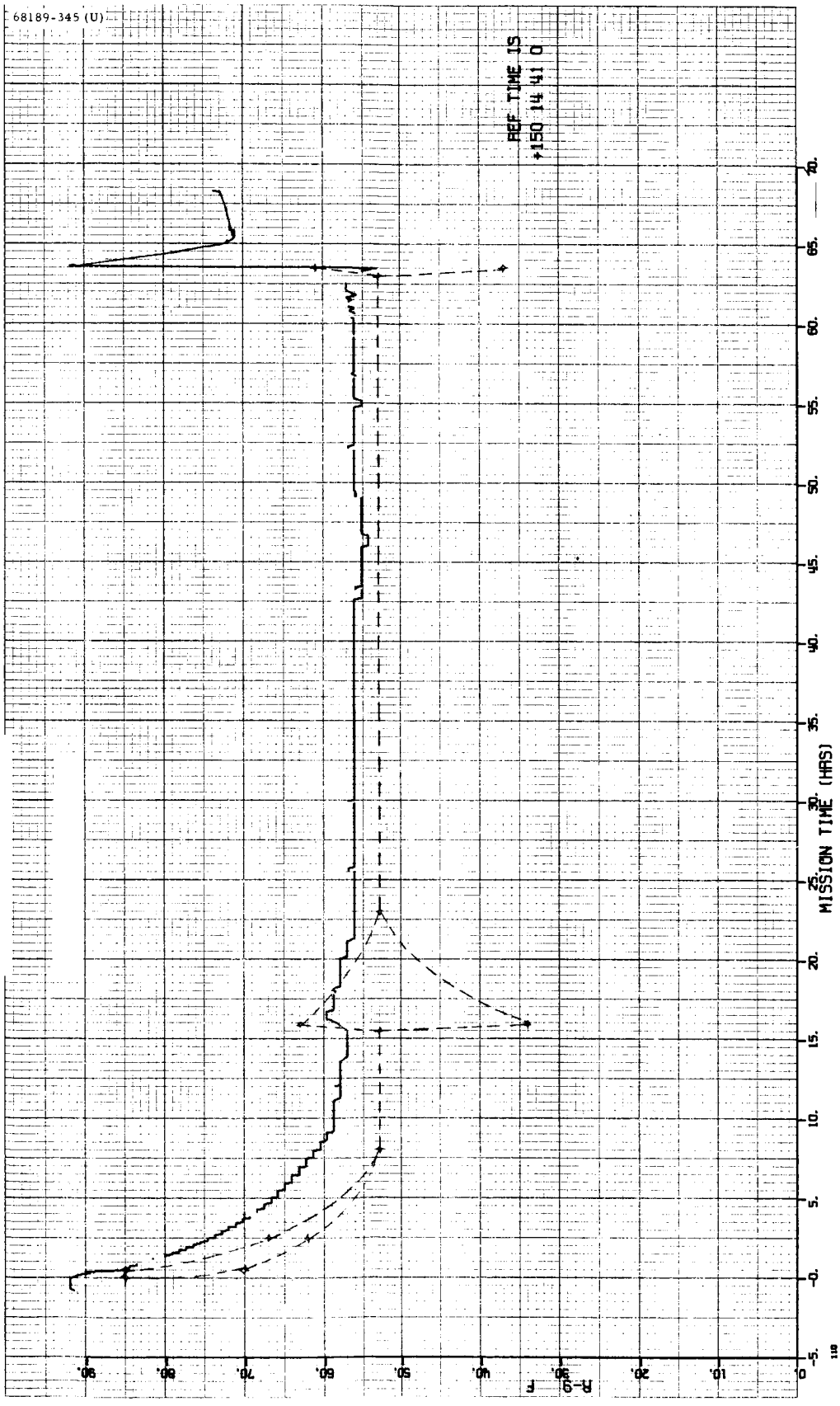


Figure A-33. RADVS Signal Data Converter

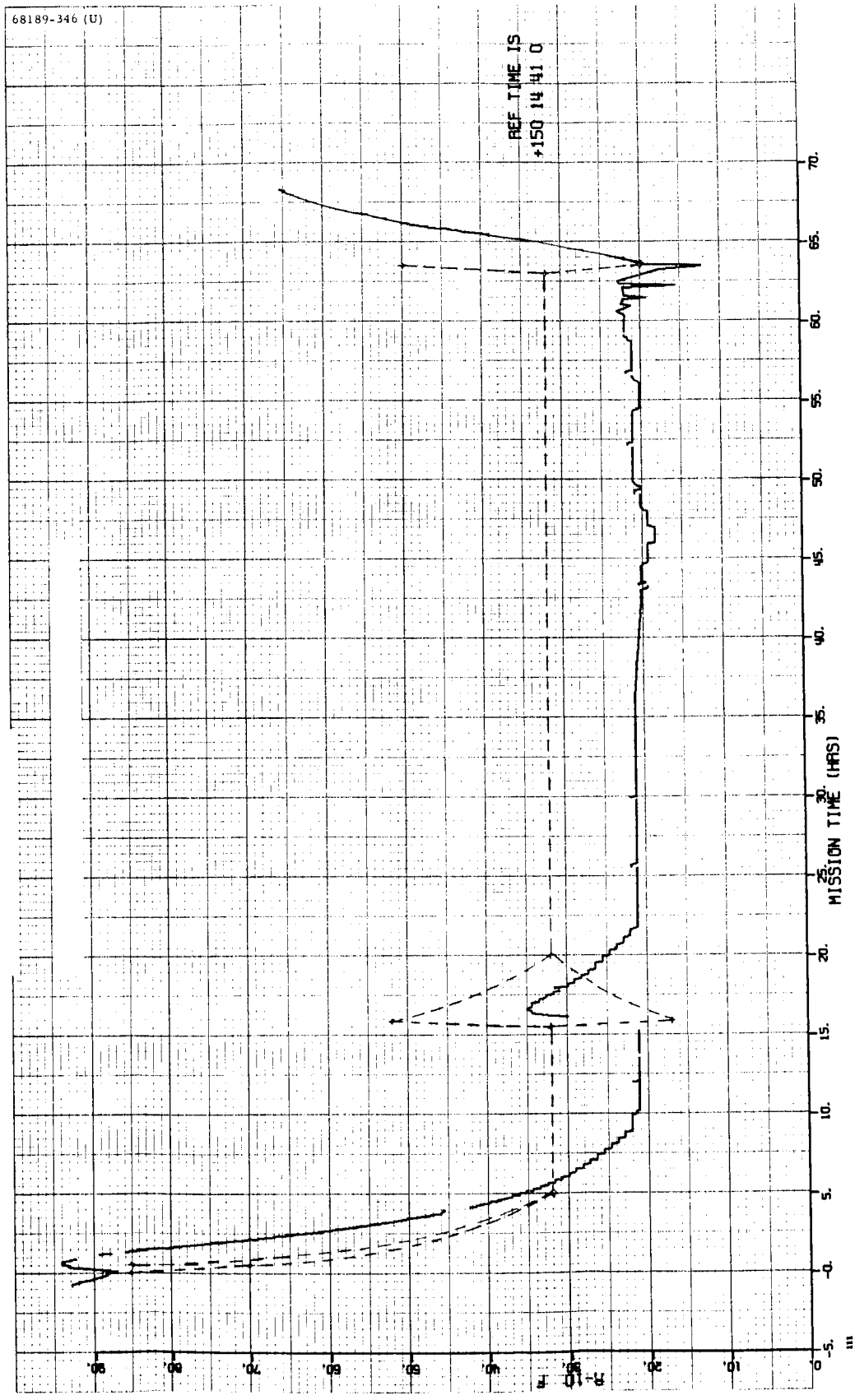


Figure A-34. RADVS Velocity Sensor Antenna Preamplifier

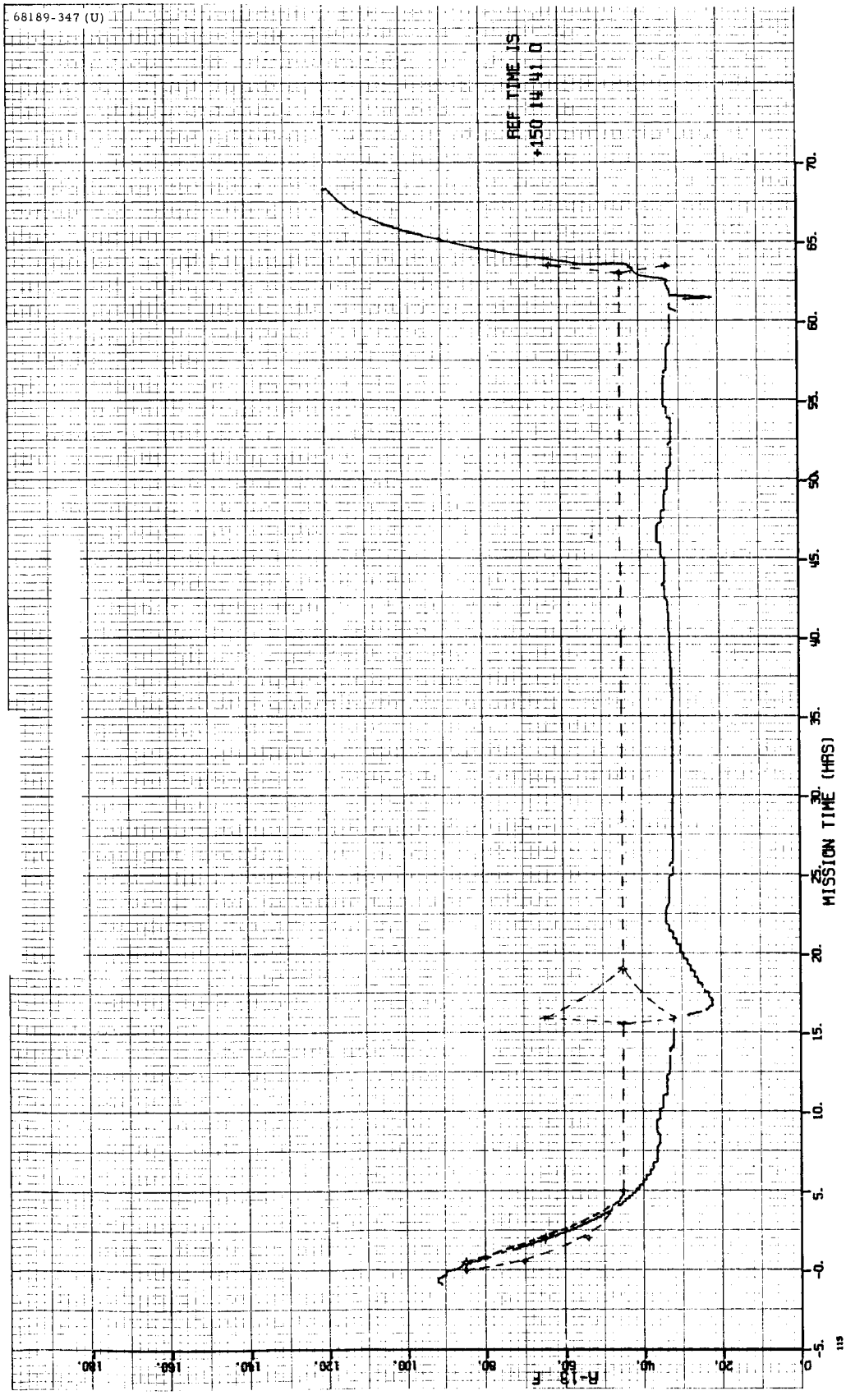


Figure A-35. Altimeter Radar Sensor Temperature (R-13)

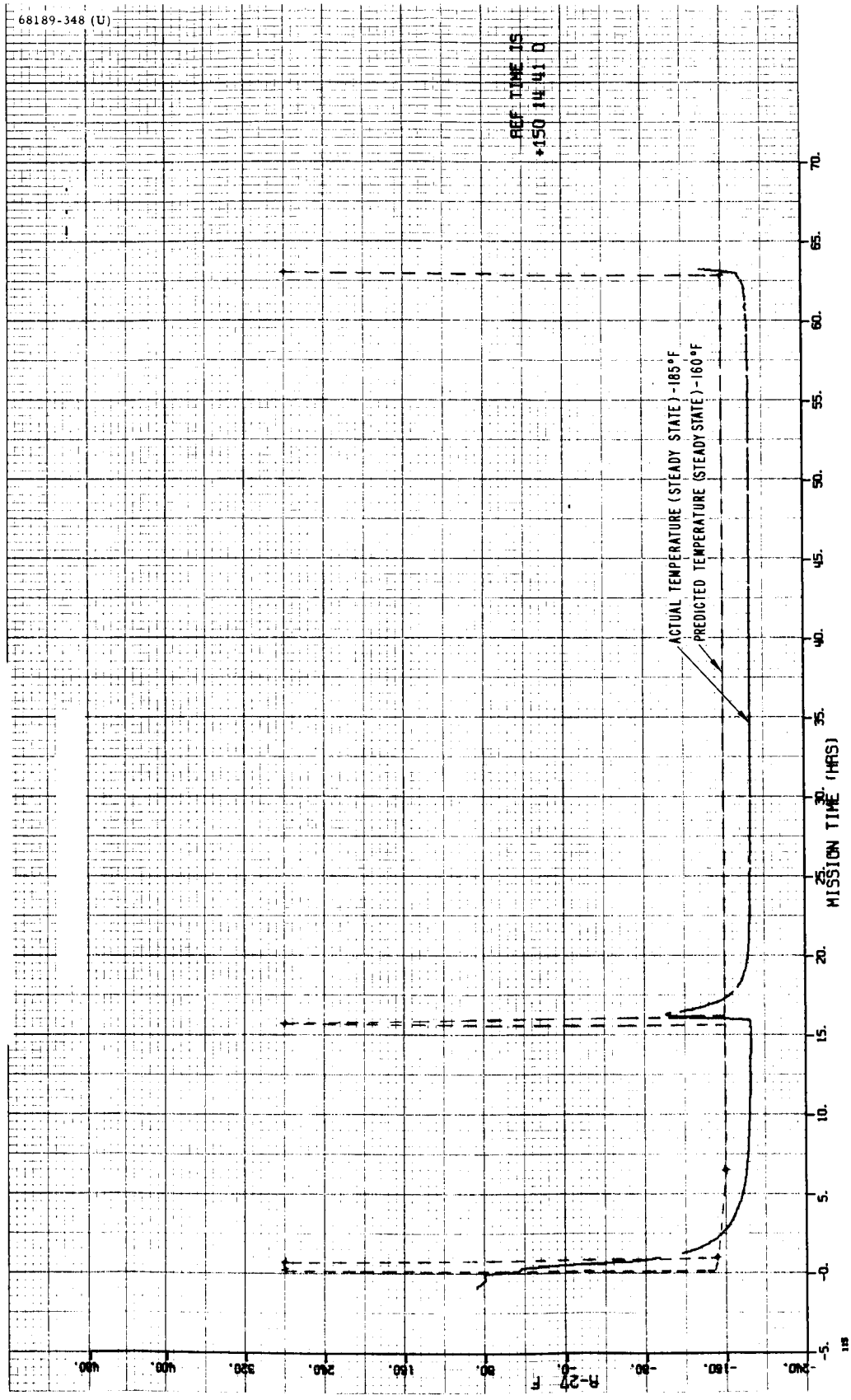
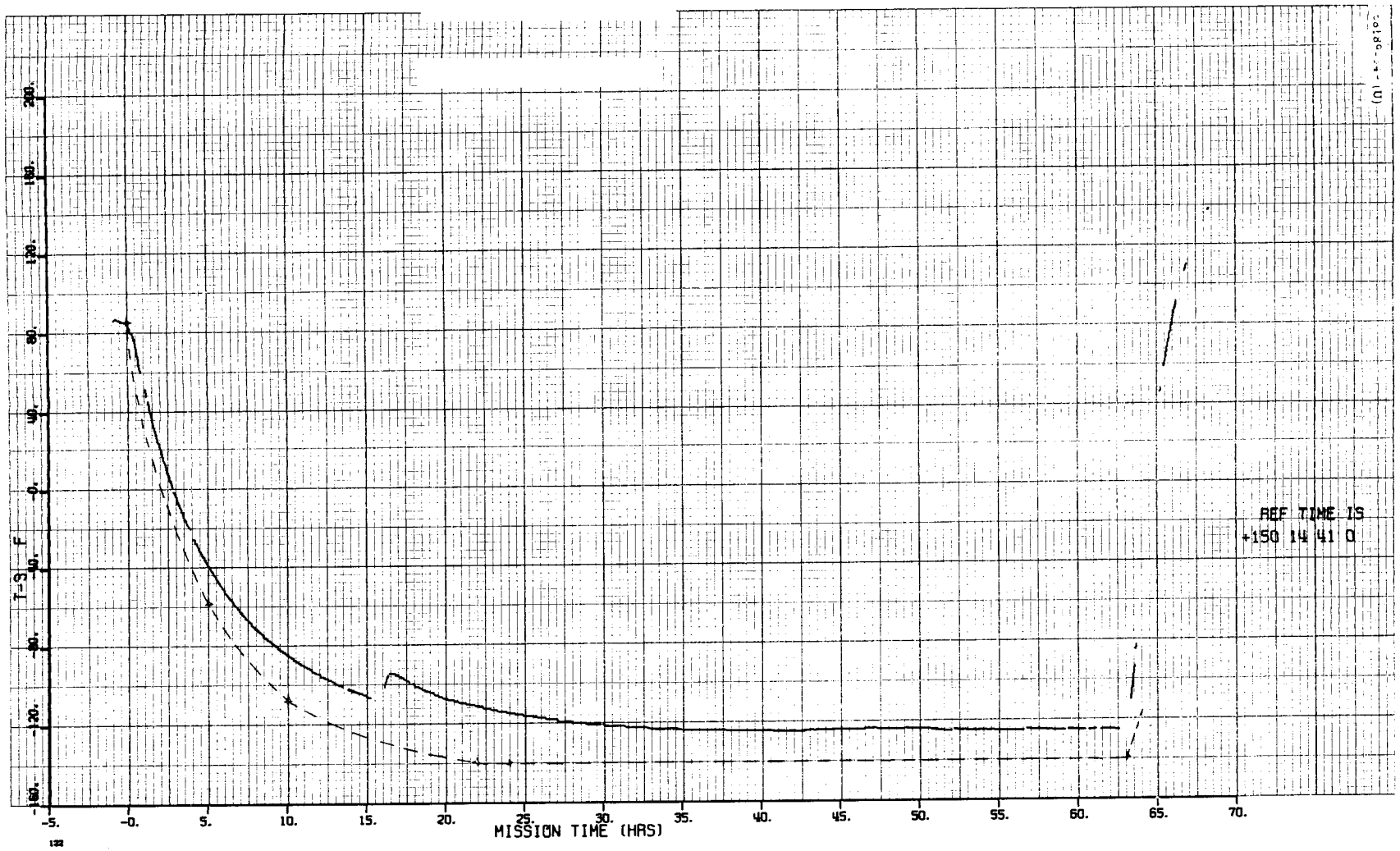
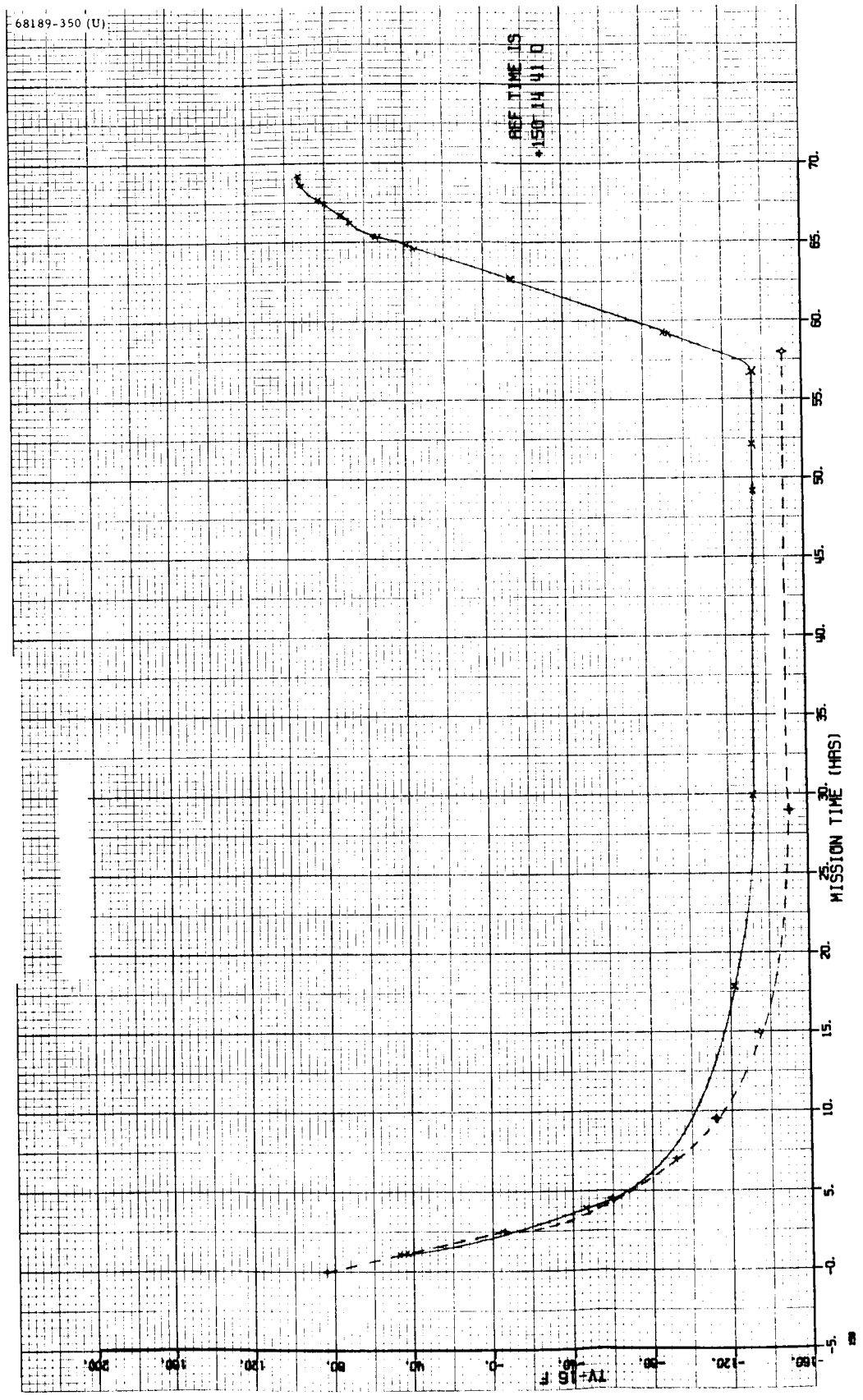


Figure A-36. AMR Edge of Antenna Dish



a) Approach

Figure A-37. TV Camera Electronics



b) Survey

Figure A-37 (continued). TV Camera Electronics

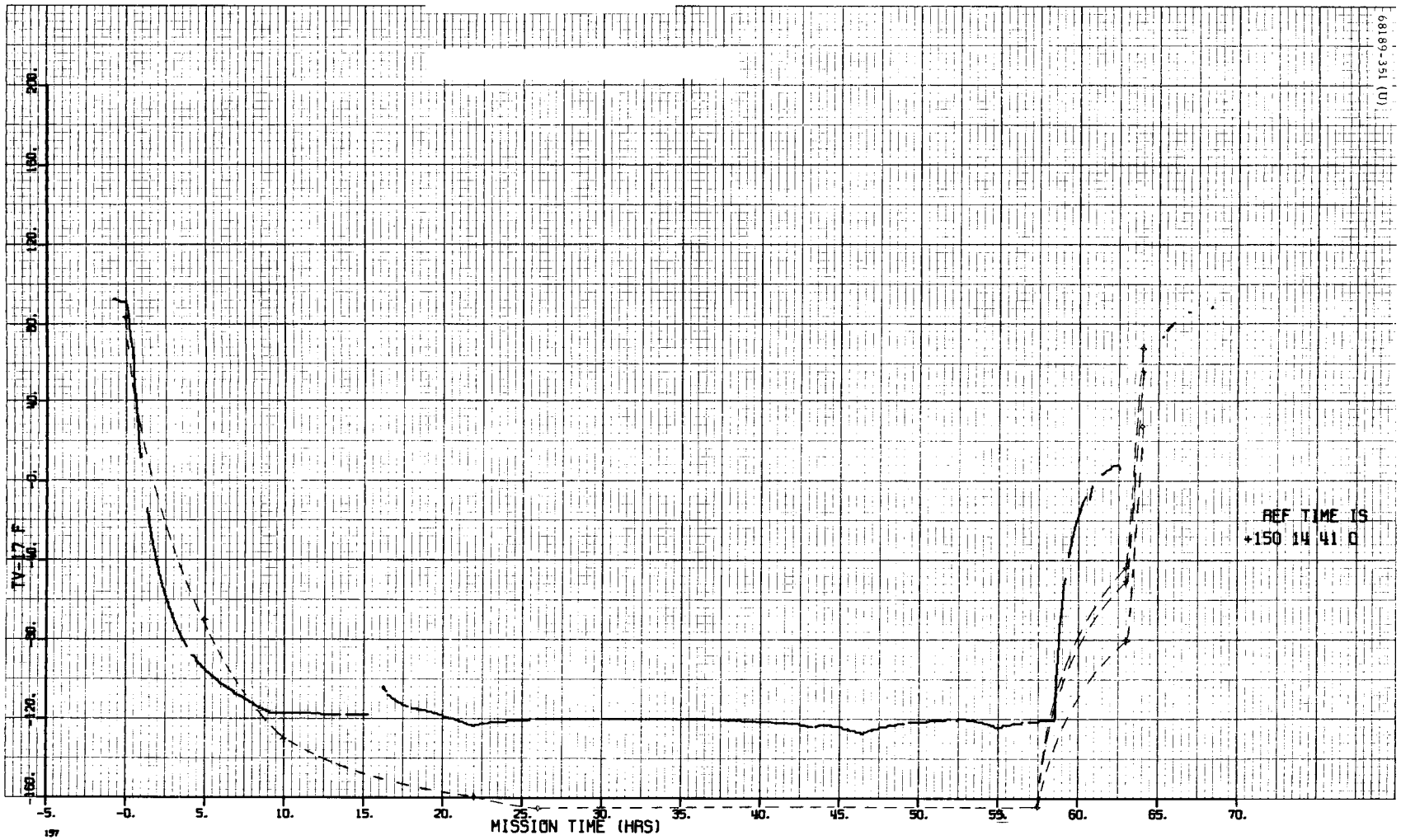


Figure A-38. Survey TV Hood and Mirror Assembly

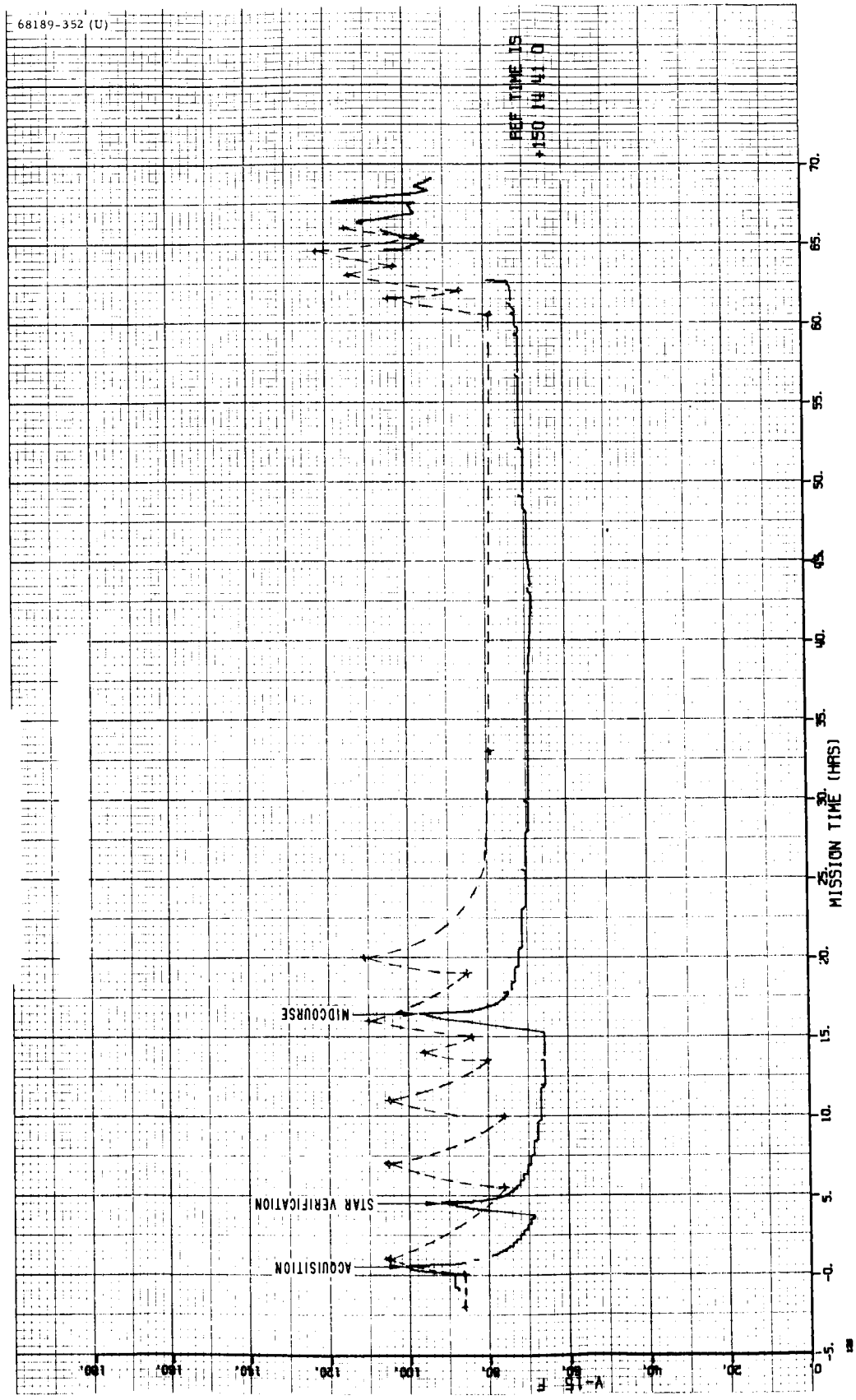


Figure A-39. Compartment A Thermal Tray Top

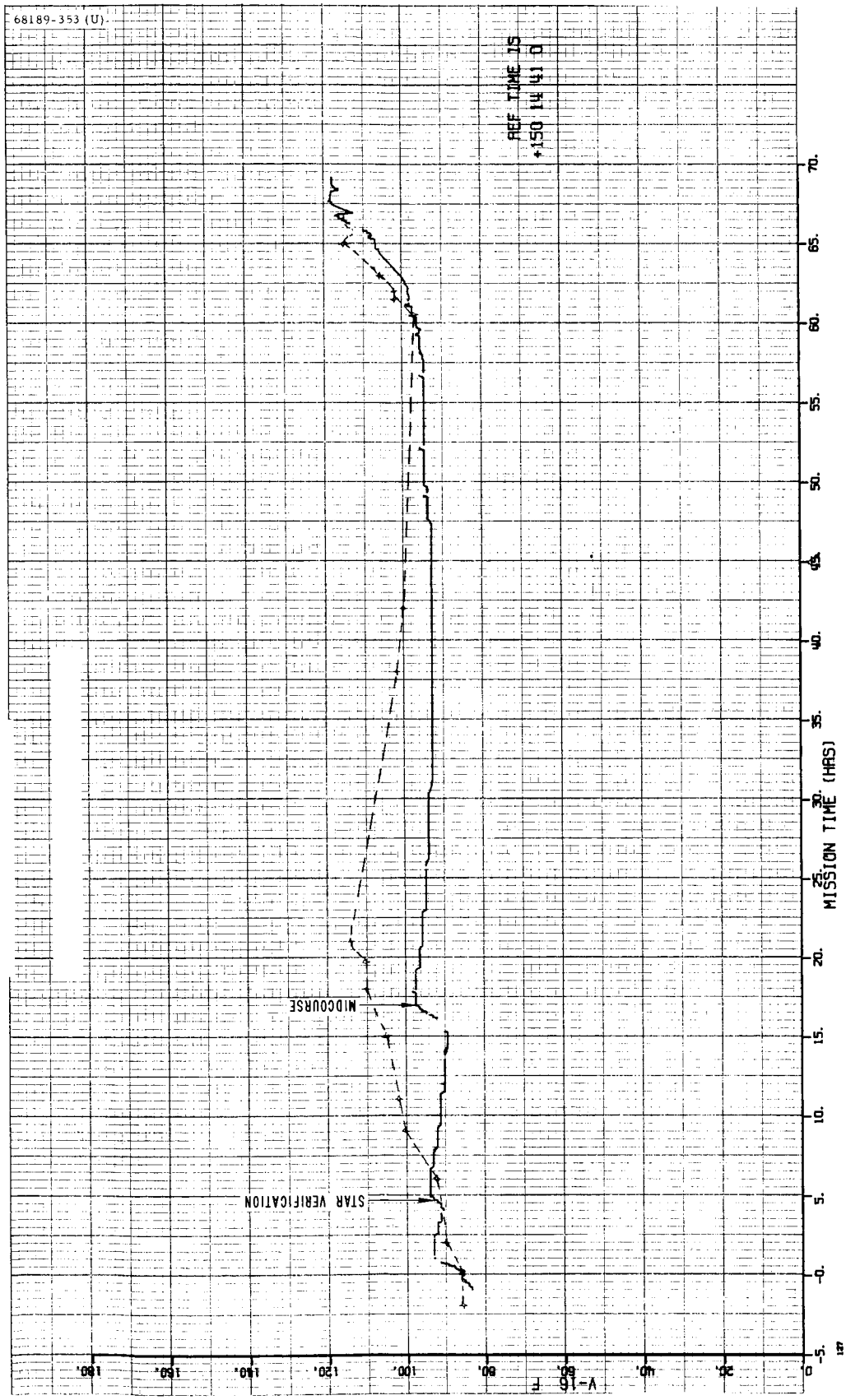


Figure A-40. Compartment A Lower Support

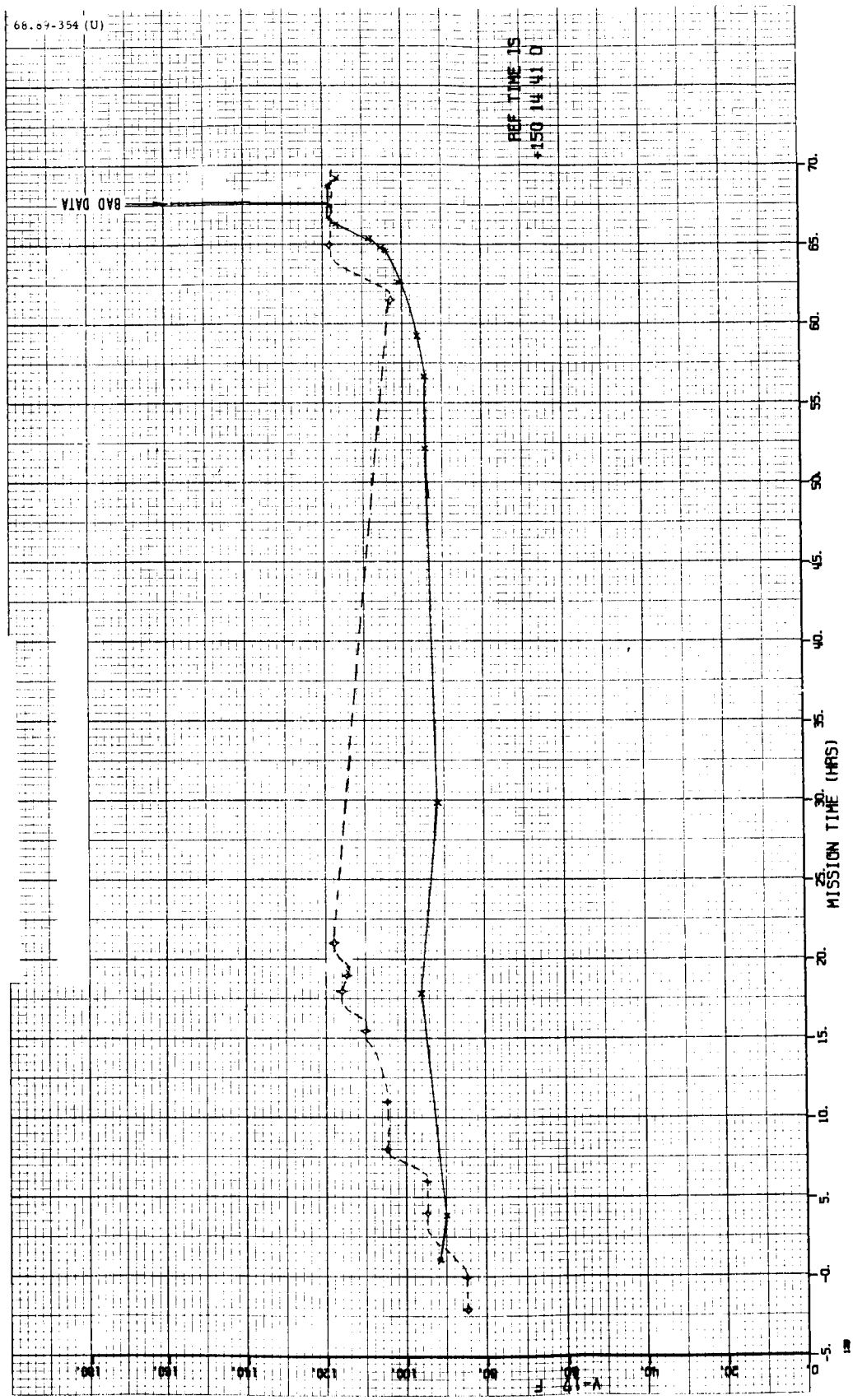


Figure A-41. Compartment A Insulation Retainer

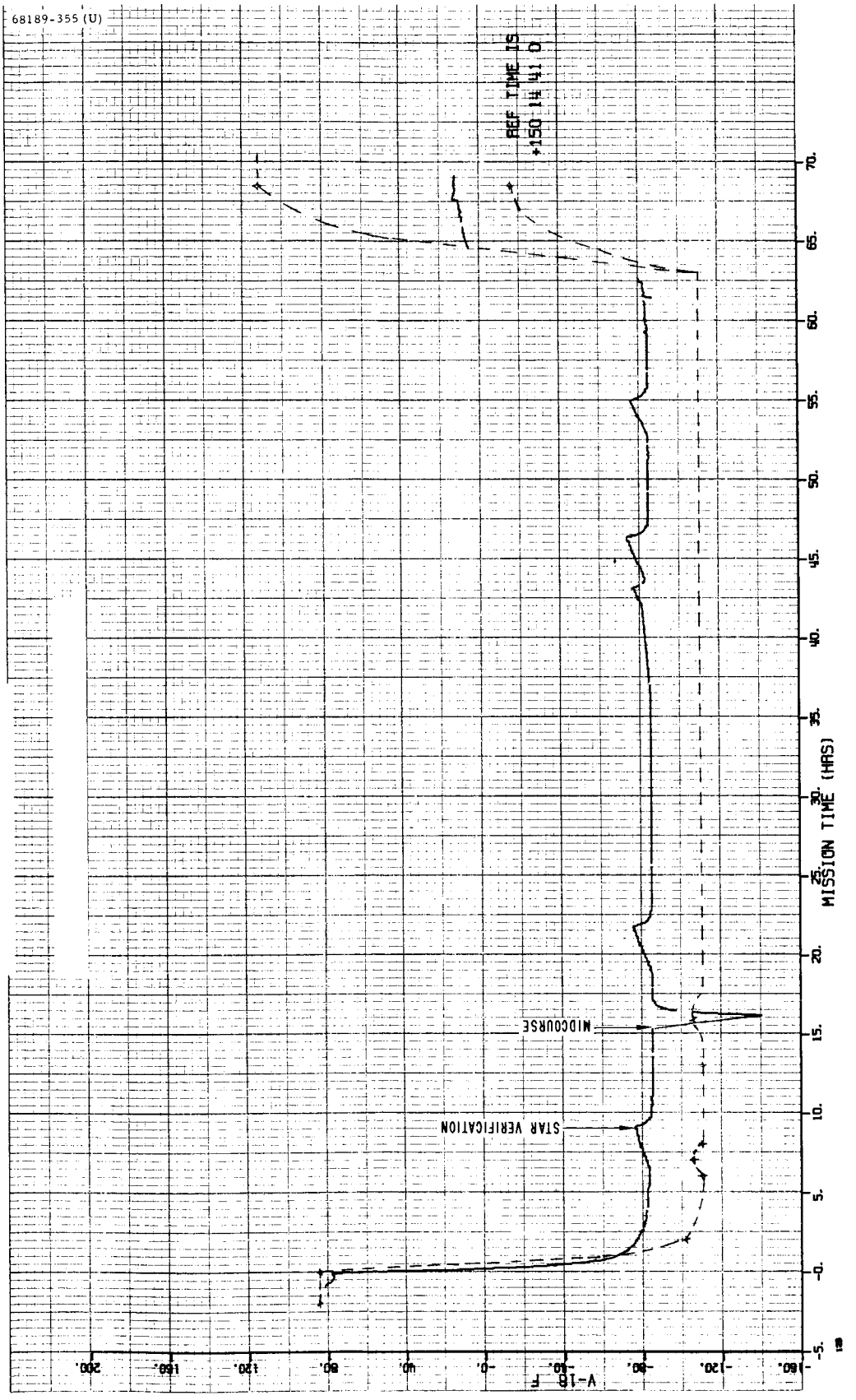
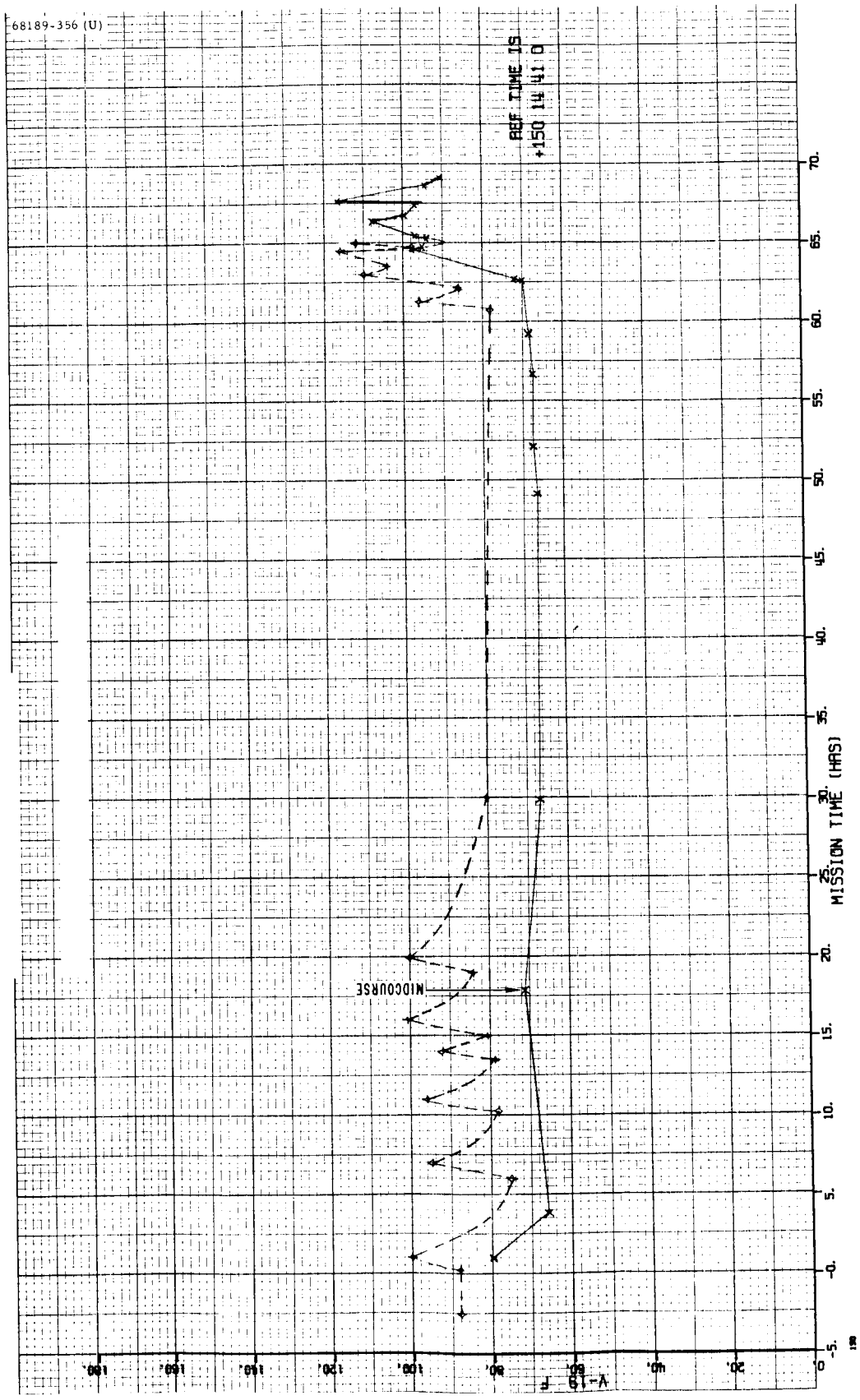
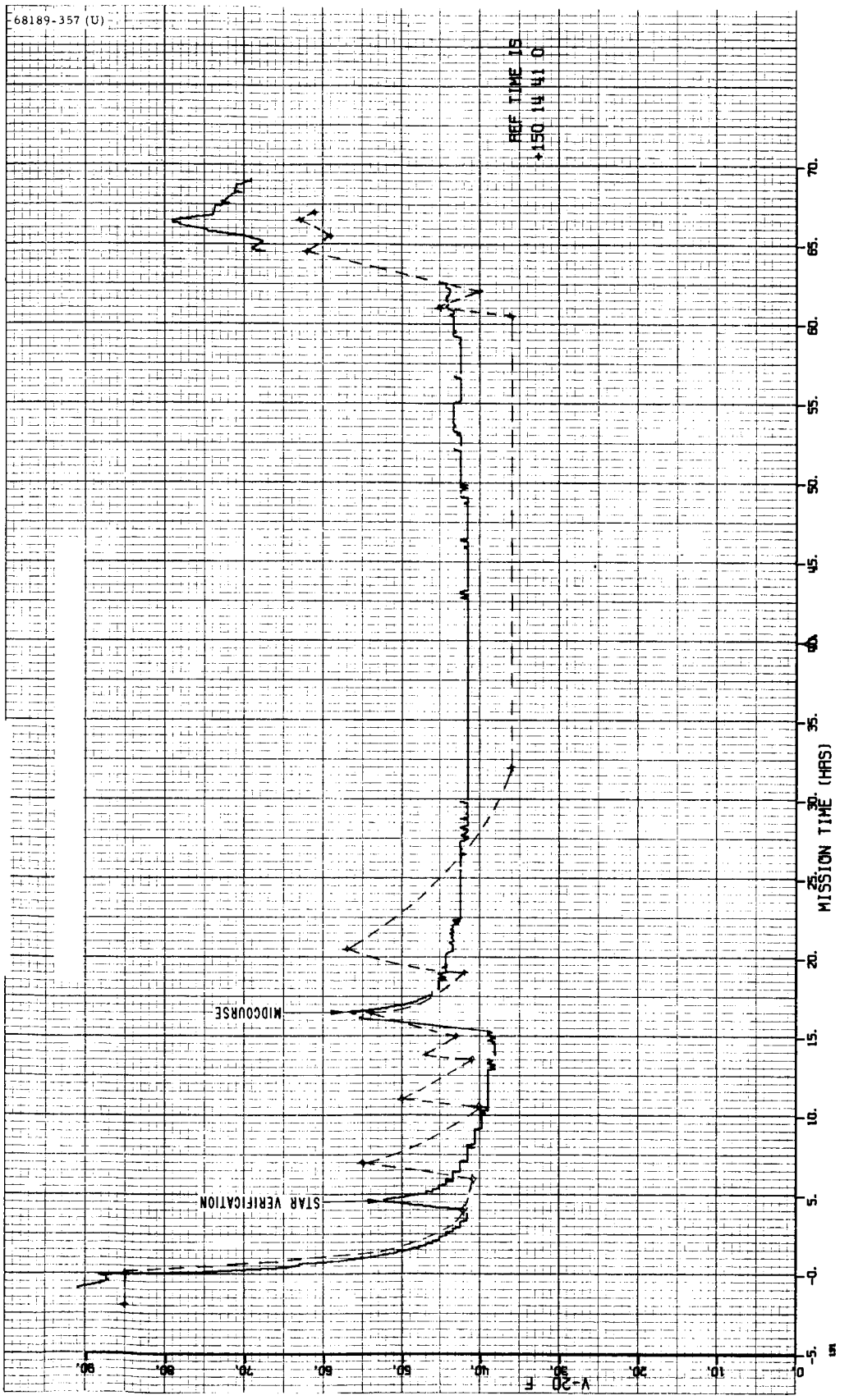


Figure A-42. Compartment A External Canister



a) Contact Ring

Figure A-43. Compartment A Thermal Switch



b) Radiator

Figure A-43 (continued). Compartment A Thermal Switch

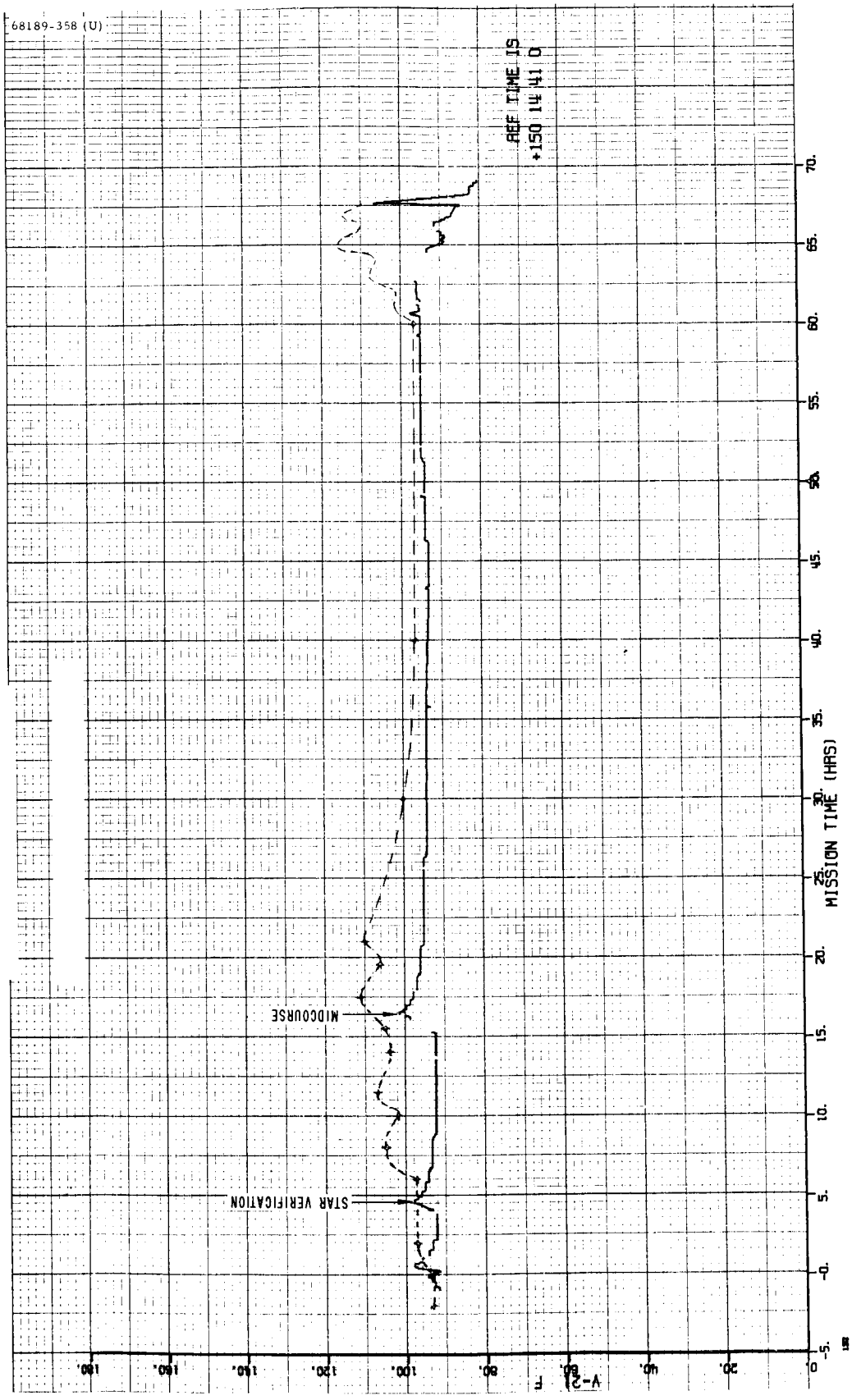


Figure A-44. Compartment A Thermal Tray – Top

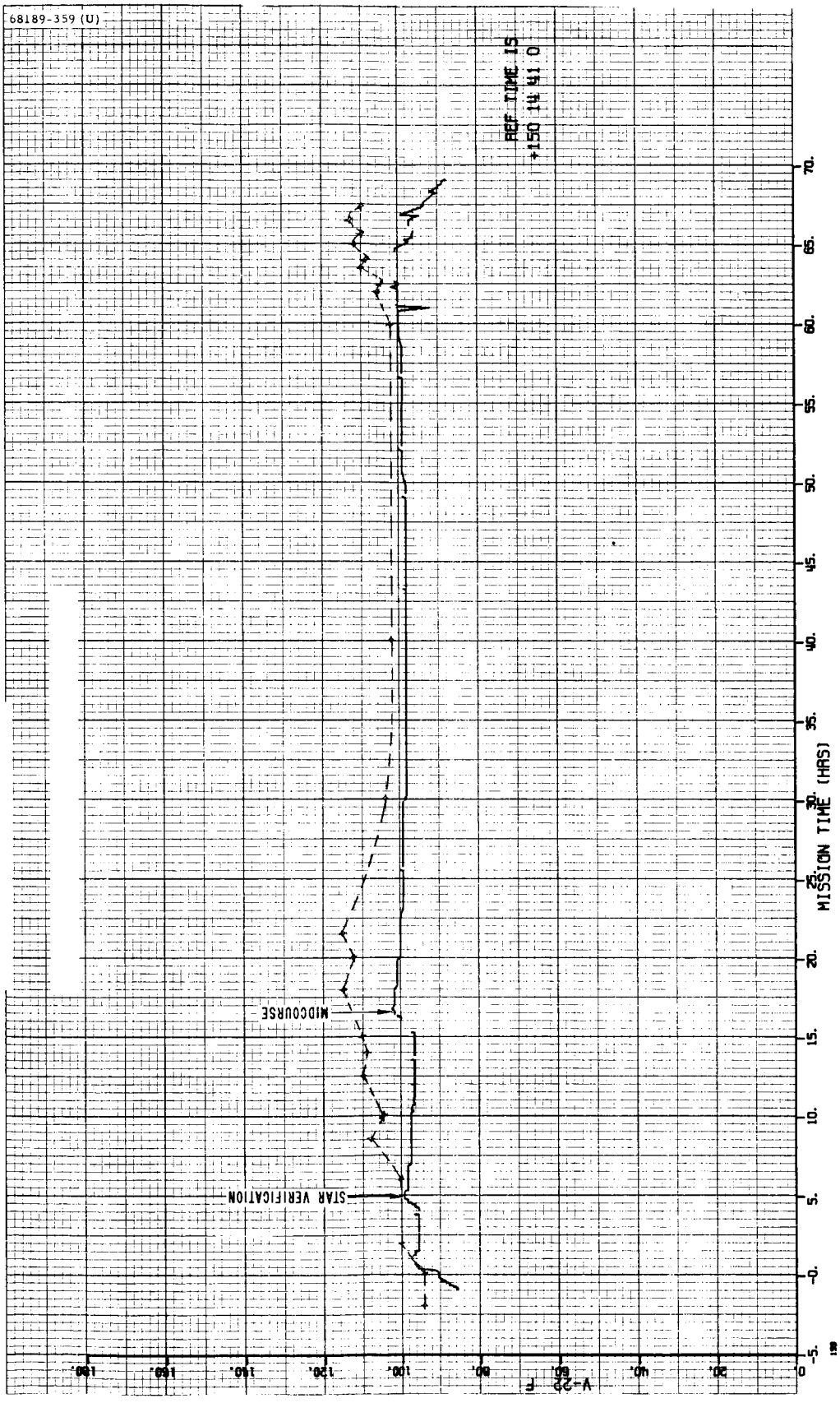


Figure A-45. Compartment B Lower Support

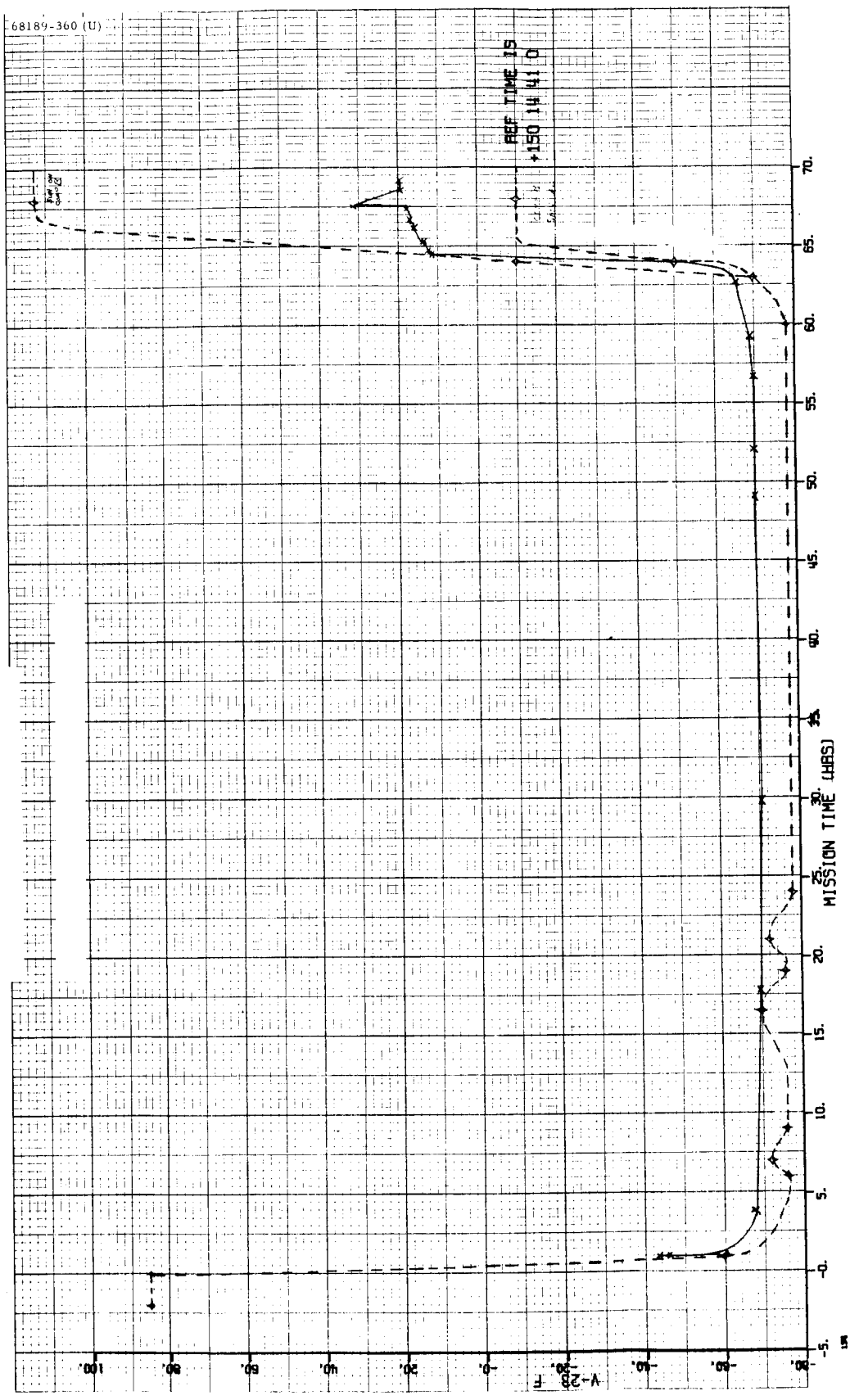


Figure A-46. Compartment B External Canister

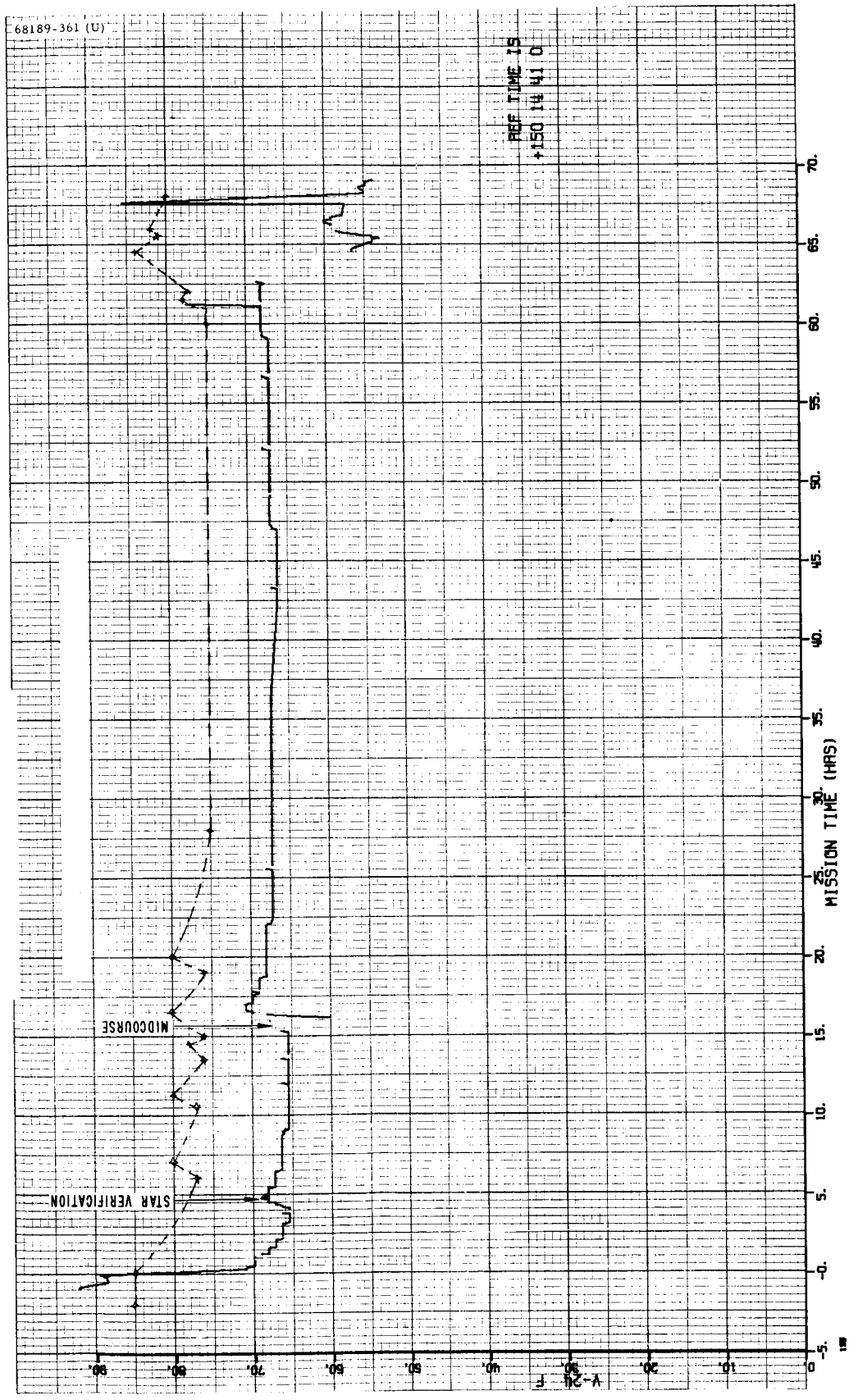


Figure A-47. Compartment B Thermal Switch 4 Radiator

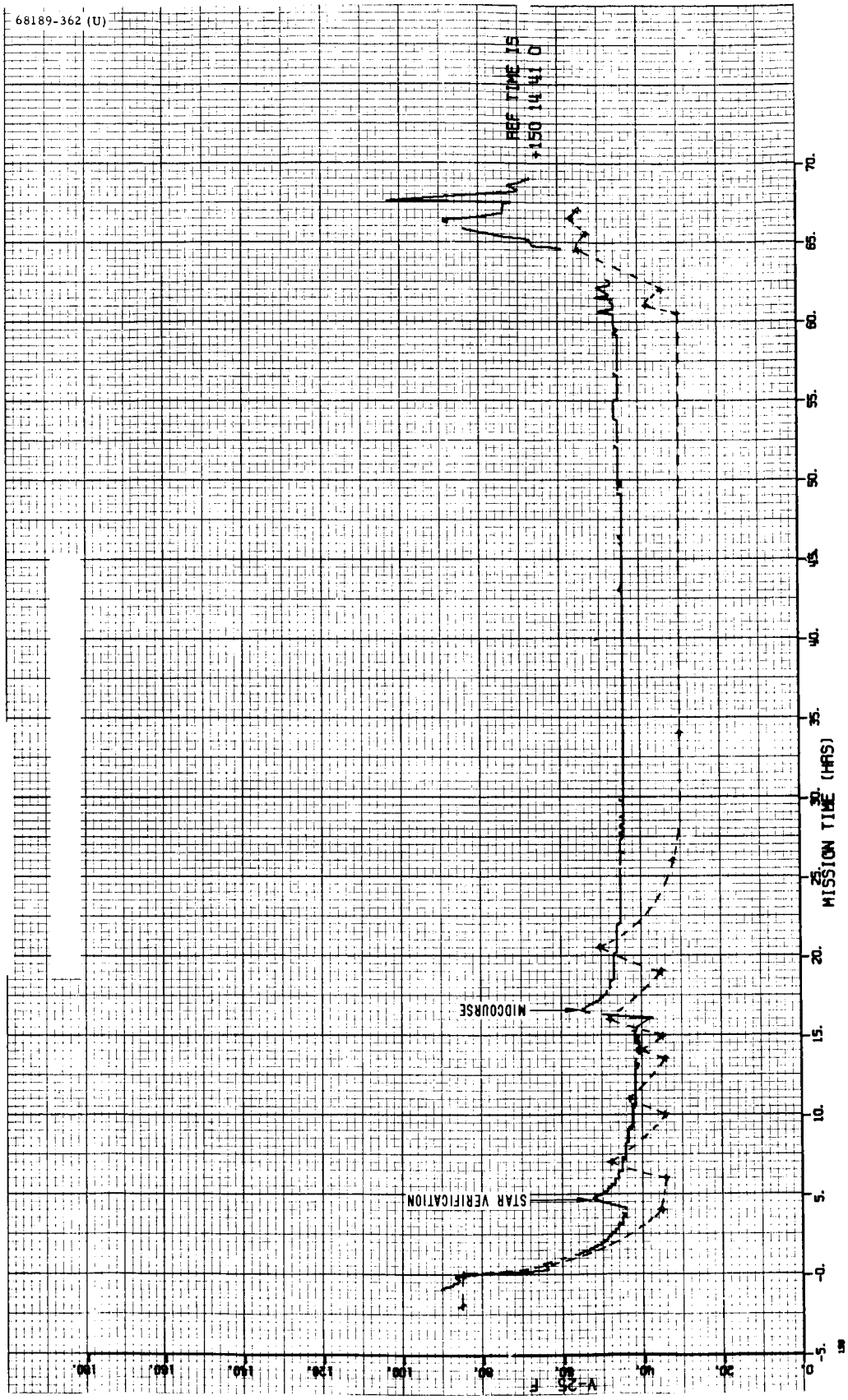


Figure A-48. Compartment A Thermal Switch 8 Radiator

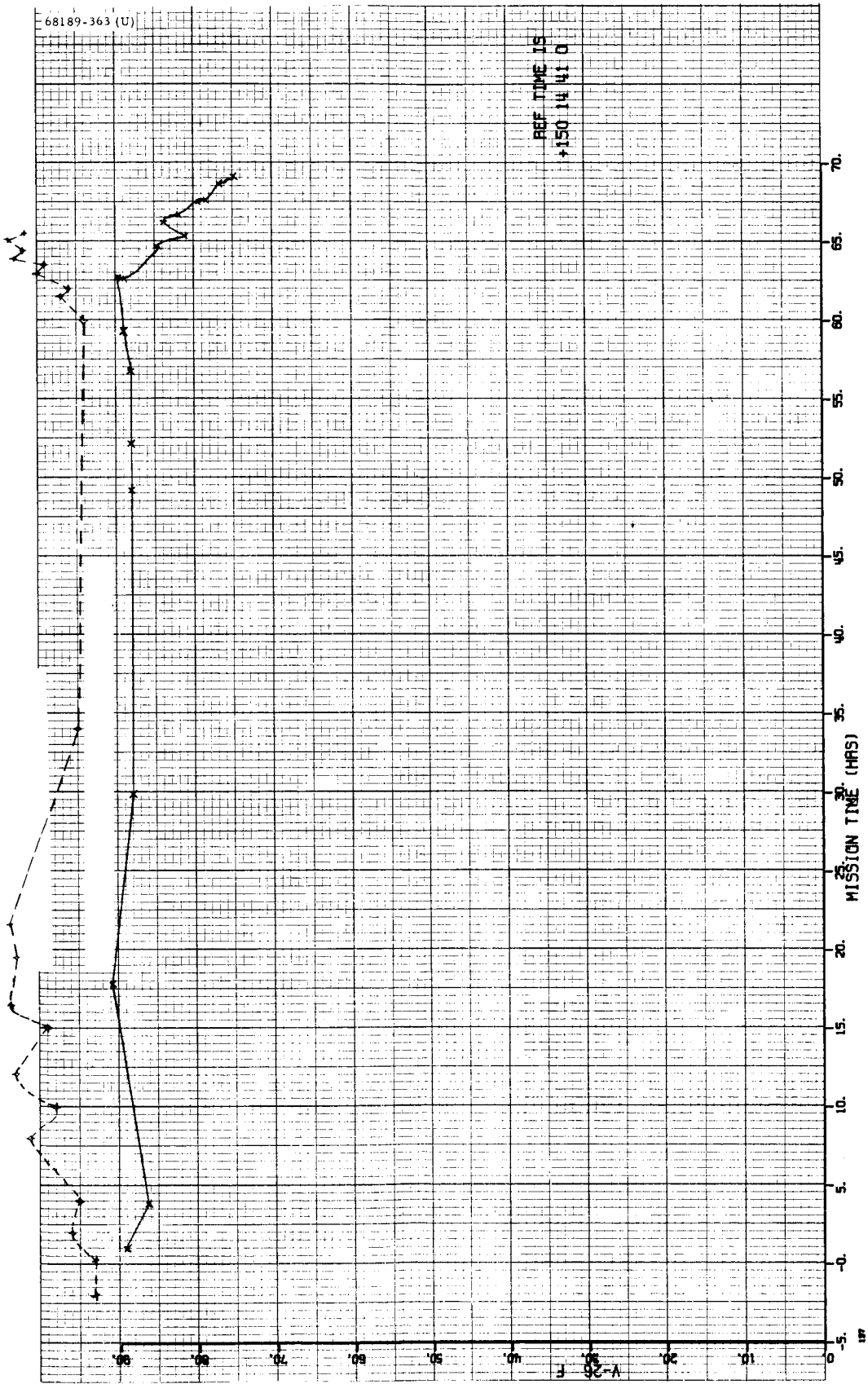


Figure A-49. Compartment B Thermal Switch 4 Contact Ring

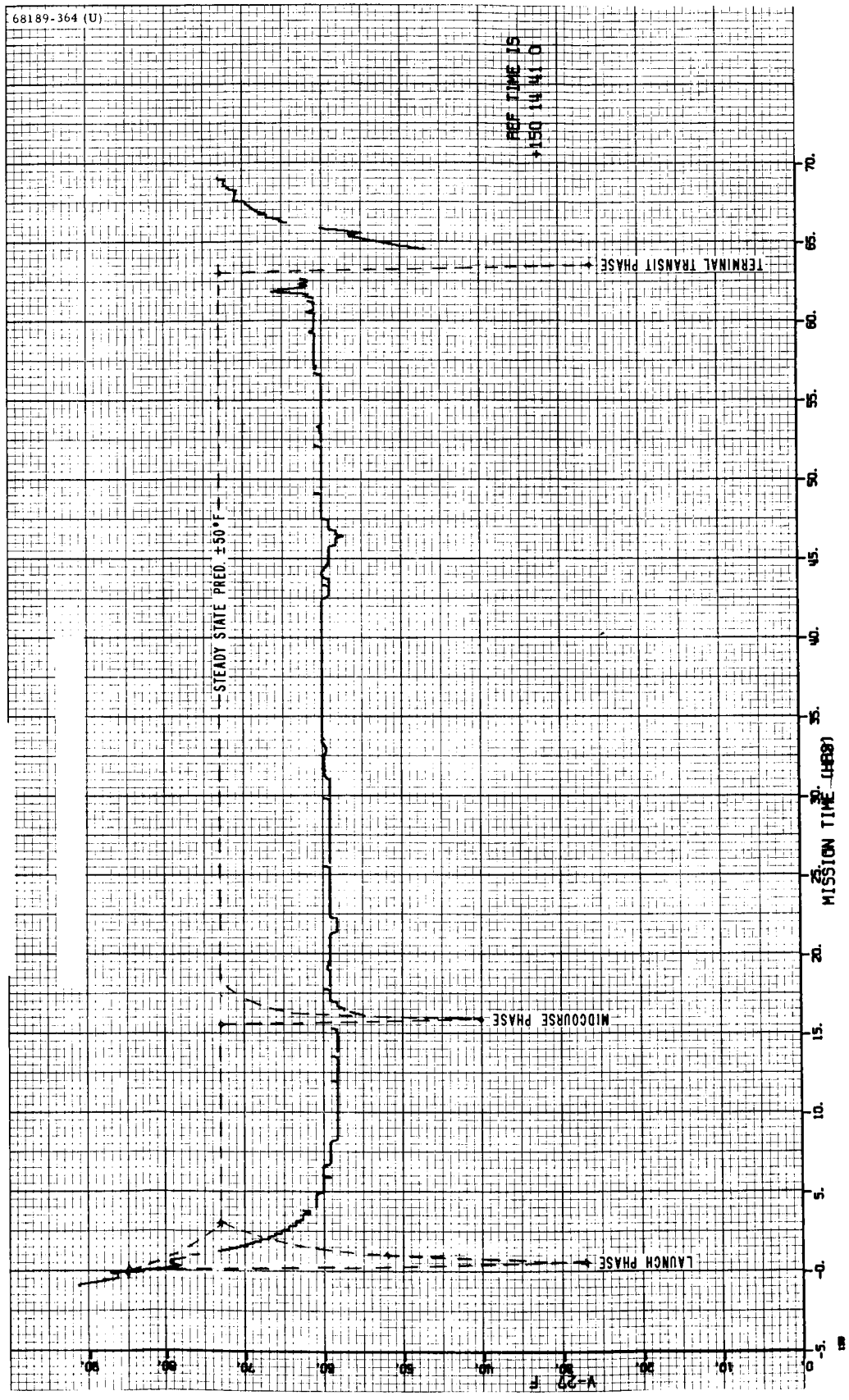


Figure A-50. Upper Spaceframe
Near leg 1

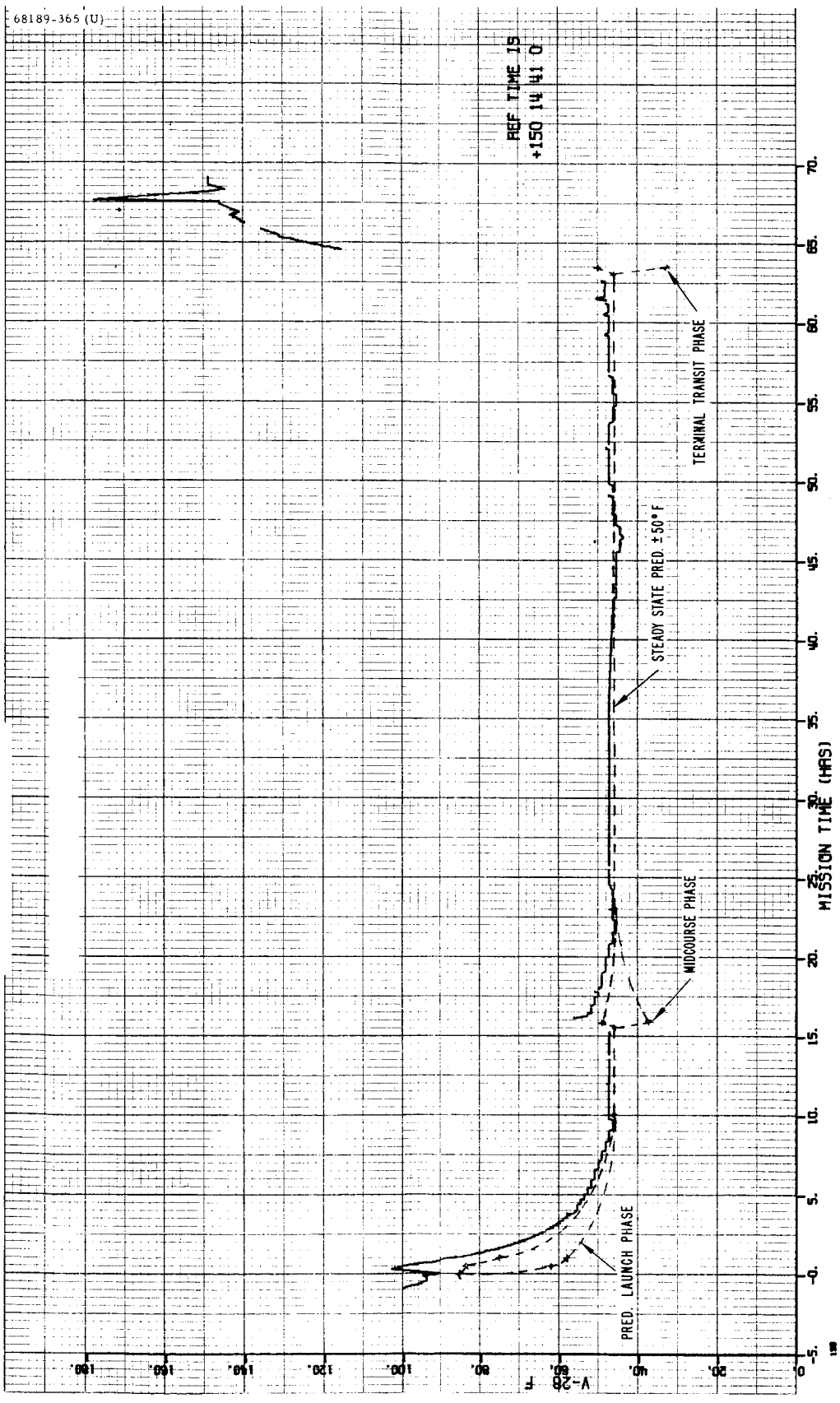


Figure A-51. Lower Spaceframe
Under compartment B

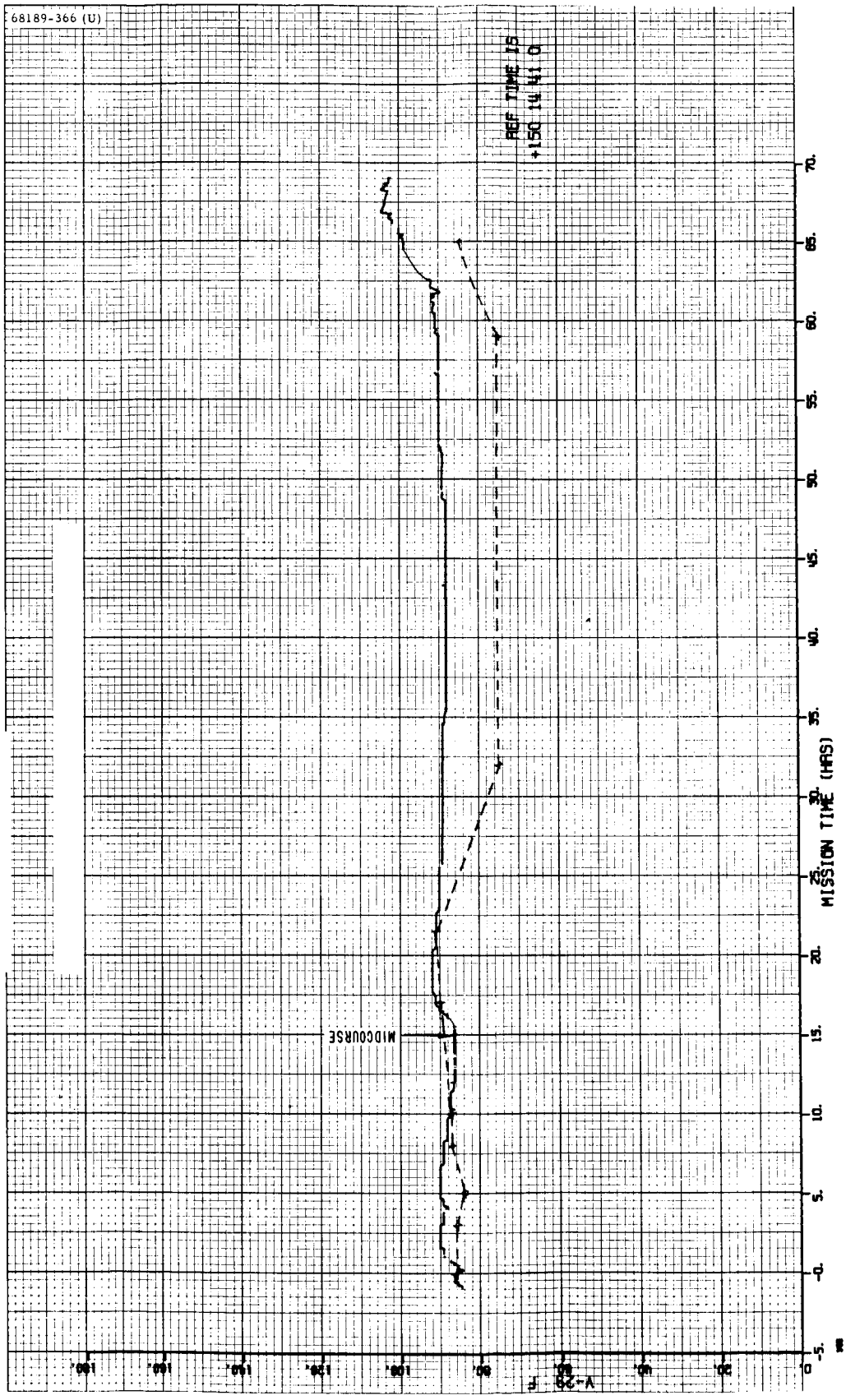


Figure A-52. Thermal Tunnel

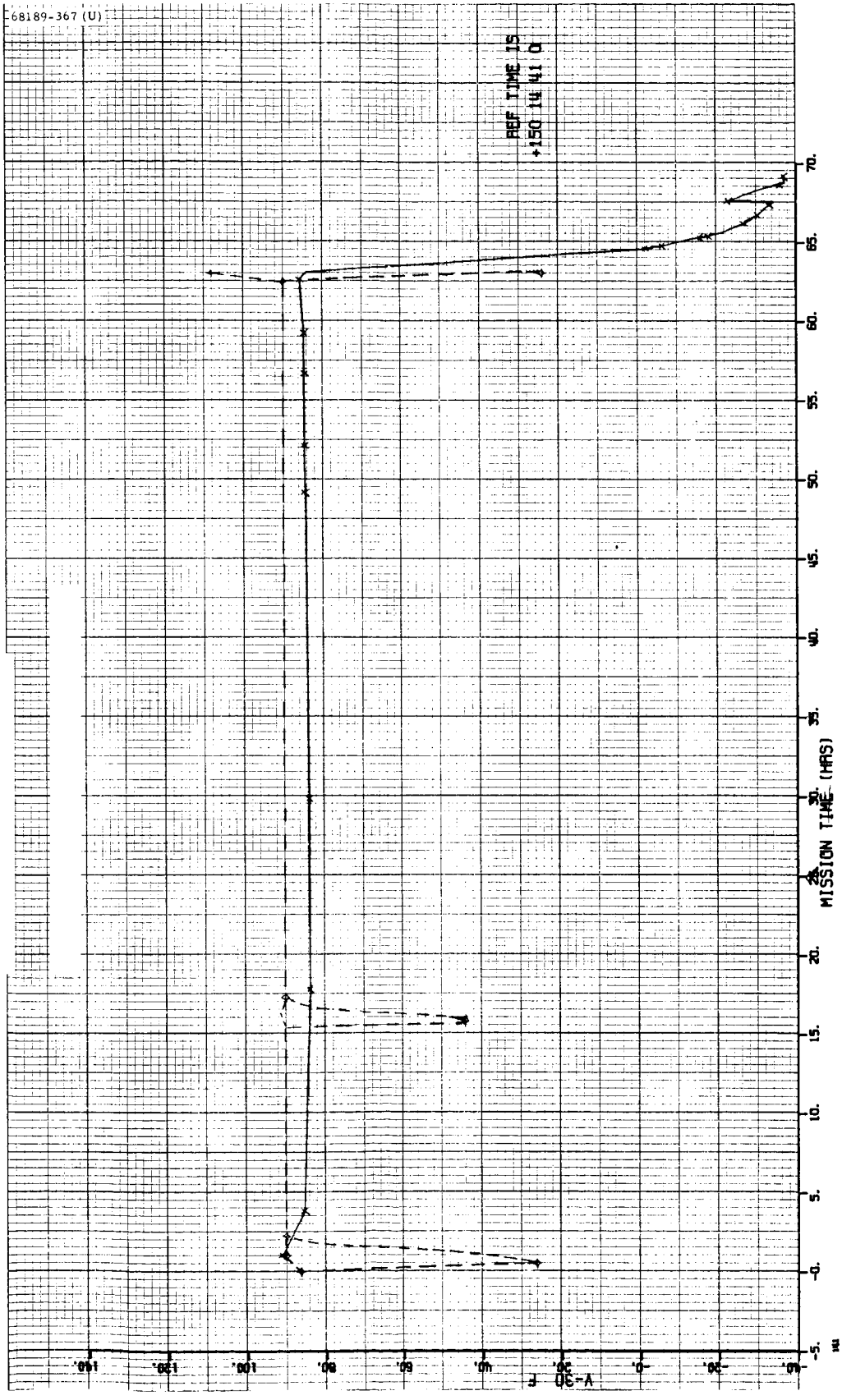


Figure A-53. Shock Absorber 1

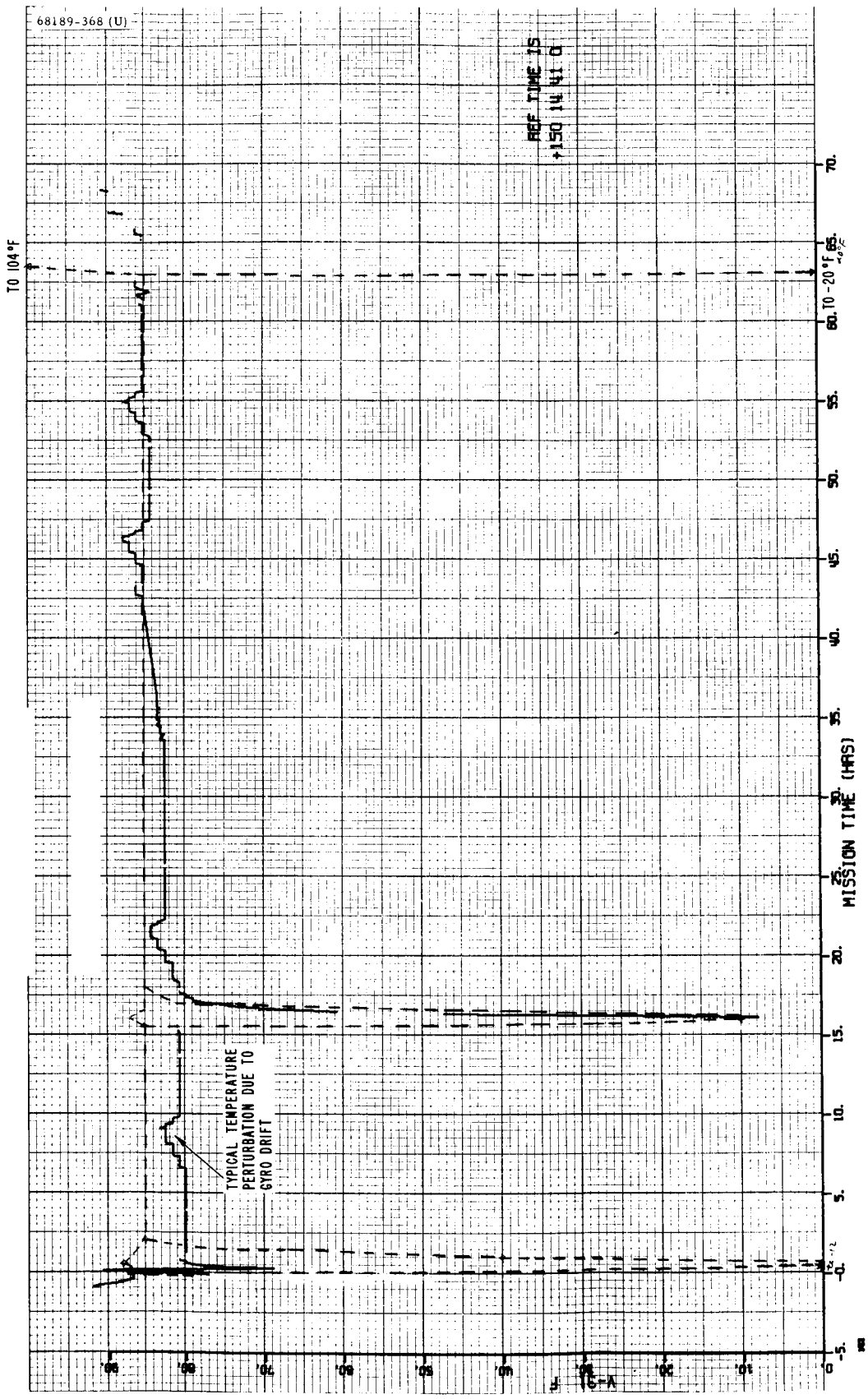


Figure A-54. Leg 2 — Upper Web

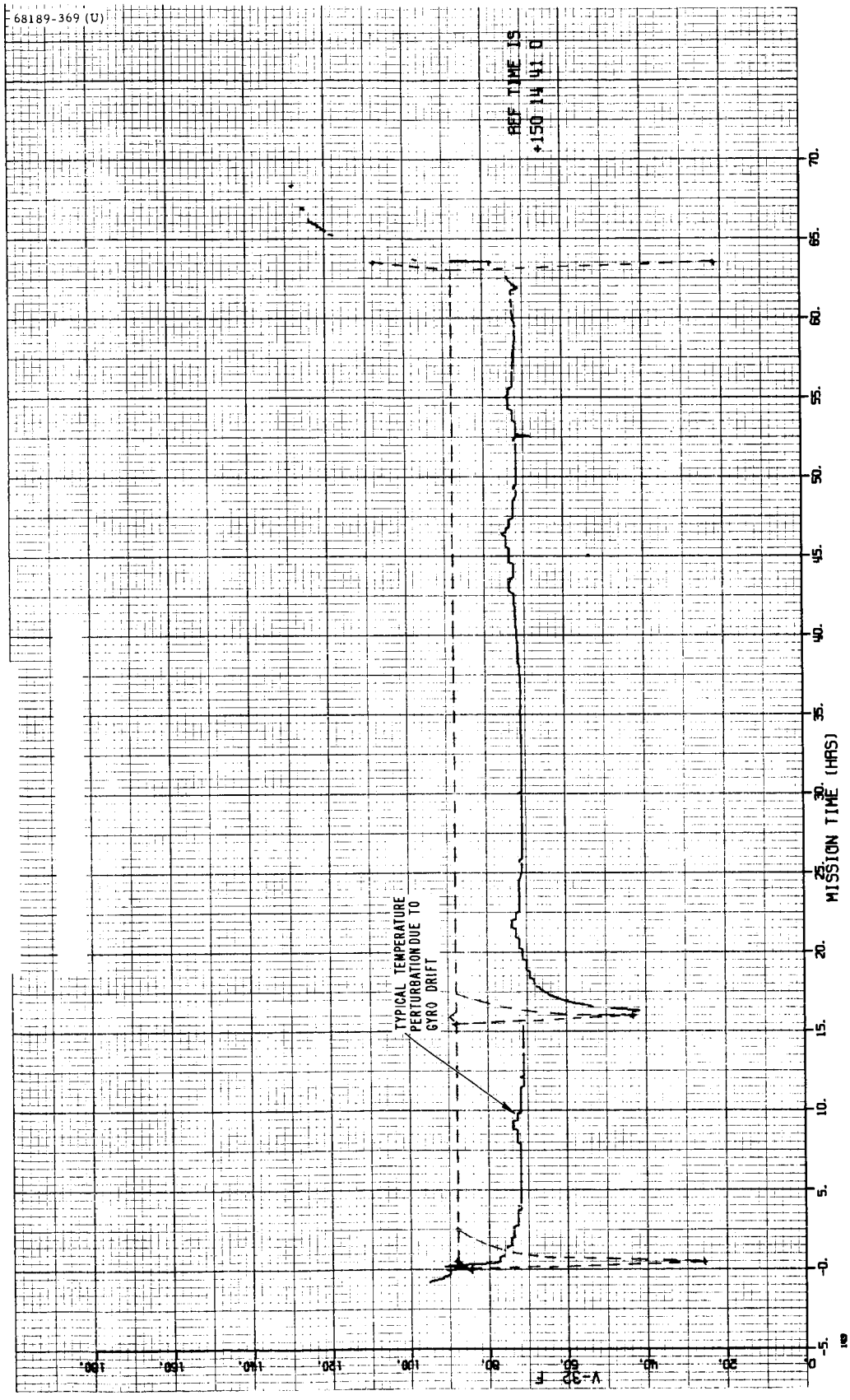


Figure A-55. Shock Absorber 2

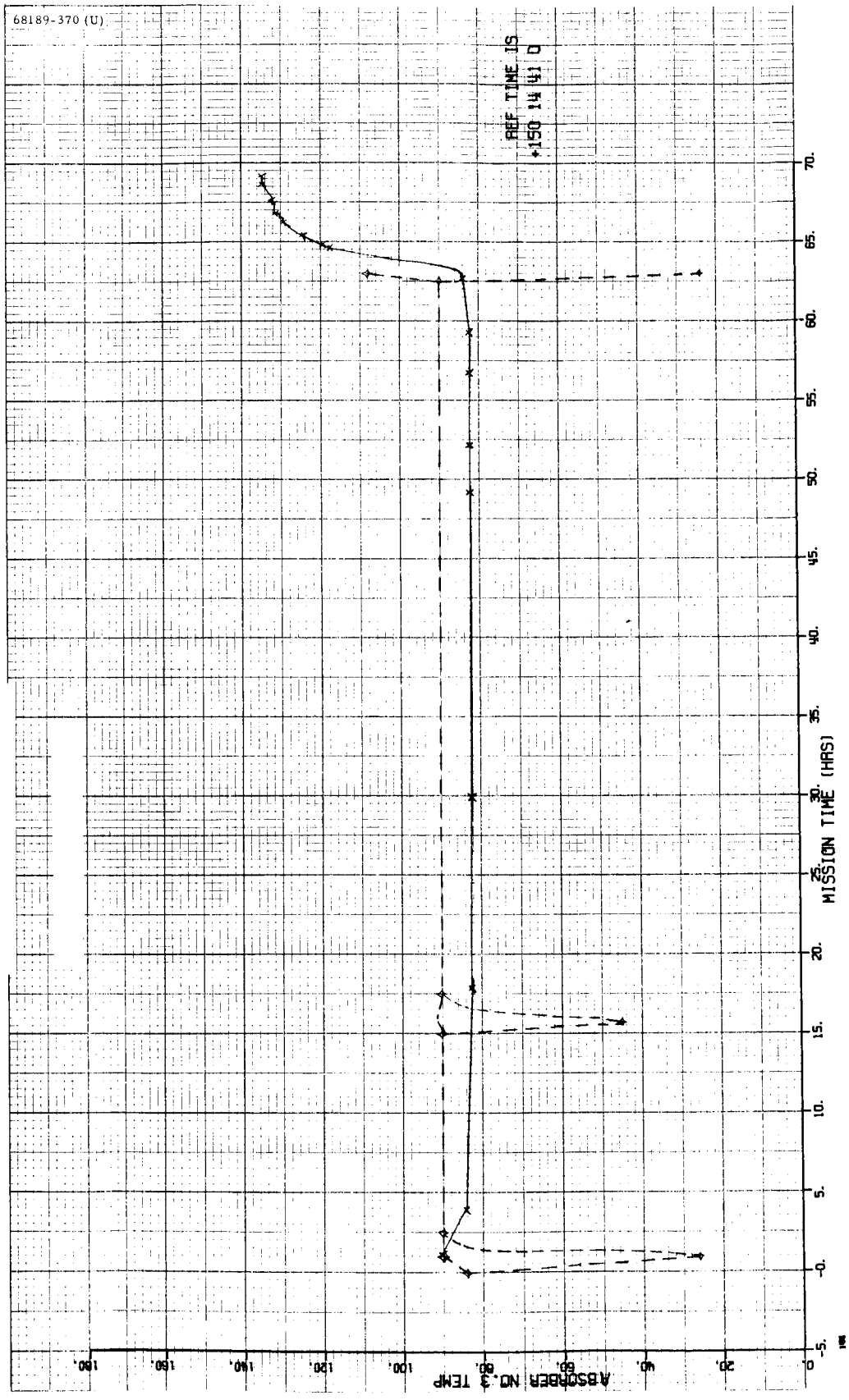


Figure A-56. Shock Absorber 3

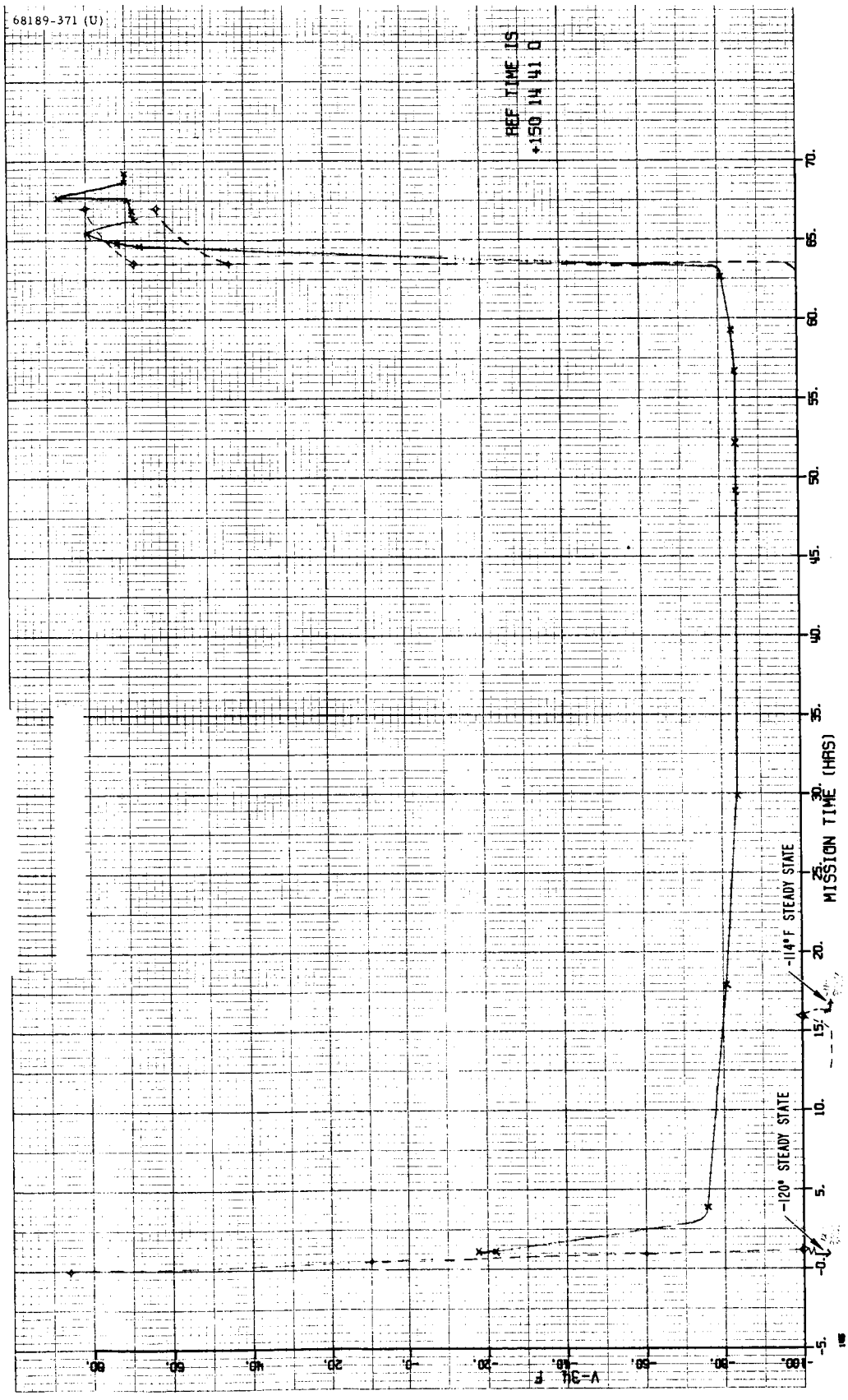
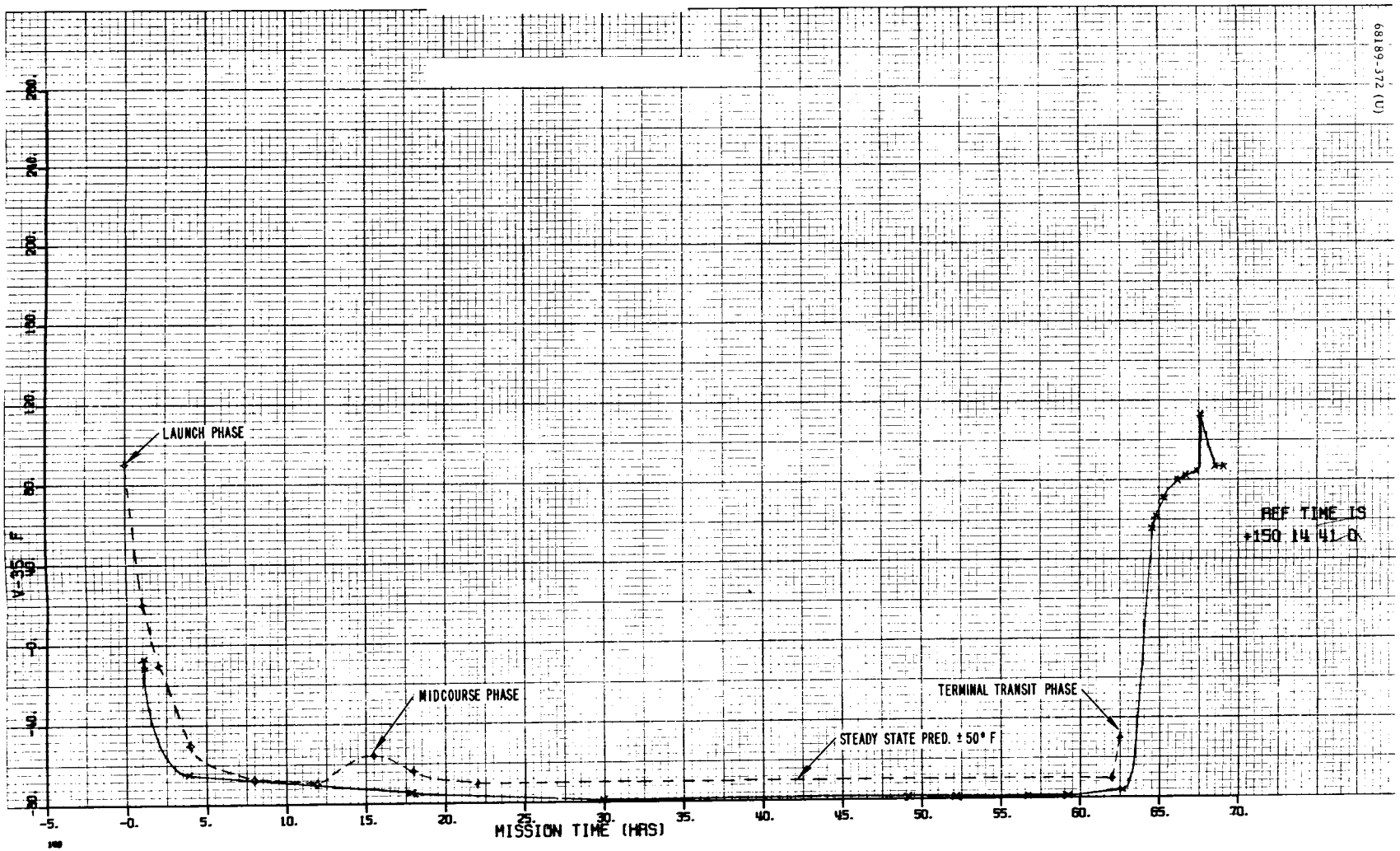


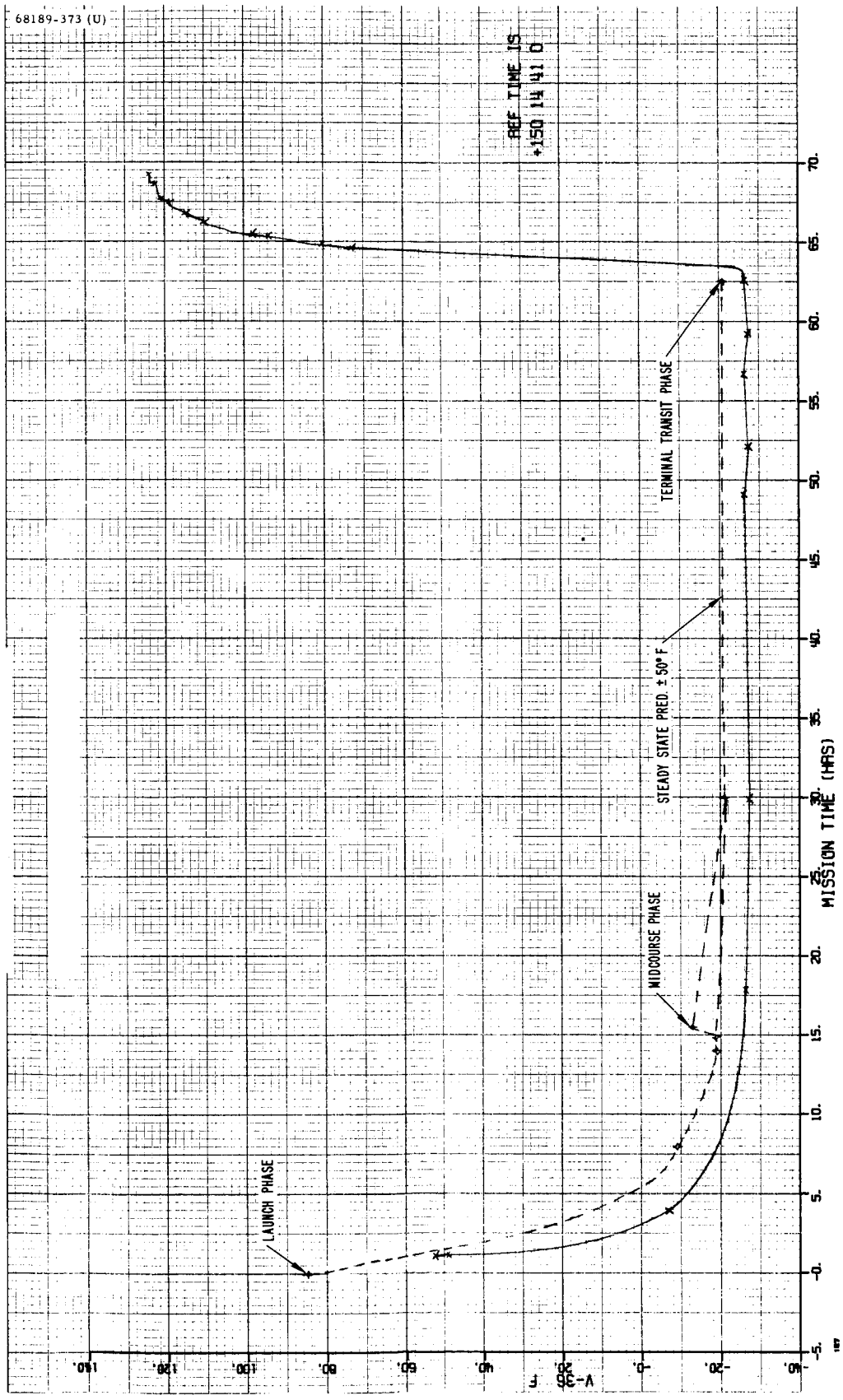
Figure A-57. A/SPP Mast



a) Upper

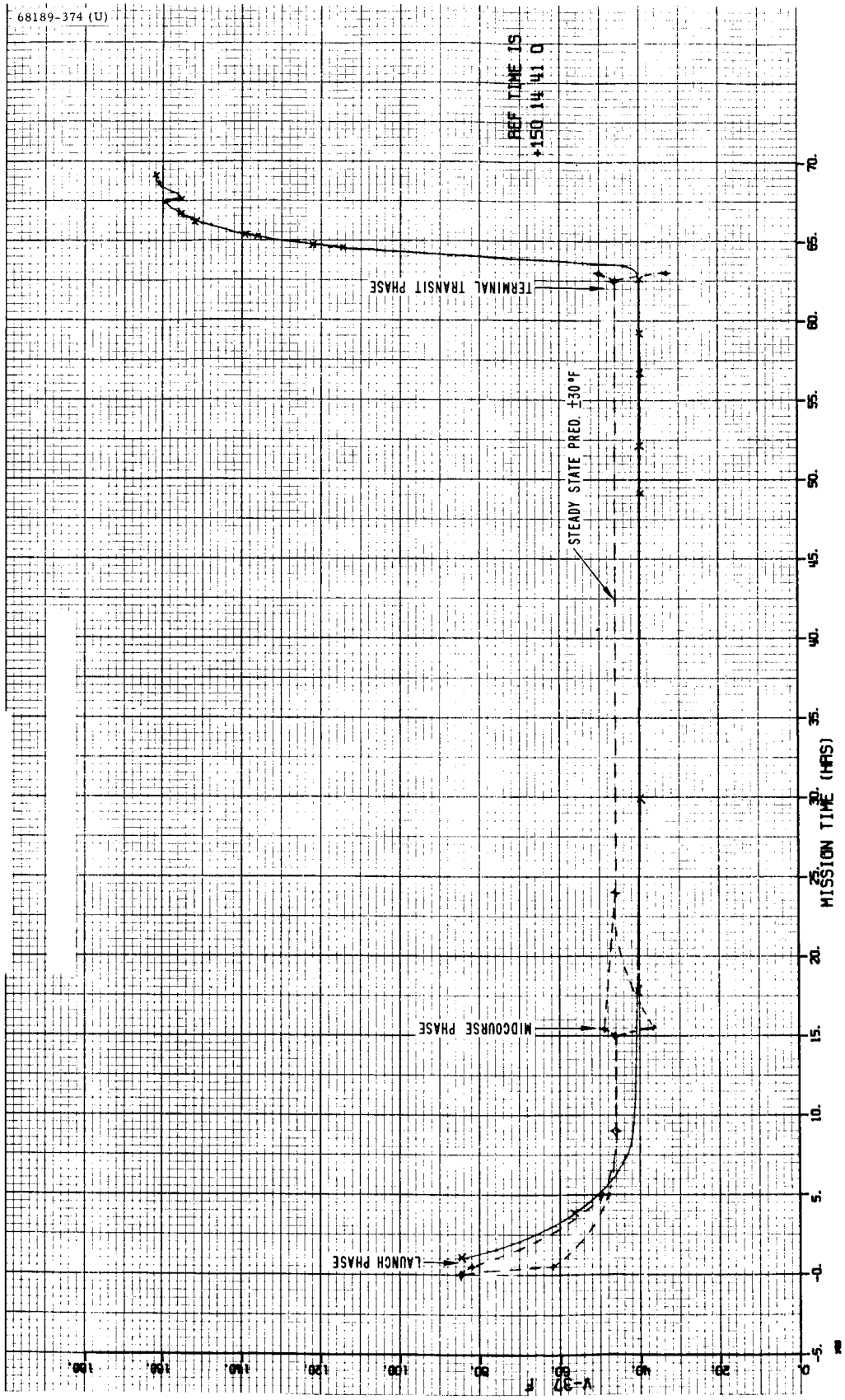
Near leg 2

Figure A-58. Spaceframes



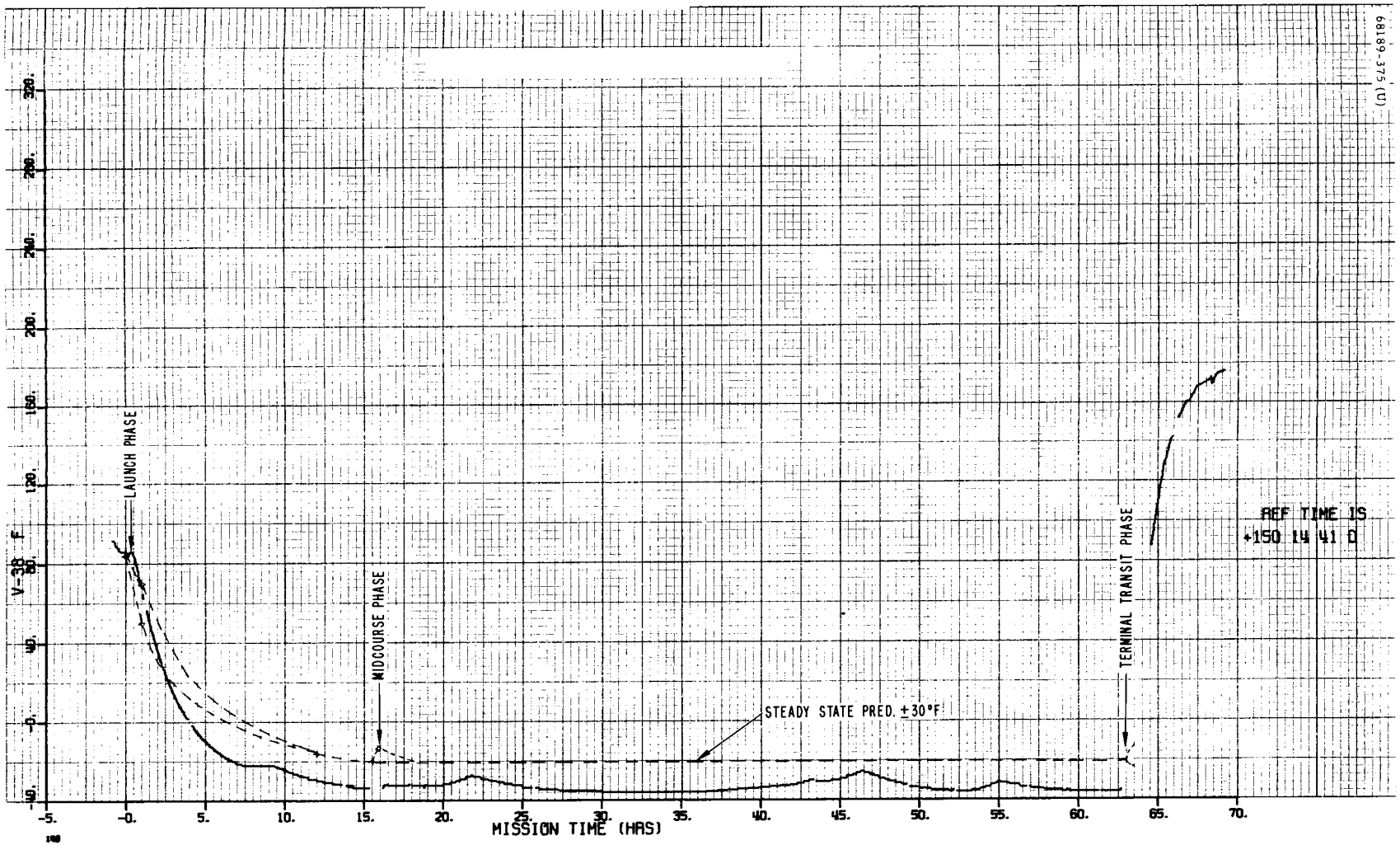
b) Lower Under compartment A

Figure A-58 (continued). Spaceframes



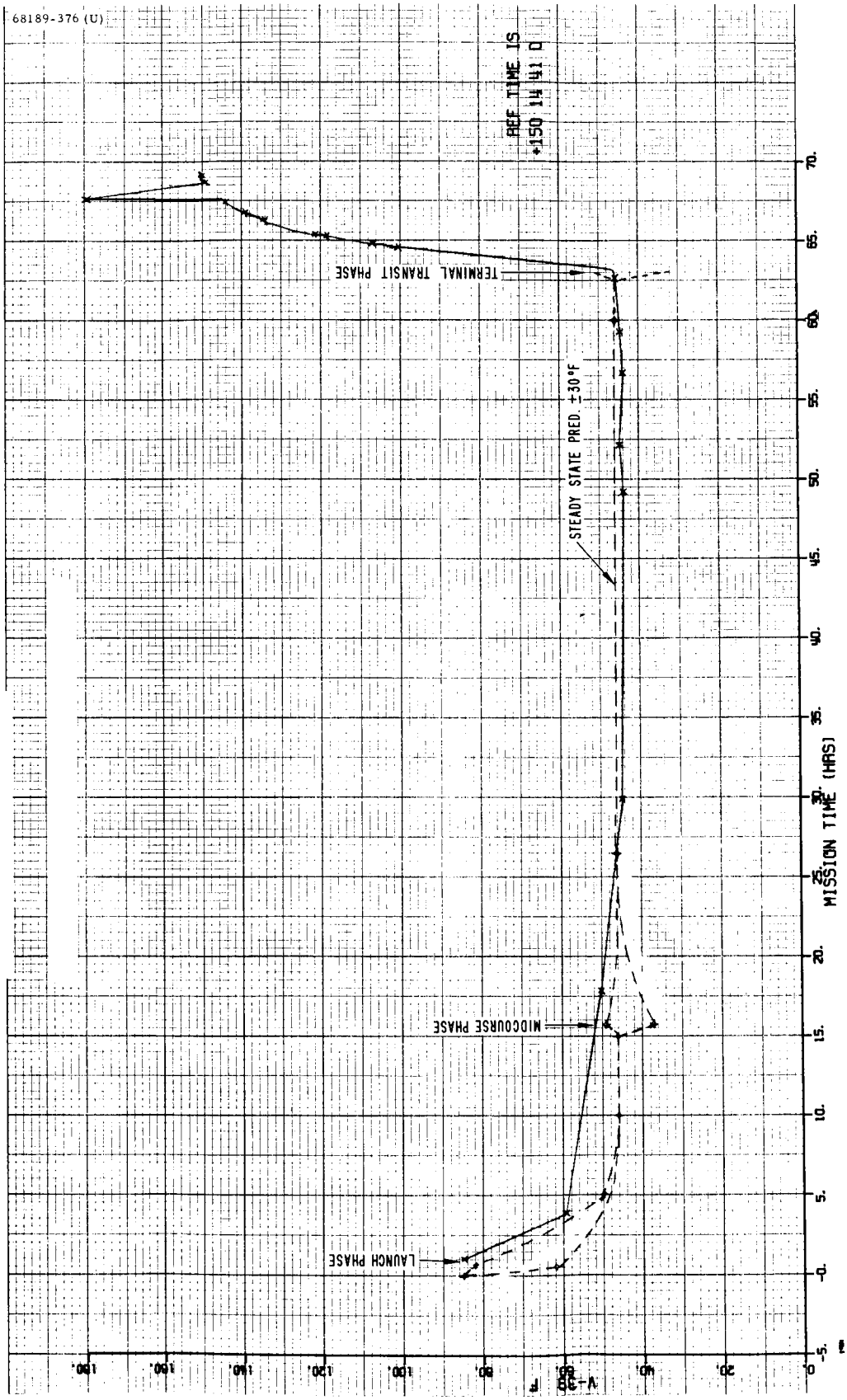
a) Point 1

Figure A-59. Retro Attach Points



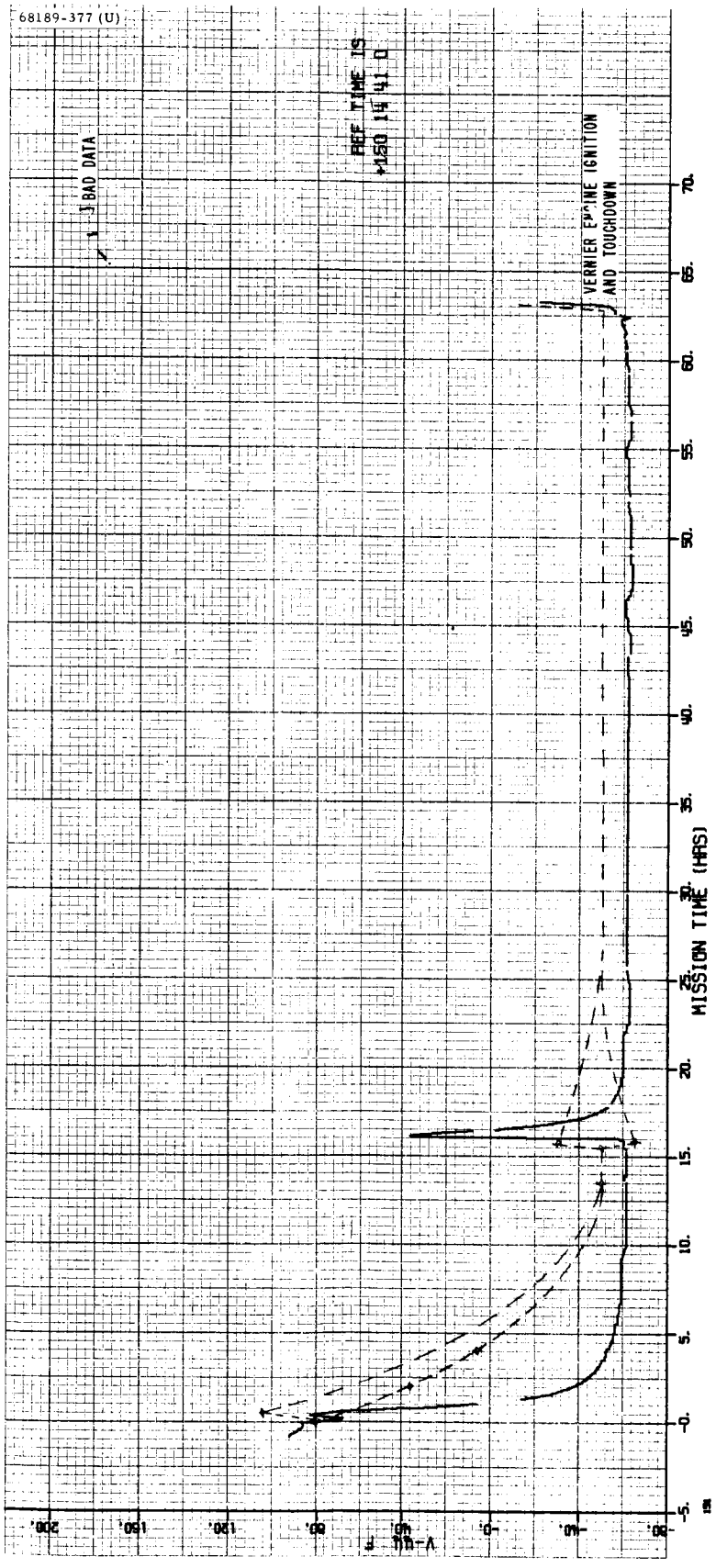
b) Point 2

Figure A-59 (continued). Retro Attach Points



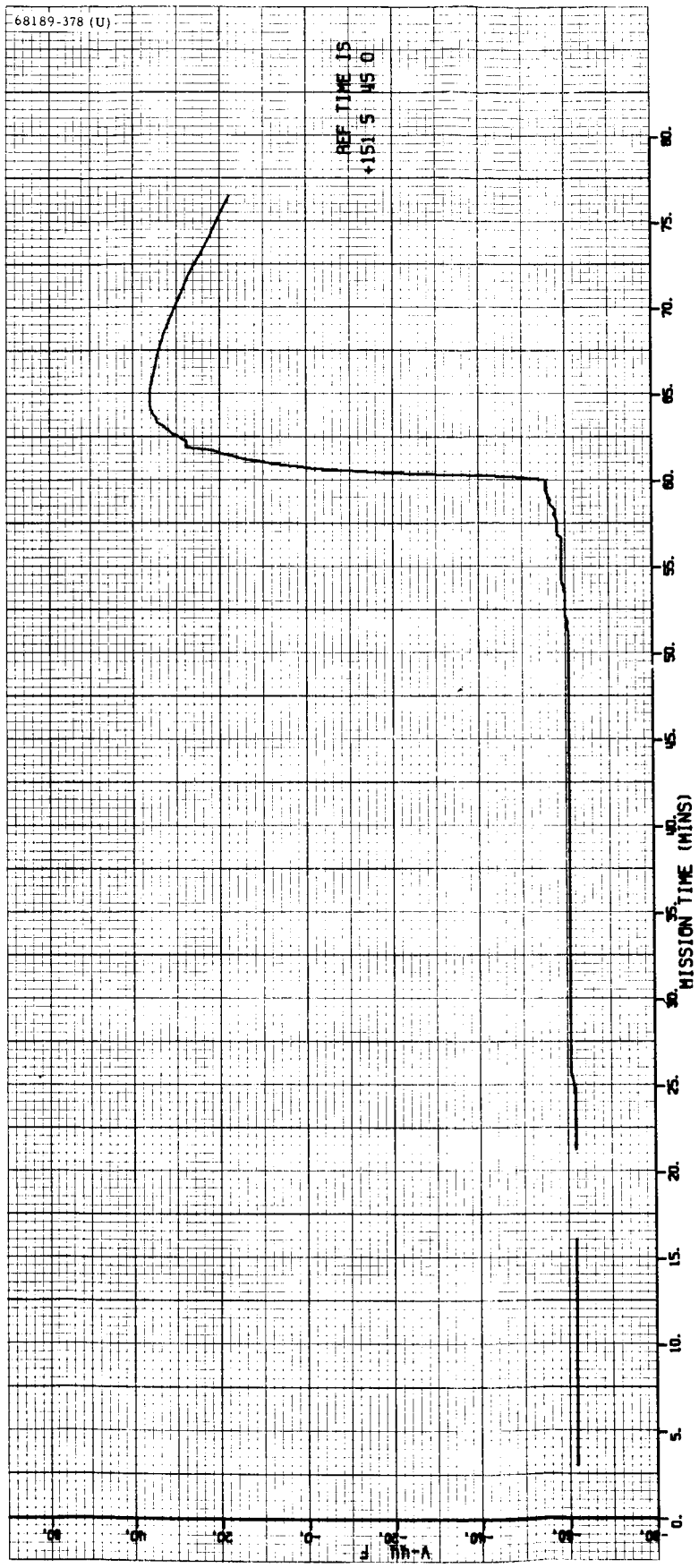
c) Point 3

Figure A-59 (continued). Retro Attach Points



a) Mission Plot

Figure A-60. Crushable Block 3



b) Midcourse

Figure A-60. Crushable Block 3

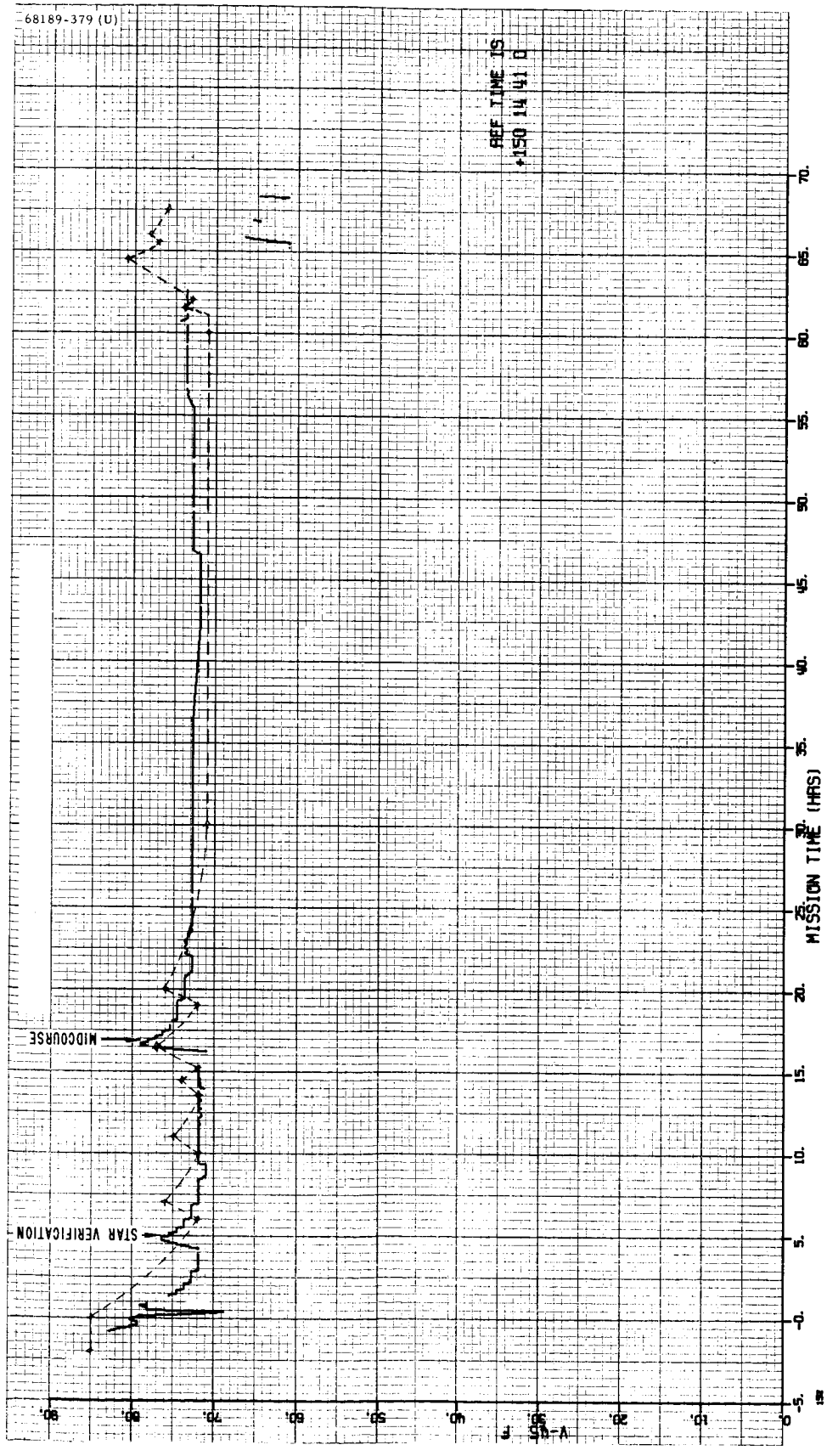


Figure A-61. Compartment B Thermal Switch 1 Radiator

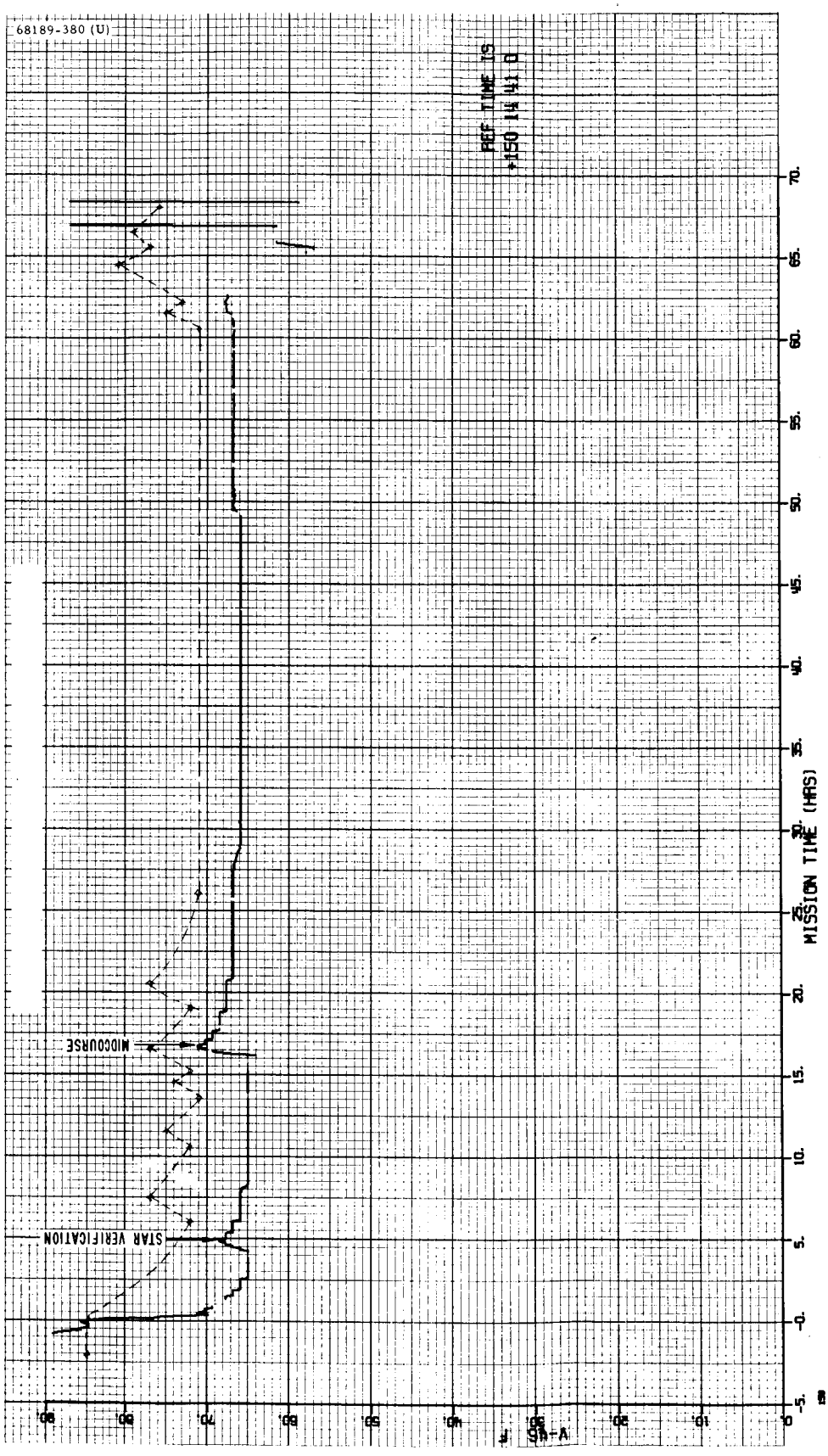


Figure A-62. Compartment B Thermal Switch 5 Radiator

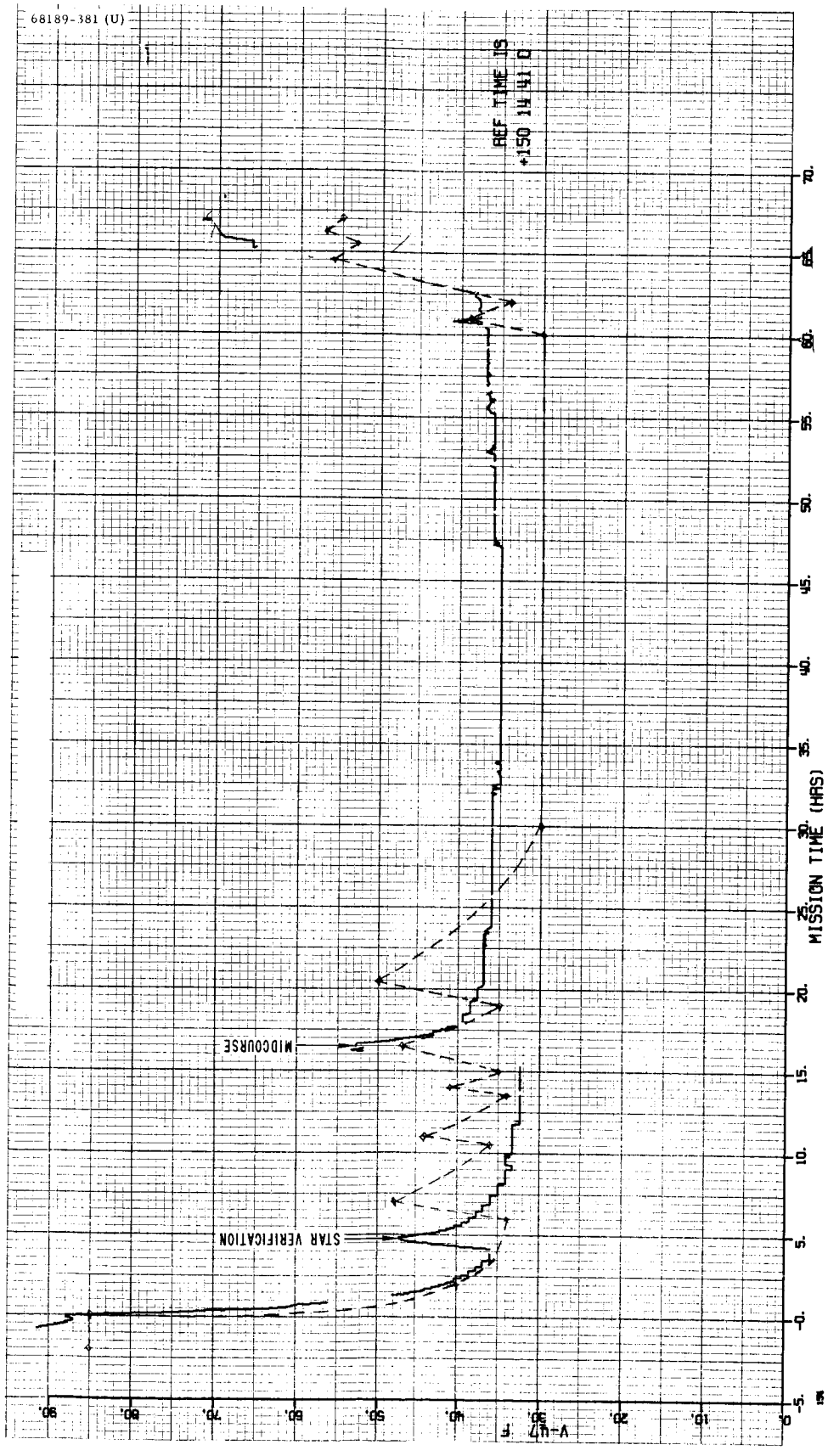


Figure A-63. Compartment A Thermal Switch 2 Radiator

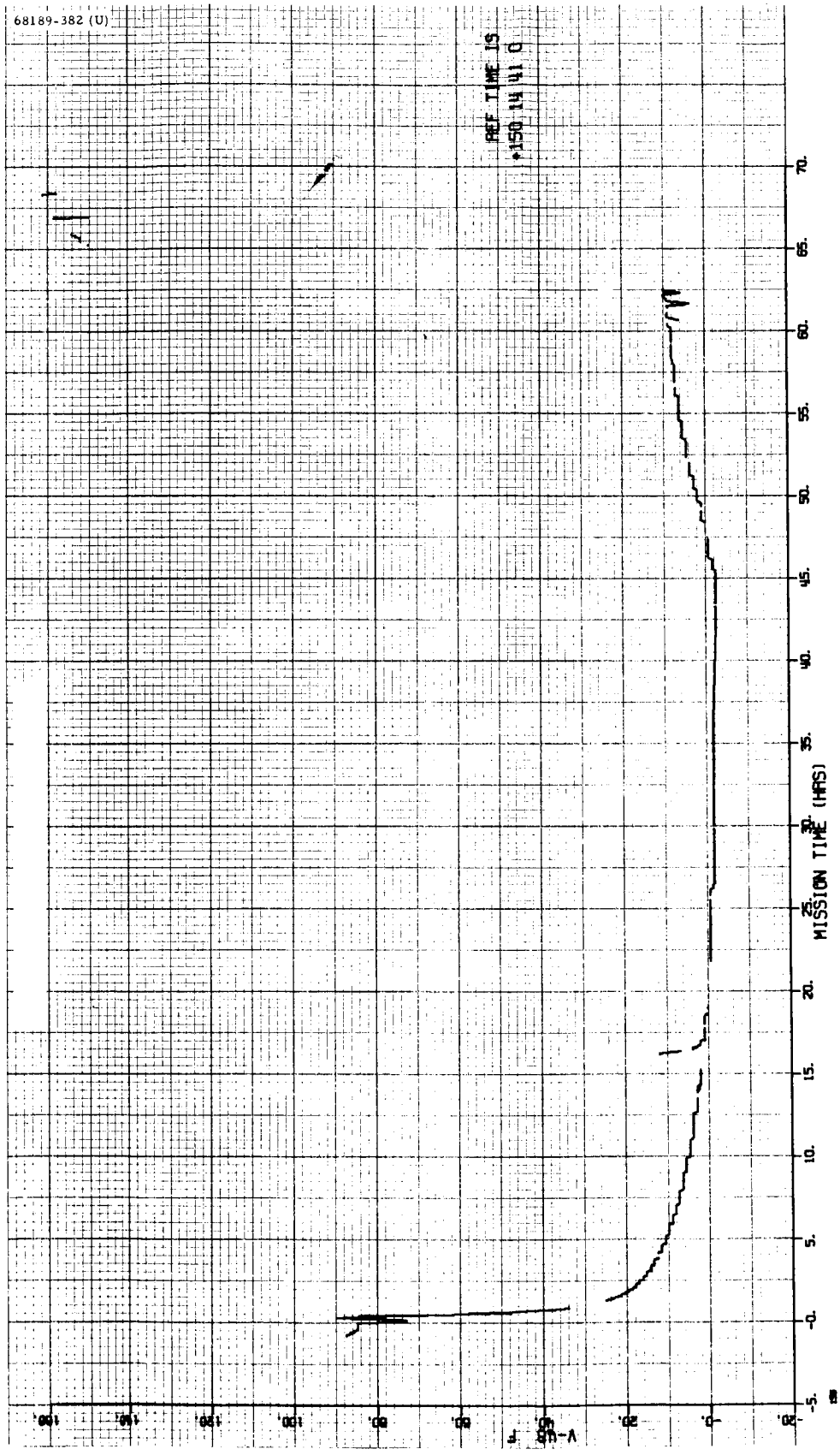


Figure A-64. Auxiliary Battery Outside Shell

APPENDIX B

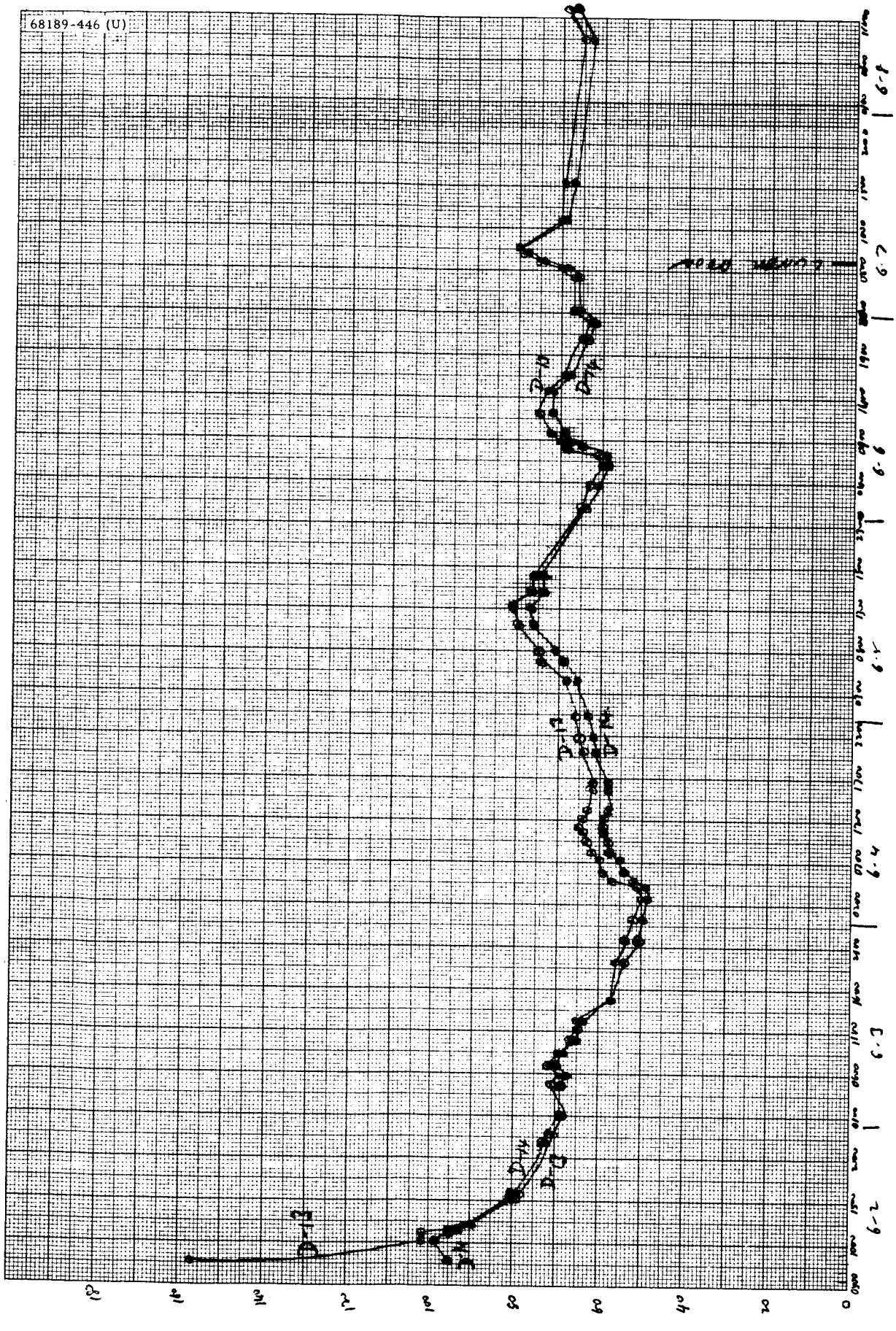


Figure B-1. Transmitters A and B

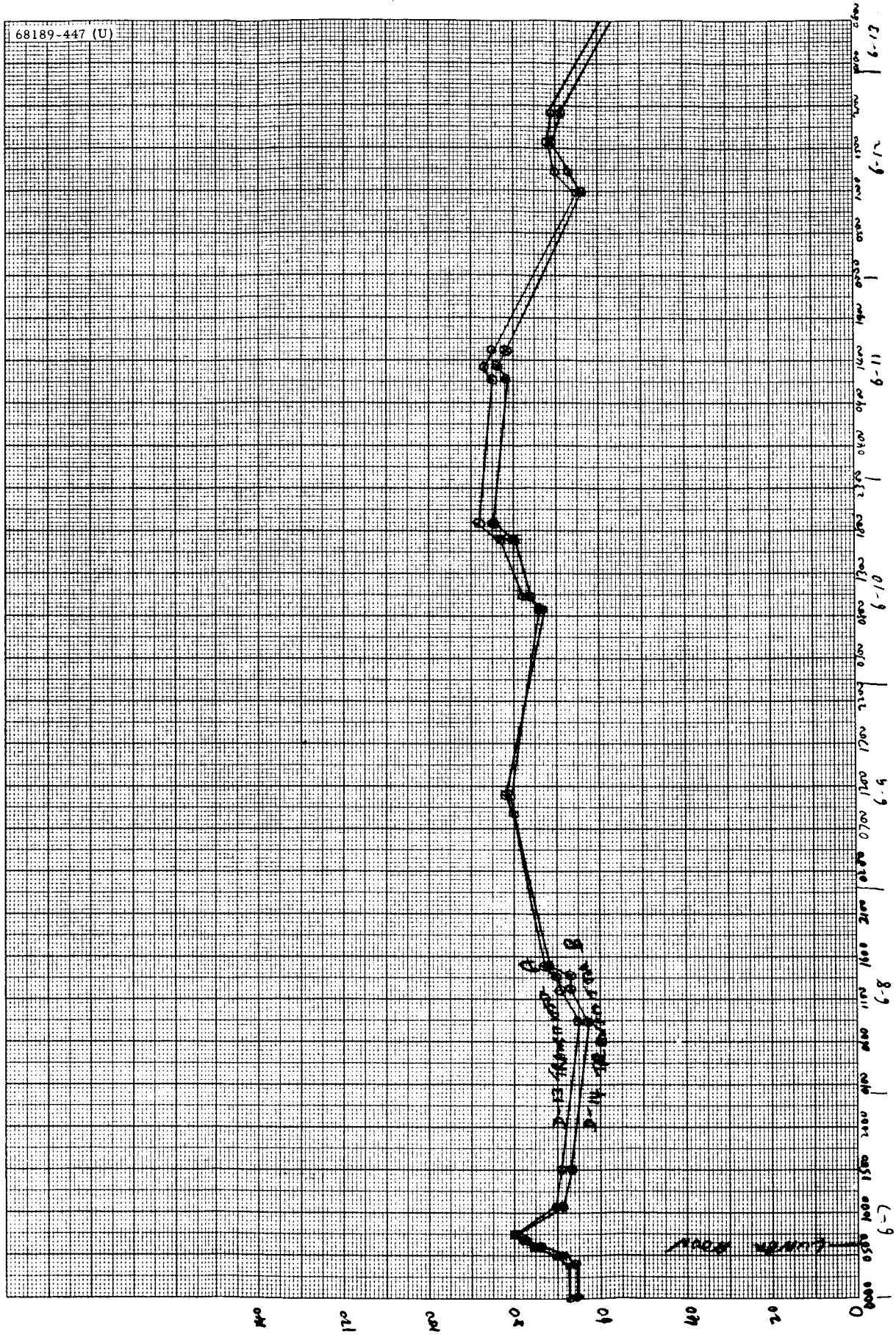


Figure B-1 (continued). Transmitters A and B

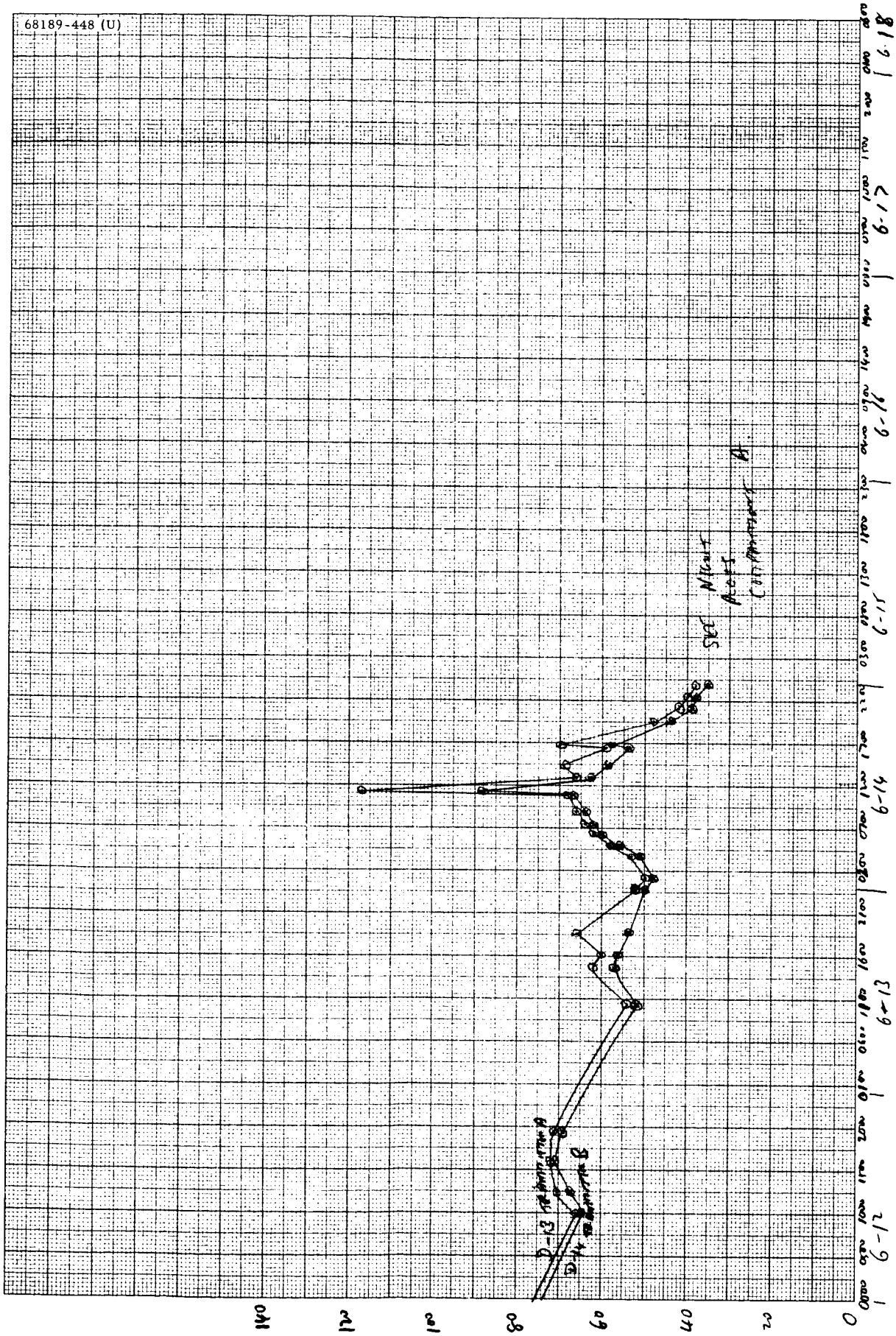


Figure B-1 (continued). Transmitters A and B

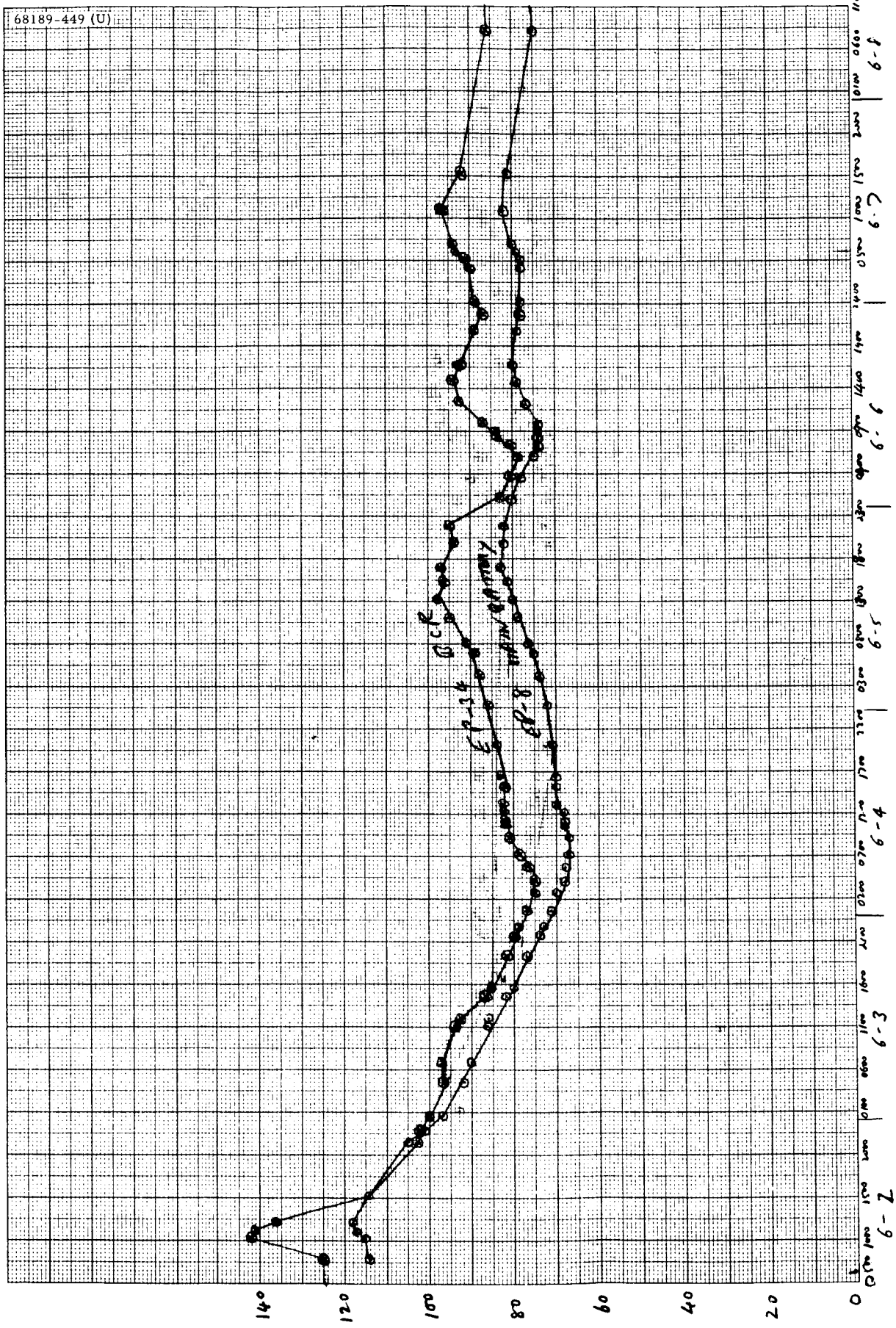


Figure B-2. Main Battery and Battery Charge Regulator

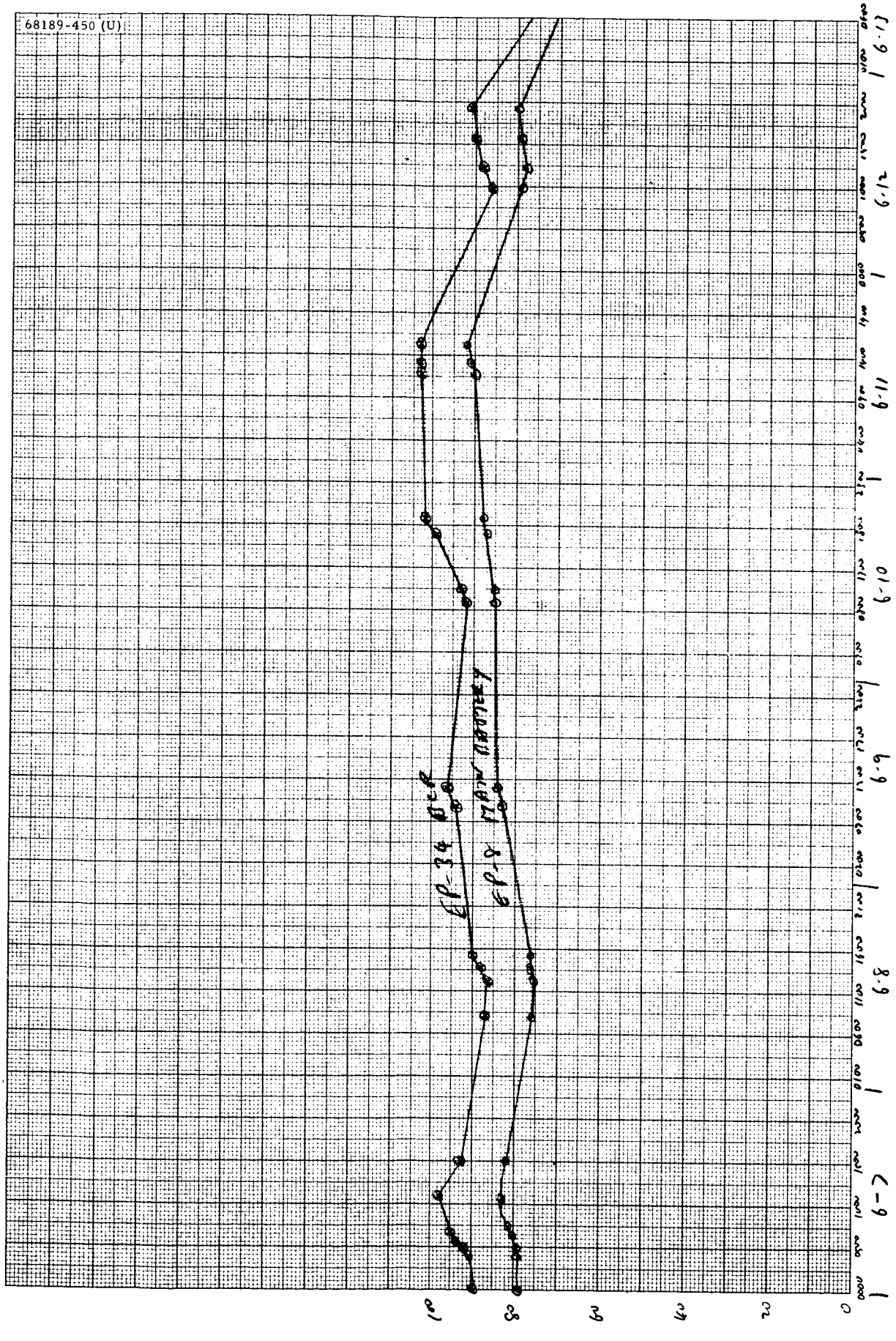


Figure B-2 (continued). Main Battery and Battery Charge Regulator

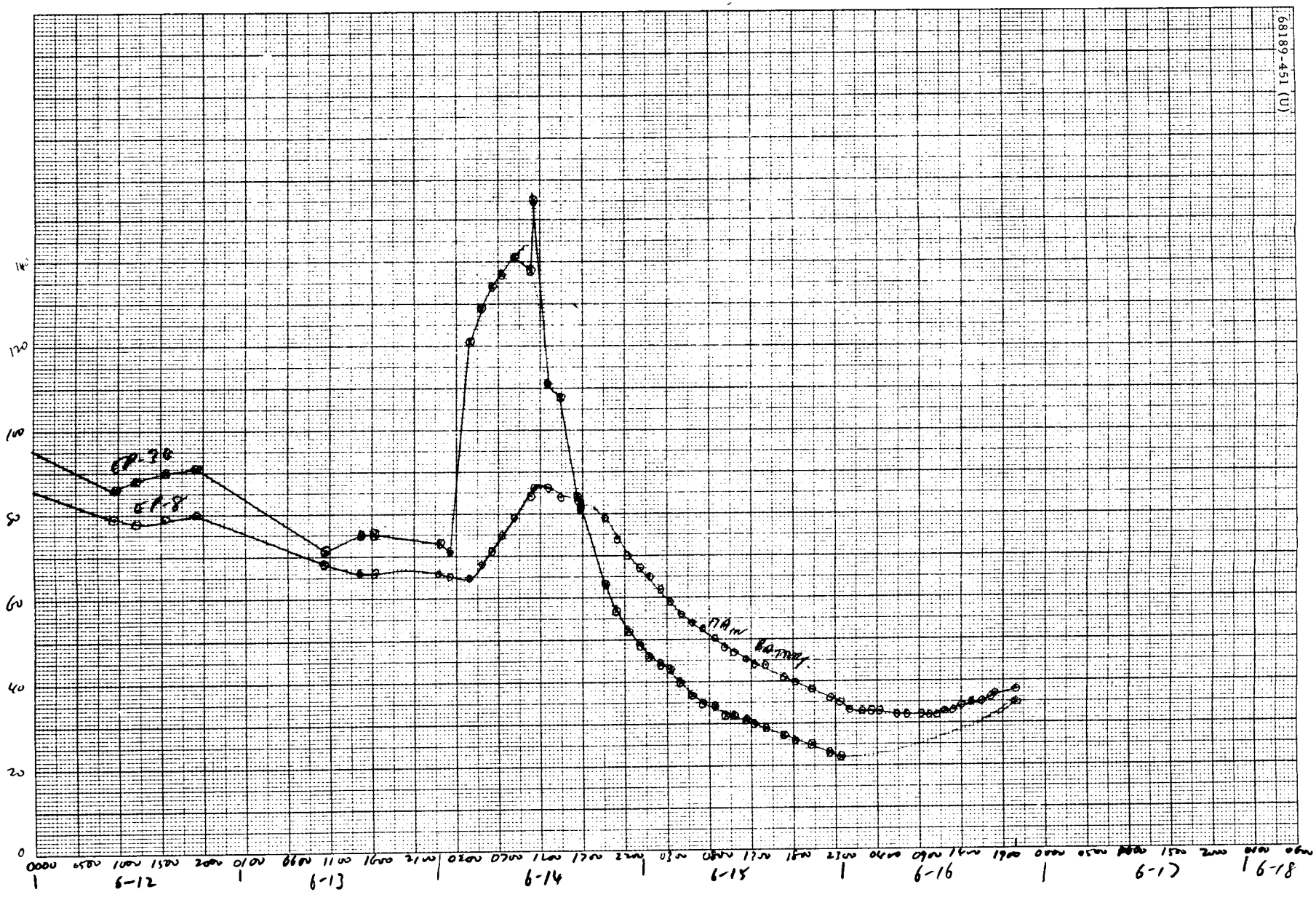


Figure B-2 (continued). Main Battery and Battery Charge Regulator

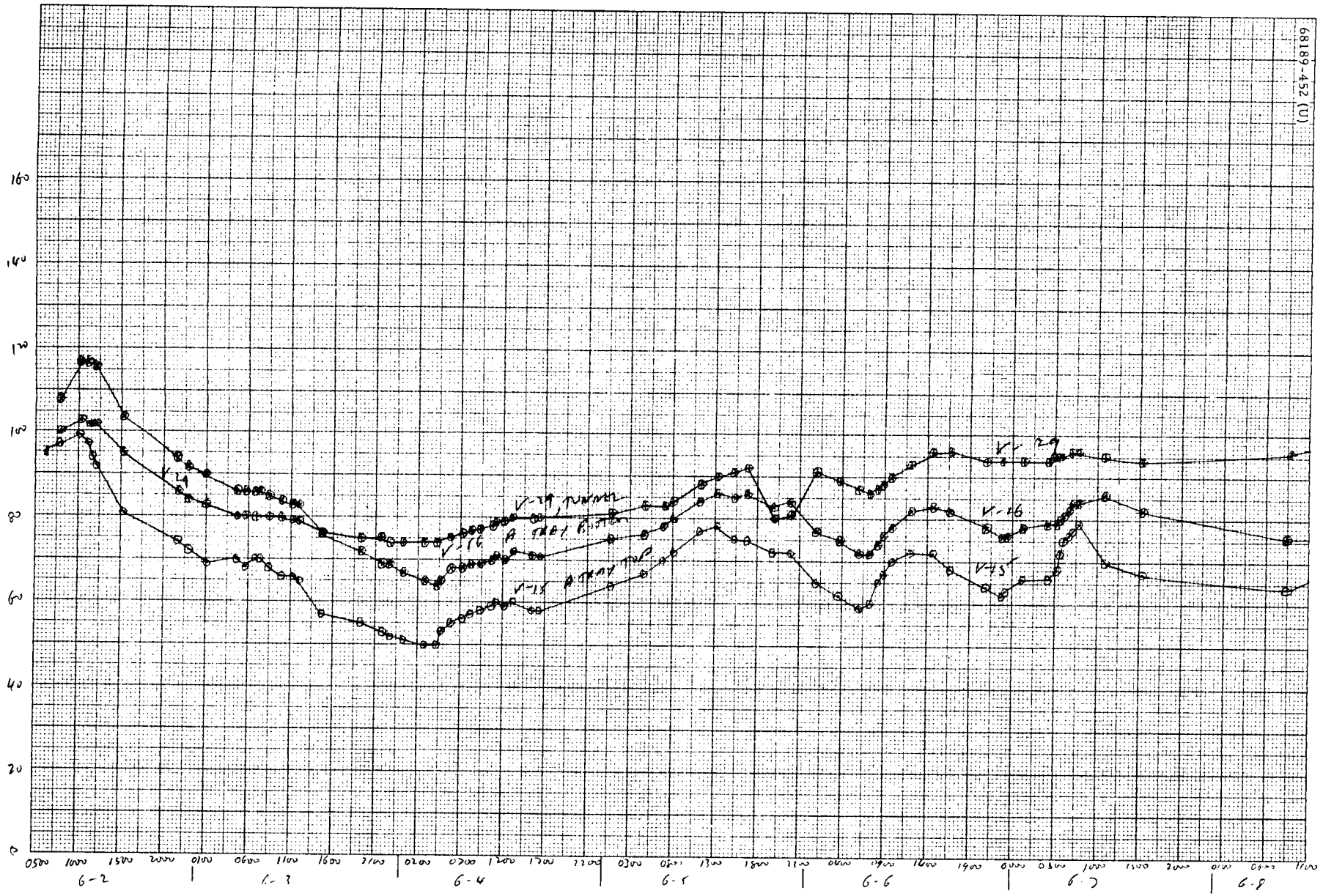


Figure B-3. Compartment A Top and Bottom Tray and Thermal Tunnel

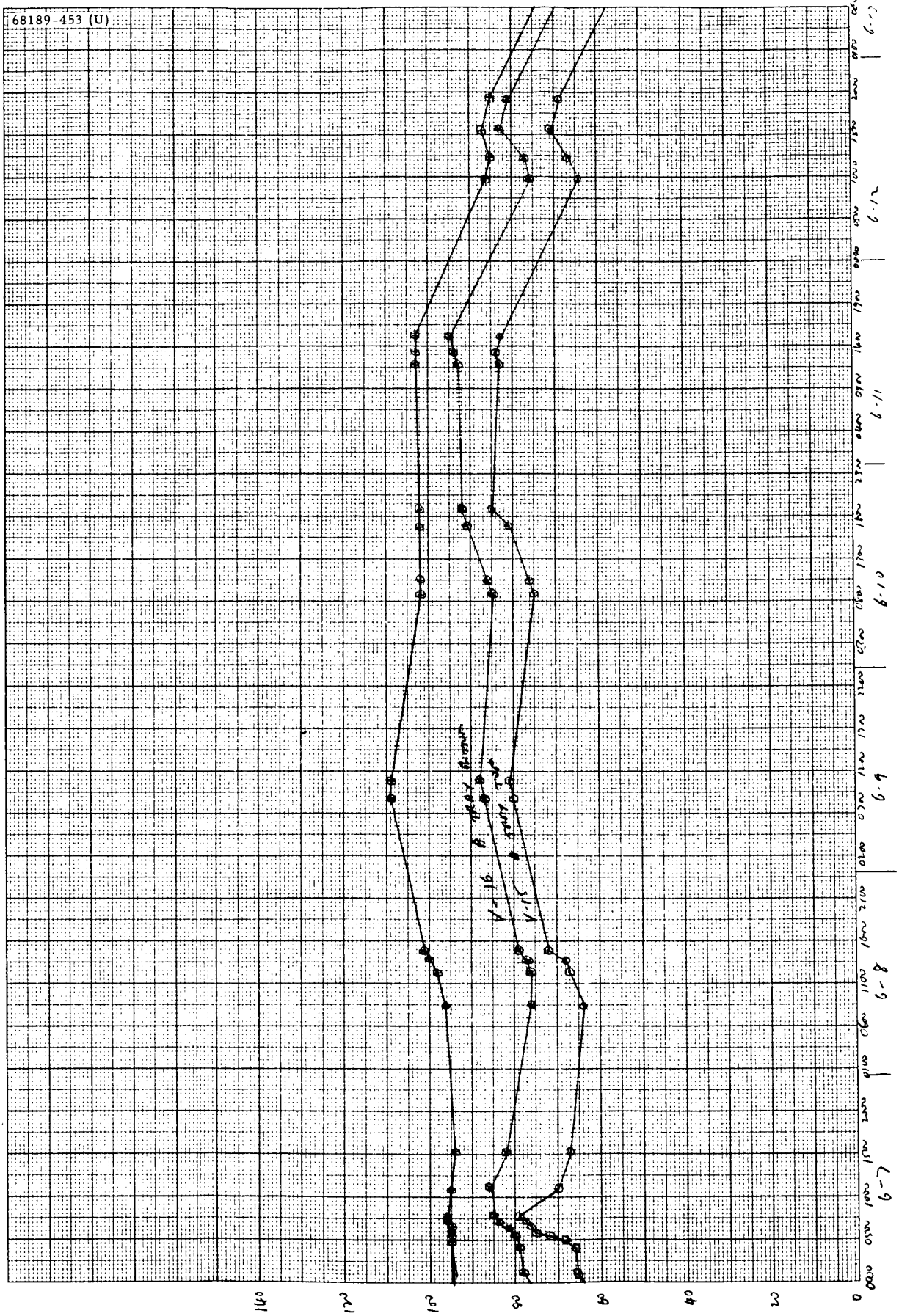


Figure B-3 (continued). Compartment A Top and Bottom Tray and Thermal Tunnel

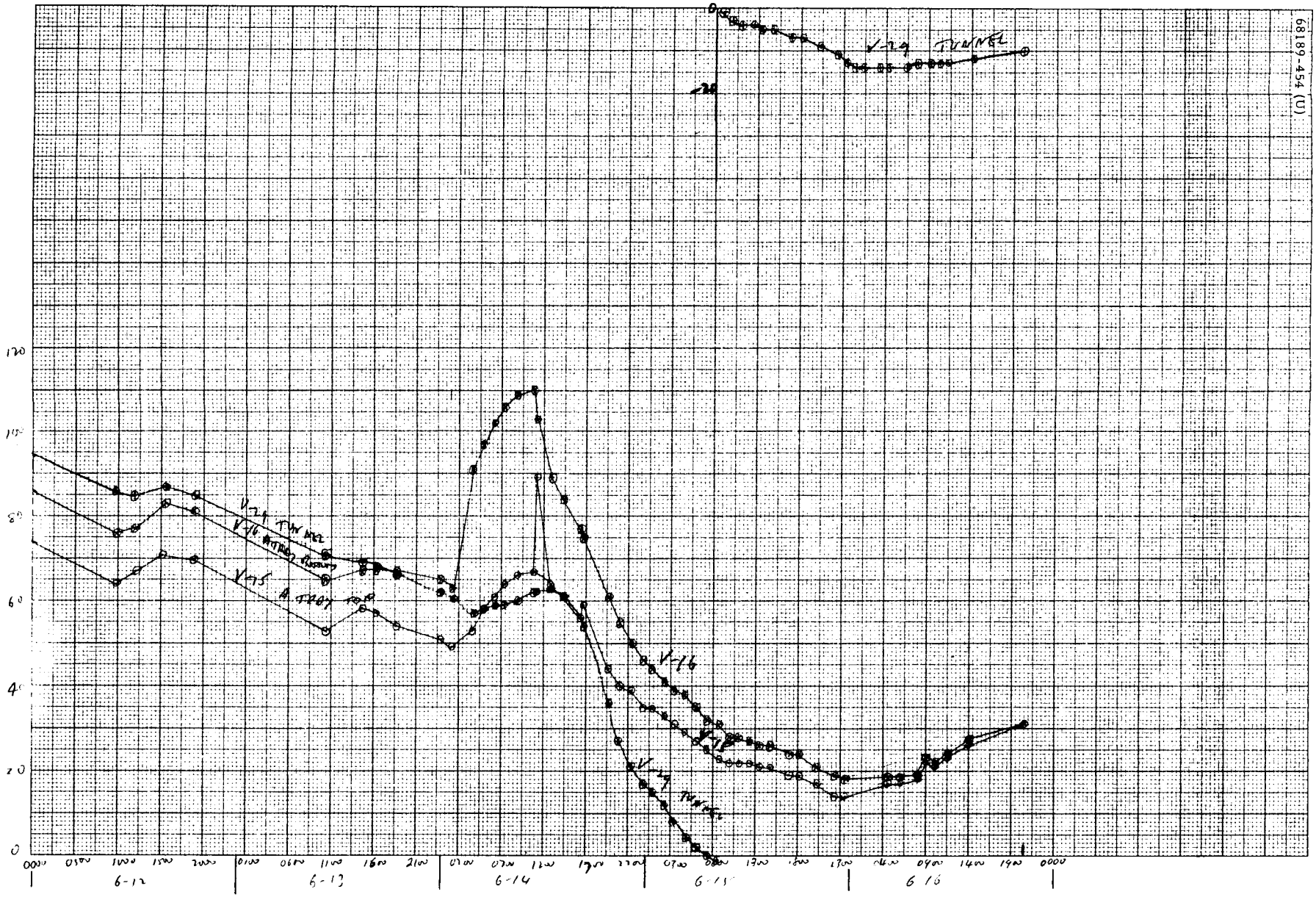


Figure B-3 (continued). Compartment A Top and Bottom Tray and Thermal Tunnel

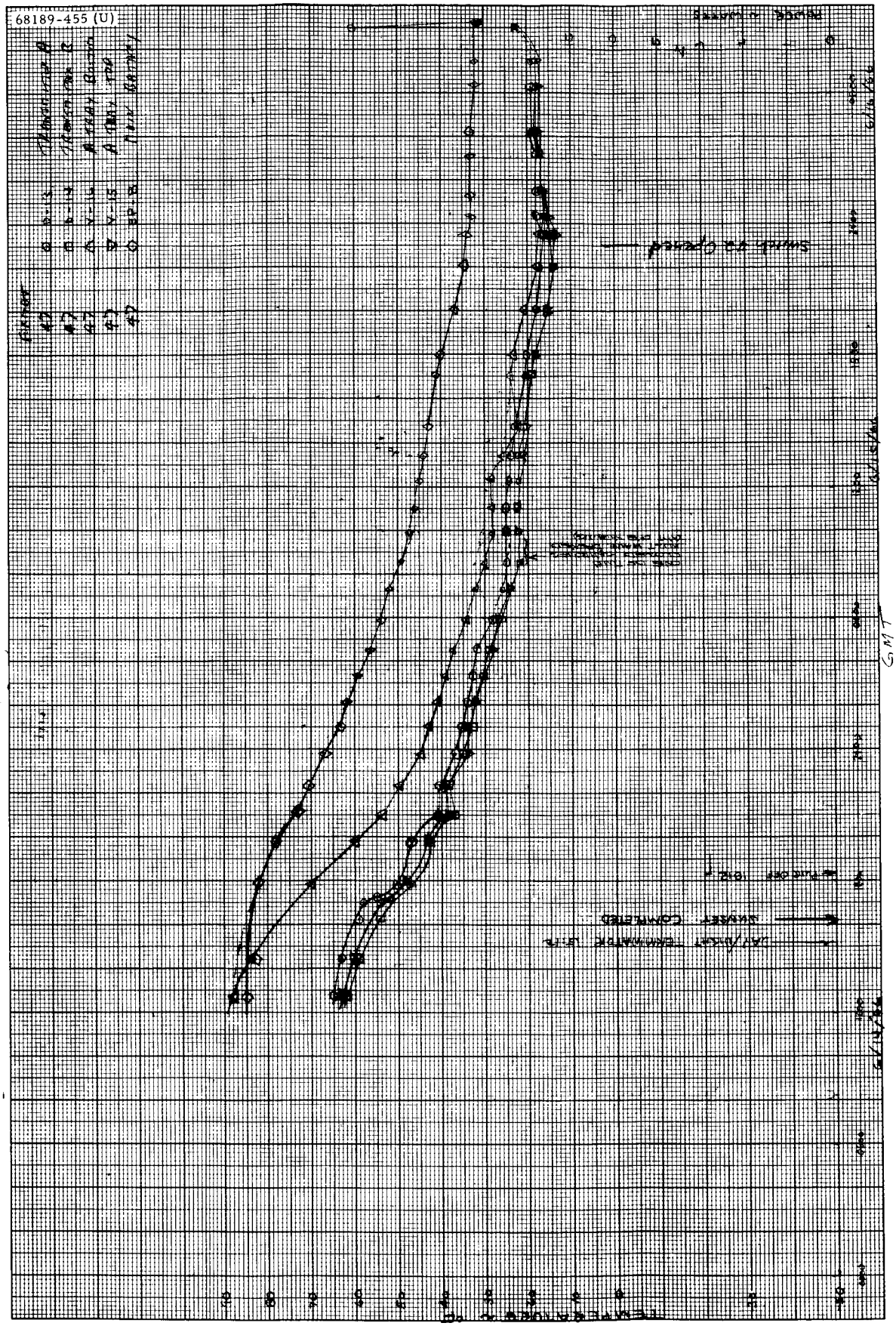


Figure B-4. Compartment A Interior (Near Day and Night Terminator)

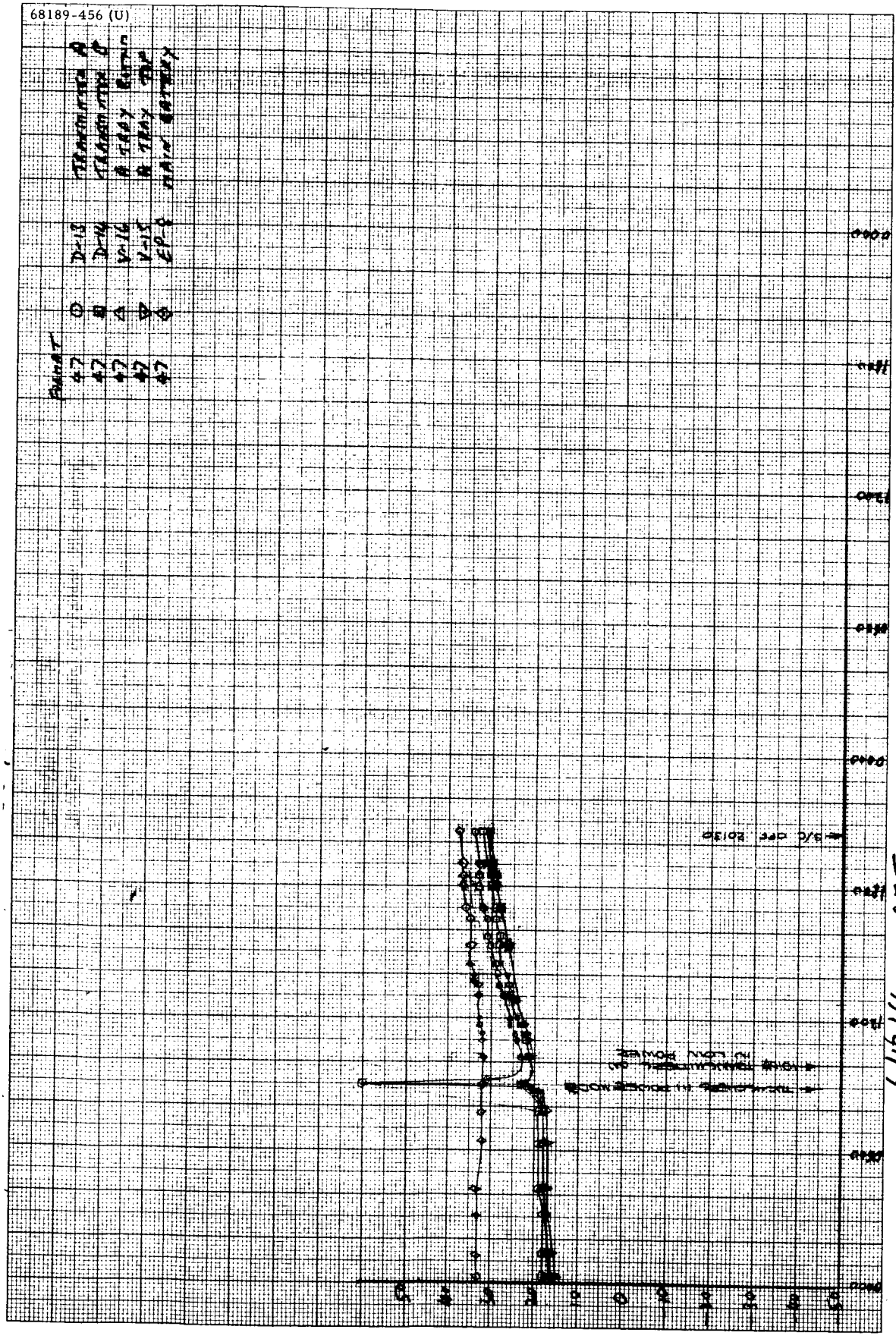


Figure B-4 (continued). Compartment A Interior (Near Day and Night Terminator)

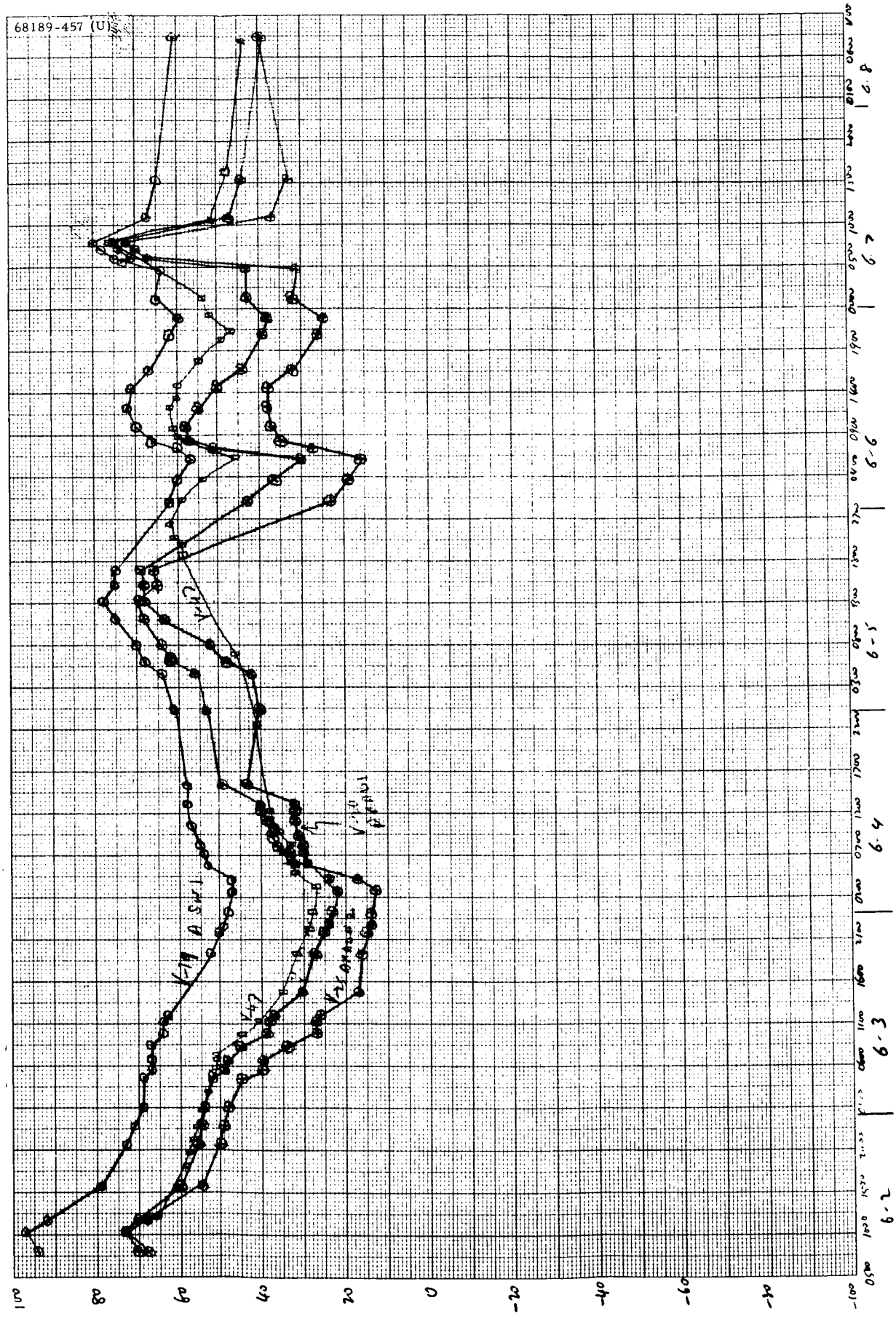


Figure B-5. Compartment A Radiators and Contact Ring

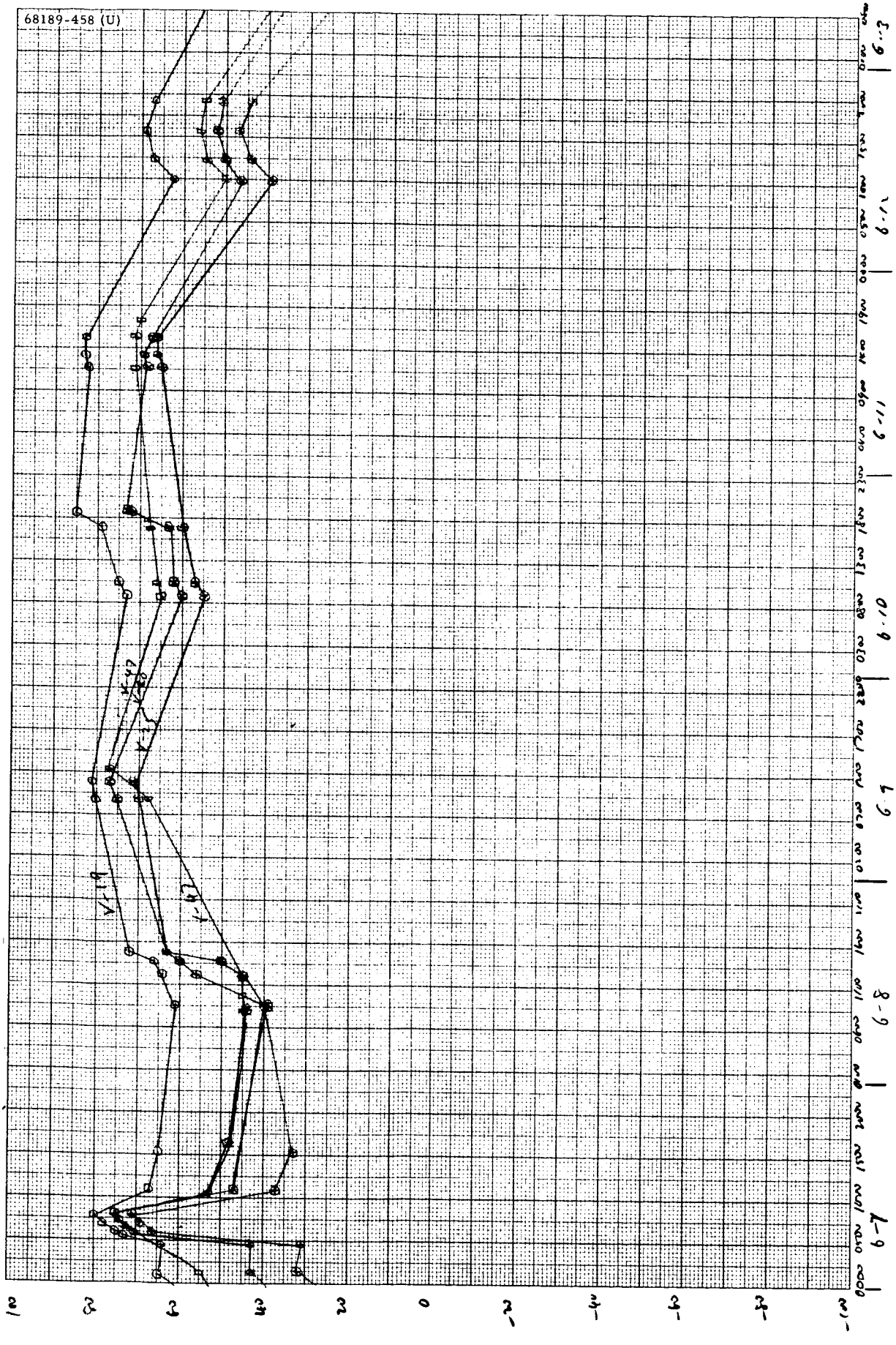


Figure B-5 (continued). Compartment A Radiators and Contact Ring

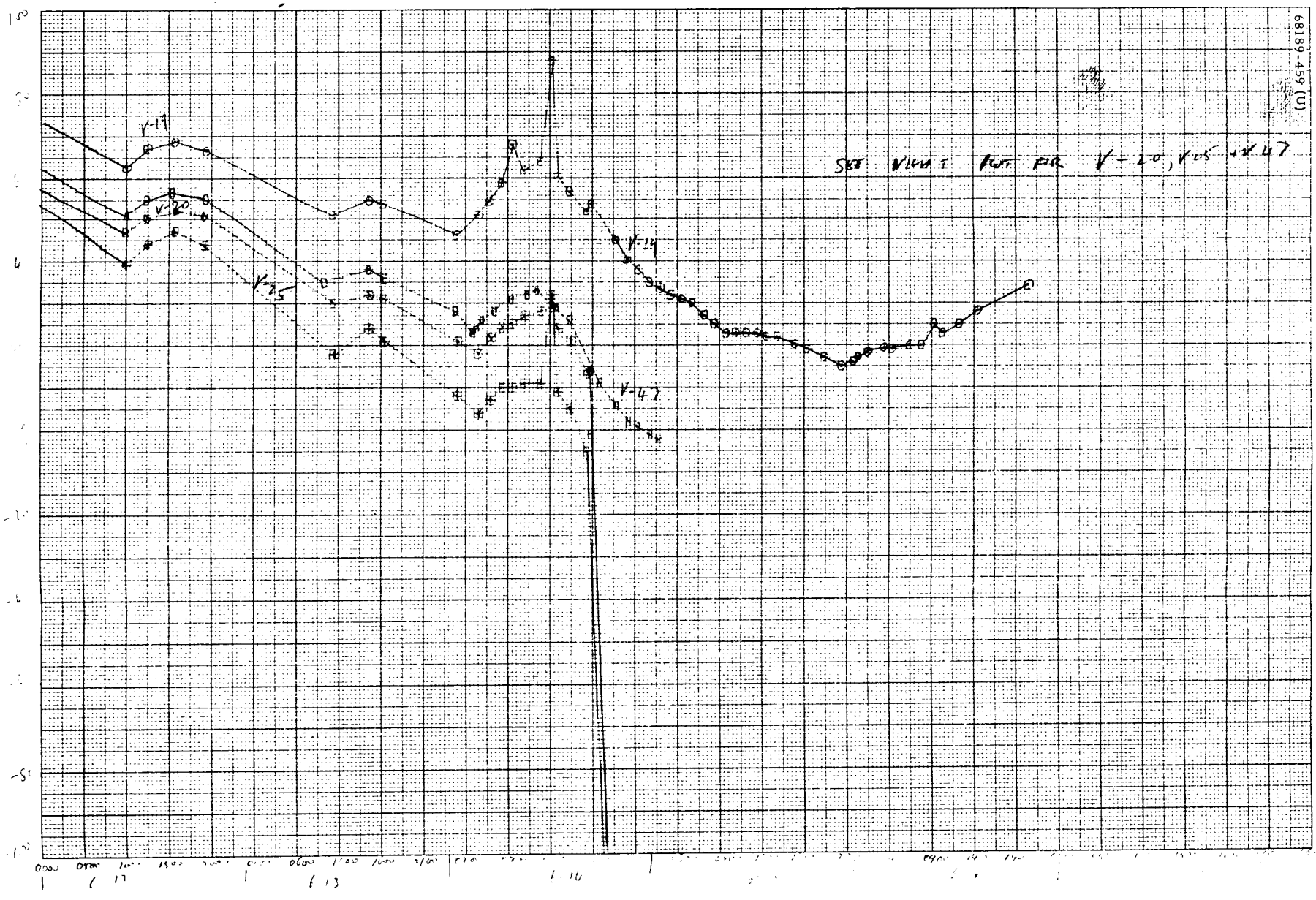


Figure B-5 (continued). Compartment A Radiators and Contact Ring

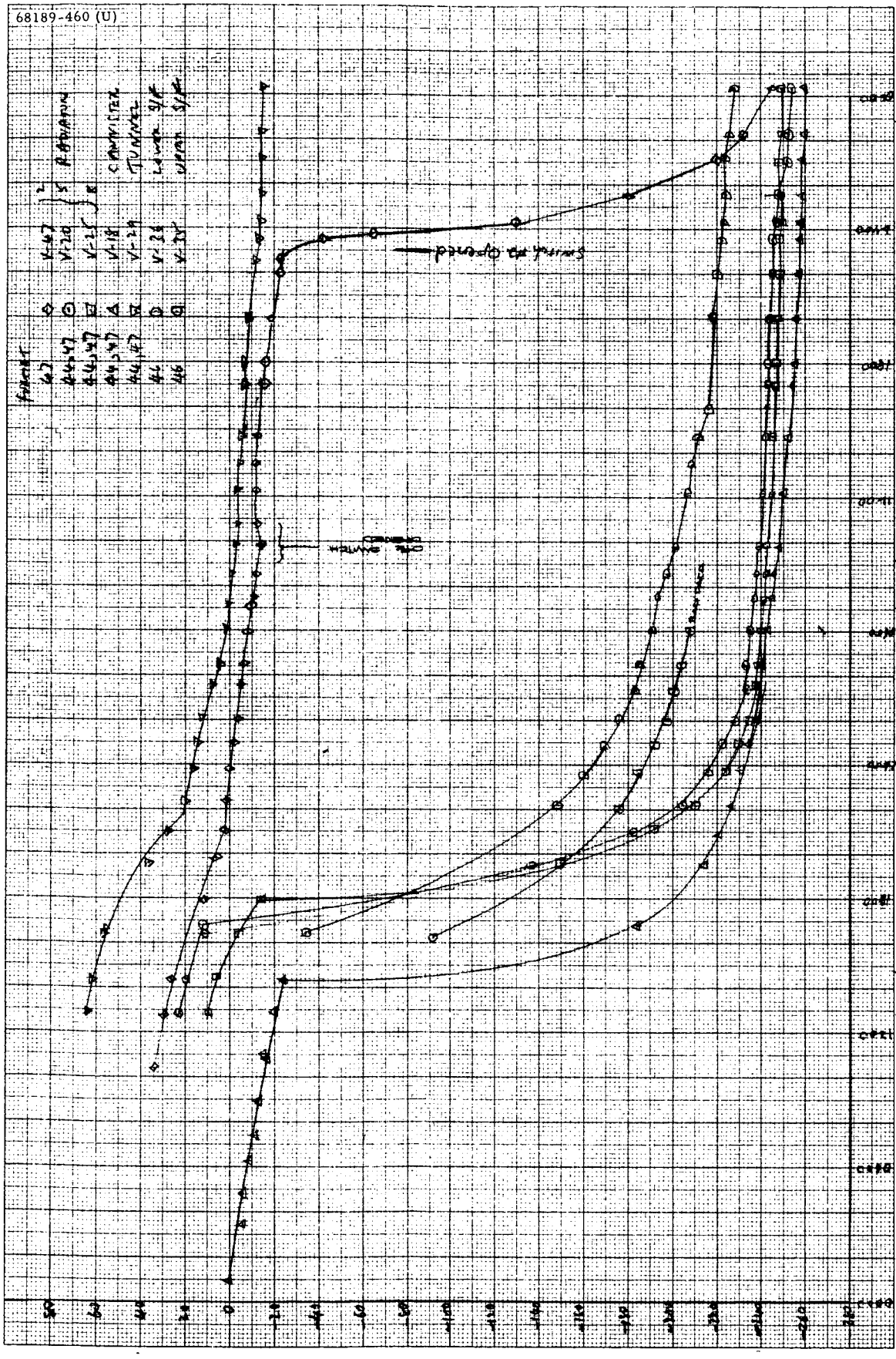


Figure B-6. Compartment A Exterior (Near Day and Night Terminator)

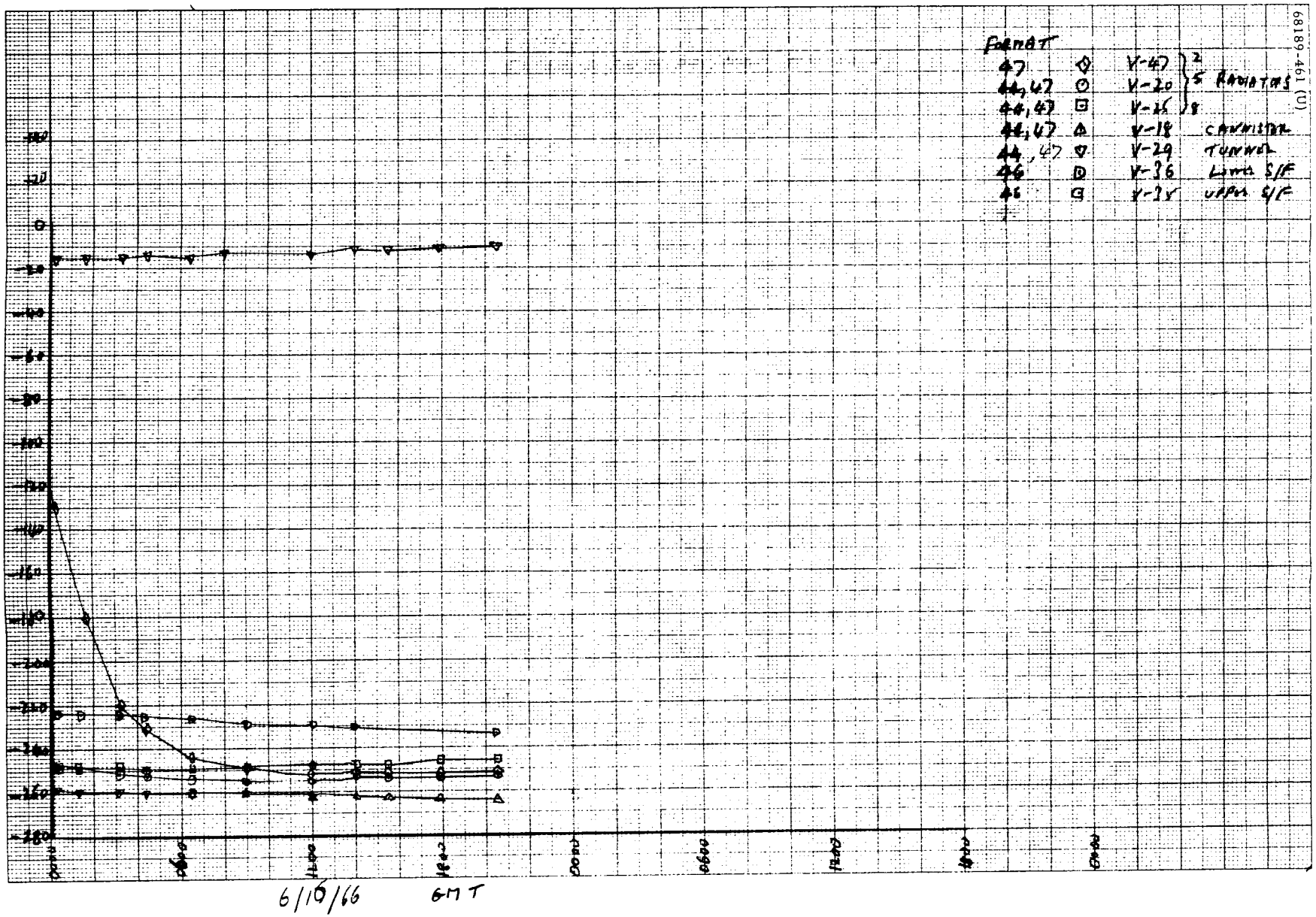


Figure B-6 (continued). Compartment A Exterior (Near Day and Night Terminator)

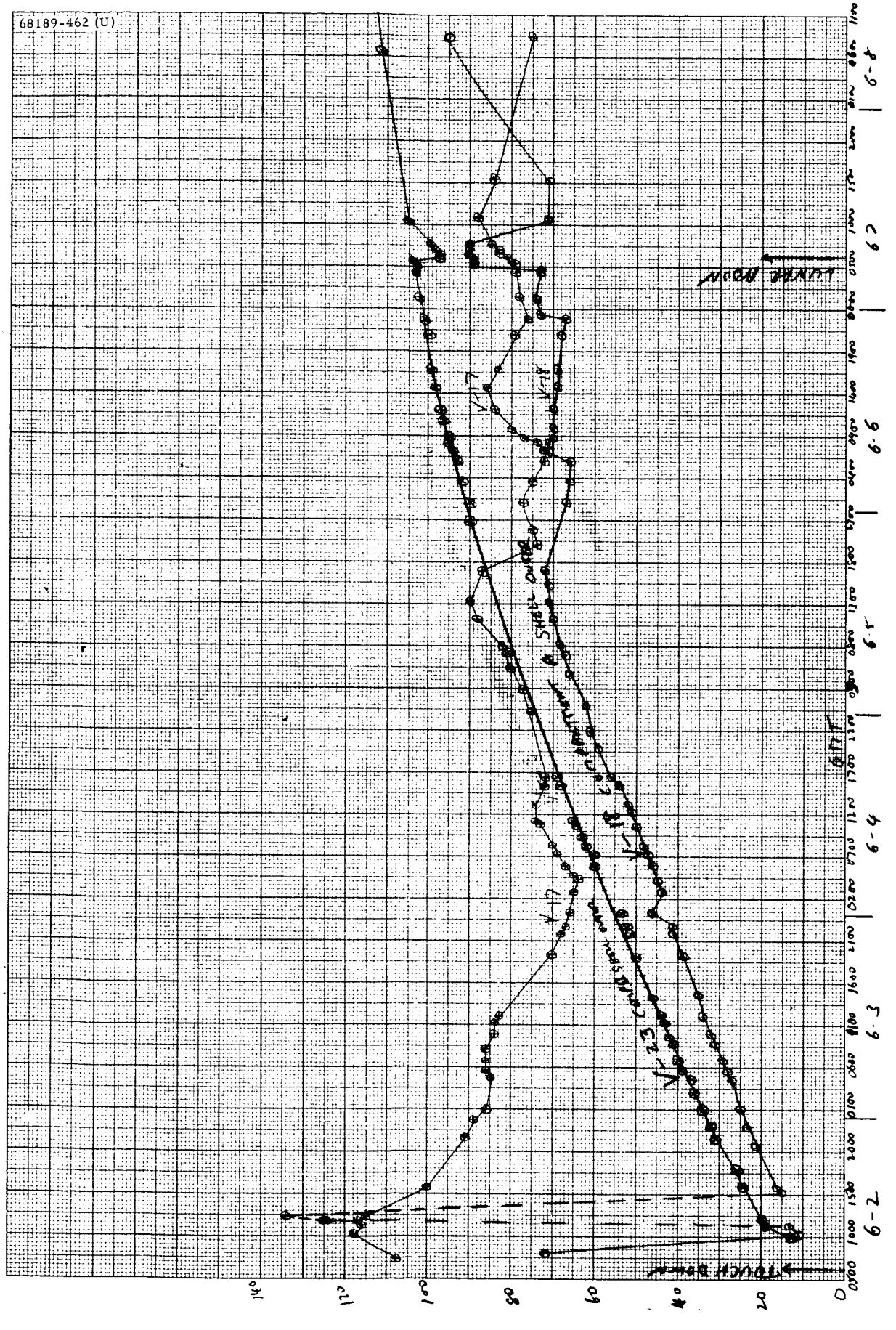


Figure B-7. Compartment A and B Outer Shells

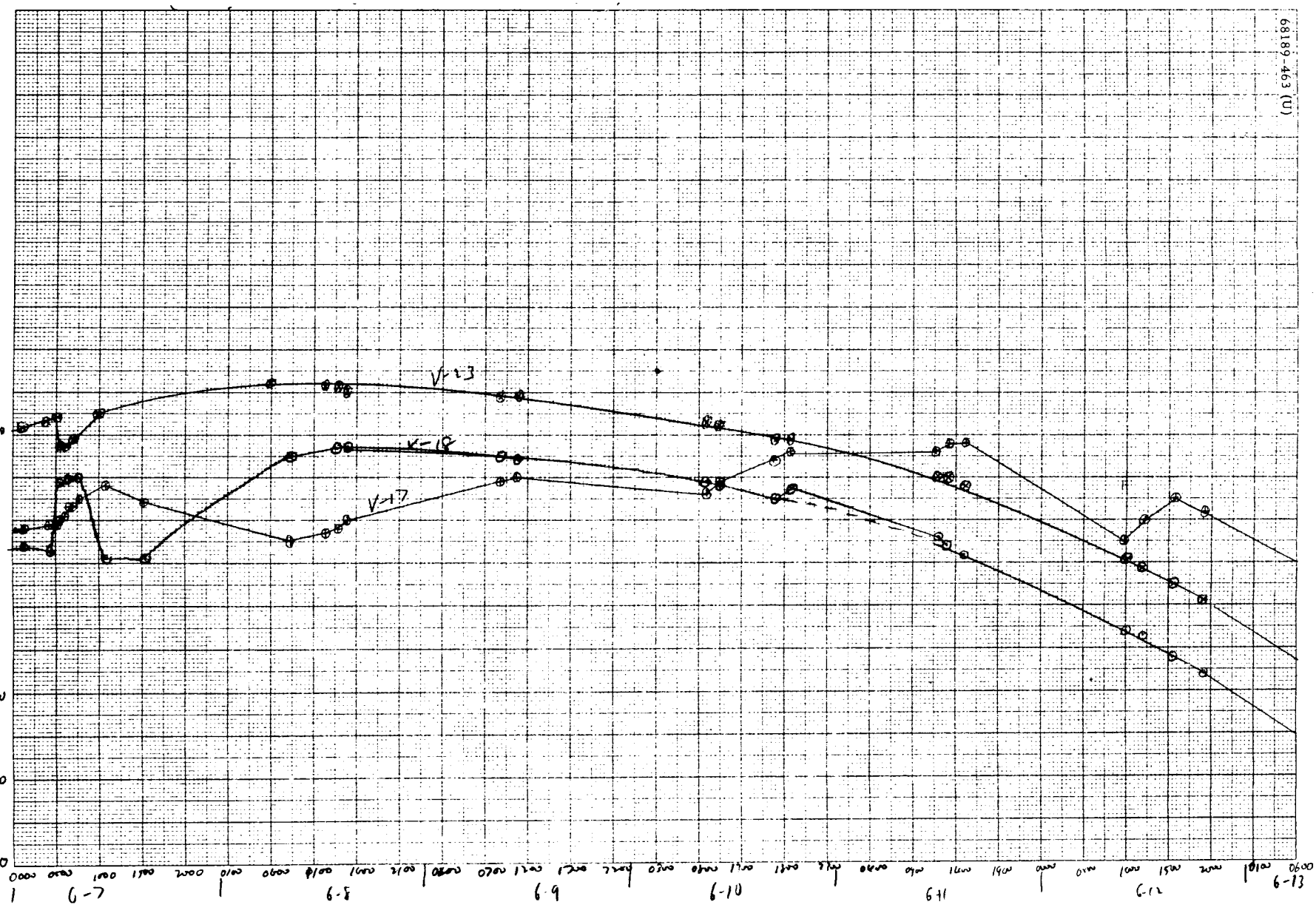


Figure B-7 (continued). Compartment A and B Outer Shells

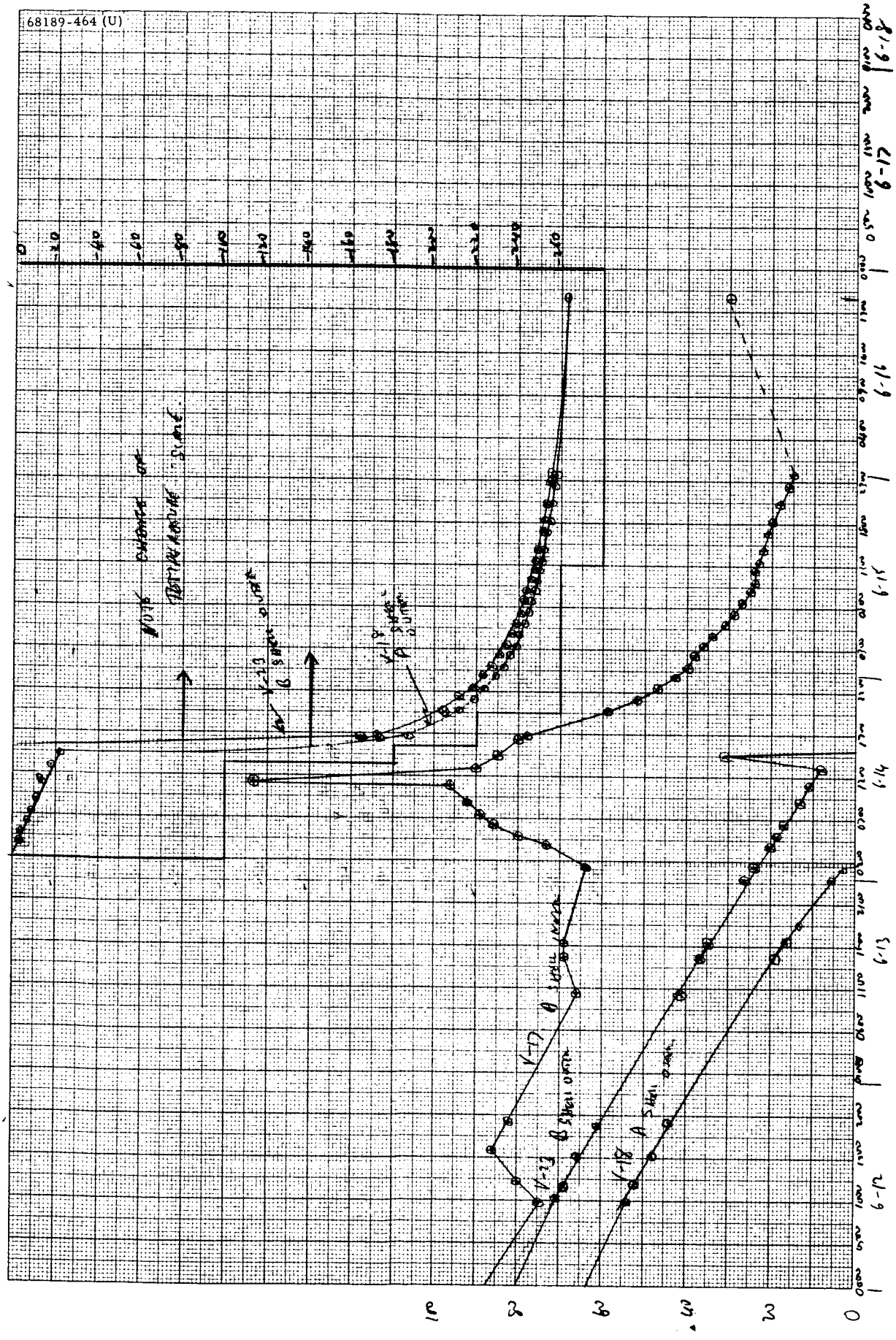


Figure B-7 (continued). Compartment A and B Outer Shells

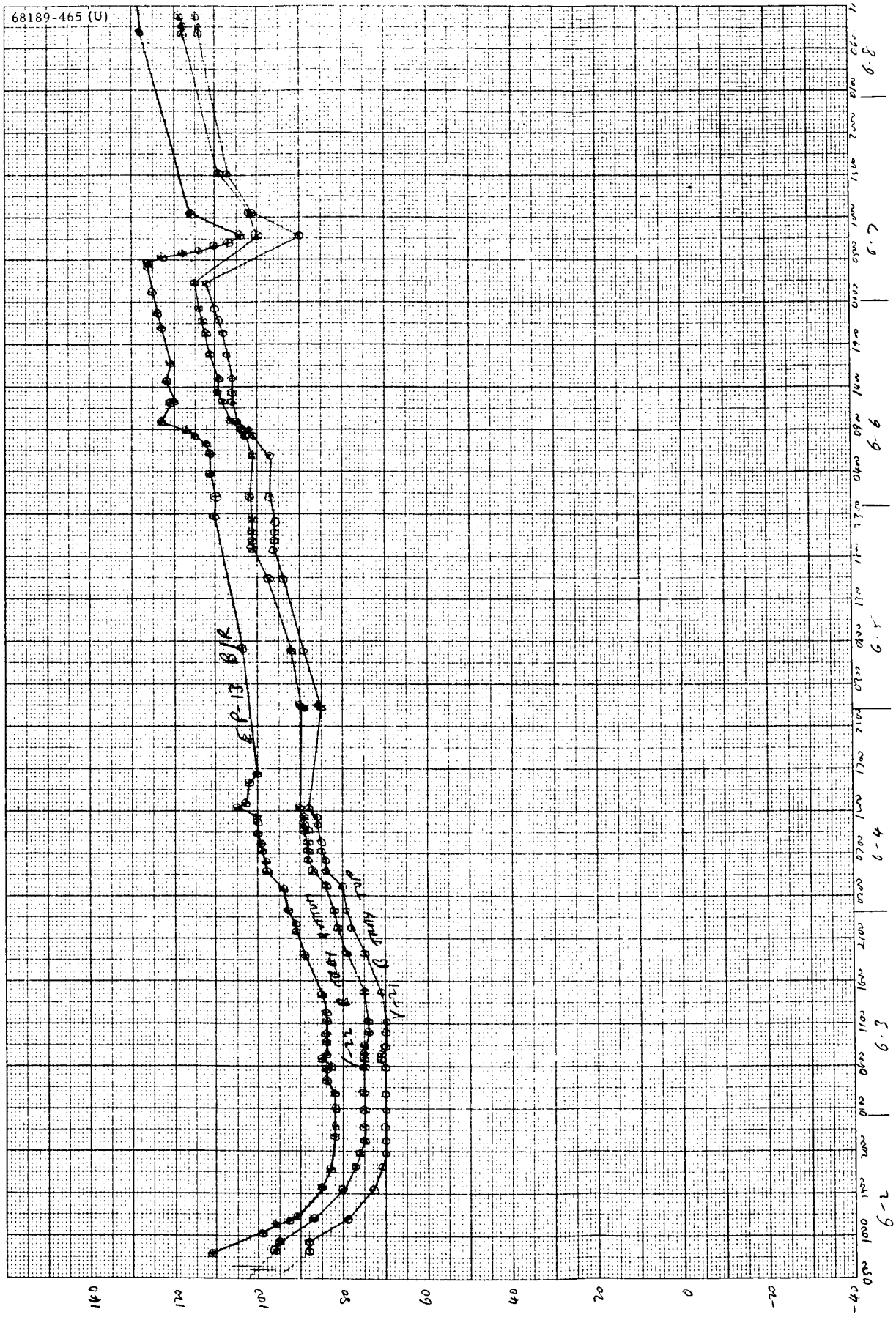


Figure B-8. Boost Regulator and Compartment B Top and Bottom Tray

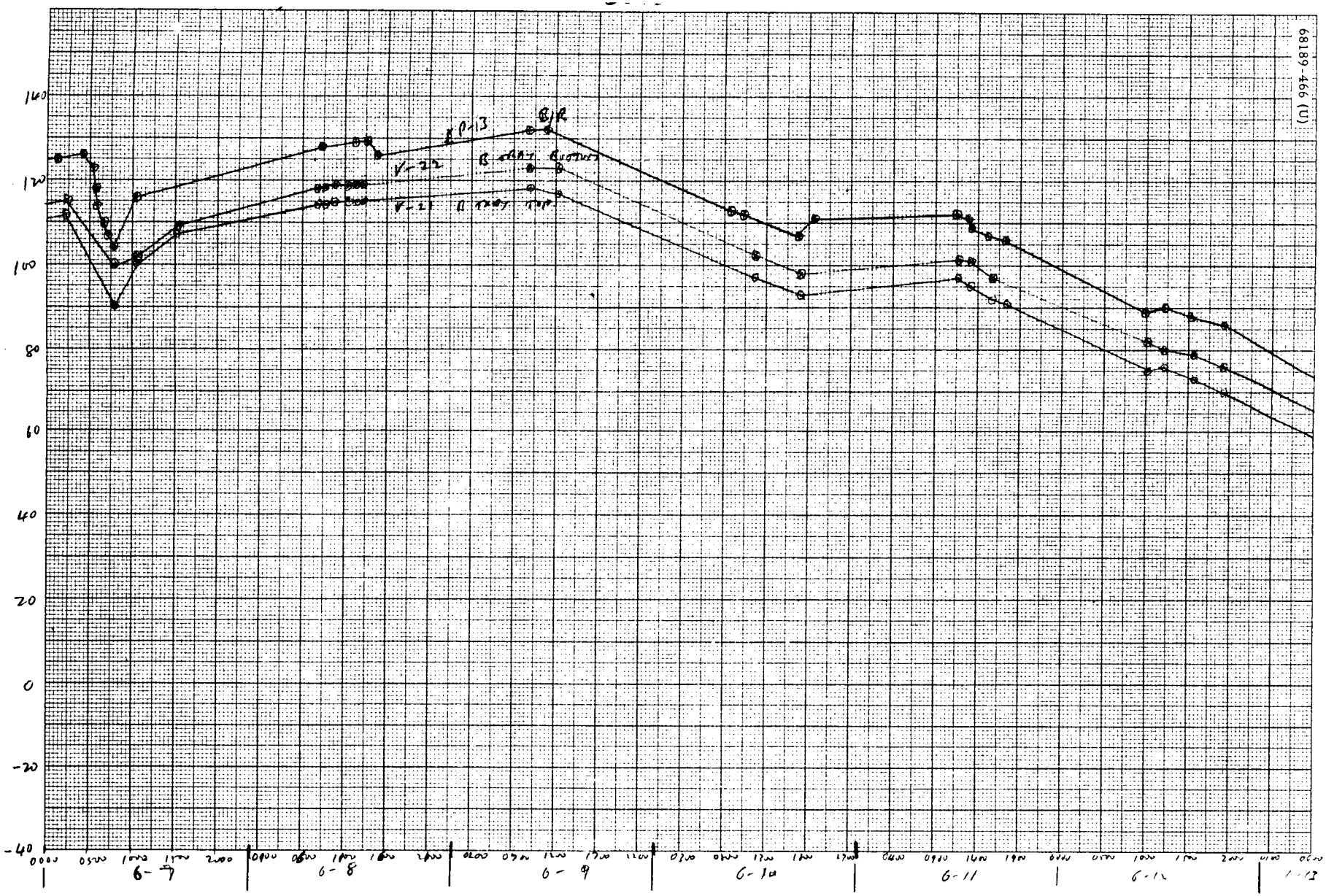


Figure B-8 (continued). Boost Regulator and Compartment B Top and Bottom Tray

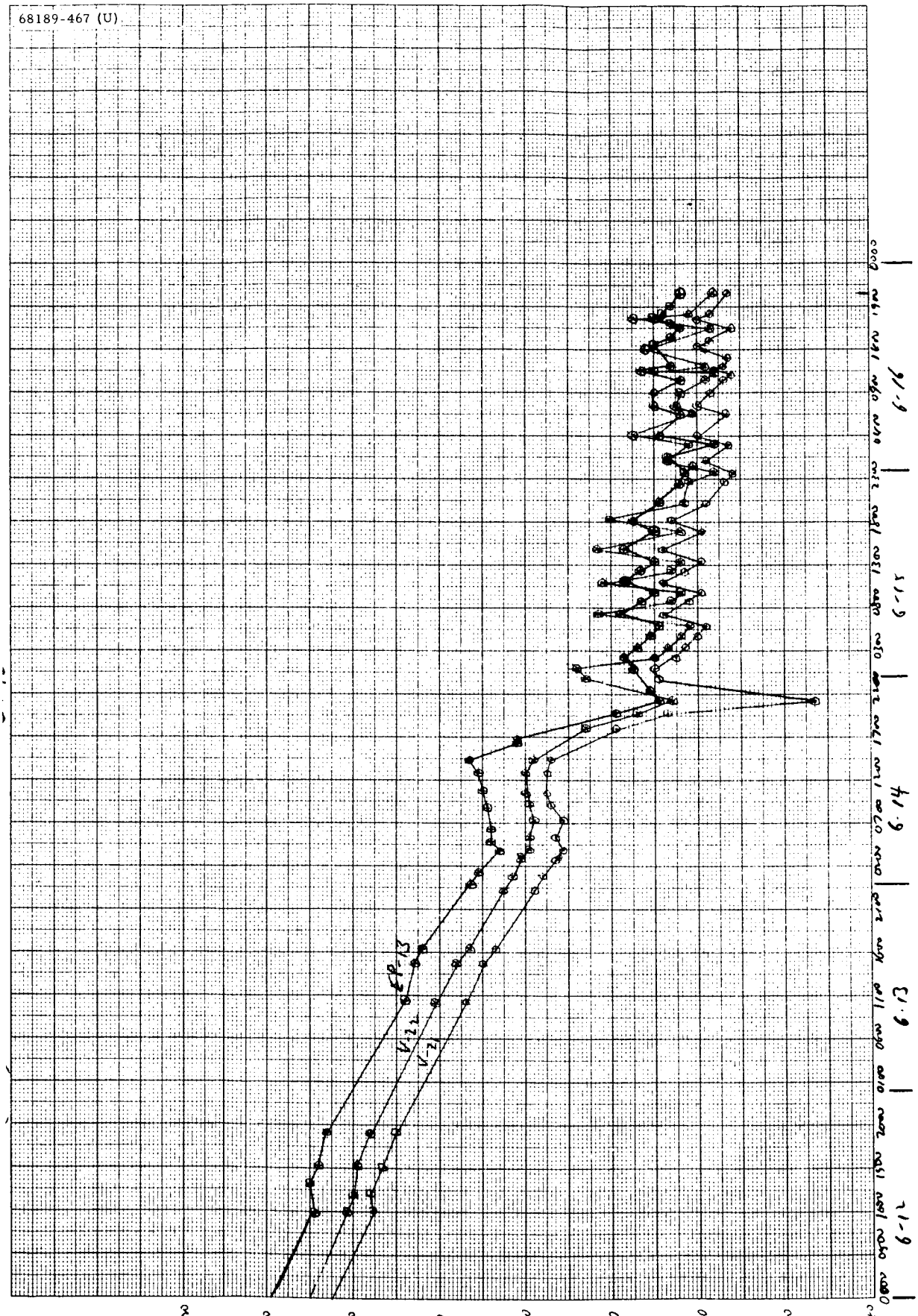


Figure B-8 (continued). Boost Regulator and Compartment B Top and Bottom Tray

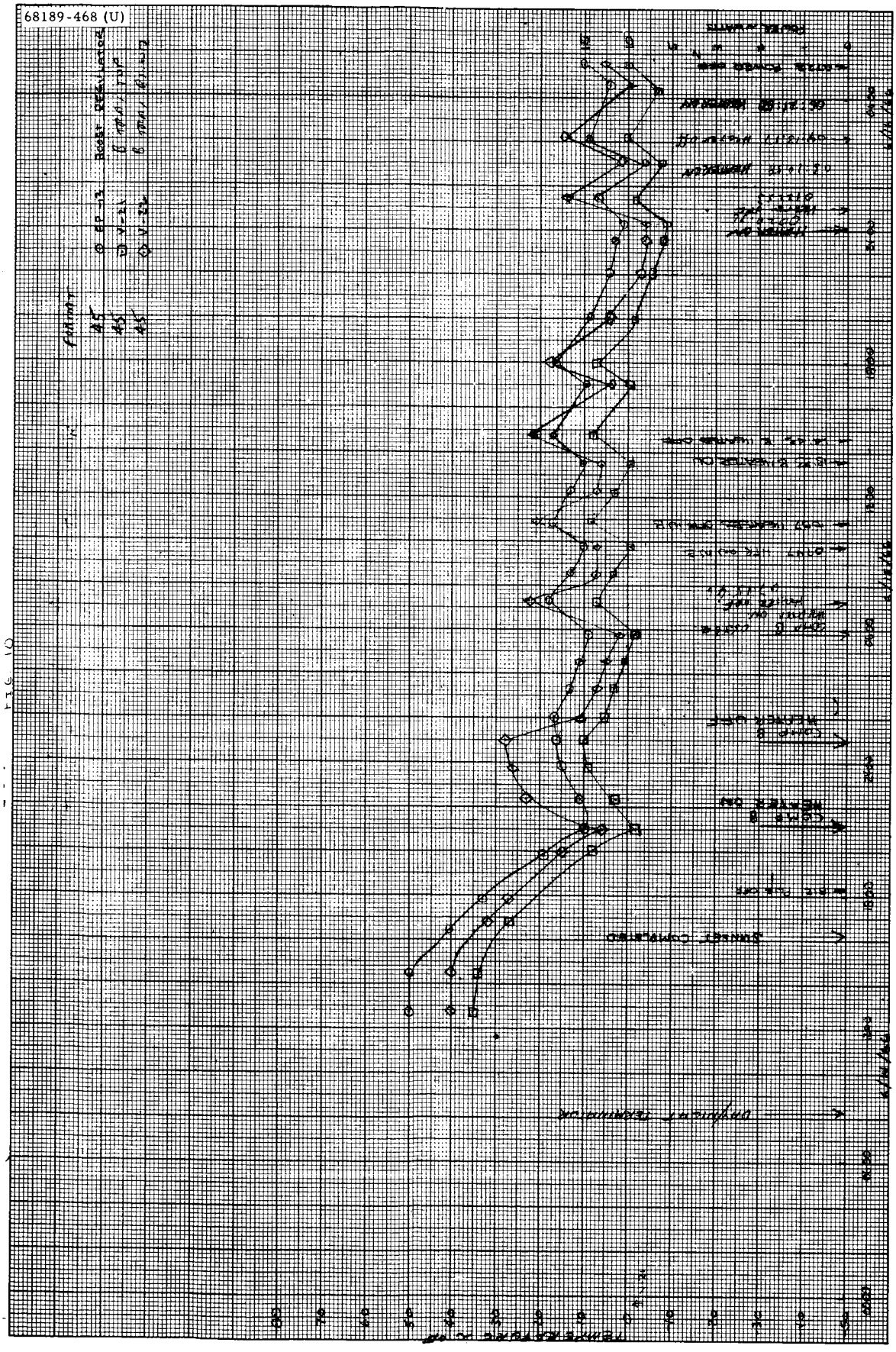


Figure B-8 (continued). Boost Regulator and Compartment B Top and Bottom Tray

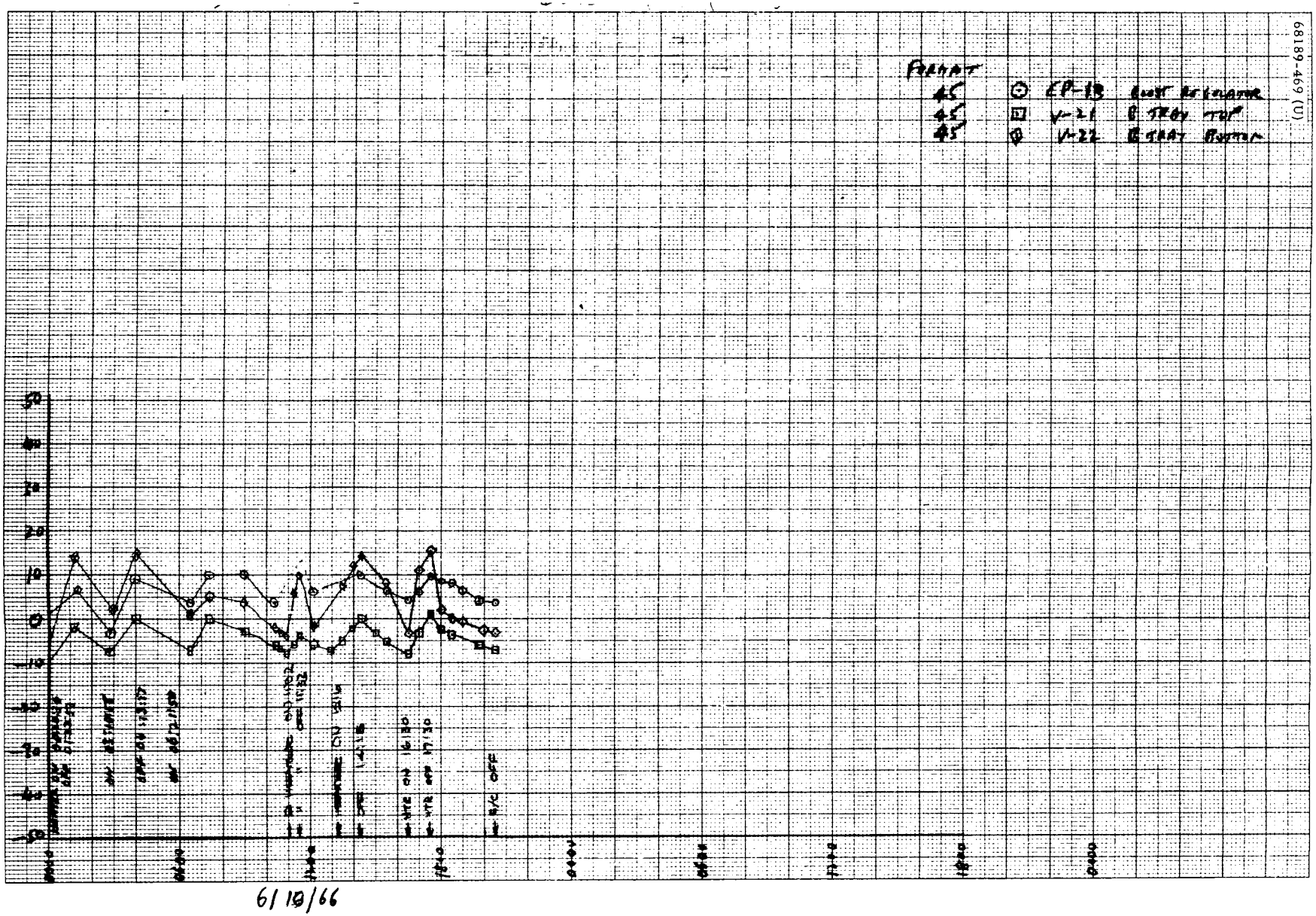


Figure B-8 (continued). Boost Regulator and Compartment B Top and Bottom Tray

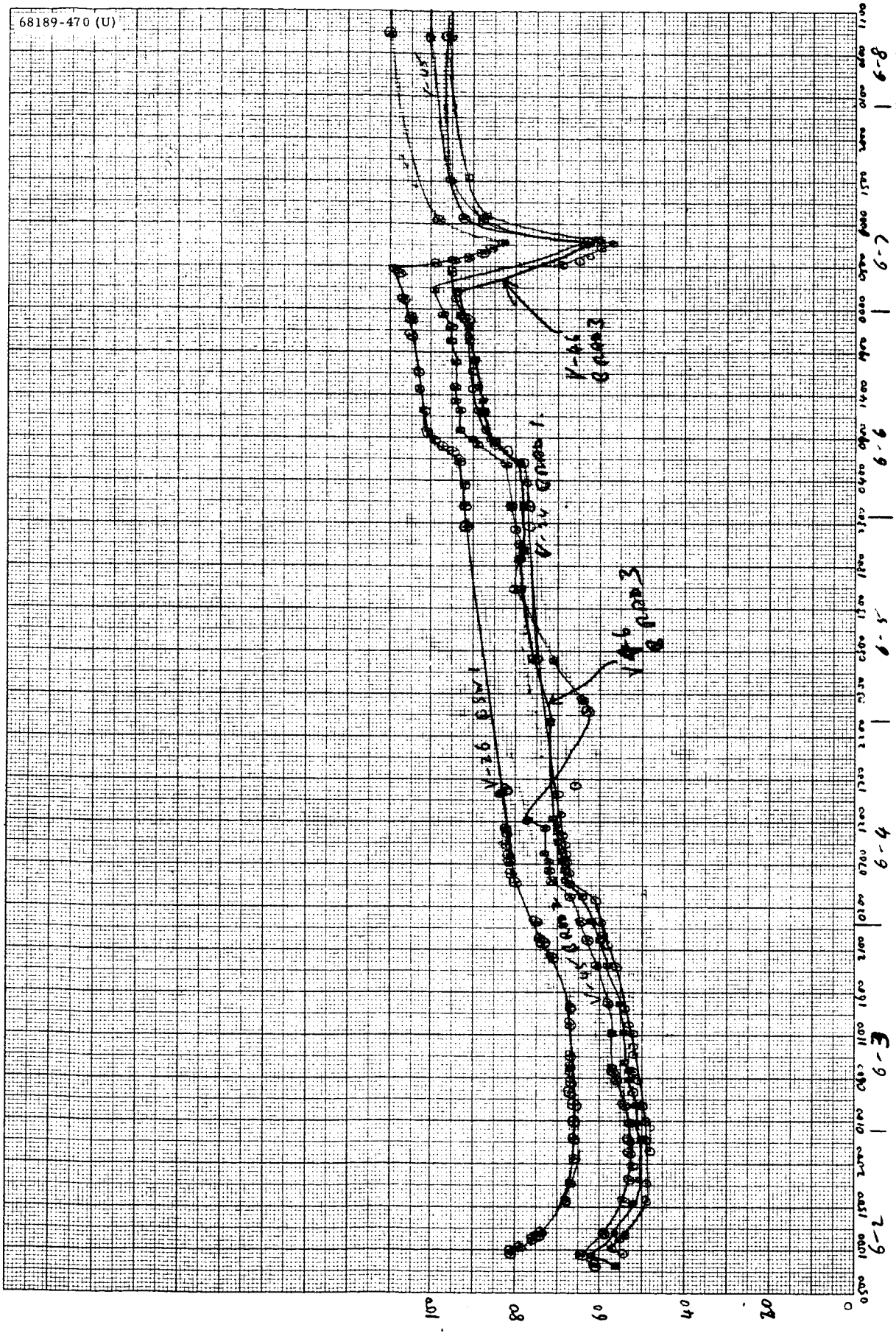


Figure B-9. Compartment B Radiators and Contact Rings

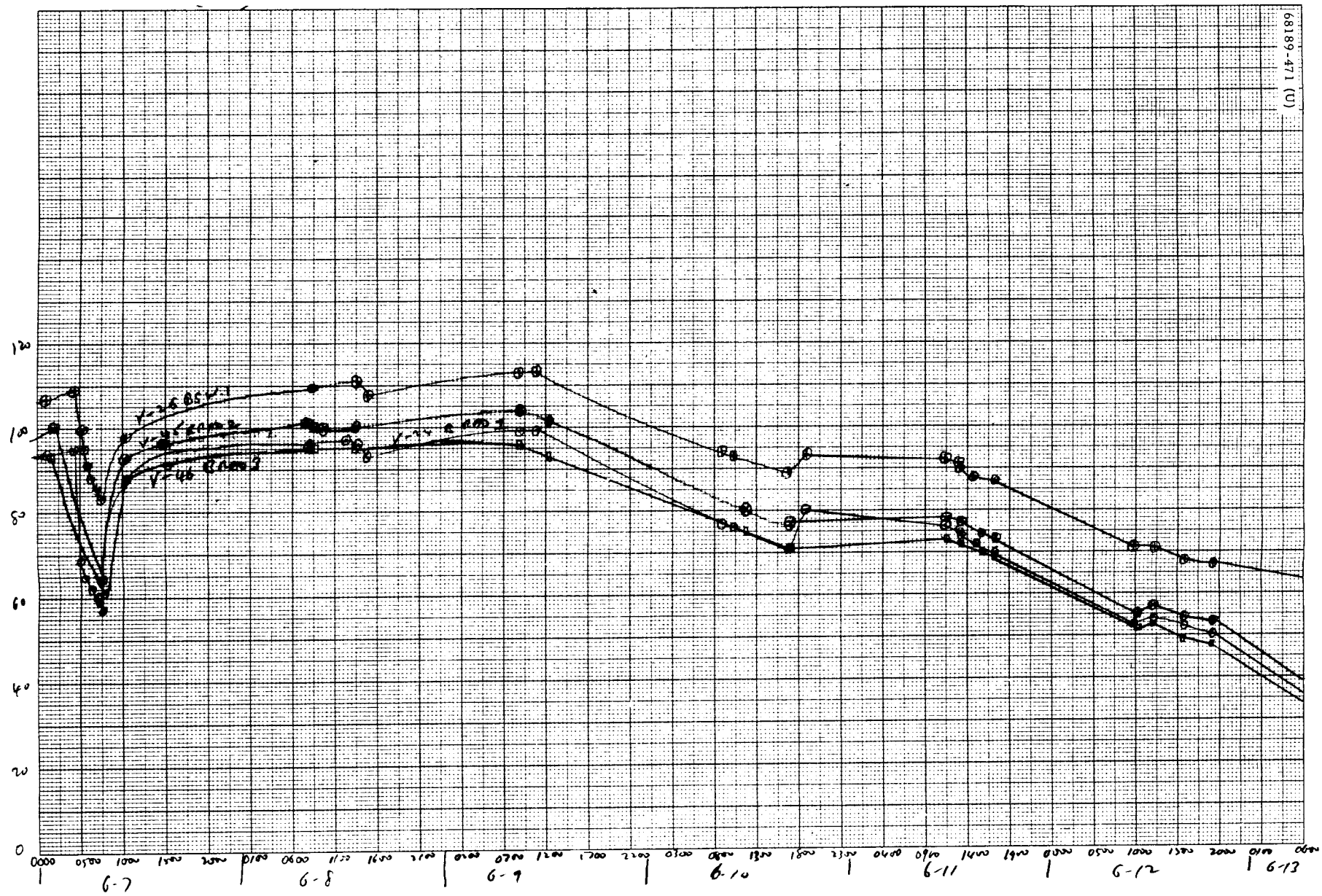


Figure B-9 (continued). Compartment B Radiators and Contact Rings

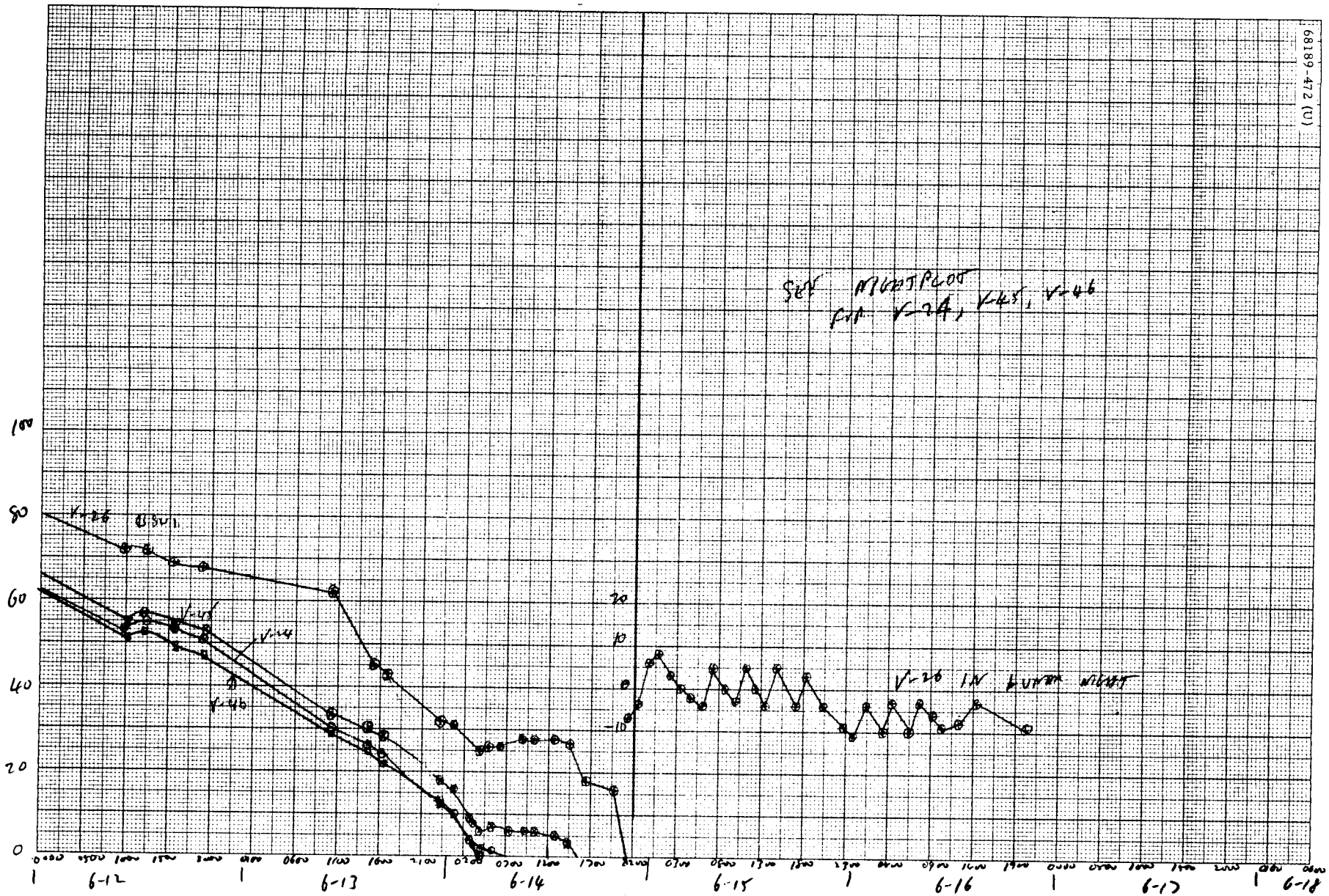


Figure B-9 (continued). Compartment B Radiators and Contact Rings

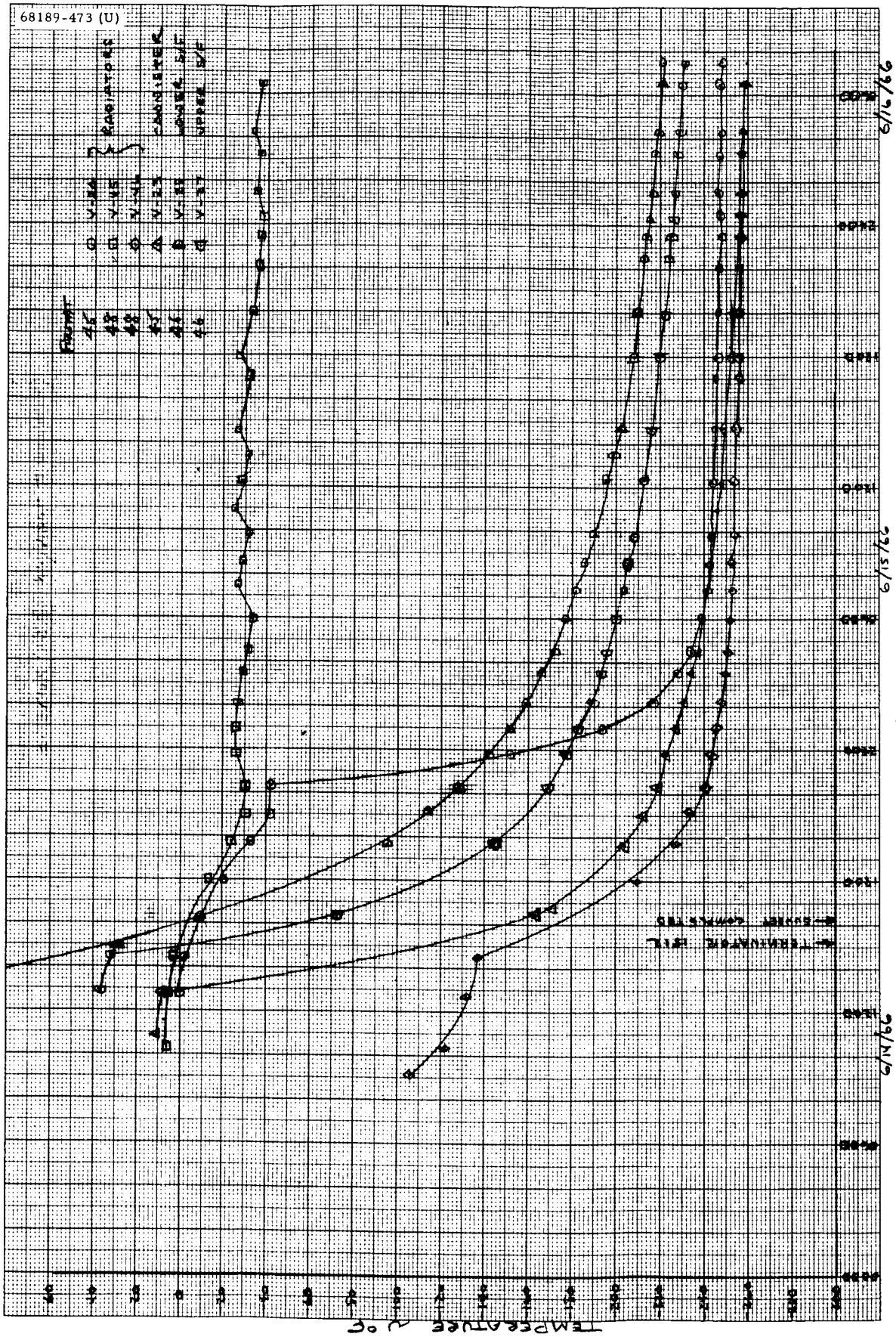


Figure B-10. Compartment B Exterior (Near Day and Night Terminator)

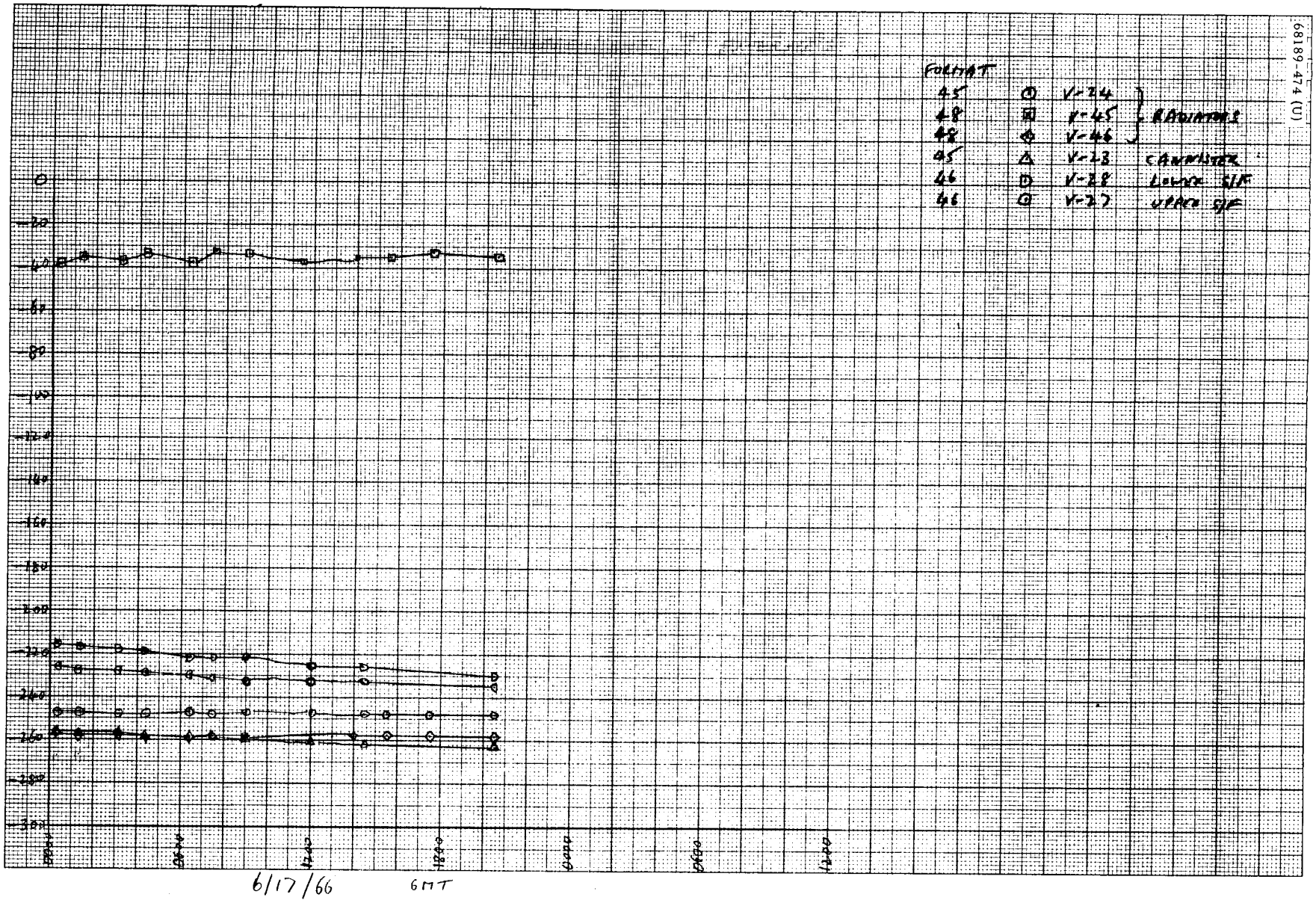


Figure B-10 (continued). Compartment B Exterior (Near Day and Night Terminator)

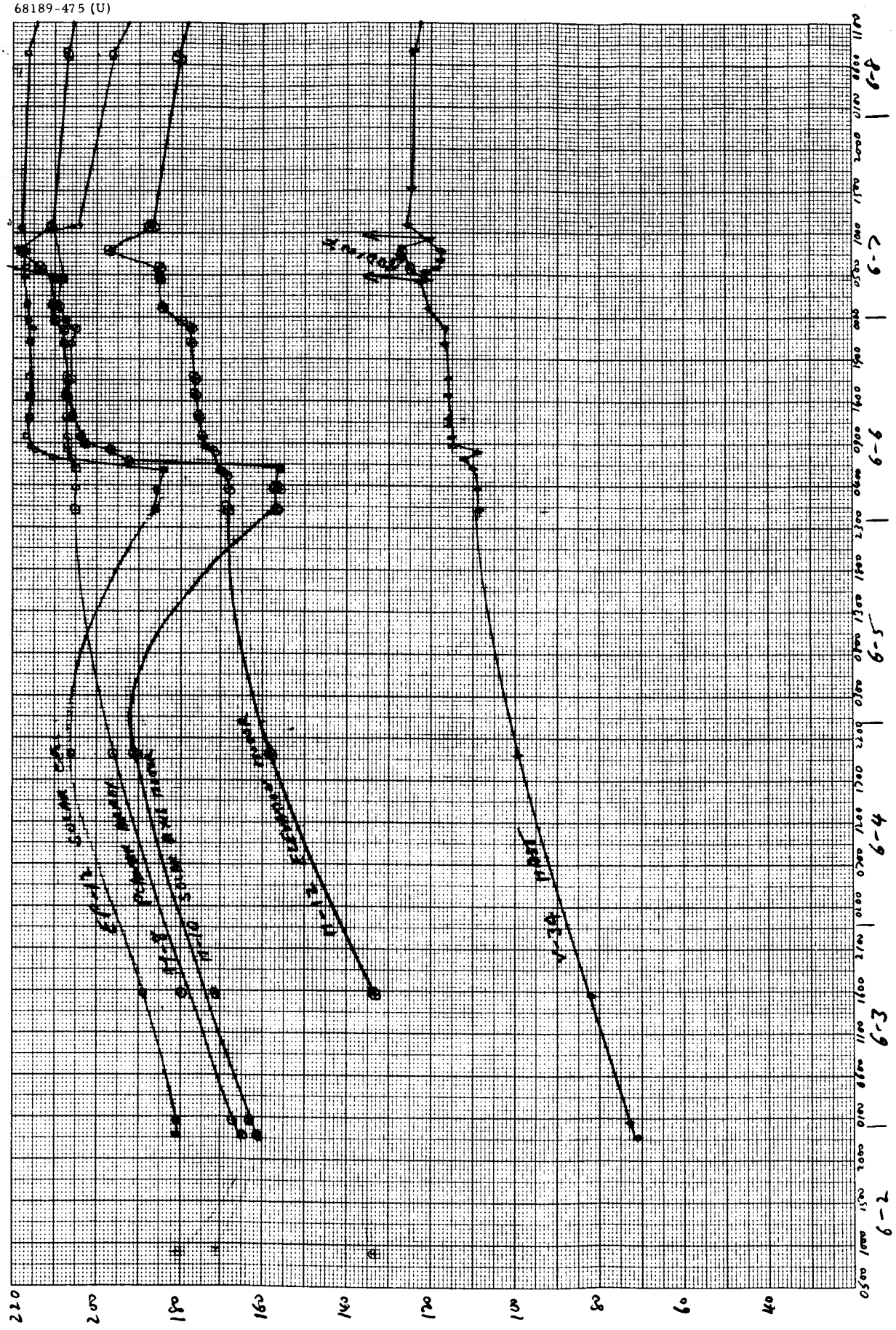


Figure B-11. Mast, A/SPP, and Solar Cells

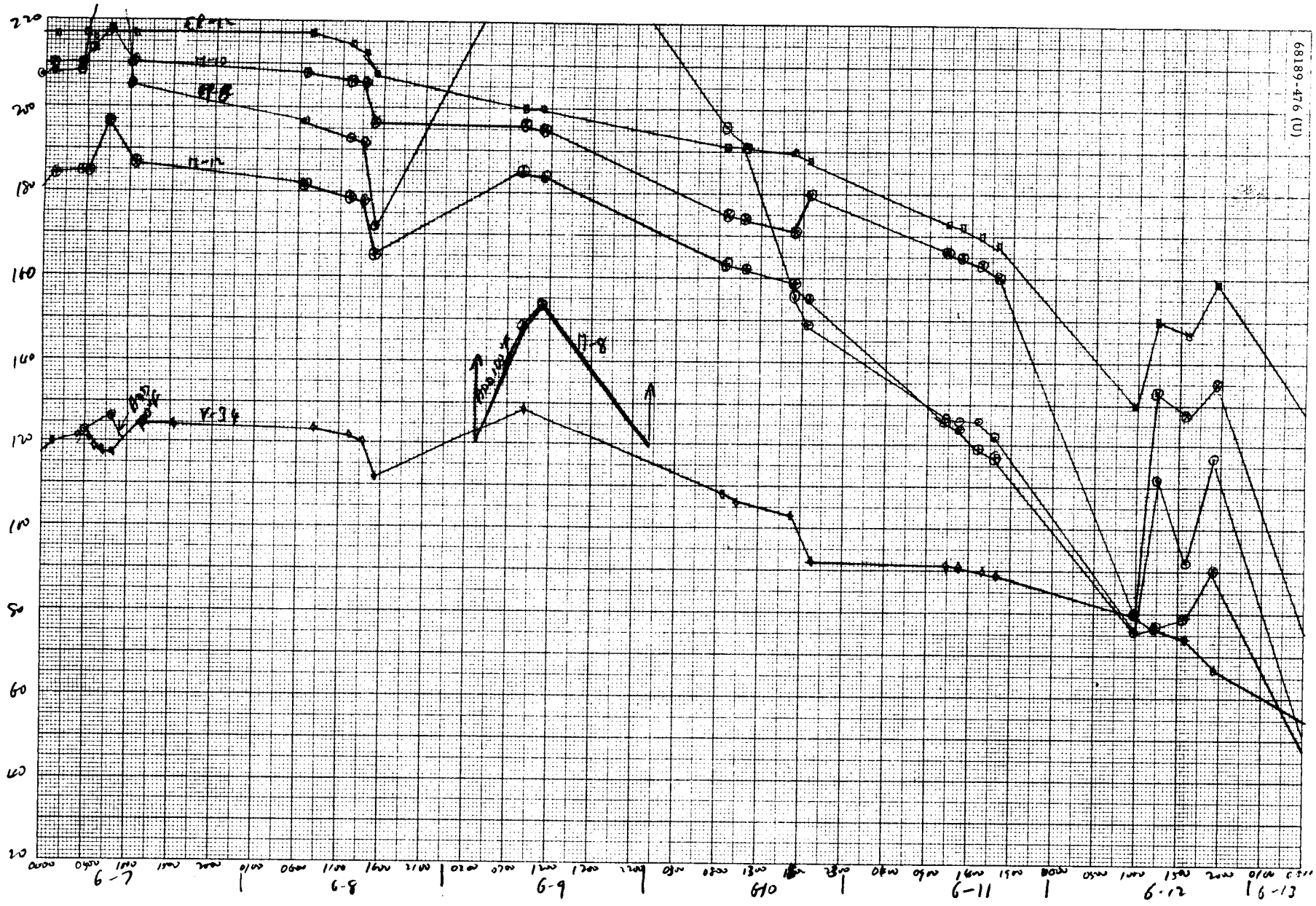


Figure B-11 (continued). Mast, A/SPP, and Solar Cells

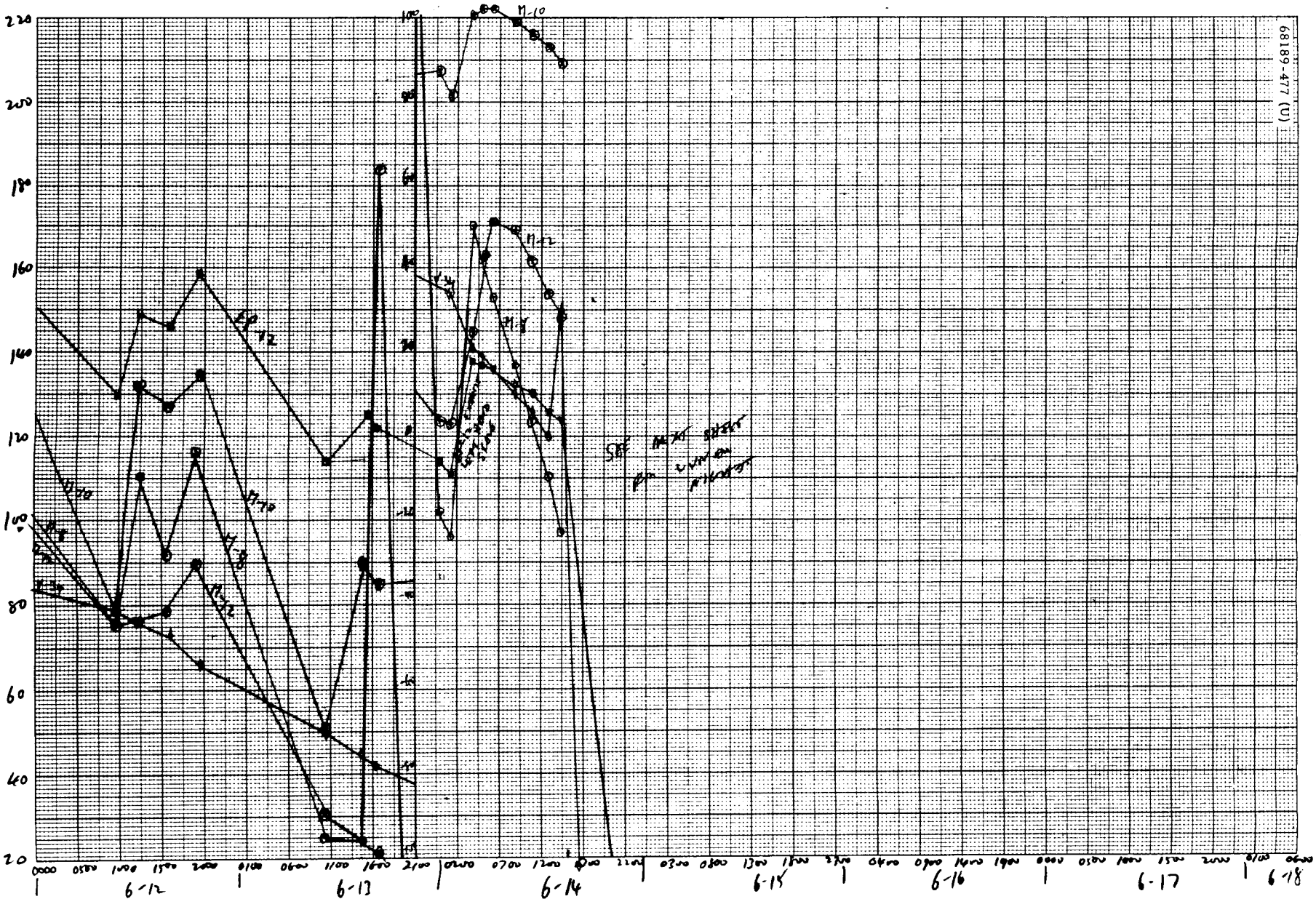


Figure B-11 (continued). Mast, A/SPP, and Solar Cells

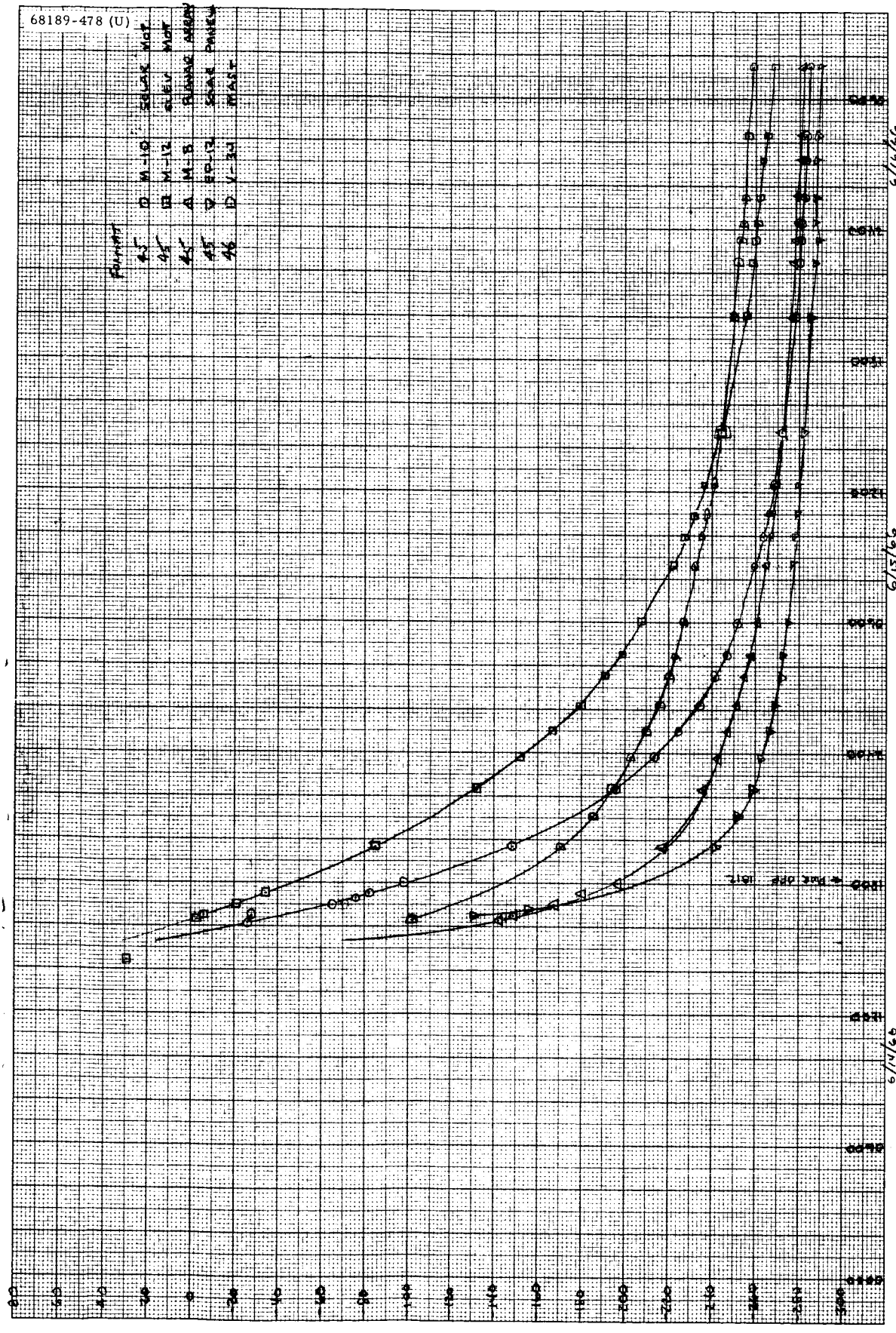


Figure B-11 (continued). Mast, A/SPP, and Solar Cells

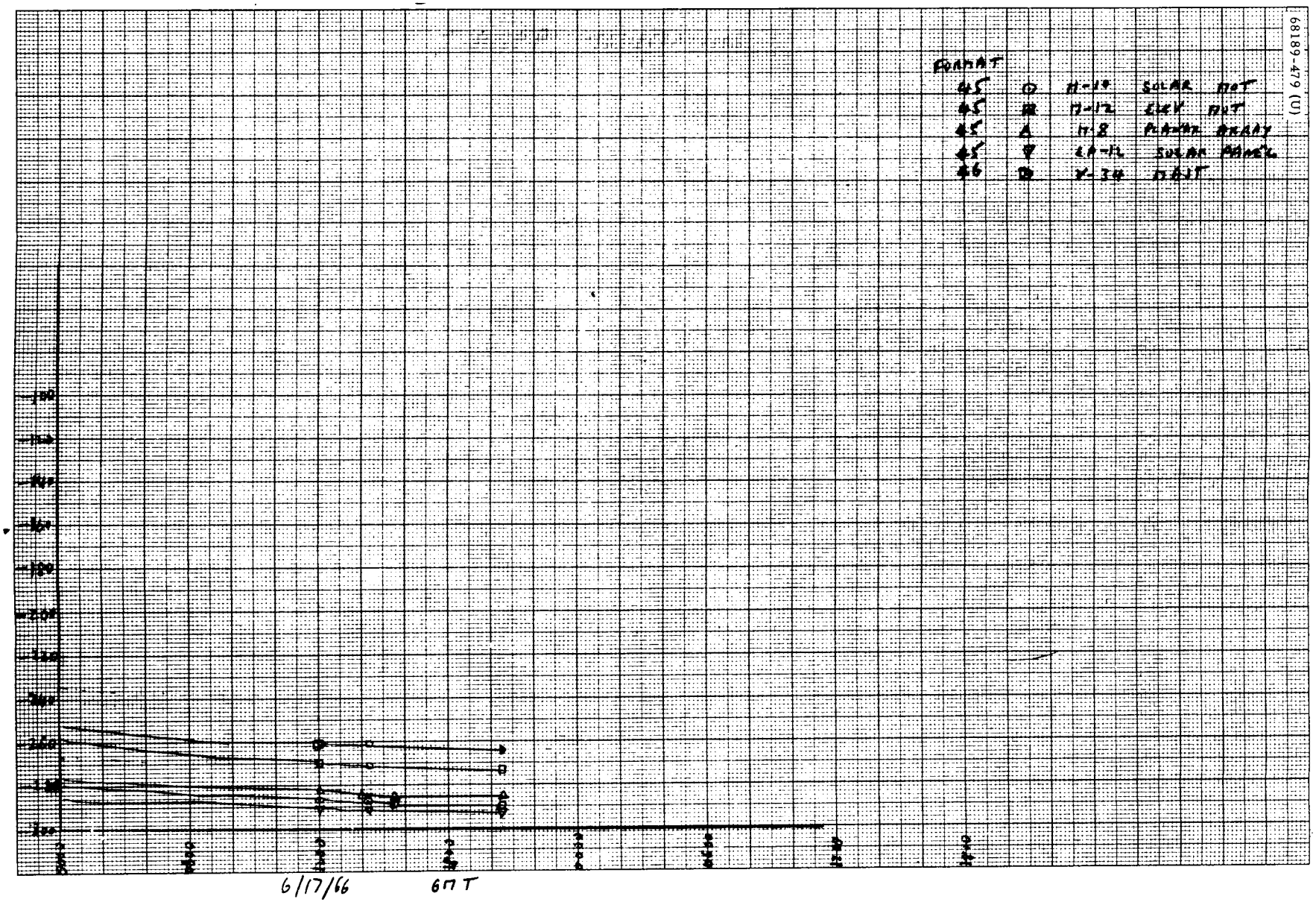


Figure B-11 (continued). Mast, A/SPP, and Solar Cells

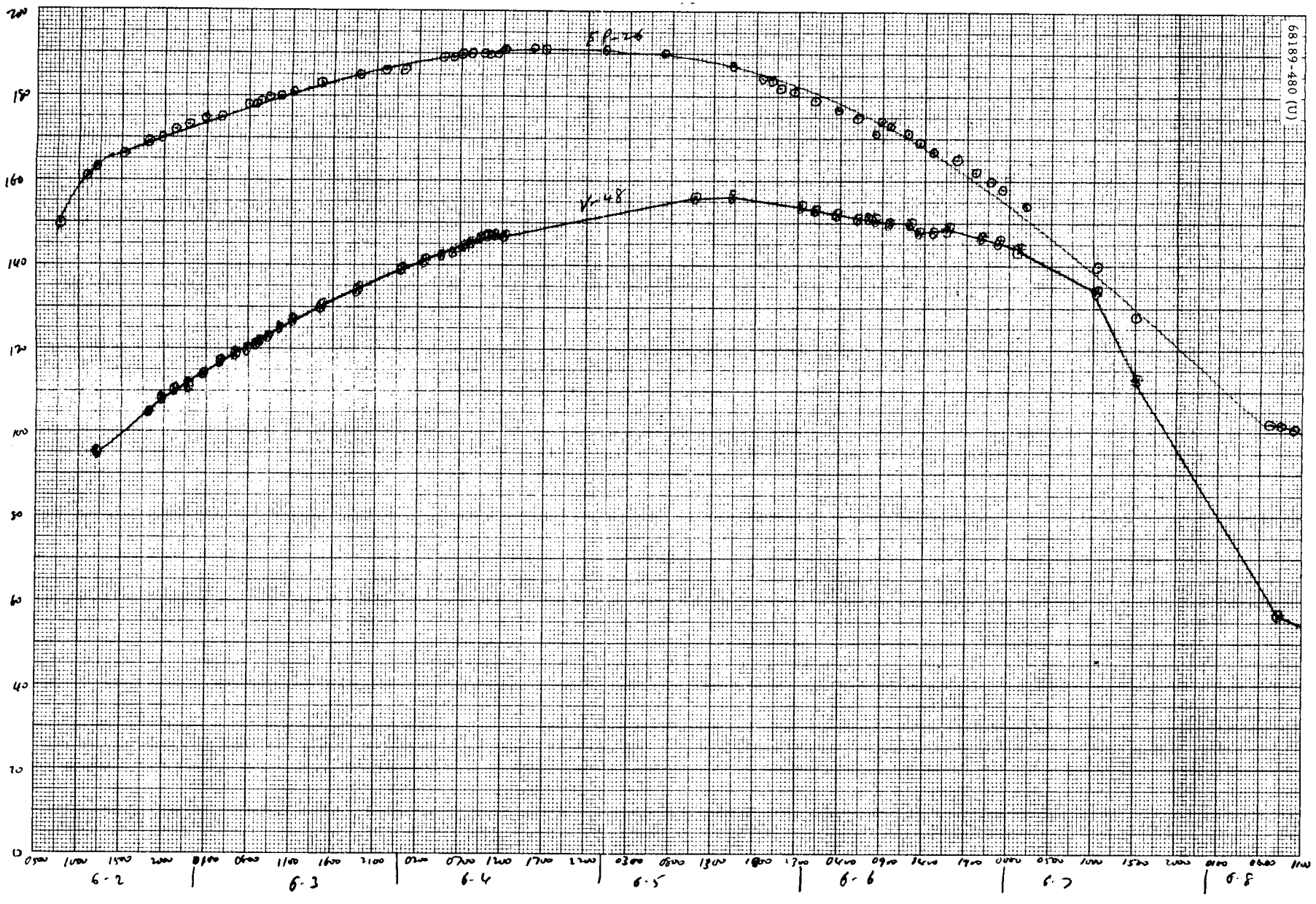


Figure B-12. Auxiliary Battery/Battery Case

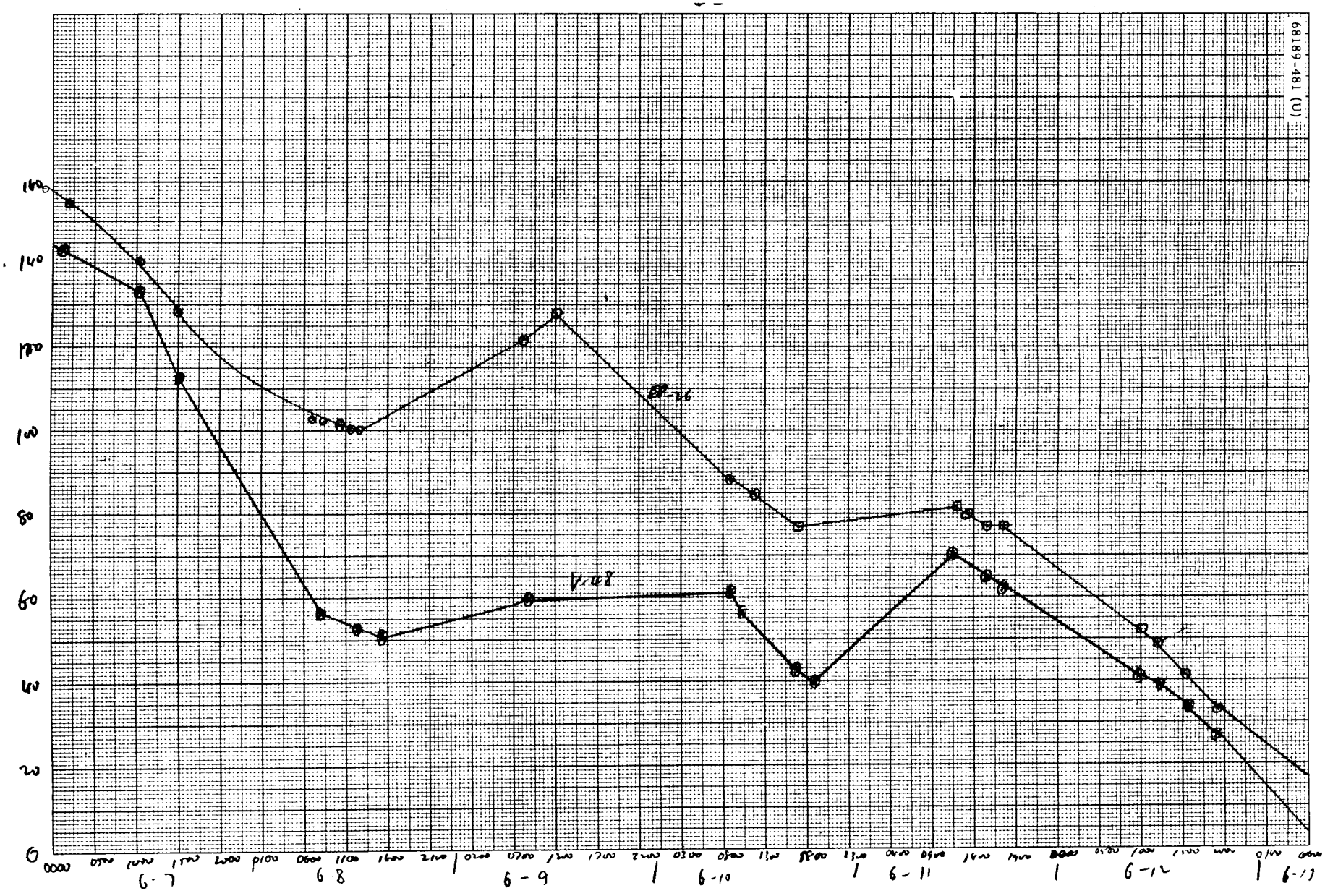


Figure B-12 (continued). Auxiliary Battery/Battery Case

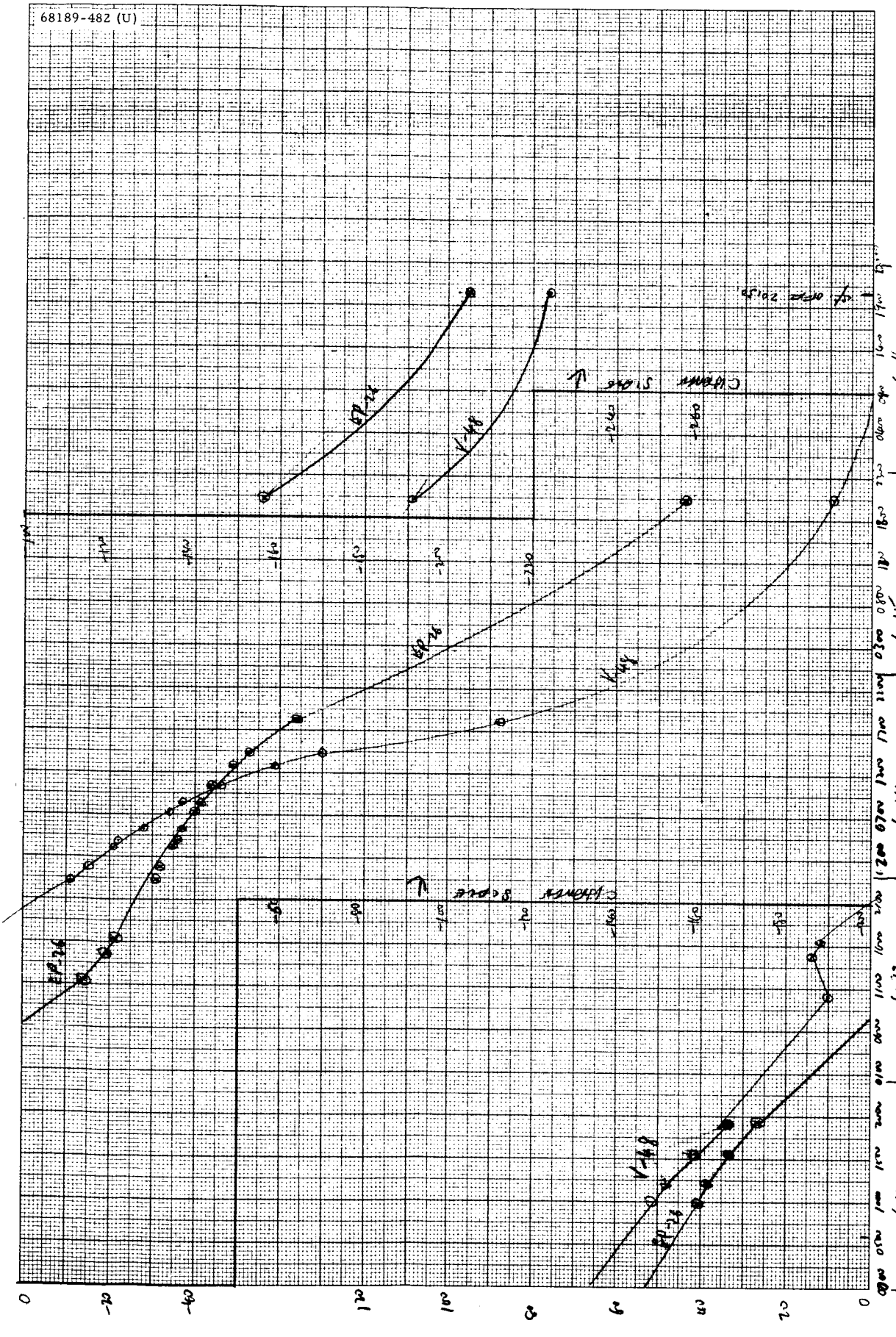


Figure B-12 (continued). Auxiliary Battery/Battery Case

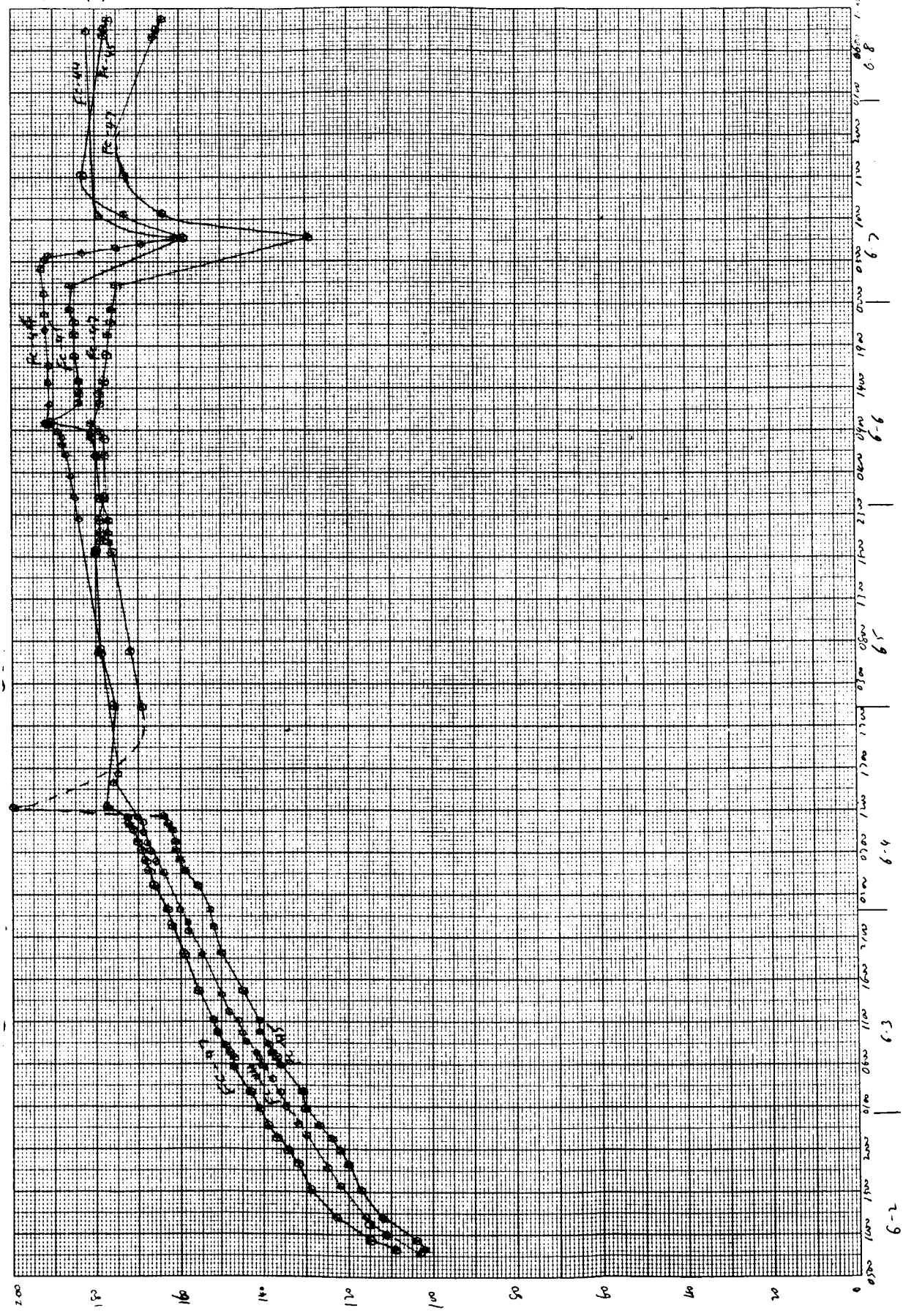


Figure B-13. Flight Control Electronics and Canopus

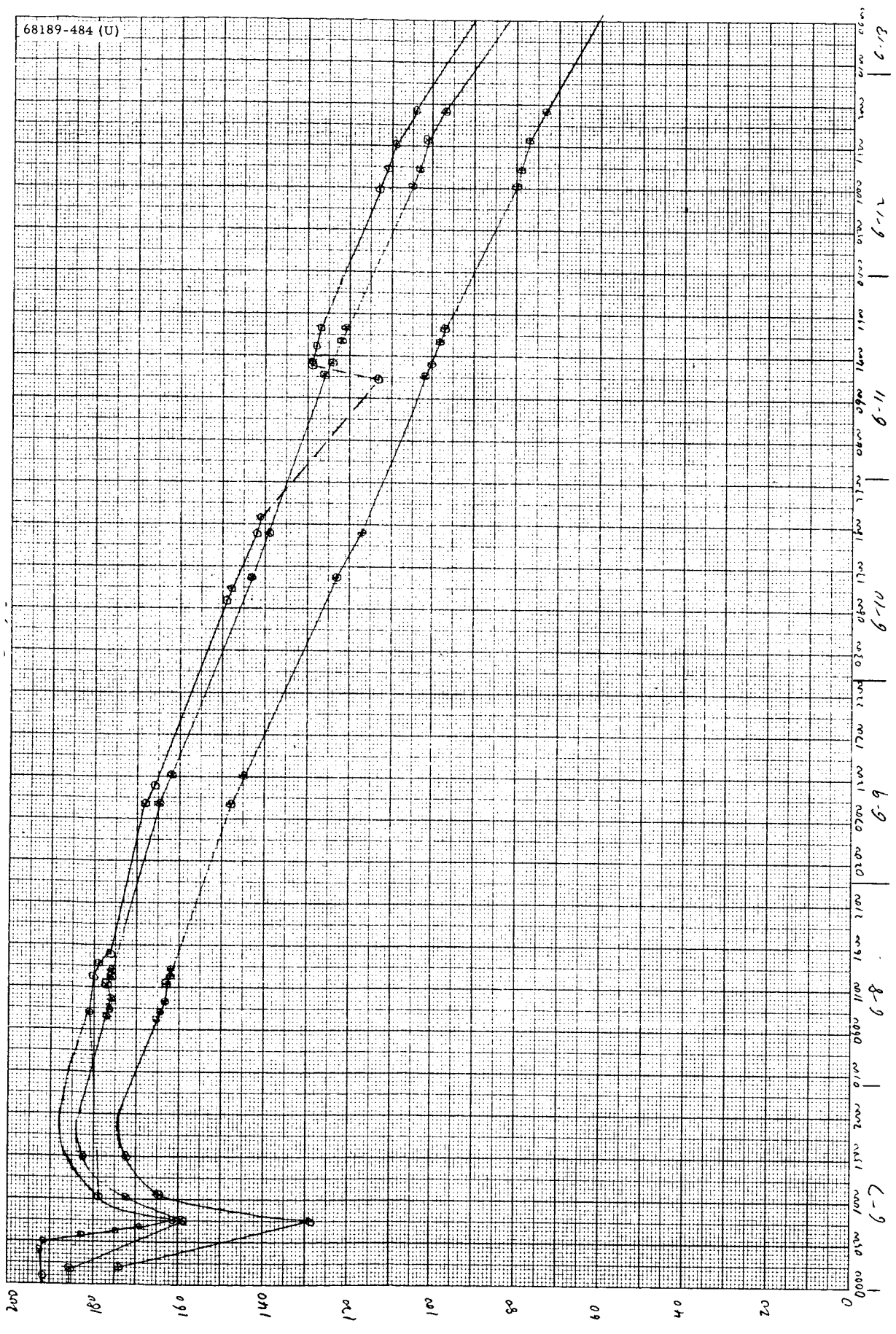


Figure B-13 (continued). Flight Control Electronics and Canopus

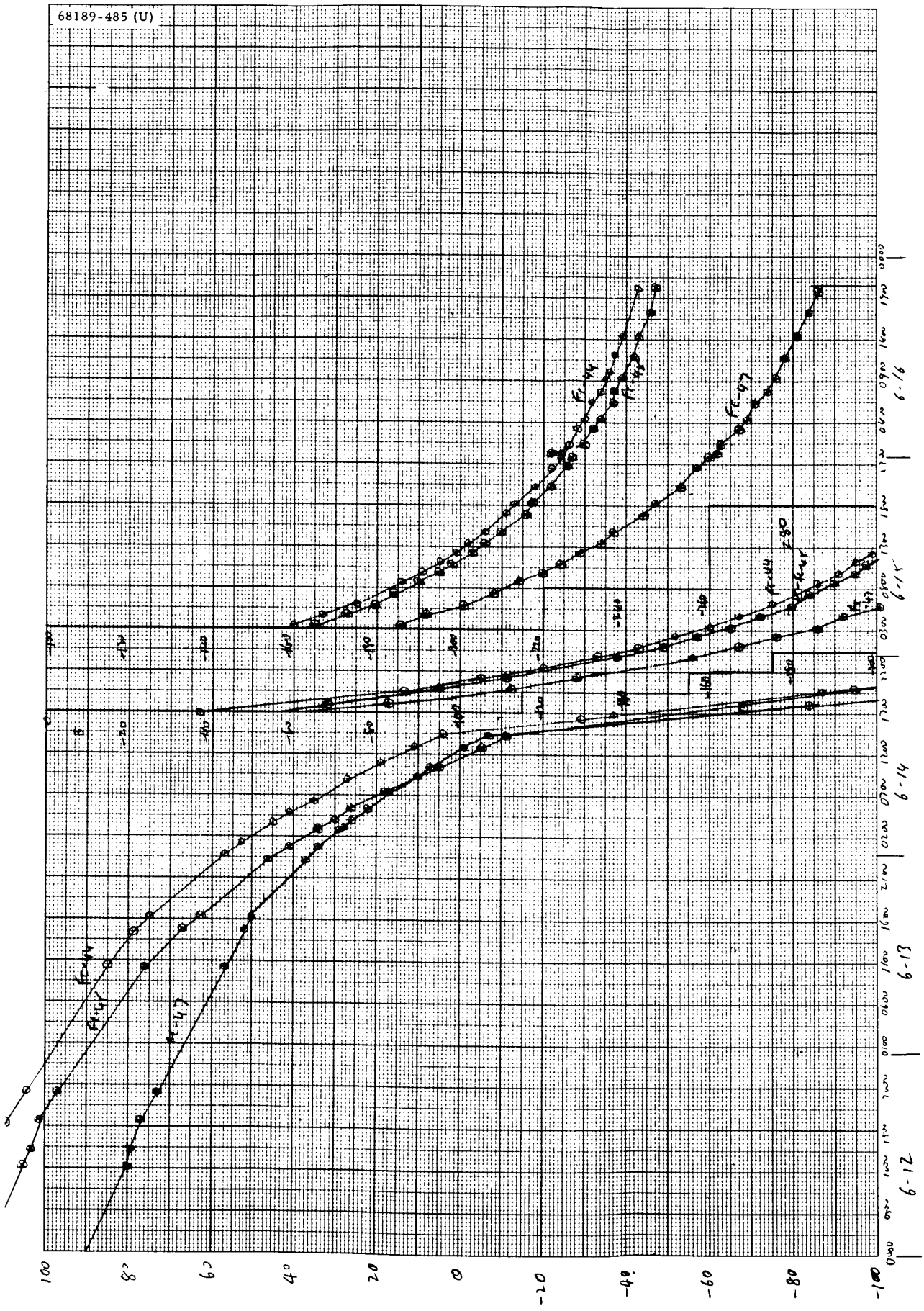


Figure B-13 (continued). Flight Control Electronics and Canopus

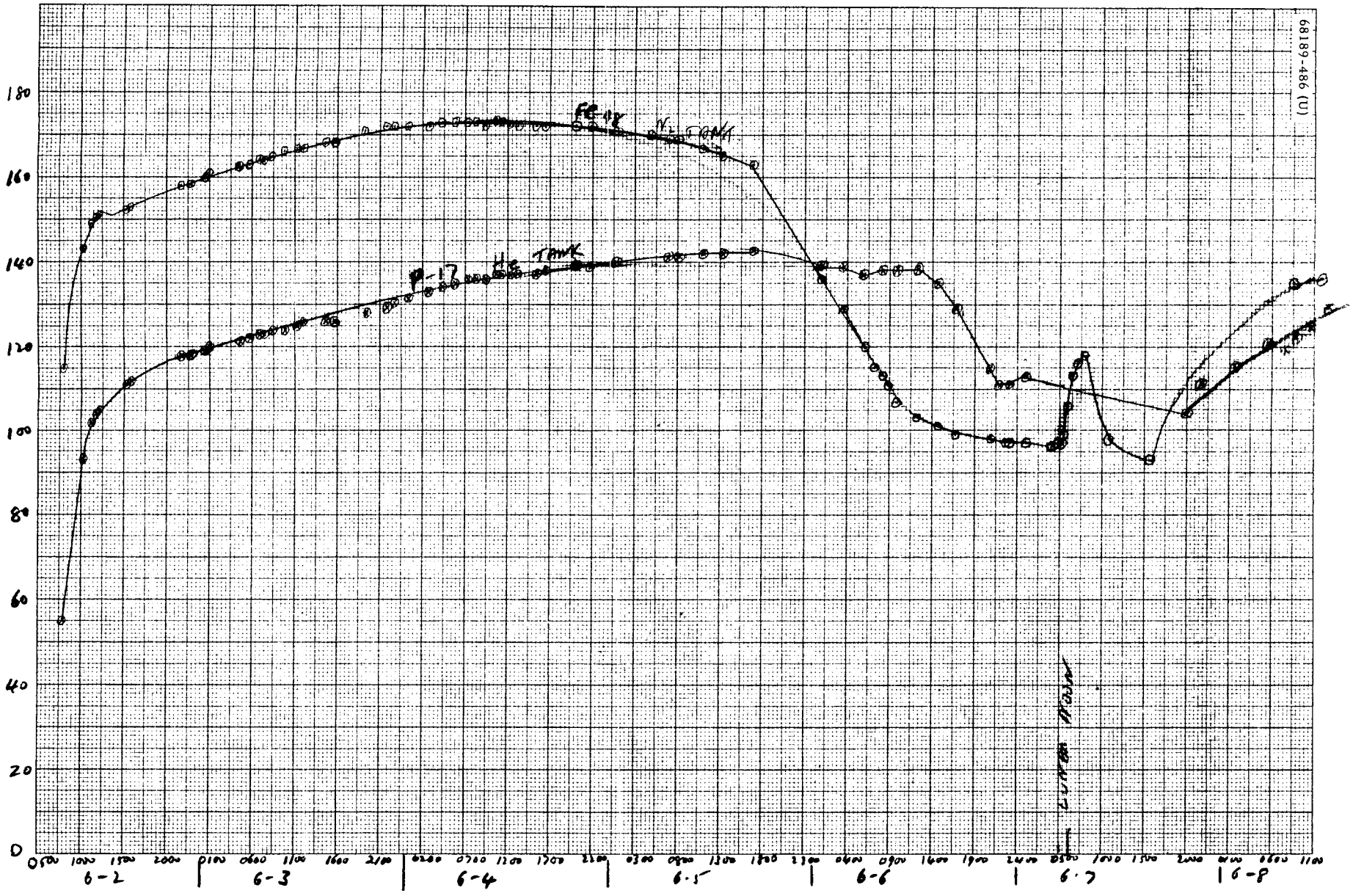


Figure B-14. Nitrogen and Helium Tanks

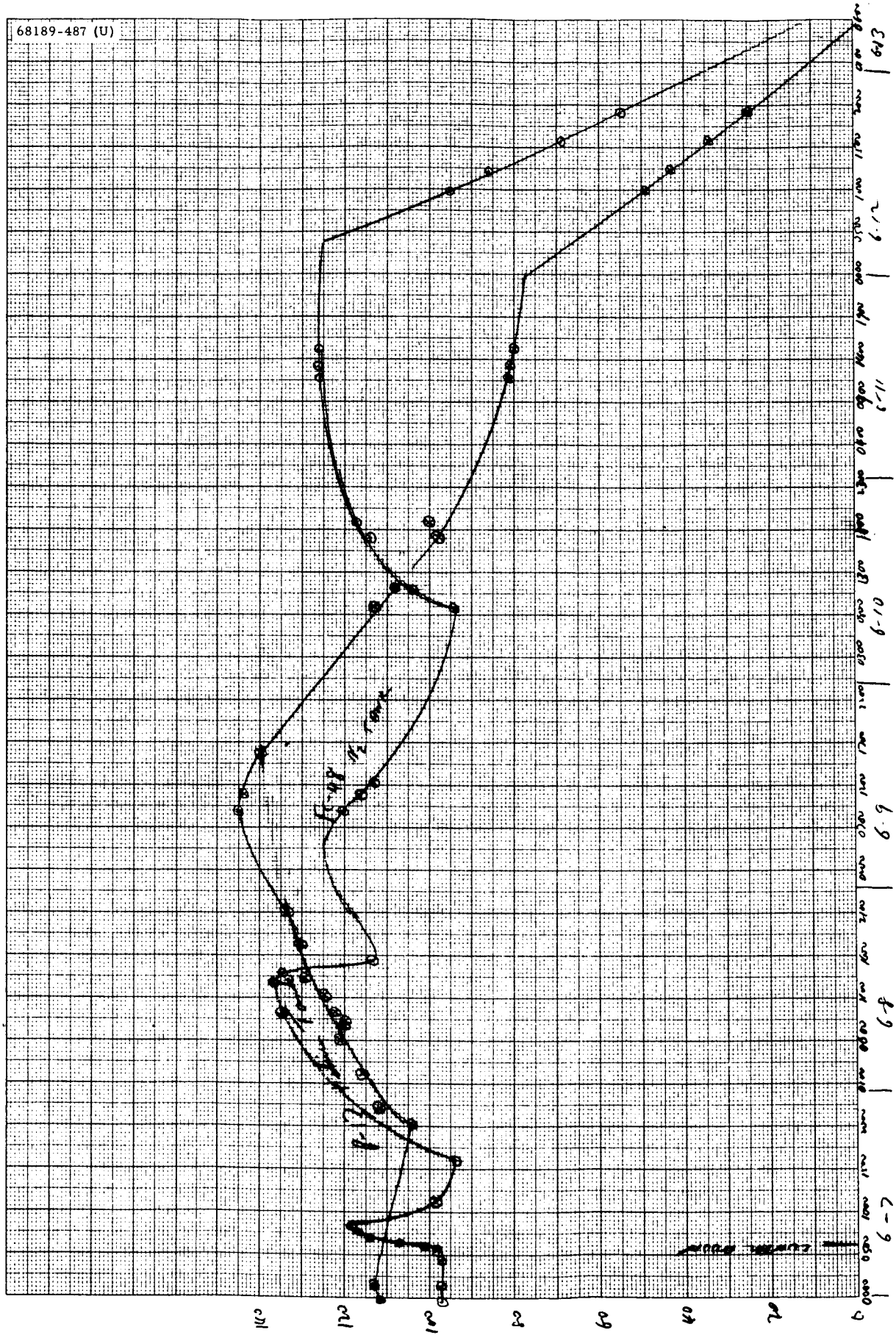


Figure B-14 (continued). Nitrogen and Helium Tanks

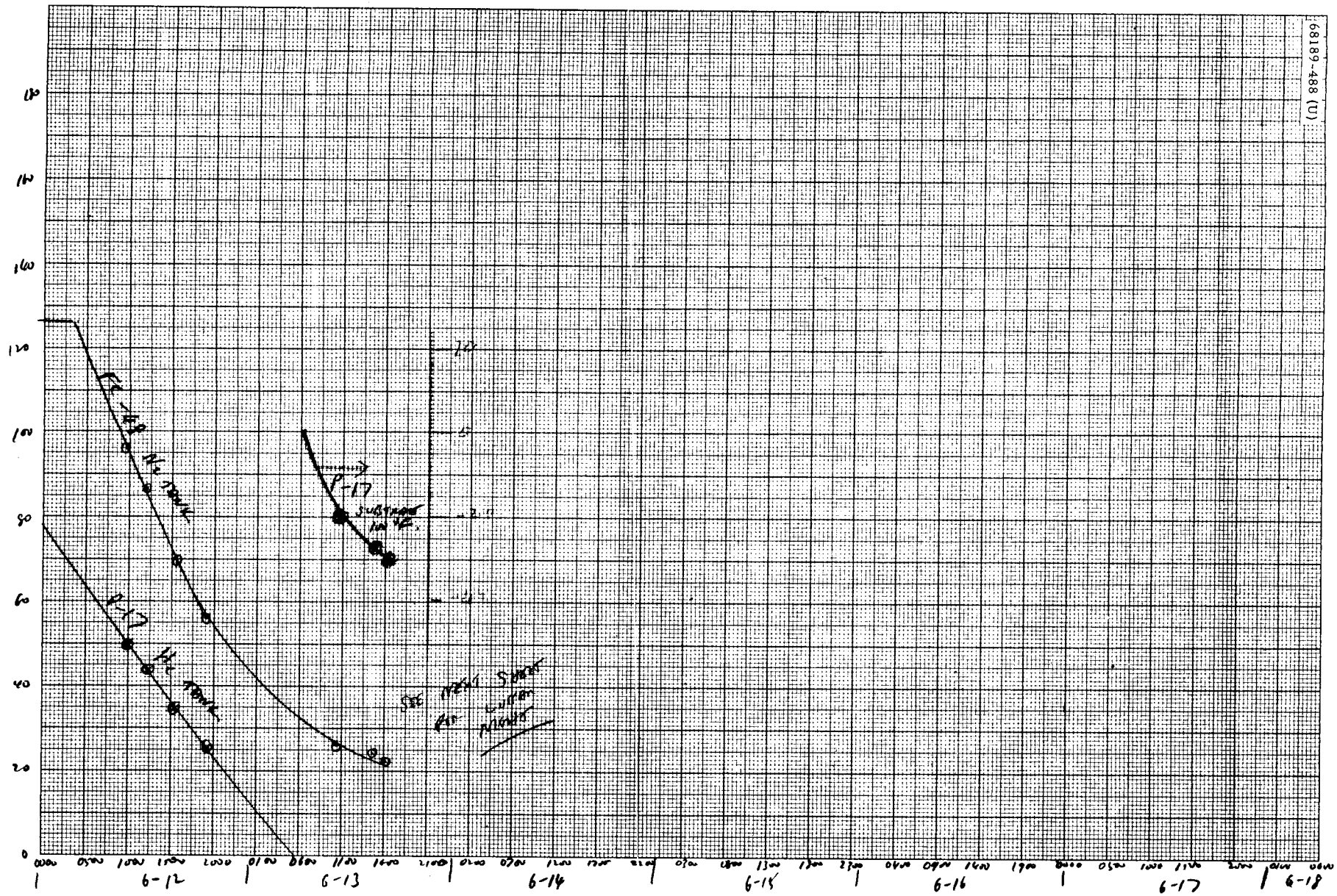


Figure B-14 (continued). Nitrogen and Helium Tanks

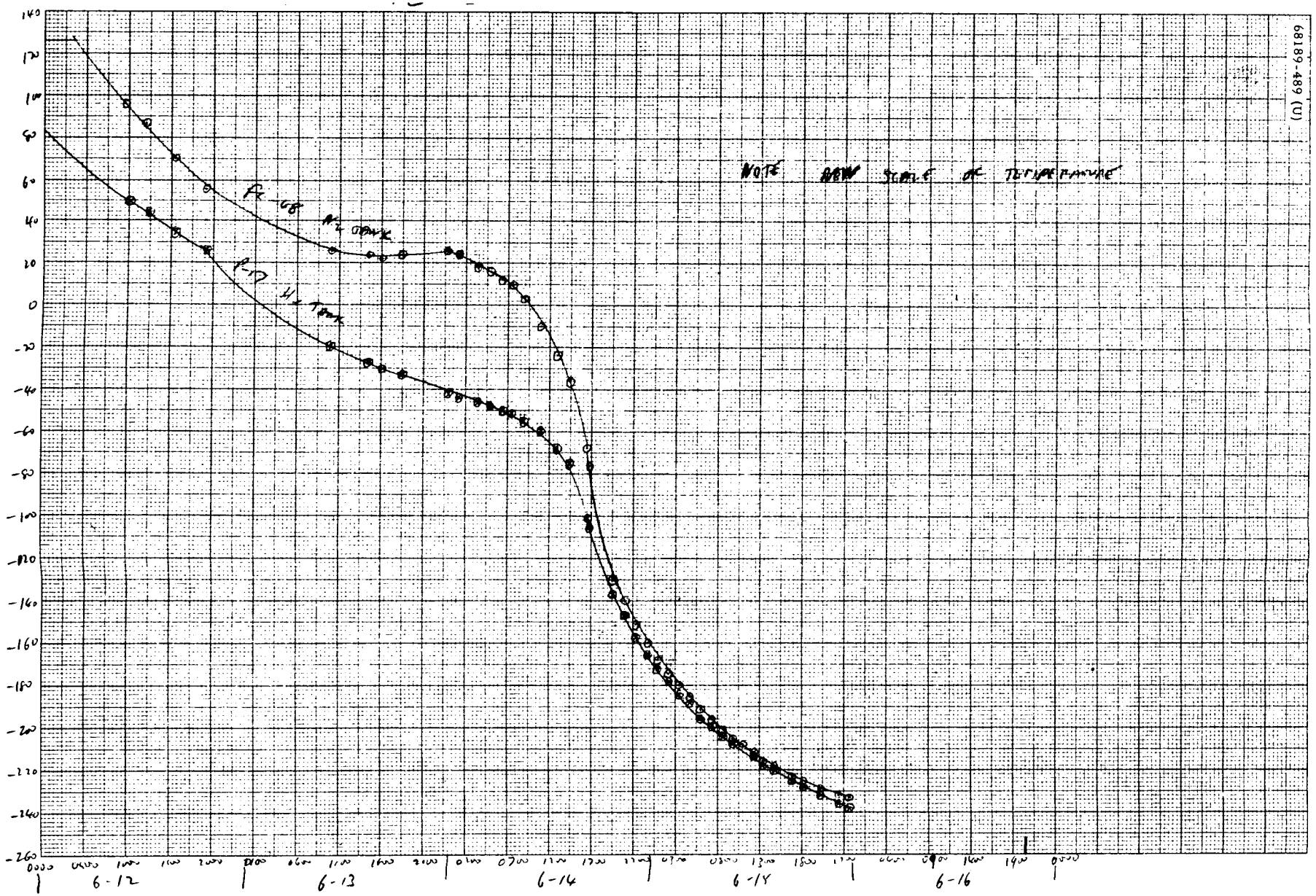


Figure B-14 (continued). Nitrogen and Helium Tanks

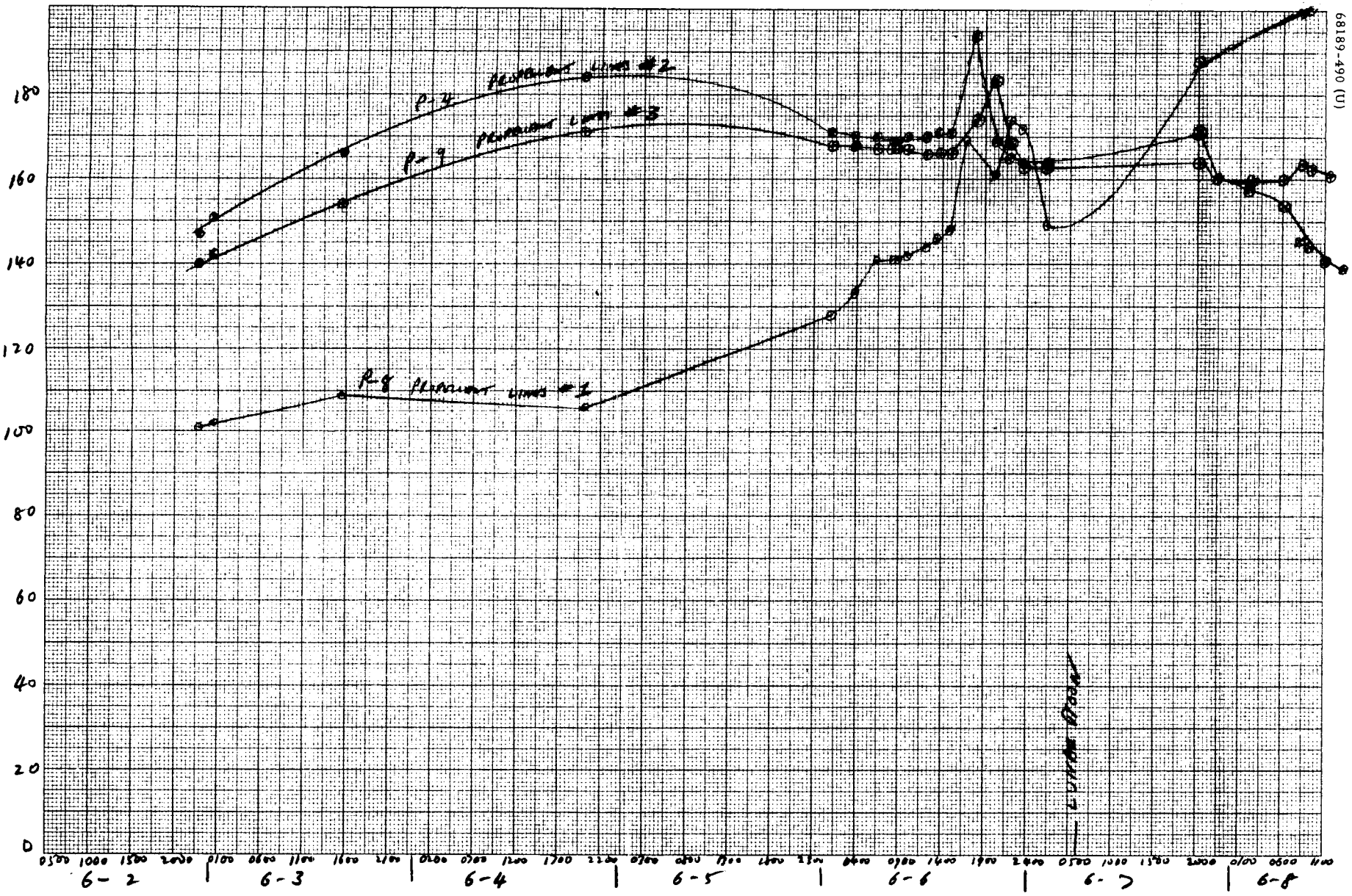


Figure B-15. Propellant Lines

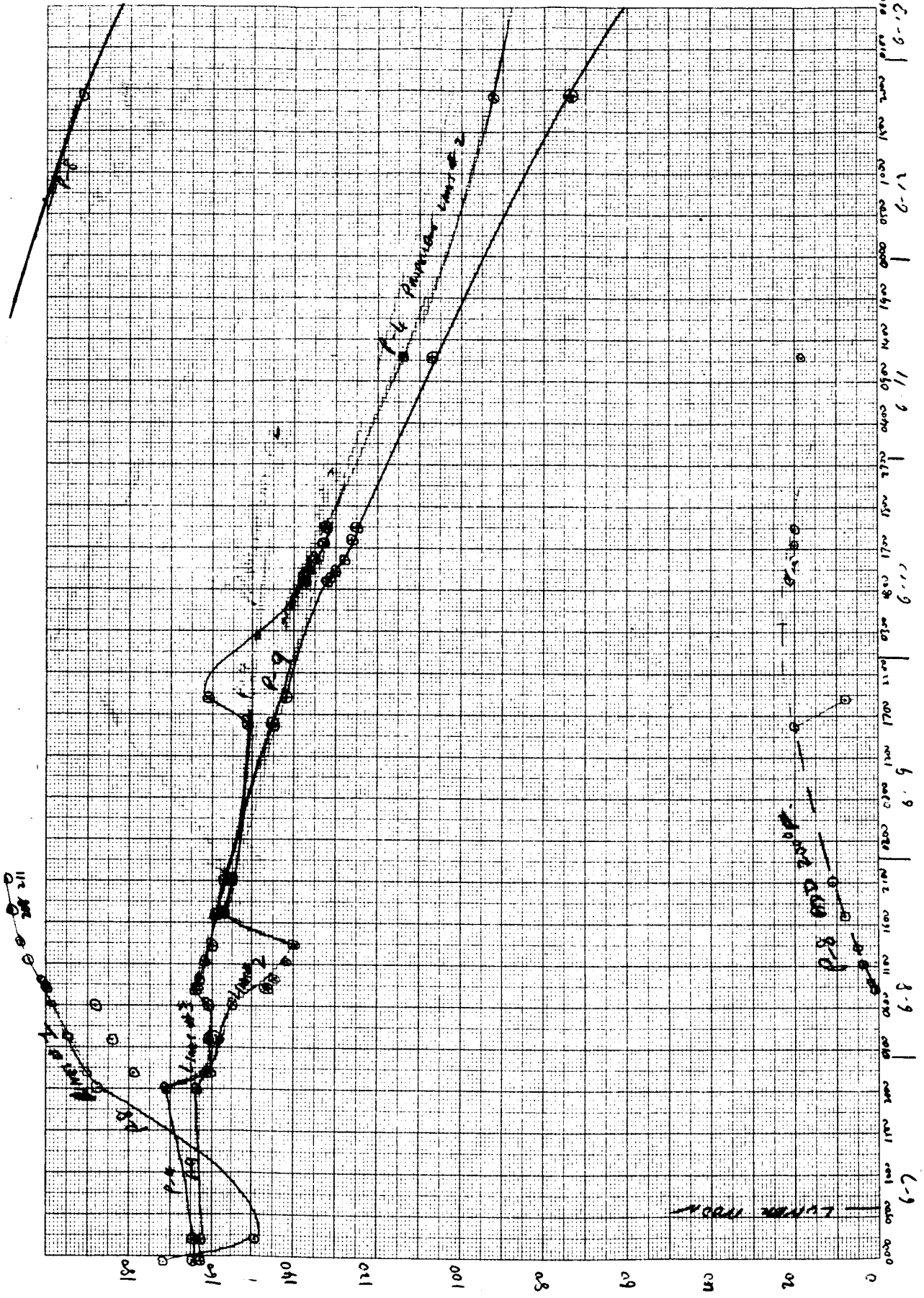


Figure B-15 (continued). Propellant Lines

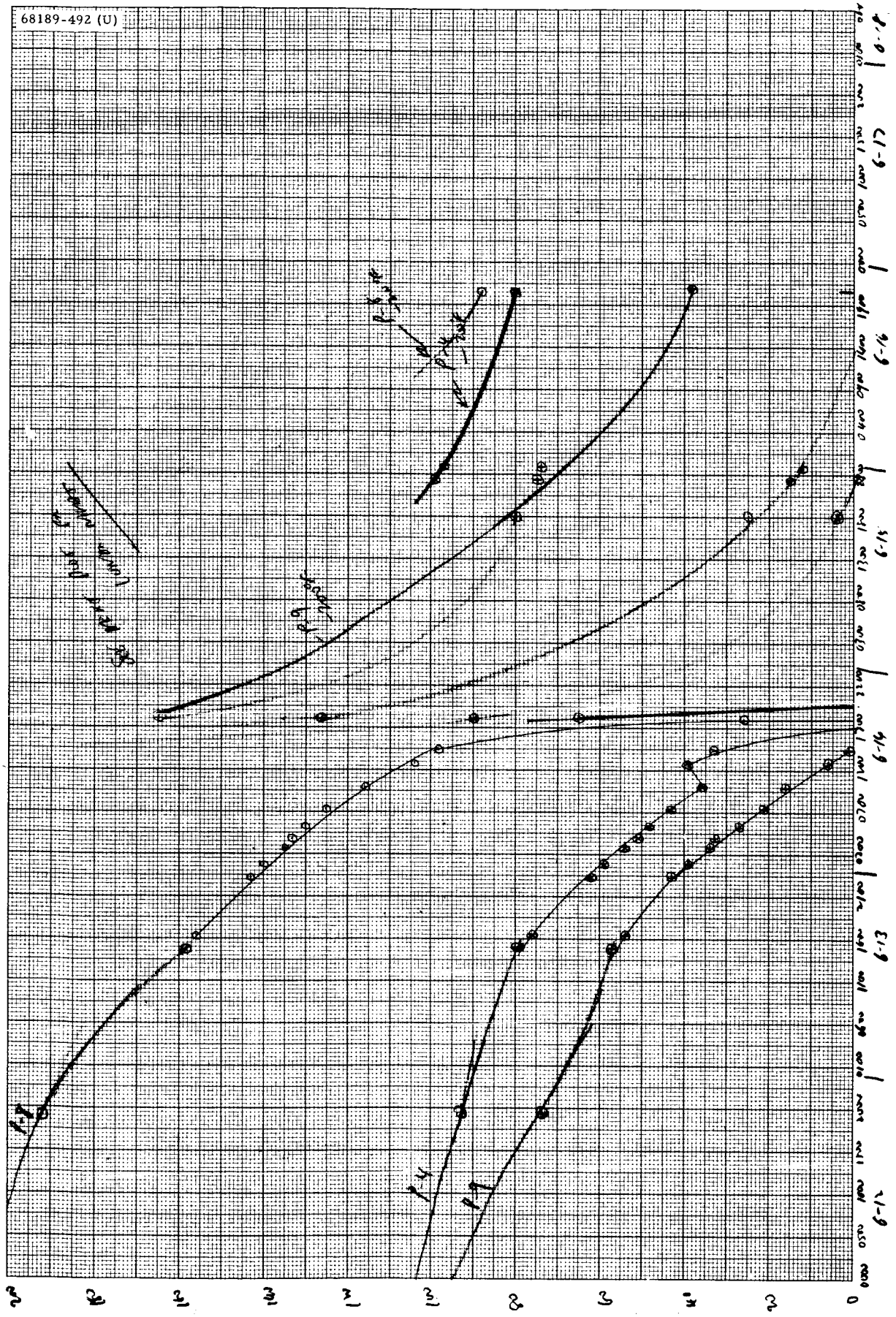


Figure B-15 (continued). Propellant Lines

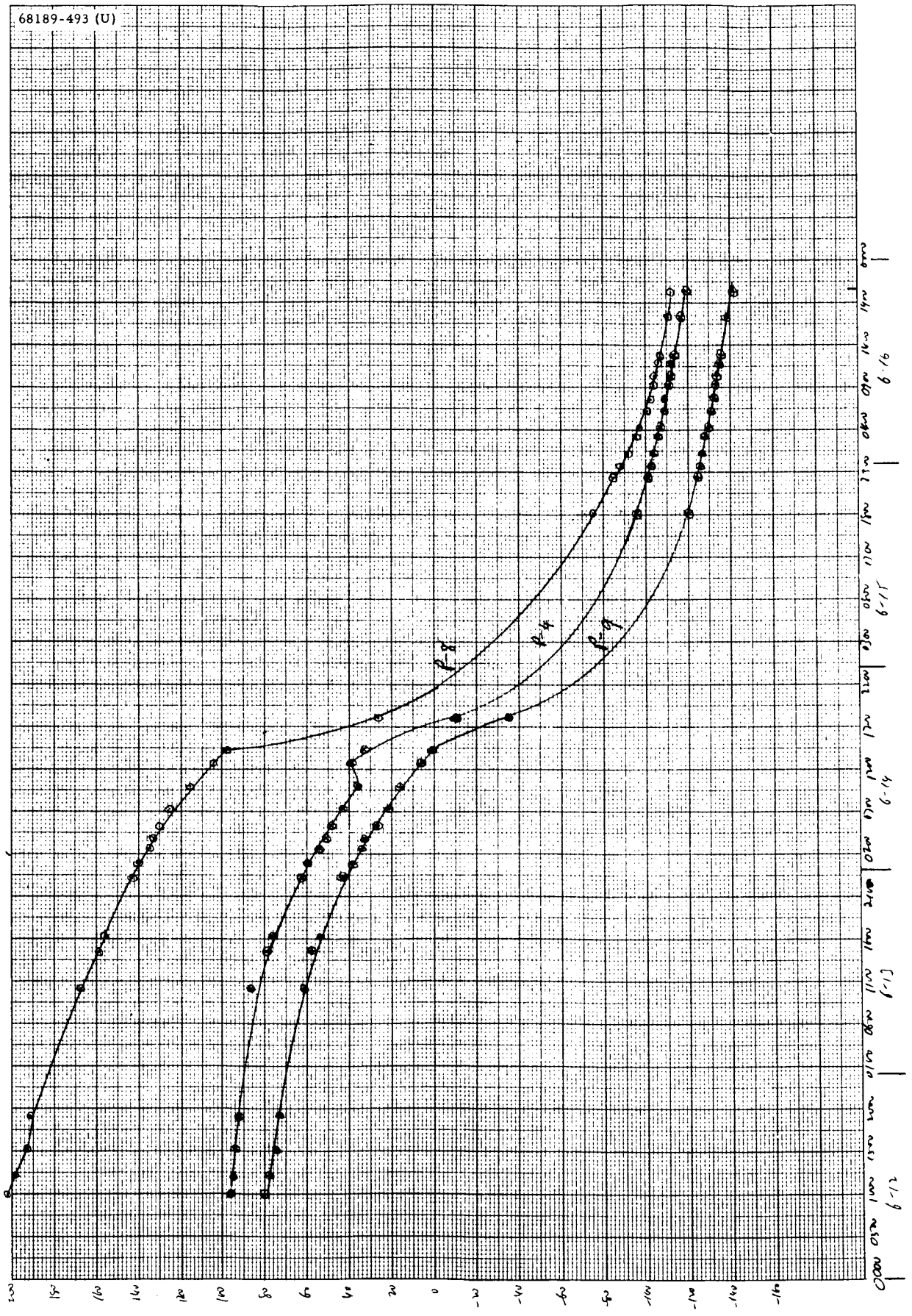
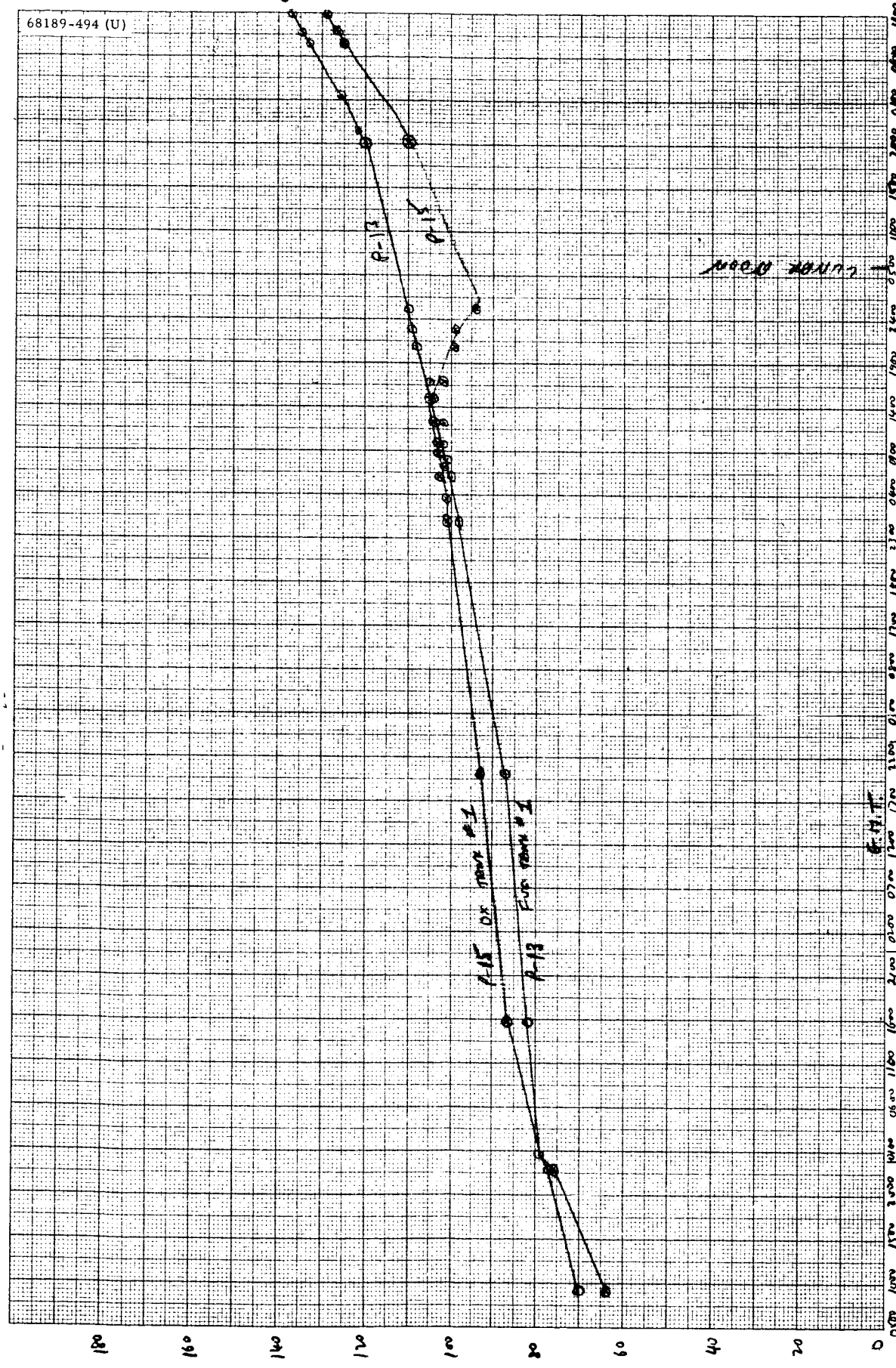


Figure B-15 (continued). Propellant Lines



a) Leg 1

Figure B-16. Fuel and Oxidizer Tanks

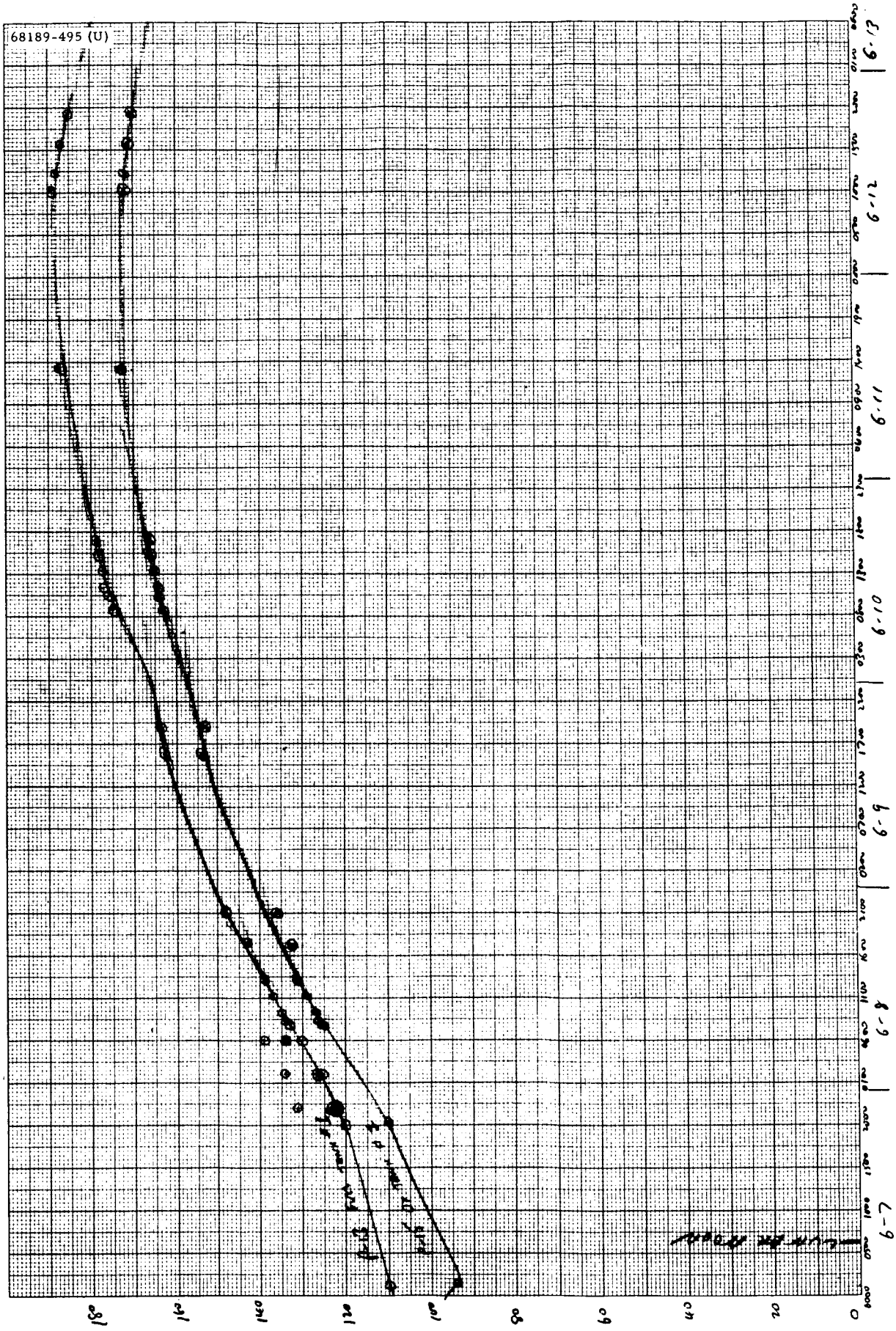


Figure B-16a (continued). Fuel and Oxidizer Tanks, Leg 1

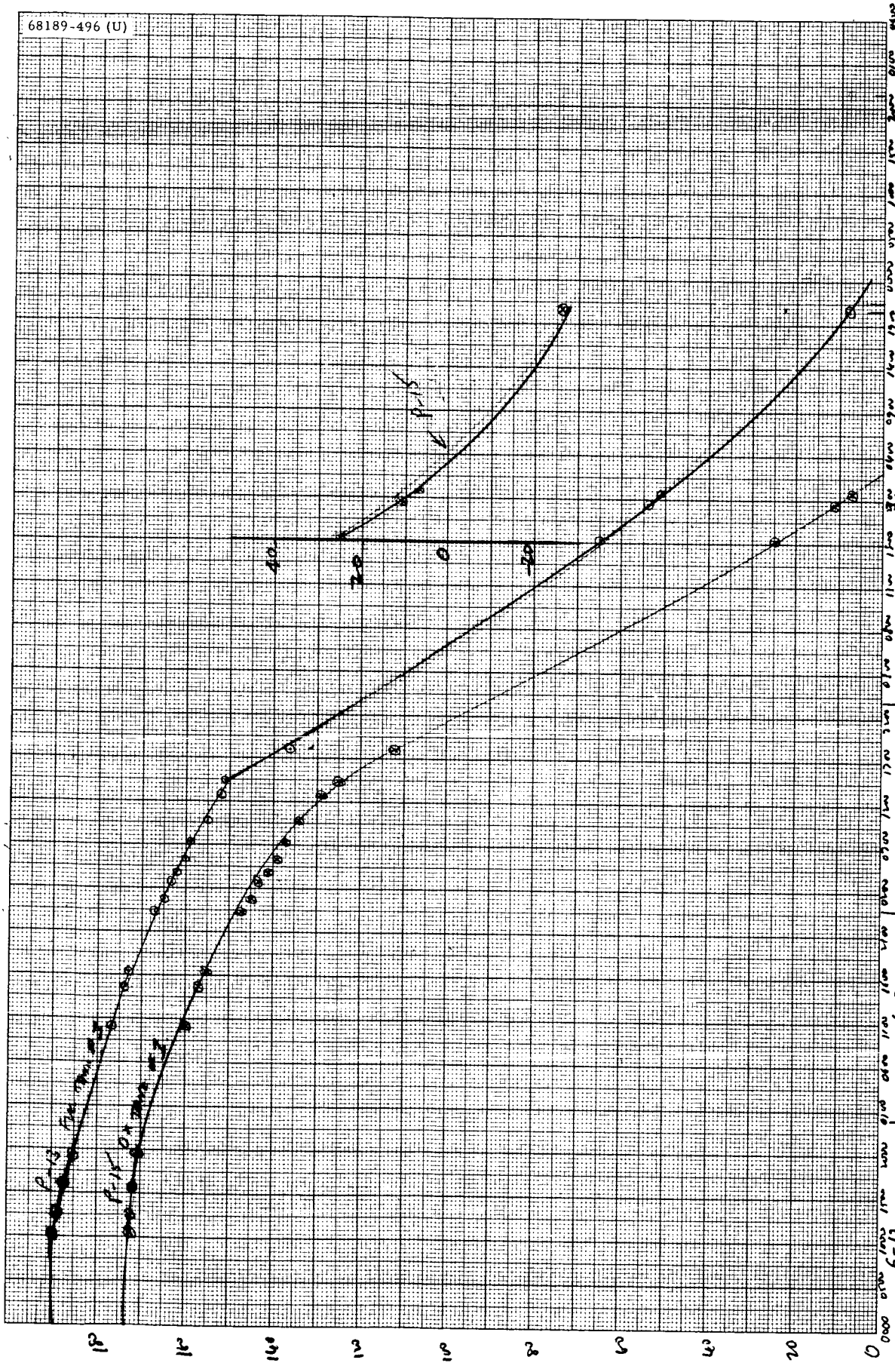
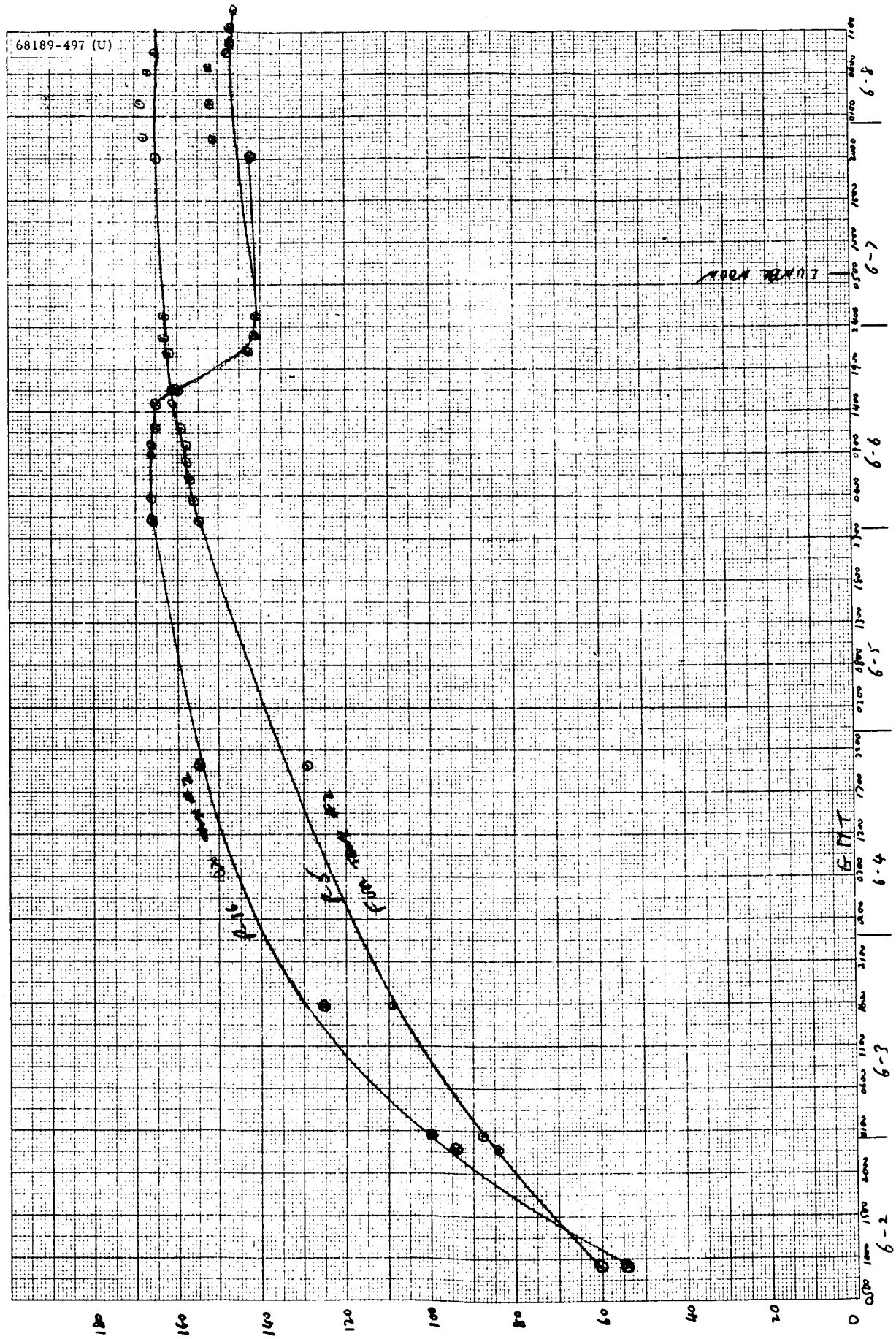


Figure B-16a (continued). Fuel and Oxidizer Tanks, Leg 1



b) Leg 2

Figure B-16 (continued). Fuel and Oxidizer Tanks

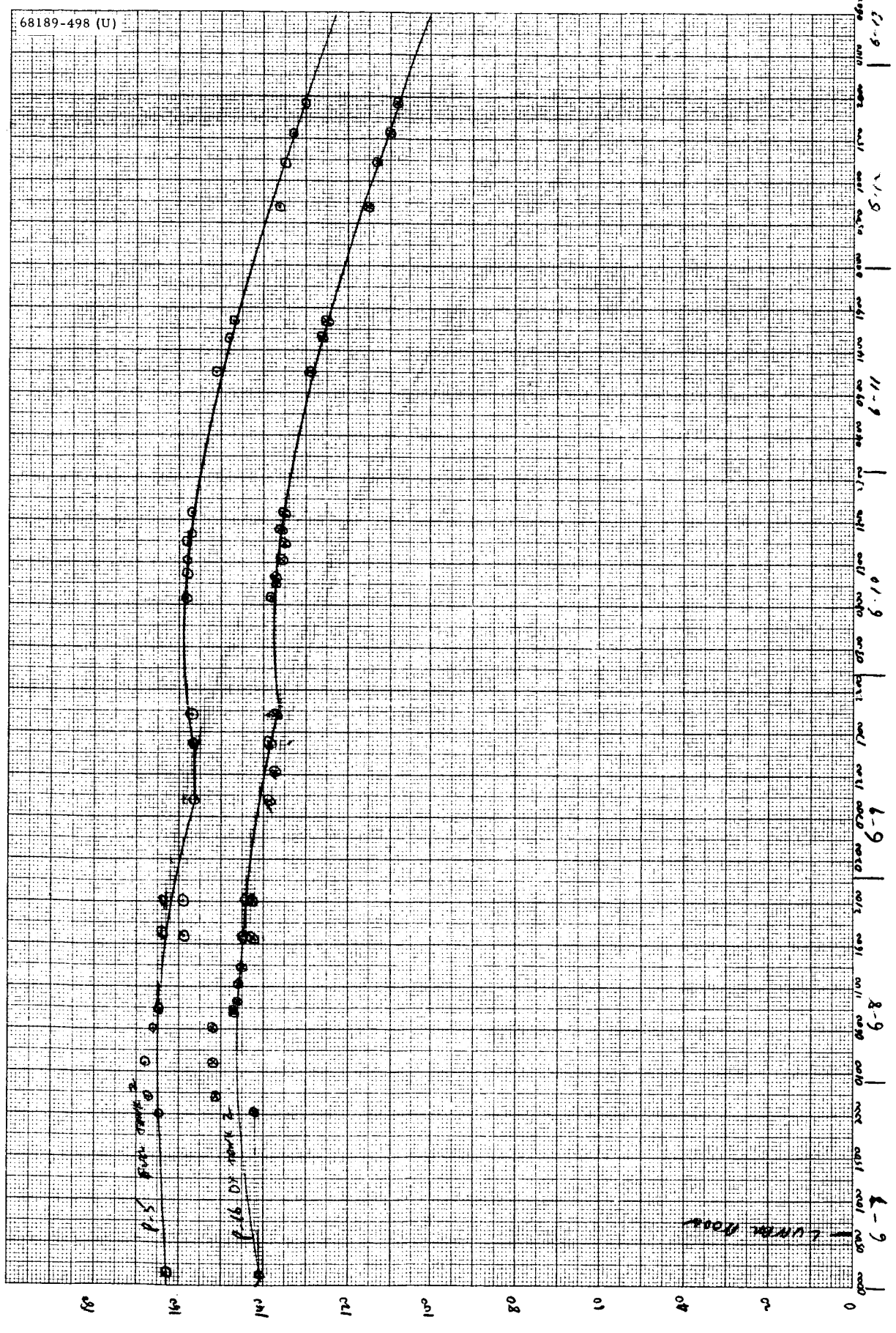


Figure B-16b (continued). Fuel and Oxidizer Tanks, Leg 2

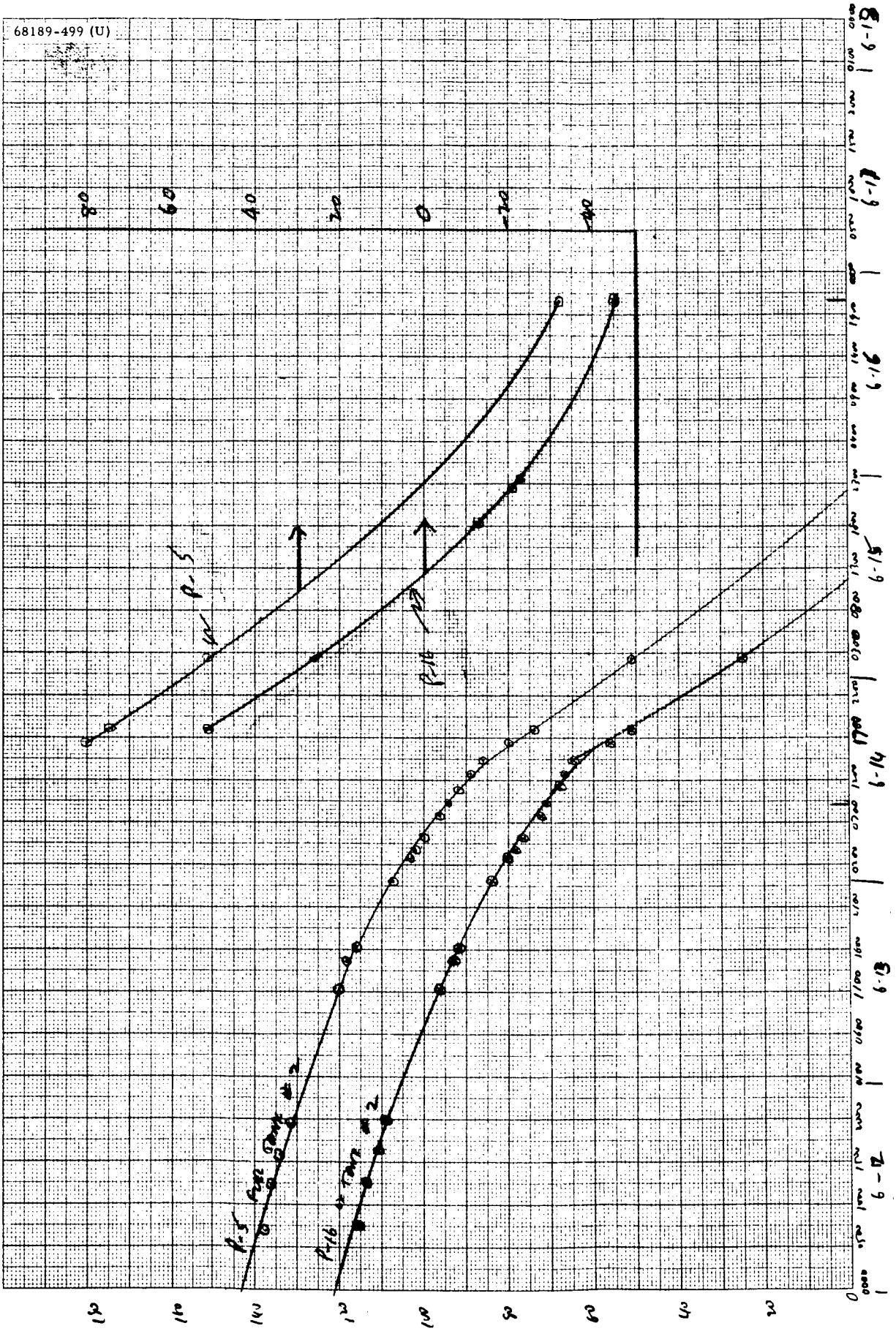
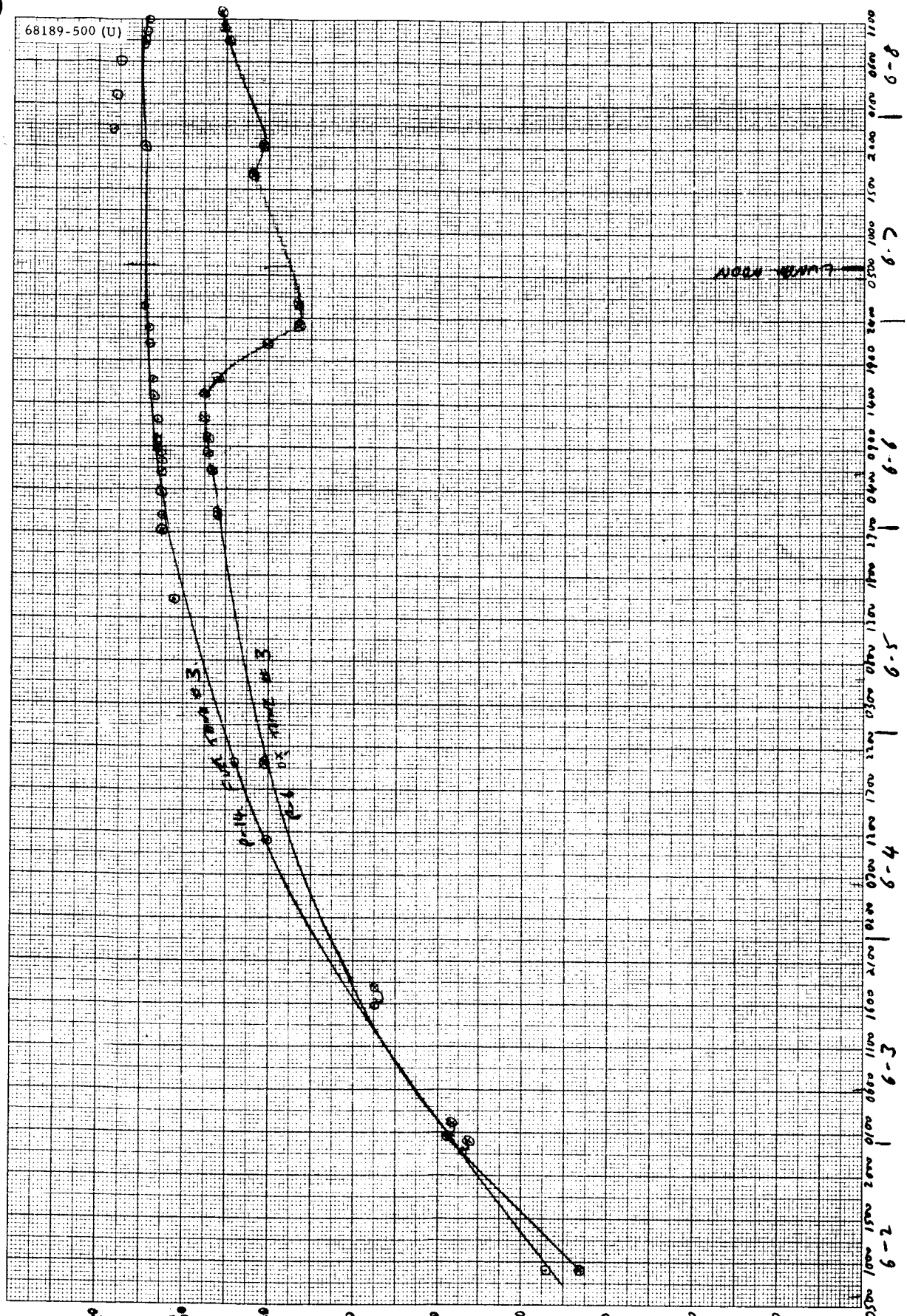


Figure B-16b (continued). Fuel and Oxidizer Tanks, Leg 2



c) Leg 3

Figure B-16 (continued). Fuel and Oxidizer Tanks

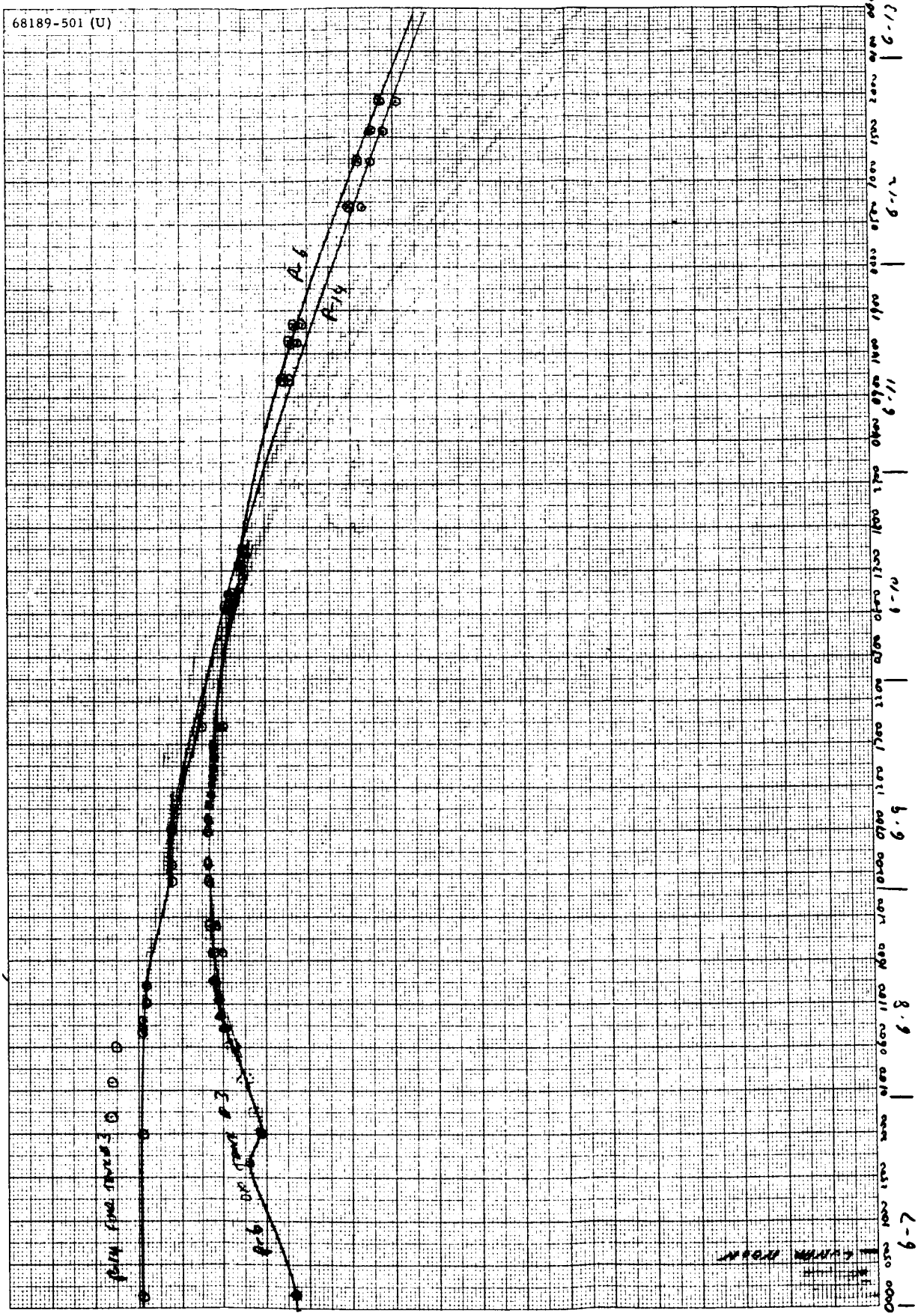


Figure B-16c (continued). Fuel and Oxidizer Tanks, Leg 3

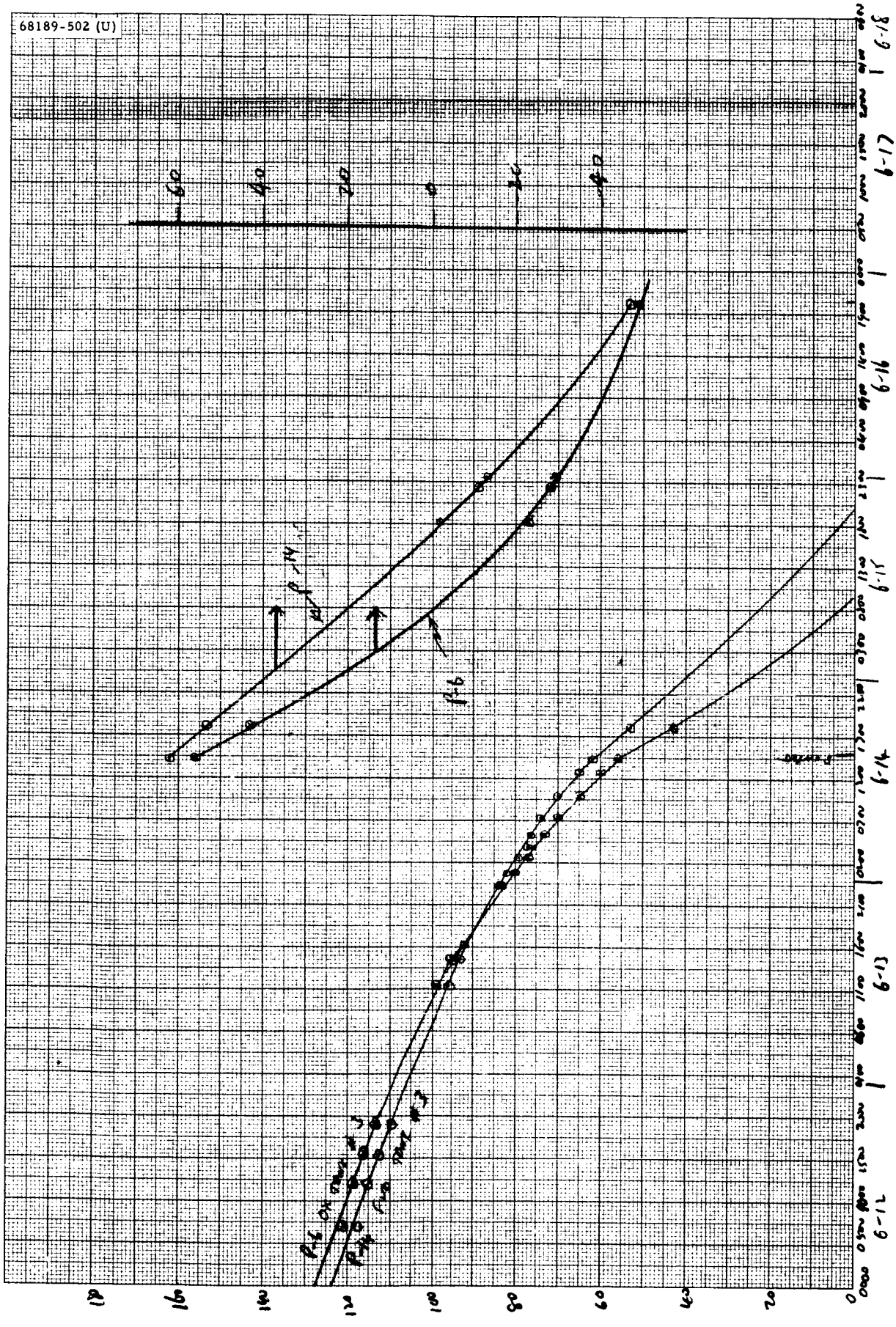


Figure B-16c (continued). Fuel and Oxidizer Tanks, Leg 3

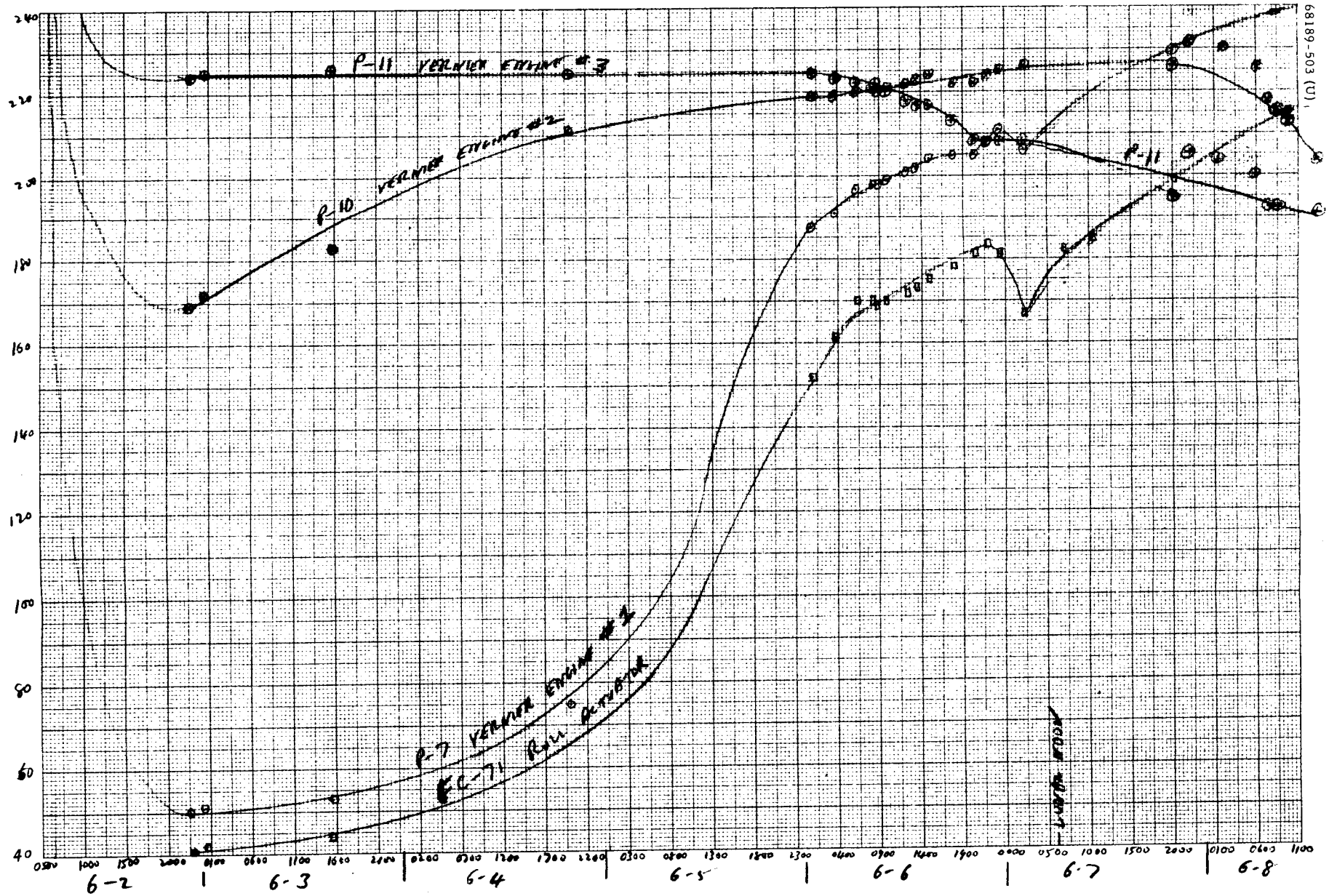


Figure B-17. Vernier Engines and Roll Actuator

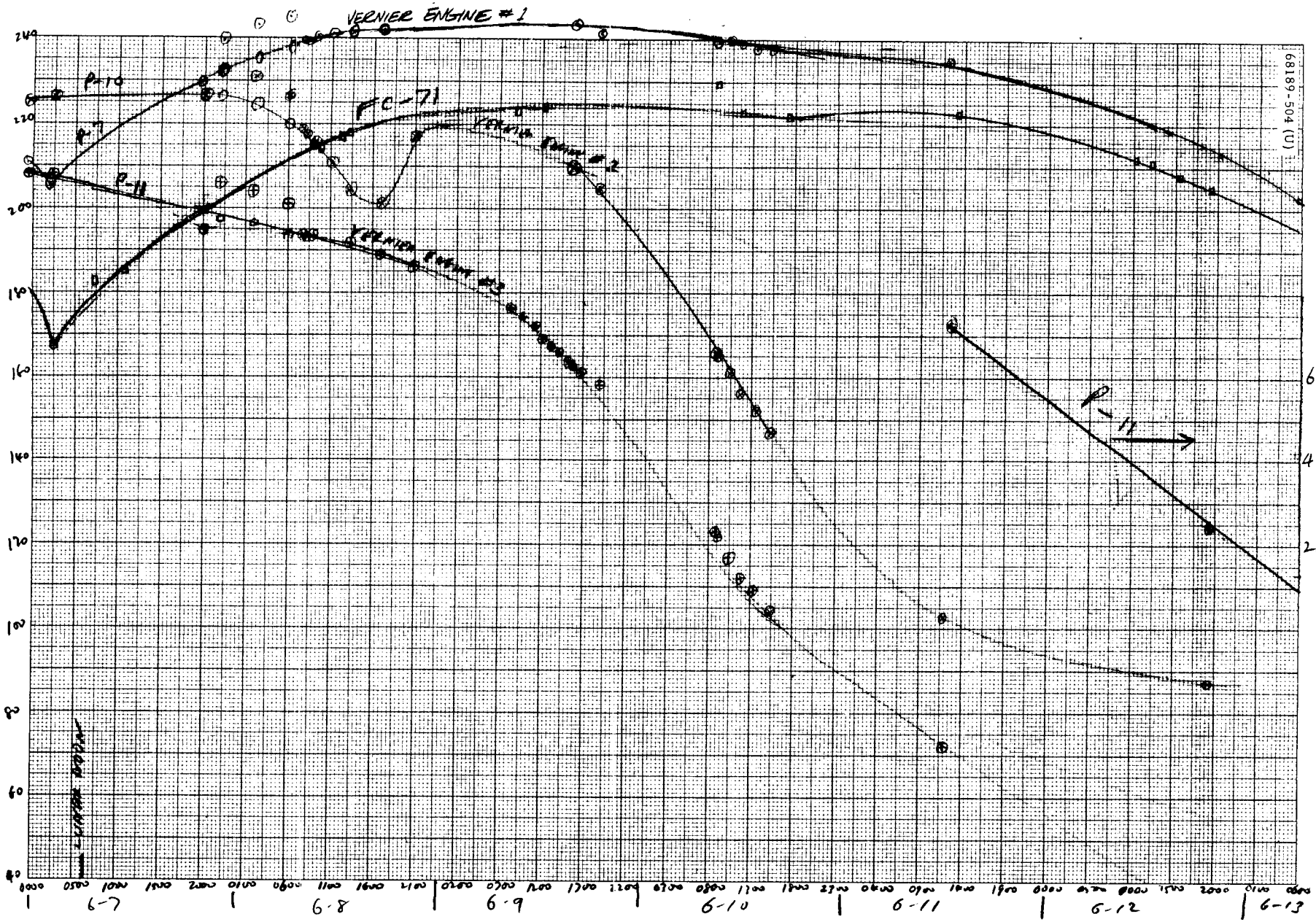


Figure B-17 (continued). Vernier Engines and Roll Actuator

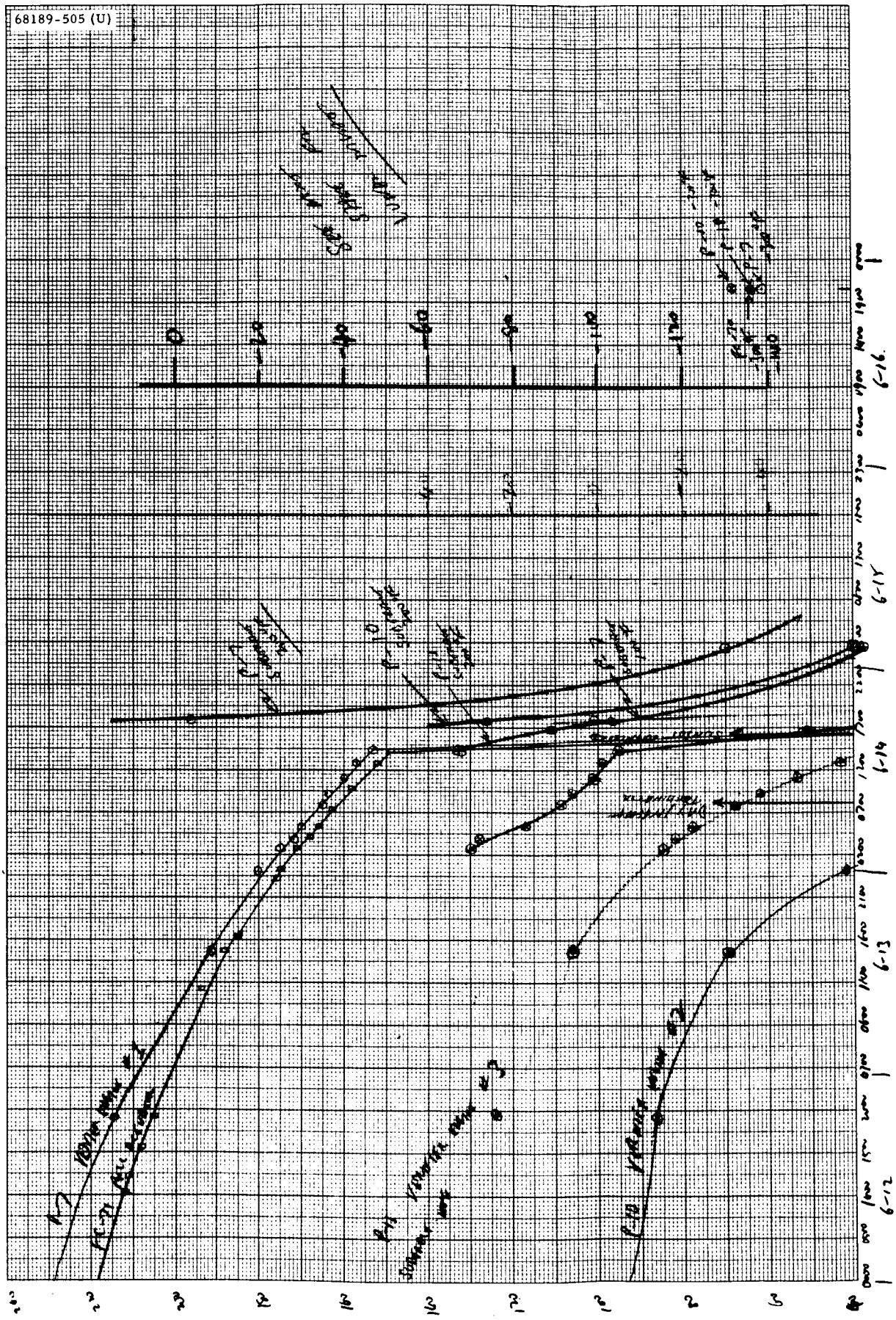


Figure B-17 (continued). Vernier Engines and Roll Actuator

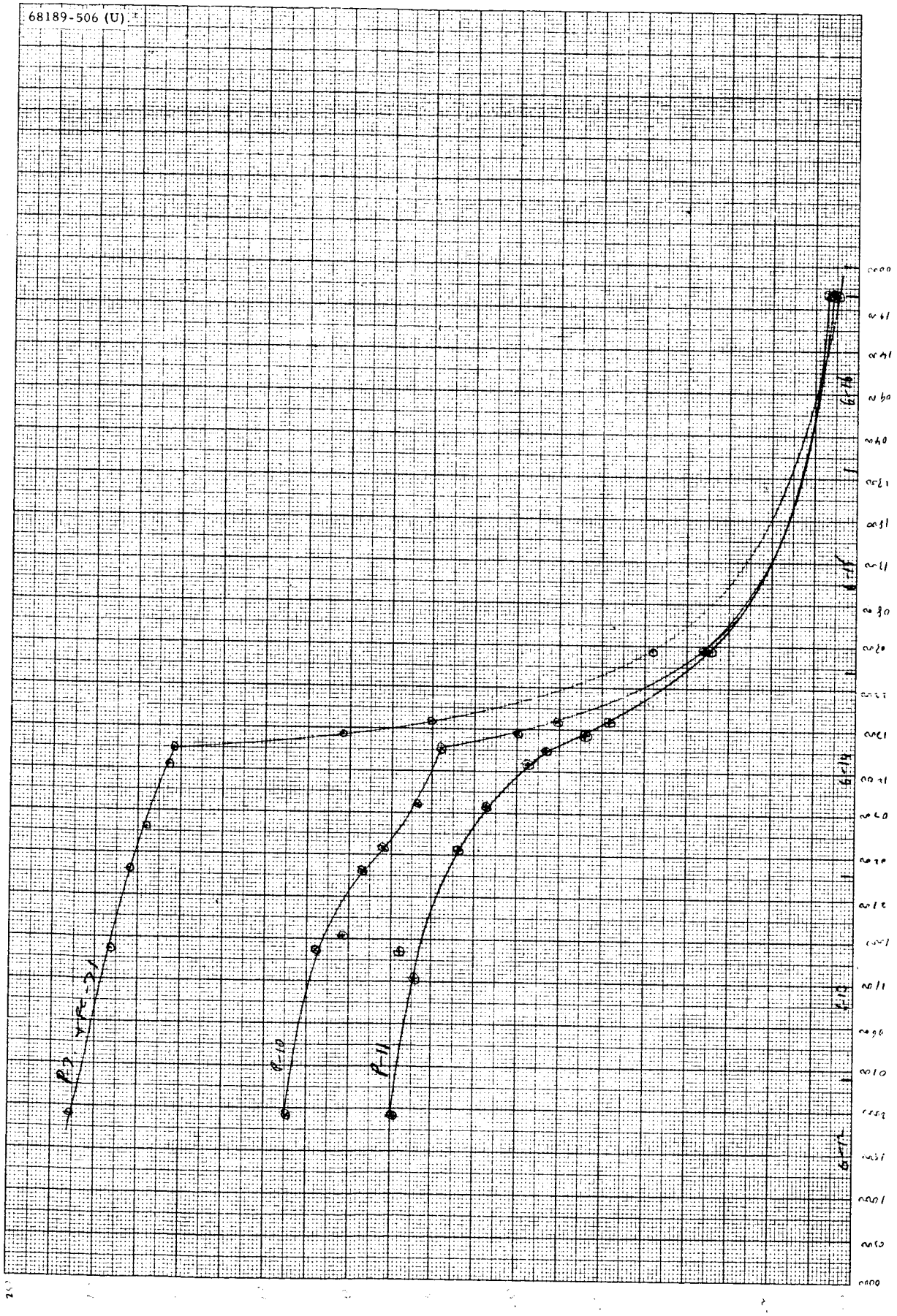


Figure B-17 (continued). Vernier Engines and Roll Actuator

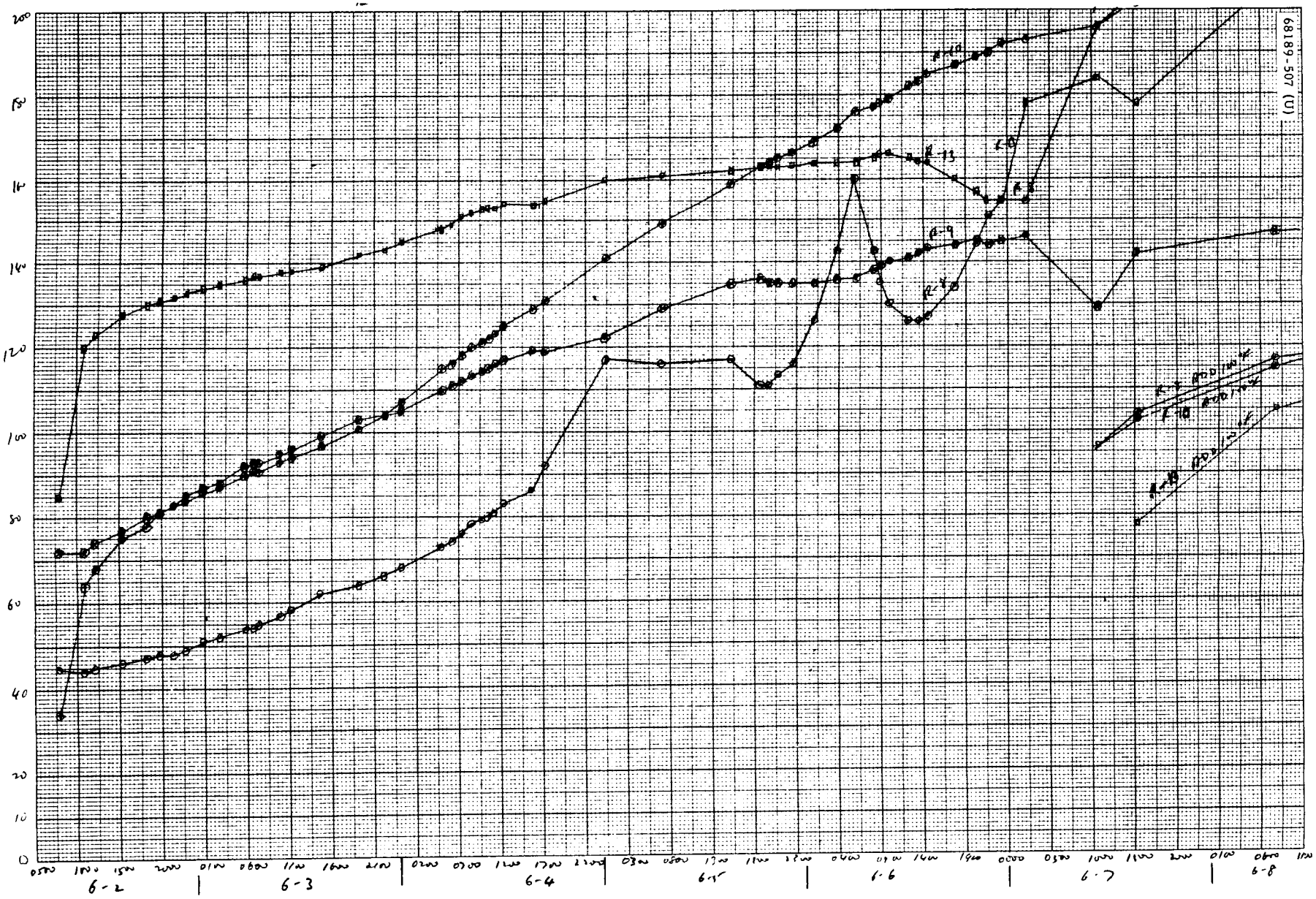


Figure B-18. RADVS System

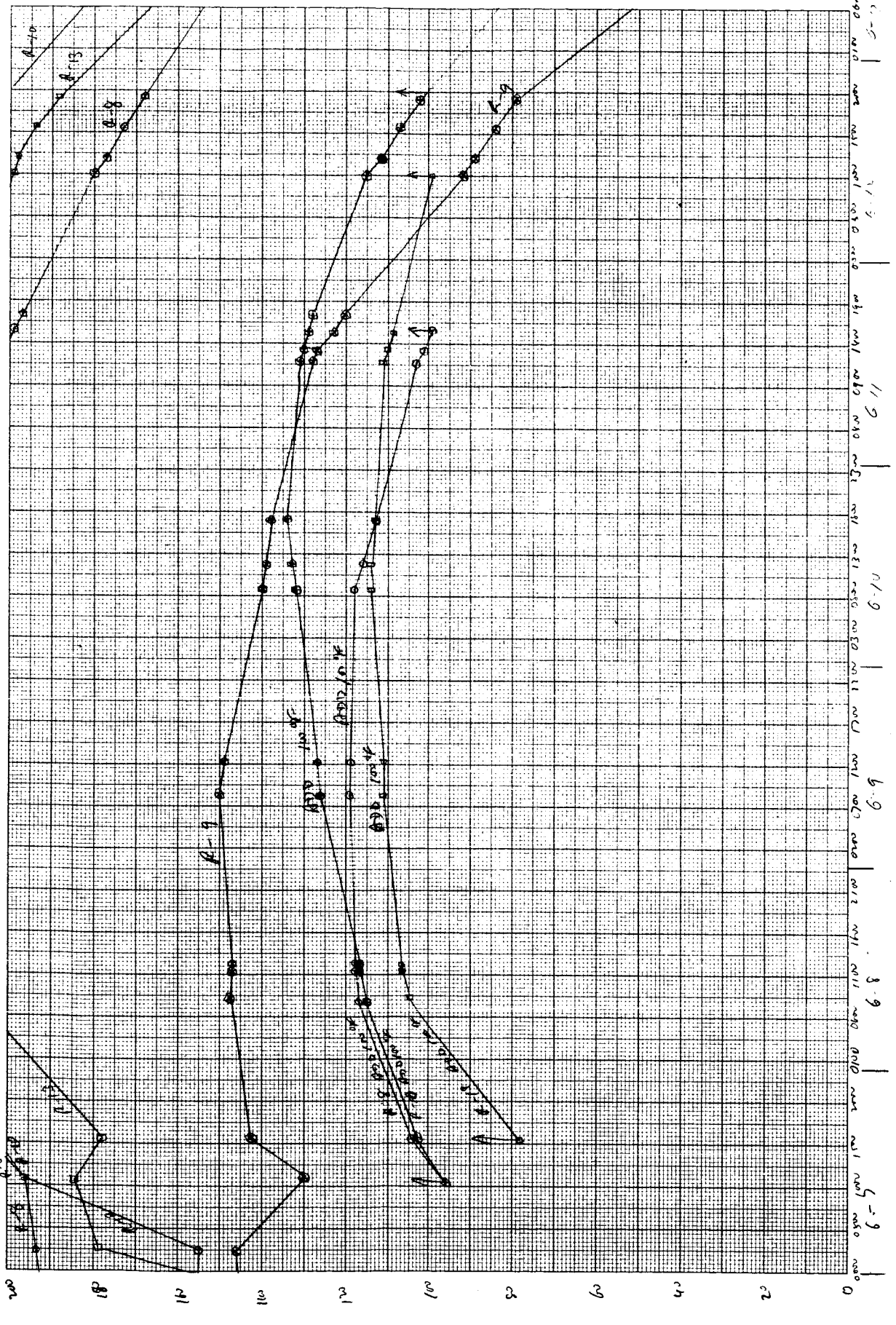


Figure B-18 (continued). RADVS System

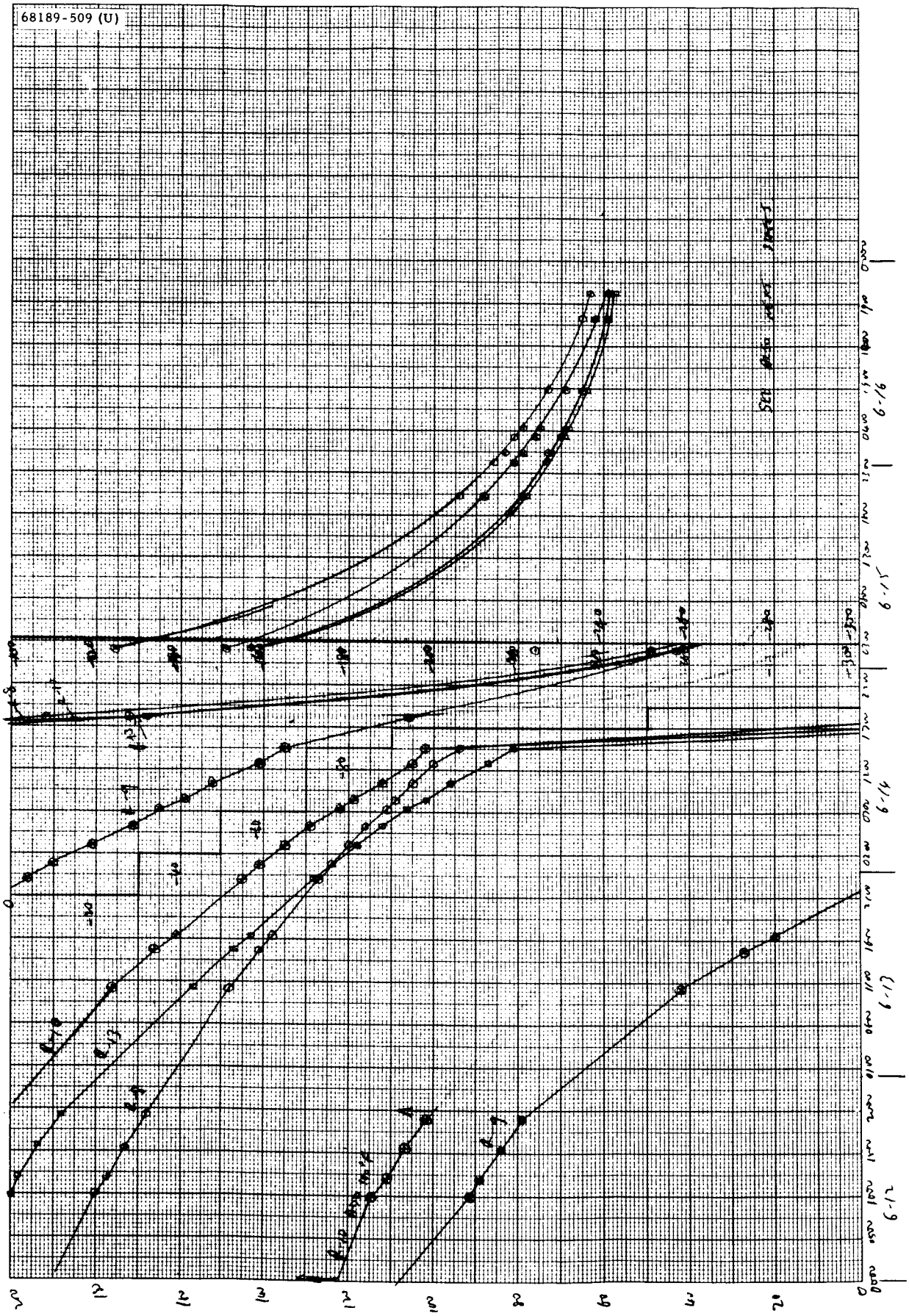


Figure B-18 (continued). RADVS System

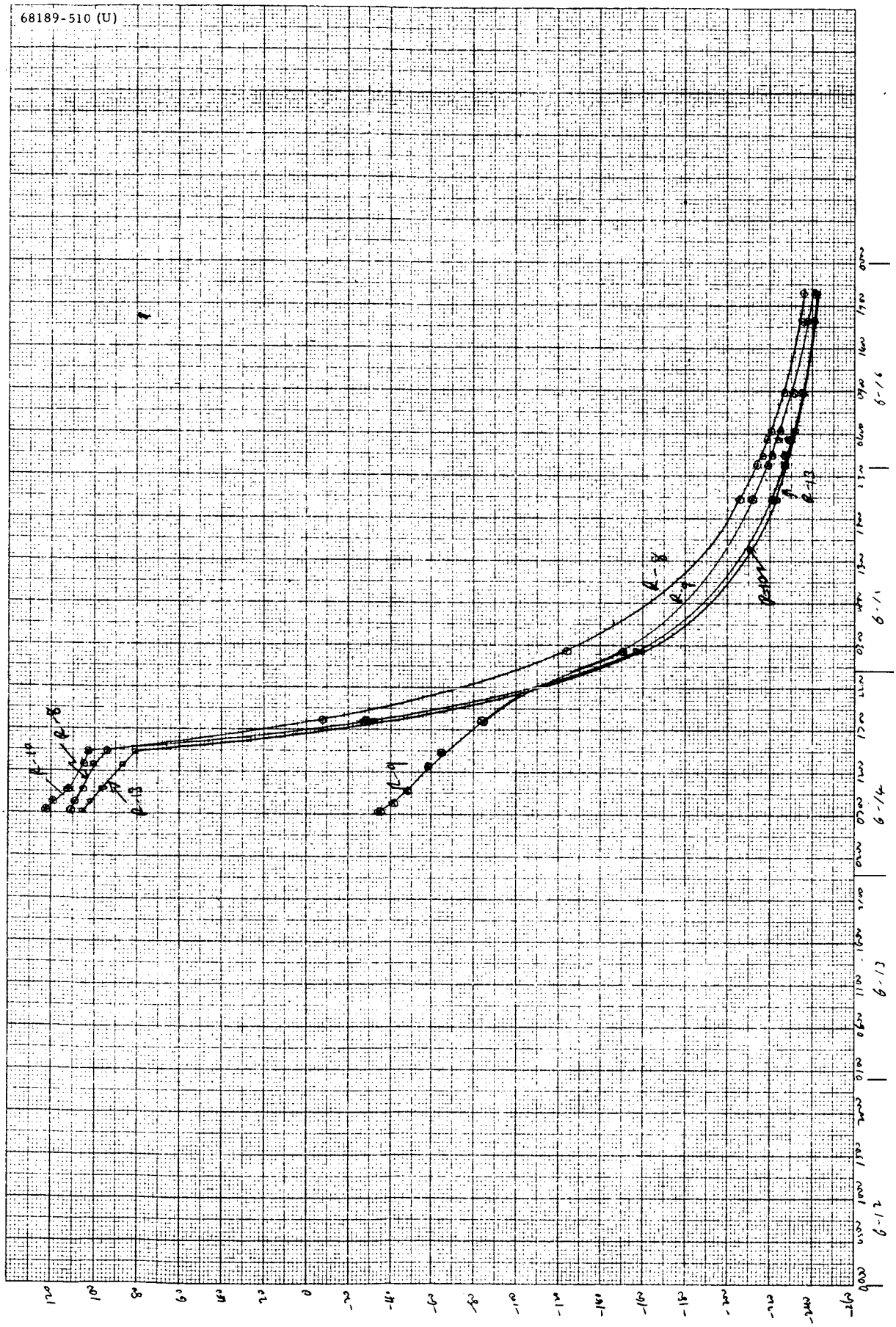
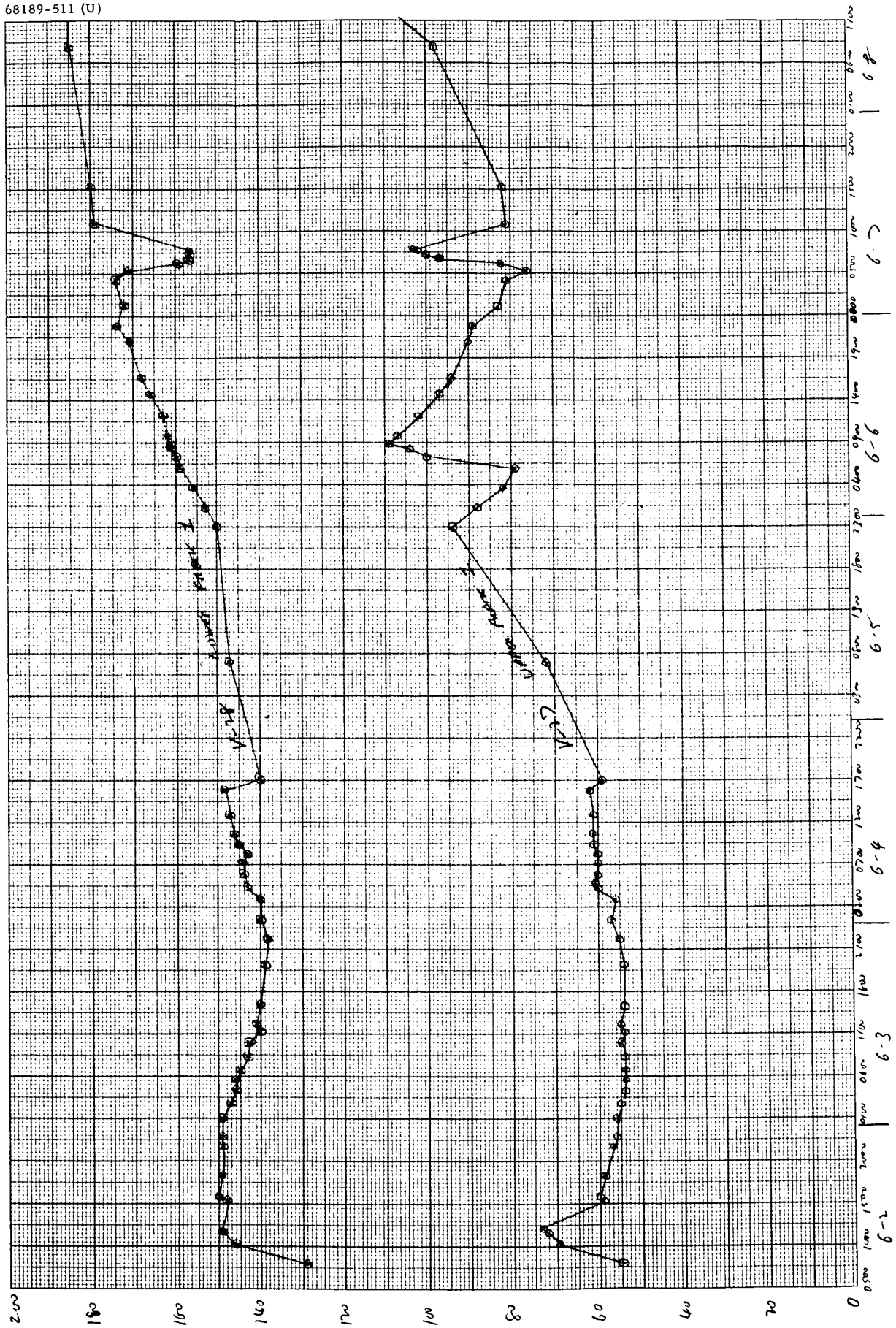


Figure B-18 (continued). RADVS System



a) Near Leg 1

Figure B-19. Upper and Lower Spaceframe

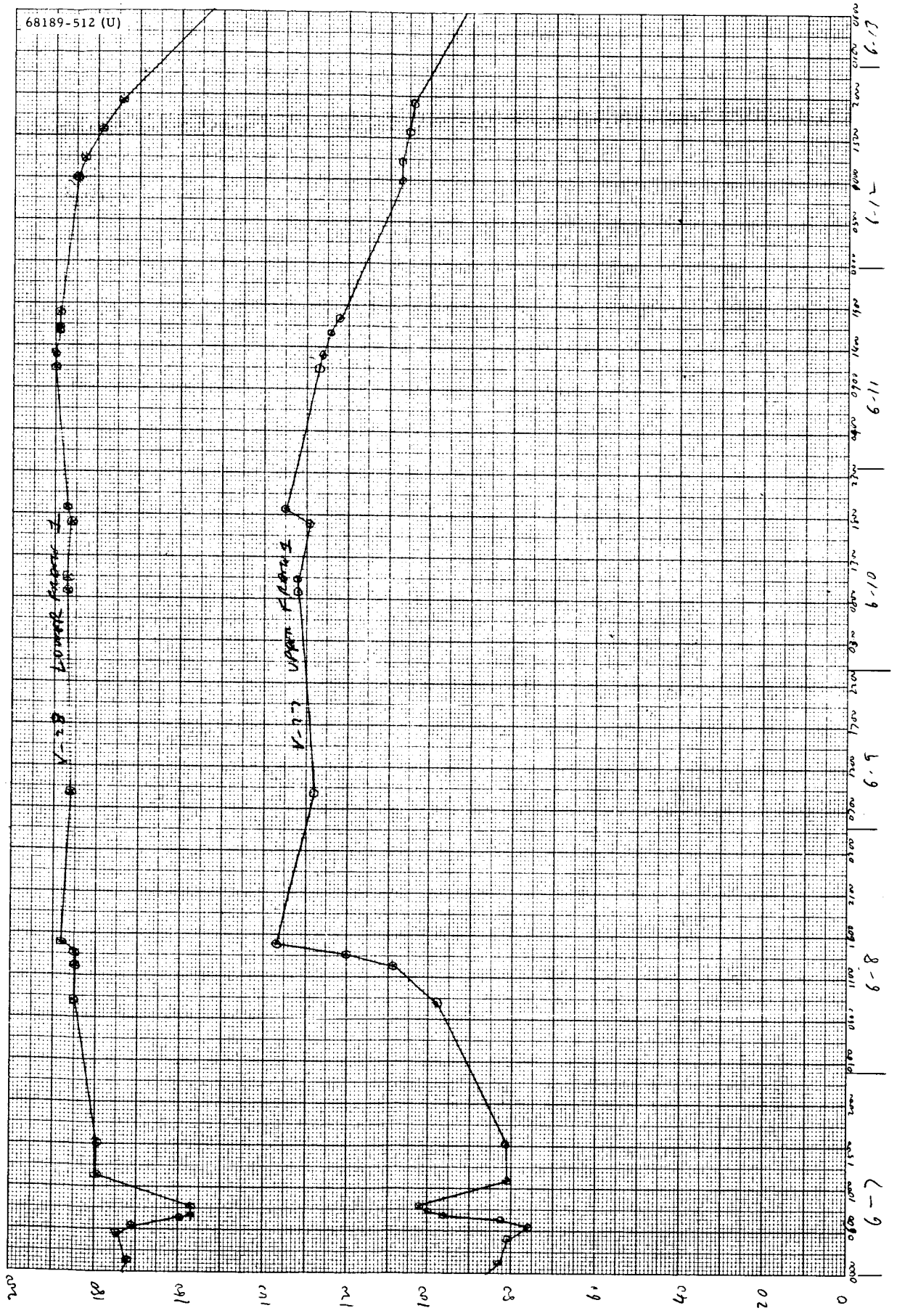


Figure B-19a (continued). Upper and Lower Spaceframe, Near Leg 1

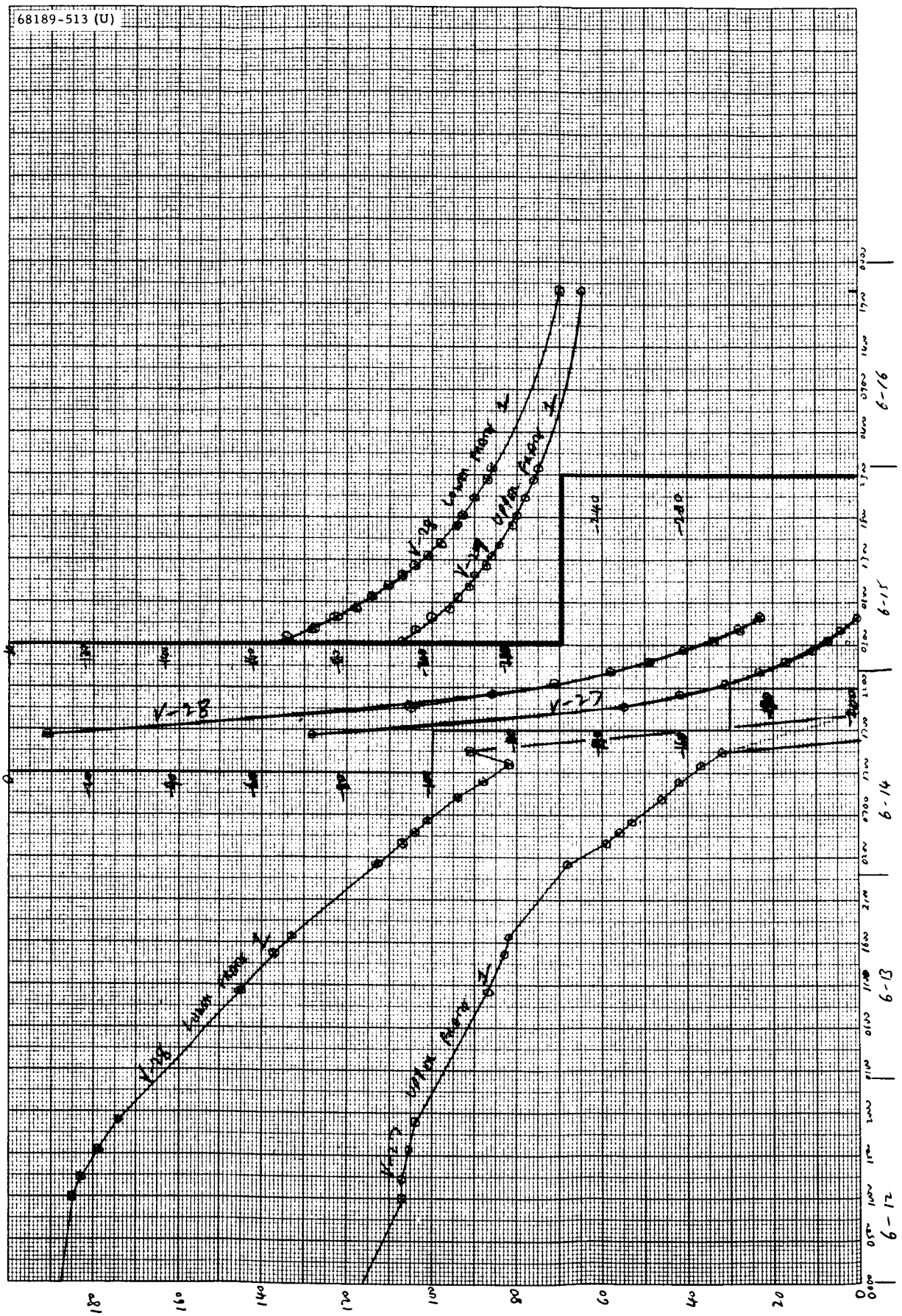
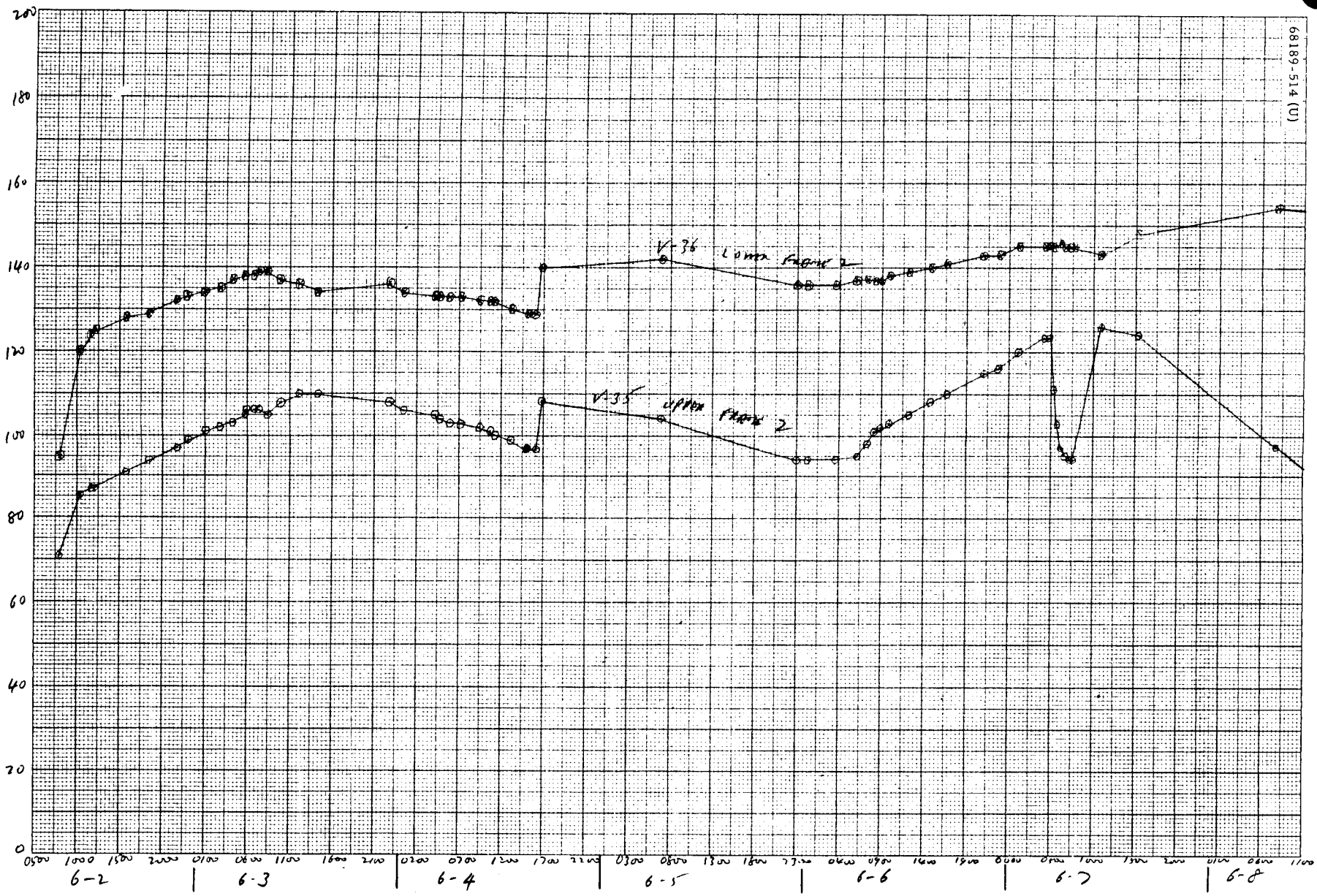


Figure B-19a (continued). Upper and Lower Spaceframe, Near Leg 1



b) Near Leg 2

Figure B-19 (continued). Upper and Lower Spaceframe

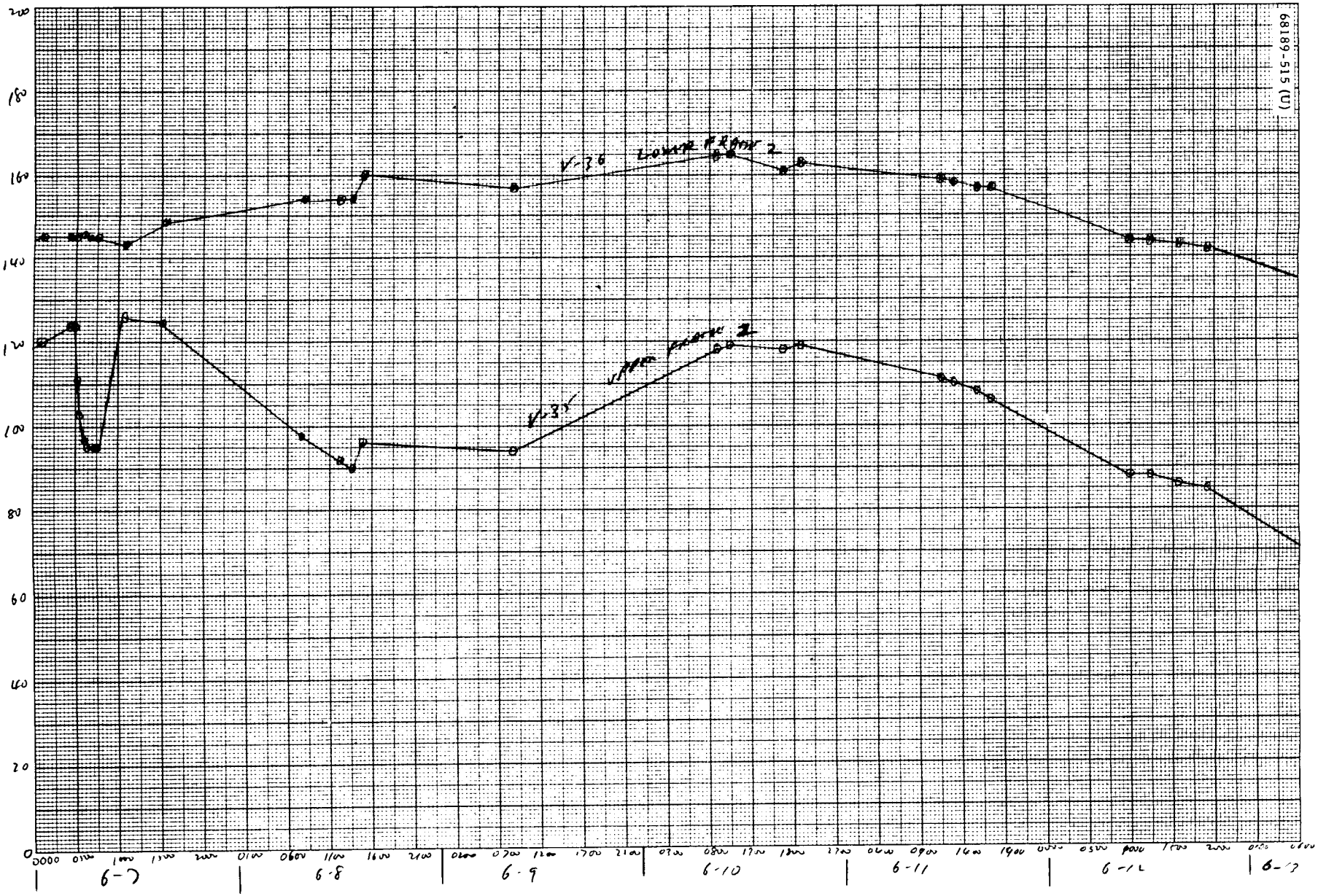


Figure B-19b (continued). Upper and Lower Spaceframe, Near Leg 2

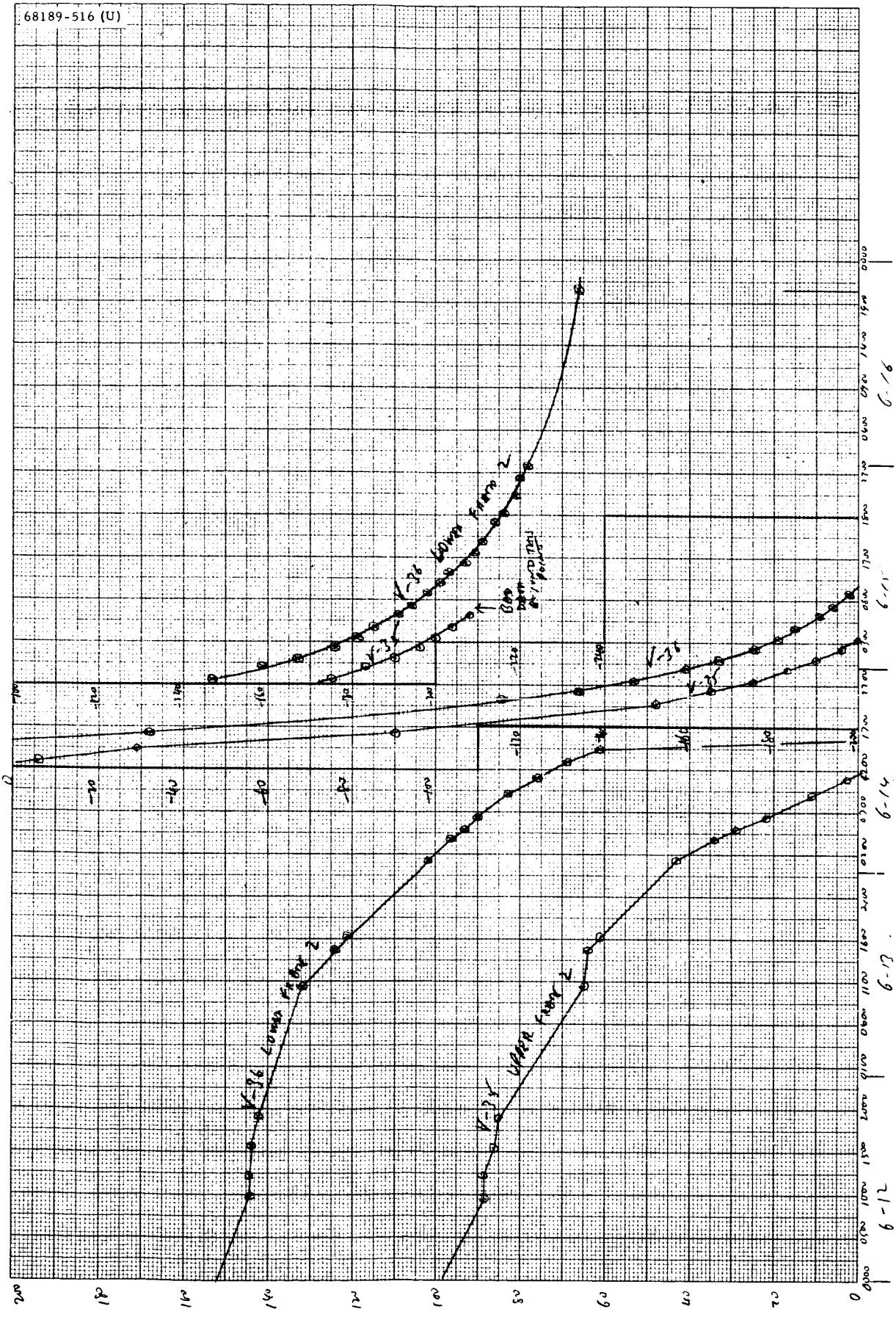


Figure B-19b (continued). Upper and Lower Spaceframe, Near Leg 2

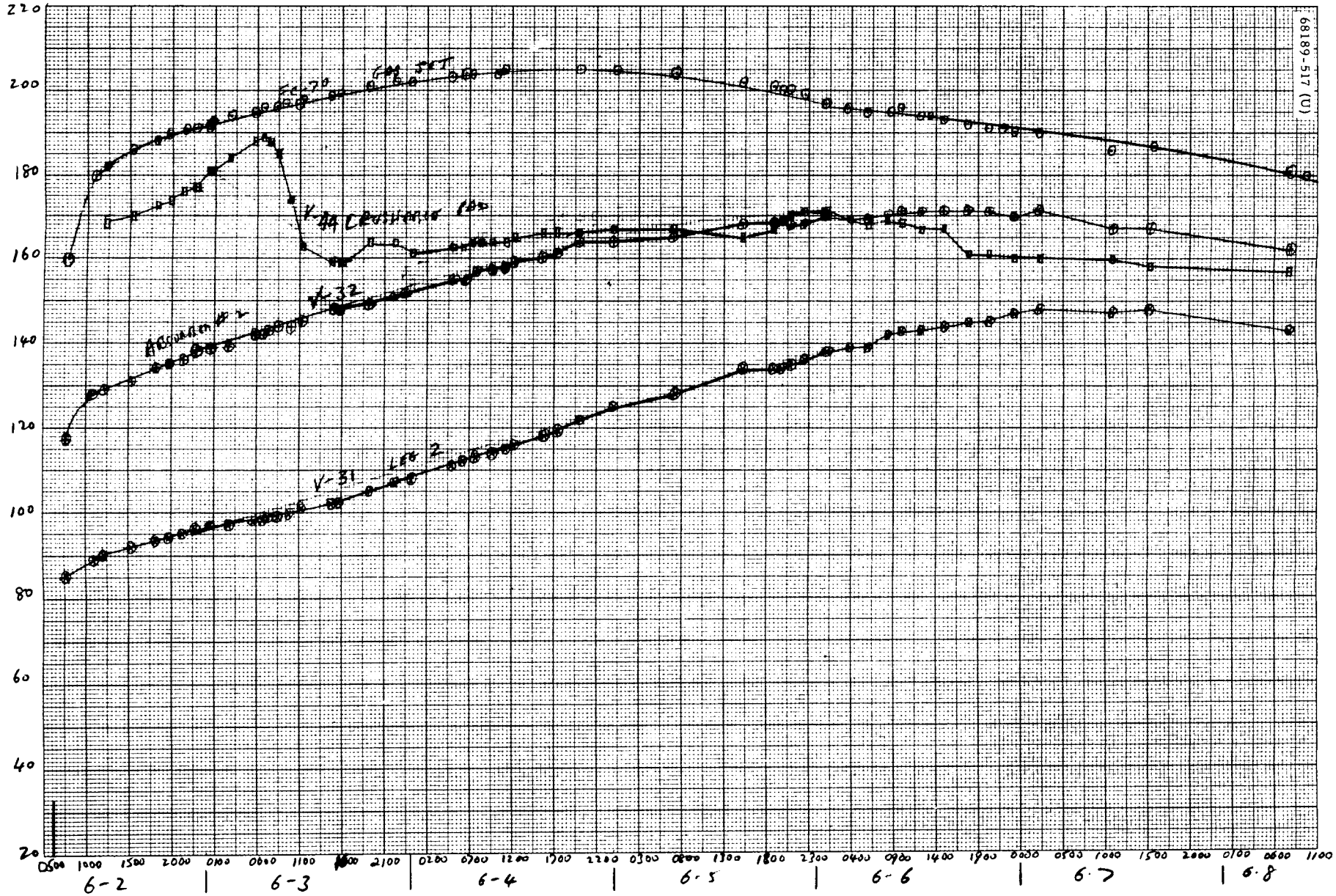


Figure B-20. Leg 2, Gas Jet 2, and Crushable Block 3

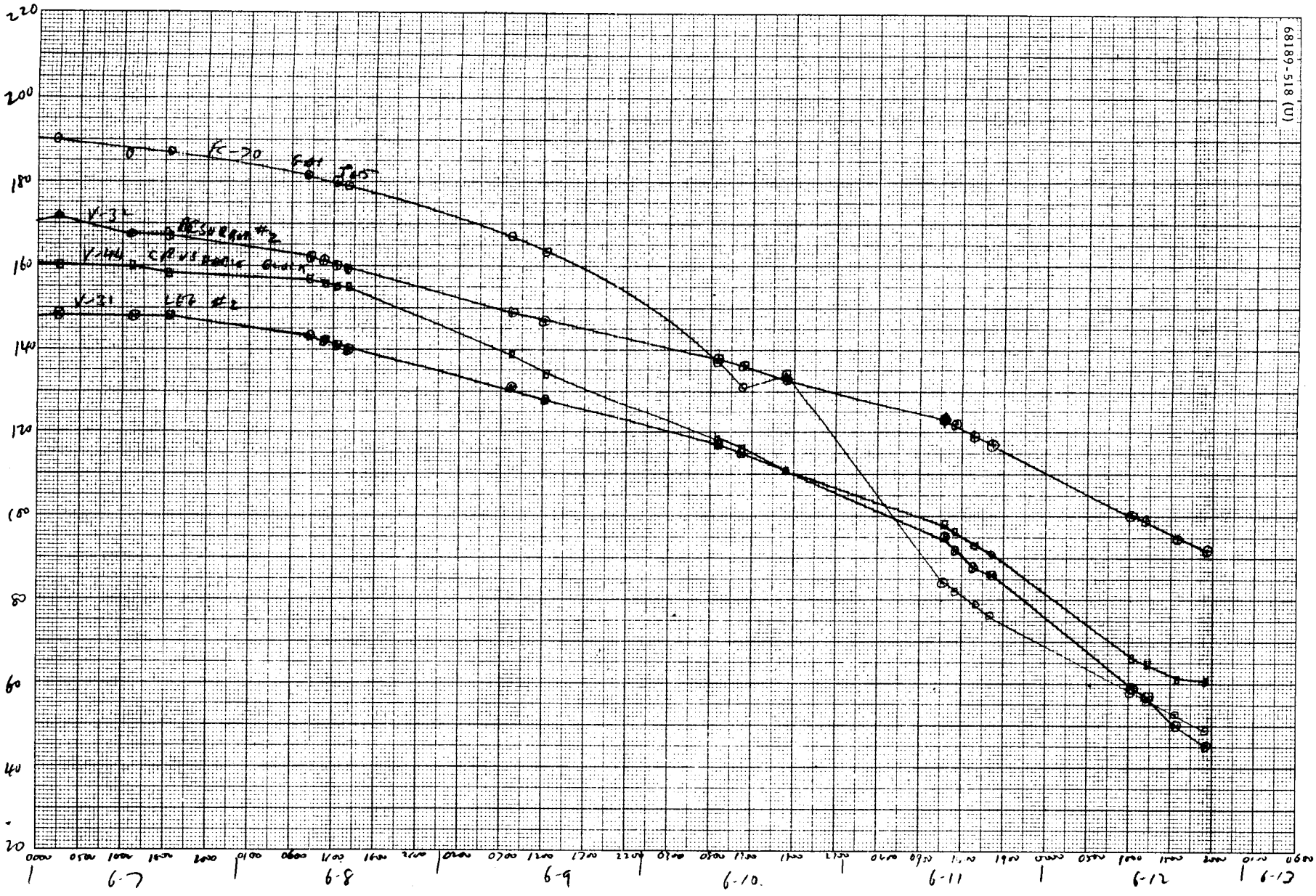


Figure B-20 (continued). Leg 2, Gas Jet 2, and Crushable Block 3

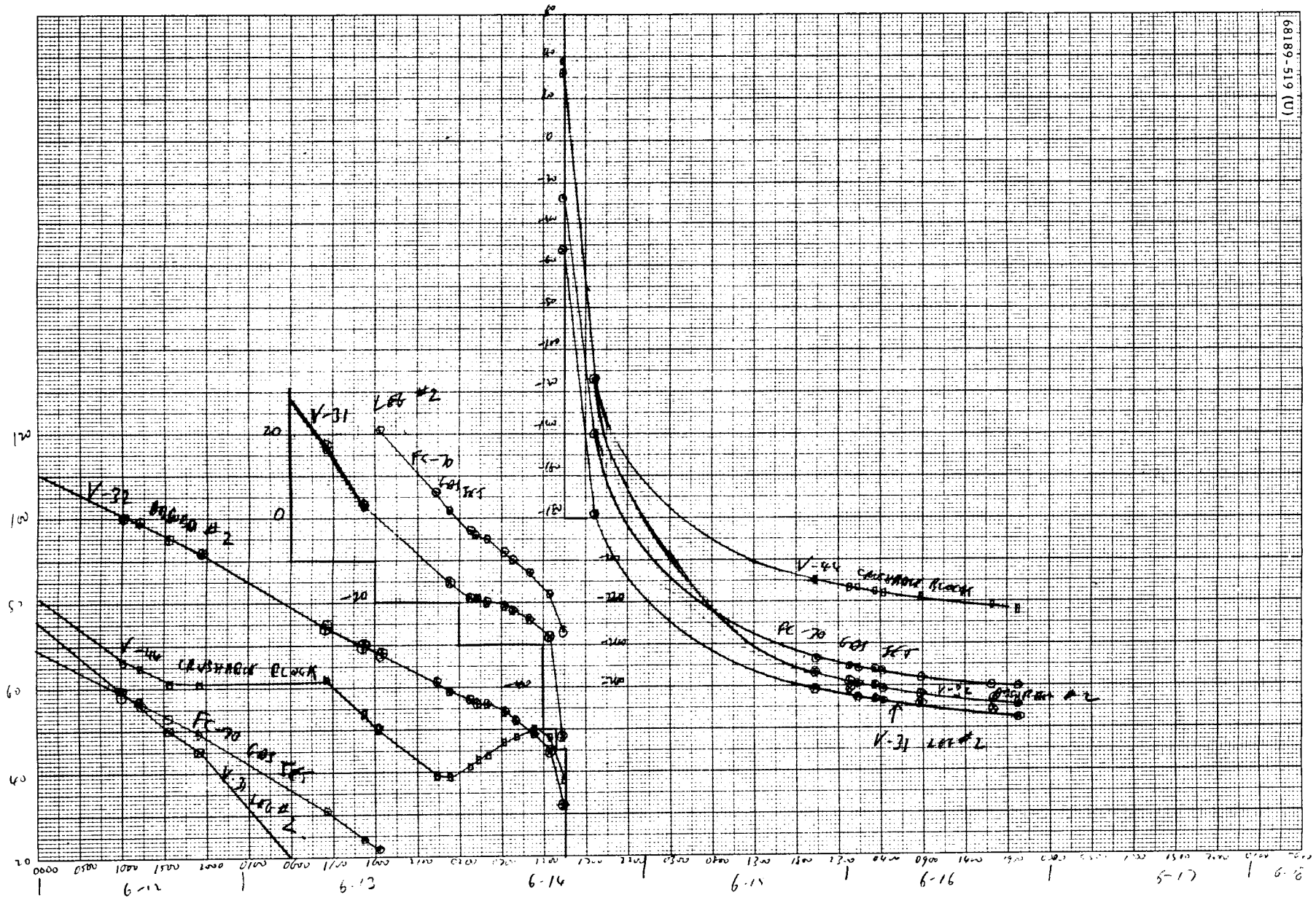


Figure B-20 (continued). Leg 2, Gas Jet 2, and Crushable Block 3

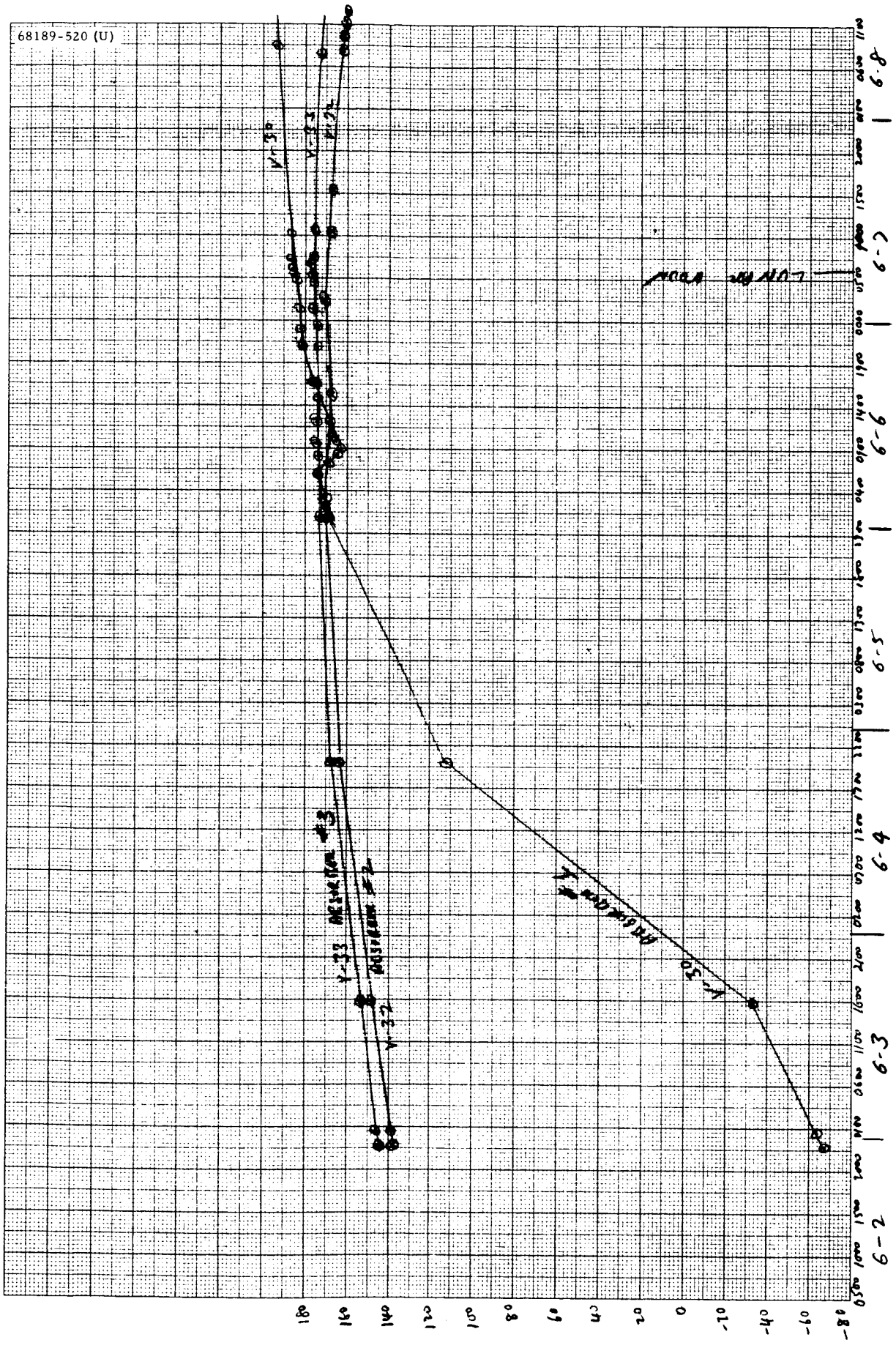


Figure B-21. Shock Absorbers

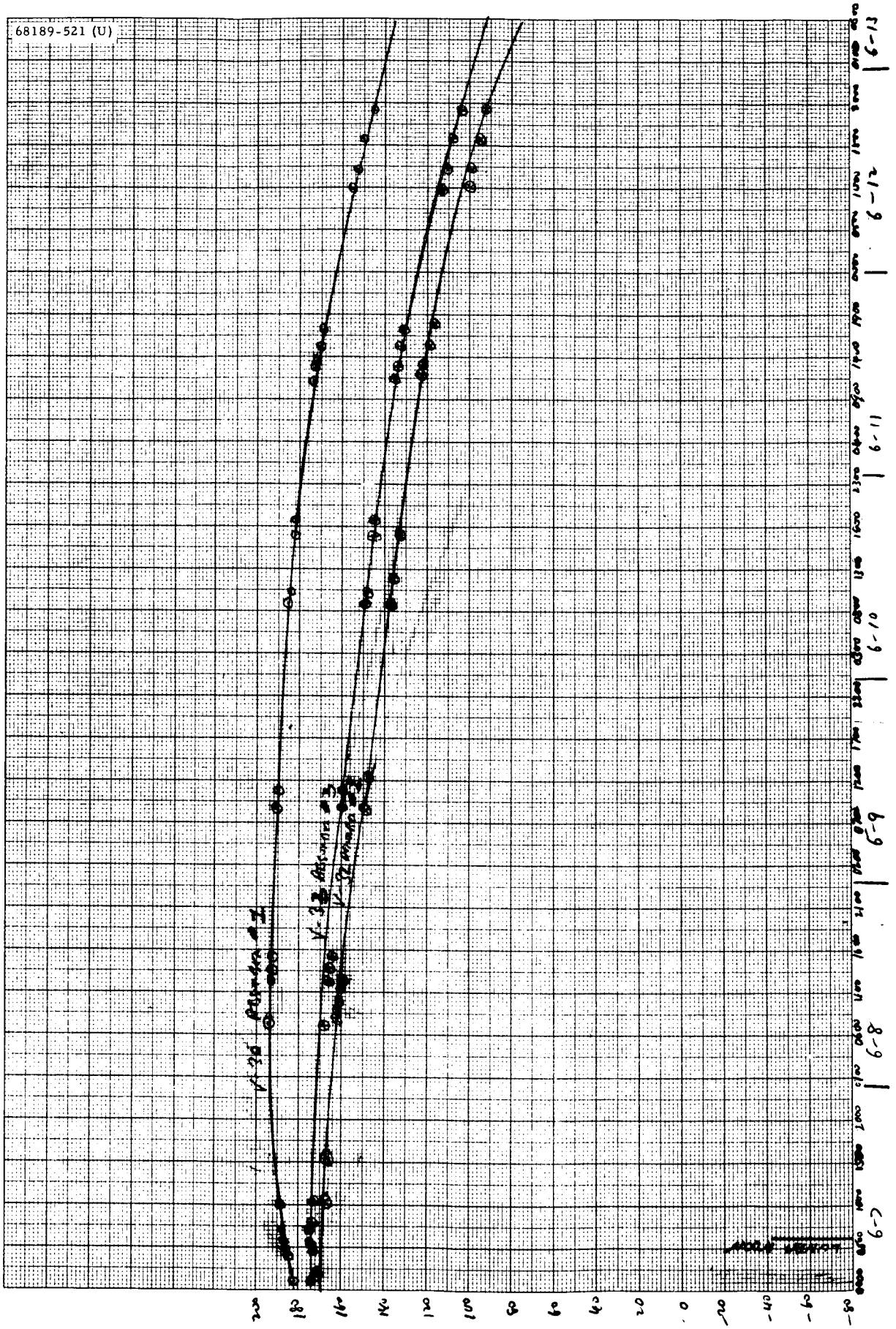


Figure B-21 (continued). Shock Absorbers

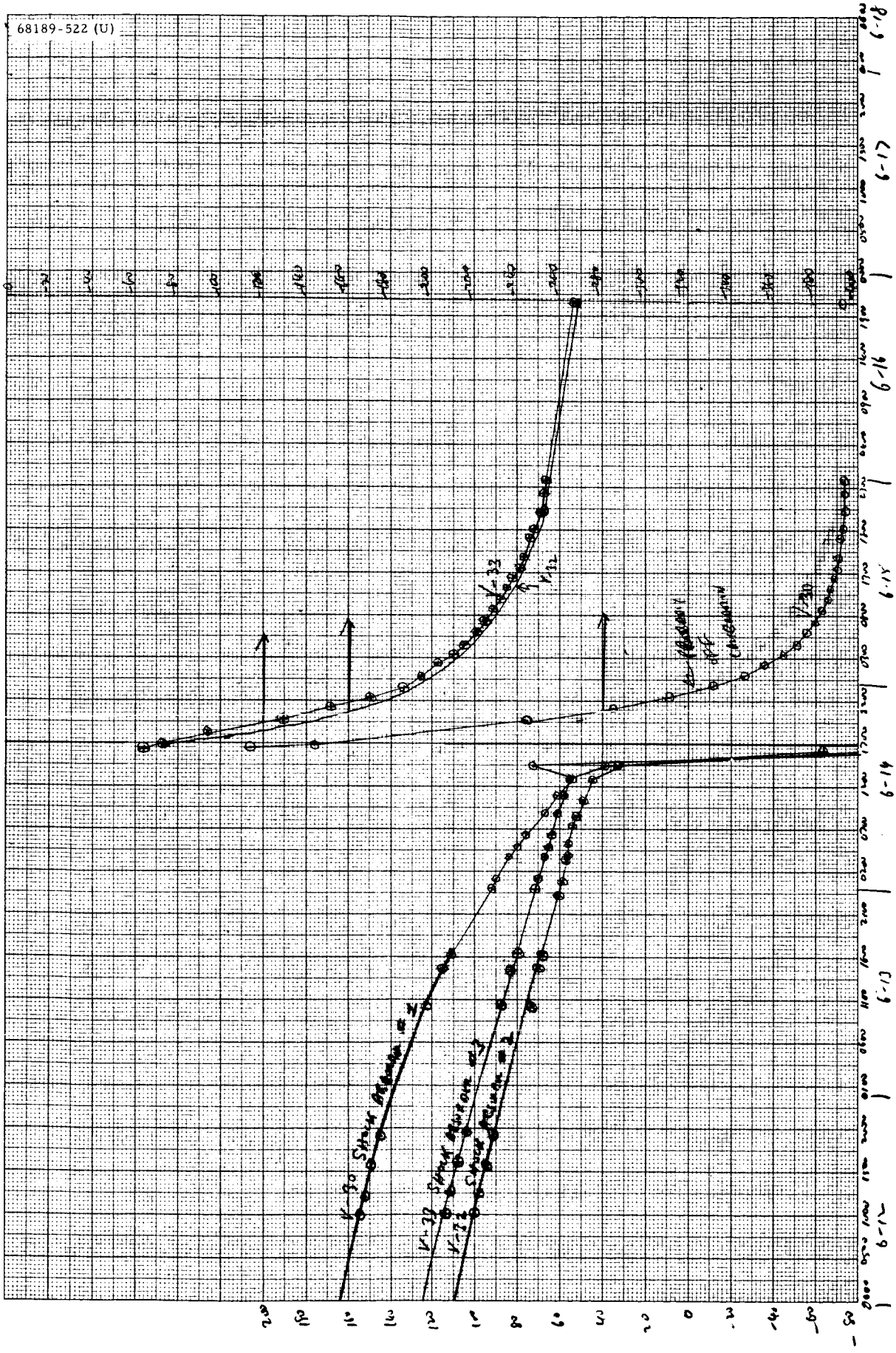


Figure B-21 (continued). Shock Absorbers

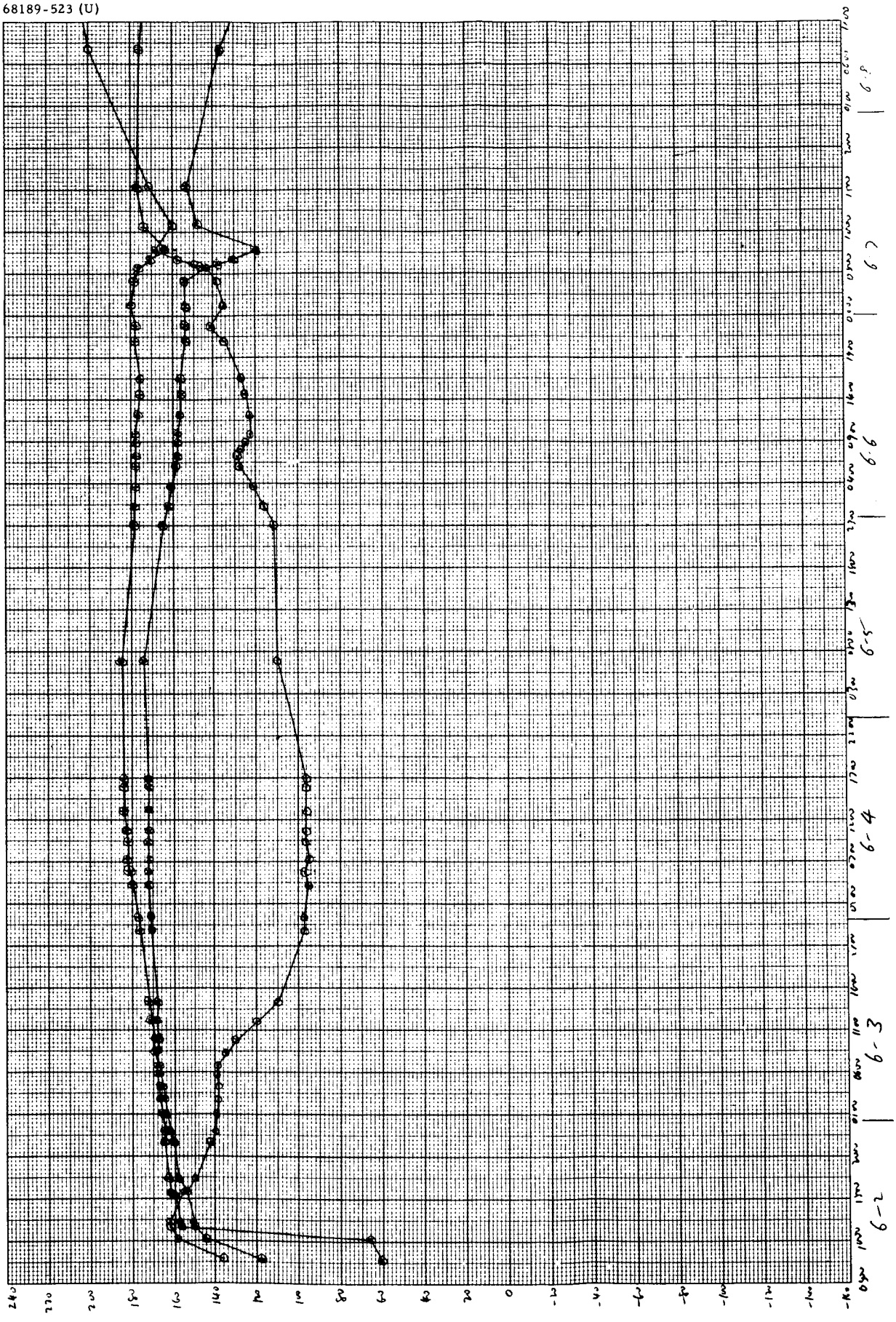


Figure B-22. Retro Attach Points 1, 2, and 3

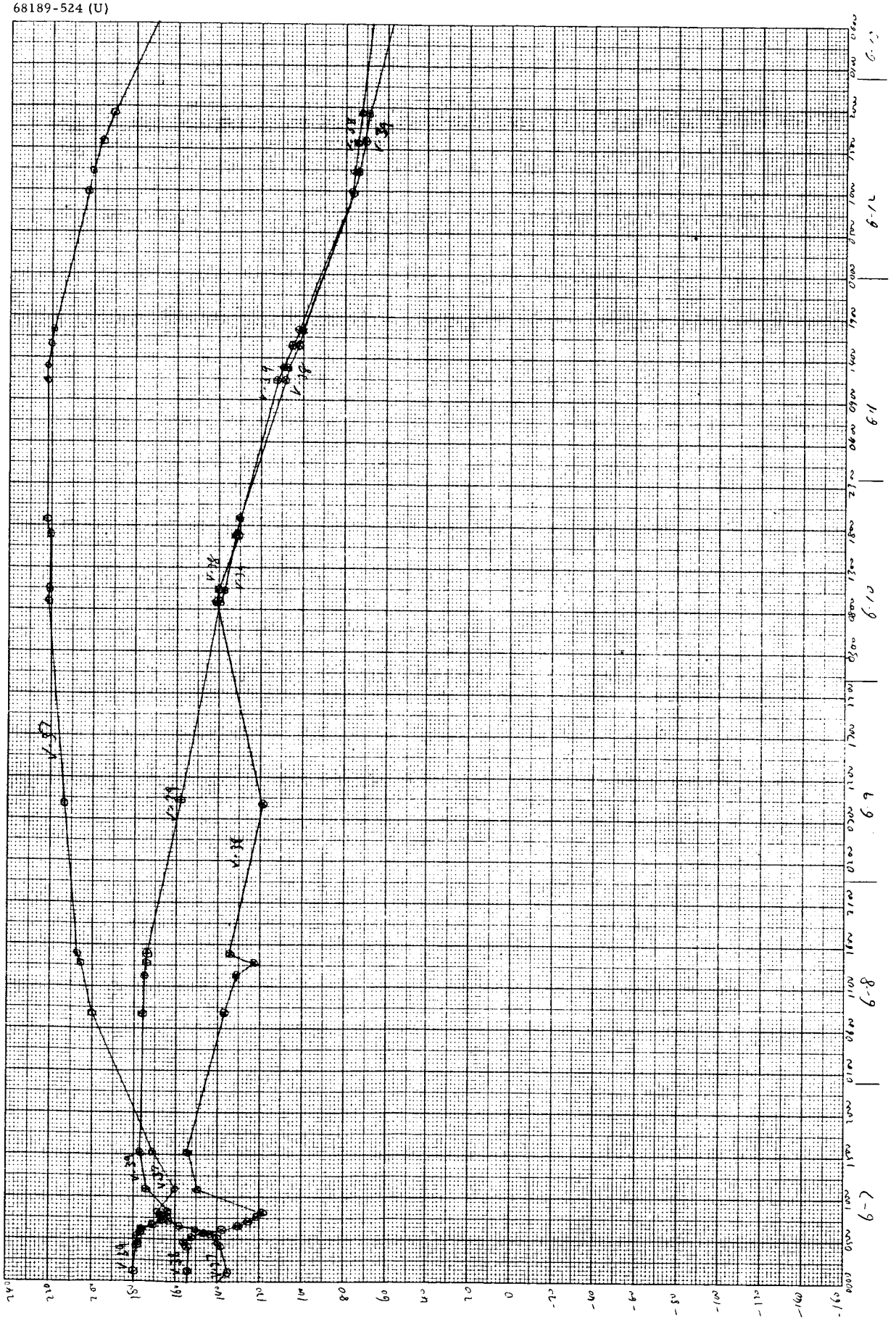


Figure B-22 (continued). Retro Attach Points 1, 2, and 3

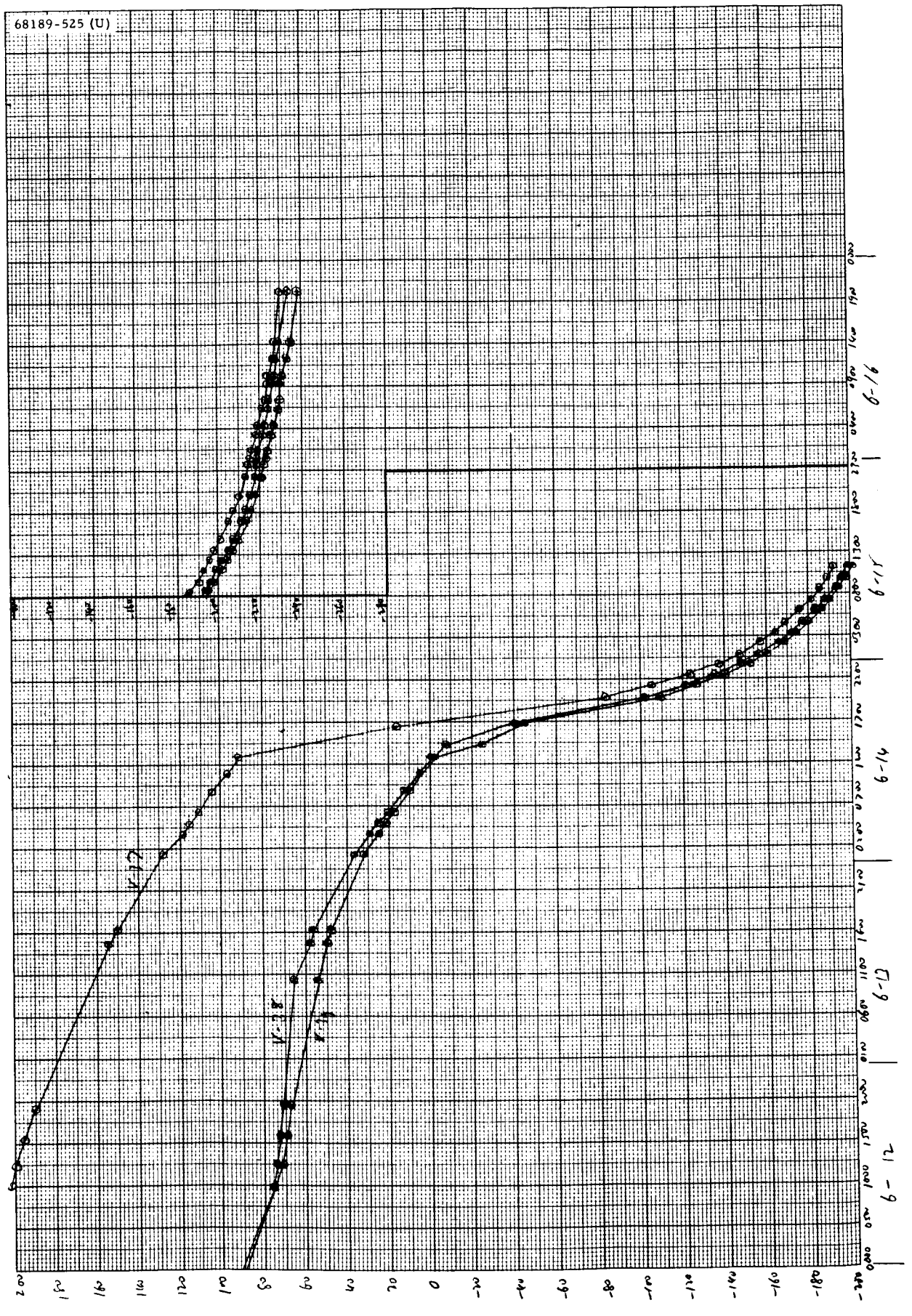


Figure B-22 (continued). Retro Attach Points 1, 2, and 3

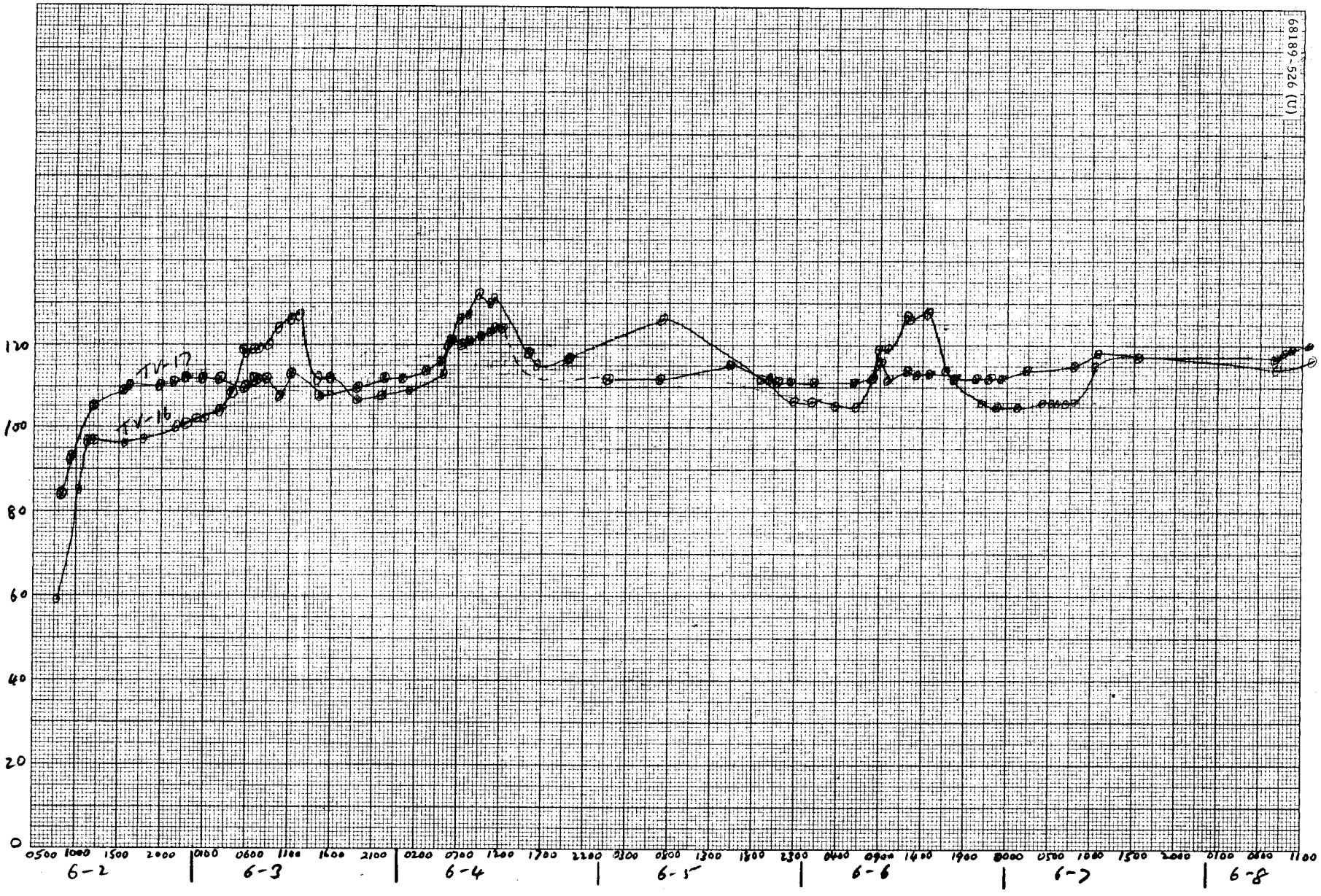


Figure B-23. Survey Camera

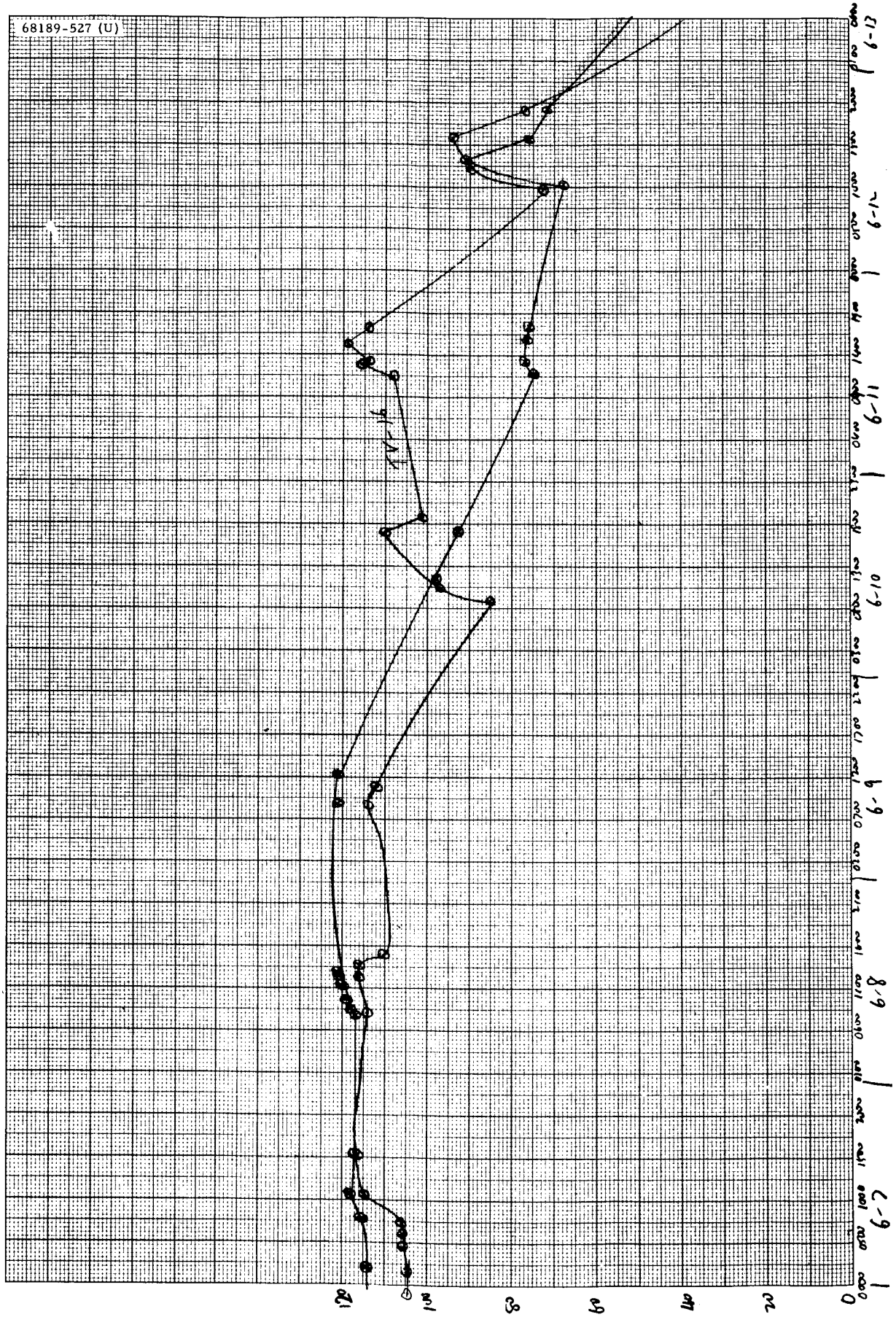


Figure B-23 (continued). Survey Camera

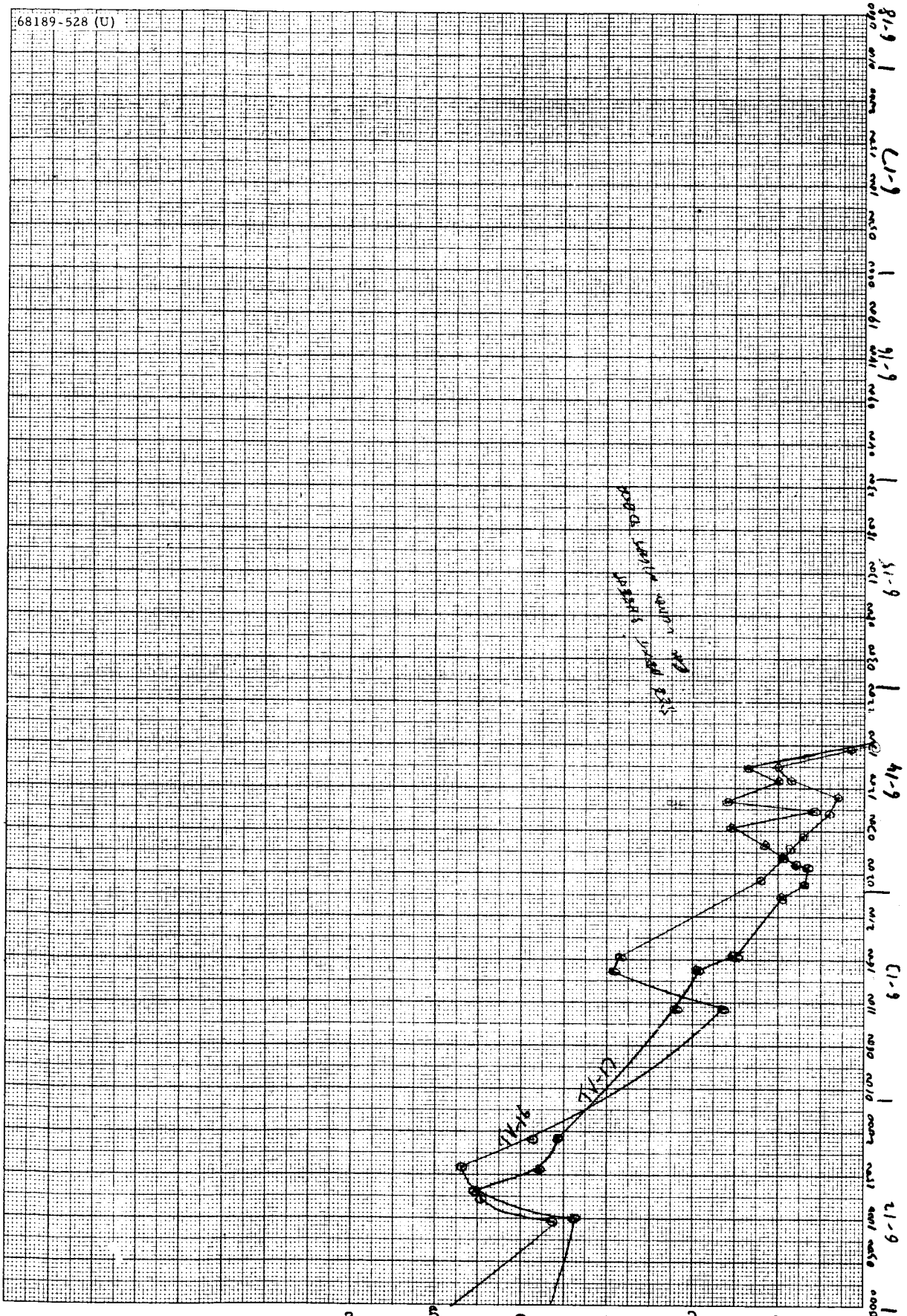


Figure B-23 (continued). Survey Camera

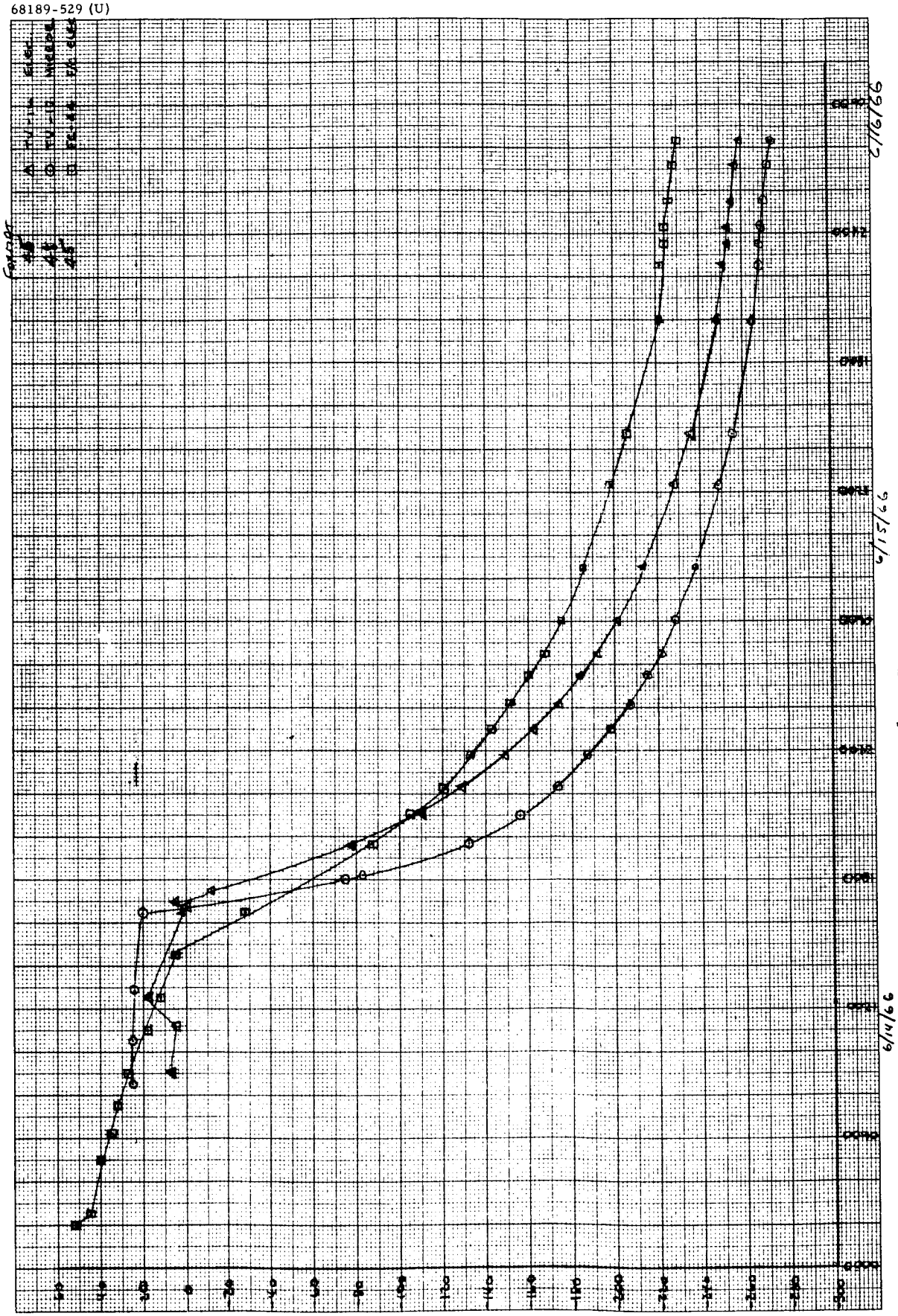


Figure B-24. TV and Flight Control

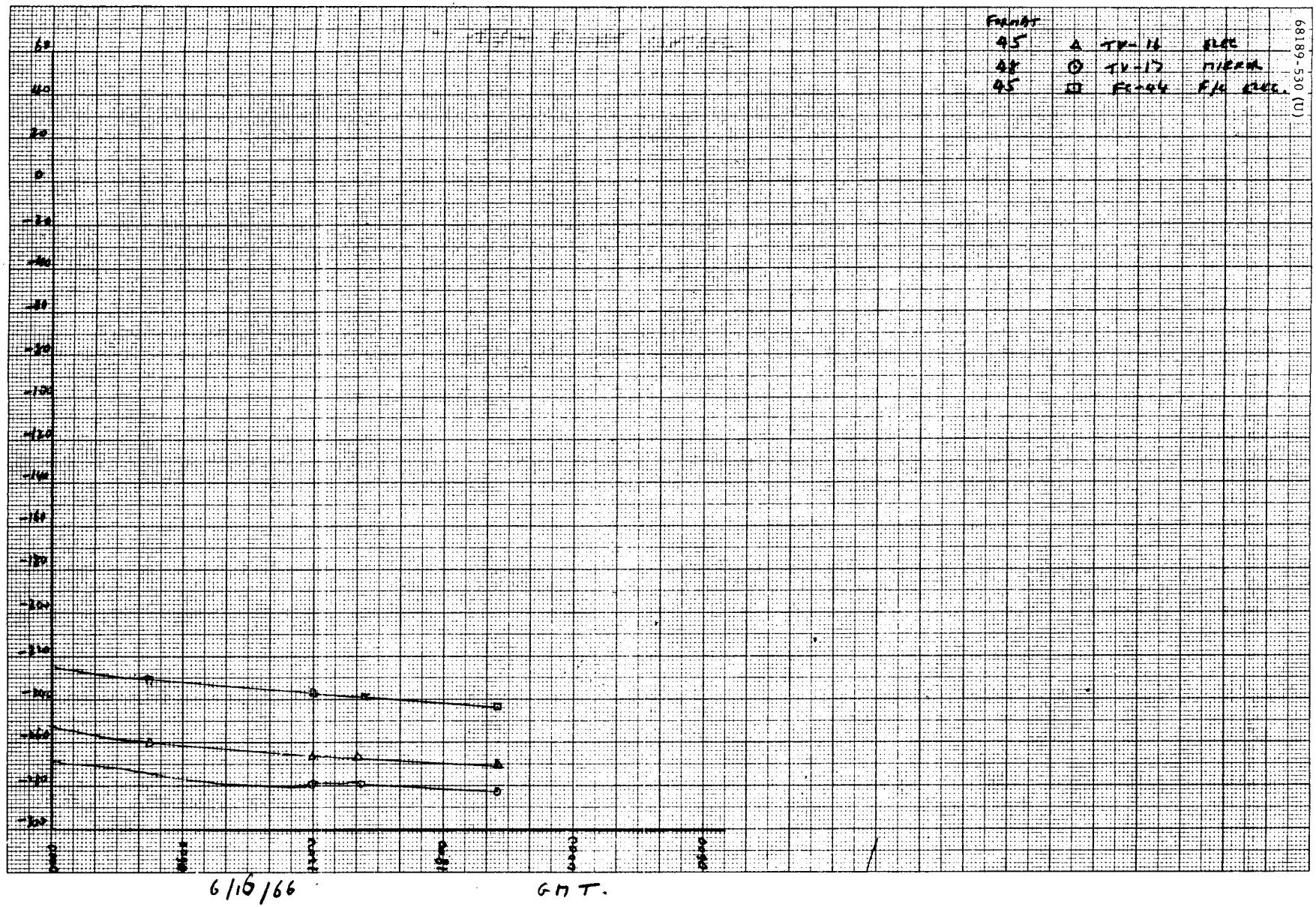


Figure B-24 (continued). TV and Flight Control